DEVELOPMENT OF NEW PHARMACOLOGICAL AGENTS FOR THE TREATMENT OF T CELL DISEASES OF THE SKIN

by

Kate O'Donnell B.Sc. (Pharm), M. Pharm.

Being a thesis submitted for the degree of Doctor of Philosophy

in Pharmacy and Pharmaceutical Sciences

Under the supervision and direction of Prof. John Gilmer

School of Pharmacy and Pharmaceutical Sciences

Trinity College Dublin

2021

Thesis Declaration

I declare that this thesis has not been submitted as an exercise for a degree at this or any other university and it is entirely my own work. I agree to deposit this thesis in the University's open access institutional repository or allow the library to do so on my behalf, subject to Irish Copyright Legislation and Trinity College Library conditions of use and acknowledgement. I consent to the examiner retaining a copy of the thesis beyond the examining period, should they so wish (EU GDPR May 2018).

Signed:

_____

Kate O'Donnell

Summary

T cell diseases of the skin fall into two distinct categories, inflammatory and malignant diseases. Examples of inflammatory T cell diseases of the skin include psoriasis, atopic dermatitis and vitiligo. Malignant T cell diseases of the skin fall under the broad name Cutaneous T Cell Lymphoma (CTCL), with the most common manifestations being Mycosis Fungoides (MF) and Sézary syndrome (SS).

This project is centred on ST0702, isosorbide-2-aspirinate-5-nicotinate, a compound containing an isosorbide group with an aspirinate and nicotinate ester attached. Prior to the work carried out in this project, ST0702 was tested in the imiquimod mouse model of psoriasis, and mice treated with ST0702 had significant reductions in all three parameters of skin inflammation; skin thickness, erythema and scaling.

Biochemical studies were carried out to determine the mechanism of action of ST0702 in the imiquimod mouse model. ST0702 exerted an effect on the proliferation of a T cell line and T cell blasts. This inhibition of proliferation was not associated with apoptosis under similar experimental conditions, indicating that the compounds exert a cytostatic effect on the cells. The antiproliferative effect of ST0702 was selective for activated T cells, as demonstrated by a lack of antiproliferative effect in the HaCaT cell line, the HEK reporter cell line and unstimulated PBMCs. The treatment of activated PBMCs and HuT78 cells with ST0702 inhibited the phosphorylation of numerous proteins involved in IL-2 signalling. ST0702 inhibited STAT3 signalling, but was not a direct inhibitor of JAK1/2/3 and the STAT3 inhibition was unlikely to be the cause of the antiproliferative effect on T cells, since the JAK inhibitor ruxolitinib had no effect on T cell proliferation at concentrations that inhibited STAT3.

ST0702 was shown to affect the metabolic activity of T cells. The rate of OXPHOS decreased, and there was a slight increase in the rate of glycolysis in T cells treated with ST0702. Several attempts were made to link the effect of the compound on the ETC to its antiproliferative effects on T cells and STAT3 inhibition. The cells were supplemented with various substrates, but none seemed to rescue the effects of ST0702 on proliferation, suggesting that the ETC disruption caused by treatment with ST0702 was not directly relevant to its antiproliferative activity.

A closer look at the proteins that were affected by ST0702 treatment led to an investigation of the compound as a potential inhibitor of the molecular chaperone HSP90. Among the HSP90 client proteins are several members of the JAK/STAT and MAPK pathway, both of which have been implicated in the pathogenesis of psoriasis.

Since it was known that ST0702 selectively affected the proliferation of T cells, and had a significant antiproliferative effect on HuT78 cells, a cell line derived from a CTCL patient, it was decided to investigate the potential of these compounds as pharmacological treatments for CTCL, and in particular, as skin-directed treatment for MF, the most common manifestation of CTCL. ST0702 and related compounds exerted antiproliferative activity on a number of T cell lines representing various manifestations and disease stages of CTCL, having modest but statistically significant effects on the proliferation of two MF cell lines, HH and MyLa.

The final part of this project involved the synthesis of new substances with potential clinical utility for skin-directed treatment of MF that had greater activity than ST0702. The anisate and anisate nicotinate compounds were identified, and they represent a key outcome of this project, being a result of careful scrutiny of the activity profile of a large family of isosorbide compounds synthesised in this work or belonging to the Gilmer lab. Several members of the compound family had greater antiproliferative activity than ST0702 in MF cell lines. Future studies will likely involve the establishment of an in vivo model of CTCL and one or more of the anisate compounds being tested in the model to assess the potential of these compounds as pharmacological agents for the treatment of CTCL.

Acknowledgements

I would like to thank many people who made it possible for me to complete this research.

I wish to thank my supervisor, Professor John Gilmer, for giving me the opportunity to do this research and for his advice and guidance over the past years. He has helped and encouraged me throughout my studies. A big thank you to Professor Aideen Long for her help and guidance and for providing me with the opportunity to use her laboratory in the TTMI.

My sincere thanks goes to Dr. Vanesa Martinez, for being a great friend and mentor and teaching me so much about being a good scientist. I would like to recognise the invaluable help she provided me throughout my studies.

I would like to thank Solvotrin Therapeutics and Trinity College Dublin for funding my PhD studies and giving me the opportunity to complete this research. Without their support and funding this project could not have reached its goal.

Thank you to everyone in lab 6.41 in TBSI, the students and postdocs, past and present, who made my time there so enjoyable. Thanks to Jinfan, Jerry, Miriam, Mark, James, Eavan, Ger, Gloria and Maria. A special thanks goes to Mark for his help with the project. Thanks also to all those in lab 2.101 in the TTMI, to Siobhan and Ismail, and to many of the other PhD students in the School of Pharmacy.

I would like to thank my friends for putting up with me talking about my thesis for what I'm sure felt like too long. The board game nights, Thursday drinks and nights out all helped me forget any of the frustration of experiments not working the way I wanted them to!

Last but definitely not least, I would like to thank my family, my parents Ciaran and Elaine, my brother Jack and sister Leah for supporting me throughout my PhD studies and my life in general. I couldn't have done it without their help and I'm sure they'll be very pleased when I start a job with an actual salary!

Table of Contents

Table of Figures ..... *vii*

List of Abbreviations ..... *xv*

1 Chapter 1: T cell diseases of the Skin *1*

1.1 Overview of Skin Components **1**

1.1.1 Epidermis 1

1.1.2 Dermis 2

1.1.3 Hypodermis 2

1.2 Immune Cells in the Skin **2**

1.2.1 Myeloid Cells 3

1.2.2 Lymphoid Cells 6

1.3 Immune Response in the Skin **9**

1.4 T cell mediated inflammatory skin diseases **10**

1.4.1 Atopic Dermatitis 10

1.4.2 Alopecia Areata 11

1.4.3 Vitiligo 13

1.4.4 Psoriasis 14

1.5 T cell Lymphomas **27**

1.6 Cutaneous T cell Lymphomas (CTCLs) **29**

1.6.1 Mycosis Fungoides 30

1.6.2 Sézary Syndrome 32

1.6.3 Clinical Staging of MF and SS 33

1.6.4 Treatment of CTCL 34

1.7 Aims and Objectives **39**

2 Chapter 2: ST0702 and the Synthesis of Analogues of ST0702 ..... *41*

2.1 Introduction **41**

2.1.1 Chemistry of 1,4:3,6-Dianhydrohexitols 41

2.1.2 Introduction to ST0702 (1) 43

2.1.3 Mouse Models in Psoriasis 45

2.2 Results and Discussion **46**

2.2.1 Aldara™ Mouse Model Experiments 46
2.2.2 Investigation into the Hydrolysis Pathways of ST0702 50
2.2.3 Initial Investigation into Effect of ST0702 on Models of the Innate Immune System 58
2.2.4 Proliferation of HaCaTs 61
2.2.5 T cell Proliferation Experiments 62
2.2.6 Synthesis of Isosorbide Analogues of ST0702 66
2.2.7 Synthesis of Isosorbide Analogues 70
2.2.8 Synthesis of Isomannide Analogues 72
2.2.9 Synthesis of Metabolites of ST0702 75
2.2.10 Physicochemical Properties of ST0702 and Analogues: Topical Administration 76
2.2.11 Lipophilicity Studies of ST0702 and Analogues 78
2.2.12 Biological Testing of New Compound Library 85
2.2.13 Testing new compounds in the Aldara™ Model 88

2.3 Conclusion 90

3 Chapter 3: Mechanism of Action of ST0702 93

3.1 Introduction 93

3.1.1 Immunology of Psoriasis 93
3.1.2 IL-2 and T cells 95
3.1.3 STAT3 and Psoriasis 97
3.1.4 IL-23/IL-17 Axis and Psoriasis 98
3.1.5 Overview of HuT78 Cells 100
3.1.6 Overview of T cell metabolism 101
3.1.7 Reactive Oxygen Species (ROS) in psoriasis 103

3.2 Results and Discussion 104

3.2.1 Phospho-kinase array: Activated PBMCs 104
3.2.2 Phospho-kinase array: HuT78 cells 108
3.2.3 Apoptosis Results for HuT78 cells treated with ST0702 or ISAL 110
3.2.4 Effect of compounds on STAT3 activation 110
3.2.5 Experiments with the JAK1/2 inhibitor ruxolitinib 115
3.2.6 Effect of ST0702 on Protein Kinase Activity 117
3.2.7 Experiments with Genistein and PP2 119
3.2.8 Direct Inhibitory Effect on JAK1/2/3 120
3.2.9 PBMC Proliferation Experiments 121
3.2.10 Glucose Experiments 128
3.2.11 Investigation into Effect of ST0702 on Metabolic Activity of the Cell 130

3.2.12 Investigation into antiproliferative activity of Complex I inhibitor rotenone 137
3.2.13 Succinate, Pyruvate, Citrate and Aspartate Supplementation 141
3.2.14 Reactive Oxygen Species (ROS) 151
3.2.15 Rescue Experiments with ROS Scavengers 154
3.2.16 HSP90 Inhibition 155

3.3 Chapter Conclusion 163

4 Chapter 4: Investigation into the potential use of developed compounds for the treatment of CTCL 167

4.1 Introduction 167
4.1.1 Molecular Pathogenesis of Cutaneous Lymphomas 167
4.1.2 Sézary Syndrome Versus Mycosis Fungoides: Single Disease Spectrum? 168
4.1.3 T cells in CTCL 169
4.1.4 Signalling Pathways in CTCL 170
4.1.5 HDAC inhibitors, HSP90 and CTCL 172
4.1.6 Cellular metabolism and ROS in CTCL 173
4.1.7 Overview of CTCL Cell Lines 174

4.2 Results and Discussion 175
4.2.1 Investigation into the activity of the compounds on MyLa cells 175
4.2.2 Investigation into the activity of the compounds on HH cells 179
4.2.3 Testing Chapter 2 Compounds on HH and MyLa Cell Lines 181

4.3 Conclusion 183

5 Chapter 5: Identification of a Potential Lead Compound for MF Therapy 187

5.1 Introduction 187
5.1.1 Library of Compounds tested 187

5.2 Results and Discussion 188
5.2.1 Library Screening for antiproliferative effect on CTCL cell lines 188
5.2.2 Library screening for antiproliferative effect on HuT78 cells 192
5.2.3 Library screening for inhibition of STAT3 activity in the IL-6 reporter 193
5.2.4 Effect of hits from CTCL inhibitors studies on OCR and role of OXPHOS 197
5.2.5 Design and synthesis of analogues of 33: Dianisates and Anisate Nicotinates 198
5.2.6 Antiproliferative activity of dianisates and anisate-nicotinates on MyLa cells 204
5.2.7 Antiproliferative effect of dianisates and anisates on HH cells 205
5.2.8 Antiproliferative effect on HuT78 cells 207

5.2.9 Inhibition of STAT3 Activation by anisate esters in the IL-6 reporter assay 209
5.2.10 Viability of HEK IL-6 Cells under STAT3 reporter assay conditions 211
5.2.11 Effect of Dianisate and Anisate Nicotinates on the proliferation of the HaCaT cell line 214
5.2.12 Measurement of levels of apoptosis in HuT78 cells 215
5.3 Discussion and Conclusion 215
5.4 Future Work 216
6 Chapter 6: Materials and Methods 219
6.1 Statistical Analysis 219
6.2 Biology 219
6.2.1 Compounds 219
6.2.2 Cell Culture 219
6.2.3 Culture of THP1-Blue NF-κB Cells 219
6.2.4 Culture of HuT78 Cells 220
6.2.5 Culture of HEK-Blue IL-6 Cells 220
6.2.6 Culture of HaCaT Cells 220
6.2.7 Culture of HH Cells 221
6.2.8 Culture of MyLa Cells 221
6.2.9 Isolation and Culture of PBMCs 221
6.2.10 Cell Counting 221
6.2.11 Cryopreservation and Revival of Cells 222
6.2.12 Preparation of T cell blasts 222
6.2.13 MTT Assay 222
6.2.14 Acid Phosphatase Assay 223
6.2.15 Alamar Blue Assay 223
6.2.16 NF-κB Activation Assay 223
6.2.17 Flow Cytometric Analysis of Cell Apoptosis 224
6.2.18 BCA Protein Assay: Calculation of Protein Concentration of Lysates 224
6.2.19 Proteome Profiler Array: Human Phospho-Kinase Array Kit 225
6.2.20 HEK IL-6 Blue Reporter Assay 225
6.2.21 IL-2 ELISA 226
6.2.22 Human Skin Microsomes 226
6.2.23 Mouse Skin Microsome 226
6.2.24 Seahorse Protocol 226
6.2.25 Preparation of Cellular Protein Extracts 228

6.2.26 Western Blotting 228
6.2.27 Cellular ROS 230
6.2.28 MitoSOX Flow Cytometry 230

6.3 Chemistry 231

6.3.1 General methods 231
6.3.2 Synthesis 231

References 271

Appendix 291

Table of Figures

Figure 1-1: Structure and cellular components of the skin in mice and humans (7). 3

Figure 1-2: Differentiation of naive T cells (20). 7

Figure 1-3: Clinical features of atopic dermatitis (41) 11

Figure 1-4: A-D Examples of well demarcated patchy alopecia areata (51)..... 13

Figure 1-5: Plaque psoriasis presentations. 16

Figure 1-6: Skin changes in psoriasis 19

Figure 1-7: Current model of the maintenance phase of psoriasis, showing the targets of approved or emerging psoriasis drugs. Modified from (91). 23

Figure 1-8: Structure of apremilast, an orally active PDE-4 inhibitor 25

Figure 1-9: Cytokine signalling through the JAK/STAT pathway (101). 26

Figure 1-10: Neoplasms corresponding to different stages of T cell differentiation (105). 28

Figure 1-11: Subtypes of mature T cell and NK cell neoplasms (106). 29

Figure 1-12: Classification of CTCLs. Adapted from (112). 30

Figure 1-13: ISCL/EORTC revision to the classification of MF and SS (117). 33

Figure 1-14: ISCL/EORTC revision to the staging of MF and SS (117). 34

Figure 1-15: Skin-directed therapies for the treatment of CTCL. 35

Figure 1-16: Systemic therapies for CTCL. Modified from (126). 37

Figure 2-1: Structure of isosorbide, isomannide and isoiodide. 42

Figure 2-2: Stereochemistry of isosorbide, isomannide and isoiodide..... 42

Figure 2-3: Structure of ST0702..... 43

Figure 2-4: Results from Aldara™ study of ST0702. 47

Figure 2-5: Structure of ST0702 (**1**), ISAL (**2**), ST0701 (**3**) and ST0703 (**4**). 48

Figure 2-6: Results from Aldara™ study for ST0701 (**3**) and ST0703 (**4**). 49

Figure 2-7: Results from Aldara™ study for ISAL (ST0702Sal). 50

Figure 2-8: General reaction scheme for hydrolysis of esters. 51

Figure 2-9: ST0702 potential hydrolysis pathways. ..... Z``52

Figure 2-10: Results from hydrolysis studies in the presence of preparations of human skin microsomes. Human skin microsomes (0.5 mg/mL) were incubated at 37˚C with 100 μM ST0702 and analysed by HPLC at designated timepoints. Points are plotted as mean ± SEM. 53

Figure 2-11: Hydrolysis pathway of ST0702 in the presence of preparations of human skin microsomes. 54

Figure 2-12: Results from hydrolysis studies in the presence of preparations of mouse skin microsomes. 55

Figure 2-13: Main hydrolysis pathway of ST0702 in mouse skin microsomes..... 56

Figure 2-14: Hydrolysis of 100 μM ST0702 in complete media (RPMI supplemented with 10% FBS and 2 mM L-glutamine) at 37˚C. 57

Figure 2-15: Hydrolysis of 100 μM ST0702 in complete media (RPMI supplemented with 10% FBS and 2 mM L-glutamine) at 37˚C. 57

Figure 2-16: Hydrolysis of 100 μM ST0702 in media (RPMI only) at 37˚C. 58

Figure 2-17: a) Overview of THP1-Blue NF-κB reporter assay and b) assay results. 59

Figure 2-18: GM-CSF, IL-10 and IL-23 production in LPS-stimulated PBMCs treated with ST0702. 60

Figure 2-19: IL-8 production in HaCaT cells in response to TNF-α. 61

Figure 2-20: Results from HaCaT proliferation studies..... 62

Figure 2-21: aCD3/CD28 activation of T cells followed by IL-2 induced T cell proliferation. 63

Figure 2-22: Proliferation of T cell blasts treated with 100 μM ST0702 (**1**), ST0701 (**3**), ISAL (**2**) or ST0703 (**4**). 63

Figure 2-23: Proliferation of T cell blasts treated with varying concentrations of ST0702. ... 64

Figure 2-24: Proliferation Results of compounds tested in HuT78 cells. 65

Figure 2-25: Annexin V Results in HuT78 treated with 100 μM compounds. 65

Figure 2-26: General reaction scheme for synthesis of isosorbide analogues of ST0702 67

Figure 2-27:Scheme for the Steglich Esterification 67

Figure 2-28: Esterification of ISMN (**8**) with the appropriate acyl chlorides. 68

Figure 2-29: Reduction of nitrate ester on C-2-esterified isosorbide compounds using H_2, Pd/C (**10a**, **10b** and **10e)** or zinc and acetic acid (**10c** and **10d).**..... 69

Figure 2-30: Esterification of isosorbide C-5 with nicotinoyl chloride..... 70

Figure 2-31: Synthesis of isosorbide-2-nicotinate-5-benzoate (**14**) 71

Figure 2-32: Structure of isosorbide-2-benzoate-5-isonicotinate (**15**) 71

Figure 2-33: Structure of isosorbide-2-aspirinate-5-salicylate (ST0701, **3**) and isosorbide 2,5-dinicotinate (16)..... 72

Figure 2-34: Approaches to the design of nicotinic acid isomannide based ester derivatives. 73

Figure 2-35:Esterification of isomannide (12) with Et_3N and appropriate acyl chlorides. 73

Figure 2-36:The addition of the nicotinate ester onto monosubstituted isomannide esters. ... 74

Figure 2-37: Structure of isosorbide-2-aspirinate (**7**) 75

Figure 2-38: Synthesis of Isosorbide-2-salicylate (**6**)..... 75

Figure 2-39: Reaction scheme for synthesis of ISAL(**2**). 76

Figure 2-40:HPLC chromatograms for the isomannide and isosorbide series. 79

Figure 2-41: Lipophilicity parameters of isomannide series obtained from RP-HPLC. 80

Figure 2-42: Lipophilicity parameters of isosorbide series obtained from RP-HPLC. 81

Figure 2-43: Lipophilicity parameters of isomannide series obtained from RP-TLC..... 82

Figure 2-44: Lipophilicity parameters for isosorbide series obtained from RP-TLC. 82

Figure 2-45: Plot of log P for isosorbide and isomannide esters. 83

Figure 2-46: Aqueous solubility results for isosorbide and isomannide compounds..... 84

Figure 2-47: HuT78 proliferation results for isosorbide and isomannide esters. 86

Figure 2-48: Results from HaCaT proliferation studies. 88

Figure 2-49: Results from Aldara study of vehicle (A), **11e** (B) and **19f** (C). 89

Figure 2-50: Overlay of 3D structure of ST0702 and 19f (isomannide-2-aspirinate-5-nicotinate). 90

Figure 3-1: Evolution of a psoriatic lesion from initiation to maintenance of disease (95). ... 95

Figure 3-2: IL-2 signalling pathway illustrating JAK-STAT signal transduction and the MAP kinase cascade (194). 97

Figure 3-3: Essential cells and molecules in the pathogenesis of psoriasis lesions, with particular emphasis on the IL-23/IL-17 axis (207). 100

Figure 3-4: Overview of cellular respiration (220). 103

Figure 3-5: PBMC proteome profiler array results. 105

Figure 3-6: Key results from proteome profiler array. 106

Figure 3-7: HuT78 proteome profiler array results. 108

Figure 3-8: Key results from HuT78 proteome profiler array. 109

Figure 3-9: Annexin V results of ST0702 and ISAL tested in HuT78 cells. 110

Figure 3-10: HEK-Blue IL-6 reporter results. 112

Figure 3-11: pSTAT3 and total STAT3 levels measured using western blotting. 113

Figure 3-12:Inhibition of STAT3 activation using decreasing concentrations of ST0702. 114

Figure 3-13: Effect of compounds on viability of HEK-Blue IL-6 cells measured using Alamar Blue. 115

Figure 3-14: HEK-Blue IL-6 results and HuT78 proliferation results for ruxolitinib. 116

Figure 3-15: Effect of PKC inhibitors on proliferation of HuT78 cells. 118

Figure 3-16: Production of IL-2 in HuT78 cells in response to PMA stimulation. 119

Figure 3-17: Results from HEK Blue IL-6 experiments with genistein and PP2. 120

Figure 3-18: Inhibitory effect of compounds on JAK1/2/3 (experiments conducted by Eurofins). 121

Figure 3-19: Design of PBMC experiments. 122

Figure 3-20: a) MTT PBMCs – CD3/CD28 and b) cell count PBMCs – CD3/CD28 only. 123

Figure 3-21: a) MTT PBMCs – CD3/CD28 + IL-2 and b) cell count PBMCs – CD3/CD28 + IL-2 124

Figure 3-22: a) MTT and b) cell count PBMCs – aCD3/CD28+IL-2 (treatment in last 24 h). 125

Figure 3-23: MTT PBMCs – CD3/CD28+IL-2 × 2 (30 min pre-treatment). 125

Figure 3-24: MTT and Cell Count PBMCs – CD3/CD28+IL-2 × 2 (treatment in last 24 h). 126

Figure 3-25: MTT from unstimulated PBMCs treated with compound for 48 h. 127

Figure 3-26:Results from glucose experiments on HuT78 cell line. 128

Figure 3-27: Results from glucose experiments on PBMCs activated with aCD3/CD28..... 129

Figure 3-28: Diagram of sensors in seahorse apparatus. 131

Figure 3-29: Seahorse experiments on activated PBMCs stimulated with IL-2. 131

Figure 3-30: Overview of Seahorse Mito-Stress test..... 132

Figure 3-31: Mito-stress Seahorse experiments on T cell blasts. 133

Figure 3-32: Seahorse experiment on T cell blasts: varying concentrations of ST0702. 134

Figure 3-33: Seahorse results for compounds tested in HuT78 cells. 135

Figure 3-34: Seahorse results for compounds tested in HaCaT cells. 135

Figure 3-35: Results from a) MTT assay and b) Acid Phosphatase assay on HuT78 cells... 136

Figure 3-36: Structure of rotenone 137

Figure 3-37: Results from MTT assay on T cell blasts testing a) rotenone and b) oligomycin. 138

Figure 3-38: a) Inhibition of STAT3 activation in HEK-Blue IL-6 cells treated with rotenone and ST0702 and b) concentration response curve for inhibition of STAT3 activation in HEK-Blue IL-6 cells treated with rotenone. 138

Figure 3-39: a) Antiproliferative effect of rotenone and ST0702 on HuT78 cells and b) concentration response curve for antiproliferative effect in HuT78 cells treated with rotenone. 140

Figure 3-40: Antiproliferative activity of rotenone on PBMCs undergoing protocol B, C, D or E. 141

Figure 3-41: Occurrences within the ETC following Complex I inhibition (263). 142

Figure 3-42: Effect of succinate supplementation on (a) proliferation of T cell blasts (b) proliferation of HuT78 cells (c) OCR and (d) STAT3 activation. 144

Figure 3-43: Antiproliferative Effect of rotenone in combination with pyruvate in T cell blasts. 146

Figure 3-44: Complex I inhibitors can affect the NAD+/NADH balance and halt the synthesis of aspartate, thereby causing a reduction in proliferation. Modified from (265). 147

Figure 3-45: Effect of aspartate supplementation on (a) proliferation of T cell blasts (b) proliferation of T cell blasts (adjusted) (c) proliferation of HuT78 cells and (d) STAT3 activation. 148

Figure 3-46: Effect of citrate supplementation on (a) proliferation of T cell blasts (b) proliferation of HuT78 cells (c) OCR and (d) STAT3 activation. 150

Figure 3-47: Levels of mROS in PBMCs ± aCD3/CD28. 151

Figure 3-48: Levels of mROS in T cells treated with ST0702 or rotenone. 152

Figure 3-49: Levels of mROS in HuT78 cells treated with ST0702, ISAL or rotenone. 153

Figure 3-50: Cellular ROS levels in HuT78 cells treated with compounds. 154

Figure 3-51: Antiproliferative effect of rotenone in combination with GSH or NAC in T cell blasts. 155

Figure 3-52: Results from pSTAT3 blot in HuT78 cells. 159

Figure 3-53: Results from HEK-Blue IL-6 cells treated with geldanamycin a) inhibitory effect on STAT3 activation and b) effect on viability measured using Alamar Blue assay. 160

Figure 3-54: HuT78 proliferation experiments with geldanamycin. 161

Figure 3-55: Results from pAkt blot with HuT78 cells. 162

Figure 3-56: Results from HSP90 blot of HuT78 cells. 163

Figure 4-1: Proliferation Results from MyLa cells treated with ST0702 or ISAL. 177

Figure 4-2: Proliferation Results from MyLa grown with/without cytokine supplementation. 178

Figure 4-3: mROS Production in MyLa following treatment with rotenone, ST0702 or ISAL. 178

Figure 4-4: Proliferation Results from HH treated with ST0702 or ISAL. 179

Figure 4-5: mROS production in HH following treatment with rotenone, ST0702 or ISAL. 180

Figure 4-6: Seahorse results in HH Cells. 181

Figure 4-7: Antiproliferative effect of chapter 2 compounds on HH cells. 182

Figure 4-8: Antiproliferative effect of chapter 2 compounds on MyLa cells 183

Figure 5-1: Examples of different carbamates. 188

Figure 5-2: Antiproliferative activity of library of compounds tested at 100 μM on MyLa cells. 189

Figure 5-3: Antiproliferative activity of broad library of compounds tested at 100 μM on HH cells. 190

Figure 5-4: Correlation curve of MyLa MTT % inhibition vs HH MTT % inhibition. 191

Figure 5-5: Compounds with greatest antiproliferative activity of HH and MyLa cells..... 192

Figure 5-6: Antiproliferative activity of library of compounds tested at 100 μM on HuT78 cells. 193

Figure 5-7: STAT3 inhibitory activity of broad library of compounds tested at 100 μM..... 194

Figure 5-8: STAT3 inhibitory activity of broad library of compounds tested at 25 μM..... 195

Figure 5-9: Correlation curve of HuT78 MTT % inhibition vs STAT3 activation. 196

Figure 5-10: Selection of compounds with greatest antiproliferative activity on HuT78 cells and STAT3 inhibitory activity..... 197

Figure 5-11: Inhibitory effect of compounds on OCR levels in HuT78 cells measured using Seahorse XF Analyser. 198

Figure 5-12: Effects of compound **33** (100 μM) in various biological assays 198

Figure 5-13: Synthesis of symmetrical dianisates (**56**) from isosorbide (**55**) via a 1-step sequence. 199

Figure 5-14: Synthesis of unsymmetrical dianisates (**59**) from ISMN (**8**) via a 3-step sequence. 200

Figure 5-15:Esterification of ISMN (**8**) with the appropriate methoxybenzoyl chlorides. ... 201

Figure 5-16: Reduction of nitrate esters on C-2 esterified isosorbide compounds (**57**) using H_2, Pd/C. 201

Figure 5-17: Esterification of isosorbide C5 with methoxybenzoyl chlorides. 202

Figure 5-18: General reaction scheme for synthesis of isosorbide-2-(o,m,p)-anisate-5-nicotinates (**60**) from ISMN (**8**). 203

Figure 5-19: Esterification of isosorbide-2-methoxybenzoate (**58**) with nicotinoyl chloride. 203

Figure 5-20: Antiproliferative activity of dianisates and anisates tested at 100 μM on MyLa cells. 204

Figure 5-21: Antiproliferative activity of dianisates and anisates at 100, 50 and 25 μM on MyLa cells. 205

Figure 5-22: Antiproliferative activity of anisates and dianisates at 100, 25 and 10 μM on HH cells. 206

Figure 5-23: Correlation curve of MyLa MTT% inhibition vs HH MTT % inhibition..... 206

Figure 5-24: Antiproliferative effect of dianisates and anisate nicotinates (100 μM) on HuT78 cells. 207

Figure 5-25: Antiproliferative activity of 100 μM anisic acids and isosorbide-2-(o,m,p)-anisate-5-hydroxyl compounds on HuT78 cells. 208

Figure 5-26: Antiproliferative effect of dianisates and anisate nicotinates (100, 50, 25, 10 μM) on HuT78 cells. 209

Figure 5-27: STAT3 inhibitory activity of dianisates and anisate nicotinates at 100, 25 and 10 μM. 210

Figure 5-28: STAT3 inhibitory activity of anisic acids and isosorbide-2-(o,m,p)-anisate-5-hydroxyl compounds tested at 100 μM. 210

Figure 5-29: Correlation curves for HuT78 % reduction in proliferation versus STAT3 % inhibition for dianisates and anisate nicotinates tested at 100 μM. 211

Figure 5-30: Effect of anisate esters (100 μM) on viability of HEK-Blue IL-6 cells. 212

Figure 5-31:Correlation curve of STAT3 inhibitory activity and decrease in % viability of HEKs for dianisates and anisate nicotinates tested at 100 μM. 213

Figure 5-32: Antiproliferative effect of dianisates and anisate nicotinates in HaCaT cells... 214

Figure 5-33: Levels of apoptosis in HuT78 cells treated with 100 μM anisate esters. 215

Figure 5-34: Key summary data for the dianisate and anisate nicotinate compounds. 216

Figure 6-1: Components of resolving and stacking gel used in Western blots. 229

List of Abbreviations

17-AAG	17-N-allylamino-17-demethoxygeldanamycin
A_3AR	A_3 adenosine receptors
AA	alopecia areata
AD	atopic dermatitis
ADP	adenosine diphosphate
AIDS	Acquired Immunodeficiency Syndrome
Akt	protein kinase B (PKB)
AMP	adenosine monophosphate
AMPK	AMP-activated protein kinase
ANOVA	analysis of variance
APC	antigen-presenting cell
ATLL	adult-T cell leukaemia
ATP	adenosine triphosphate
BCA	bicinchoninic acid
Bcl-2/6/x	B cell lymphoma-2/6/x
BSA	bovine serum albumin
CBCL	cutaneous B cell lymphoma
CCR	C-C chemokine receptor
cDC	conventional dendritic cell
CLA	cutaneous lymphocyte-associated antigen
CMOP	committed monocyte progenitor
CMP	common myeloid progenitor
CNS	central nervous system
CSF-1	colony stimulating-factor 1
CTCL	cutaneous T cell lymphoma
CTD	C-terminal domain
CVD	cardiovascular disease
CYP	cytochrome
DAG	diacylglycerol
DC	dendritic cell
DCA	deoxycholic acid
DCC	dicyclohexylcarbodiimide
DCF	2',7'-dichlorofluorescein

DCFDA	2’,7’-dichlorofluorescin diacetate
DCM	dichloromethane
DETC	dendritic epidermal T cells
DMAP	4-dimethylaminopyridine
DMEM	Dulbecco's modified eagle media
DMF	dimethyl fumarate
DMSO	dimethyl sulfoxide
DNA	deoxyribonucleic acid
Δp	protonmotive force
EBV	Epstein-Barr virus
ECAR	extracellular acidification rate
ECM	extracellular matrix
EDTA	ethylenediaminetetraacetic acid
EGFR	epidermal growth factor receptor
EID	erythrodermic inflammatory dermatoses
ELISA	enzyme-linked immunosorbent assay
EORTC	European Organisation for Research and Treatment of Cancer
ER	endoplasmic retuculum
ERK	extracellular signal-regulated kinases
ERRα	estrogen-related receptor alpha
ESI	electrospray ionisation
ETC	electron transport chain
FADH	flavin adenine dinucleotide (reduced)
FAK	focal adhesion kinase
FAO	fatty acid oxidation
FBS	fetal bovine serum
FCCP	carbonyl cyanide-p-trifluoromethoxyphenylhydrazone
FDA	U.S Food and Drug Administration
FITC	fluorescein isothiocyanate
GDP	guanosine diphosphate
GM-CSF	granulocyte-macrophage colony-stimulating factor
GMP	granulocyte-macrophage progenitor
GSH	glutathione
GSK-3	glycogen synthase kinase-3
GTP	guanosine triphosphate

GWAS	genome-wide association studies
H_2O	water
HCA_2	hydroxycarboxylic acid receptor 2
HCl	hydrochloric acid
HDAC	histone deacetylase
HDL	high-density lipoprotein
HIF-1α	hypoxia-inducible factor 1-alpha
HIV	human immunodeficiency virus
HLA	human leucocyte antigen
HPLC	high performance liquid chromatography
HRMS	High resolution mass spectrometry
HRP	horseradish peroxidase
HSC	hematopoietic stem cells
HSF-1	heat shock factor-1
HSP	heat shock protein
HSR	heat shock response
HSV	herpes simplex virus
HTLV-1	human T cell lymphotropic virus type 1
ICAM-1	intercellular adhesion molecule 1
iDC	inflammatory dendritic cell
IFN	interferon
IFN-α	interferon-alpha
IFN-γ	Interferon-gamma
Ig	immunoglobulin
IIMN	L-isoiodide mononitrate
IκK	inhibitor of kappa B kinase
IL	interleukin
ILC	innate lymphoid cells
IMMN	isomannide mononitrate
IMQ	imiquimod
IP_3	inositol 1,4,5-triphosphate
ISCL	International Society for Cutaneous Lymphoma
ISMN	isosorbide mononitrate
JAK	Janus kinases
LC	Langerhans cells

LDH	lactate dehydrogenase
LDL	low-density lipoprotein
LFA	lymphocyte function-associated antigen
LPS	lipopolysaccharide
mAb	monoclonal antibody
MAPK	mitogen-activated protein kinase
mDC	myeloid dendritic cell
MDP	macrophage and dendritic cell precursor
MeOH	methanol
MF	mycosis fungoides
MHC	major histocompatibility complex
miRNA	microRNA
MMAE	monomethyl auristatin E
MMF	monomethyl fumarate
mRNA	messenger RNA
mSWAT	modified Severity-Weighted Assessment Tool
mTOR	mechanistic or mammalian target of rapamycin
NAC	N-acetyl cysteine
NAD+	nicotinamide adenine dinucleotide (oxidised)
NADH	nicotinamide adenine dinucleotide (reduced)
NADPH	nicotinamide adenine dinucleotide phosphate
NaOH	sodium hydroxide
NFAT	nuclear factor of activated T cells
NF-κB	nuclear factor-kappa B
NK	natural killer
NMR	nuclear magnetic resonance
NO	nitric oxide
NOX	NADPH oxidases
NTD	N-terminal domain
OXPHOS	oxidative phosphorylation
PASI	psoriasis area and severity index
PBL	peripheral blood lymphocytes
PBMC	peripheral blood mononuclear cells
PBS	phosphate-buffered saline
pDC	plasmacytoid dendritic cells
PDE-4	phosphodiesterase-4

PDGFR	platelet-derived growth factor receptor
PHA	phytohaemagglutinin
PI	propidium iodide
PI3K	phosphoinositide 3-kinase
PIAS	protein inhibitors of activated STATs
PIP_2	phosphatidylinositol (3,4)-bisphosphate
PIP_3	phosphatidylinositol (3,4,5)-trisphosphate
PKA	protein Kinase A
PKC	protein Kinase C
PKG	protein Kinase G
PMA	phorbol myristate acetate
PMSF	phenylmethylsulfonyl fluoride
PTP	protein tyrosine phosphatase
RIPA	radioimmunoprecipitation assay
RNA	ribonucleic acid
RNS	reactive nitrogen species
ROS	reactive oxygen species
RP-HPLC	reverse phase-HPLC
RP-TLC	reverse phase-TLC
RT	room temperature/retention time
SA	staphylococcus aureus
SAR	structure activity relationship
SC	stratum corneum
SCID	severely combined immunodeficiency
SD	standard deviation
SDS	sodium dodecyl sulfate
SDS-PAGE	sodium dodecyl sulfate polyacrylamide gel electrophoresis
SEAP	secreted embryonic alkaline phosphatase
SEER	surveillance, epidemiology, and end results
SEM	standard error of the mean
SFK	Src family kinases
SOCS	suppressors of cytokine signalling
SS	Sézary syndrome
STAT	signal transducer and activators of transcription
$t_{1/2}$	half-life
TBS	tris-buffered saline

TBST	tris-buffered saline with saline
TCA	tricarboxylic acid cycle
TCGF	T cell growth factor
TCIPA	tumour cell-induced platelet aggregation
T_{CM}	central memory T cells
TCR	T cell receptor
T_{EM}	effector memory T cells
TEMED	tetramethylethylenediamine
Tfh	T follicular helper cells
TGF-b	transforming growth factor beta
Th1	T helper type 1
Th17	T helper type 17
Th2	T helper type 2
Th9	T helper type 9
TIGAR	TP53-inducible glycolysis and apoptosis regulator
TLC	thin layer chromatography
TLR	toll-like receptor
TNF-α	tumour necrosis factor alpha
TNMB	tumour, node, metastasis, blood
TOR	target of rapamycin
Treg	regulatory T cells
T_{RM}	tissue resident T cells
TSEB	total skin electron beam therapy
TTNT	time to next treatment
TYK2	tyrosine kinase 2
UVA	ultraviolet A
UVB	ultraviolet B

Chapter 1: T cell diseases of the Skin

1.1 Overview of Skin Components

The skin is the largest and heaviest human organ (1). The primary function of the skin is to act as a formidable physical barrier, protecting the body from environmental hazards, noxious substances and pathogens. In addition to its mechanical barrier function, the skin forms an active barrier that provides the first line of immunological defence against infection. The skin is composed of three main layers; the epidermis, the dermis and the subcutaneous fat tissue (hypodermis).

1.1.1 Epidermis

The epidermis is subdivided into the stratum corneum, stratum lucidem, stratum granulosum and stratum basale. The epidermis is primarily composed of keratinocytes (90-95%). These keratinocytes usually proliferate within the stratum basale and differentiate as they move through the epidermal layer, producing a stratification of cell type, and leading to a highly keratinised dead cell (corneocyte) at the skin surface. Under normal conditions, there is a balance between stem keratinocyte proliferation, terminal differentiation and the continuous desquamation of corneocytes from the skin surface (about 50 billion daily) (1).

The epidermis is also home to a subset of tissue-resident macrophages called Langerhans cells (LCs) which can present antigens (2). LCs are tightly bound to keratinocytes through dendritic processes that radiate in all directions (3). They can be both anti-inflammatory or inflammatory. In addition to LCs, $CD8^+$ memory T cells can also reside in the epidermis, these appear following the resolution of skin inflammation, such as that caused by the herpes simplex virus (HSV) infection (3).

The outermost layer of the epidermis is an impermeable layer known as the stratum corneum. It consists of layers of dead keratinocytes, called corneocytes, and intercellular lipids. The thickness ranges from 10 to 30 μm, but this varies depending on the body site. The stratum corneum functions as a barrier but contains many holes for skin appendages, such as hair follicles and sweat ducts (2). The corneocyte ‘bricks’ and the intercellular lipids ‘mortar’ provide a highly hydrophobic barrier against the environment, whilst the skin appendages provide a route for small molecule drugs and chemicals to penetrate the skin and allows for trans-epidermal water loss (2). LCs can extend their dendrites through tight junctions just beneath the stratum corneum to capture external antigens (4). Beneath the stratum corneum is

the stratum lucidum, which is a thin, clear layer of dead keratinocytes. Keratinocytes in the stratum lucidum contain eleidin rather than keratin. The stratum granulosum is a thin layer between the stratum lucidum and the stratum basale and the keratinocytes here contain cysteine- and histidine-rich granules, which bind keratin filaments together. The stratum basale contains basal keratinocytes, immune cells such as LCs and T cells, and melanocytes that confer pigmentation to the skin (5).

1.1.2 Dermis

The dermis primarily consists of extracellular matrix proteins that give the skin structure and elasticity (3). This abundant extracellular matrix (ECM), comprising collagen and elastin fibres provides a scaffold for immune cell migration. The dermis is composed of fibroblasts, which produce structural proteins and provide a supporting scaffold, endothelial cells, and neurons. It also contains many types of innate immune cells including dermal dendritic cells and macrophages. The macrophages present in the dermis are highly efficient at capturing dead cells and presenting antigens. Natural killer (NK) cells, monocytes, and neutrophils are some of the other components of the innate population of the dermis. Additionally, eosinophils and mast cells are present in the dermis and they are mainly involved in allergic responses (3). In the steady state, small numbers of neutrophils, monocytes and T cells survey the dermis for pathogens and, upon detection of inflammatory stimuli many more immune cells infiltrate the dermis (2).

1.1.3 Hypodermis

The subcutaneous fat layer or hypodermis is found under the dermis and consists of fibrocytes and adipocytes. It is rich in proteoglycans and glycosaminoglycans, which attracts fluids into the tissue and gives it mucous-like properties (6). The hypodermis has an important role in adipose homeostasis and serves as an insulating layer for the body (5).

1.2 Immune Cells in the Skin

Immune cells interact with skin cells to maintain tissue homeostasis and to induce immune responses. Diverse and functionally specialised immune cells populate the skin (7). Nearly every skin cell type can, upon stimulation, produce chemokines, cytokines and other inflammatory mediators that activate the innate and adaptive immune system and promote leucocyte recruitment from blood (7, 8).

With all of these different cells working in parallel the immune response in skin can become dysregulated. This dysregulation can lead to chronic inflammatory skin diseases such as

psoriasis and atopic dermatitis, in addition to the development of neoplastic diseases with a T cell origin such as cutaneous T cell lymphomas (CTCLs) (7).

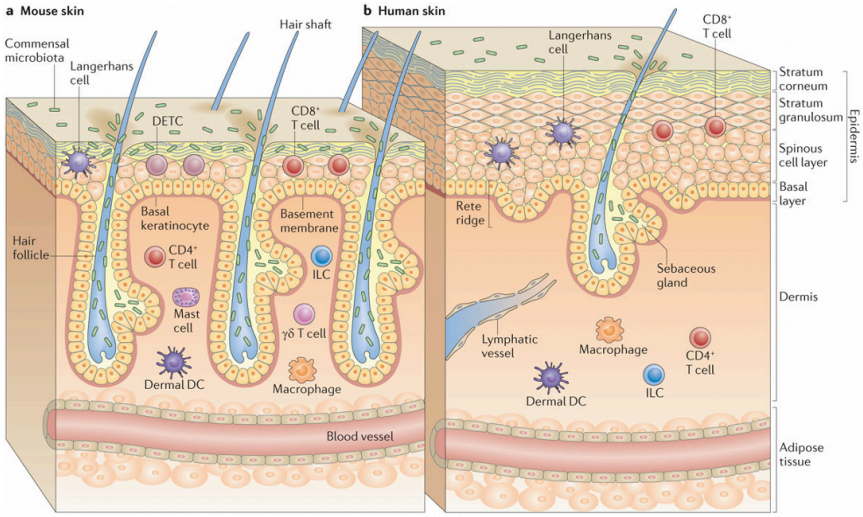

Figure 1-1: Structure and cellular components of the skin in mice and humans (7).
Mouse skin has more densely packed hair follicles, while human skin has a thicker epidermis and dermis. The most prevalent immune cells in human epidermis are LCs and CD8+ T cells. In murine epidermis, there is a prominent population of dendritic epidermal T cells (DETCs), which are absent in human epidermis. Human and mouse skin are both populated by dendritic cells, macrophages, mast cells, natural killer (NK) cells, αβ T cells and ILCs.

1.2.1 **Myeloid Cells**

1.2.1.1 *Dendritic Cells*

Dendritic cells (DCs) are bone-marrow cells derived from the lymphoid-myeloid system, and are specialised antigen presenting cells with a superior capacity to induce T cell responses. DCs in the dermis and epidermis participate in the recognition of invading pathogens. They are antigen-presenting cells (APCs) and have a role in the initiation of the adaptive and innate immune response. The skin contains a complex network of DCs, mainly composed of epidermal Langerhans cells, bone-marrow derived dermal conventional DCs, plasmacytoid DCs and inflammatory DCs (9).

Langerhans cells make up approximately 3% of all epidermal cells and are found regularly spaced out throughout the epidermis. Conventional dermal DCs are present in the dermis, at the level of the capillaries and in the higher part of the reticular dermis (10). As APCs, cDCs have various properties such as stimulation of naïve CD4+ T cells and presenting exogenous antigens to CD8+ cells in a process known as cross presentation (9). Migration of DCs from

the skin is one of the first steps in the initiation phase of an immune response in the skin. Skin contact with antigens stimulates the production of cytokines such as IL-6, tumour-necrosis factor alpha (TNF-α), granulocyte-macrophage colony-stimulating factor (GM-CSF), IL-1β, among which TNF-α and IL-1β are essential in DC migration. The DCs migrate through the afferent lymphatic vessels to the skin-draining lymph nodes (10). Conventional DCs are activated by numerous cytokines, including IL-6, TNF-α, IFN- α and LL-37-RNA complexes (9).

Plasmacytoid DCs (pDCs) are a unique subpopulation of DC that originate at bone marrow and migrate to the skin under pathological conditions (11). pDCs are not present in peripheral tissues under normal conditions, but migrate to skin that has been damaged by infection, injury, autoimmunity or cancer. pDCs are able to detect viral nucleic acid and initiate protective immunity through the production of type I interferons (IFNs). Unlike conventional myeloid DCs, pDCs express the Toll-like receptors (TLRs), TLR7 and TLR9, which recognise viral and self-nucleic acids and when activated, lead to the secretion of large amounts of type I IFNs. The migration pattern for the pDCs involves migration from the blood to the T cell-rich areas of the secondary lymphoid organs such as lymph nodes, and is in contrast to the migration pattern for myeloid DCs, which migrate first into peripheral non-lymphoid tissue such as the skin and then, upon activation, migrate into the T cell-rich areas of lymph nodes (11).

Inflammatory DCs (iDCs) are thought to derive from monocytes rather than conventional DC precursors. There are normally very few iDCs in healthy tissues, but the number increases after inflammatory insults. iDCs are involved in the polarisation of Th1, Th2 and Th17 cells by the production of inflammatory cytokines (9).

1.2.1.2 *Macrophages and Monocytes*

Monocytes are a group of cells circulating in the blood, bone marrow and spleen and consist of 10% of the total leukocytes in humans. Monocytes can remain in the circulation for up to 1-2 days, after which time, if they have not been recruited, they die and are removed (12). Monocytes originate in the bone marrow from hematopoietic stem cells (HSCs) and develop through a series of sequential differentiation stages: the common myeloid progenitor (CMP), the granulocyte-macrophage progenitor (GMP), the common macrophage and DC precursor (MDP) and the committed monocyte progenitor (cMoP). MDP also give rise to common DC progenitors (CDP) whose differentiation potential is restricted to DC lineage. The homeostatic control of monocyte/macrophage development is mostly influenced by colony stimulating factor-1 (CSF-1), while GM-CSF is also involved in phagocyte development, but only during the inflammatory state (12).

Resident macrophages are found in virtually all tissues of adult mammals, where they can represent up to 15% of the total cell number in quiescent conditions. Macrophages can take different names according to their tissue location, such as osteoclasts (bone), alveolar macrophages (lungs), microglial cells (CNS) and LC (skin). The traditional view that tissue macrophages originate from circulating peripheral blood monocytes needs to be reconsidered as new evidence has shown that macrophages have self-renewal capacity and can populate tissues before birth (13).

The dynamics of the macrophage and monocyte populations in the skin are not completely understood, however it is known that skin resident macrophages can originate from the yolk sac and can self-renew within the tissue (14). Monocytes and macrophages have been divided into three major populations: classically activated M1 macrophages, regulatory M2 macrophages and wound-healing macrophages. There is much evidence that M1 macrophages contribute to both acute and chronic inflammation in the skin (7).

1.2.1.3 *Mast Cells*

Mast cells are present in the dermis and are specialised for first-line surveillance functions, due to the presence of large amounts of preformed pro-inflammatory mediators that are stored within their cytoplasmic granules and can be rapidly released upon mast cell contact with antigens (7). Under normal conditions, mast cells do not circulate in the bloodstream, but mast cell progenitors migrate into tissues where they differentiate into mast cells under the influence of the tissue-environment. The cytoplasm of the mast cell contains 50-200 large granules that store inflammatory mediators, including histamine, heparin and a variety of cytokines. In the skin, antigens, via IgE, can activate mast cells. The cells release histamine and other vasoactive molecules, which cause urticaria. If the antigen activates mast cells in deeper tissue, angioedema can occur, and if the response is prolonged, atopic dermatitis or eczema can occur (15).

1.2.1.4 *Neutrophils*

Neutrophils are polymorphonuclear and phagocytic leukocytes that comprise the first line of host immune response against invading pathogens. They are important effector cells during tissue injury-induced inflammation. When an infection occurs there is a rapid influx of neutrophils from peripheral blood to the inflammatory site. They can kill microorganisms and clear infections by a number of mechanisms including chemotaxis, phagocytosis, release of reactive oxygen species (ROS), release of granular proteins and the production and release of

cytokines (16). They are also involved in the modulation of the adaptive immune response, through interactions with T and B cells, and possibly APCs (17).

1.2.2 **Lymphoid Cells**

1.2.2.1 *T cells*

Healthy skin contains approximately 20 billion T cells, almost double the number of T cells found in the circulation (18). Adult human skin is home to abundant populations of memory αβ T cells, as well as lesser numbers of natural killer (NK) cells, γδT cells and innate lymphoid cells (ILCs) (8).

T cells play a central role in the adaptive immune system. T cells mature in the thymus, where they undergo somatic gene rearrangement resulting in the expression of a unique T cell receptor (TCR). T cells are activated by foreign antigen to proliferate and differentiate into effector cells only when the antigen is displayed on the surface of antigen-presenting cells in peripheral lymphoid organs. T cells recognise protein fragments that have been degraded by the APC. The peptides are then carried to the surface of the presenting cell on molecules called major histocompatibility complex (MHC) proteins. Antigens are held in a structure called the MHC complex, on the surface of the MHC. During the positive selection process, detection of antigens presented by the APC on MHC Class 1 (MHCI) or class 2 (MHCII) by the rearranged TCR implements either a CD8+ (cytotoxic T cell) or CD4+ (T-helper cells) T cell lineage fate, respectively. Presentation of autoantigens in the thymic medulla ensures the elimination of autoreactive T cells, and the remaining T cells enter the circulation where they patrol blood and lymph as naïve T cells (CD45RA+CCR7+) (19).

Activation of T cells occurs in the peripheral lymphoid organs, where APCs (dendritic cells, macrophages and B cells) display foreign antigen complexed with MHC proteins on their surface. APCs display three types of protein molecules on their surface that have a role in activating naïve T cells: the MHC proteins, costimulatory proteins and cell-cell adhesion molecules. Following the interaction of the T cells with the APC, costimulatory molecules such as LFA-1, CTLA-4, CD28, CD2 and CD40 ligand are induced on the T cells (20). These can then bind to the upregulated costimulatory molecules on the APC which include ICAM-1, CD86, CD80, LFA-3 and CD40. Activation of the naïve T cell requires two signals, as without the costimulatory molecular interactions, the binding of the T cell receptor with the MHC presented antigen would result in T cell anergy rather than stimulation (20).

There are two main classes of T cells, cytotoxic T cells (CD8+) and helper T cells (CD4+). The effector CD8+ T cells directly kill cells that are infected with a virus or another intracellular

pathogen. Effector helper T cells are involved in stimulating the responses of other cells, primarily macrophages, B cells and CD8+ T cells.

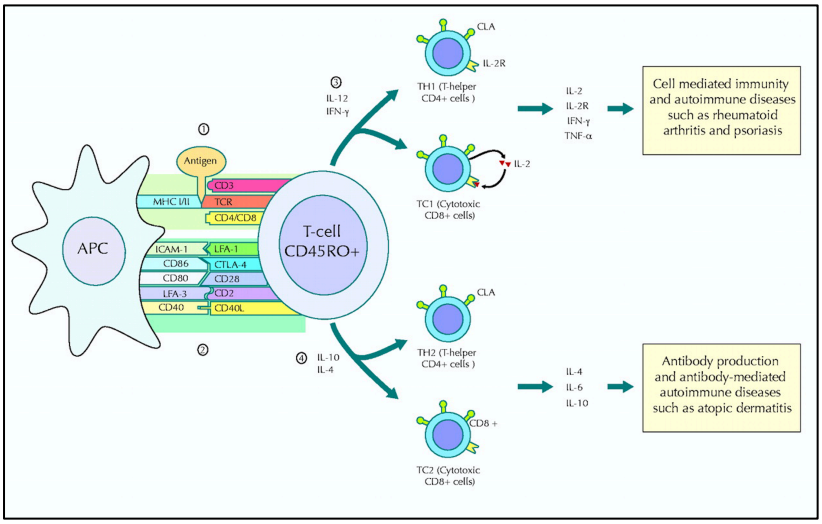

Figure 1-2: Differentiation of naive T cells (20).

1.2.2.2 *Cytotoxic T cells (CD8+)*

Once a cytotoxic T cell has been activated by an infected APC to become an effector cell it can destroy any target cell infected with the same pathogen. Cytotoxic T cells can induce the target cell to undergo apoptosis, and the cytotoxic T cell usually releases a pore-forming protein called perforin, which is stored in the secretory vesicles of the T cell and is released by local exocytosis at the point of contact with the target cell. These vesicles also contain serine proteases such as granzyme B, which can activate the caspase family of proteases that mediate apoptosis. These caspases then activate other caspases, and produce a proteolytic cascade that can kill the cell. Another method by which cytotoxic T cells induce apoptosis is through the Fas ligand on the surface of the T cell binding to the Fas receptor on the target cell, again triggering the caspase cascade (19).

1.2.2.3 *Helper T cells (CD4+)*

Different subsets of T helper cells can develop from naïve CD4+ T cells, namely Th1, Th2, Th17 or Th22 cells. Th1 cells produce IFN-γ and are thought to be primarily responsible for cell mediated immune responses, whilst Th2 cells produce IL-4, IL-5 and IL-13 and are primarily involved in humoral immunity, including allergic reactions. Th17 cells produce IL-17 and IL-22 and are involved in both inflammatory and autoimmune diseases. Th22 cells produce IL-22 only. T follicular helper (Tfh) and regulatory T cells (Tregs) have also been identified. Tregs express the transcription factor FOXP3 and have immunosuppressive effects

on immune cells (21). Tfh upregulate the B cell lymphoma 6 (Bcl6) transcription factor and migrate into B cell follicles. They play an essential role in the formation of germinal centres (22, 23). In more recent years, a novel class of Th cells, designated Th9 cells were identified. Most memory Th9 cells have been found to be skin-tropic or skin-resident (24). The role of these IL-9 secreting cells in skin diseases is not fully understood, however they have been linked to diseases such as psoriasis and CTCL (25).

The different Th subsets are implicated in the pathogenesis of a variety of diseases. In CTCL the malignant cell is thought to derive from a Th2 polarised origin. In early stage atopic dermatitis, Th2 cells are thought to drive the disease, however Th1 cells are implicated in the chronic disease stages. Psoriasis is predominantly associated with memory type Th1 polarised lymphocytes, with neutrophils, macrophages and dendritic cells all present in the inflammatory infiltrate. Th17 cells have also been implicated in psoriasis (26).

1.2.2.4 *Memory T cells*

Memory T cells, are by definition, derived from naïve T cells that have undergone multiple rounds of clonal expansion (8). After pathogen clearance, 95% of the effector cells undergo apoptosis, the remaining T cells give rise to a highly specialised set of memory cells that have lost CD45RA expression and instead express CD45RO (1). The effector T cell populations that are generated during an acute immune response are far more numerous than the memory T cell populations that survive long term in the skin, but the precise relationship between these populations is unknown, with one model suggesting that memory T cells are a distinct lineage that derive from an early activated T cell subpopulation that has not gone through T cell expansion, whilst another model suggests that memory T cells derive from a subset of surviving effector T cells (27).

Based on their migratory properties, memory T cells can be categorised into four major subsets: central memory T cells (T_{CM}), effector memory T cells (T_{EM}) and the more recently identified tissue resident T cells (T_{RM}), of which two populations have been identified (28). T_{EM} provide rapid effector function upon reactivation (1). T_{CM} cells express the chemokine receptor CCR7 and the vascular addressin L-selectin (CD62L) enabling them to circulate between lymph nodes and blood. T_{EM} cells express tissue-homing receptors that grant them access to peripheral tissues. Skin-homing T_{EM} cells, for instance, express the E-selectin ligand Cutaneous Lymphocyte-Associated Antigen (CLA) which allows them to enter the skin. CLA is therefore a marker that identifies skin specific T cells, but it also has a role as an adhesion molecule that facilitates the initial tethering of T cells to the epithelium. T_{RM} cells are non-recirculating memory T cells that reside indefinitely in epithelial barrier tissues and provide rapid front-line

immune protection in peripheral tissues. Studies of immune surveillance in a model of HSV infection have shown that skin-resident memory T cells achieved superior protection compared with circulating memory CD4+ T cells (29).

1.2.2.5 *B-cells*

B cells mature in the bone marrow and are involved in the humoral immune response. They are responsible for mediating the production of antibodies, antigen-specific immunoglobulins (Ig), directed against invasive pathogens. Mature B cells recirculate between secondary lymphoid organs in search of antigens. When they encounter an antigen, B cells receiving T cell help can enter a number of different developmental possibilities. In addition to the production of antibodies, B lymphocytes also act as APCs, and can produce cytokines with potent effects on both localised and systemic immunity.

Similar to T cells, the migration of B cells from the peripheral circulation into tissue sites is governed by interactions between selectins, chemokine receptors, and integrins with their cognate ligands (30). B cells have been shown to exhibit both proinflammatory and suppressive roles in the pathophysiology of inflammatory skin disorders in animal models and clinical studies in human subjects. In humans, treatment with rituximab, a monoclonal antibody (mAb) that targets the B cell surface antigen CD20 and depletes CD20+ B cells, has been reported to improve Atopic Dermatitis (AD) lesions (31). As AD is considered to be a T cell driven disease, it is unclear if this activity is related to antibody production by B cells or through the impact of B cells on T cell function. Interestingly, treatment with rituximab has been reported to result in the development of psoriasis in patients undergoing B cell depletion therapy for other indications such as rheumatoid arthritis or non-Hodgkin lymphoma, findings that suggest that B cells might play a suppressive role in the development of T cell mediated inflammatory skin diseases (32, 33).

1.3 Immune Response in the Skin

Keratinocytes, and skin resident immune cells, such as DCs, mast cells and macrophages can sense epidermal trauma, infection or exposure to UV radiation, and they can become activated, typically via the NF-κB and MAP kinase dependent pathways. This response can be mediated by pathogen components that are recognised by Toll-like receptors (TLRs) on these cells. The downstream results of the activation of these pathways are proinflammatory responses that leads to additional recruitment of inflammatory cells to the skin and migration of activated APCs to local skin-draining lymph nodes. DCs are specialised APCs that express high levels of co-stimulatory molecules and are capable of activating naïve T cells in lymph nodes. They

are able to internalise macromolecules introduced after skin disruption and, following processing, the antigens are bound to antigen presenting molecules and the resulting complex is expressed on the cell surface for presentation to T cells. The DCs then migrate and collect in lymph nodes where they come into contact with, and subsequently activate, naïve T cells (34). Antigen detection by CD4+ cells is restricted to MHCII expressed on APCs including dendritic cells, B cells and macrophages (1). The T cells become antigen-specific effector/memory cells and acquire the ability to home to the skin. Antigen specific memory T cells are also generated and circulate through the lymph nodes to provide a long-term reservoir for immune surveillance (35).

1.4 T cell mediated inflammatory skin diseases

1.4.1 Atopic Dermatitis

Atopic dermatitis (AD), commonly known as eczema, is an inflammatory skin disease. Atopy is defined as an inherited tendency to produce immunoglobulin E (IgE) antibodies in response to minute amounts of common environmental proteins, such as pollen, house dust mites and food allergens. Dermatitis refers to an inflammation of the skin. Symptoms include pruritus, dry skin, oedema, excoriations, lichenification and oozing (36). AD primarily affects young children but can persist into adulthood. It has a lifetime prevalence of approximately 20% (37).

There are two main hypotheses proposed to explain the inflammatory lesions in atopic dermatitis, the first being an immune hypothesis (38). This proposes that atopic dermatitis is the result of an imbalance of T cells, especially Th1, Th2, Th17 and Th22 and also Tregs. In the atopic dermatitis state naïve CD4+ T cells are preferentially differentiated into Th2 cells, which leads to an increased production of interleukins, primarily IL-4, IL-5 and IL-13, which then lead to an increase in the levels of IgE (38). The other hypothesis centres on skin barrier defects, since it has been observed that individuals with mutations in the filaggrin gene are at increased risk of developing AD. The filaggrin gene encodes structural proteins in the stratum corneum and stratum granulosum which help bind keratinocytes together, thereby maintaining an intact skin barrier and keeping the stratum corneum hydrated. When less filaggrin is produced, the skin barrier is no longer intact, excessive water loss occurs, there is increased penetration of allergens into the skin and eczema can result (38).

Psoriasis and AD are similar in that, in both diseases, epidermal keratinocytes respond to T cell derived cytokines by altering growth and differentiation responses. Psoriasis is largely driven by Th17 cells and associated IL-17 production, whereas AD has a strong Th2 component associated with IL-4 and IL-13 activation. Both diseases have activation of Th22 T cells and Th1 pathways with increased IL-22 and IFNγ.

The most common treatment options for AD include corticosteroids, emollients (to treat the dry skin associated with the condition), topical calcineurin inhibitors (such as tacrolimus), oral antihistamines, and UV light (39). Dupilumab, a mAb against IL-4Rα has shown efficacy in a large number of patients and is the first biological agent to be approved for the treatment of patients with moderate to severe AD (40).

Figure 1-3: Clinical features of atopic dermatitis (41)

1.4.2 **Alopecia Areata**

Alopecia Areata (AA) is one of the most prevalent autoimmune diseases in the USA, affecting approximately 4.5 million people. It is the most frequent cause of inflammation-induced hair loss. AA can affect both adults and children and has a worldwide prevalence of 0.1 to 0.2%, with a calculated lifetime incidence of approximately 2% (42). AA has historically been classified as an autoimmune disease of the hair follicle due to the characteristic T cell accumulation at the hair bulb (43). It manifests in the form of non-scarring, patchy hair loss, with a narrowing of the hair shaft near the scalp as a hallmark (44). AA can eventually lead to the loss of all the hair of the scalp (alopecia totalis), or, in its most severe form, the loss of hair of the whole body (alopecia universalis) (45).

The diagnosis of AA is normally straightforward, especially when it presents in its classical form with focal or multifocal patches of acute non-scarring alopecia, and a positive hair-pull test (43). If a skin biopsy is required, AA is associated with a histopathological finding of a peribulbular immune infiltrate of CD8+ T cells (known as a 'swarm of bees'), and CD4+ T cells around the hair follicles (44).

Similar to the CNS or the placenta, the hair follicle is considered an immune privileged site, and it is the loss of this immune privilege which leads to the hair follicles being attacked by autoreactive CD8+ and NK cells. Loss of immune privilege (IP) is considered a cornerstone in the pathogenesis of AA (44). IP is a revolutionary adaptation to protect organs in the body that have limited regenerative ability. IP protects these organs by creating an anergic state that could even tolerate a foreign graft within the tissue. Evidence for the hair follicles being immune privileged sites comes from two studies; the first which demonstrates the ability of melanocytes of a black guinea pig to survive in hair follicles grafted onto albino guinea pig recipients (46), and the second, which demonstrates the survival of human dermal sheath tissues within a sex-mismatch transplantation (47). The presence of lymphocytes, dendritic cells and NK cells in the peribulbar area of the anagen hair follicle, which is usually sparse of immune cells, serves as proof of IP collapse in AA (48). There are two main theories explaining the initial events that lead to IP collapse, the first emphasises local defects in hair follicles, whereas the second implicates a dysregulated immune system (48).

AA was initially believed to be a Th1 disease, due to the role of IFN-γ, but AA has also been epidemiologically associated with atopy, which is a classic Th2 condition defined by a predominance of IL-4 and IL-13. Mouse studies have demonstrated that CD8+ cells are important effector cells in AA, but maximal induction of AA also requires the help of CD4+ lymphocytes (49).

Treatment options for AA are limited and are not always effective. Treatment options fall within two categories: use of an immunosuppressive regimen (used for patients with acute and rapidly progressing AA) or an immune deviation strategy that manipulates the intracutaneous inflammatory milieu (used for patients with chronic, relapsing AA) (45). Treatment options include corticosteroids (to suppress the immune system), minoxidil, anthralin, topical immunotherapy, PUVA or cyclosporin (42). Topical minoxidil, a potassium channel facilitator that is used as a general hair-growth stimulant in androgenetic alopecia, can be used in alopecia areata, but ideally in combination with other treatments such as dithranol cream and corticosteroids (45).

Recently, the important role of the JAK-STAT pathway in AA has been discovered, and trials are currently underway to test the effectiveness of JAK inhibitors such as ruxolitinib and tofacitinib in the treatment of AA (50).

Figure 1-4: A-D Examples of well demarcated patchy alopecia areata (51).

1.4.3 **Vitiligo**

Vitiligo occurs in about 1% of the population globally and is the most common cause of acquired skin, hair and oral depigmentation. It involves the destruction of the melanocytes of the skin and is characterised by the occurrence of white depigmented patches of skin. Generally, vitiligo develops initially on hands, wrists, body folds and orifices such as eyes, nose and mouth (52). The histology of lesional skin is characterised by a dermal inflammatory infiltrate along with hypopigmentation in the basal layer of the epidermis, the latter being caused by the destruction of melanocytes (44).

Vitiligo can be classified as nonsegmental (generalised) or segmental. Nonsegmental vitiligo is the most common form (80-90% of cases). In completely depigmented areas, inflammation is usually absent, but mononuclear cells have been identified at the margin of the depigmented areas in cases of nonsegmental vitiligo (53).

Vitiligo is a complex disease, as it appears to associate environmental and genetic factors together with metabolic and immune alterations (54). Oxidative stress has been suggested to be the initial pathogenic event in melanocyte degeneration. Elevated levels of reactive oxygen species (ROS) have been observed in lesional and non-lesional skin of vitiligo patients, with several studies suggesting that mitochondria could be the main source of ROS in vitiligo (55). Increased levels of ROS can create a pro-inflammatory environment that can promote activation of the immune system, and can alter the signal transduction pathways in melanocytes (54). The involvement of the innate immune system in vitiligo has also been shown, with

damage to melanocytes and keratinocytes inducing the production of pro-inflammatory cytokines (54).

In terms of adaptive immunity, there is much evidence for the role of T cells and their related cytokines in the development of vitiligo, with CD4+ and CD8+ T cells consistently found at the edge of actively depigmenting skin of vitiligo patients (56). Studies carried out using melanocyte-specific TCR transgenic mouse models suggest that CD4+ T cells are involved in depigmentation and reports have shown that both CD4+ and CD8+ T cells produce mainly IFN-γ and TNF-α in vitiligo, which is indicative of a Th1/Tc1 cell polarisation (57). The precise role of Th17 cells in vitiligo is not known, but higher levels of IL-17 expression are observed in both blood and perilesional skin of vitiligo patients (58, 59). CD8+ T cells specific for melanocyte antigens have been detected in the blood and perilesional skin of patients with vitiligo and it has been shown that CD8+ T cells from perilesional skin of vitiligo patients can recognise melanocyte antigens, express granzyme B and the pro-inflammatory cytokines IFN-γ, TNF-α and IL-17 and can induce autologous melanocyte apoptosis in normally pigmented skin in vitro, suggesting the involvement of a cytotoxic response to melanocytes (57, 60).

Treatment success is usually assessed in terms of the proportion of treated patients in whom a specified degree of repigmentation is achieved, with more than 50% or more than 75% (depending on the study) considered to be a good response. Treatment options include phototherapy (narrowband UV-B), topical therapies such as corticosteroids and calcineurin inhibitors or surgical grafting (50, 53). Most of these therapeutic options have limited efficacy. With regard to emerging therapies, the use of JAK inhibitors to treat vitiligo patients is currently being examined, the evidence for which being that IFN-γ, a key cytokine in vitiligo, translates its intracellular signal through STAT1 (50).

1.4.4 **Psoriasis**

The word psora comes from the Greek, meaning “to itch”. The term psoriasis has been in use since *c* 133 AD, and the disease was grouped with leprosy until the 19th century (61). It has been suggested that biblical leprosy was, in fact, the disorder known today as psoriasis. The identification of psoriasis as a distinct disease did not occur until the 19th century.

Psoriasis is a chronic inflammatory autoimmune skin disease that is characterised by T cell mediated hyper-proliferation of keratinocytes (62). It is a disease of the immune cells, discovered when psoriasis patients were observed to respond to the immunosuppressant cyclosporin. Psoriasis affects over 73,000 people in Ireland, with over 9,000 of those suffering

from severe psoriasis (63). It is estimated that over 6,000 new psoriasis cases are diagnosed annually in Ireland.

Psoriasis can develop at any age, but it has two peak periods of onset; between 15 and 25, and between 50 and 60 years of age (64). The severity of psoriasis varies greatly between patients, with many patients having psoriasis that affects only a small area of the skin (< 2% Body Surface Area (BSA)) whereas in other patients the disease can be much more severe (64).

1.4.4.1 *Psoriasis Presentations*

There are no exact diagnostic criteria for psoriasis so the diagnosis is made clinically through pattern recognition and careful examination of the morphology of the skin (65). The clinical phenotype of the psoriasis can then be deduced. Psoriasis has a broad spectrum of clinical presentations, and involves many different morphologies, including plaque lesions, guttate type eruptions, erythrodermic psoriasis, and the formation of pustular lesions (65).

Plaque psoriasis is the most prevalent type of psoriasis, and affects approximately 90% of all psoriasis patients (65). Plaque psoriasis can affect any part of the body but is often localised to the elbows and knees in a symmetrical pattern. The scalp is also commonly affected. Plaque psoriasis lesions are characterised by dry, sharply demarcated round or oval plaques with silvery white scales that are loosely adherent (65).

Guttate psoriasis occurs more frequently in children and young adults. It can occur on its own (termed acute guttate psoriasis) or can complicate existing chronic plaque psoriasis (66). It is characterised by round erythematous exanthema of generally less than 1 cm size over the trunk and the extremities (65). The lesions appear as ‘gutta’ or droplets. It has a strong association with preceding or concurrent streptococcal infection, and typically erupts 1–2 weeks following an episode of acute tonsillitis. If left untreated, guttate psoriasis may clear spontaneously but there is a risk that it could develop into chronic plaque psoriasis (66).

Pustular psoriasis is characterised by the formation of white pus-filled pustules that are surrounded by red skin. The pus consists of white blood cells. It is non-contagious and is primarily seen in adults and generally affects most of the body. It is a quite a rare clinical subtype of psoriasis (67).

It has been suggested that the different clinical presentations of psoriasis are linked to the activation of different arms of the immune system, with the adaptive immune system being dominant in chronic plaque psoriasis whilst the innate immune and autoinflammatory responses are dominant in generalised pustular psoriasis (67). Autoimmunity involves the activation of the adaptive immune system, such as T or B cells, whereas autoinflammatory

reactions are driven by endogenous danger signals, metabolic mediators and/or cytokines. In psoriasis, autoimmunity and auto-inflammation co-exist (67).

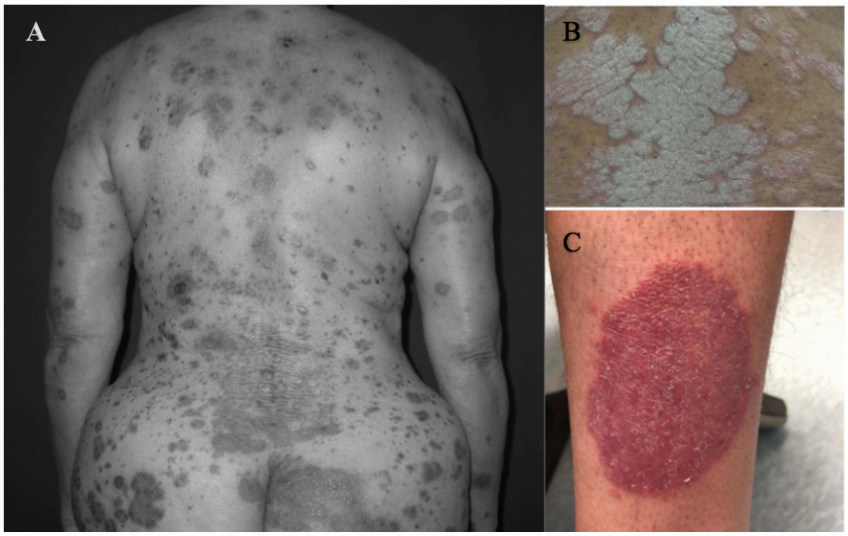

Figure 1-5: Plaque psoriasis presentations.
A: Plaque psoriasis disseminated on the back, upper limbs, and sacral area (68). B: Discrete plaques with thick silvery scale characteristic of plaque psoriasis (69). C: Psoriasis plaques may be associated with significant erythema (69).

1.4.4.2 *Psoriasis Classifications*

Generally, psoriasis is classified as mild, moderate or severe. This classification is based on the amount of body surface that is affected. Mild psoriasis affects less than 5% of BSA, moderate psoriasis affects between 5 and 10% of BSA, whilst in severe psoriasis greater than 10% of BSA is affected (65). There are a number of different clinical phenotypes of psoriasis, which are based on different factors, including age of onset (age of onset before 40 years is Type I, age of onset after 40 years is Type II), pattern of distribution, morphology, anatomical site and stage of development (65).

The severity of psoriasis can be assessed using the psoriasis area and severity index (PASI) which was developed in 1978 as a means to clinically assess psoriasis severity. The index involves grading based on three main criteria: erythema, thickening of skin, and scaling, all of which are graded from 0–4, in addition to an assessment of the percentage area affected (70). The PASI score is the cumulative score for all these parameters. A score of 0 would indicate no pathology whereas a higher score (to a maximum of 72) indicates more severe disease (71).

1.4.4.3 *Psoriasis Comorbidities*

There are a number of co-morbidities associated with psoriasis, including psoriatic arthritis, diabetes and cardiovascular disease. It is estimated that between 25 and 34% of patients with psoriasis have psoriatic arthritis (72). Psoriatic arthritis is an inflammatory disease of the peripheral and axial skeleton and presents with various clinical features such as enthesitis (inflammation of the entheses, the site where the tendons or ligaments insert into bone), dactylitis (inflammation of a digit, either finger or toe), nail dystrophy, uveitis (inflammation of the uvea of the eye) and osteitis (inflammation of the substance of a bone), in addition to comorbidities such as obesity, metabolic syndrome and cardiovascular disease (CVD) (73). The skin disease usually manifests before the arthritis, with psoriasis symptoms preceding joint symptoms by an average of 10 years (72).

Young people with severe psoriasis are three times more likely to suffer cardiac events. Studies have suggested that the more severe the psoriasis, the greater the risk of CVD. There have been a number of studies that have compared serum lipid levels in patients with psoriasis to those of control subjects. In general, there is a tendency for an increase in levels of serum triglycerides (TGs) and a decrease in high density lipoproteins (HDL) in patients with psoriasis (64). Studies have also shown an increase in low density lipoproteins (LDL) levels in patients with psoriasis.

The impact of psoriasis on heath related quality of life and patient reported outcomes has been shown to be similar to those reported for chronic diseases such as depression, post-myocardial infarction, congestive heart failure and even some cancers (64).

1.4.4.4 *Genetic Basis for Psoriasis*

The genetic basis for psoriasis has been supported by numerous twin and family studies. It has been shown that there is a higher incidence of psoriasis in relatives of patients with psoriasis compared to the general population (74). In epidemiological studies, the recurrence risk for affected siblings was estimated to be between 4 and 10 (75). The recurrence risk ratio is a measure of familial aggregation of disease, and is defined as the ratio of risk of disease manifestation in other family members compared with the disease prevalence in the general population. Twin studies have shown that there is a concordance rate of between 62 and 70% for monozygotic twins compared to 21–23% for dizygotic twins (76).

With regard to the mode of inheritance, psoriasis is consistent with a multifactorial pathway of inheritance. Linkage studies and association studies have been carried out to attempt to deduce the genes that underlie susceptibility to disease. Linkage studies examine the tendency for genes which are located nearby on the same chromosome to co-segregate. Using this method,

there have been a number of psoriasis susceptibility loci mapped, the strongest association being a locus within the MHC on chromosome 6p21(PSORS1)(74). Psoriasis has also been associated with alleles in the MHC region for many years, and there have been numerous association studies for psoriasis with HLA alleles (75). The first psoriasis-associated signal identified was the MHC class I molecule HLA-Cw*0602, which remains one of the prominent genetic risk factors for psoriasis susceptibility that has been identified to date. It has a particularly strong association in patients with an early age at onset and in patients with guttate psoriasis. Other examples include class I antigens HLA-B13, HLA-B17 and its split HLA-B57, and HLA-Cw6 which have all shown a positive association with psoriasis in population studies (75).

Genome Wide Association Studies (GWAS) have been carried out to identify psoriasis genes. In a large scale European study, 1,409 European ancestry psoriasis cases and 1,436 controls were genotyped (77). The study found association between at least seven genetic loci and psoriasis. Loci with confirmed association encode HLA-C, three genes involved in IL-23 signalling (IL-23A, IL-23R, IL-12B), two genes that act downstream of TNF-α and regulate NF-κB signalling (TNIP1, TNFAIP3) and two genes involved in the Th2 pathway (IL-4, IL-13).

The genetic susceptibility to disease must also be considered with regard to environmental factors. There are a variety of environmental risk factors that are associated with psoriasis. Risk factors include streptococcal pharyngitis (guttate psoriasis), HIV infection, trauma, smoking, stressful life events, and obesity (74).

1.4.4.5 *Pathogenesis of Psoriasis*

The exact cause of psoriasis is poorly understood to this day, with a variety of factors, including genetics, environmental conditions, skin barrier disruption and immune dysfunction all believed to play a role in the course of the disease (65).

Psoriasis is characterised by abnormal keratinocyte hyperproliferation which results in thickening of the epidermis (producing plaques) and thickening of the stratum corneum (SC) (producing scale). In its classical presentation (psoriasis vulgaris) the disease presents as well circumscribed reddish and scaly papules and plaques. These plaques typically appear on the elbows, knees and scalp; in addition to other cutaneous sites. Psoriasis vulgaris is generally easy to diagnose based on the clinical features of the disease, and therefore a skin biopsy to examine histopathology is not usually necessary (78). Fingernails are involved in up to 50% of patients with psoriasis skin lesions, and toenails are involved in 35% of patients. Nail

involvement occurs in up to 80% of patients with psoriatic arthropathy (78). Psoriasis is generally characterised by the presence of four abnormalities. The first involves vascular changes where the papillary blood vessels become dilated and tortuous, resulting in erythema. The second abnormality involves inflammation where the polymorphonuclear leukocytes from the dermal vessels enter the epidermis, and lesions rich in CD4+ and CD8+ T cells release pro-inflammatory cytokines. The third abnormality involves hyperproliferation of the keratinocyte layer (acanthosis), whilst the fourth involves parakeratosis, an altered epidermal differentiation whereby corneocytes retain their nuclei in the cornified layer and the granular layer is lost (79).

The hyperproliferation of keratinocytes is a key feature of psoriasis. In non-diseased skin the ratio of proliferating to non-proliferating keratinocytes is around 60% whereas in psoriasis it is almost 100% (62). Additionally, the mean cell cycle time is reduced from 311 h to 36 h in psoriatic lesions (62).

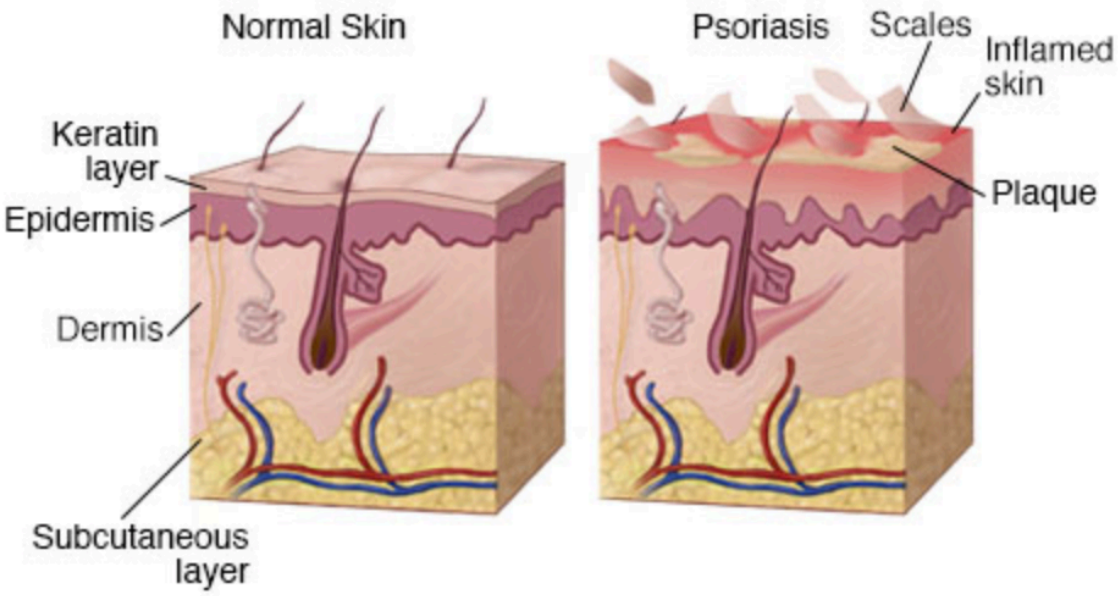

Figure 1-6: Skin changes in psoriasis
Psoriasis is characterised by epidermal thickening (producing plaques), thickening of the stratum corneum (producing scales), dilated blood vessels (leading to erythema) and skin inflammation (80).

1.4.4.6 *Current Therapies for Psoriasis*

There is no cure for psoriasis, however symptom relief can be provided by a variety of treatment strategies. Current treatments available for psoriasis patients can be divided into three major categories: topical, phototherapy and systemic (including biologics).

1.4.4.6.1 Topical Treatments for Psoriasis

Topical treatment is the preferred treatment strategy for mild to moderate psoriasis due to its local route of delivery (81). There are disadvantages and limitations to topical treatment for psoriasis. Firstly, patients often dislike topical products as they can be messy and time-consuming to apply. Additionally, if the psoriasis is localised to particular locations, patients can find it difficult to find an acceptable topical medication.

Topical therapies such as creams, ointments, gels and shampoos for the skin and the scalp are prescribed for mild to moderate cases of psoriasis, or in combination with other treatments for more severe cases. Topical agents that are currently in use for the treatment of psoriasis include corticosteroids, vitamin D analogues, retinoids, dithranol and coal tar products.

Emollients, in addition to their effects on drying, scaling and cracking, may have anti-proliferative effects in psoriasis and, as such, may be the only treatment necessary for mild psoriasis (82).

Vitamin D and its analogues (calcipotriol, tacalcitiol and calcitriol) are often used first line for the long term treatment of plaque psoriasis, they do not smell or stain and are more acceptable to patients than tar or dithranol products (82). Within the skin, Vitamin D has been shown to inhibit keratinocyte proliferation and promote differentiation (83). It can also induce apoptosis and promote the formation of a permeability barrier, and has been shown to have a role in the suppression of T cell proliferation, in addition to other immunomodulatory roles (83). Vitamin D analogues can be irritant to perilesional skin, causing redness, soreness, peeling and pruritus in up to 35% of patients during the first week of treatment.

Coal tar has anti-inflammatory and anti-scaling properties. Crude coal tar (1–10% w/w) is often prepared in a soft paraffin base, often patients do not like the smell or mess. However, cleaner proprietary products have been shown to be less effective and improvement takes longer. Coal tar is a by-product created in the process of making coke from coal (84). It has been described as having as many as 10,000 ingredients, of which only about 400 have been identified, those are predominantly carbon, water and polycyclic aromatic hydrocarbons. The mechanism by which coal tar has its effect is largely unknown, however current evidence points to the role of aryl hydrocarbons as being responsible for the therapeutic effect (84). Coal tar has been used since 1925 as part of the Goeckerman regimen, which typically involves combining phototherapy with topical crude coal tar, coal tar derivatives and corticosteroids.

Topical corticosteroids are the most widely prescribed treatment for psoriasis worldwide (85). They have anti-inflammatory, immunosuppressive, and antiproliferative activities. Short-term

studies have confirmed the efficacy of topical corticosteroids in psoriasis (85). They are not suitable for long-term use or as the sole treatment for extensive chronic plaque psoriasis; any early improvement is not usually maintained and there is a risk of the condition deteriorating or precipitating an unstable form of psoriasis upon withdrawal (82).

Calcineurin inhibitors are immunomodulators. There are two types currently available as topical treatments for psoriasis; tacrolimus and pimecrolimus. They act by inhibition of the activity of calcineurin phosphatase and blocking the production of inflammatory substances (86). Their efficacy in the treatment of psoriasis is limited, unless they are used under occlusion or on the thinner skin of the face, as penetration of these agents can be quite poor (85).

Tazarotene is a topical retinoid used in the treatment of psoriasis. It acts to modulate three major pathogenic factors in psoriasis: keratinocyte hyperproliferation, abnormal keratinocyte differentiation, and dermal and epidermal inflammatory infiltration (87). There are a number of adverse effects associated with the use of tazarotene, the most serious being teratogenicity.

1.4.4.6.2 Ultraviolet Light for Psoriasis

Light therapy for psoriasis treatment usually involves exposure to short wavelengths of UV light, called UVB. In the case of resistant moderate to severe psoriasis, a combination of oral or topical psoralen and a longer wavelength UVA light is used (PUVA). Phototherapy is used to treat patients who do not respond to topical therapies or who have widespread disease. Adverse effects of this form of treatment includes the burning of skin, photo-ageing, and potentially an increased risk of skin cancers (85).

1.4.4.6.3 Systemic Therapies for Psoriasis

Systemic treatments include both orally and parenterally administered agents for the treatment of more severe psoriasis. Examples of systemic drugs used for psoriasis include methotrexate, ciclosporin, fumarates and biological agents such as TNF-α inhibitors.

Methotrexate is a folate acid antagonist. It acts by interfering with DNA synthesis and also has specific T cell immunosuppressive activities. Despite the potential for severe side effects (teratogenicity, bone marrow suppression, liver fibrosis, pulmonary fibrosis), methotrexate remains the mainstay of treatment for refractory psoriasis and psoriatic arthritis (85).

Cyclosporin is a short-term treatment for moderate-to-severe psoriasis. It is a macrocyclic immunosuppressant that binds immunophilin and inhibits the calcineurin phosphatase-initiated activation of T cells (85). Cyclosporin is not nephrotoxic or teratogenic, but it can cause

nephrotoxicity and hypertension. It is commonly used in combination or in rotation with other treatments for psoriasis.

Oral retinoids such as acitretin can bind to nuclear receptors and thereby alter gene transcription and reduce keratinocyte hyperproliferation. These agents are useful for erythrodermic or pustular psoriasis. As they are non-immunosuppressive, they can be used by patients for whom immunosuppressants may be contraindicated. Oral retinoids are teratogenic, and other adverse effects include hyperlipidaemia and osteoporosis, in addition to mucocutaneous effects (cheilitis, dry skin, conjunctivitis, hair loss) (85).

Oral fumaric acid esters are also used for the treatment of psoriasis. The two fumaric acid esters in current use are monomethyl fumarate (MMF) and dimethyl fumarate (DMF). Monomethyl fumarate has been identified as a hydroxycarboxylic acid receptor 2 (HCA_2) receptor agonist (88). The HCA_2 receptor also binds nicotinic acid and fumaric acid esters have a similar effect to nicotinic acid, in that they cause a flushing response mediated through the activation of HCA_2 receptors found in epidermal cells.

1.4.4.6.4 Biologics used in the treatment of psoriasis

The immunological activation of psoriasis involves several critical steps, the activation of Langerhans cells, T cell activation, differentiation and expansion of Th1 cells, T cell migration to the skin, and induction of an inflammatory cytokine and chemokine cascade in skin lesions. Intervention is possible at each of these steps, with the emergence of engineered biologic agents (89).

Biologics have revolutionised the treatment of severe psoriasis. Psoriasis area severity index (PASI) 75, defined as a 75% reduction in PASI, had for decades been the gold standard for primary outcome in randomized controlled trails of therapies for psoriasis. The PASI75 response rate for methotrexate, a conventional first-choice small molecule drug for systemic treatment of psoriasis, is typically 35.5–41%. However, with the development of biologics, these highly targeted and effective therapies have meant that PASI90 and PASI100 have become the new, realistic gold standard endpoint measurements in clinical trials (90).

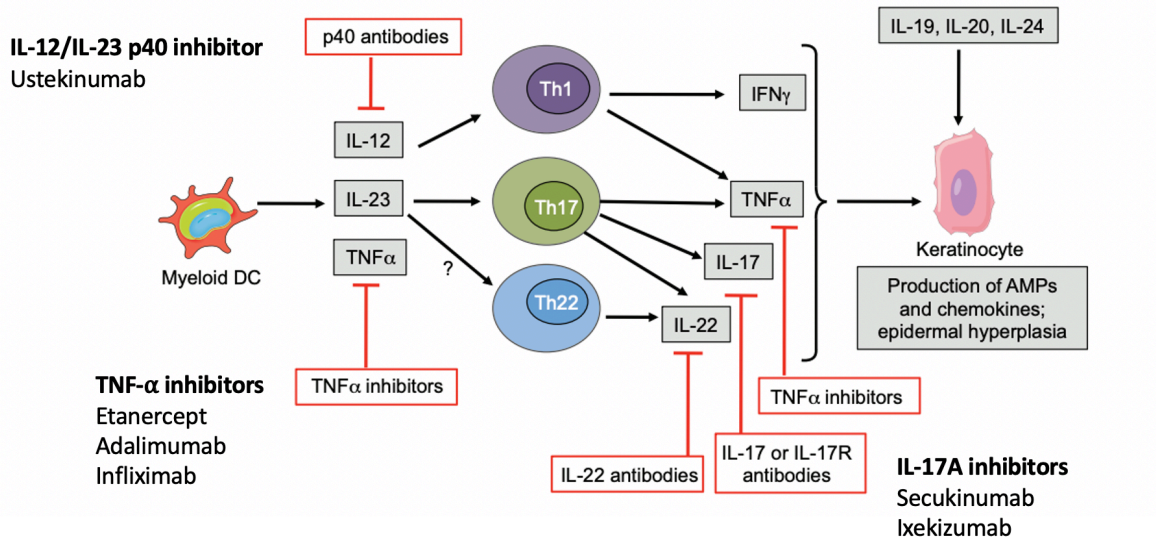

Figure 1-7: Current model of the maintenance phase of psoriasis, showing the targets of approved or emerging psoriasis drugs. Modified from (91).

There are two main classes of biologic agents used in the treatment of psoriasis, biologics targeted at T cells and cytokine targeting agents. The first biological agent that was developed specifically for the treatment of psoriasis was alefacept, a T cell targeting agent (92). It was then joined by efalizumab. These agents have validated the concept of a role of T cells in established disease. They targeted the activation and migration of T cells.

Alefacept is a human lymphocyte function-associated antigen (LFA)-3/immunoglobulin (Ig) 1 fusion protein. It binds to CD2 molecules on the surface of activated T cells and thereby blocks the co-stimulation of T cells by the antigen presenting cell. This impedes the activation and proliferation of T cells. Alefacept also induces a selective reduction of memory effector T cells by apoptosis (92). Alefacept had modest efficacy, but as more efficacious biologics were developed, the poor cost effectiveness of alefacept led to it being withdrawn from the market in 2011.

Efalizumab is another biologic that targets T cells. It is a humanised IgG1 mAb that binds to CD11a, a subunit of LFA-1. It leads to blockade of the interaction between LFA-1 and ICAM-1, which interferes with the co-stimulation of T cells by APCs. Efalizumab had superior efficacy to alefacept, but safety issues arose during the post-marketing phase, and efalizumab was withdrawn from the market (90).

The first TNF-α inhibitor approved for the treatment of psoriasis was etanercept. It can bind two TNF-α molecules and acts as a competitive inhibitor of endogenous TNF-α. TNF-α is produced by a number of cells involved in the pathogenesis of psoriasis. TNF-α inhibitors are considered to be targeted therapy, but with a widespread target. Other TNF-α inhibitors used

in the treatment of psoriasis include infliximab and adalimumab. TNF-α inhibitors all share the same target, but they have different mechanisms of action, and therefore have different efficacy and adverse events. Of the three inhibitors, studies conducted have shown that infliximab is the most effective, whilst etanercept is the least effective (93).

Ustekinumab is an IL-12/IL-23 inhibitor. It is a human IgG1 mAb that targets the shared protein subunit p40 of IL-12 and IL-23, inhibiting the actions of these two cytokines. Both IL-12 and IL-23 are secreted by dendritic cells following the activation and differentiation of naïve T cells into Th1 and Th17 cells. More recently, the selective IL-23p19 subunit inhibitors Guselkumab, Tildrakizumab and Risankizumab have been developed, with the aim of increasing safety by preserving the IL-12 mediated Th1 response against human pathogens (94).

Secukinumab is an IL-17A inhibitor, and was the first inhibitor of IL-17 to be licensed for psoriasis. The IL-17 cytokine family comprises 6 members, IL-17A-F. Th17 cells secrete IL-17A and IL-17F, IL-17A being about 10-30 fold more potent than IL-17F. Secukinumab has a faster onset of action than older biologics and has higher PASI90 and PASI100 response rates than ustekinumab.

Despite their efficacy in the treatment of severe psoriasis, biologics are associated with a multitude of issues, including questions about long-term efficacy, relapse after drug withdrawal, safety, and costs. These issues are driving the search for newer and better therapies for the treatment of severe psoriasis (95).

1.4.4.7 *Novel Therapies*

1.4.4.7.1 PDE-4 Inhibitors

Type-4 cyclic nucleotide phosphodiesterase (PDE-4) is a phosphodiesterase present in many immune cell types (96). It acts via the degradation of cAMP. It is highly expressed in immunological cells including T cells, macrophages, dendritic cells and monocytes. cAMP causes a downregulatory signal in immune cells, suppressing the production of proinflammatory mediators such as TNF-α, IL-17 and IL-23, as well as enhancing the production of the anti-inflammatory cytokine IL-10. Inhibition of PDE-4 results in an increase in cAMP levels and leads to the inhibition of the NF-κB pathway. Apremilast is an oral PDE-4 inhibitor that has been approved for the treatment of psoriasis and psoriatic arthritis. Adverse events associated with its use include intestinal intolerability and gastrointestinal effects (97).

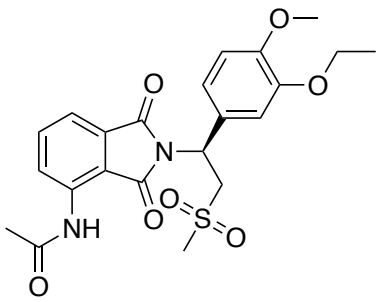

Figure 1-8: Structure of apremilast, an orally active PDE-4 inhibitor

1.4.4.7.2 JAK Inhibitors

The Janus Kinases (JAKs) are a family of intracellular tyrosine kinases. Originally given the acronym JAK to represent 'Just Another Kinase' the name was subsequently changed to Janus kinases in recognition of the Roman god Janus who had two opposing faces, suggestive of the organisation of the JAK kinase and pseudokinase regions (98). They play a key role in the signalling of numerous inflammatory cytokines and therefore were identified as promising therapeutic targets. There are four members of the JAK family: JAK1, JAK2, JAK3 and TYK2.

The tyrosine kinase activity of JAK is activated when the cytokine binds and brings two receptor molecules together to form a dimer. This dimerisation brings the two JAKs into close proximity, where they can phosphorylate each other. Phosphorylation further activates JAK, allowing it to phosphorylate the receptor. The phosphotyrosine residues on the receptor proteins are binding sites for latent STAT (signal transducer and activators of transcription) proteins. When a STAT binds to the receptor it is phosphorylated by JAK. Once phosphorylated, two STATs can form a STAT dimer which is an active transcription factor. There are a number of different STAT proteins in cells, and activation of different cytokine receptors will result in the formation of different STAT dimers, each of which will bind to a specific DNA sequence. In this way, different cytokines can activate a specific set of genes that cause a response in the cells.

A number of JAK inhibitors have been developed, the first of which was tofacitinib, which has affinity for JAK3, JAK1 and JAK2. Intracellularly, JAKs signal in pairs and tofacitinib inhibits signalling in receptors that are associated with JAK3 and/or JAK1 with selectivity over receptors that signal via pairs of JAK2 (99). The structure of tofacitinib mimics that of ATP without the triphosphate group and it can bind to the adenosine triphosphate (ATP) binding site in the catalytic cleft of the kinase domain of JAK (99). Upon binding to the ATP-binding pocket, tofacitinib inhibits the phosphorylation and activation of JAK, which prevents activation of STATs and thereby gene transcription. Other examples of JAK inhibitors in current use are ruxolitinib (JAK1/2) and baricitinib (JAK1/2) (100).

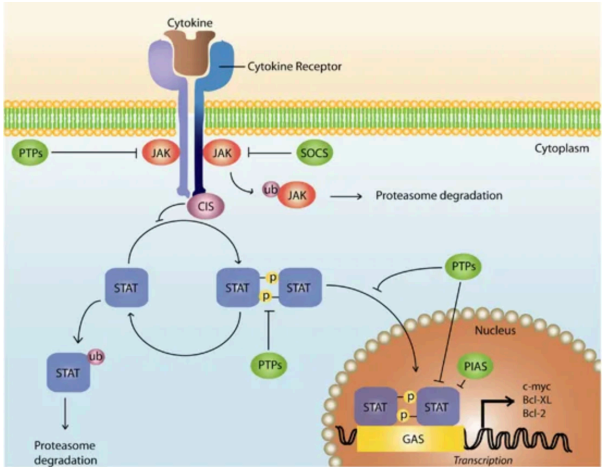

Figure 1-9: Cytokine signalling through the JAK/STAT pathway (101).

The cytokine binds to the receptor, causing receptor dimerisation and resulting in JAK activation and the phosphorylation of tyrosine residues on the intracytoplasmic region of the cytokine receptor. These phosphorylated tyrosine residues serve as docking sites for STATs. Once recruited, STATs are phosphorylated on specific tyrosine residues by JAKs, which leads to their dimerisation, STAT dimers translocate to the nucleus, where they can direct the transcription of their target genes. The JAK-STAT pathway is regulated by protein inhibitors of activated STATs (PIAS) and protein tyrosine phosphatases (PTPs).

1.4.4.7.3 A3 adenosine receptor agonists

A_3 adenosine receptors (A_3ARs) are G-protein-coupled receptors that are involved in a variety of intracellular signalling pathways and physiological functions. The choice of the A_3AR as a target for inflammation is based on two findings. The first is that A_3ARs are highly expressed in peripheral blood mononuclear cells (PBMCs) isolated from patients with psoriasis. Secondly, A_3AR activation with a specific agonist (CF101) downregulates the NF-κB signalling pathway, inhibits the proliferation of specific autoreactive T lymphocytes and induces apoptosis of inflammatory cells (97). CF101 has been tested in clinical trials and showed promising efficacy in the treatment of moderate-to-severe plaque psoriasis (102).

1.4.4.7.4 Need for New Therapies for Mild-Moderate Psoriasis

It has been a number of years since a new chemical entity has been discovered for the treatment of psoriasis. Many topical products available have a role in the treatment of mild-moderate plaque psoriasis, but remain ineffective for severe plaque psoriasis. The topical products available to treat mild-moderate psoriasis have varying success.

The systemic products available for the treatment of severe forms of psoriasis can be successful, but many have serious adverse effects associated with their use. For example, methotrexate can

cause blood dyscrasias, while phototherapy can increase the risk of developing skin cancer. Biologics have revolutionised the treatment of severe psoriasis, but the risk and cost involved in these therapies outweigh their use in patients with small, localized lesions that could be managed with a topical drug (69). Risk-benefit assessments do not favour the use of systemic products for the treatment of mild-moderate psoriasis, and therefore these patients cannot always access more efficacious therapies should their topical therapies fail.

To summarise, despite the large number of treatment types available it is clear that there is still much scope for the development of more efficacious treatments for mild-moderate psoriasis.

1.5 T cell Lymphomas

Lymphomas are a type of cancer that begin with a malignant change in a lymphocyte, lymph node cell or lymphatic tissue of the marrow. Classification of lymphomas usually takes three elements into consideration; whether or not the lymphoma is Hodgkin's or non-Hodgkin's, if it is B cell, T cell or NK cell derived, and the site from which the cell arises. Hodgkin Lymphomas accounts for 15-25% of all lymphomas and represents the most common lymphoma subtype in children and young adults in the Western world. They are characterised by the presence of Hodgkin and Reed-Sternberg (HRS) cells, which are outnumbered by reactive immune cells in the tumour environment, including T and B-lymphocytes, eosinophils, macrophages, mast cells, plasma cells and stromal cells. The cell of origin is considered to be a postgerminal B cell (103).

Non-Hodgkin lymphomas account for the majority of lymphomas and represent a wide spectrum of illnesses that range from the most indolent to the most aggressive malignancies. It is estimated that about 85-90% of non-Hodgkin lymphomas are derived from B cells, with the remaining lymphomas derived from T cells or NK cells. Non-Hodgkin lymphomas occur at extranodal sites in approximately 27% of cases, the most common site of extranodal involvement is the gastrointestinal tract, with the skin being the second most common (104).

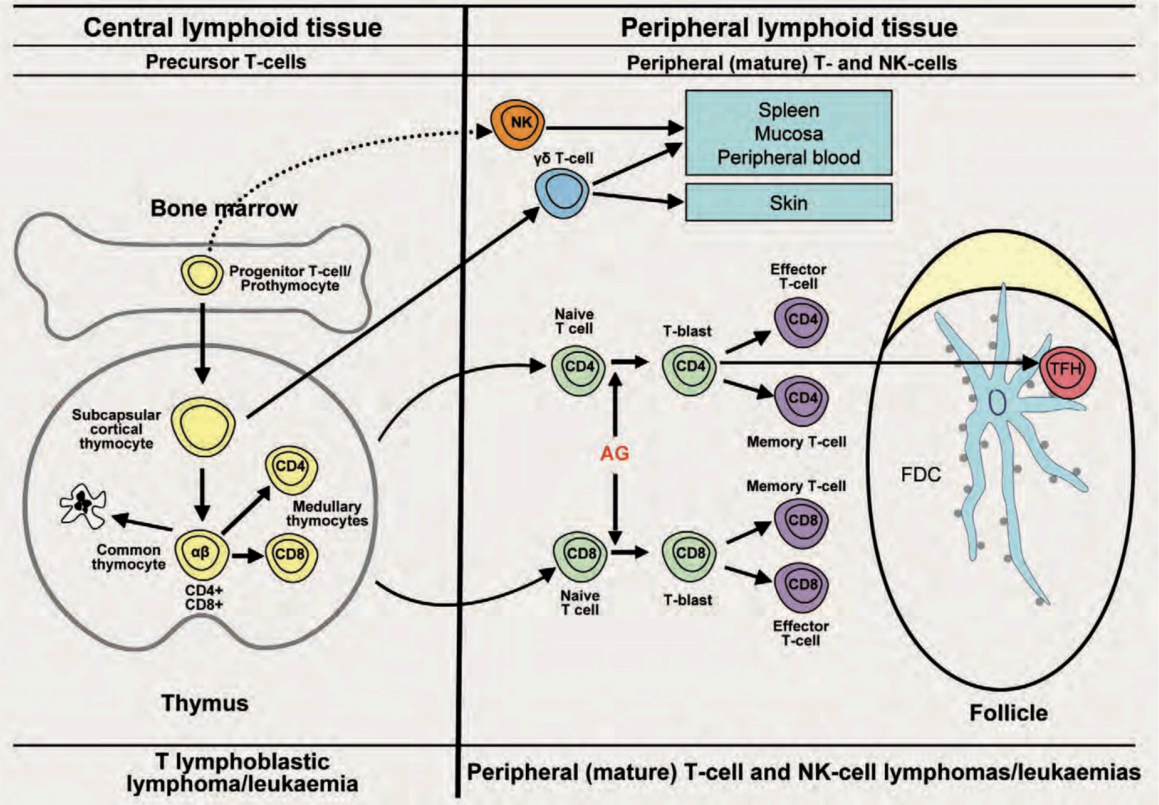

Figure 1-10: Neoplasms corresponding to different stages of T cell differentiation (105).
T cell neoplasms can be lymphoblastic or peripheral, corresponding to different stages of maturation. Lymphoid progenitors enter the thymus where the precursor cells develop into varied naïve T cells. The exact maturation path of NK cells and γδ T cells is not fully understood. The αβ T cells leave the thymus and upon exposure to antigen (AG) they develop further into CD4+ and CD8+ effector and memory cells, or follicular helper T cells, which are found in germinal centres.

T cell lymphomas are therefore a rare form of non-Hodgkin lymphoma. They can develop in lymphoid tissues such as the lymph nodes and spleen, or outside of lymphoid tissues, such as in the GI tract, liver, nasal cavity and skin. The classification of T cell non-Hodgkin lymphoma is complex, and many of the recognised distinct entities are characterised by relatively specific clinical features, morphological aspects, immunophenotypes and recurrent genetic alterations. Classification is based on the distinction between lymphocytes of the innate immune system (NK cells and γδ cells), which are not antigen specific, versus those of the adaptive immune system, which are antigen specific. Additionally, they can be further subdivided into nodal, extranodal, cutaneous or leukaemia. The different T cell lymphomas are outlined in the WHO classification scheme (105).

Mature T cell and NK-cell neoplasms
T-cell prolymphocytic leukaemia
T-cell large granular lymphocytic leukaemia
Chronic lymphoproliferative disorder of NK cells
Aggressive NK-cell leukaemia
EBV+ T-cell lymphoproliferative diseases of childhood, including cutaneous chronic active EBV infection, hydroa vacciniforme-like lymphoma, severe mosquito-bite hypersensitivity, systemic chronic active EBV infection, and systemic EBV+ T-cell lymphoma of childhood
Adult T-cell leukaemia or lymphoma
Nasal-type extranodal NK–T-cell lymphoma
Enteropathy-associated T-cell lymphoma
Monomorphic epitheliotropic intestinal T-cell lymphoma
Indolent T-cell lymphoproliferative disorder of the gastrointestinal tract
Hepatosplenic T-cell lymphoma
Subcutaneous panniculitis-like T-cell lymphoma
Mycosis fungoides
Sézary syndrome
Primary cutaneous CD30+ T-cell lymphoproliferative disorders
Lymphomatoid papulosis
Primary cutaneous anaplastic large cell lymphoma
Primary cutaneous γδ T-cell lymphoma
Primary cutaneous CD8+ aggressive epidermotropic cytotoxic T-cell lymphoma
Primary cutaneous acral CD8+ T-cell lymphoma
Primary cutaneous CD4+ small or medium T-cell lymphoproliferative disorder
Peripheral T-cell lymphoma, not otherwise specified
Angioimmunoblastic T-cell lymphoma
Follicular T-cell lymphoma
ALK-positive anaplastic large cell lymphoma
ALK-negative anaplastic large cell lymphoma
Breast implant-associated anaplastic large cell lymphoma

Figure 1-11: Subtypes of mature T cell and NK cell neoplasms (106).

1.6 Cutaneous T cell Lymphomas (CTCLs)

Primary cutaneous lymphomas are defined as non-Hodgkin lymphomas presenting in the skin with no evidence of extracutaneous disease at the time of diagnosis (107). They include both CTCLs and cutaneous B cell lymphomas (CBCLs). In Western countries, CTCLs account for approximately 75-80% of all primary cutaneous lymphomas, whilst the other 20-25% are CBCLs. The incidence of CTCL is approximately 6.4 per million persons, based on Surveillance, Epidemiology, and End Results (SEER) registry data (108). In the US, from 2005-2008 the age-adjusted incidence rate per 100,000 person-years for Mycosis Fungoides

(MF) was 0.55 and for Sézary syndrome (SS) was 0.01, with incidence higher among males and black patients (109).

CTCLs have been recognised for over 200 years, the first description of mycosis fungoides (MF) coming from French dermatologist Jean Louis Alibert, publishing his observations about a malady affecting the skin with unsightly mushroom-like skin tumours. However, it was not until the 1970s that MF was defined as a lymphoma of T cell origin, leading Edelson to introduce the more precise term CTCL (110). CTCL is caused by a mutation in T cells, distinguishing it from most non-Hodgkin lymphomas, which are generally B cell related.

The vast number or T cells residing in the skin underlie the significant potential for neoplasia. Genetic factors such as an individual's human leukocyte antigen (HLA) type may predispose some people to develop CTCL by allowing the inappropriate activation and accumulation of T cells via antigen presentation (111).

Classification of Different CTCLs	
Indolent	**Aggressive**
Mycosis Fungoides	Sézary syndrome
Variants and subtypes of MF • Folliculotropic MF • Pagetoid reticulosis • Granulomatous slack skin	Primary cutaneous NK/T cell lymphoma, nasal-type
Primary cutaneous anaplastic large-cell lymphoma	Primary cutaneous aggressive CD8+ T cell lymphoma
Lymphomatoid papulosis (CD30+)	Primary cutaneous γ/δ T cell lymphoma
Subcutaneous panniculitis-like T cell lymphoma	Primary cutaneous peripheral T cell lymphoma, unspecified
Primary cutaneous CD4+ small/medium T cell pleomorphic T cell lymphoma	

Figure 1-12: Classification of CTCLs. Adapted from (112).

1.6.1 Mycosis Fungoides

Mycosis fungoides is an indolent epidermotropic, primary cutaneous T cell lymphoma characterised by infiltrates of small to medium sized T lymphocytes with cerebriform nuclei. The term mycosis fungoides originally referred to the mushroom-like nodules seen in the tumour stage of the disease. MF is the most common type of CTCL, and accounts for approximately 50% of CTCL cases (105). Even so, due to the relatively low incidence of CTCL, MF is considered a rare disease.

Most patients are adults/elderly, but the disease can be observed in children and adolescents. The male: female ratio is 2:1. MF is limited to the skin with widespread distribution. The initial

diagnosis of MF presents challenges as the disease initially presents as flat erythematous patches or plaques covering a limited area of skin and mimics to non-malignant inflammatory skin disorders such as chronic eczema, allergic contact dermatitis and psoriasis. The long-standing, scaly, patch lesions preferentially involve the buttocks and body areas infrequently exposed to sunlight ('bathing trunk') (113). Lesions are unlikely to be found on the face, except in tumour-stage disease or with folliculotropic variants (112). The disease is insidious in onset, and it is not uncommon for it to be unrecognised or misdiagnosed for many years. The lesions many become thickened, may coalesce to from larger plaques or may undergo partial involution, leaving residual annular plaques. The patches or plaques may show hypopigmentation or hyperpigmentation, atrophy and petechiae, as well as a variety of tropisms in which the malignant cells accumulate in specialised areas of the epidermis, such as hair follicles or sweat glands (114).

In advanced stages extracutaneous dissemination may occur mainly to lymph nodes, liver, spleen, lungs and blood. Bone marrow involvement is rare. The progression of the disease is quite slow, and can involve the transition from patches to more infiltrated plaques and then eventually tumours.

Patients with tumour stage MF characteristically show a combination of patches, plaques and tumours, which often show ulceration. The typical phenotype is CD2+, CD3+, TCRβ+, CD5+, CD4+, CD8-. CLA, which is associated with lymphocyte homing to the skin is expressed in most cases. Rare cases may be positive for CD8, this is observed more frequently in paediatric MF. The clinical behaviour of CD8+ MF is similar to that of the CD4+ phenotype.

The prognosis in MF is dependent on the extent of cutaneous and extracutaneous disease as reflected in the clinical stage. Patients with limited disease generally have an excellent prognosis, and a similar survival rate to that of the general population. In more advanced cases, the prognosis is poor, especially in patients with skin tumours and/or extracutaneous dissemination. Accurate staging, based on TNMB (tumour, node, metastasis, blood) is required because of its prognostic value, with early stages having a good prognosis (52-100% 10 year overall survival) and a low risk of disease progression (12-33% in 10 years). However, advanced stages have a worse prognosis (<38% 10-year survival) and more than 58% of them progress (115).

Infectious agents, occupational exposures and genetic mutations have all been evaluated as possible etiological factors in relation to MF, but the exact cause remains unidentified. Viruses have been identified as contributing agents in some other cutaneous lymphomas (human T cell lymphotrophic virus-associated adult T cell lymphoma-leukaemia and Epstein-Barr virus-

associated nasal natural-killer-T-cell lymphoma), but no virus has been identified as playing an aetiological role in MF.

The lesions formed in MF contain dermal infiltrates composed of multiple inflammatory cells including T cells with normal morphology, as well as atypical T cells with distinctive neoplastic morphology. The malignant cells infiltrate the epidermis and form Pautrier microabscesses, which are collections of T cells adherent to dendritic processes of Langerhans cells. During disease progression, the composition of the dermal infiltrate changes and the malignant cells eventually predominate, leading to the development of tumours. The prognosis for transformed MF is very poor.

1.6.2 **Sézary Syndrome**

Discovered by the French dermatologist Albert Sézary in 1938, Sézary syndrome (SS) is a rare aggressive leukemic variant of CTCL. SS accounts for approximately 2% of all cutaneous lymphomas and in the past was defined by the triad of generalised erythroderma, generalised lymphadenopathy and the presence of clonally related neoplastic T cells with cerebriform nuclei (Sézary cells) in skin, lymph nodes and peripheral blood. However, the International Society for Cutaneous Lymphoma (ISCL) has now proposed that the diagnosis of SS should be primarily based on molecular and flow cytometric evidence of a large clonal population of abnormal T cells in the blood, in addition to erythroderma (now defined as affecting >80% BSA). Lymphadenopathy is usually present but is not regarded as essential to the diagnosis of SS (112). In terms of clinical features, the bright red skin of these patients can be very pruritic. Patients can have fine scaling, and the palms and soles of the feet are sometimes thickened, scaly and fissured. Patients can also develop alopecia, nail dystrophy and eye changes with advanced disease (112). The typical phenotype of the malignant T cell is CD2+, CD3+, TCRβ+, CD5+, CD4+, CD8- (105).

The diagnosis of SS presents a number of difficulties. The histological features of SS may be similar to those in MF, and differentiation between early-stage SS and erythrodermic inflammatory dermatoses (EIDs) may be very difficult. Patients with MF can develop erythroderma, leading to a disorder called erythrodermic MF which can be difficult to distinguish clinically from SS.

SS generally occurs in adults, characteristically presents over the age of 60 and has a male predominance (105). It is an aggressive disease with an overall survival rate at 5 years of approximately 36% (116), and a median survival of three years. Most patients die of opportunistic infections. Prognosis factors include the degree of lymph node and peripheral blood involvement.

1.6.3 Clinical Staging of MF and SS

For clinical staging of MF and SS, the revised TNMB staging system is used. For example, a patient with generalised patch/plaque (T2), no clinically abnormal peripheral lymph nodes (N0), no visceral organ involvement (M0) and low blood tumour burden (B1) would be have a disease classification of IB. Apart from the clinical stage, older age, larger cell transformation and increased lactate dehydrogenase (LDH) values have been identified as independent unfavourable prognostic factors in MF and SS. Due to the indolent nature of MF, patients do not invariably progress from one stage to the next.

Classification	Description
S (Skin)	
T1	Limited plaque/patch (involving < 10% of total skin surface)
T2	Generalised patch/plaque (involving ≥ 10% of total skin surface)
T3	Tumour(s), one or more
T4	Erythroderma
N (lymph node)	
N0	No clinically abnormal peripheral lymph nodes
N1	Clinically abnormal peripheral lymph nodes; histologically uninvolved
N2	Clinically abnormal peripheral lymph nodes; histologically involved (nodal architecture effaced)
N3	Clinically abnormal peripheral lymph nodes; histologically involved (nodal architecture (partially) effaced)
Nx	Clinically abnormal peripheral lymph nodes; no histological confirmation
M (viscera)	
M0	No visceral organ involvement
M1	Visceral involvement
B (blood)	
B0	No circulating atypical (Sézary) cells (or < 5% of lymphocytes)
B1	Low blood tumour burden (≥ 5% of lymphocytes are Sézary cells, but not B2)
B2	High blood tumour burden (≥ 1000/μL Sézary cells and positive clone)

Figure 1-13: ISCL/EORTC revision to the classification of MF and SS (117).

Clinical stage				
IA	T1	N0	M0	B0-1
IB	T2	N0	M0	B0-1
IIA	T1-2	N1-2	M0	B0-1
IIB	T3	N0-2	M0	B0-1
III	T4	N0-2	M0	B0-1
IVA1	T1-4	N0-2	M0	B2
IVA2	T1-4	N3	M0	B0-2
IVB	T1-4	N0-3	M1	B0-2

Figure 1-14: ISCL/EORTC revision to the staging of MF and SS (117).

1.6.4 **Treatment of CTCL**

To date, there is no cure for SS or MF, with the possible exception of patients with disease confined to small areas of the skin. The goal of therapy is to induce long-term remission without further compromising a patient's immune system or quality of life.

Decisions surrounding patient treatment should consider disease characteristics, comorbidities, treatment availability and potential adverse effects. For patients with early stage disease, with patches and or plaques covering < 10% (stage IA), or ≥ 10% of the skin surface (stage IB) treatment generally begins with skin-directed therapies, such as PUVA, narrowband UVB radiation, topical corticosteroids and occasionally topical chemotherapies (118). Local radiotherapy is also commonly used.

Patients with a more advanced stage of the disease, or in an early stage but for whom skin-directed therapies couldn't control disease progression, are usually started on systemic treatments. A number of treatments have shown efficacy in MF/SS, however no treatment regimen has been identified as superior. In terms of treatment durability, a retrospective study was carried out that analysed the treatment history of 198 MF/SS patients, with the primary endpoint being time to next treatment (TTNT) (118). The patients all had a biopsy-proven diagnosis of MF/SS requiring at least one systemic therapy. The median TTNT for single- or multiagent chemotherapy was only 3.9 months, while IFN-α gave a median TTNT of 8.7 months and histone deacetylase inhibitors just 4.5 months (118). PUVA was used first line in 75.8% of patients and was associated with the longest TTNT, however many of these patients had early-stage disease.

1.6.4.1 *Skin-directed therapies*

Skin-directed therapies
Corticosteroids
Nitrogen mustard
Carmustine
Topical retinoids
Topical rexinoid (bexarotene)
Ultraviolet light therapy
Electron beam radiation (localised and total skin)
Topical tacrolimus
Imiquimod
Photodynamic therapy

Figure 1-15: Skin-directed therapies for the treatment of CTCL.

The calcineurin inhibitor tacrolimus is approved for use in atopic dermatitis and it is as effective as mid- to low-potency glucocorticoids when used on facial skin and intertriginous areas in MF patients. Tacrolimus has an advantage over steroids, in that it does not suppress collagen synthesis and therefore does not cause skin atrophy (119), however the use of calcineurin inhibitors should be limited in CTCL patients because their use has been associated with an increased risk of lymphoma (120).

Topical corticosteroids as monotherapy or in combination with other therapies are widely used in the treatment of MF. They are often used as monotherapy in early stage MF (Stages I-IIA) or as part of combination therapy in more advanced stages. The first study examining the efficacy of steroid monotherapy was carried out in 1998. The uncontrolled study prospectively evaluated the twice daily use of mainly high-potency topical steroids in 79 patients with stage IA/B disease and observed a response rate of 94% (121). Since that study, a further retrospective study of 37 patients with early and late stage MF who received front-line topical steroid monotherapy was carried out, and showed that topical steroid monotherapy can achieve measurable improvement in affected BSA and the modified Severity-Weighted Assessment Tool (mSWAT), and achieve complete remission in a limited subset of patients (122). Another prospective study examined 13 patients treated with topical clobetasol propionate as monotherapy for early stage MF and particularly focused on cutaneous adverse events observed with topical corticosteroid use (123). The study concluded that superpotent topical corticosteroids such as clobetasol propionate should remain the first choice for patients with early-stage MF (stage IA).

Topical mechlorethamine is an alkylating agent that is approved for the treatment of IA and IB MF in patients who have received prior skin-directed therapy. A phase II study looked at 260 patients with stage IA-IIA MF who had not used topical mechlorethamine within 2 years and were naïve to treatment with topical carmustine and were randomly allocated to a commercial gel preparation or a 0.02% compounded mechloethamine ointment (124). The gel proved non-inferior to the ointment, with a shorter time to response. The response rate was approximately 50%. No drug-related serious adverse events occurred within a treatment duration of up to 12 months, however more than 50% of patients experienced skin related adverse events, most commonly irritant contact dermatitis. The gel has orphan drug designation in Europe (125).

Bexarotene is a retinoid that selectively binds and activates retinoid X receptors ('rexinoid'). These rexinoid receptors have biological activity distinct from that of retinoic acid receptors. Bexarotene can regulate various cellular processes including cellular differentiation, proliferation, apoptosis and insulin sensitisation (126). It is available as a systemic therapy and as a 1% gel formulation for topical application. The product is approved by the FDA for topical treatment of lesions in CTCL patients (Stage IA and IB) who have refractory disease, but it is not approved in Europe (125). Response rates have been reported as being from 44% (127) to 63% (128). The toxicity is mild and usually restricted to skin irritation.

8-Methoxypsoralen plus ultraviolet A (PUVA) and ultraviolet B (UVB) are both commonly used for the treatment of MF, both as a monotherapy and as part of a multimodality therapeutic regimen. The immediate relief that many patients get in terms of a decrease in lesion size and in pruritus can be very gratifying to patients (129).

In total skin electron beam therapy (TSEB), electrons, generated in a linear accelerator, are attenuated to penetrate the skin to a limited depth, thereby avoiding toxicity to internal organs including the bone marrow. Evidence from retrospective studies have shown that a standard treatment course consisting of 30-36 Gy applied over a period of 8 to 10 weeks is able to induce high remission rates. TSEB can be associated with nodal and localised skin irritation and the toxicity of TSEB is dose dependent (125).

Localised radiotherapy is used for palliative treatment for individual lesions and may induce long-term remission in unilesional disease. It can be used alone or in combination with other skin-directed therapies (125).

Imiquimod is an immunomodulatory agent approved for the topical treatment of extragenital and perianal warts and superficial basal cell carcinomas in adults. It binds to TLR7 and TLR8 and can induce Th1 cytokines, including IFN-α (130). An open-label pilot study evaluating 5% imiquimod cream in six patients with stage IA to IIB MF induced a clinical response rate of

50% and was well tolerated (131). Other studies have also reported modest effects (132), and a study combining imiquimod with PUVA resulted in complete clearance of a PUVA- and retinoid-resistant MF plaque on a patient's face (133).

In terms of novel skin-directed therapies for limited stage disease, topical resiquimod, a TLR7/8 agonist that is structurally related to imiquimod, has been granted orphan designation by the European Commission. In a trial of 12 patients with stage IA-IIA CTCL treated with 0.03% and 0.06% topical resiquimod gel, lesions significantly improved in 75% of patients and cleared in 30% of patients (134). Topical alitretinoin, a vitamin A derivative has also shown positive results in the treatment of CTCL.

1.6.4.2 *Systemic Therapies for CTCL*

Therapy	Agents
Biologic response modifiers	Retinoids (bexarotene) and IFNs
Folic acid metabolism inhibitors	Methotrexate and paltrexate
Histone deacetylase inhibitors	Vorinostat and romidepsin
Antibodies	Brentuximab, mogamulizumab and alemtuzumab
Targeted therapy	Denileukin diftitox
Standard chemotherapy agents	Liposomal doxorubicin, gemcitabine, pentostatin and combination chemotherapies

Figure 1-16: Systemic therapies for CTCL. Modified from (126).

There is no standard systemic therapy for patients with advanced stage MF and SS, with a variety of agents being used as monotherapy or in combination with other agents.

Oral bexarotene has been shown to be an effective therapy for CTCL. In a multi-centre clinical study involving 94 patients with advanced stage CTCL (IIA-IVB), the overall clinical response was between 45 and 55% (135). It also showed similar efficacy in patients with early stage CTCL (IA-IIA), with efficacy in 15 of the 28 patients treated with oral bexarotene (136). Bexarotene is quite well tolerated, but the most frequent adverse effects reported were hyperlipidaemia, hypercholesterolemia and hypothyroidism.

Alemtuzumab is a recombinant DNA-derived humanised IgG mAb that is directed against the CD52 surface antigen expressed on malignant B and T cells and promotes antibody-dependent cytotoxicity and lysis (137). It appears to deplete central memory T cells from the circulation, but does not diminish effector memory cells that are confined within the skin (138). A phase 2 study with alemtuzumab involving 22 patients with advanced MF or SS showed a 55% response rate, with 32% of patients in complete remission (139). However 50% of patients had infectious complications.

Brentuxumab vedotin is an anti-CD30 mAb-drug conjugate in which the mAb is linked via a protease-cleavable linker to monomethyl auristatin E (MMAE), an anti-tubulin agent. CD30 is a cell surface receptor that is part of the TNFR superfamily, and is found on Hodgkin Reed-Sternberg cells, activated monocytes, activated B and T natural killer cells, and B and T cell non-Hodgkin lymphomas (137). After targeting the CD30 receptor, brentuxumab vedotin is internalised within the cells and the peptide linker is cleaved, releasing the antimitotic MMAE inside the cells (140). MF and SS lesions have variable levels of CD30 expression, however studies have shown that brentuxumab vedotin demonstrated significant clinical efficacy in treatment-refractory or advanced MF or SS with a range of CD30 expression levels (141). The response rate was 70% in the 30 patients tested. Brentuxumab vedotin is approved by the FDA for CD30+ expressing MF.

Mogamulizumab is a humanised anti-CCR4 mAb with a defucosylated Fc region leading to enhanced antibody-dependent cell-mediated cytotoxicity. CCR4 is expressed on malignant T cells, preferentially on Th2 and Treg cells, and stimulates T cell migration to the skin and other extranodal sites. Targeting CCR4 depletes malignant cells, but also decreases the surrounding Tregs, further enhancing the therapeutic effect (137). In a phase 2 study of CTCL patients treated with mogamulizumab the global response rate was reported as 37%, with more responders in the SS group than the MF group (142). The rate of serious adverse effects was 24%. Mogamulizumab has been granted approval in Europe for the treatment of adult patients with MF or SS who have received at least one prior systemic therapy.

The interferons (IFNs) are naturally produced polypeptides that have antiviral, immune modulatory and cytostatic. There are three types, IFN-α, IFN-β and IFN-γ. IFN-α acts by activating CD8+ T cells and NK cells and suppressing the production of the Th2 cytokines by malignant lymphoma cells. This results in an improvement of the Th1/Th2 balance.

Histone deacetylases (HDACs) are overexpressed in many lymphomas. They are involved in catalysing the removal of acetyl groups from histones, thereby leading to decreased DNA accessibility and gene silencing (143). The inhibition of HDACs can lead to altered gene expression, cell cycle disruption, increased apoptosis, inhibition of angiogenesis, increased oxidative stress and reduced proliferation in tumour cells (137). The two HDAC inhibitors (HDACi) used in the treatment of CTCL are romidepsin and vorinostat. In a phase 2 trial of romidepsin involving 96 CTCL patients with stage IB to IVA disease the response rate was 34%, with 6% reaching complete remission (144). The most common adverse events reported were mild and included nausea and vomiting, with severe drug related adverse events being rare. A phase IIB trial of vorinostat involving 74 patients with persistent, progressive or refractory stage IB-IVA CTCL had a response rate of almost 30% (145). 48% of patients with

stage IIB or higher disease had clinical improvement, but did not meet objective response criteria. The most common adverse events were diarrhoea, fatigue and anorexia.

Denileukin diftitox is an immunotoxin that is a fusion molecule combining an enzymatically active portion of the diphtheria toxin with an IL-2 protein targeting the CD25 subunit of the IL-2 receptor (137). It was granted orphan drug designation by the European Medicines Agency in 2001, but it does not appear to be commercially available currently. The approval was based on a phase 3 trial treating 71 relapsed/refractory CD25+ CTCL patients showing an objective response rate of 30%, with 10% achieving complete remission (146).

1.7 Aims and Objectives

This project is centred on ST0702, isosorbide-2-aspirinate-5-nicotinate. Prior to the work carried out in this project ST0702 was tested in the imiquimod mouse model of psoriasis, where mice treated with ST0702 had significant reductions in all three parameters of skin inflammation; skin thickness, erythema and scaling.

The overall aim of this thesis is to investigate ST0702 and analogues as potential pharmacological treatments for both inflammatory and malignant T cell diseases of the skin, building on the fact that ST0702 has demonstrated efficacy in the treatment of psoriasis, an inflammatory T cell driven disease of the skin.

The aims of the thesis will be broadly achieved through the following actions:

1. Determine the mechanism of action of ST0702 in the imiquimod mouse model of psoriasis.
2. Identify an assay/assays that can be used to screen analogues for activity.
3. Synthesise analogues of ST0702.
4. Screen the analogues for activity.
5. Compound optimisation.

Chapter 2: ST0702 and the Synthesis of Analogues of ST0702

2.1 Introduction

This chapter focuses on ST0702, a new drug in development for the treatment of psoriasis. Prior to the commencement of this project, ST0702 was tested in the Aldara™ mouse model of psoriasis-like inflammation. ST0702 was shown to reduce the PASI score in a dose dependent manner. Before determining the mechanism of action of ST0702 it was first decided to investigate the metabolism pathways that ST0702 might follow in various skin settings. This chapter also described synthetic efforts towards analogues of ST0702 that were developed to identify analogues with greater activity or to give an increased understanding of the structure-activity relationship (SAR), especially with respect to the aspirin moiety. The physicochemical characteristics of these novel compounds were profiled, and preliminary biochemical characterisation was carried out on the new compounds in order to identify biochemical measures that could be predictive of effect, and which might be used to guide subsequent efforts to identify more potent analogues.

2.1.1 Chemistry of 1,4:3,6-Dianhydrohexitols

2.1.1.1 *Isosorbide Skeleton and Chemistry*

1,4:3,6-Dianhydrohexitols are a family of isomeric carbohydrates derived as by-products from the starch industry. The family of compounds include isosorbide (also known as 1,4:3,6-dianhydro-D-glucitol), isomannide (1,4:3,6-dianhydro-D-mannitol) and isoiodide (1,4:3,6-dianhydro-L-iditol). The 1,4:3,6-dianhydrides are formed from the hexitols D-mannitol, D-glucitol and L-iditol under acidic conditions (147). The dianhydrides, D-isomannide, isosorbide and D and L-isoiodide all have two free hydroxyl groups located at the C-2 and C-5 positions. The three isomers differ according to the stereochemistry of the two hydroxyls at the carbon atoms on position 2 and position 5 of the two cis-fused five membered tetrahydrofuran rings. Isosorbide is very hydrophilic and is only poorly soluble in many organic solvents (148).

2.1.1.2 *Stereochemical Reactivity: Regioselective Substitution*

According to molecular models the 1,4:3,6-dianhydrides have two nearly planar cis-fused five membered tetrahydrofuran rings in the form of a V with the two free hydroxyl groups situated at the C-2 and C-5 positions either inside or outside the V shaped wedge at an angle of approximately 120° (147). Isomannide has two endo-hydroxyl groups at C-2 and C-5, isosorbide has one endo at C-5 and one exo at C-2 hydroxyl groups, and isoiodide has two exo-

hydroxyl groups. The ditosylates of isomannide, isosorbide and isoiodide have been shown to have different reactivity, with both tosylate groups of isomannide shown to have reactivity, one tosylate group in the isosorbide is reactive, whilst both tosylates in isoiodide are extremely unreactive (147). These differences have been attributed to the differences in the configuration of the hydroxyl groups in the dianhydrides. In isosorbide, the endo hydroxyl group at C-5 is more reactive than the hydroxyl at C-2 due to an intramolecular hydrogen bond between the H atom on the 5-hydroxyl group and the oxygen atom of the adjacent cis-fused five membered ring. Thus, the oxygen-hydrogen bond at C-5 is weaker than that at C-2 and more prone to nucleophilic attack. In isomannide, both hydroxyl groups are stereochemically equivalent and thus do not possess any difference in reactivity. They are both involved in intramolecular hydrogen bonding, a feature that is not evident in isoiodide. Therefore, it is expected that these molecules demonstrate different reactivity compared to each other. Other than different reactivity, compounds bearing these molecules as building blocks are also expected to have different interaction character with protein binding pockets due to the stereochemical difference of the carbons at position 2 and 5. This in turn may also change the physical and chemical properties of the same analogues derived from isosorbide, isomannide or isoiodide as building blocks. The substitution of the tosylate probably involves SN2 reactions, which require the nucleophile to have access to the back side of the carbon. The access to the rear of the carbon atom bearing the exo-tosylate models has been shown in molecular modelling to be somewhat hindered, whereas access to a carbon atom that bears the endo group is sterically unhindered.

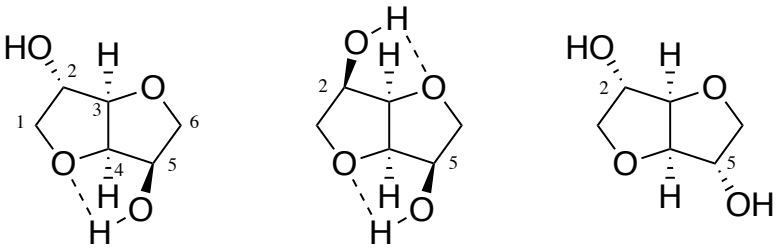

Figure 2-1: Structure of isosorbide, isomannide and isoiodide.

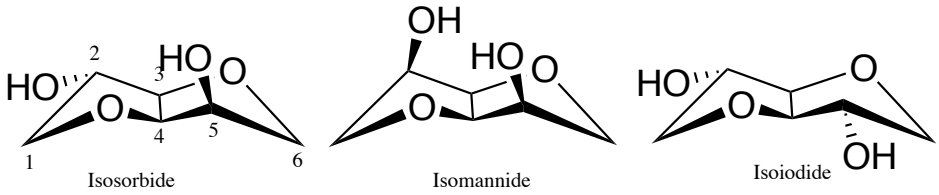

Figure 2-2: Stereochemistry of isosorbide, isomannide and isoiodide.

2.1.2 **Introduction to ST0702 (1)**

This project is focused on a novel aspirin prodrug, isosorbide-2-aspirinate-5-nicotinate (ST0702), which incorporates nicotinic acid and aspirin connected to isosorbide. ST0702 undergoes metabolism in human blood, releasing niacin and aspirin (149).

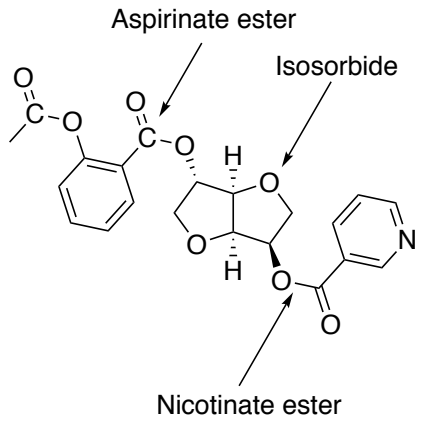

Figure 2-3: Structure of ST0702

This compound was found to be significantly more effective than nicotinic acid on markers of dyslipidaemia including LDL in cynomolgus monkeys. Its administration also led to reduced prostaglandin D2, the lipid metabolite that is thought to cause flushing, one of the major drawbacks of niacin usage (149). ST0702 demonstrated potential for providing enhanced efficacy and reduced side effects compared to immediate release niacin pharmacotherapy for dyslipidaemia.

Researchers in the Gilmer group have shown that ST0702 has superior antiplatelet properties to aspirin in its ability to block tumour cell-induced platelet aggregation (TCIPA), a phenomenon that is thought to be critical to the spread of cancer during metastasis. Aspirin had no effect at the concentrations used in this model (150). Further studies on ST0702 demonstrated that the compound inhibited deoxycholic acid (DCA)-induced IL-8 mRNA, the most generally recognised readout of proinflammatory bile acids (151).

It was suggested that the anti-inflammatory effects of ST0702 were due to the anti-inflammatory properties of the intact compound rather than its byproducts. A potential problem associated with oral administration of ST0702 was identified, as the three ester groups (the acetyl group of the aspirin group as well as the esters linking the nicotinate and the aspirinate group to the 2- and 5- positions of the isosorbide) would be susceptible to hydrolysis. The decision was made to test ST0702 in a topical formulation which could be applied directly to inflamed tissue to examine the potential functional significance of the effects seen in vitro. The

compound would still be acted on by esterases in the skin, but the local effects might have occurred prior to the metabolism of the compound.

ST0702 had been tested in two models of mouse skin inflammation, the Aldara™ Psoriasis Model and the MC903 Model of Atopic Dermatitis. ST0702 did not demonstrate activity in the MC903 dermatitis model, but had good activity in the Aldara™ Model, which will be discussed in a later section. The compound demonstrated a specific effect on the inflammatory conditions in the psoriasis-like inflammation.

Salicylic acid was presumed to be one of the breakdown products of ST0702 in mouse skin. It is used topically for its keratolytic properties and it has been shown to reduce the rate of keratinocyte proliferation. Warts and localised hyperkeratosis can be treated with salicylic acid concentrations of between 10-40%, and at lower concentrations it is used for the treatment of plaque psoriasis (152).

Nicotinic acid is also known as niacin or Vitamin B3. Medication and supplemental niacin are primarily used to treat high blood cholesterol and pellagra (niacin deficiency). It is a derivative of pyridine, with a carboxylic acid at the 3-position. Nicotinic acid is known to have favourable activity on the entire lipid panel. It has been shown to raise HDL-C in a dose dependent manner by approximately 25%. It also acts to reduce LDL-C by 15-18% and triglycerides by 20-40% at the 2g/day dose (153).

Nicotinic acid is used in high doses to raise HDL and reduce LDL, but it causes intense peripheral flushing, which consists of cutaneous vasodilatation accompanied by a burning sensation. Although harmless, this led to limitations in the use of nicotinic acid for the treatment of hypercholesterolemia due to issues of poor adherence and toxicity that arose from both flushing and gastrointestinal. The flushing that occurs following the administration of nicotinic acid is attributed to the activation of the HCA_2 receptor (formerly known as the GPR109A receptor) (154). In 2014, the Heart Protection Study 2: Treatment of HDL to reduce the incidence of Vascular Events (HPS2-Thrive) was published (155). This study was a randomised controlled trial involving 25,673 adults with vascular disease which found that the effects of extended release niacin combined with laropiprant did not significantly reduce the risk of major vascular events but did significantly increase the risk of serious adverse events. The study authors felt that these results were generalizable to all high-dose niacin preparations. An editorial on this trial drew the conclusion that, based on randomised clinical trials, niacin carries an ‘unacceptable toxicity profile for the majority of patients and should not be used routinely’(156).

2.1.3 **Mouse Models in Psoriasis**

Psoriasis is generally not observed in mammals other than man, and this lack of suitable animal model has greatly hindered research into the pathogenesis of psoriasis (157). There have been two reported cases of psoriasis in animals, a rhesus monkey (158) and a cynomolgus monkey (159). Many transgenic, knockout and reconstituted models of psoriasis have been developed over the past few decades. These models all have their limitations, but have shown that keratinocyte hyperplasia, vascular hyperplasia, and cell-mediated immunity in skin are closely interrelated. Mouse models that mirror aspects of psoriasis have been identified or created by genetic engineering (157).

A good psoriasis model should be able to reflect the clinical and histological features, in addition to reflecting proven insights into psoriasis pathogenesis and treatments (160). A good pre-clinical model of psoriasis will demonstrate the following:

- Epidermal hyperproliferation of keratinocytes and altered keratinocyte differentiation to include acanthosis, hyperparakeratosis and partial loss of the stratum granulosum.
- Regular and symmetrical extension of rete ridges separated by elongated dermal papillae and thinning of the suprapapillary plate (papillomatosis).
- Infiltration of dendritic cells, T cells, monocytes, macrophages, neutrophils and mast cells.
- Support the important functional role of T cells in disease pathogenesis.
- Altered dermal vascularity such as the presence of tortuous capillaries and increased number of CD31+ endothelial cells.
- Responsive to standard anti-psoriatic therapies such as corticosteroids (160).

There exists profound differences between mouse and human skin. Apart from the size difference, the epithelium in fur-covered mice skin is disproportionately composed of hair follicles, whilst the epithelium in human skin is to a much larger extent interfollicular. Mouse epidermis generally comprises of only 2–3 keratinocyte layers and is only one quarter of the thickness of human epidermis. It also has a faster epidermal turnover. Human dermis is much thicker than mouse dermis, and wounding is very different as mouse skin regenerates effectively without significant scarring (157).

The immune system in mice also differs from that of humans. For example, mice have several subtypes of dendritic cells, including the CD8+ dendritic cells and other inflammatory cells, such as the dendritic epidermal T cells and NK1.1+ T cells that are not found in humans (157).

Topical application of imiquimod (IMQ), a Toll-like receptor 7 (TLR7) and Toll-like receptor 8 (TLR8) ligand, is used for the treatment of genital and perianal warts caused by the human papilloma virus, in addition to the treatment of other virus-associated skin abnormalities and

pre-cancerous skin lesions such as actinic keratoses and superficial basal cell carcinomas. IMQ has been shown to exacerbate psoriasis in patients with well-controlled psoriasis during the topical treatment of basal cell carcinomas. The exacerbations occur at both the treated areas and at distant sites that were previously unaffected.

Since its initial description in 2009 the IMQ-induced model of acute skin inflammation has become the most widely used pre-clinical murine model of psoriasis, with a large increase in the number of publications using this model since 2009 (161). It has been shown that IMQ-induced dermatitis in mice closely resembles human psoriatic lesions in terms of the phenotypic and histological characteristics, and that the development of lesions is dependent on the IL-17/IL-23 axis (161). The advantages of the IMQ model are its ease of use, its relative inexpensiveness compared to transgenic or xenotransplatation mouse models and the relatively quick and reproducible inflammatory skin response (162).

There are some limitations to the use of the IMQ model. IMQ ingestion can be an issue due to the grooming behaviours of mice. There has been a suggestion that preventing oral intake of Aldara™ through placing an 'Elizabethan collar' on the mice blocks not only the cutaneous effect, but also the local inflammation, indicating that the systemic response might be considered to be an amplification loop (163). Additionally, the mechanism of action by which IMQ induces acute skin inflammation in mice is poorly understood. Its effect on the skin cannot be due solely to the activation of TLR receptors, because keratinocytes lack expression of TLR7/8. Another limitation is that prolonged treatment is not tolerated. Mice treated with topical IMQ develop a systemic inflammatory response and are prone to dehydration. This observation may be due in part to the additive effects of ongoing IMQ ingestion by treated mice. Most mice treated with IMQ daily for periods longer than two weeks die. This hinders the study of psoriasis comorbidities, such as psoriatic arthritis, metabolic syndrome and cardiovascular disease. It is worth noting that the mouse model is an acute, localised model of skin inflammation and doesn't reflect the chronic nature of human disease (162).

2.2 Results and Discussion

2.2.1 Aldara™ Mouse Model Experiments

2.2.1.1 *ST0702 (**1**)*

Prior to the commencement of this project, a number of compounds were screened for efficacy in the Aldara™ model of psoriasis, including ST0702. The experiments were carried out in the Fallon lab in TCD. The dorsal skin of mice was shaved and depilated and the mice were randomly allocated to either treatment or vehicle group. On Day 0, mice were scored for disease

signs. Following this 62.5 mg of Aldara™ Cream (5% imiquimod, equivalent to daily dose of 3.125 mg imiquimod) was applied to a defined area of the shaved dorsal skin surface. Next, 30 min after the Aldara™ application, ST0702 (mixed in petroleum jelly vehicle) was applied to the dorsal flank, to cover the entire Aldara™ challenged surface, with an even layer of the white petroleum. This was repeated for a further five days. The mice were scored according to three parameters: erythema, skin thickening and scaling, with scores from 0–4 for each parameter. No pathology would be scored 0, while severe pathology would be scored 4. The total score, or PASI score was the cumulative score for all three parameters and can range between 0–12.

The results, outlined in Figure 2.4, showed that application of ST0702 significantly reduced the progressive development of psoriasis-like skin inflammation in mice in two separate experiments and demonstrated a dose-dependent response. Mice treated with ST0702 had significant, and dose-dependent reductions in the development of all three parameters of skin inflammation; skin thickness, erythema and scaling.

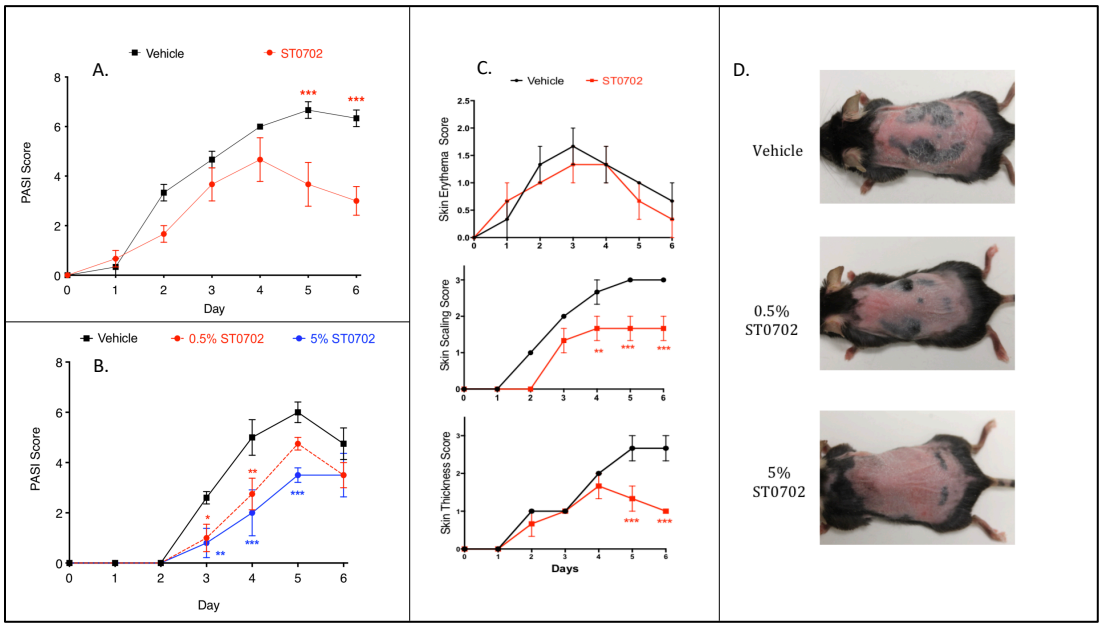

Figure 2-4: Results from Aldara™ study of ST0702.

***A:** PASI Score of Mice exposed to vehicle or 3% ST0702. Data are mean ± SEM from 3 mice per group. **B**: PASI score of Aldara™-treated mice exposed to Vehicle (white petroleum jelly), 0.5 or 5% ST0702. Data are mean ± SEM from 6 mice per group. **C.** Skin scaling, erythema and thickness scores of Aldara-treated mice exposed to Vehicle or 3% ST0702. ANOVA and Dunnett's multiple comparisons test were used to test for statistical differences between groups. Statistical differences between Vehicle group and ST0702 group are shown. Data is presented as mean ± SEM from 3 mice per group *P<0.05, **P<0.01, ***P<0.001. **D.** Representative photographs of the shaved back skin of mice exposed to Vehicle, 0.5 or 5% ST0702.*

2.2.1.2 *ST0701, ST0703 and ST0702Sal*

There were three other compounds tested in the Aldara model in addition to ST0702. These were:

- ISAL (ST0702Sal, **2**): isosorbide-2-salicylate-5-nicotinate
- ST0701 (**3**) isosorbide-2-aspirinate-5-salicylate
- ST0703 (**4**): isosorbide-2-aspirinate-5-isonicotinate

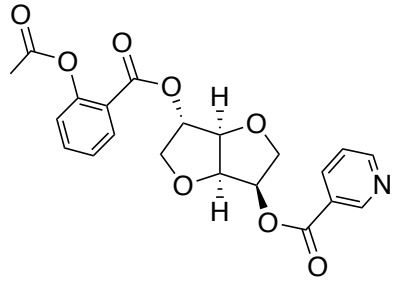

ST0702 (**1**)

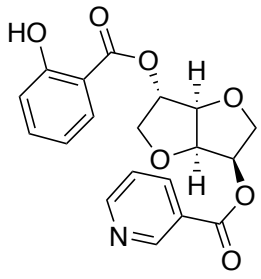

ISAL (**2**)

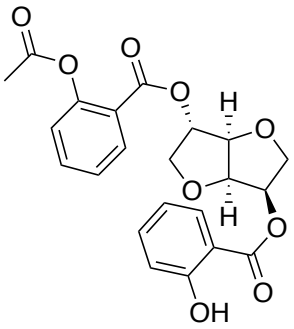

ST0701 (**3**)

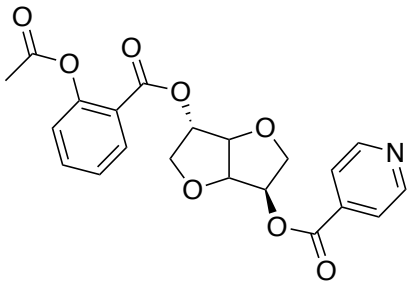

ST0703 (**4**)

*Figure 2-5: Structure of ST0702 (**1**), ISAL (**2**), ST0701 (**3**) and ST0703 (**4**).*

These compounds were tested as they were structurally similar to ST0702. ST0701 (**3**) has an aspirinate ester at the 2-position and a salicylate ester instead of the nicotinate ester at the -5 position. ST0703 (**4**) also has an aspirinate group at the 2- position and it has an isonicotinate ester at position 5, where the nitrogen is in the 4- position of the pyridine ring, instead of the 3-position as is the case with ST0702. ST0701 and ST0703 did not appear to inhibit disease in the mouse psoriasis model. The difference in reduction in PASI score was only significant for both compounds on day 3 compared to vehicle control. There was some reduction of skin thickness and erythema seen with both compounds, with ST0701 more effective than ST0703 at reducing thickness.

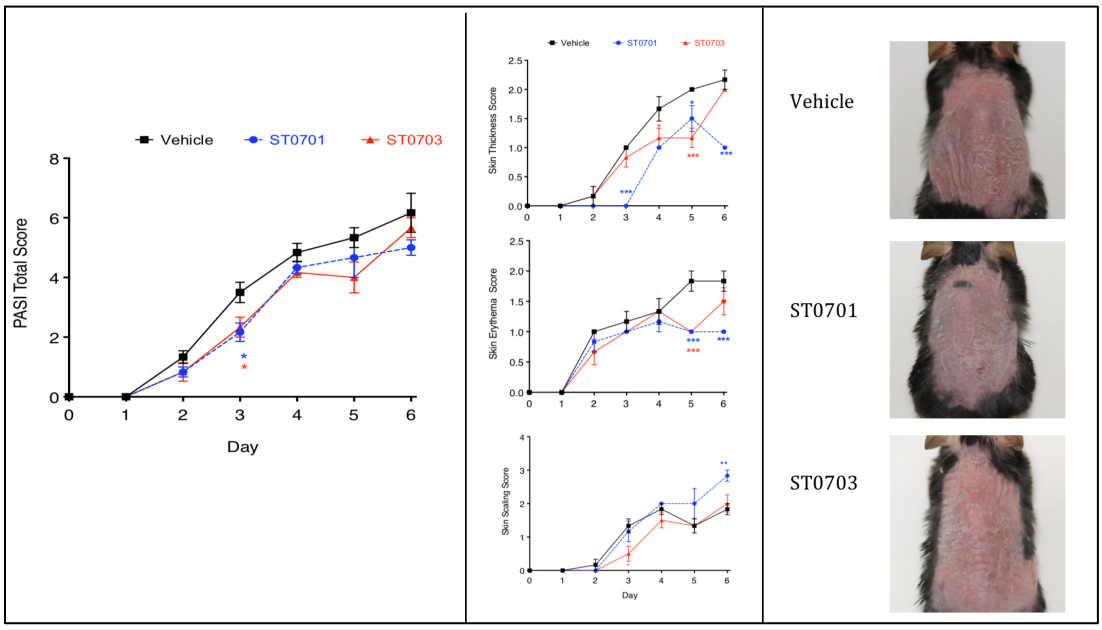

*Figure 2-6: Results from Aldara™ study for ST0701 (**3**) and ST0703 (**4**).*
***A:** PASI score of Aldara-treated mice exposed to Vehicle (white petroleum jelly), ST0701 and ST0703. Data are mean ± SEM from 6 mice per group. *P<0.05, **P<0.01, ***P<0.001. **B:** Skin scaling, erythema and thickness scores of Aldara-treated mice exposed to Vehicle, ST0701 or ST0703. ANOVA and Dunnett's multiple comparisons test was used to test for statistical differences between groups. Statistical differences between Vehicle group and ST0701 (*) and (*) ST0703 groups are shown. Data is presented as mean ± SEM from 6 mice per group. **C:** Representative photographs of the shaved back skin of Aldara-treated mice exposed to Vehicle, 3% ST0701 or 3% ST0703.*

ISAL (ST0702Sal, **2**) was studied as it was expected to be the primary metabolite of ST0702, with the expectation that the acetyl ester of the aspirinate group would be hydrolysed by esters in the skin. This would then leave the salicylate ester as the main metabolite. Treatment with ISAL caused a reduction in the PASI score, but to a lesser degree than the reduction achieved by ST0702. ISAL had very little effect on skin thickness or erythema, but had a pronounced effect on scaling.

From the results of these studies it was determined that of the four compounds tested in the mouse model of psoriasis, ST0702 had the most potential for further development for the treatment of psoriasis.

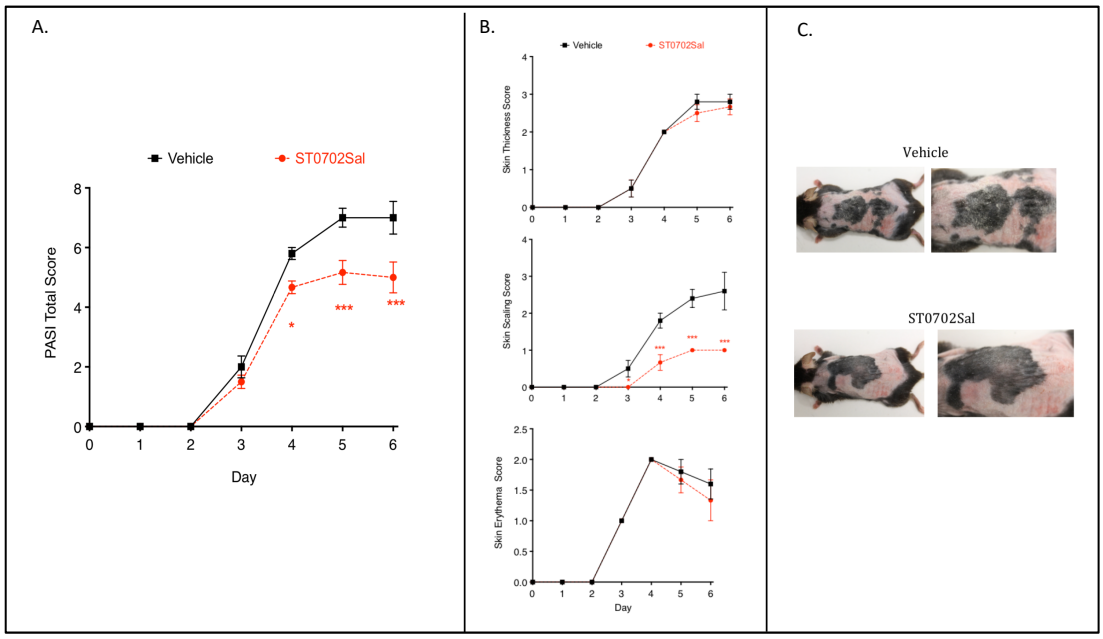

Figure 2-7: Results from Aldara™ study for ISAL (ST0702Sal).

***A**: PASI score of Aldara-treated mice exposed to Vehicle (white petroleum jelly) and ST0702Sal. Data are mean ± SEM from 6 mice per group. **B**: Skin scaling, erythema and thickness scores of Aldara-treated mice exposed to Vehicle or ST0702Sal. ANOVA and Dunnett's multiple comparisons test was used to test for statistical differences between groups. Statistical differences between Vehicle group and ST0702Sal group are shown. Data is presented as mean ± SEM from 6 mice per group. *P<0.05, **P<0.01, ***P<0.001. **C:** Representative photographs of the shaved back skin of Aldara-treated mice exposed to Vehicle or ST0702Sal.*

2.2.2 Investigation into the Hydrolysis Pathways of ST0702

In order to understand the effects of ST0702 in the psoriasis model it was decided to investigate its hydrolysis in vitro under conditions predictive of its metabolism in skin. It is known that ST0702 is capable of rapidly releasing aspirin, salicylic acid, or nicotinic acid under the influence of blood esterases (149). It is important both for *in vitro* biological studies and to assess the results of the *in vivo* Aldara™ study in mice to know how quickly ST0702 is metabolised under particular conditions. The question of whether the activity of ST0702 depends on the metabolites or the intact compound could be more easily answered if it were known whether or not the compound was immediately hydrolysed upon penetration into the mouse skin. Similarly, for in vitro assays, if the compound was immediately hydrolysed following incubation in media supplemented with the cell growth media this would affect the

analysis of any results obtained from cell studies in which the compound was incubated in media.

Esterases are hydrolases that hydrolyse ester bonds as well as peptides, amides and halides, in the presence of water, and therefore play an important role in the metabolism of a number of compounds used as drugs in humans. Esterases contribute to the metabolism of approximately 10% of therapeutic drugs (164) and are responsible for ester prodrug activation and drug detoxification. Esterases can be classified as carboxyl, aryl or acetylcholine esterases. They are found in various tissues and organs including the mammalian skin, liver and plasma. In the skin, esterases have particularly high activity in the epidermis, the hair follicles and the perspiratory glands; there is no esterase activity in the stratum corneum (165). Studies with mono and diesters of salicylic acid in cryostat sections of human skin transplanted onto hairless mice and of human cadaver skin have found that there is higher esterase activity in the upper skin layers (166). Furthermore, nicotinate esters have been shown to undergo incomplete metabolism upon transport through the skin (167). Esterases follow the general hydrolysis pattern:

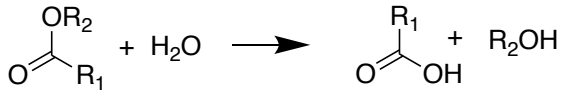

Figure 2-8: General reaction scheme for hydrolysis of esters.

ST0702 has three esters, all of which are susceptible to cleavage. The acetyl functional group of the aspirinate ester would be expected to be the first to hydrolyse, followed by the two esters attached to the isosorbide functional group. The potential paths of metabolic hydrolysis are outlined in Figure 2.9.

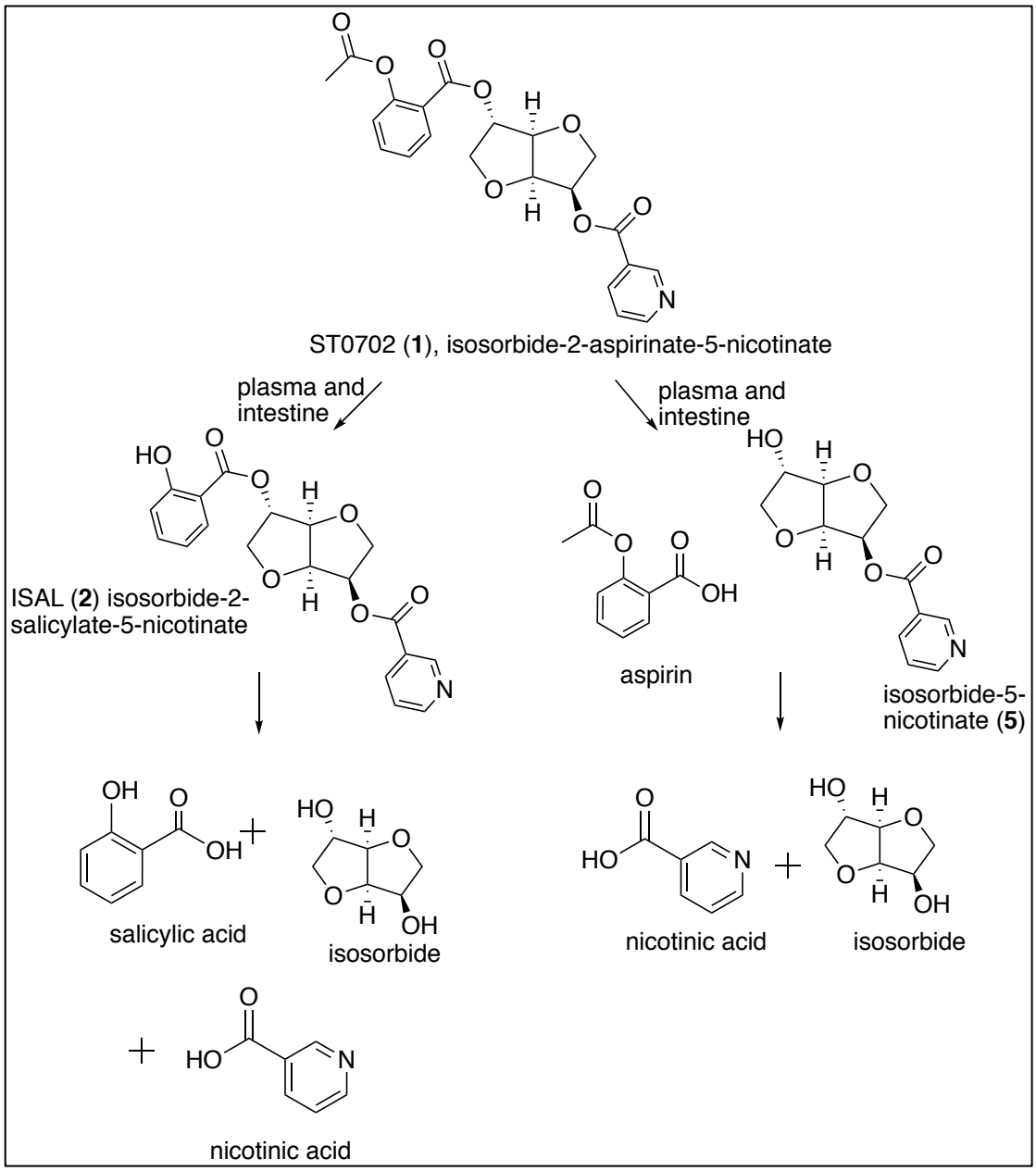

Figure 2-9: ST0702 potential hydrolysis pathways.

2.2.2.1 *Microsomal Study*

Microsomes are vesicle-like artifacts that are reformed from pieces of the endoplasmic reticulum (ER) when eukaryotic cells are broken up in the lab. Microsomes are not present in healthy, living cells. Microsomes can be concentrated and separated from other cellular debris by differential centrifugation. Unbroken cells, nuclei and mitochondria sediment out at 10,000 g, whereas soluble enzymes and fragmented ER, which contains CYP450 enzymes, remains in solution. At 100,000 g, the endoplasmic reticulum fragments sediment out of solution as a pellet, but the soluble enzymes remain in the supernatant. In this way, CYP450 enzymes are

concentrated and isolated. The S9 fraction used in the experiments outlined here contains the cytosol and microsomes. The microsome component contains CYP450 isoforms and other enzymes. CYP metabolism can vary greatly from one species to another, and interspecies differences in drug metabolism can be predicted by studying the in vitro metabolism of a drug via microsomes from different species. For example, a comparison of the CYP metabolism profile of different species with those of human microsomes can assist in the identification of the most relevant model for pharmacokinetic studies (168).

2.2.2.2 *Study of Hydrolysis Pathway of ST0702 in Human Skin Microsomes*

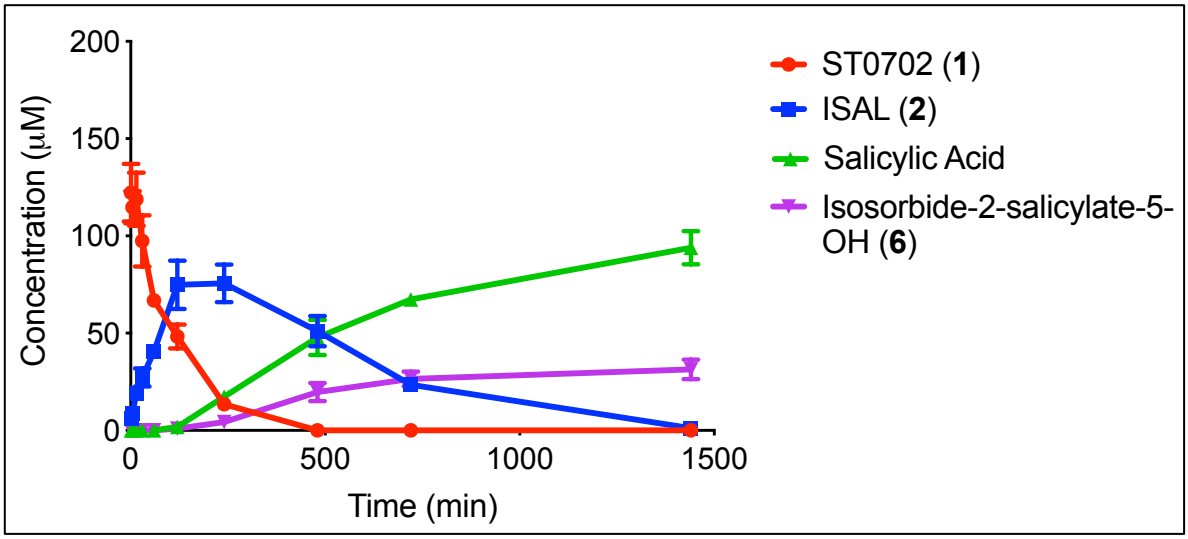

Figure 2-10: Results from hydrolysis studies in the presence of preparations of human skin microsomes. Human skin microsomes (0.5 mg/mL) were incubated at 37˚C with 100 μM ST0702 and analysed by HPLC at designated timepoints. Points are plotted as mean ± SEM.

The stability of ST0702 upon incubation with both human and mouse skin microsomes was studied. The progression curve for the hydrolysis in human skin microsomes is presented in Figure 2.10. Based on the results obtained it is thought that the primary metabolic pathway in human skin is as outlined in Figure 2.11. Using first order kinetics, the half-life ($t_{1/2}$) of ST0702 varied from 75.34 -76.17 min in human skin microsomes. The main metabolite of ST0702 initially was ISAL (**2**)**,** as it can be observed that as the concentration of ST0702 reduced, the concentration of ISAL (**2**) increased. ISAL was then metabolised further and as its concentration declined there was an increase in concentration of salicylic acid. This accounts for the period in which ST0702 was falling in concentration, but the concentration of ISAL remained constant. At this point, ISAL was being formed, but was also undergoing further metabolism. There was also some formation of isosorbide-2-salicylate (**6**), which is formed from the hydrolysis of the nicotinate ester, however this only started to appear after

approximately 4 h and reached a peak of about 40 μM in the 24 h period. The formation of salicylic acid appears to be favoured over the formation of isosorbide-2-salicylate (**6**). This is in line with what would be expected in studies in human plasma, where it would have been predicted that following the cleavage of the acetyl group of the aspirin, the next cleavage would be of the salicylic acid group, leaving isosorbide-5-nicotinate. The isosorbide-5-nicotinate (**5**) was too polar to be detected using this HPLC method, however, it is likely that the formation of the salicylic acid coincides with the formation of isosorbide-5-nicotinate and then subsequent metabolism yields nicotinic acid.

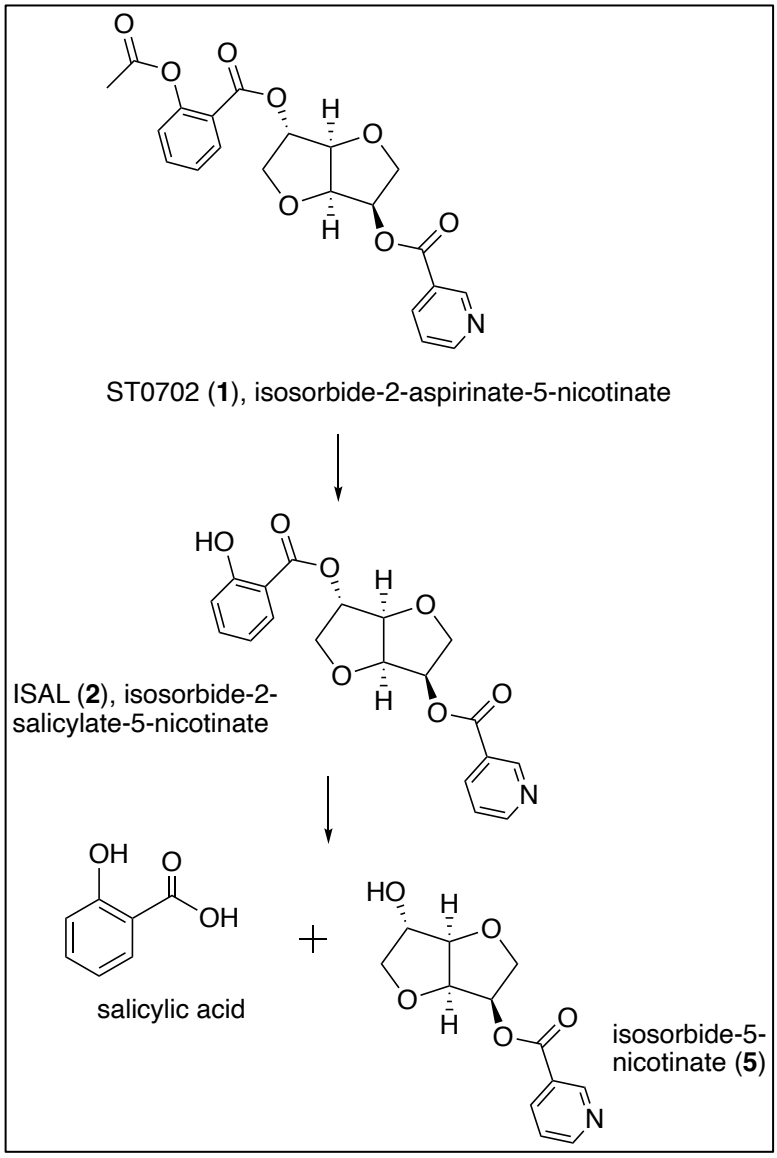

Figure 2-11: Hydrolysis pathway of ST0702 in the presence of preparations of human skin microsomes.

2.2.2.3 *Study of Hydrolysis Pathway of ST0702 in Mouse Skin Microsomes*

The metabolism of the compound in the mouse skin microsome was investigated over a 24 h period. It was observed that all of the ST0702 had been consumed after 60 min. The hydrolytic pathway of ST0702 in mouse skin microsomes was quite different to that observed in the human skin, with ST0702 appearing to undergo metabolism at a slower rate in human skin compared to mouse skin. After 8 h, all of the ST0702 exposed to the human skin microsome preparation had been metabolised which is in contrast to the 1 h required for total metabolism in the mouse skin microsome. First order kinetics analysis produced a $t_{1/2}$ of ST0702 in mouse microsomes in the range 4.43–7min, indicating rapid metabolism of ST0702. The metabolism of ST0702 saw the formation of ISAL (**2**), which was then further metabolised to isosorbide-2-salicylate (**6**). The isosorbide-2-salicylate was then relatively stable over the 24 h time period, with concentrations of 80 µM still present after 24 h. The formation of salicylic acid was also observed, but at quite a low rate, potentially due to the apparent stability of isosorbide-2-salicylate (**6**).

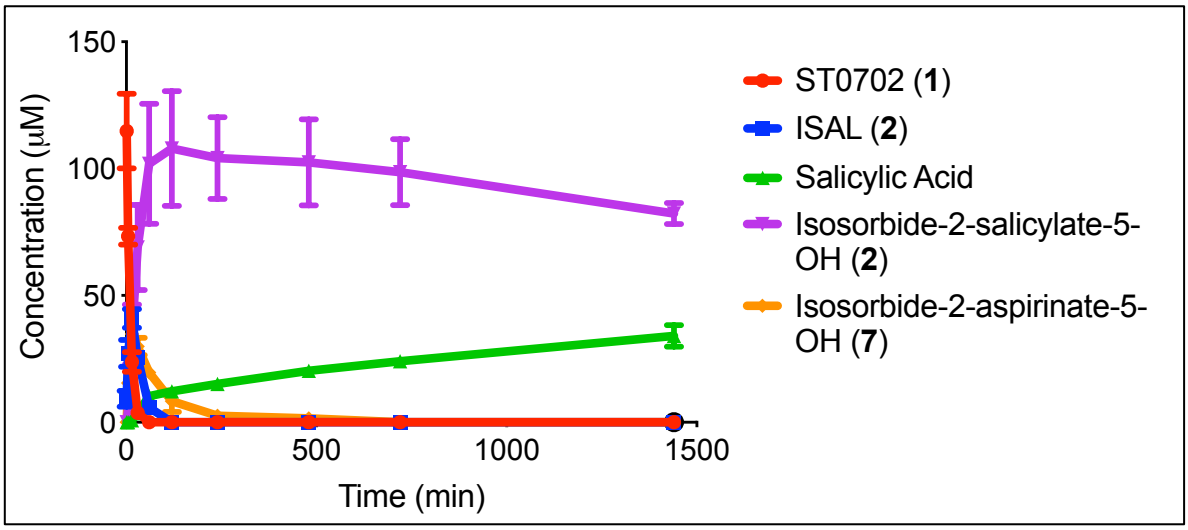

Figure 2-12: Results from hydrolysis studies in the presence of preparations of mouse skin microsomes.

Mouse skin microsomes (0.5 mg/mL) were incubated at 37˚C with 100 µM ST0702 and analysed by HPLC at designated timepoints. Points are plotted as mean ± SEM.

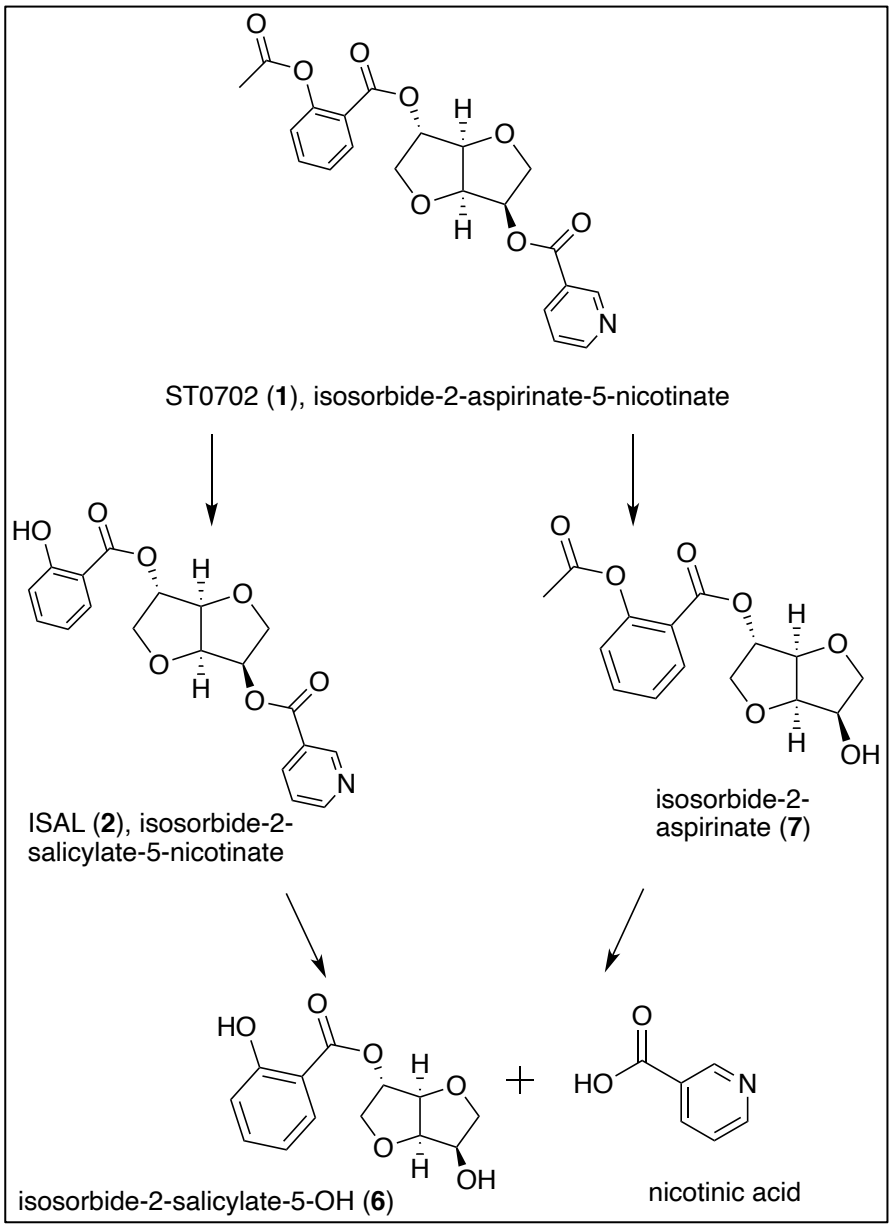

Figure 2-13: Main hydrolysis pathway of ST0702 in mouse skin microsomes.

2.2.2.4 *Study of Hydrolysis Pathways of ST0702 in Media*

Prior to the commencement of biological studies into the activity of ST0702 studies were carried out to investigate the stability of ST0702 in media. Biological studies to test the activity of ST0702 and related compounds were to be carried out in media containing serum, so it was important to know how long the intact compound was stable in media before undergoing hydrolysis. Initial experiments observed the disappearance of ST0702 and the appearance of its metabolite ISAL in complete media. The progression curves for the hydrolysis can be seen in Figure 2.14. The $t_{1/2}$ for ST0702 was found to be 29.6 min. After 4 h, no ST0702 remained as it had all been transformed into ISAL, or further hydrolysed to the other probable

metabolites. It can be seen that at the 2 h point the amount of ISAL being produced begins to decline, presumably as very little ST0702 is present for hydrolysis to occur and the salicylate itself is further metabolised to other more polar metabolites.

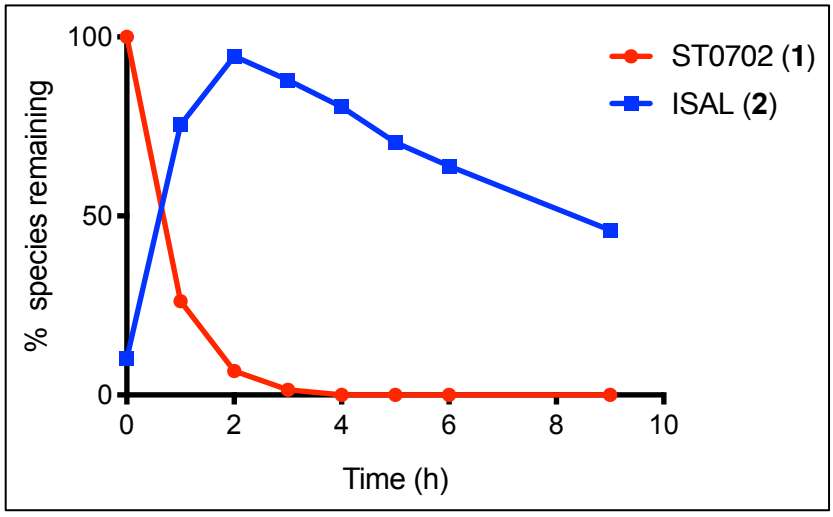

Figure 2-14: Hydrolysis of 100 µM ST0702 in complete media (RPMI supplemented with 10% FBS and 2 mM L-glutamine) at 37˚C.

In an additional study of the behaviour of ST0702 in serum-supplemented media, which involved a more detailed study of hydrolysis products and longer incubation times (from 0 – 48 h) the following results were observed (Figure 2.15). The $t_{1/2}$ of ST0702 was seen to be 37 min, which was similar but slightly longer to the 29.6 min observed previously. The difference can be perhaps explained by the slight differences in enzymatic activity of the serum. After 2 h, all the ST0702 had been hydrolysed. Initially, the main metabolite produced was ISAL. However, after 30 h, all of the ISAL had been metabolised. The main compound remaining after 48 h was salicylic acid.

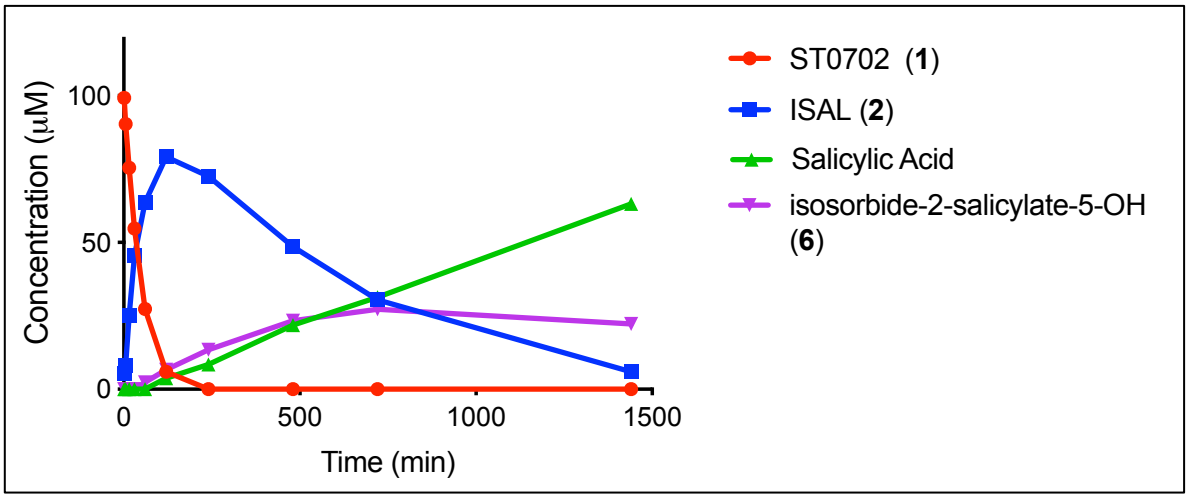

Figure 2-15: Hydrolysis of 100 µM ST0702 in complete media (RPMI supplemented with 10% FBS and 2 mM L-glutamine) at 37˚C.

The metabolism of ST0702 in serum-free media was also investigated. As some of the subsequent mechanistic studies were carried out under serum-starving conditions it was necessary to know whether ST0702 or its metabolites were present under these conditions. The progression curves are documented in Figure 2.16. ST0702 was metabolised much more slowly in serum-free media. This was expected due to the lack of enzymatic activity. The $t_{1/2}$ was seen to be 495 min. Serum-starving of cells pre-treatment could therefore be investigated as a possible method of ensuring ST0702 persisted in the media for long enough to have an effect on cells.

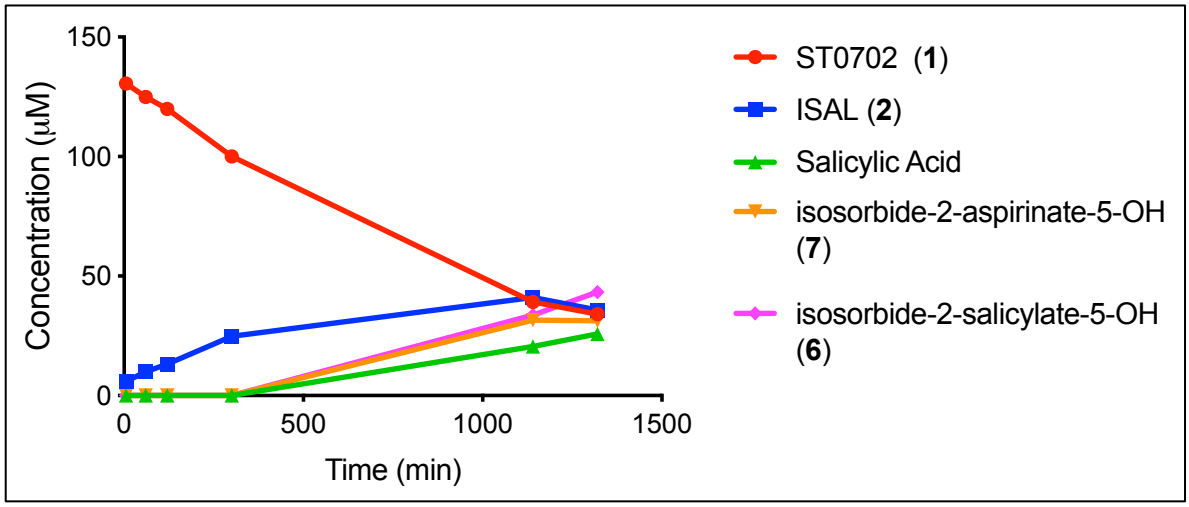

Figure 2-16: Hydrolysis of 100 μM ST0702 in media (RPMI only) at 37˚C.

The conclusion drawn from these stability experiments was that ST0702 is not particularly stable in complete media, and care will have to be taken when carrying out biological assays, as were the compound to be diluted in media prior to addition to cells there is a chance that the cells will not be exposed to the ST0702, but rather its metabolites, and inferences into the activity of the compounds when tested under these circumstances could not be made.

2.2.3 Initial Investigation into Effect of ST0702 on Models of the Innate Immune System

The first step in the investigation into the biological activity of ST0702 involved experiments examining the effect of ST0702 on the innate immune system. The first signalling pathway investigated was the NF-κB pathway. NF-κB is a protein transcription factor that is heavily involved in the regulation of inflammatory processes (169). Activation of NF-κB is rapidly and transiently induced by viral and bacterial infections, necrotic cells products, DNA damage, oxidative stress and pro-inflammatory cytokines (170). The activation of NF-κB results from the phosphorylation of the inhibitor of kappa B kinase (IκK) complex. The importance of NF-κB signalling in psoriasis has been shown, with lesional and non-lesional psoriatic skin

demonstrating elevated levels of activated, phosphorylated NF-κB (171). NF-κB has the ability to link altered keratinocyte and immune cell states through its effects on cellular proliferation, differentiation and apoptosis, as well as cytokine and chemokine production. Current biological treatments for psoriasis alter NF-κB signalling, with TNF-α and IL-12/23 inhibitors blocking cytokines that rely on NF-κB signalling as a downstream transcription factor (169).

ST0702 was tested in an NF-κB THP-1 reporter cell line. These experiments involved stimulation of the cells with a variety of inflammatory stimulants and cytokines, including TNF-α, phorbol myristate acetate (PMA), IL-1β and lipopolysaccharide (LPS). ST0702 (100 μM) did not reduce NF-κB activation in response to any of these inflammatory stimulants.

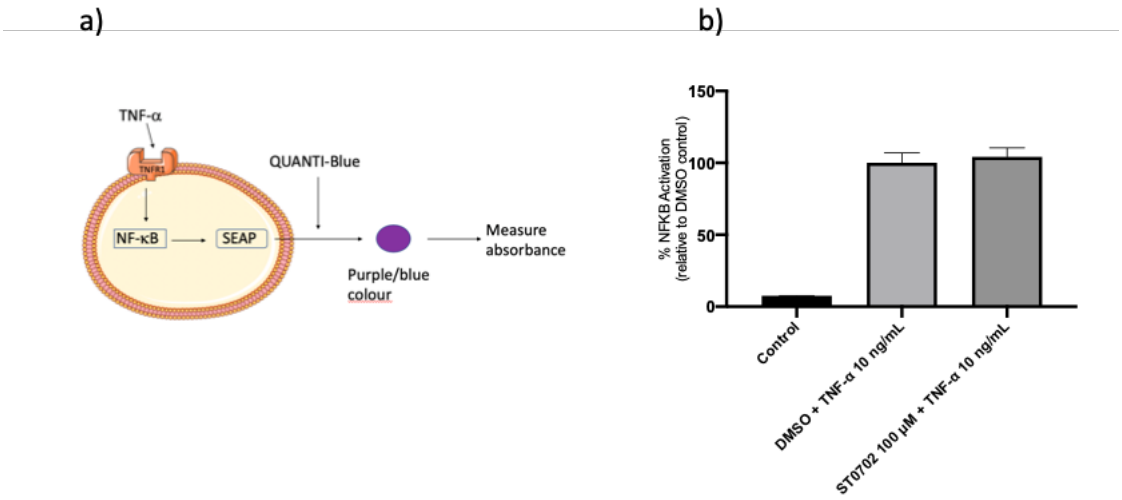

Figure 2-17: a) Overview of THP1-Blue NF-κB reporter assay and b) assay results. For b) Cells were plated at 1 × 10^5 cells/mL, preincubated with ST0702 or 0.5% DMSO for 30 min, then stimulated with 10 ng/mL TNF-α for 24 h. Cells in the control wells were untreated and were not stimulated with TNF- α. Following this SEAP levels were determined using Quantiblue. Data is expressed as mean ± SEM of three independent experiments.

The release of a number of inflammatory cytokines following treatment with ST0702 (100 μM) was investigated. IL-23, GM-CSF and IL-10 levels were examined. There were no consistent changes in levels of cytokines conventionally believed to be involved in psoriasis such as IL-23 and GM-CSF. However, the levels of IL-23 production by the PBMCs following stimulation with LPS were quite low, so this was perhaps not the best model to study the effect on this cytokine. Levels of IL-10 produced by PBMCs were increased following stimulation with LPS in cells that had been pre-treated with ST0702 compared to pre-treatment with DMSO.

IL-10 is an anti-inflammatory cytokine that plays an important role in immune mediation. Macrophages are the most important source of IL-10, but it is also secreted by B cells, T cells,

mast cells, DCs, keratinocytes, eosinophils and NK cells (172). Studies have linked psoriasis with mutations in the promoter region of the IL-10 gene (173, 174) and levels of IL-10 have been found to be decreased in the serum of psoriasis patients (175).

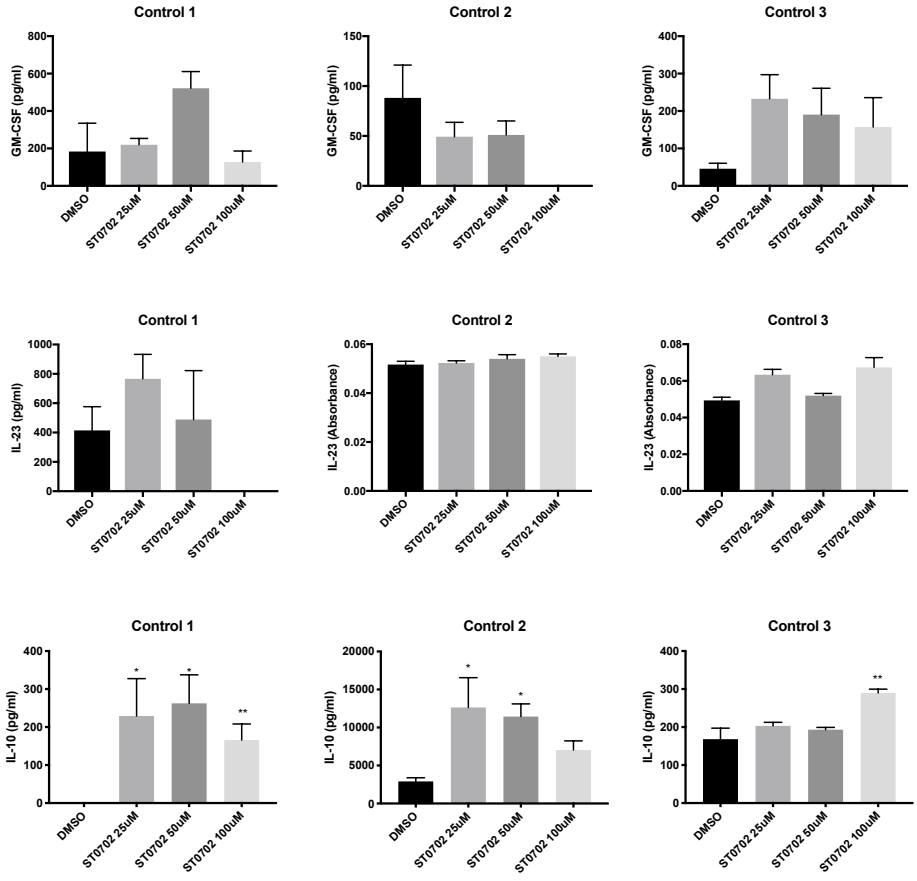

Figure 2-18: GM-CSF, IL-10 and IL-23 production in LPS-stimulated PBMCs treated with ST0702.

PBMCs were treated with compounds for 6 h before being stimulated with LPS 1 ug/ml for 24 h. ELISA was then carried out to test levels of GM-CSF, IL-10 and IL-23. Data is expressed as mean ± SEM.

ST0702 was also tested in HaCaT cells, a keratinocyte cell-line. Levels of IL-8 produced by HaCaT cells following treatment with TNF-α were not reduced by treatment with ST0702 (100 μM). Instead, a small increase was observed. IL-8 levels were tested as previous studies had shown that ST0702 (50 μM) significantly decreased the increase in IL-8 mRNA expression and IL-8 protein secretion in response to DCA (200 μM) stimulation in Het-1A cells, an oesophageal cell line (151). The same study also showed a decrease in IL-6 levels in DCA-stimulated Het-1A cells treated with ST0702 (50 μM). It was therefore interesting that there was no decrease in IL-8 observed here.

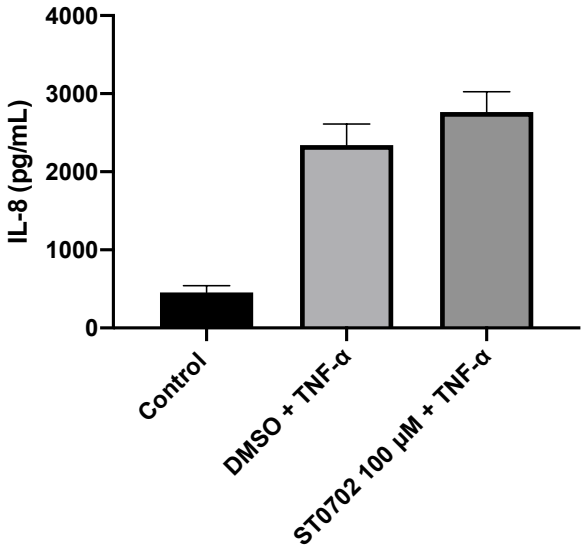

Figure 2-19: IL-8 production in HaCaT cells in response to TNF-α.
HaCaTs were plated at 1 × 10^5 cells/well in a 96 well plate. The cells were incubated overnight to adhere. The cells were pretreated with DMSO or ST0702 100 µM for 30 min, then stimulated with 10ng/mL TNF-α. Cells in the control wells were untreated and were not stimulated with TNF- α. The supernatants were removed after 18 h and the amount of IL-8 present was then measured by ELISA. The experiment was carried out in triplicate and data is expressed as mean ± SEM.

2.2.4 **Proliferation of HaCaTs**

The next experiments conducted investigated whether the compounds had an effect on the proliferation of keratinocytes. Psoriasis is characterised by abnormal keratinocyte hyperproliferation which results in thickening of the epidermis (18), so a direct effect of the compounds on keratinocyte proliferation would be a potential mechanism for the observed effect in psoriasis models. Cultured human keratinocytes can be difficult to work with for a number of reasons. Firstly, fresh human keratinocytes require supplementary growth factors to survive and proliferate in vitro. Also, donor-to-donor variability in growth characteristics and in vitro responses can complicate the interpretation of experimental data (176). For those reasons, HaCaT cells, a keratinocyte cell line, were employed in this instance. HaCaTs are a spontaneously immortalised human cell line from adult skin that has been proposed as a model for the study of keratinocyte function. The cells exhibit normal morphogenesis and express all the major surface markers and functional activities of functional keratinocytes (176). The MTT colorimetric assay was used to measure proliferation of HaCaT cells (177).

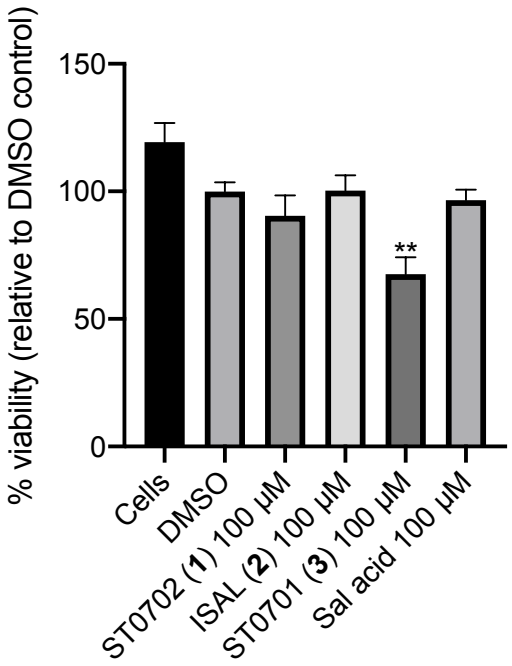

Figure 2-20: Results from HaCaT proliferation studies.
Cells were plated at 1 × 10^4 cells per well of a 96-well plate and left to adhere for 24 h. The compounds were then added and the plate was incubated for 48 h. Following this MTT was carried out. Data is expressed as mean ± SEM of three independent experiments.

The compounds do not appear to be having a significant anti-proliferative effect on the keratinocyte cell line, with compound **3** the only compound to have a statistically significant effect on proliferation, causing a reduction of approximately 30%. Salicylic acid was also tested in this assay, as it is a known keratolytic agent. It did not have effect in the assay, but this was expected as it would only be expected to have keratolytic activity at higher concentrations than those utilised here. Abnormal hyperproliferation of keratinocytes is one of the hallmarks of psoriasis, so the fact that ST0702 and related compounds are not that effective here is interesting, and suggests that the mechanism by which ST0702 has anti-inflammatory effects in psoriasis-like mouse models is unlikely to be due to its antiproliferative activity on keratinocytes.

2.2.5 **T cell Proliferation Experiments**

The next set of experiments carried out were designed to examine the effects of the compounds on T cells. T cell blasts were obtained by activating PBMCs with aCD2/CD28 and then stimulating the cells with two successive treatments of IL-2. Psoriasis is considered to have a T cell mediated inflammatory pathology, so inhibition of the proliferation of T cells was speculated to be the cause of the effect of ST0702 in the IMQ mouse model.

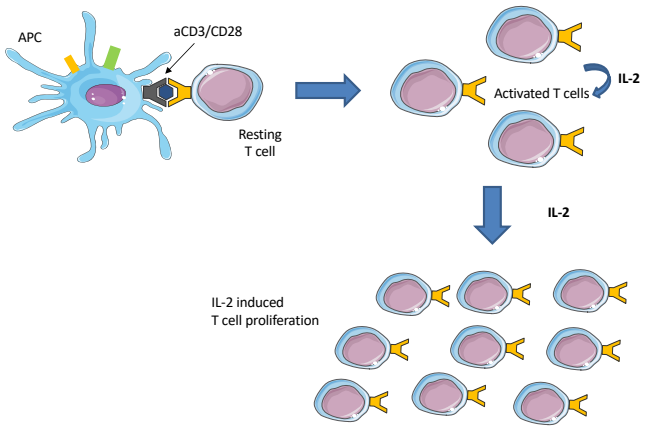

Figure 2-21: aCD3/CD28 activation of T cells followed by IL-2 induced T cell proliferation.

The T cells were treated with compounds for the last 24 h and then proliferation was measured using MTT (Figure 2.22) The compound with the largest inhibitory effect on the proliferation of the T cell blasts was ST0701(**3**), but ST0702 (32% reduction) and ISAL (50% reduction) were also inhibitory.

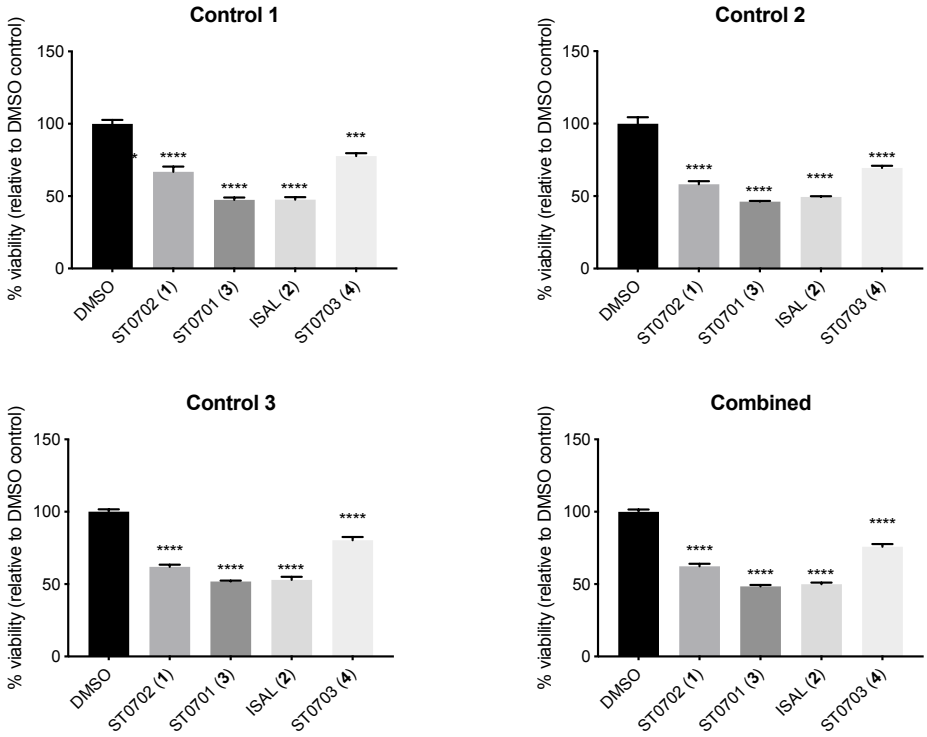

*Figure 2-22: Proliferation of T cell blasts treated with 100 µM ST0702 (**1**), ST0701 (**3**), ISAL (**2**) or ST0703 (**4**).*

PBMCs (5 × 10^5 cells/well in a 24-well plate) were stimulated with aCD3/CD28 beads for 72 h before adding two successive rounds of IL-2 (20 ng/ml) for 48 h. Cells were then treated with either DMSO, ST0702, ST0701, ST0703 or ISAL 100 µM for the last 24 h of stimulation. MTT was then carried out. Data is presented of mean ± SEM of 3 donors performed in triplicate.

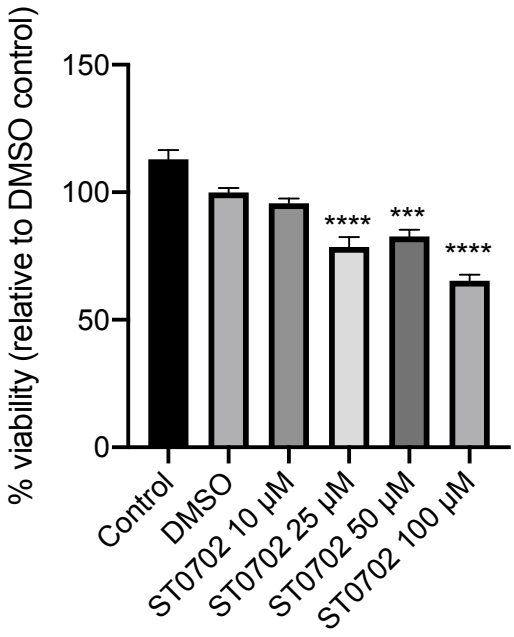

Figure 2-23: Proliferation of T cell blasts treated with varying concentrations of ST0702. PBMCs (5 × 10^5 cells/well in a 24-well plate) were seeded and stimulated with aCD3/CD28 beads for 72 h before adding two successive rounds of IL-2 (20 ng/ml) for 48 h. Cells were then treated with either 100, 50, 25 or 10 µM ST0702 for the last 24 h of stimulation. MTT was then carried out. Data is presented of mean ± SEM of 4 donors performed in triplicate.

The effect of ST0702 on T cell blasts was concentration dependent between 10 µM and 100 µM (Figure 2.23). The effect of 100 µM ST0702 was highly reproducible, with an inhibition of proliferation of approximately 35% observed in all experiments on T cell blasts.

A T cell line, HuT78 cells, was used for more efficient screening of the effect of the compounds on T cell proliferation. HuT78 could be cultured and produced in sufficient quantities to enable rapid experimental turnover. The results observed in the HuT78 cell line mimicked the results from the T cell blast experiments, with ST0702 causing an inhibition of proliferation of approximately 35%, and **3** (ST0701) being the most active compound, causing about 50% inhibition (Figure 2.24). Again, the results seem to be somewhat concentration dependent, but, as was also the case with the HuT78 cells, there is not much difference between the effect of 50 µM and 25 µM ST0702, with both concentrations having modest effects.

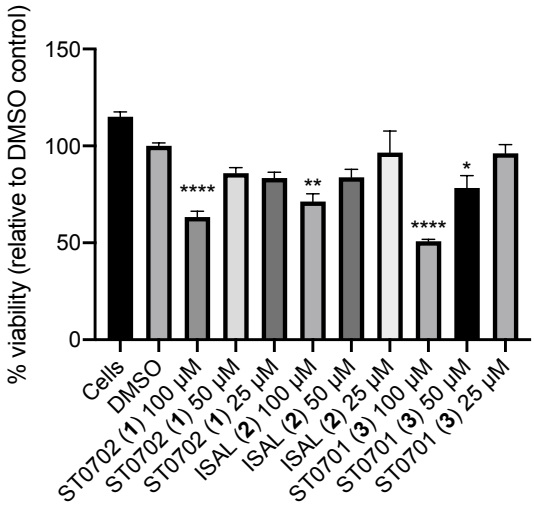

Figure 2-24: Proliferation Results of compounds tested in HuT78 cells.
HuT78 cells were plated at 1 × 10^4 cells per well of a 96-well plate. The cells were treated with 100 µM, 50 µM or 25 µM compound and incubated for 48 h. After this time, MTT was carried out. Results for each concentration are expressed as mean ± SEM of three experiments performed in triplicate.

To determine if the effect observed was due to a cytostatic or a cytotoxic effect on cell proliferation and growth, the amount of apoptosis that the cell was undergoing in response to treatment with the compounds was measured. The compounds did not appear to be very cytotoxic, with ST0701 (**3**) causing the most apoptosis, but the percentages of apoptotic cells were quite low (Figure 2.25). The implication of these experiments was that the results in the proliferation assay reflected a cytostatic rather than cytotoxic effect.

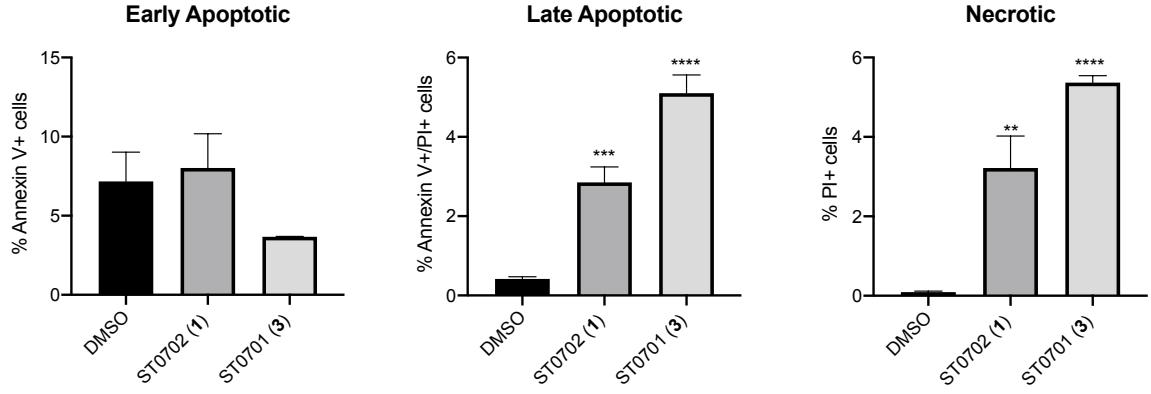

Figure 2-25: Annexin V Results in HuT78 treated with 100 µM compounds. .
HuT78 cells were plated at 1 × 10^4 cells per well (of a 96-well plate) with DMSO, 100 µM ST0702, or 100 µM ST0701 ***(3)*** *and incubated at 37℃ for 48 h. The cells were stained with Annexin V and PI. The samples were analysed by flow cytometry. Data is presented as mean ± SEM of three independent experiments performed in triplicate.*

2.2.6 **Synthesis of Isosorbide Analogues of ST0702**

The next part of the project involved the synthesis of a library of novel nicotinic acid ester derivatives based on ST0702 using isosorbide or isomannide as building blocks. The purpose of synthesising the analogues was to try to identify analogues that were even more active than ST0702 and to try to understand the SAR of ST0702, especially with respect to the aspirin/salicylate moiety. The presence of salicylic acid as a potential metabolite complicates the determination of the mechanism of action of ST0702 in the inflammatory models including the in vivo model. Salicylate toxicity must also be considered if this compound were to be applied topically, as toxicity can occur with topical use of 6% salicylic acid over 40% body surface area (152).

At this point of the project, the biological activity of ST0702 was not fully understood and it was unclear whether the activity was due to the effect of the intact ST0702 or whether it was its hydrolysis products. It was decided to probe the SAR at position-2 to obtain an idea as to whether it was the aspirinate ester group (or metabolites: aspirin or salicylic acid) that was having the effect, or if it were the intact molecule. The analogues retained the nicotinate ester group at C-5, with the ester groups at C-2 varying between the analogues.

The synthesis of the analogues with varying components at position 2 was a three-step sequence. The starting material for this was isosorbide mononitrate (ISMN) (**8**). ISMN contains an isosorbide group with a nitrate ester group attached at position-5. ISMN is composed of two cis-fused five membered tetrahydrofuran rings. It has an endo-nitrate and an exo-hydroxyl group (178).

ISMN is an organic nitrate that is used clinically for the treatment of angina, but serves as a useful material for the production of isosorbide compounds because the difficult step of introducing regioselectivity has already been achieved and the nitrate is easily removed by reduction following the elaboration of the 2-position (179).

The first step in the pathway involves the esterification of ISMN at the C-2, the second involves the reduction of the nitrate ester group at the C-5 of ISMN, whilst the third involves the esterification of the free hydroxyl at C-5 of the isosorbide group by nicotinic acid.

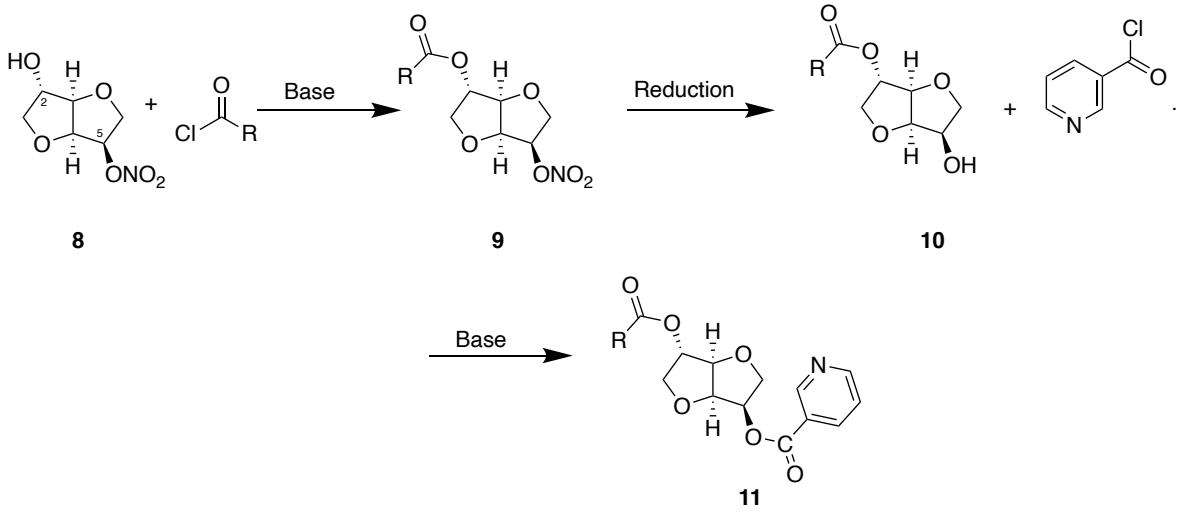

Figure 2-26: General reaction scheme for synthesis of isosorbide analogues of ST0702

2.2.6.1 *Esterification at C-2*

The synthesis of the ester intermediates can be achieved by many different approaches. The first possible approach was the Steglich Esterification using the appropriate carboxylic acid and DCC (dicyclohexylcarbodiimide) coupling procedure as shown in Figure 2.27. The reaction involves the formation of an O-acylisourea intermediate. The O-acylisourea intermediate has similar reactivity to that of the corresponding carboxylic acid anhydride. Following the addition of alcohol, a stable dicyclohexylurea and a corresponding ester are formed. In this method, DMAP (4-dimethylaminopyridine) is added as a catalyst to ensure efficient formation of esters. As a strong nucleophile, DMAP reacts with the O-acylisourea intermediate to form a reactive amide. This reactive amide intermediate reacts rapidly with alcohols and avoids intramolecular side products.

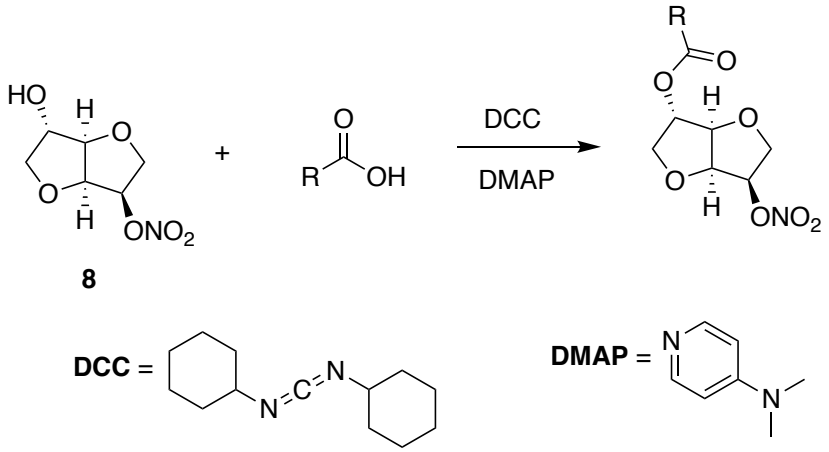

Figure 2-27:Scheme for the Steglich Esterification

The second approach involves the reaction of acyl chlorides with the free –OH group in ISMN under basic conditions, to produce the corresponding ester. This method was used to synthesise the esters for these compounds.

The esterification of the C-2 position of isosorbide was carried out and involved the reaction of acyl chlorides with a free –OH group in isosorbide under basic conditions, to produce the corresponding ester together with hydrogen chloride as shown in Figure 2.28. The first acyl chloride used was acyl chloride, to give the acetate ester, and the length of the carbon backbone increased with each of the next analogues, up to the valeroate ester. These esters were chosen to try the maximise the inference that could be gained from SAR studies, and to examine the importance of the ester substituent at the C-2 position. The benzoate ester was also a chosen analogue, as it could provide an insight into the importance of the aspirinate group, especially if it had similar efficacy to that of ST0702. This synthetic route of generating an ester from an alcohol is relatively easy and irreversible, compared to the route involving an alcohol and carboxylic acid. The esterification was monitored using TLC, and the formation of the correct product was confirmed using ^{1}H-NMR. Yields for this reaction ranged from 85-90%.

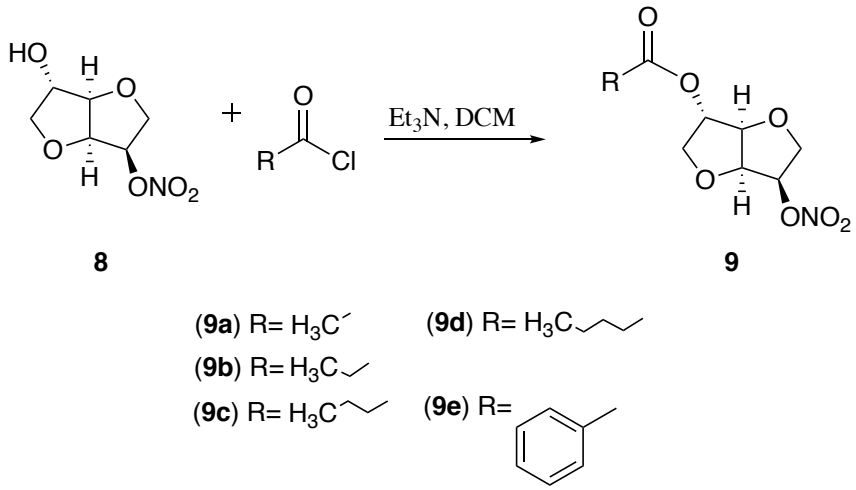

*Figure 2-28: Esterification of ISMN (**8**) with the appropriate acyl chlorides.*

2.2.6.2 *Reduction of the Nitrate Ester*

Nitrate ester reduction to secondary alcohol can be accomplished in many different ways. The oldest and most common method is to use reductive hydrolysis of alkali metal sulfide or hydrosulfide (such as sodium or ammonium sulphide or sulfur hydride) (180). The alcohol can also be produced through hydrogenation with palladium as a catalyst, and this was the method utilised for the majority of the present work.

The nitrate group at C-2 can be reduced by catalytic hydrogenation with palladium, nickel, rhodium or ruthenium. The hydrogenation takes place on the surface of the finely divided metal. Palladium on an inert charcoal support is widely used for this kind of reaction.

For the production of **10c** and **10d** a different method was used to reduce the nitrate ester group (Figure 2.29). The reducing agent utilised was zinc and acetic acid. The initial intention was to use this method to reduce the nitrate ester on all of the compounds, however the polarity of the acetate and propionate substituted compounds meant that isolation of the product following the completion of the reduction reaction was difficult, so hydrogenation using Pd(C) was the method used for the remainder of the compounds.

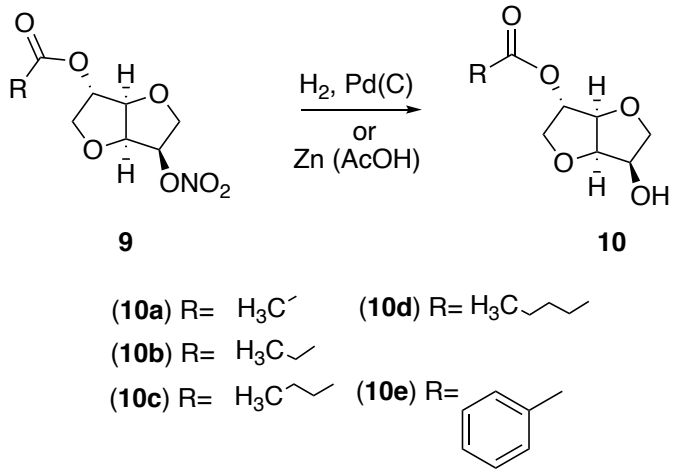

*Figure 2-29: Reduction of nitrate ester on C-2-esterified isosorbide compounds using H_2, Pd/C (**10a**, **10b** and **10e**) or zinc and acetic acid (**10c** and **10d**).*

2.2.6.3 *Addition of the Nicotinate Group at C-5*

The final stage of the synthesis of the nicotinic acid isosorbide-based ester derivatives was to introduce the nicotinate function onto the available hydroxyl group at position-5 of the isosorbide esters. This was achieved by the reaction of nicotinoyl chloride with a free –OH group at position-5 of the isosorbide ester in the presence of a triethylamine and DMAP, in a solution of DCM producing the corresponding nicotinic acid isosorbide-based ester derivatives.

The reaction was monitored using TLC with both vanillin staining and UV detection. For some of the reactions, extra portions of nicotinoyl chloride and triethylamine were added to ensure complete formation of the target compound. Since the addition of the nicotinate functional group to the molecule does not alter the overall polarity to a greater extent, the products would have similar polarity to the starting materials and consequently very close R_f values on the TLC plate. After the reaction reached completion, these compounds were purified by column

chromatography to give the final desired compounds in good yields. No washing was completed as many of the products were water soluble.

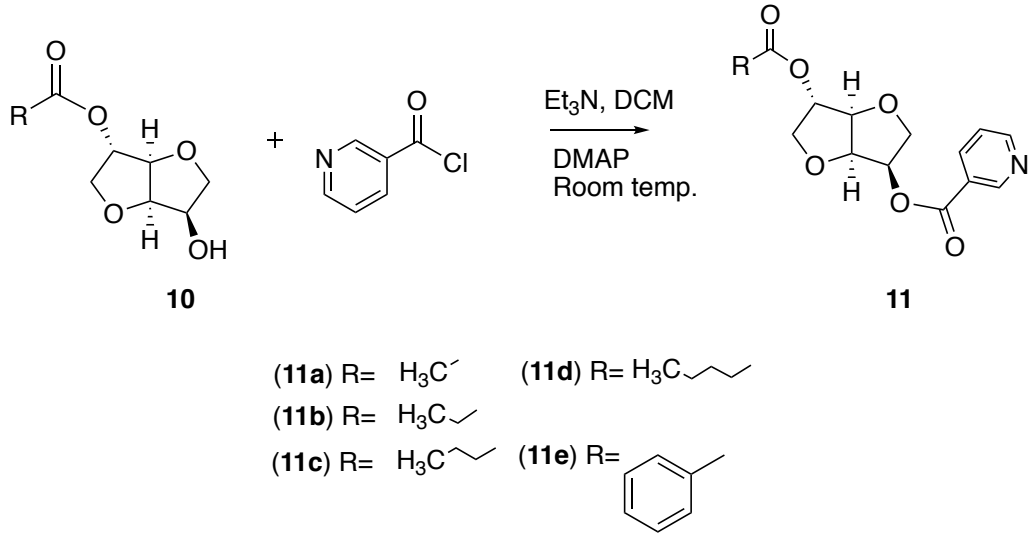

Figure 2-30: Esterification of isosorbide C-5 with nicotinoyl chloride.

2.2.7 **Synthesis of Isosorbide Analogues**

A number of other isosorbide analogues were synthesised. These were also of similar structure to ST0702 but had modifications other than that at the C-2 position. They were synthesised in a similar way to the C-2 analogues, with an initial esterification, followed by a reduction using H_2, Pd/C and then a final esterification.

Isosorbide-2-nicotinate-5-benzoate (**14**) was synthesised from ISMN in a three-step process, first the addition of the nicotinate ester at C-2, followed by the reduction of the nitrate group at C-5, followed by the addition of the benzoate ester group at C-5.

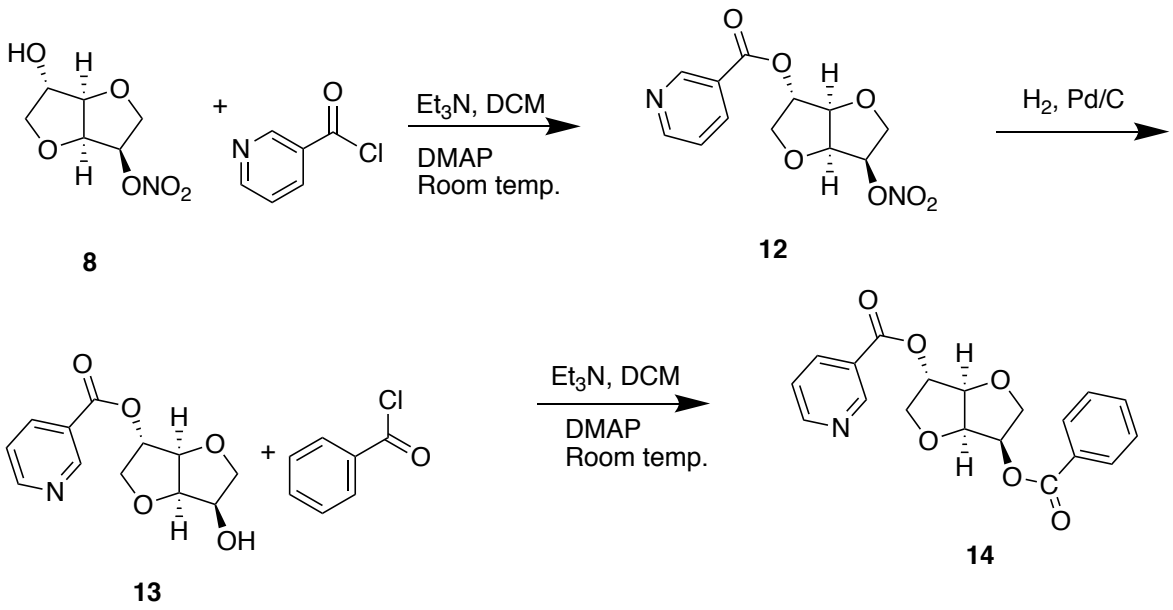

*Figure 2-31: Synthesis of isosorbide-2-nicotinate-5-benzoate (**14**)*

Isosorbide-2-benzoate-5-isonicotinate (**15**) was synthesised from ISMN in a three-step process, first the addition of the benzoate ester at C-2 to produce isosorbide-2-benzoate-5-nitrate (**9e**) followed by the reduction of the nitrate group at C-5 to give isosorbide-2-benzoate (**10e**), and then the addition of the isonicotinate ester group at C-5.

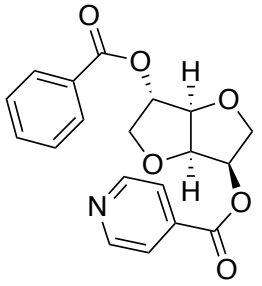

*Figure 2-32: Structure of isosorbide-2-benzoate-5-isonicotinate (**15**)*

Isosorbide-2-aspirinate-5-salicylate (ST0701, **3**) and isosorbide 2,5-dinicotinate (**16**) had previously been synthesised from ISMN by researchers in the Gilmer lab and were tested along with the other isosorbide analogues.

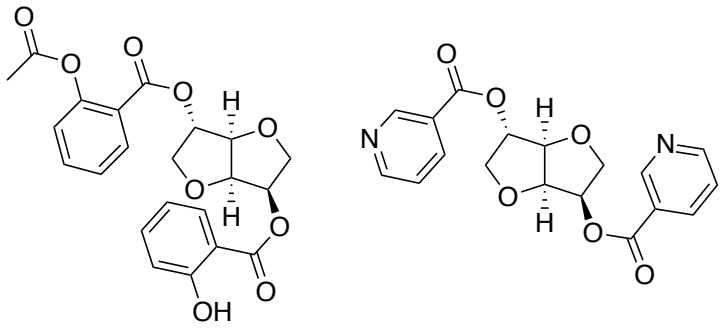

ST0701 (**3**) (**16**)

*Figure 2-33: Structure of isosorbide-2-aspirinate-5-salicylate (ST0701, **3**) and isosorbide 2,5-dinicotinate (16).*

2.2.8 **Synthesis of Isomannide Analogues**

The synthesis of isomannide analogues was approached slightly differently from the synthesis of the isosorbide compounds, primarily because the starting materials were different. For the isosorbide compounds the starting material was ISMN, which had a nitrate ester group already on the -5 position of the isosorbide skeleton. For the isomannide compounds, the starting material was isomannide (**17**), so there were two free endo hydroxyl groups. For isomannide compounds, the 2 and the 5 position are the same, as both are endo hydroxyl groups. For isosorbide, the 2 and the 5 position are different, as the 2 position has an exo-hydroxyl group while the 5 position has an endo-hydroxyl group. For simplicity, the 2- and 5-position of isomannide will be referred to, however it should be noted that these positions are interchangeable.

The synthetic strategy in preparing nicotinic acid isomannide based ester derivatives involved modifying the hydroxyl group of isomannide with a range of ester groups at either position-2 or position-5 with retention of configuration.

Two approaches could be taken to synthesise these compounds. The first approach was to achieve mono-substitution of one of the free hydroxyl groups of isomannide with appropriate ester derivatives, so that a nicotinate ester can be introduced onto the remaining available hydroxyl group in the later stage to complete the synthesis. The second approach to the synthesis of these compounds involves the addition of nicotinate functional group at either C-2, or C-5 with retention of configuration at first, then followed by esterification on the remaining available hydroxyl group with appropriate ester derivatives as shown in Figure 2.34. The first approach was chosen for the synthesis of these compounds.

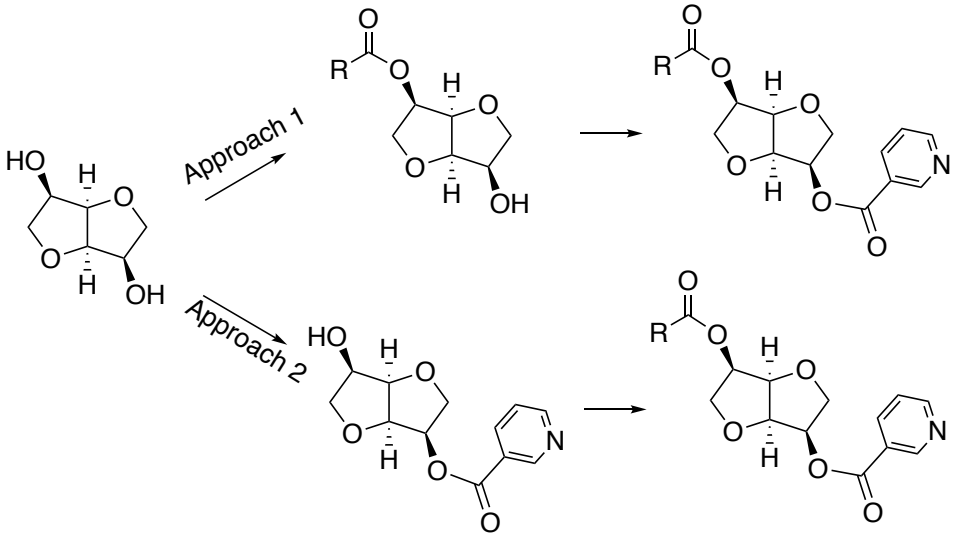

Figure 2-34: Approaches to the design of nicotinic acid isomannide based ester derivatives.

2.2.8.1 *The synthesis of mono-substituted isomannide ester*

To achieve monosubstitution of the isomannide group, stoichiometric amounts of the relevant acyl chlorides were reacted with a free –OH group in isomannide under basic conditions, to produce the corresponding ester together with HCl as shown in Figure 2.35. This synthetic route of generating an ester from an alcohol is relatively easy and irreversible.

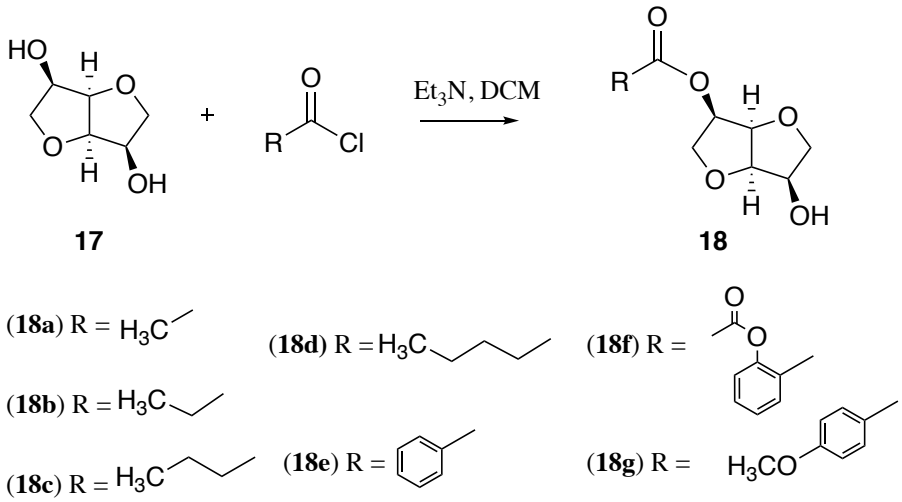

Figure 2-35:Esterification of isomannide (12) with Et_3N and appropriate acyl chlorides.

The reaction involves the selective esterification of one of the available hydroxyl groups of isomannide at either C-2 or C-5 using an acyl chloride. Isomannide has two free endo-hydroxyl groups at C-2 and C-5 which share the same reactivity. However, only one of the positions was required to be esterified so mono-substitution needed to be achieved. The selective formation of the mono-substituted ester isomannide was achieved by carrying out the reaction at 0°C in

order to slow down the reaction and favour the formation of mono-substituted esters from isomannide rather than the formation of di-substituted ones. A lower temperature allows greater control over the reaction, so that it can be stopped before excessive formation of di-substituted esters.

This approach was therefore applied to the synthesis of the 2-acetate (**18a**), 2-propionate (**18b**), 2-butyrate (**18c**), 2-valeroate (**18d**) and 2-benzoate (**18e**), 2-aspirinate **(18f)** and 2-methoxybenzoate **(18g)** which were prepared using appropriate acyl chlorides.

2.2.8.2 *The synthesis of nicotinic acid isomannide based ester derivatives*

The final stage of the synthesis of the nicotinic acid isomannide based ester derivatives was to introduce the nicotinate ester group onto the available hydroxyl group at position-5 of the mono-substituted isomannide esters. This synthesis was achieved relatively easily by the reaction of nicotinoyl chloride with a free –OH group at position-5 of the mono-substituted isomannide in the presence of a base, triethylamine, and a catalyst, DMAP, in a solution of DCM to produce the corresponding nicotinic acid isomannide based ester derivatives together with hydrogen chloride (Figure 2.36).

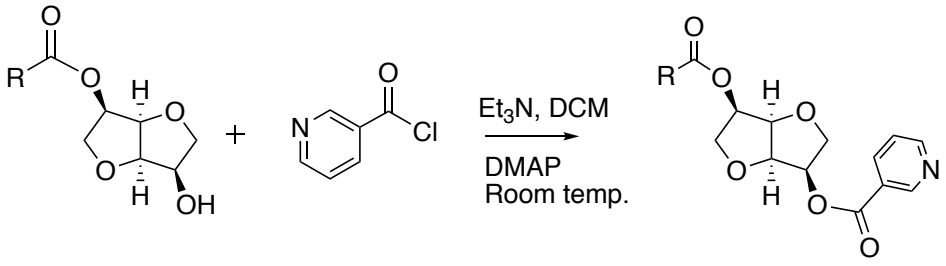

18 **19**

(**19a**) R = H_3C

(**19b**) R = H_3C

(**19c**) R = H_3C

(**19d**) R = H_3C

(**19e**) R =

(**19f**) R =

(**19g**) R = H_3CO

Figure 2-36:The addition of the nicotinate ester onto monosubstituted isomannide esters.

The reaction was monitored using TLC with both vanillin staining and UV detection. Extra portions of nicotinoyl chloride and triethylamine were added to ensure the complete formation of the desired compound and complete consumption of the starting materials. The reaction was challenging to monitor because of the similarity of the secondary alcohol and the nicotinate ester R_f values. Particular attention was given in the reaction with 2-benzoate isomannide and

2-aspirinate isomannide, as both of their starting materials and finished products were UV detectable which made it challenging to conclude whether the reaction was completed.

2.2.9 **Synthesis of Metabolites of ST0702**

As part of the metabolism studies for ST0702, it was necessary to obtain its potential hydrolysis products to act as standards for high performance liquid chromatography (HPLC).

Isosorbide-2-aspirinate (**7**) had been synthesized by previous researchers in the Gilmer group and was synthesized from ISMN in a similar way to the C-2 analogues, just forgoing the addition of the nicotinate ester as the final step. Esterification occurs at the C-2 position, with the formation of the aspirinate ester, followed by reduction using H_2, Pd/C.

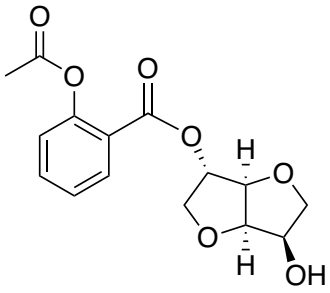

Figure 2-37: Structure of isosorbide-2-aspirinate (7)

Isosorbide-2-salicylate (**6**) was synthesised via a two-step sequence from ISMN. ISMN was first reacted with 2-benzyloxybenzoic acid via DCC coupling to form isosorbide-2-benzyloxybenzoate-5-nitrate (**20**). Following this a reduction reaction with H_2, Pd/C was carried out and the nitrate ester and benzyloxybenzoate ester were both reduced, yielding isosorbide-2-salicylate (**6**).

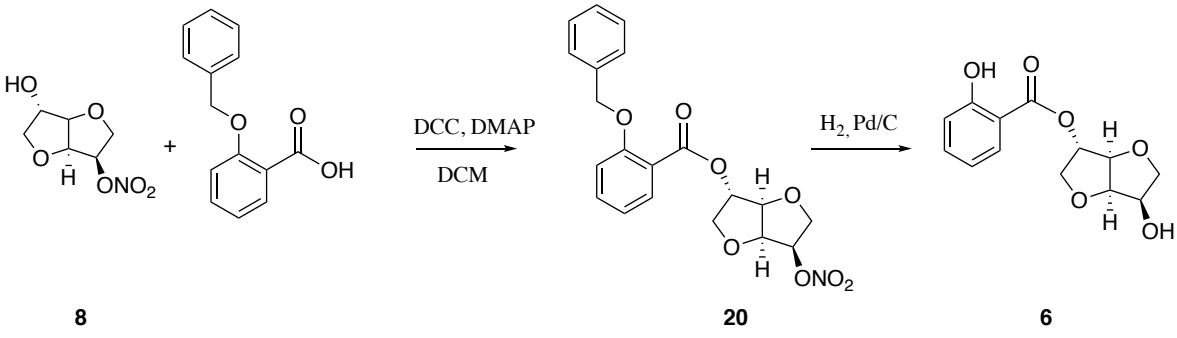

8 **20** **6**

*Figure 2-38: Synthesis of Isosorbide-2-salicylate (**6**).*

Isosorbide-2-salicylate-5-nicotinate (ISAL, **2**) was synthesised using two different methods. The first method utilised the known enzyme mediated reaction**.** Following a study of the metabolism of ST0702 it was determined that one of the main metabolites of ST0702 incubated

in FBS-supplemented media was isosorbide-2-salicylate-5-nicotinate, which arose from the cleavage of the acetyl ester of aspirin. As an alternative to synthesising isosorbide-2-salicylate-5-nicotinate (ISAL), which involved quite a complex synthesis protocol, it was decided to obtain the compound by treating a solution of ST0702 with 10% FBS in aqueous buffer and monitoring the production of ISAL, formed from the cleavage of the acetyl ester of aspirin, by HPLC. ISAL was then isolated by flash column chromatography.

The second method involved a four step sequence, the first step involved DCC coupling of the free hydroxy group of ISMN with 2-benzyloxybenzoic acid to form isosorbide-2-benzyloxybenzoate-5-nitrate. The nitrate ester was then selectively reduced using zinc and acetic acid. The nicotinate ester was then added onto the available hydroxyl group at position-5. The last step involved the reduction of the benzyloxybenzoate ester using hydrobromic acid and acetic acid, to yield isosorbide-2-salicylate-5-nicotinate.

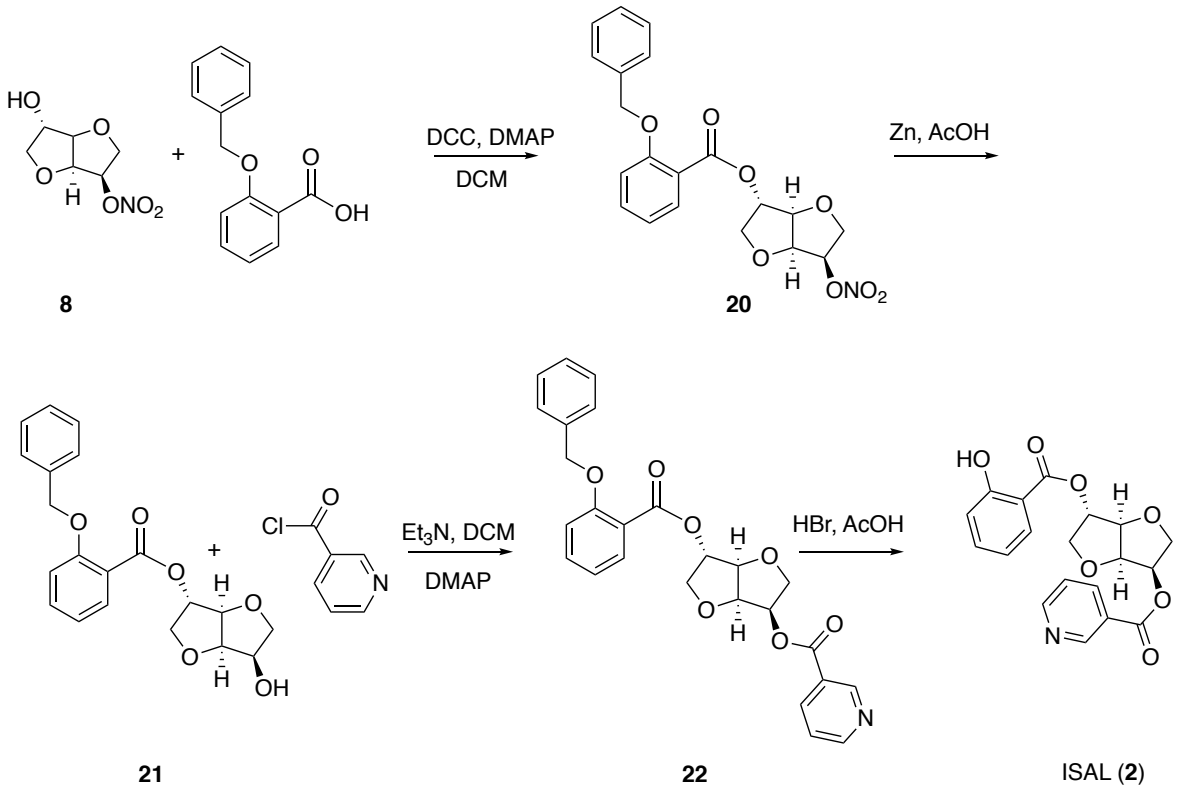

*Figure 2-39: Reaction scheme for synthesis of ISAL(**2**).*

2.2.10 **Physicochemical Properties of ST0702 and Analogues: Topical Administration**

ST0702 was being studied as a potential topical therapy for psoriasis. The topical route of administration has been chosen for several reasons. Firstly, ST0702 is apparently intrinsically active but tends to break down rapidly in skin conditions producing innocuous or well characterised byproducts. Additionally, ST0702 has shown efficacy when applied topically

(suspended in a petroleum jelly vehicle) in the IMQ mouse model of psoriasis. The decision to investigate the potential of ST0702 and analogues means it is necessary to study the physicochemical properties of these compounds.

For lead compounds being considered for oral administration, Lipinski's 'Rule of 5' should be considered (181). The rules state that poor absorption or permeability are more likely when:

- There are more than 5 H bond donors (expressed as the sum of OHs and NHs)
- The molecular weight is greater than 500 Da.
- The *log P* is greater than 5.
- There are more than 10 H-bond acceptors (expressed as the sum of Ns and Os)

ST0702 will be delivered topically so these Lipinski rules do not apply, however, for a drug to be suitable for transdermal delivery, it has been suggested that modification of these rules might lead to the identification of more feasible drug candidates, these new rules are as follows (182):

- Modest molecular weight (MW < 400–500 Da)
- A balanced lipophilicity (*log P* ideally around 2 or 3)
- A measurable solubility in both oil and water (as the drug will need to pass through the SC)

As ST0702 was considered for potential local administration, transdermal drug delivery may not be the desired outcome, as drug delivery to the systemic circulation may not be necessary if the compound is only having local effect. However, it may be desirable to have some transdermal delivery as psoriasis is thought to induce a chronic systemic inflammatory state.

To be considered as a potential treatment for psoriasis the lead compound would need to have suitable properties as to allow permeation and penetration into the epidermis and dermis, and to do so it would need to first pass through the SC. The SC is the main barrier to drug penetration.

Topical delivery of psoriasis medications can be limited by poor penetration of drugs through psoriatic skin. Psoriatic skin has been described as 'rigid' due to the thick scaly plaques, increased levels of cholesterol and decreased levels of ceramides, and a deficiency of natural moisturising factors such as water. The state of hydration of the SC is an important factor in determining the rate of percutaneous absorption of a drug (183). An increase in the level of hydration in the SC can decrease the diffusional path length and protein network density, favouring the drug transport. The reverse is true when SC hydration levels are low. As a result of these factors, adequate penetration through psoriatic tissues to achieve therapeutic effectiveness remains a significant challenge. Additionally, the metabolic capacity of the skin

needs to be considered, as does the possibility that the drug or the excipients in the formulation may cause increased irritation at the site of action. Studies in mice have shown that IMQ-induced psoriatic skin can lead to enhanced drug penetration and skin accumulation (184, 185), which suggests that it is the defect in barrier function, and not the elongation in the delivery pathlength that dominates drug absorption through psoriatic skin (185).

Absorption of drug into the skin falls under the influence of a number of different physiological factors relating firstly to the skin, including skin age, anatomical location, temperature, race, skin hydration, skin condition (diseased/healthy) and skin metabolism (186). In terms of physicochemical factors, drug lipophilicity, molecular size, and the ionisation and pH of the formulation, all have a large influence on the degree of penetration (186). In general, molecules of size larger than 500 Da are too large to penetrate the SC (187). An example of a drug with too high a molecular weight would be cyclosporin (1202 Da) which was found to be ineffective when applied topically in psoriasis, atopic dermatitis and allergic contact dermatitis (188). However, when injected intralesionally it was effective in psoriasis, suggesting that a molecular weight of 1202 Da is too high to achieve sufficient skin penetration (189). To achieve optimal permeability the lipid/water partition coefficient is expected to be 1 or greater. Higher logP values are associated with greater accumulation in the SC. pH must also be considered as the use of formulations with either very high or very low pH values can damage the skin.

2.2.11 **Lipophilicity Studies of ST0702 and Analogues**

Before testing the biological activity of the newly synthesised compounds the physicochemical properties were examined to assess if they were suitable for topical drug delivery. It was known that the compounds all have a molecular weight of less than 500 Da, which is required for adequate penetration through the SC. To get greater insight into the potential penetration ability, the log P and water solubility of the compounds was measured. The logP was measured using two different methods, HPLC and RP-TLC, and water solubility was measured using a supersaturation method and HPLC analysis.

2.2.11.1 *Determination of Log P using HPLC Method*

A suitable RP-HPLC method was developed for simultaneous estimation of lipophilicity in the isomannide and isosorbide series. Different chromatographic conditions were applied and optimised in order to get a short sampling time and high sensitivity. An isocratic elution method was used, so the composition of the mobile phase was kept constant throughout the HPLC separation. The mobile phase used was a combination of acetonitrile and water (and included 0.1% formic acid). Various concentrations of the acetonitrile/water mixture were tested until

the components of the mixture are separated cleanly in a reasonable amount of time. The optimised mobile phase contained 40: 60 acetonitrile and water.

Typical chromatograms obtained with the final conditions are shown in Figure 2.40.

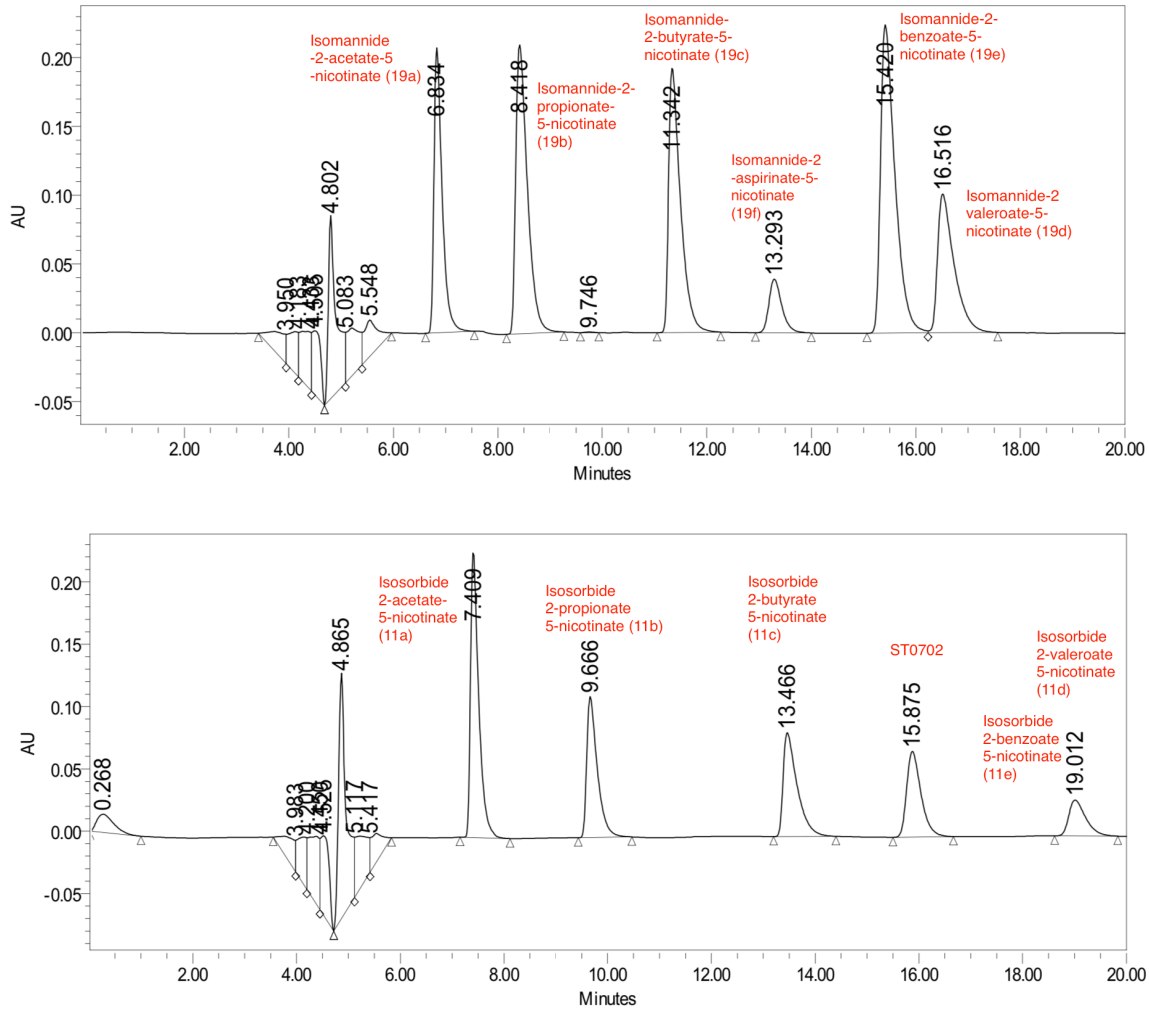

Figure 2-40:HPLC chromatograms for the isomannide and isosorbide series.
Data was obtained by RP-HPLC. An optimised HPLC method was used with an isocratic mobile phase containing 40: 60 acetonitrile and water.

As observed from the chromatograms, the method was capable of separating all related compounds within the series with the exception of the benzoate ester (**11e**) and valeroate ester (**11d**) of isosorbide, which have a retention time of 18.583 min and 19.012 min, respectively. The order of elution in both chromatograms are as follows: acetate ester (**11a**)(**19a**) > propionate ester (**11b**)(**19b**) > butyrate ester (**11c**)(**19c**) > aspirinate ester (ST0702)(**19f**) > benzoate ester (**11e**)(**19e**) > valeroate ester (**4d**)(**19d**) derivatives. The elution order is governed by the carbon content for a related series, as well as the water solubility of the solute. For compounds in an analogous series, retention time usually decreases with decreasing the number

of carbon atoms and increasing water solubility. Retention time also decreases with unsaturation due to *pi* electron dipoles in the double bond which makes it more polar and thus elute faster. The acetate ester is the least retained in the system due to its structure bearing a straight carbon chain with the fewest carbon atoms, it is then followed by the propionate esters and butyrate esters. Interestingly, the valeroate esters eluted more slowly than the benzoate esters, even though the latter has more carbon atoms. This is because the valeroate ester contains a saturated straight carbon chain, whereas the benzoate ester contains unsaturated carbon double bonds. The *pi* bond electrons are more polarisable and thus contribute to instantaneous dipole moments which makes it slightly more polar than the straight carbon chain that contains a similar number of carbon atoms. The aspirinate esters eluted faster than the benzoate esters which can be attributed to the fact that there is an extra ester functional group on the ring structure of the aspirinate ester.

The literature *Log P* values for three reference compounds (aspirin, benzyl methacrylate and ethyl benzoate) were plotted against the logarithm of their capacity factors to form a linear relationship. The capacity factor is equal to *(Tr - To) / To*, where *Tr* is the retention time of the desired analyte and *To* is the retention time of the unretained peak.

This linear slope could then be used to estimate *Log P* values for the isomannide and isosorbide series. The capacity factor and lipophilicity parameters obtained in both series from the HPLC method are presented in Figures 2.41 and 2.42. In RP-HPLC, the lipophilicity of an analyte is the primary predictor of retention times. As was expected from the rate of retention of these compounds, the calculated *Log P* values were higher for the valeroate esters, followed by benzoate esters and aspirinate ester, then aliphatic esters with decreasing carbon chains.

Isomannide-series	Retention Time (min)	Capacity Factor (*k'*)	Log *k'*	*Log P*
Acetate (**19a**)	6.83	0.42	-0.37	1.21
Propionate (**19b**)	8.42	0.75	-0.12	1.71
Butyrate (**19c**)	11.34	1.36	0.13	2.22
Valeroate (**19d**)	16.52	2.44	0.39	2.73
Benzoate (**19e**)	15.42	2.21	0.35	2.64
Aspirinate (**19f**)	13.30	1.77	0.25	2.45

Figure 2-41: Lipophilicity parameters of isomannide series obtained from RP-HPLC.

Isosorbide-series	Retention Time (min)	Capacity Factor (*k'*)	Log *k'*	*Log P*
Acetate (**11a**)	7.41	0.52	-0.28	1.39
Propionate (**11b**)	9.67	0.99	-0.01	1.94
Butyrate (**11c**)	13.47	1.77	0.25	2.45
Valeroate (**11d**)	19.01	2.91	0.46	2.88
Benzoate (**11e**)	18.59	2.82	0.45	2.86
ST0702	15.88	2.26	0.36	2.66

Figure 2-42: Lipophilicity parameters of isosorbide series obtained from RP-HPLC.

2.2.11.2 *Determination of Log P using RP-TLC Method*

The partition coefficient (*P*) is used to describe the lipophilicity of a drug. It is defined as the ratio of equilibrium concentrations of a drug in an organic phase (C_{org}) and an aqueous phase (C_{aq}).

$$P = \frac{Corg}{Caq}$$

Most commonly the organic solvent is n-octanol and the other solvent is water. Hydrophobic molecules will have a high *P* value while hydrophilic molecules will have a low *P* value.

Reverse phase TLC (RP-TLC) was performed on pre-coated C18 reverse-phase high performance TLC plates. The plates were developed in a closed chamber across a development distance of 15 cm at room temperature. Methanol (MeOH) as an organic modifier was used at three concentration levels (40, 50 and 60% MeOH in water). The retention of each compound in this system is referred as R_M. The R_M value can be calculated using the following equation:

$$R_M = \log\left(\frac{1}{Rf} - 1\right)$$

The relationship between the concentrations of the organic modifier and their corresponding R_M values were found to be linear with $R^2 > 0.95$ in all cases. The theoretical R_M value at 0% organic modifier was calculated by extrapolating from the calibration curves that were obtained. These values were then correlated to the literature *log P* of two reference compounds (methyl benzoate and paracetamol). This linear slope could then be used to calculate the *Log P* values for the isomannide and isosorbide series.

Isomannide-series	R_{M0}	*Log P*
Acetate (**19a**)	1.47	1.73
Propionate (**19b**)	1.53	1.76
Butyrate (**19c**)	2.11	2.03
Valeroate (**19d**)	2.62	2.26
Benzoate (**19e**)	3.21	2.53
Aspirinate (**19f**)	3.29	2.57

Figure 2-43: Lipophilicity parameters of isomannide series obtained from RP-TLC. Compounds were spotted onto RP-TLC plates. 3 mobile phases were used (40, 50 and 60% MeOH in water). The R_M was found and was compared to R_M of three reference compounds for which log P was known.

Isosorbide-series	R_{M0}	*Log P*
Acetate (**11a**)	1.43	1.72
Propionate (**11b**)	1.91	1.93
Butyrate (**11c**)	2.56	2.24
Valeroate (**11d**)	2.92	2.40
Benzoate (**11e**)	3.36	2.60
ST0702	3.18	2.52

Figure 2-44: Lipophilicity parameters for isosorbide series obtained from RP-TLC. Compounds were spotted onto RP-TLC plates. 3 mobile phases were used (40, 50 and 60% MeOH in water). The R_M was found and was compared to R_M of three reference compounds for which log P was known.

Compared to the determination of their lipophilicity using the HPLC method, the overall rank retention order obtained in this method showed very close similarity. As expected, the lipophilicity parameters are increased with more rigid molecular structure and longer straight carbon chain. However, using the RP-TLC method the *Log P* values for the valeroate esters in both series are lower than the benzoate and aspirinate esters, which contradicts the results from HPLC study. This is presumably because of small accuracy problems encountered with the TLC method, notably a slightly uneven solvent front and large spot diameter that could have influenced the R_f values and consequently their retention parameters. As discussed, both retention parameters (R_M) and capacity factor (k') can reflect the lipophilic character of the analytes. A plot of capacity factor obtained from HPLC and retention parameters obtained from TLC was completed. Theoretically, these two parameters should be in linear relationship since the lipophilic property of any compounds should be constant. However, R^2 values of 89% and

72% were obtained within the two correlations. The differences in the log P values determined using each method can be attributed to factors involved in different system conditions such as the mobile phase composition and temperature. The HPLC was set to run at 50°C using a mobile phase of 60:40 v/v water and acetonitrile, whereas the TLC was performed at room temperature using different concentrations of methanol in water. In RP-HPLC, a change in mobile phase and column temperature can change the selectivity of the separation, which in turn has an influence on the retention time of certain analytes. Therefore, the capacity factor may be affected. Nevertheless, both studies were able to successfully evaluate the lipophilicity of isomannide and isosorbide series and more importantly, similar *Log P* values were established.

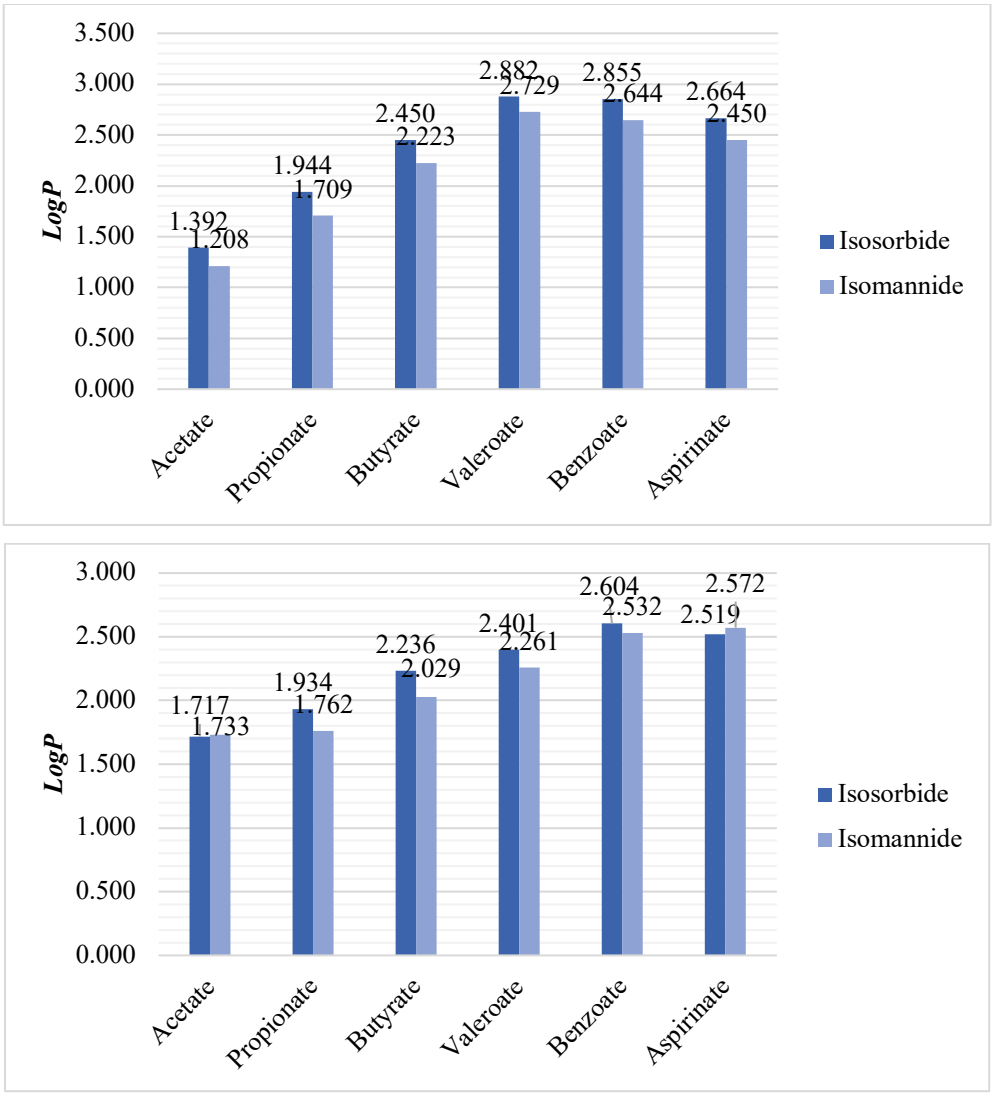

Figure 2-45: Plot of log P for isosorbide and isomannide esters.

Top: Comparison of Log P from HPLC between isosorbide and isomannide series. Bottom: Comparison of Log P from RP-TLC between isosorbide and isomannide series.

It was observed that compounds with the same ester functional group in the isosorbide series are generally more lipophilic than those in isomannide series. Compounds in the isomannide and isosorbide series with the same functional group are diastereomers, so it is no surprise that they appear to have different physicochemical properties. The difference in their physicochemical properties can be attributed to the different orientations in space of the ester functional groups at C-2. The ester function at position-2 is in the exo orientation in the isosorbide series and in the endo orientation in the isomannide series. This different orientation leads to an increased surface area in the isosorbide compounds. This increase hydrophobic surface area in turn decreases their polarity and increases their lipophilicity.

2.2.11.3 *Determination of Water Solubility of ST0702 and Analogues*

Aqueous solubility is one of the key physicochemical properties in drug discovery. In this study, aqueous solubility was measured using a HPLC method. The method used is similar to that of a UV absorption method as the UV detector on the HPLC is used. Samples of both the isosorbide and the isomannide compounds were added to a small amount of water until they reached supersaturation state and were then incubated for 24 h at room temperature. The saturated solutions were centrifuged, and the supernatants were analysed by HPLC. The concentrations of the dissolved compounds in the saturated solution were calculated with reference to a standard. The collected data is presented in Figure 2.46.

Isosorbide		Isomannide	
Compound	mg/mL	**Compound**	mg/mL
Acetate (**11a**)	16.28 ± 1.45	Acetate (**19a**)	48.75 ± 2.27
Propionate (**11b**)	21.04 ± 0.36	Propionate (**13b**)	46.64 ± 3.30
Butyrate (**11c**)	7.81 ± 0.07	Butyrate (**13c**)	11.93 ± 0.51
Valeroate (**11d**)	2.39 ± 0.01	Valeroate (**13d**)	10.95 ± 0.01
Benzoate (**11e**)	0.05 ± 0.01	Benzoate (**13e**)	0.22 ± 0.01
ST0702	0.05 ± 0.01	Aspirinate (**13f**)	1.22 ± 0.09

Figure 2-46: Aqueous solubility results for isosorbide and isomannide compounds. Compounds were added to water until supersaturation was reached, they were then incubated for 24 h at room temperature. The saturated solutions were centrifuged and the supernatants were analysed by HPLC. Data are presented as mean ± SD.

The above results in Figure 2.46 indicate that the isosorbide compounds are less water soluble than their corresponding isomannide compounds. For example, the isosorbide acetate compound has a water solubility of 16.3 mg/mL, whereas the isomannide acetate compound

has a solubility of 48.7 mg/mL. These results are in agreement with those obtained during the lipophilicity study where it was observed that the isosorbide compounds were, in general more lipophilic and had a higher *log P* value than their corresponding isomannide counterpart.

2.2.12 **Biological Testing of New Compound Library**

2.2.12.1 *HuT78 Proliferation*

The first biological assay carried out on the new library of compounds was a determination of the antiproliferative activity of the compounds on the HuT78 cell line. This assay was chosen as ST0702 had demonstrated good antiproliferative activity in this model and it seemed likely to be linked to the effect of ST0702 in the IMQ mouse model, as psoriasis is a T cell driven disease.

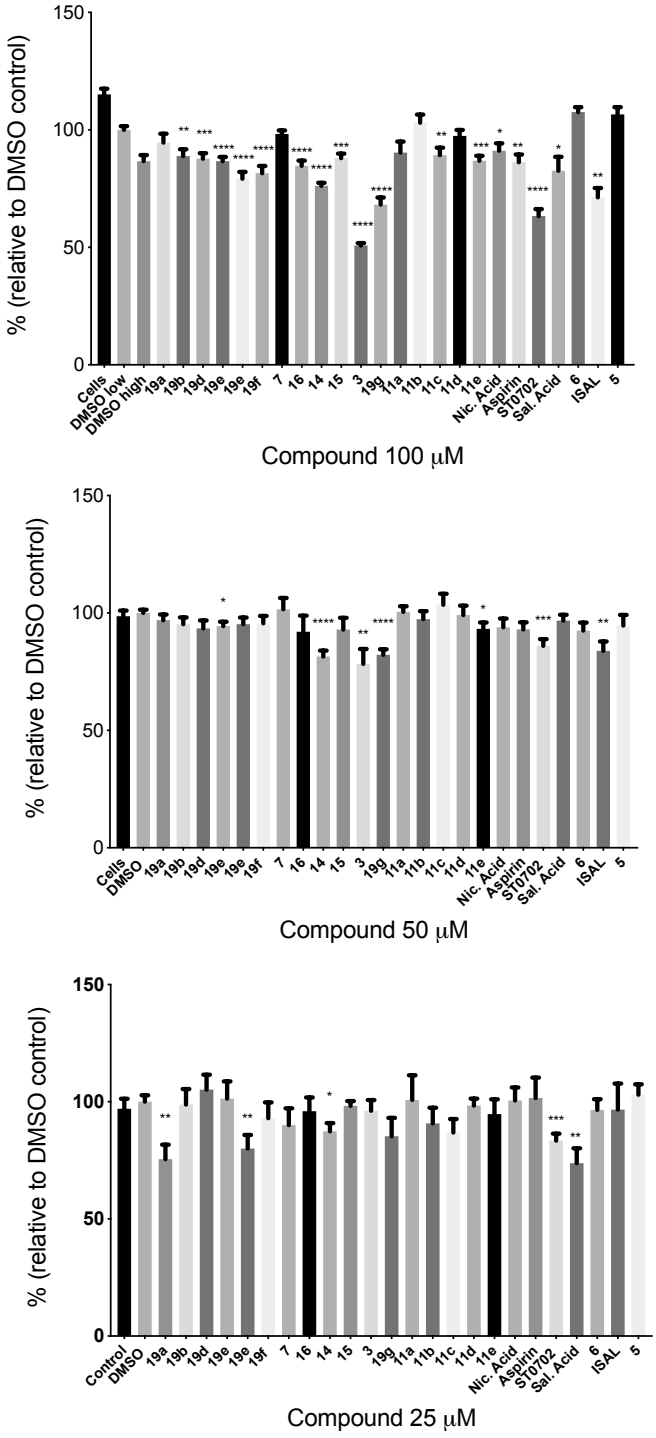

Figure 2-47: HuT78 proliferation results for isosorbide and isomannide esters.
HuT78 cells were plated at 1 × 10^4 cells per well of a 96-well plate. The cells were treated with 100 μM, 50 μM or 25 μM compound and incubated for 48 h. After this time, MTT was carried out. Results for each concentration are expressed as mean ± SEM of three experiments performed in triplicate.

Interestingly, the most effective compounds at inhibiting HuT78 proliferation were **3**, ST0702, and ISAL (Figure 2.47). These compounds had been tested in the HuT78 model previously (Figure 2.24). None of the new compounds demonstrated greater activity than these compounds, with **3** showing 50% inhibition, ST0702 almost 40% and ISAL producing inhibition of 30%. Of the newly synthesised compounds, the compounds containing the acetate, propionate, butyrate and valeroate esters had virtually no effect in the assay. Isomannide-2-aspirinate-5-nicotinate (**19f**), which differs from ST0702 only in the stereochemistry of the hydroxyl group at the 2-position of the isosorbide ring, had about 20% activity, significantly less than that of ST0702. Isomannide-2-methoxybenzoate-5-nicotinate (**19g**) caused a reduction of approximately 30% when tested at 100 μM. Isosorbide-2-benzoate-5-nicotinate (**11e**), isomannide-2-benzoate-5-nicotinate (**19e**) and isosorbide-2-nicotinate-5-benzoate (**14**) all had an inhibitory effect of approximately 20%. These compounds are all quite similar structurally, differing only in the stereochemistry. The necessity for active compounds to have a salicylate ester in order to have an effect in the model of HuT78 proliferation seems to be suggested by these results. However, it should be noted that isomannide-2-methoxybenzoate-5-nicotinate (**19g**) is also quite active, causing a reduction of approximately 30% when tested at 100 μM, so a substituted aryl group at position 2 may be sufficient for activity.

2.2.12.2 *HaCaT Proliferation Studies*

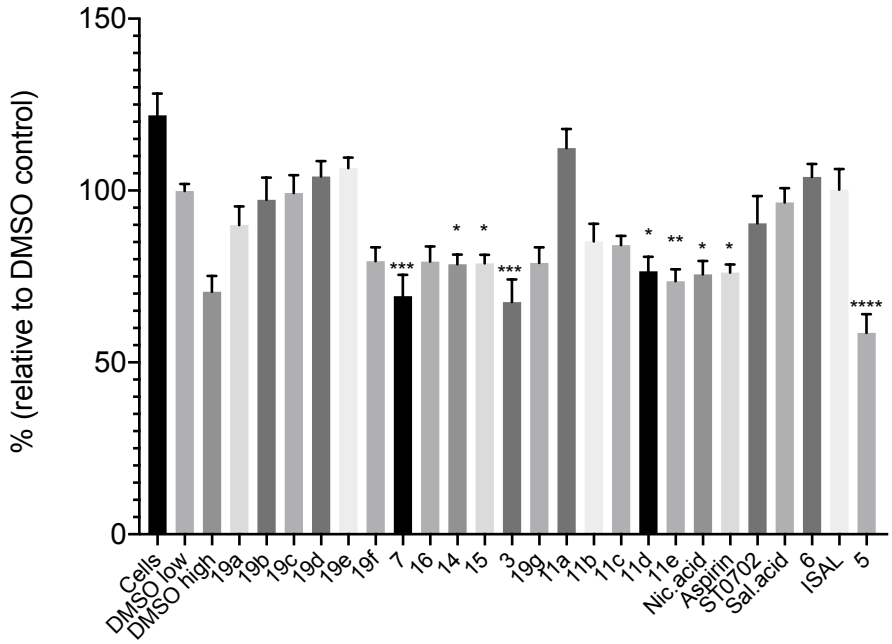

Figure 2-48: Results from HaCaT proliferation studies.
Cells were plated at 1 × 10^4 cells per well of a 96-well plate and left to adhere for 24 h. The compounds (100 μM) were then added and the plate was incubated for 48 h. Following this MTT was carried out. Two separate DMSO controls (low and high) were set up to match the quantity of DMSO being added to some of the wells. Results are expressed as mean ± SEM of three experiments performed in triplicate.

The activity of the compounds at inhibiting the proliferation of a keratinocyte cell line were also tested (Figure 2.48). It had been shown previously (Figure 2.20) that ST0702 and ISAL did not inhibit the proliferation of the HaCaT cells. In this assay there were other compounds that had not previously demonstrated efficacy in other models, such as aspirin and nicotinic acid which did show some effect here (approx. 25% reduction). Compounds **14** and **3** and, which had shown efficacy in the HuT78 proliferation models were also active in this assay.

2.2.13 **Testing new compounds in the Aldara™ Model**

Based on the findings with the new compounds, and to gain further insight into the SAR of the compounds and assess the appropriateness of the biological assays being used to screen the compounds, another mouse study, again with the Aldara™ model, was carried out. On this occasion, the experimental conditions were slightly different, with IMQ being applied daily to the mouse right ear, rather than the shaved dorsal skin surface, as was the case in the earlier studies. Apart from the location of the application of the Aldara™ cream, and the compounds being tested, the same procedure was followed as was outlined in Section 2.2.1.

Two compounds were chosen to be tested, isosorbide-2-benzoate-5-nicotinate (**11e**) and isomannide-2-aspirinate-5-nicotinate (**19f**). Compound **11e** differs from ST0702 only in the 2-position, where it has a benzoate ester rather than an aspirinate ester. With both an aspirinate and a nicotinate ester, **19f** has a very similar substituent pattern to ST0702, but the stereochemistry of the sugar skeleton is different, with isomannide having two endo-hydroxyl groups at C-2 and C-5, whereas the isosorbide in ST0702 has one endo-hydroxyl at C-5 and one exo-hydroxyl at C-2.

As presented in Figure 2.49, compound **11e** had no significant effect in the model. There was no statistically significant reduction in the PASI score, nor were the individual components of the PASI scale, namely scaling, erythema and thickness, significantly reduced relative to vehicle. This suggests that the aspirinate group at position-5 might be necessary for activity, or that a salicylate is a requirement for activity in the model.

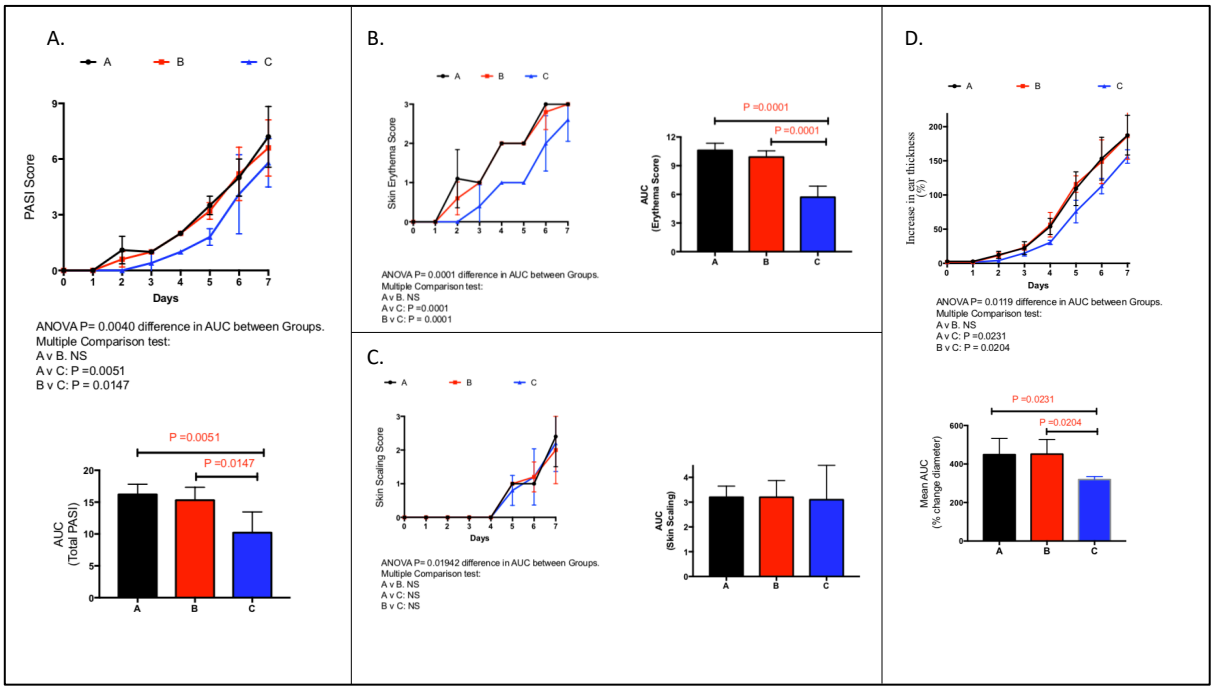

*Figure 2-49: Results from Aldara study of vehicle (A), **11e** (B) and **19f** (C).*
***A:** PASI Score of Mice exposed to vehicle (white petroleum jelly), or 3% B or C. **B**: Skin Erythema score of Aldara-treated mice exposed to Vehicle, 3% B or 3% C. **C.** Skin scaling scores of Aldara-treated mice exposed to Vehicle 3% B or 3% C. **D.** Increase in ear thickness scores of Aldara-treated mice exposed to Vehicle 3% B or 3% C. Data are mean ± SEM from 5 mice per group. *<P0.05, **P<0.01, ***P<0.001. ANOVA and Dunnett's multiple comparisons test were used to test for statistical differences between groups.*

Compound **19f** had a greater effect in the model. The PASI score is significantly reduced compared to the vehicle, and there is a decrease observed in erythema and thickness. There is

no significant reduction in scaling. The results suggest that this compound is somewhat effective in the model.

To gain further insight into the potential reasons for the differences in activity observed between ST0702 and isomannide-2-aspirinate-5-nicotinate (**19f**) some molecular modelling was carried out. It was found that the two compounds occupy a very similar space, with a similarity score of 0.851. The main difference observed was the orientation of the aspirinate esters, which suggests that this ester at position 2 could be important for activity. The isosorbide core did appear to be more folded over than the isomannide core, and occupied a different regional space. The nicotinate ester was slightly offset but the pyridine ring aligns the same way in both compounds. The tail of the aspirinate group also occupies the same regional space in both compounds. In one sense the results were reassuring because they showed that the effects of the two compounds could have a common biochemical explanation since they have similar spatial arrangement and potential for protein target binding.

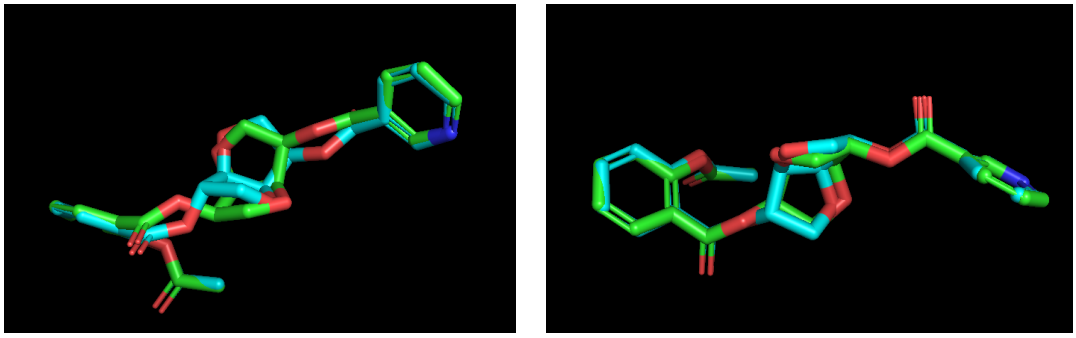

Figure 2-50: Overlay of 3D structure of ST0702 and 19f (isomannide-2-aspirinate-5-nicotinate).

2.3 Conclusion

ST0702 has proven to be effective in the IMQ mouse model of psoriasis-like inflammation, with significant and dose dependent reductions in the development of all three parameters of skin inflammation, skin thickness, erythema and scaling. The objectives of the work carried out in this chapter were to investigate its hydrolytic metabolism pathways, to perform preliminary investigations into its biochemical effects in relevant models and to survey the chemical space related to ST0702 in relation to the biochemical or pharmacological effects. This was to try and understand better the mechanism of action of ST0702 and the potential for more potent or efficacious compounds.

Previous studies by others in the Gilmer group had shown that ST0702 was capable of rapidly releasing aspirin, salicylic acid and nicotinic acid in vivo (149). The effect of ST0702 in the IMQ mouse model could be attributed to one or more of the hydrolysis products, or it could be the intact compound that was having the effect. Since the subsequent cell-based studies suggested that the intact compound is responsible for its effect, rather than the metabolites, the activity in the murine model of inflammation becomes more impressive considering the short half-life of the intact compound. Conversely, the compound was more stable in the presence of human microsomes suggesting that it might be more active in human skin inflammation than suggested by the mouse model. The main metabolites produced differed in the human and mouse model, with the isosorbide-2-salicylate (**6**) persisting for longer in the mouse model. The production of salicylic acid is favoured in the human skin microsome. Isosorbide-2-salicylate (**6**) was tested for biological activity in the HuT78 proliferation assay and found to be inactive.

Initial biological testing of ST0702 has shown that it doesn't appear to be having a large effect on several relevant aspects of the innate immune system, with no inhibitory effect on the NF-κB pathway, no reduction in IL-8 secretion by the HaCaT cell line and no reduction in the secretion of the pro-inflammatory cytokines IL-23 and GM-CSF. ST0702 treatment did cause an increase in the secretion of the anti-inflammatory cytokine IL-10, which is the only evidence discovered of an anti-inflammatory effect on the innate immune system.

ST0702 exerted an effect on the proliferation of a T cell line, and on the proliferation of T cell blasts produced from donor PBMCs. This inhibition of proliferation was not associated with apoptosis under similar experimental conditions, indicating that the compounds exert a cytostatic effect on the cells. If this were the case, then a 50% reduction could represent a complete inhibition of proliferation. The population doubling time of HuT78 is described in the literature as varying between 26 (190) and 65 h (ATCC), which means that with a treatment time of 48 h, the cells would only be expected to undergo one population doubling. Similarly, in the T cell blast experiments, the cells are only treated with the compound for the last 24 h, so several population doublings within that timeframe would be unlikely.

A larger panel of compounds were synthesised and tested to explore the SAR, but none were identified that were more active than ST0702. The metabolites of ST0702, such as aspirin, nicotinic acid and salicylic acid were not found to have effect in the biological pathways examined here, however ISAL did have very similar effects to ST0702, which suggests that a compound containing the salicylate ester is a requirement for efficacy and that the effects of ST0702 itself are probably due to the salicylate ester given its preponderance in assay media according to the hydrolysis studies.

It is evident from the physicochemical testing carried out that the majority of these compounds should prove suitable for use as topical agents. They all have a molecular weight of less than 500 Da. The apparently ideal lipophilicity range of logP 2–3 was observed for the butyrate, valeroate, benzoate and aspirinate esters of the isosorbide and isomannide compounds, as the acetate and propionate esters have logP values under 2. The water solubility was inversely related to the lipophilicity, as expected. Based on its physicochemical properties, ST0702 is a suitable candidate for topical administration. The compounds broadly fall into the physicochemical range considered ideal for topical administration in dermatology. Their physical properties may be useful in guiding and interpreting future SAR studies.

The second IMQ mouse model experiment gave further insight into the SAR, again demonstrating the apparent importance of the salicylate ester and the compound having isosorbide stereochemistry. Unfortunately, as the experiment with ST0702 was carried out under different conditions to this study, direct comparisons examining the magnitude of effect of these compounds is not possible. However, based on a crude estimation, it would appear that ST0702 is the more effective compound, with a greater reduction in PASI score observed.

Concluding this chapter, several insights have been gained into the mechanism of action of ST0702. There have been insights gained into the SAR of the compounds, with the development of a promising biological assay that appears to relate to the effects in the Aldara™ model and which could be used to guide the design of new compounds possessing the characteristic properties of ST0702 and which are potentially effective in psoriasis. The next chapter describes studies designed to understand the cytostatic effect of ST0702 which appears to be a property of the intact compound and potentially its primary hydrolysis product in tissue, its salicylate ester, ISAL.

Chapter 3: Mechanism of Action of ST0702

3.1 Introduction

The aim of this chapter is to elucidate the mechanism of action of ST0702, a substance that has shown activity in the IMQ mouse model of psoriasis. In the previous chapter it was shown that ST0702 acts as an inhibitor of T cell proliferation and this effect appears to correlate with and explain its activity in the IMQ model. However, the mechanism by which ST0702 is inhibiting T cell proliferation is unknown and therefore this chapter describes experiments seeking to elucidate the biochemical pathways involved in the actions of ST0702 and related compounds. This was in part due to curiosity in relation to ST0702, but also due to the instinct that the pathway, if identified, might be novel and interesting in itself and a potential target for compounds that could be produced from ST0702 or for other compound families entirely. The investigations described in this chapter culminated in the identification of a novel target for inflammatory disorders of T cells, including psoriasis.

3.1.1 Immunology of Psoriasis

Until the late 1970s, psoriasis was thought to be a disease primarily of dysfunctional epidermal keratinocytes. The first clinical evidence to suggest a potential role of T cells in psoriasis was the successful treatment of psoriasis patients with cyclosporin A, an immunosuppressive agent that inhibits both the proliferation and cytokine release of T cells (191). Even though psoriasis is considered a T cell mediated inflammatory pathology, cells that belong to both adaptive and innate immunity as well as non-immune cells are all involved in the pathogenesis of the disease. Dendritic cells, NK cells and macrophages play an important role, as do the non-immune keratinocytes and endothelial cells (172).

Psoriasis pathogenesis is often considered in two phases, the initiation phase and the maintenance phase. In the initiation phase, initial triggers such as physical trauma start a cascade of events that leads to the development of psoriatic lesions. Stressed keratinocytes release self-DNA that forms complexes with the cathelicidin antimicrobial peptide LL37. LL37 is typically not expressed in healthy skin under steady state conditions, but is produced by keratinocytes or released by infiltrating neutrophils in response to skin wounding or infections (11). Epidermal trauma, which induces LL37 expression in the skin, is also a typical trigger of psoriasis development known as the Koebner phenomenon. High levels of LL37 appear to persist in the skin of psoriatic lesions (192). The LL37/DNA complexes trigger the activation of plasmacytoid DCs to produce IFN-α (11). The IFNs produced by pDCs lead to an

uncontrolled maturation of myeloid dendritic cells (mDCs), which are key stimulators of autoreactive T cells in autoimmunity (11). Keratinocyte derived IL-1β, IL-6, TNF-α, and DC derived IFN-α activate dermal DCs.

During the maintenance phase, activated DCs can migrate to lymph nodes to present antigen (either of self or microbial origin) to naïve T cells and promote their differentiation into Th1 or Th17 cells. Th1 and Th17 cells then migrate into psoriatic dermis, attracted by keratinocyte derived chemokines. Th17 cells secrete IL-17A, IL-17F and IL-22 which stimulate keratinocyte proliferation, whilst inflammatory DCs (iDCs) produce IL-23, NO and TNF (95).

Evidence of a pivotal role of T cells in the pathogenesis of psoriasis has come from both experimental and clinical data. The inflammatory infiltrate in psoriasis is dominated by an influx of CD4+ and CD8+ T cells and infiltration of these cells is one of the earliest events in the evolution of psoriatic plaques (193).

In terms of cytokine involvement, the Th1 cytokines IL-2, IFN-γ and TNF-α are predominant in the psoriatic lesions. IL-2, IFN-γ and TNF-α are produced by CD8+ and CD4+ T cells, and these cytokines then stimulate the recruitment of more inflammatory cells and the epidermal changes that are characteristic of psoriasis (193). Immune cells including dendritic cells in the skin, as well as keratinocytes also produce large amounts of cytokines. IFN-γ and TNF-α can induce keratinocytes to produce the cytokines IL-6, IL-7, IL-8, IL-12, IL-15, and IL-18, among others (62).

Neutrophils have also been suggested as potential role-players in psoriasis (67). Neutrophils are the most abundant leukocyte in humans and are involved in driving the innate immune responses against pathogen. Neutrophils are a minor inflammatory population in chronic plaque psoriasis, however the presence and infiltration of neutrophils into the epidermis is one of the main histologic features of psoriasis. Neutrophils are found in low numbers in the epidermis and SC in chronic plaque lesions but are the predominant leukocyte population in pustular psoriasis skin lesions. Neutrophil chemo-attractants are highly expressed in plaque psoriasis and about 5–10 times higher in pustular psoriasis. One of the key inflammatory cytokines driving neutrophil inflammation in psoriasis is IL-36. IL-36 belongs to the IL-1 family of cytokines and is highly expressed in plaque psoriasis. The effect of IL-36 is mainly on keratinocytes and not T cells as they lack an IL-36 receptor (67).

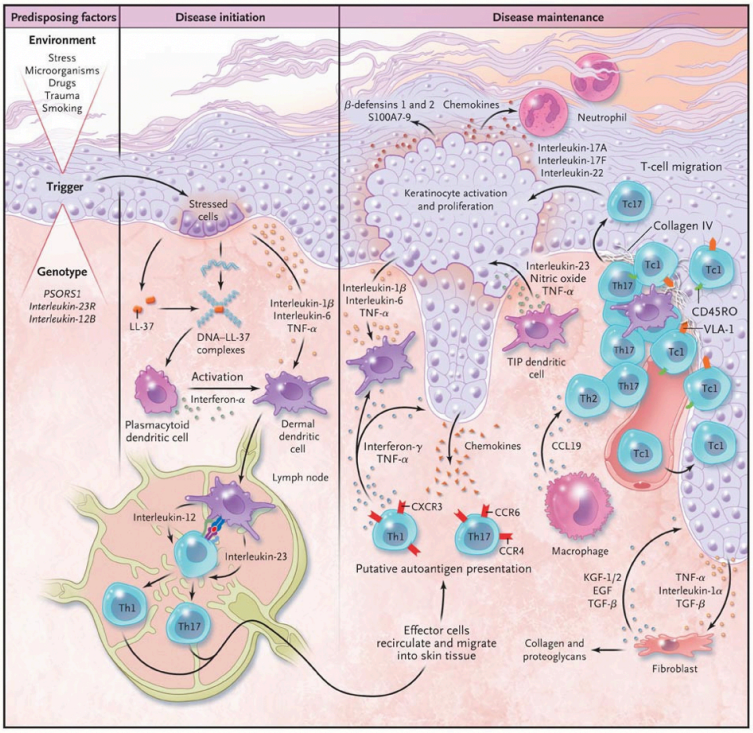

Figure 3-1: Evolution of a psoriatic lesion from initiation to maintenance of disease (95).

3.1.2 **IL-2 and T cells**

IL-2 was first described as a T cell growth factor (TCGF) and was identified as a potent mitogen and growth regulator of T cells in vitro (194). IL-2 is a cytokine that exerts its effects on many cell types, the most prominent of which is the T lymphocyte.

The high affinity IL-2 receptor (IL-2R) is composed of three polypeptides: IL-2Rα (CD25), IL-2Rβ (CD22) and the γ–subunit (γ_c, CD132) and co-expression of all three are needed for high affinity IL-2 binding (194). IL-2 is critical for the development of $CD4^+FoxP3^+$ Tregs and it has been shown that the severe immune autoreactivity of IL-2 knockout mice were due to a loss of Tregs.

IL-2 influences effector T cell differentiation and is critical for determining the fates of antigen receptor activated cells, that is, whether they will differentiate into Th1, Th2, Th17 or Tfh cells. $CD4^+$ αβ T cells differentiate following immune activation to produce distinct effector subpopulations that can be distinguished based on cytokine production, expression of lineage-specific master regulators and cytokine requirements.

Th1 cells produce IFN-γ and depend on signals from IL-12 and activation of the transcription factors STAT4 and T-bet. Th1 cells are therefore dependent on expression of the IL-12R. Th2 cells produce IL-4, IL-5 and IL-13 and depend on IL-4 signals and transcriptional activities of

STAT6 and GATA3. Th2 cells are therefore dependent on the expression of the IL-4 receptor. Th17 cells, which control neutrophil function and epithelial barrier integrity produce IL-17A, IL-17F and IL-22 and depend on signals from IL-6 in combination with TGF- β, IL-23 and IL-21. These signals result in the activation of STAT3 and expression of the transcription factor RORγt to promote Th17 differentiation. Expression of the IL-6 receptor is therefore very important for Th17 differentiation. Tfh cells support B cell mediated immune responses and germinal centre formation in spleen. Tfh cells require IL-21 and IL-6 for development, and BCL6 acts as the master regulator (194). IL-2 can control the fate of CD4+ cells by controlling the expression of key cytokine receptors, transcription factors, chromatin regulators and effector cytokines.

IL-2 is also an important cytokine for CD8+ effector cells. In response to infection, naïve antigen-specific CD8+ T cells differentiate into effector cytotoxic T cells that make proinflammatory cytokines such as IFN-γ and acquire the ability to kill infected cells. IL-2 can influence the effector activities of these CD8+ cells by inducing the expression of IFN-γ, TNF-α and lymphotoxin-α, and by stimulating the expression of the cytolytic molecules perforin and granzyme B (194).

Following T cell activation the cells rapidly start producing IL-2. A major function of IL-2 is to promote proliferation of CD4+ and CD8+ T cells (195). Both CD4+ and CD8+ T cells play a role in psoriasis, with evidence that there is a predominance of CD8+ T cells in the epidermis of the psoriatic lesion, whereas CD4+ T cells are more common in the upper dermis (62).

Upon IL-2R stimulation, a variety of downstream events occur. The IL-2Rβ chain binds JAK1 and the γ–subunit binds to JAK3, and occupancy of the IL-2 receptor results in activation of JAK1/3. IL-2 can induce the tyrosine phosphorylation and DNA binding of proteins of the STAT family, the most important being STAT5A Y694 and STAT5B Y699. IL-2 induced serine phosphorylation of STAT5A S127 and S128 can also occur. STAT3 can be phosphorylated at Y705 or S727 and STAT1 phosphorylation on Y701 can also be induced.

The activation of JAK1/3 can induce tyrosine phosphorylations on the IL-2Rβ chain, which allows the recruitment of STAT5A and STAT5B transcription factors and their subsequent tyrosine phosphorylation. After this phosphorylation, the STAT5 proteins dissociate from IL-2Rβ and form dimers, which induces their transcriptional activation and translocation to the nucleus.

In addition to JAK/STAT signalling, the adaptor SHC becomes tyrosine phosphorylated in response to IL-2 receptor activation. SHC then forms a complex with the SH2 domain of the adaptor GRB2, which binds to the Ras guanine nucleotide exchange protein SOS. This complex

catalyses the exchange of GDP for GTP on Ras, allowing an accumulation of Ras in its GTP-bound state leading to the activation of the Ras-Raf-MEK-ERK cascade (194).

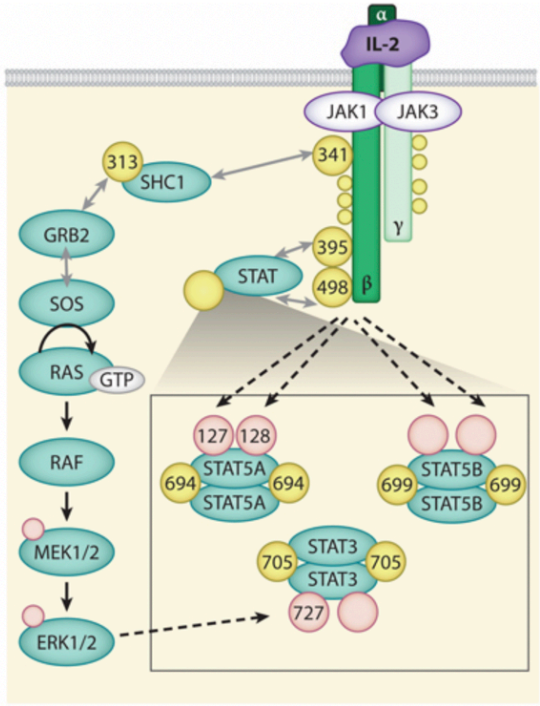

Figure 3-2: IL-2 signalling pathway illustrating JAK-STAT signal transduction and the MAP kinase cascade (194).

3.1.3 **STAT3 and Psoriasis**

STAT3 is a member of the STAT family of proteins. In non-stimulated cells, STAT3, like other STAT proteins, is kept in an inactive cytoplasmic form (4). Typically, STAT3 becomes activated after phosphorylation of tyrosine 705 in response to such ligands as EGF, IL-5, IL-6 or IL-2. Multiple tyrosine kinases have been described as intracellular activators of STAT3 activity (such as EGFR, Src and ERK), however the phosphorylation of STAT3 on tyrosine 705 is mainly regulated by JAK1.

Additionally, activation of STAT3 may occur via phosphorylation of serine 727 by MAP kinases and through c-Src non-receptor tyrosine kinase. The third mechanism of STAT3 activation is through the reverse acetylation of STAT3 by histone acetyltransferase on a single lysine residue (Lys 685).

STAT3 activation is regulated by negative regulators such as PIAS (protein inhibitor of activated STAT) and SOCS (suppressors of cytokine signalling) proteins in addition to protein tyrosine phosphatases.

STAT3 is abundantly overexpressed in psoriasis (196). Transgenic mice that overexpress STAT3 in keratinocytes exhibit a psoriasis-like phenotype. STAT3 hyperactivation has been reported in almost every cell type involved in psoriasis initiation and maintenance. This is consistent with the prominent role that is played by STAT3 in the biology of Th17 lymphocytes, and of the Th17 cytokines IL-6, IL-23 and IL-22.

3.1.4 **IL-23/IL-17 Axis and Psoriasis**

In recent years there has been increasing interest in the role of the IL-23/Th17 (T helper 17 cell) axis in psoriasis patients, arising out of elevated levels of IL-23 and Th17-related cytokines being found in psoriasis lesions and serum from psoriasis patients (197). IL-17 mRNA protein levels are shown to be increased in the blood or skin biopsies from human psoriatic lesions (198). The IL-17 family includes at least six homo-dimeric cytokines, IL-17A through IL-17F, while 5 members of the IL-17 receptor (IL-17R) family have been identified (198). IL-17A and IL-17F are most relevant to psoriatic disease. IL-17 is primarily produced by Th17 cells, but innate immune cells, including γδT cells, neutrophils and mast cells have been found to be involved in IL-17 secretion in psoriasis. IL-17 has been shown to be a direct potentiator in enhancing keratinocyte proliferation and inhibiting keratinocyte differentiation via the downstream mediator REG3A, a protein with antimicrobial functions involved in wound repair. Data has shown that IL-17 stimulates the production of chemokines and antimicrobial peptides by keratinocytes. Keratinocytes then promote Th17 cell recruitment and produce more IL-17, resulting in a positive feedback loop.

The increase in IL-17 and IL-17 secreting cells is related to the altered balance between IL-23 and Th17 cells. IL-23 is critical in the survival and proliferation of Th17 cells and contributes to keratinocyte proliferation. Dendritic cells and macrophages are the main sources of IL-23, the levels of which are increased in psoriatic skin. IL-23 activates a number of STAT molecules, including STAT1, STAT3, STAT4 and STAT5. STAT3 is the main player in the IL-23 signalling pathway (197). Notably, IL-17 does not rely on JAK/STAT signalling, but the blockade of upstream IL-23 using JAK inhibitors indirectly results in decreased IL-17 (199).

IL-22 is also involved in this pathway. Elevated levels of IL-22 are found in the blood of psoriatic patients, the levels of which correlated with disease severity (200). IL-22 is preferentially produced by IL-23 driven Th17 cells (201) and induces IL-23 mediated keratinocyte hyperproliferation *in vivo* and *in vitro*, through STAT3 signalling. The combination of IL-22 and IL-17 inhibits the differentiation of keratinocytes and increases their proliferation and mobility, which leads to parakeratosis, acanthosis and elongation of the epidermal rete ridges (papillomatosis) which are the hallmarks of skin psoriatic plaques.

Reports of a unique subpopulation of memory T cells that make IL-22 alone have led to the classification of Th22 cells (202). Th22 cells produce IL-22 without IL-17 or IFN-γ and are characterised by the expression of certain chemokine receptors, including CCR4 and CCR6, which can influence homing to the skin. Like Th17 cells, Th22 cells are also influenced by IL-23, which is required for their maintenance and expansion (203).

The pharmacological agent, ustekinumab works by targeting this IL-23/IL-17 axis and has been studied for the treatment of psoriasis. It is an IL-12/23 p40 antibody. IL-12 and IL-23 share a common p40 subunit, and both cytokines are produced by inflammatory myeloid cells and influence the development of Th1 and Th17 cell responses, respectively (204). IL-12 signals through JAK2 and TYK2 and leads to the phosphorylation of predominantly STAT4, but also STAT1, STAT3 and STAT5 homodimers (205). IL-23 also activates JAK/STAT but it predominantly activates STAT3 (205). IL-12 induces the production of IFN-γ, which is required for the development of the Th1 immune response, whilst IL-23 induces IL-17A, IL-17F and/or IL-22 and stabilises Th17 cells. IL-12 promotes the differentiation of naïve T CD4 T cells into IFN-γ producing Th1 cells, but IL-23 does not directly promote Th cell differentiation, due to the absence of an IL-23R on naïve T cells. In mice (and it is likely similar in humans), exposure to cytokines such as TGF-β, IL-1 and IL-6 induces expression of RORγt, a transcription factor that promotes the expression of the IL-23R and IL-17a (206). This will then determine the transformation of CD4+ naïve cells to Th17, which will produce IL-17, IL-22 and TNF−α (172). The therapeutic rationale for the use of IL-12/23p40 antibody in psoriasis stems from the fact that cytokines produced by IL-12 (such as IFN-γ) and IL-23 (such as IL-17A, IL-17F and IL-22) are elevated in lesional plaques (204), and preclinical models have shown that IL-23 exposure in mouse skin leads to hyperproliferation and abnormal differentiation of keratinocytes (161).

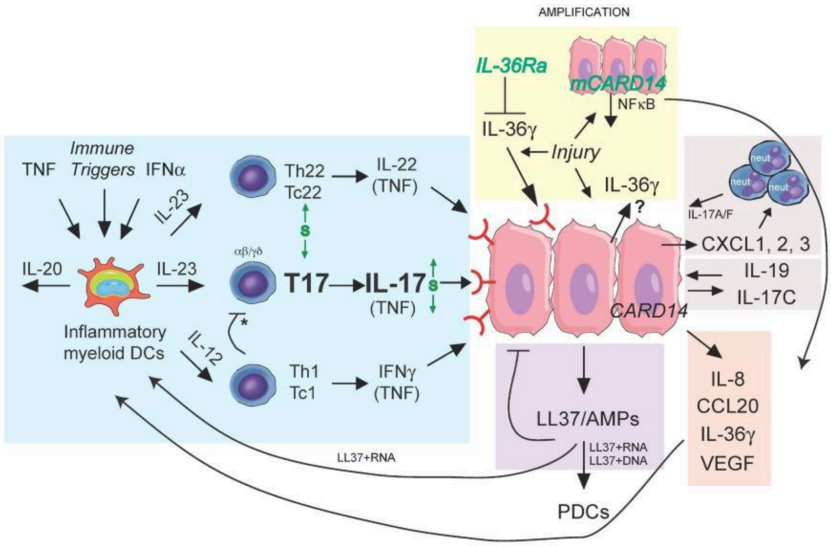

Figure 3-3: Essential cells and molecules in the pathogenesis of psoriasis lesions, with particular emphasis on the IL-23/IL-17 axis (207).

Inflammatory and resident myeloid dendritic cells become activated to produce IL-23. This drives production of IL-17 ligands (IL-17A, IL-17F) from αβ and γδ T cells (T17), and IL-22 by subsets of CD4+ (Th22) and CD8+ (Tc22) cells, while IL-12 drives production of IFNγ. Some of these cytokines will recruit cells into the skin, such as IL-8, CXCL1, 2 & 3 which are all neutrophil chemotaxins. There is synergy (green S) between IL-17 and TNFα, as well as between IL-17 and IL-22. There are abundant IL-36 cytokines in psoriasis, which are also involved in neutrophil chemotaxis, and IL-36Ra is the natural antagonist for this effect (207).

3.1.5 **Overview of HuT78 Cells**

HuT78 cells are an established T cell lymphoma cell line developed from the peripheral blood of a patient with SS involving 'skin, blood, lymph nodes and liver'. A clone of HuT78, H9 has been used to isolate and propagate HIV-1 from the blood of AIDS patients. They are a constitutively activated T cell line.

Studies have demonstrated that HuT78 cells do not express the high affinity (αβγ) IL-2R (208), however, some expression of the IL-2 receptor β subunit and γ subunit has been detected (209). They do not express the IL-2 receptor at baseline or after exposure to mitogens such as PHA (208). Several Src-related tyrosine kinases have been shown to be overexpressed in HuT78 lines, including c-Src, Lck (lymphocyte-specific protein tyrosine kinase) and Fyn. HuT78 have been shown to have constitutively activated STAT3, and knockdown of STAT3 can induce apoptosis (210). When expression of STAT3 and phosphorylated STAT3 was measured in HuT78 and compared to levels in normal peripheral blood lymphocytes isolated from healthy

volunteers it was found that the expression of STAT3 was 2.6 times higher in the HuT78 cells and the levels of tyrosine phosphorylated STAT3 was 5.2 times higher (210).

3.1.6 Overview of T cell metabolism

It is known that throughout the life of an immune cell, energy and substrate requirements change dramatically, and this means that metabolic pathways can have profound effects on immunity (211). It has been observed that immune cells transform from a state of relative metabolic quiescence to a highly active metabolic state during the activation phase of the immune response.

The two main cooperative processes that supply ATP within cells are glycolysis and oxidative phosphorylation (OXPHOS). In the glycolysis pathway, glucose is broken down into pyruvate. Glycolysis generates ATP but also provides metabolic intermediates that can enter other metabolic pathways.

In mitochondria, the tricarboxylic acid (TCA) cycle incorporates substrates from various cytosolic and mitochondrial metabolic pathways to generate reducing equivalents, which donate electrons to the electron transport chain (ETC) and lead to the generation of ATP through OXPHOS. Substrates that are oxidised in the TCA cycle include pyruvate from glycolysis and metabolites derived from the oxidation of amino and fatty acids.

Fatty acid oxidation (FAO) involves the translocation of free fatty acids into the mitochondrial matrix, where they are cleaved, producing acetyl-CoA that enters the TCA cycle. FAO also generates NADH that can be reoxidised in the mitochondria by Complex I of the ETC, which together with the oxidation of $FADH_2$ leads to the generation of a proton gradient across the inner mitochondrial membrane that is essential for OXPHOS.

In the ETC electrons are moved through a series of electron transporters that undergo redox reactions, which causes hydrogen ions to accumulate within the matrix space. A concentration gradient forms in which hydrogen ions diffuse out of the matrix space by passing through ATP synthase. The current of protons powers the catalytic action of ATP synthase, which phosphorylates ADP, producing ATP.

A consequence of ETC dysfunction is impaired cell proliferation, and human cells in culture arrest upon pharmacological or genetic inhibition of Complex I or III. Changes in ATP or reactive oxygen species (ROS) levels have been suggested to underlie the anti-proliferative effects of ETC inhibition, but the exact reason why ETC function is a requirement for proliferation is not well understood (212).

The metabolism of T cells varies with effector function and developmental state. Naïve T cells metabolise glucose, amino acids and fats to drive the TCA cycle and OXPHOS, which highlights the importance of respiring mitochondria for T cell function. Naïve T cells are activated by ligation of the cell-surface T cell receptor (TCR), in combination with co-stimulation of other cell-surface receptors (e.g. CD3 and CD28) which leads to proliferation and differentiation. As a result of activation, T cells must alter their metabolic activity to meet the increased energy demands associated with cell growth, proliferation, differentiation and effector function. T cells transition from the primary use of OXPHOS to meet metabolic needs to the use of glycolysis. The increase in glycolytic flux appears to be regulated by the PI3K and the Akt pathway, as well as the transcription factor Myc and ERRα (213). Activated T cells take up large amounts of glucose and simultaneously produce lactate, leading to the theory that activated T cells are primarily glycolytic despite ample oxygen supply. This preference by rapidly proliferating cells for glycolysis over OXPHOS despite sufficient oxygen availability for OXPHOS is termed aerobic glycolysis or the Warburg effect as it was first described by Otto Warburg when characterising the metabolism of cancer cells (214). Despite the fact that glycolysis is a less efficient means of producing ATP compared to OXPHOS, it is thought that T cells prefer glycolysis because the production of ATP is expedited (100 times faster) and because it provides building blocks required for the biosynthesis of fatty acids, amino acids and nucleic acids.

However, glycolysis is insufficient to provide the full complement of factors needed for cell proliferation, with evidence that the mitochondrial substrate glutamine (which fuels the TCA cycle) is required for T cell proliferation (215). Activated T cells have been shown to upregulate both glycolysis and OXPHOS, with glycolysis as the dominant pathway (216). Pharmacological inhibition of mitochondrial OXPHOS or glycolysis in vitro has been shown to diminish T cell proliferation (217, 218). The different T cell subtypes have also been shown to have distinct metabolic phenotypes, for example Tregs show higher levels of OXPHOS and AMPK-dependent FAO, whereas Th17 cells rely mostly on glycolysis (219). Mitochondrial oxygen consumption has been shown to increase during T cell activation, and fuelling mitochondria was sufficient to support T cell activation. Mitochondrial ROS is critical for activation of nuclear factor of activated T cells (NFAT) and subsequent IL-2 production (211), in addition to being required for optimal T cell activation and expansion (218).

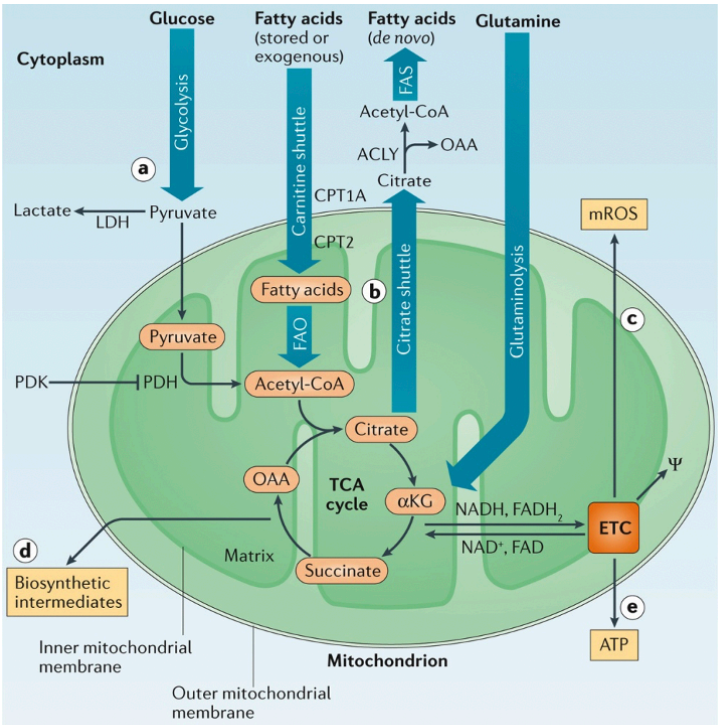

Figure 3-4: Overview of cellular respiration (220).

a) Glycolysis produces pyruvate from glucose, and the pyruvate can then be secreted as lactate, or can be oxidised to acetyl CoA by pyruvate dehydrogenase (PDH). Acetyl CoA can condense with oxaloacetate (OAA) and enter the TCA cycle as citrate. b) Citrate can alternatively be exported via the citrate shuttle, which leads to the regeneration of acetyl CoA and OAA. Fatty acids can then be generated from acetyl CoA by fatty acid synthase (FAS). c) mROS are produced by the ETC through the production of superoxides. d) TCA cycle intermediates can act as building blocks for the synthesis of macromolecules. e) The ETC uses the reducing equivalents formed from the TCA cycle to drive ATP production.

3.1.7 Reactive Oxygen Species (ROS) in psoriasis

ROS are chemically reactive species containing oxygen. They are formed from the partial reduction of oxygen and are free radicals with one unpaired electron in their outer orbit (219). Examples include hydrogen peroxide, the superoxide anion and hydroxyl radicals. Cellular ROS are generated endogenously as in the process of mitochondrial oxidative phosphorylation, or they may arise from interactions with exogenous sources such as xenobiotic compounds.

Endogenous sources of ROS in mammals include seven isoforms of NADPH oxidases (NOXs) that are differentially expressed in diverse cells and species, the mitochondrial respiratory chain, the flavoenzyme ERO1 in the endoplasmic reticulum, in addition to many other enzymes (221).

ROS production by the mitochondria is regulated by several factors, including reactive nitrogen species (RNS), mechanistic or mammalian target of rapamycin (mTOR), p53, SHC1, ROMO1, B cell lymphoma-2 (Bcl-2) family members and uncoupling proteins. Hypoxia also promotes mitochondrial ROS generation.

Important ROS regulating enzymes include superoxide dismutases, catalases and the enzymes of the glutathione redox cycle, which couples the reduction of peroxide to the oxidation and regeneration of reduced glutathione.

Two sites in the respiratory chain, complex I and complex III have been suggested as the major source of mROS. Rotenone, a complex I inhibitor, has been shown to increase levels of mROS (222). Rotenone inhibits the transfer of electrons from iron-sulfur centres in Complex I to ubiquinone. This interferes with NADH during the creation of ATP. Complex I is unable to pass off its electrons to CoQ, creating a back-up of electrons within the mitochondrial matrix. Cellular oxygen is reduced to the radical, creating ROS.

There are two modes of operation by isolated mitochondria that result in significant $O_2^{\bullet-}$ production, predominantly from Complex I. The first occurs when the mitochondria are not making ATP and consequently have a high Δp (protonmotive force) and a reduced CoQ (Coenzyme Q) pool. The second mode of operation is when there is a high $NADH/NAD^+$ ratio in the mitochondrial matrix (223).

In T cells, upon TCR cross-linking, mitochondrial ROS are generated within 15 min, and at low levels, ROS have been associated with increased cell proliferation and survival. However, upon accumulation, these ROS can influence gene expression and can lead to DNA damage, permeabilization of mitochondrial membranes and apoptosis (216). Oxidative stress is thought to play a role in the pathogenesis of psoriasis, particularly in the imbalanced differentiation of Th1 and Th2 cells that is a feature of psoriasis. T cell commitment to Th1 or Th2 cells has been shown to be dependent on the activation of redox-sensitive signalling cascades, where oxidative conditions support Th1 development (224, 225). Additionally, ROS can act as second messengers and can have an effect on several inflammatory pathways in psoriasis. Signalling pathways relevant to psoriasis that are known to be influenced by ROS levels include the MAPK, NF-κB and JAK-STAT pathways (224) .

3.2 Results and Discussion

3.2.1 Phospho-kinase array: Activated PBMCs

It had been previously observed that ST0702 and related compounds were having an effect on T cell proliferation. The mechanism by which this inhibition was happening was unidentified,

however, following on from the results of the T cell migration assay, and in particular, the reduction in cell number observed in ST0702 treated T cells, the IL-2 receptor was identified as a potential target for ST0702. It was decided to investigate its effect on phosphorylation profiles of a number of kinases and their protein substrates related to the signalling pathways involved in T cell proliferation. A multiplex antibody array was used that permitted the simultaneous detection of the relative site-specific phosphorylation of 43 kinases and 2 related proteins. Many kinases present downstream of the IL-2R were present in the array. The array was carried out in PBMCs stimulated with PHA to induce IL-2 responsiveness and then stimulated with IL-2. The ability of IL-2 to induce phosphorylation of particular proteins was observed, as was the effect of ST0702 on the relative levels of protein phosphorylation (Figure 3.5).

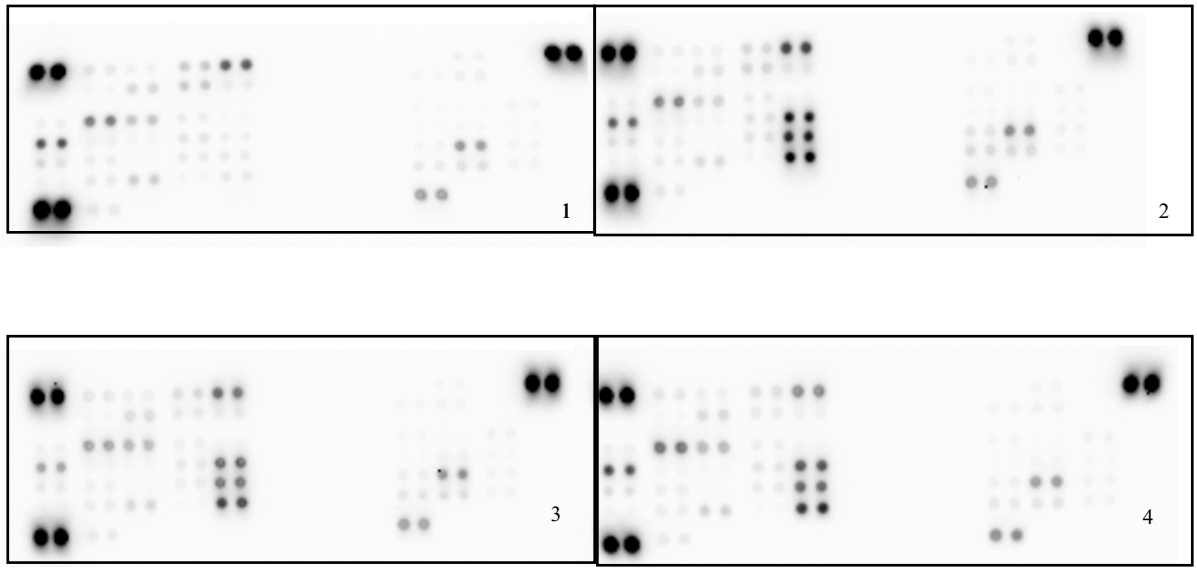

Figure 3-5: PBMC proteome profiler array results.
PBMCs were seeded at 1 × 10^6 cells/mL and activated with 10 µg/mL PHA over a 72 h period. They were then serum-starved (1% serum) for 4 h, for the last 30 min of this they were exposed to either 100 µM ST0702 or DMSO control. 20 ng/mL IL-2 was then added for 15 min. The cells were lysed and the manufacturer's protocol was then followed. Figure 1 corresponds to basal conditions (no IL-2 added). Figure 2 is the vehicle control (DMSO+ 20 ng/mL IL-2) whilst Figure 3 and 4 are replicates of ST0702 100 µM+ 20 ng/mL IL-2).

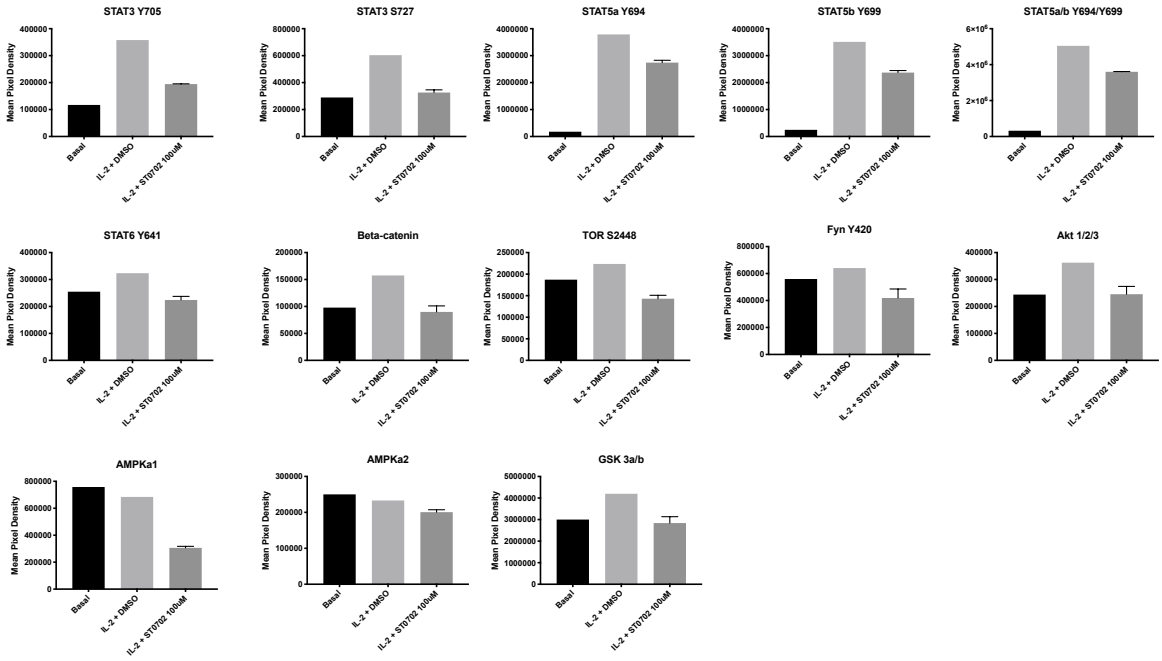

Figure 3-6: Key results from proteome profiler array.
Results are presented for STAT3, STAT6, STAT5a, STAT5b, GSK-3a/b, AMPKa1/2, Akt 1/2/3 and β-catenin.

The key results from the array are outlined in Figure 3.6. Treatment with 100 μM ST0702 was shown to cause a reduction in the phosphorylation levels of STAT3, STAT6 and STAT5a/b in comparison with IL-2 alone. In the case of STAT3 and STAT6, the levels of phosphorylation were reduced to almost basal levels. For STAT5a/b there was approximately a 30% reduction in levels of phosphorylation. As there were no JAKs included in the array it was not known whether or not the effect of ST0702 on the STATs was due to a downstream effect and the possibility that ST0702 was acting directly on the JAK receptors could not be excluded.

Levels of phosphorylated GSK-3a/b (Glycogen Synthase Kinase-3) were also reduced back to basal levels, as were levels of β-catenin. GSK-3 is a serine/threonine protein kinase that mediates the addition of phosphate molecules onto serine and threonine amino acid residues. Phosphorylation of a protein by GSK-3 usually inhibits the activity of its downstream target. GSK-3 is active in a number of central intracellular signalling pathways, including cell proliferation, migration, glucose regulation and apoptosis (226). Active (unphosphorylated) GSK-3α/β has been shown to phosphorylate β-catenin, targeting it for degradation. The degradation of β-catenin leads to an increase in T cell proliferation. Therefore, by reducing the amount of active GSK-3α/β, ST0702 could in theory be inhibiting proliferation.

Levels of phosphorylated AMP-activated protein kinase (AMPK) α1 and AMPKα2 were reduced following treatment with 100 μM ST0702. AMPK levels were not increased following

stimulation with IL-2. AMPK is a serine/threonine kinase that can sense low cellular ATP levels. Under conditions of low energy AMPK phosphorylates specific enzymes and growth control nodes to increase ATP generation and decrease ATP consumption. AMPK is activated following changes in the ATP: ADP or ATP: AMP ratio and is able to redirect metabolism towards increased catabolism and decreased anabolism through the phosphorylation of key proteins in multiple pathways, including mTOR complex 1, lipid homeostasis, glycolysis and mitochondrial homeostasis (227). AMPK has been shown to play a role in the metabolic reprogramming of naïve T cells to support the increased demands of effector T cell function (228, 229). The predominant metabolic phenotype of activated CD4+ and CD8+ effector T cells in vitro is a shift to aerobic glycolysis, also known as the Warburg effect (230). Activated T cells were found to possess a glucose-sensitive metabolic checkpoint controlled by AMPK that regulates mRNA translation and glutamine-dependent mitochondrial metabolism to maintain T cell bioenergetics and viability. T cells lacking AMPKα1 displayed reduced mitochondrial bioenergetics and cellular ATP in response to glucose limitation in vitro, and AMPKα1 was shown to be essential for Th1 and Th17 cell development (228).

Fyn is one of the Src family kinases (SFKs) that is expressed in T cells. In terms of SFKs, T cells primarily express Lck and Fyn-T (a haematopoietic cell-specific isoform that contains an alternatively spliced form of exon 7 that encodes a part of the kinase domain). Both Lck and Fyn are involved in early TCR signal transduction events. Fyn-deficient splenic T cells show mild impairment in CD3 stimulated proliferation, but secrete little, if any, IL-2 (231). There was no decrease observed in Lck, but there was also no increase observed in Lck phosphorylation levels from basal levels following IL-2 stimulation.

Levels of phosphorylated Akt1/2/3 were also reduced following treatment with 100 μM ST0702. Akt (also known as Protein Kinase B) is a serine/threonine kinase that has three isoforms, Akt 1, Akt 2 and Akt3. Akt is a downstream component in phosphoinositide 3-kinase (PI3K) signalling. The PI3K pathway is a signal transduction pathway that promotes survival and growth in response to extracellular signals. PI3K is a ubiquitous enzyme family that is activated by stimulation of G-protein coupled receptors, autophosphorylation of receptor tyrosine kinases induced by ligands and activation of integrin signalling (232). Following activation, it attaches a phosphate group to position 3 of PIP_2 to form PIP_3. PIP_3.can then serve as a docking site for numerous proteins, including Akt. Once activated, Akt moves to the cytoplasm and nucleus, where a number of downstream targets are phosphorylated, activated or suppressed to provide a survival signal that protects cells from apoptosis induced by various stresses, and also mediates a variety of metabolic effects (233). The pathway is frequently deregulated in malignancies, and it also has been shown to have clinical relevance in

inflammatory skin diseases such as psoriasis. PI3K is upstream of mTOR, and Akt is known to phosphorylate mTOR. Studies have shown that mTOR is involved in the regulation of CD4+ T cell differentiation (234). The PI3K/mTOR pathway likely plays a role in Th1 and Th17 upregulated differentiation in psoriasis, and a reduction in the phosphorylation levels of Akt can be seen as a potential mechanism for the activity of ST0702 in the imiquimod mouse model. In general the effects of ST0702 were primarily on proteins activated through phosphorylation downstream of IL-2 activation, with some notable exceptions, such as AMPK.

3.2.2 **Phospho-kinase array: HuT78 cells**

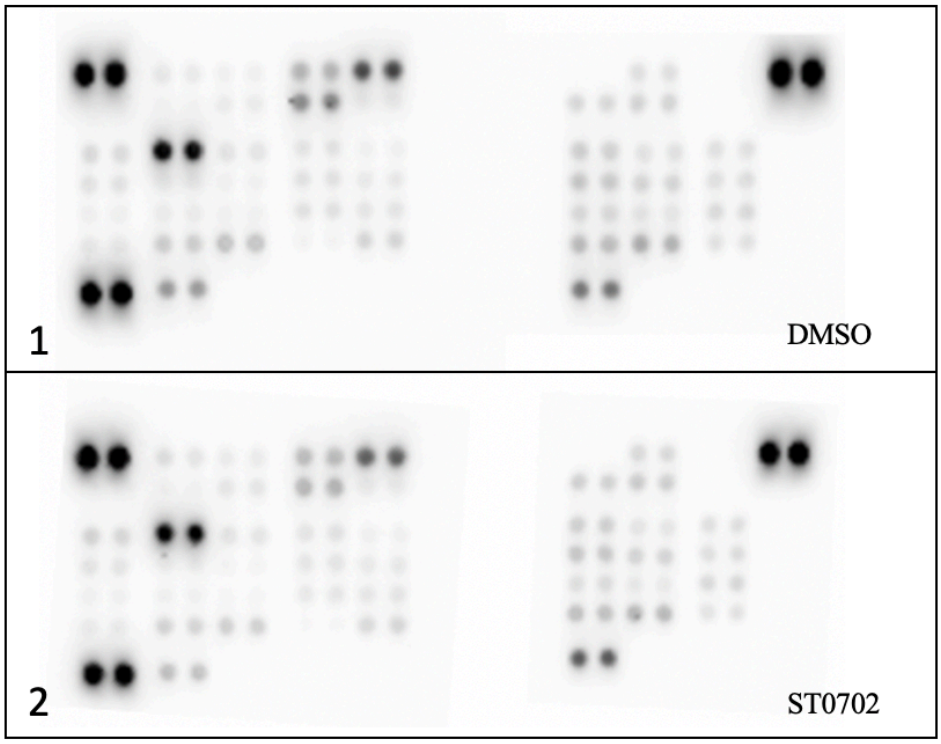

Figure 3-7: HuT78 proteome profiler array results.
HuT78s were seeded in T25 flasks at a density of 1 × 10^6 cells/mL and treated with 100 μM ST0702 or DMSO control for 30 min. The cells were lysed (following protocol outlined in kit). The protocol was then followed as outlined in the manual. Figure 1 corresponds to the DMSO control, and Figure 2 corresponds to cells treated with ST0702 100 μM. The above images were obtained using a visualiser with an exposure time of 20 min.

It has been shown (Figure 2.23) that ST0702 has an effect on the proliferation of HuT78 cells, but the mechanism of this inhibition of proliferation was unknown. Similar to the experiment carried out on PBMCs, a kinase array was used to try to deduce the mechanism of action of ST0702 on the HuT78 cells. The assay was expected to provide greater insight into the mechanism of action of ST0702. The results are shown in Figure 3.7, with key proteins affected

outlined in Figure 3.8. The HuT78 cells are constitutively activated, so no stimulation was required.

The results show that phosphorylation of STAT3 (Y705 and S727), STAT6, STAT2, GSK3α/β and AMPKα1 were all reduced, although to a slightly lesser degree than that observed in the PBMC experiment. Levels of phosphorylated Chk-2, and FAK were also reduced, these were not affected in the PBMC model. Phosphorylation levels of a number of other proteins, including Akt, p27, PDGFR-β, WNK1 and Yes were all reduced. Notably, the phosphoprotein inhibition in this experiment affected proteins that were not apparently related and the pattern appeared to be random or unconnected.

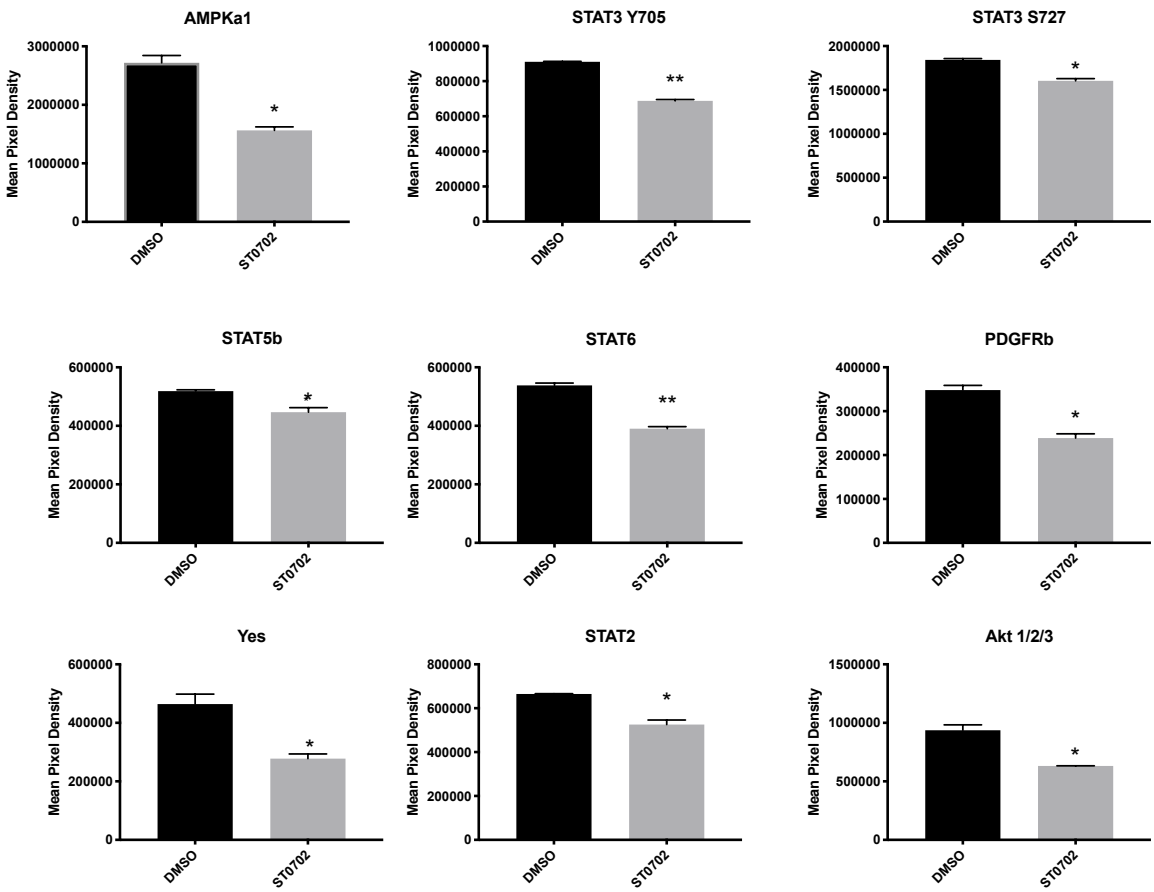

Figure 3-8: Key results from HuT78 proteome profiler array.
Results are presented for AMPKa1, STAT3, STAT5, STAT2, Akt1/2/3, Yes and PDGFRβ.

3.2.3 **Apoptosis Results for HuT78 cells treated with ST0702 or ISAL**

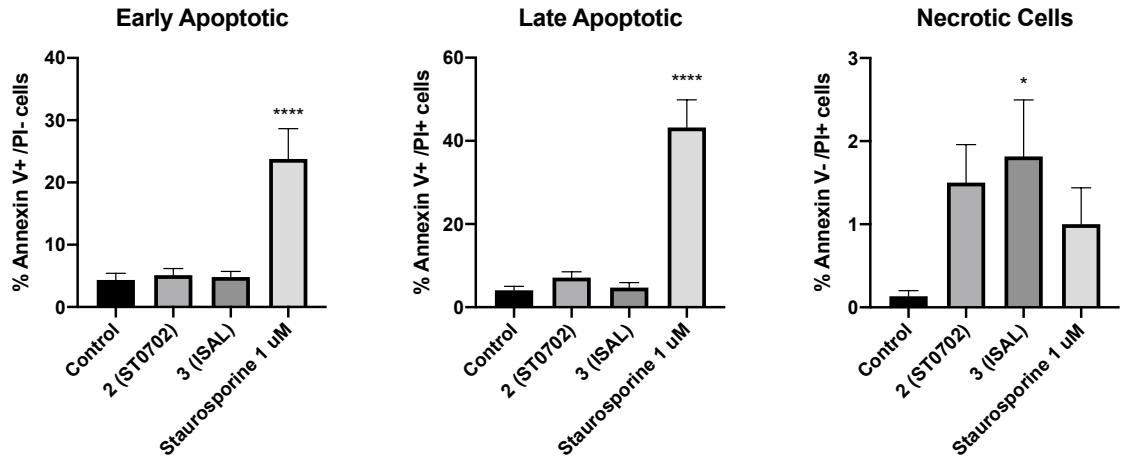

Figure 3-9: Annexin V results of ST0702 and ISAL tested in HuT78 cells.
HuT78 cells were plated at 1 × 10^4 cells per well of a 96-well plate with DMSO, 1 μM staurosporine or 100 μM compound and incubated at 37℃ for 48 h. The cells were stained with Annexin V and PI. The samples were analysed by flow cytometry. Results are expressed as mean± SEM of three independent experiments.

As can be seen in Figure 3.9, ST0702 or ISAL do not appear to be reducing the proliferation of cells by causing apoptosis of the cells. The non-selective protein kinase inhibitor staurosporine was used as a positive control as it is known to induce apoptosis by an undetermined mechanism. Levels of early and late apoptotic cells observed in HuT78 cells treated with 100 μM ST0702 or ISAL were less than 10%, in contrast to cells treated with staurosporine, where the percentage of early and late apoptotic cells exceeded 60%. These results mirrored the results observed in earlier studies of apoptosis (Figure 2.25).

3.2.4 **Effect of compounds on STAT3 activation**

Having identified from the array that the JAK-STAT family of proteins were affected by the compounds, and knowing the importance of these pathways in the regulation of the immune system it was decided that an assay was needed that would allow for the efficient screening of a large number of compounds for effects on this family of proteins. A reporter cell line was used that reports on the activation of STAT3. The cell line has a receptor for IL-6 and if a compound is an inhibitor of the IL-6R, JAK1, JAK2, Tyk2 or STAT3 there will be a reduction in the amount of SEAP that is measured which can be attributed to a reduction in the activation of the JAK/STAT3 pathway.

This cell line was chosen because a cell line with an IL-2R was not available, and the IL-6R does signal through JAK/STAT. Additionally, IL-6 has a role in the IL-23/IL-17 axis, which has a large role in the pathology of psoriasis, so studying the effects of the compound on this receptor could also provide additional insight into the mechanism of action.

IL-6 signalling occurs through the assembly of a receptor complex with two subunits; IL-6Rα, which binds the ligand, and gp130, which is involved in signal transduction. The binding of IL-6 to its receptor complex triggers the activation of the associated JAK kinases, leading to the phosphorylation of five tyrosine residues on the cytoplasmic portion of gp130. gp130 can bind to JAK1, JAK2 and TYK2 and of these, it appears that JAK1 is the most essential, with cells lacking in JAK1 having highly impaired IL-6 signal transduction (235). The phosphotyrosine residues lead to the recruitment and activation of STATs, and also the recruitment of the SHP2 adaptor, which leads to the activation of the Ras-MAP kinase pathway. SOCS3, a STAT3 immediate early target gene, is recruited to the same phosphotyrosine residue as SHP2, mediating a negative feedback effect via the inactivation of JAKs. In terms of STAT involvement, all members of the IL-6 cytokine family are able to activate STAT3, and to a lesser extent, STAT1, with STAT3 recognised as the primary mediator of the functions of IL-6 (236).

The IL-6 receptor can be compared to the IL-2 receptor, which has already been discussed in detail. They are structurally and functionally related receptors. The IL-2 receptor subunits bind JAK1 and JAK3, and the main STAT proteins involved are STAT5a/b, with some STAT3 and STAT1 activation. In contrast, the IL-6 receptor binds JAK1, JAK2 and TYK2, with STAT3 activation being the most important for signal transduction. There is no JAK3 involvement in the IL-6 receptor, but it is involved in IL-2 signal transduction. These differences could prove important when trying to ascertain the mechanism of action.

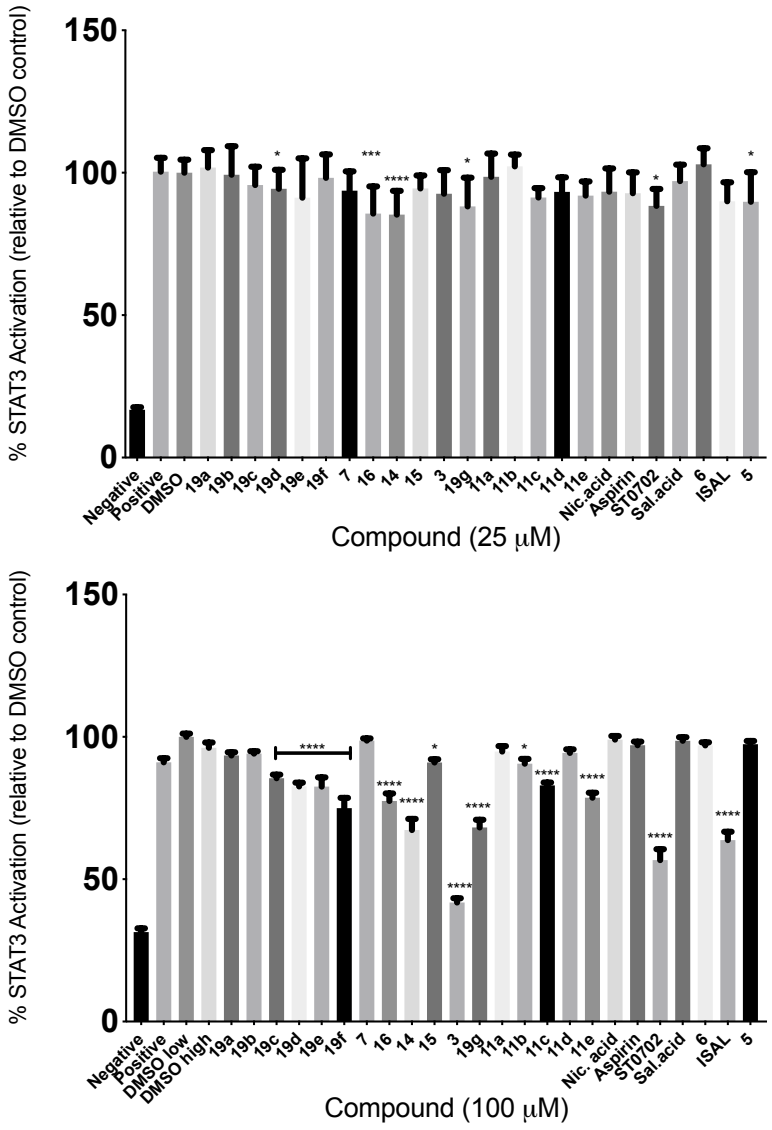

Figure 3-10: HEK-Blue IL-6 reporter results.
HEK-Blue IL-6 cells were plated at 5 × 10^4 cells per well of a 96-well plate. The cells were treated with 25 μM or 100 μM compound or DMSO vehicle. After 30 min incubation, the cells were stimulated with 1 ng/mL IL-6. After 24 h Quantiblue Reagent was added and SEAP levels were determined, and this was used to quantify STAT3 activation. Two separate DMSO controls (low and high) were set up to match the quantity of DMSO being added. Results are expressed as mean± SEM of three independent experiments.

In the above Figure 3.10 it can be seen that a number of compounds caused a reduction in the levels of SEAP being produced, thereby indicating a reduction in the activation of the JAK/STAT3 pathway. The most active compound was **3**, followed by ST0702 and then ISAL**.** Compound **3**, isosorbide-2-aspirinate-5-salicylate showed a >50% reduction in JAK-STAT activation compared to the DMSO control, while ST0702 reduced activation by 40%.

Reduction in STAT3 activation following ST0702 treatment is comparable with the reduction observed in the proliferation of HuT78 cells following treatment with ST0702. Previous studies (237) have identified mutations in JAK1 and JAK3 which result in constitutive activation of the JAK-STAT pathway; inhibition of this pathway results in decreased HuT78 cell proliferation. The results seen here therefore suggested that STAT inhibition might be at least one of the mechanisms of action of ST0702.

The compounds demonstrating the most activity in this assay were ST0702, **14**, **3**, **19g** and ISAL. These compounds also showed an inhibitor effect in the HuT78 proliferation assay. The correlation between results suggested that there could be a link between the ability of the compounds to reduce the activation of STAT3 and their ability to inhibit the proliferation of HuT78 cells.

To validate the effect of the compounds on STAT3 activation, a Western blot was carried out and the results are outlined in Figure 3.11. The reduction in the amount of phosphorylated STAT3 in cells treated with ST0702 can be clearly observed. Of note, the selective JAK1 and JAK2 inhibitor, ruxolitinib was also included and it can be seen that it had a much larger effect at decreasing pSTAT3 levels than the compounds.

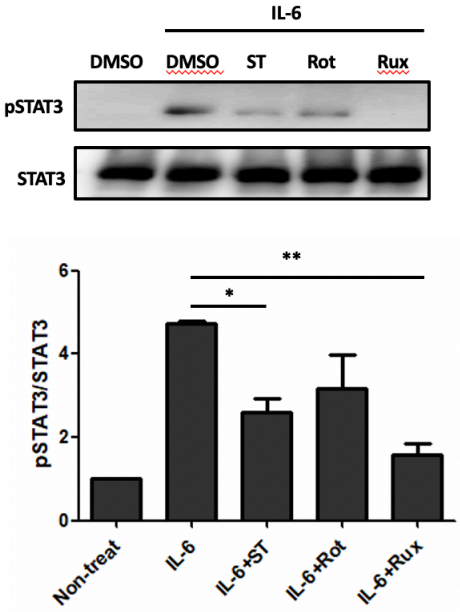

Figure 3-11: pSTAT3 and total STAT3 levels measured using western blotting.
HEK-Blue IL-6 cells were plated at 2 × 10^5 cells in a six well plate and incubated for 48 h. Following this, cells were treated for 30 min with DMSO, ST0702 100 μM, Rotenone 100 nM, or Ruxolitinib 1 μM. The cells were then stimulated for 30 min with IL-6 (1 ng/mL). Lysates were then prepared, and western blots were carried out. Results are expressed as mean± SEM of three experiments.

A study was carried out to examine the concentration-response relationship of ST0702 in these cells, and to determine if the STAT3 inhibitory effect was concentration dependent (Figure 3.12). Concentrations greater than 100 μM were not tested, as it seemed that these levels would not be relevant to the interpretation of the in vivo models. Concentrations of ST0702 as low as 25 μM were found to have a statistically significant effect on STAT3 activation (20%). There was some effect seen at 0.1 μM, but as 10 μM and 1 μM had no effect this could just be a chance occurrence.

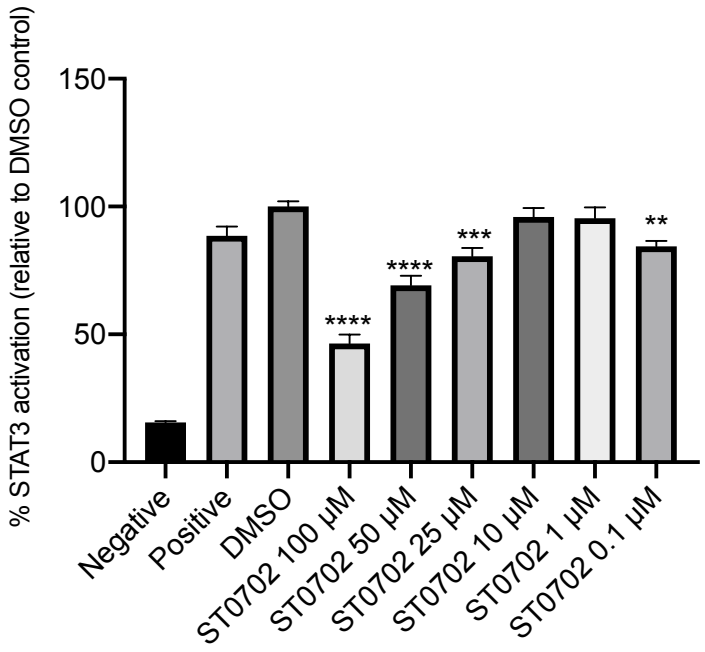

Figure 3-12:Inhibition of STAT3 activation using decreasing concentrations of ST0702. HEK-Blue IL-6 cells were plated at 5 × 10^4 cells per well of a 96-well plate. Cells were treated with 25 μM or 100 μM compound or DMSO vehicle. After 30 min incubation, the cells were stimulated with 1 ng/mL IL-6. The cells in the negative wells did not receive IL-6 stimulation. After 24 h Quantiblue Reagent was added and SEAP levels were determined. Results are expressed as mean± SEM of three experiments.

The effect of the compounds, in particular ST0702, its related metabolite ISAL, and **3** on STAT3 activation seemed promising. However, it was important to validate that the effect that the compounds were having on the HEK STAT3 reporter cell line was a true effect and was not due to any apoptotic effect that the compounds might be having. To that end, it was necessary to determine the viability of the HEK reporter cells. Initially MTT was used, however the HEKs are loosely adherent so it was not possible to use MTT to accurately investigate viability. MTT requires the cell supernatant be removed and this could not be done with the

HEK cells as removing the supernatant caused some disruption of the attached cells. This was leading to large variation in results in the MTT experiments.

It was decided to use Alamar Blue as an indicator of viability in these cells instead. With this method, the Alamar Blue reagent was added directly to the well containing the cells. There was no cause for removing the supernatant so the cells were not disrupted and an accurate measure of viability could be obtained. From Figure 3.13 it can be observed that the most toxic compound was **3**. This corresponded with the results that had been seen in the HuT78 apoptosis experiments, where compound **3** caused more apoptosis than ST0702 (Figure 2.25). Here the reduction in cell viability when cells were treated with compound **3** was approximately 30%, whereas for ST0702 and ISAL the approximate reduction in viability was closer to 10% and was not statistically significant. This indicates that some of the inhibitory effect of compound **3** on STAT3 activation could be attributed to a loss in cell viability. In the next experiments confirmation was sought that STAT3 inhibition at the level observed could be responsible for the cytostatic effects in the HuT78 cell line.

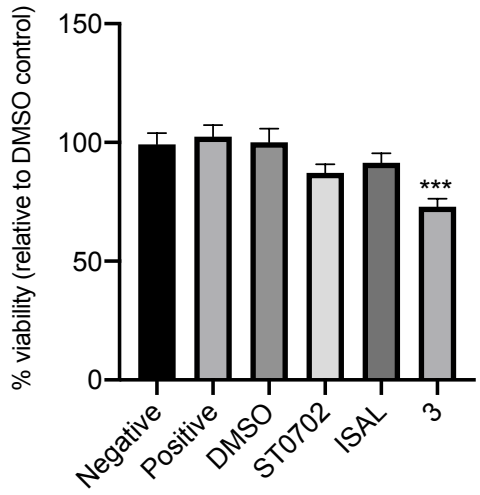

Figure 3-13: Effect of compounds on viability of HEK-Blue IL-6 cells measured using Alamar Blue.

HEK-Blue IL-6 cells were plated at 5 × 10^4 cells per well of a 96-well plate. Cells were treated with 100 µM compound or DMSO vehicle. After 30 min incubation, the cells were stimulated with 1 ng/mL IL-6. The cells in the negative control wells were not stimulated with IL-6. After 24 h the viability was determined using Alamar Blue assay.

3.2.5 **Experiments with the JAK1/2 inhibitor ruxolitinib**

Ruxolitinib is a JAK1/2 inhibitor. It was tested in two separate experiments, the HEK-Blue IL-6 assay (Figure 3.14a) and the HuT78 proliferation assay (Figure 3.14b). In the HEK-Blue IL-

6 cells, concentrations of ruxolitinib as low as 1 μM show a marked effect on the activation of the JAK-STAT pathway induced by IL-6. STAT3 activation was reduced by up to 85%. However, when 1 μM ruxolitinib was tested in the HuT78 proliferation model, no inhibition of proliferation was observed. This is in line with results seen by other researchers, where the IC_{50} for ruxolitinib activity in HuT78 proliferation was seen to be 24 μM (237). A possible reason for the lack of effect on proliferation is that it has been found previously that ruxolitinib caused a marked and rapid inhibition of STAT activation that was abolished after 3 h of treatment (237). For the MTT proliferation experiment, there was a 48 h incubation period before the effects were measured. This was potentially too long, and the cells might have been able to overcome the effects of ruxolitinib and continue to proliferate. In contrast to this, the HEK-Blue IL-6 assay has a 24 h incubation period, and it is the amount of SEAP that is produced throughout the entire experiment that is being measured, not just the amount that is being produced at the endpoint. Another potential reason for a lack of response is that there is no JAK2 mutation in HuT78 cells, and ruxolitinib acts on both JAK1 and JAK2. The IL-6 receptor has both JAK1 and JAK2, which could explain why we see an effect in the IL-6 model, but not the HuT78 model. The overall implications of these findings is that STAT3 inhibition in the HuT78 cell line may not directly lead to an inhibitory effect on proliferation.

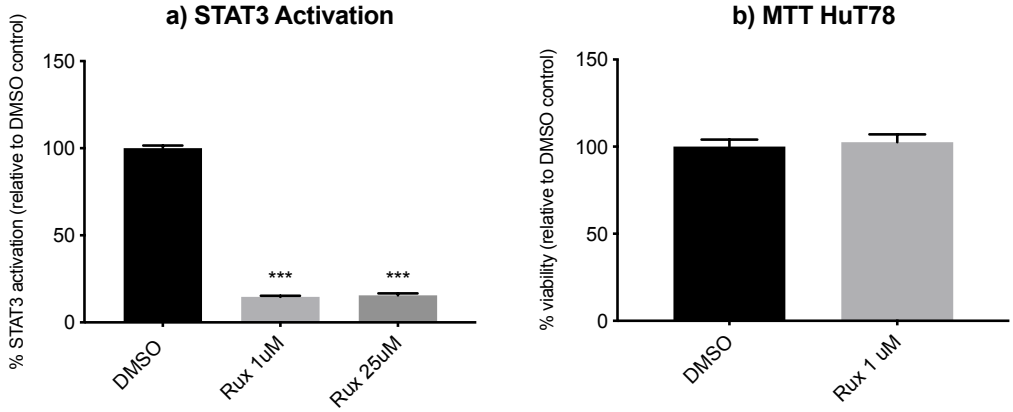

Figure 3-14: HEK-Blue IL-6 results and HuT78 proliferation results for ruxolitinib.
a) HEK-Blue IL-6 cells were plated at 5 × 10^4 cells per well of a 96-well plate. Cells were treated with 1 μM or 25 μM ruxolitinib. After 30 min incubation, the cells were stimulated with 1 ng/mL IL-6. After 24 h Quantiblue reagent was added and SEAP levels were determined. b) HuT78 cells were plated in flat-bottomed 96 well plates at 1 × 10^4 cells per well of a 96-well plate. The cells were treated with 1 μM ruxolitinib and incubated for 48 h. After this time, MTT was carried out. Results for each assay are expressed as mean± SEM of three independent experiments.

3.2.6 **Effect of ST0702 on Protein Kinase Activity**

As a further investigation into the effect of ST0702 on the IL-2 receptor, an experiment was carried out to test the hypothesis that ST0702 was having an inhibitory effect on Protein Kinase C (PKC). Protein kinase C is a serine/threonine kinase which participates in T cell transduction in a wide variety of cell types. In T cells, antigen binding to its receptor results in the hydrolysis of the membrane phospholipid, phosphatidylinositol 4,5-bisphosphate with the production of inositol 1,4,5-triphosphate (IP_3) and diacylglycerol (DAG). IP_3 raises intracellular calcium stores while DAG activates PKC. HuT78 cells express PKCα and β.

PKC is the cellular receptor for phorbol esters and other tumour promoters which bind directly and activate the enzyme. PMA is a specific activator of PKC. When T cells are stimulated with PMA this leads to the phosphorylation of various T cell proteins, including the CD4, CD8 and CD45 molecules and the γ subunit of the CD3 complex (238).

The activity of three different PKC inhibitors on proliferation of HuT78 cells was measured, with Gö6976, BisIM and BioX being tested (Figure 3.15). Gö6976 is a potent PKC inhibitor, selective for PKCα and PKCβ. Bisindolylmaleimide I is a selective cell permeable PKC inhibitor that is structurally similar to staurosporine. It shows selectivity for PKCα, β_I, β_{II}, γ, δ and ε isozymes. It may inhibit protein kinase A at higher concentrations. BioX (GSK-3 inhibitor IX, 6-bromoindirubin-3-oxime) is a specific inhibitor of Glycogen synthase 3 (GSK-3). GSK-3 is a constitutively activated serine/threonine kinase involved on a wide variety of cellular processes including glycogen metabolism, transcription, translation, cell cycle and apoptosis.

When the effect of each inhibitor on proliferation was measured, Gö6976 was the most effective inhibitor. BisIM achieved approximately 50% inhibition, and BioX had a small but significant effect on proliferation. The results observed with the GSK-3 inhibitor, BioX is in line with a published study that tested the effect of three different GSK-3 inhibitors (not BioX) on the rate of apoptosis in HuT78 cells, and saw that none of the inhibitors significantly affected the rate of apoptosis (239).

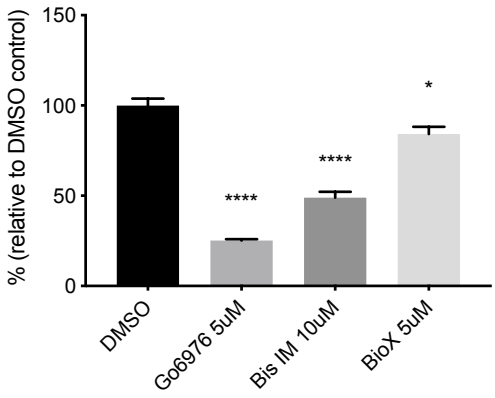

Figure 3-15: Effect of PKC inhibitors on proliferation of HuT78 cells.
HuT78 cells were plated in 96 well plates at 1 × 10^4 cells per well of a 96-well plate. The cells were treated with inhibitors and incubated for 48 h. Cell counting was then carried out. Results for each concentration are expressed as mean ± SEM of four independent experiments.

The hypothesis being tested by this experiment was whether PKC inhibition could cause a decrease in the proliferation of HuT78, and by extension, whether the inhibitory effects of ST0702 could be due to it having an inhibitory effect on PKC. Based on the results of this first set of experiments this seemed plausible.

HuT78 cells stimulated with the PKC activator PMA will secrete IL-2. To investigate directly whether or not ST0702 was acting as a PKC inhibitor, and blocking the effects of PMA, an experiment was set up with HuT78 cells stimulated with PMA (Figure 3.16). A PKC inhibitor, Gö6976, was used as a positive control, as it was expected that it would block PKC signalling and inhibit the production of IL-2.

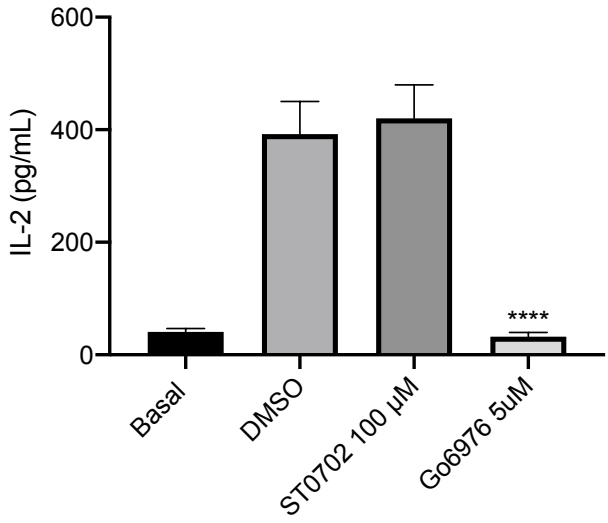

Figure 3-16: Production of IL-2 in HuT78 cells in response to PMA stimulation.
HuT78 cells were plated in a 24 well plate at 1 ×10^6 cells/well. Cells were treated with DMSO, 100 µM ST0702 or 5 µM Gö6976. Following 30 min incubation cells were stimulated with PMA 10 ng/mL (except the cells in the basal wells) and incubated overnight. The amount of IL-2 in the supernatant was then measured by ELISA. The experiment was carried out in triplicate and results are expressed as mean ± SEM. .

As can be seen in Figure 3.16, PMA stimulation caused a large increase in IL-2 production. ST0702 did not inhibit this production of IL-2, while Gö6976 brought IL-2 levels back to pre-stimulation levels. This is quite conclusive evidence that ST0702 does not act as a PKC inhibitor, however it has previously been shown that another PKC inhibitor, H-7 (which inhibits cyclic AMP-dependent protein kinase) does not inhibit IL-2 secretion by HuT78 (240), so it cannot be dismissed as a potential mechanism, but it seems unlikely given the results here. H7 is a very broad protein kinase inhibitor, inhibiting protein kinase A (PKA), protein kinase G (PKG) and PKC, among others, whilst Gö6976 is a potent selective PKC inhibitor.

3.2.7 **Experiments with Genistein and PP2**

Genistein is a natural isoflavone that acts as a broad tyrosine kinase inhibitor. PP2 is a substance that has frequently been used in cancer research as a selective inhibitor for Src family kinases. It strongly inhibits the kinases Lck, Fyn, Hck, shows weaker inhibition of EGFR and practically no inhibition of JAK2. Studies have shown that genistein can inhibit the growth of a number of tumour cells in vitro but can enhance the mitochondrial reductions of tetrazolium salts, leading to a underestimating of the growth inhibitory activity of the substance when the MTT assay is used as the indicator (241).

Genistein, when used at concentrations of 100 μM or above, inhibited STAT3 activation in the HEK IL-6 reporter cell line (Figure 3.17a). Genistein is a tyrosine kinase inhibitor, and since IL-6 signalling and STAT3 activation requires tyrosine phosphorylation, this effect was expected.

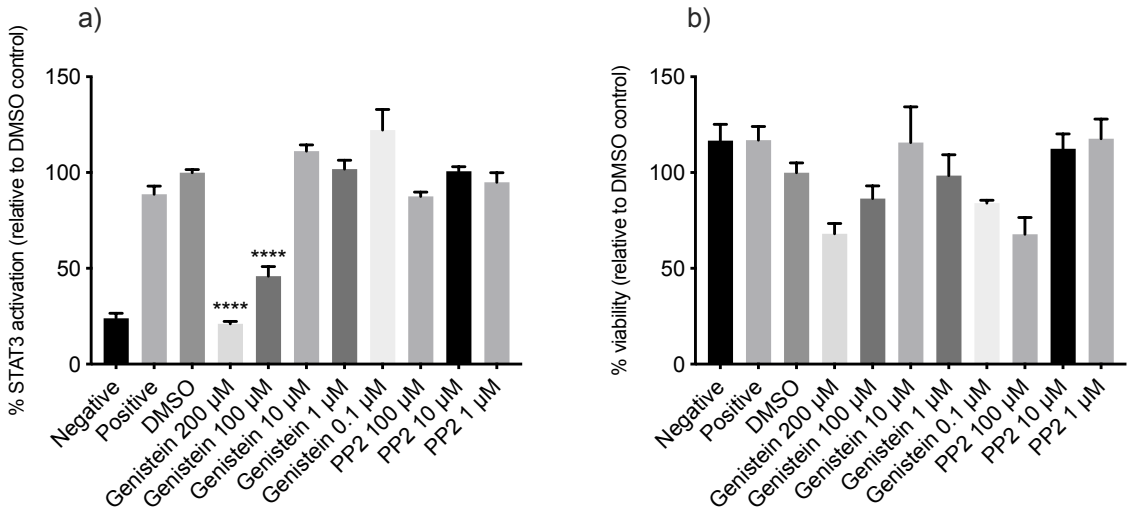

Figure 3-17: Results from HEK Blue IL-6 experiments with genistein and PP2.
HEK-Blue IL-6 cells were plated at 5 × 10^4 cells per well of a 96-well plate. Various concentrations of PP2 or Genistein were added. After 30 min incubation, the cells were stimulated with 1 ng/mL IL-6 and incubated for 24h. The cells in the negative control wells were not stimulated with IL-6. Following this, Quantiblue reagent was added and SEAP levels were determined. The results are shown in graph a). MTT was also carried out to determine the viability of these cells, and the results are shown in graph b).

There has been evidence that the Src and JAK family kinases cooperate to mediate constitutive STAT3 activation in breast cancer cell lines, and the biological effects of Src and JAK tyrosine kinase inhibitors are partly mediated by blocking STAT3 signalling (242). PP2 is a selective inhibitor of Src, and the intention behind its inclusion was to rule out the possibility that ST0702 was a Src inhibitor, and that this was responsible for the inhibitory activity on STAT3 observed in the HEK IL-6 cells. This does not appear to be the case, as treatment of the cells with concentrations of PP2 known to inhibit Src tyrosine kinases, does not have any effect on STAT3 activation in the reporter assay.

3.2.8 **Direct Inhibitory Effect on JAK1/2/3**

At this point there was evidence that ST0702 was having an effect on the JAK/STAT signalling pathway, the first set of evidence being the multiplex antibody array, where reductions were

observed in IL-2 stimulated phosphorylation of STAT3 and STAT5. Add to this the reduction in STAT3 activity being seen in the IL-6 reporter assay, and the reduction in proliferation of the HuT78 cell lines, a cell line which has constitutively activated STAT3, and there points to an effect of the compounds on STAT3. To try to pinpoint the exact mechanism of these compounds, and how exactly the STAT3 inhibitory effect was being achieved, it was hypothesised that the compounds might be inhibiting upstream of STAT3, and having a direct effect on JAK1, 2 or 3.

The work to determine whether the compounds were having an inhibitory effect on JAK1/2 or 3 was outsourced to Eurofins, a commercial company who offer these assays as a service. The company used purified enzymes in solution with synthetic substrates, so it was measuring a direct inhibitory effect on JAKs, in contrast to the reporter assays where events both upstream and downstream of JAKs could be responsible for the reduction in STAT3 activation observed. ST0702 and its main metabolite, ISAL were tested. The results that came back were conclusive, neither compound was an inhibitor of JAK1, JAK2 or JAK3.

Target	**Activity (% Control)**		
Sample	**JAK1**	**JAK2**	**JAK3**
ST0702 @ 50µM	116	98	107
ST0702 @ 100µM	129	88	107
ISAL @ 50µM	114	91	105
ISAL @ 100µM	112	110	100

Figure 3-18: Inhibitory effect of compounds on JAK1/2/3 (experiments conducted by Eurofins).

3.2.9 **PBMC Proliferation Experiments**

To validate the results of the cell line experiments, analysis was carried out on T cells expanded from PBMCs, a more physiological model. Once again, ST0702 caused a decrease in T cell numbers, suggesting an inhibitory effect on T cell proliferation. However, it is likely that this effect was not due to the ability of ST0702 to inhibit the JAK/STAT pathway, as treatment of T cells with ruxolitinib did not result in similar decreases in cell numbers.

A different mechanism of action was then sought which might explain these results. Five different treatment protocols were carried out. A number of different experimental protocols were used to determine whether or not ST0702 or some of the more promising analogues had effects on PBMC proliferation. All of the protocols involved initial activation of the PBMCs using anti-CD3/CD28 for a period of 72 h. Some of the protocols then involved further stimulation of proliferation using IL-2 for a 48 h period, and then other protocols involved a

further stimulation with IL-2 for an additional 48 h. The compounds were added at different timepoints of the experiments. A scheme detailing the different protocols investigated can be seen in Figure 3.19. Proliferation was measured using two different methods, MTT and manual cell counting.

The logic behind the design of these experiments was to determine the point at which the compound was having an effect on the proliferation of the T cell blasts. It was necessary to determine whether the compound was affecting the activation of the T cells with a CD3/CD28 or if it was having an inhibitory effect on the IL-2R or a signalling pathway downstream of the IL-2R.

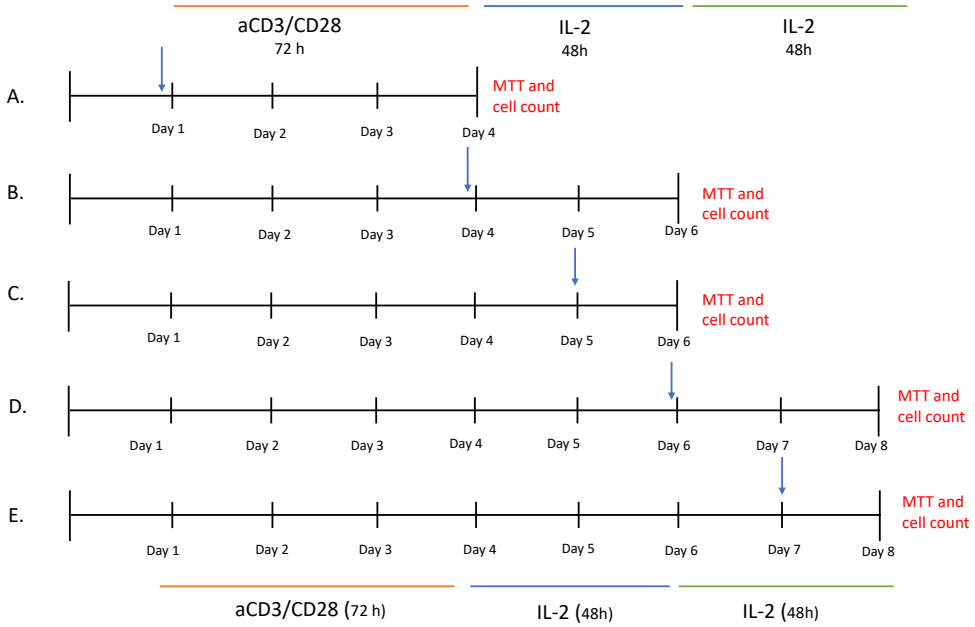

Figure 3-19: Design of PBMC experiments.
For all protocols, PBMCs (5×10^5 cells/well in a 24-well plate) were seeded. The blue arrow indicates the point in each protocol that the compounds were added, for Protocol A, the compounds were incubated 30 min prior to the addition of aCD3/CD28, for Protocol B the compounds were incubated 30 min prior to the addition of IL-2, for Protocol C the compounds were incubated 24 h following the addition of IL-2, for Protocol D the compounds were incubated 30 min prior to the addition of the second cycle of IL-2 and for Protocol E the compounds were incubated 24 h following the addition of the second cycle of IL-2.

3.2.9.1 *Protocol A: aCD3/CD28 only*

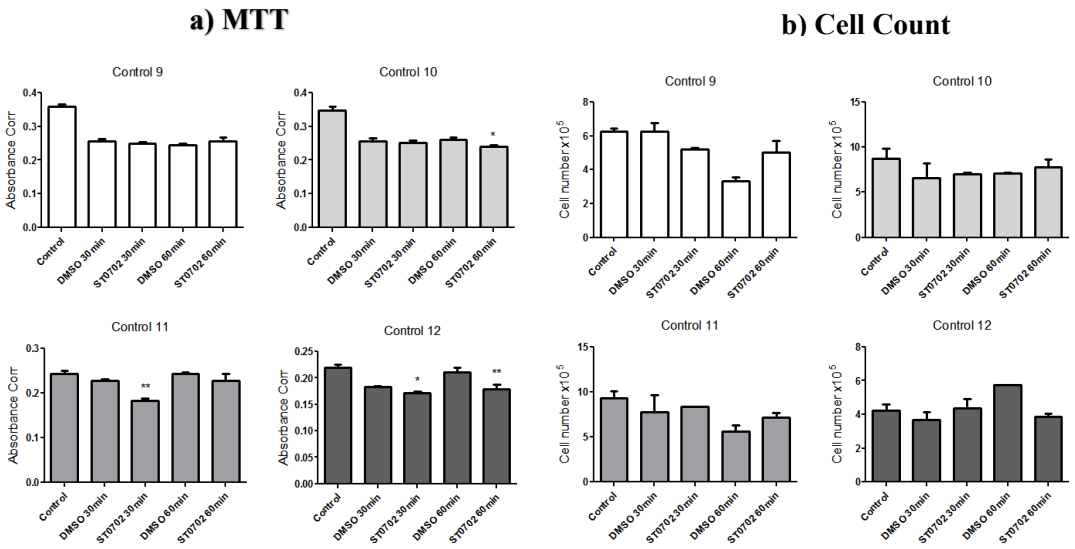

Figure 3-20: a) MTT PBMCs – CD3/CD28 and b) cell count PBMCs – CD3/CD28 only. PBMCs (5 × 10^5 cells/well in a 24-well plate) were pre-treated with either DMSO or ST0702 100 μM for 30 min or 60 min, then stimulated with aCD3/CD28 beads for 72 h. MTT and cell counting was then carried out. Data for each donor is expressed as mean ± SEM.

The effect of ST0702 on inhibition of T cell proliferation was minimal when Protocol A was used (Figure 3.20). Protocol A only involves the activation of the PBMCs, and no IL-2 is added. Therefore the cells might not be expected to undergo much proliferation.

For the MTT results, ST0702 exerted a statistically significant decrease in two of the four donors after an incubation period of 60 min and in two of the donors with a 30 min incubation period. The effects seen were modest and inconsistent. Similarly, for the manual cell counting there were no statistically significant results observed for ST0702 treatment. The conclusion can therefore be drawn that the compound does not affect proliferation unless the cells are stimulated or otherwise dividing rapidly.

3.2.9.2 *Protocol B: aCD3/CD28 + IL-2 x 1 (treatment 30 min pre IL-2 addition)*

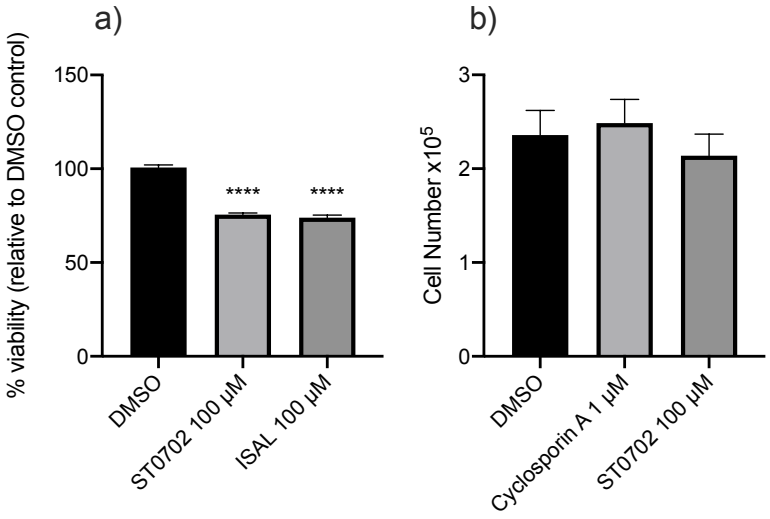

Figure 3-21: a) MTT PBMCs – CD3/CD28 + IL-2 and b) cell count PBMCs – CD3/CD28 + IL-2

PBMCs (5 × 10^5 cells/well in a 24-well plate) were seeded and stimulated with aCD3/CD28 beads for 72 h. They were then pre-treated with either DMSO, ST0702 100 µM or Cyclosporin A 1 µM for 30 min before adding IL-2 (20 ng/ml) and incubated for 48 h. Manual cell count and MTT was then carried out. Data is expressed as mean± SEM of 4 donors, carried out in triplicate.

For Protocol B, the cells were activated and then stimulated with one round of IL-2, so it would be expected that the T cell blasts would be undergoing rapid expansion. ST0702 and ISAL both had effect on proliferation here, as measured using the MTT (Figure 3.21a). This effect was not as clear in the cell count, where the immunosuppressant cyclosporin A was also tested, and also had no effect on T cell proliferation as measured using manual cell counting (Figure 3.21b). It has been shown previously that T cell proliferation induced by CD28 and PMA stimulation is resistant to cyclosporine (243), and this appears to be the case for proliferation induced by aCD3/CD28 stimulation and IL-2.

3.2.9.3 *Protocol C: aCD3/CD28 + IL-2 x 1 (treatment 24 h post IL-2 addition)*

For protocol C, ST0702 (100 µM) had an inhibitory effect of 28% on proliferation as measured via MTT (Figure 3.22a). A statistically significant decrease in cell number, as measured via manual cell counting, was also observed (Figure 3.22b) This reduction in cell count was not observed for protocol B. The difference between protocol B and C is that in protocol B the compound is added 30 min prior to IL-2 stimulation, when the cells have not begun to actively

proliferate and expand, whereas in protocol C, ST0702 was added 24 h post IL-2 stimulation, when the cells would have expected to be rapidly expanding. ISAL was also tested in the MTT here, and cells treated with ISAL (100 μM) showed a 32% reduction in proliferation.

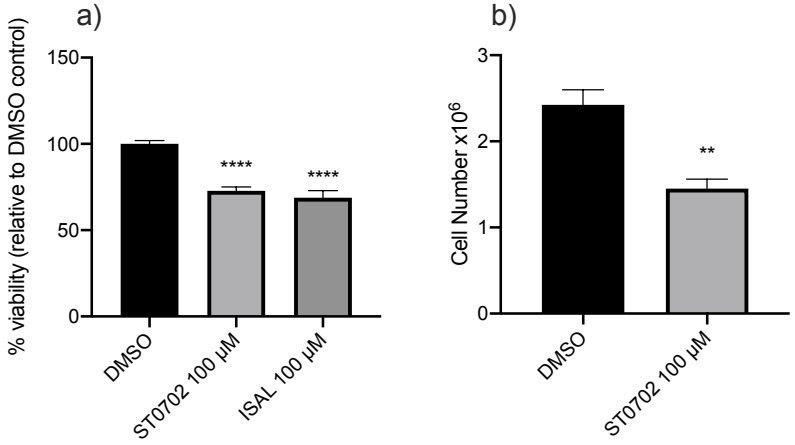

Figure 3-22: a) MTT and b) cell count PBMCs – aCD3/CD28+IL-2 (treatment in last 24 h). PBMCs (5 × 10^5 cells/well in a 24-well plate) were seeded and stimulated with aCD3/CD28 beads for 72 h before adding IL-2 (20 ng/ml) for 48 h. Cells were then treated with either DMSO or compounds at 100 μM for the last 24 h of stimulation. Cells were then counted manually or MTT was carried out. Data is expressed as mean± SEM of 4 donors, carried out in triplicate.

3.2.9.4 *Protocol D: aCD3/CD28 + IL-2 x 2 (treatment 30 min pre second IL-2 addition)*

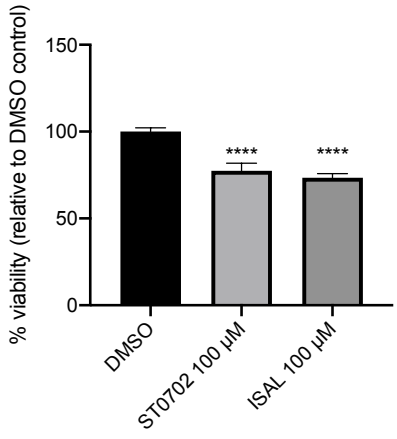

Figure 3-23: MTT PBMCs – CD3/CD28+IL-2 × 2 (30 min pre-treatment).
PBMCs (5 × 10^5 cells/well in a 24-well plate) were seeded and stimulated with aCD3/CD28 beads for 72 h before adding two successive rounds of IL-2 (20 ng/mL) for 48 h. Cells were treated with either DMSO or ST0702 100 μM for 30 min before the second round of IL-2. MTT was then carried out. Data is expressed as mean± SEM of 4 donors, carried out in triplicate.

For protocol D, the PBMCs were activated with aCD3/CD28 beads for 72 h before adding two successive rounds of IL-2 (20 ng/mL) for 48 h, with compound added 30 min before the second round of IL-2. For this protocol, treatment with ST0702 did result in a statistically significant reduction in T cell proliferation in three of the four donors (Figure 3.23). However, this inhibition of proliferation was much less than was observed in Protocol C, suggesting that incubation with ST0702 30 min prior to stimulation of T cells is not the optimal protocol. A possible theory as to why this is the case could be that the compound works best at inhibiting proliferation when the cells are actively proliferating just as the compound is added. Previous metabolism studies outlined in Chapter 2 have revealed that ST0702 has a very short half-life when added to complete media, as was the case here. It is possible that a large proportion of ST0702 had been metabolised by the time that the IL-2 stimulation was added and the cells began to actively proliferate.

3.2.9.5 *Protocol E: aCD3/CD28 + IL-2 x 1 (treatment 24 h post second IL-2 addition)*

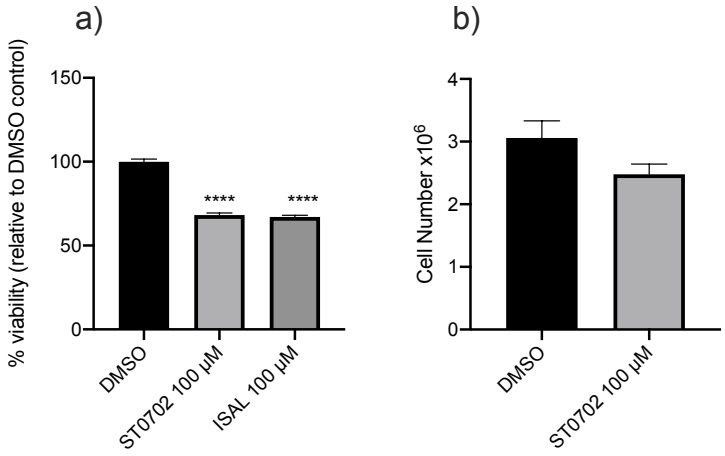

Figure 3-24: MTT and Cell Count PBMCs – CD3/CD28+IL-2 × 2 (treatment in last 24 h). PBMCs (5 × 10^5 cells/well in a 24-well plate) were seeded and stimulated with aCD3/CD28 beads for 72 h before adding two successive rounds of IL-2 (20 ng/ml) for 48 h. Cells were then treated with either DMSO, ST0702 or ISAL 100 µM for the last 24 h of stimulation. Manual cell count and MTT was then carried out. Data is expressed as mean± SEM of 4 donors, carried out in triplicate.

ST0702 showed promising activity in this protocol, where the compound was added 24 h into the second cycle of IL-2 stimulation (Figure 3.24). These results are in agreement with those seen when the compounds were added 24 h after the first cycle of IL-2 was added, which gives strength to the theory that the compounds have a greater effect when the cells are actively proliferating when they are added. When the compounds are added 30 min prior to stimulation,

as was the case for Protocols B and D, the inhibition of proliferation seen with ST0702 was not nearly as pronounced.

3.2.9.6 *Effect of ST0702/ISAL on proliferation of unstimulated PBMCs*

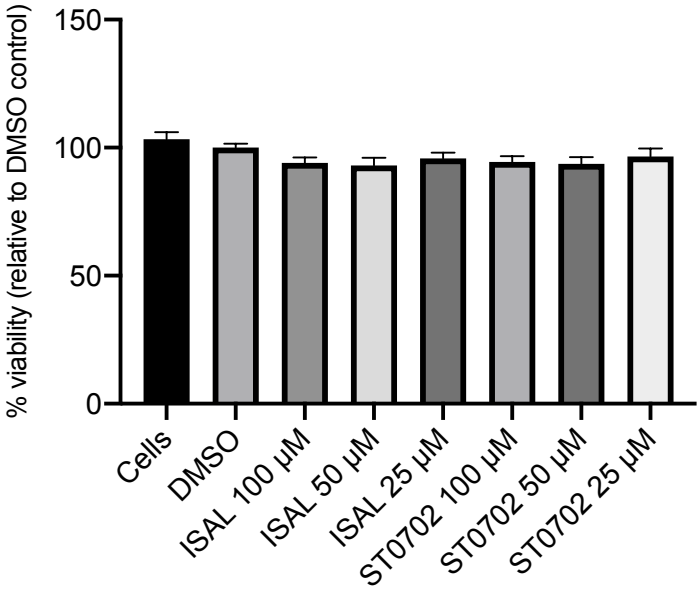

Figure 3-25: MTT from unstimulated PBMCs treated with compound for 48 h.
PBMCs (1 × 10^5 cells/well in a 96-well plate) were seeded and treated with compound for 48 h. Following this, MTT was carried out. Data is presented as mean ± SEM of three different donors.

When the PBMCs were not activated with aCD3/CD28 neither ST0702 nor ISAL (100 µM) had any effect on the proliferation of the cells (Figure 3.25). Non-activated PBMCs would not be expected to proliferate, so this test was less a measure of the effect of the compounds on proliferation, and more a measure of the ability of the compounds to cause cell death. It can be seen from the results that neither ST0702 nor ISAL had any effect on the viability of unstimulated PBMCs.

The two protocols that demonstrated the best results, Protocols C and E, involved ST0702 being added 24 h following IL-2 stimulation, when the cells were actively proliferating. Protocols A, B and D saw ST0702 being added 30 min before the cells were stimulated with either aCD3/CD28 or IL-2. This gave rise to a theory that the activity of ST0702 could potentially depend on the metabolic activity of the cells at the time at which the compound was added. As further support for this theory, it was noted that phosphorylation levels of AMPKα1 were reduced by a significant amount in the array (Figures 3.6 and 3,8). AMPKα1 is involved in the regulation of energy demanding/consuming metabolic pathways (244). Once activated,

AMPKα1 regulates catabolism/anabolism, switching off ATP consuming pathways and supporting ATP generating pathways.

3.2.10 **Glucose Experiments**

To further test the hypothesis put forward that perhaps ST0702 and related compounds were having an effect on the metabolism of T cells, which could in turn impact on their rate of proliferation, experiments were carried out to examine the effects of the compounds in low and high glucose conditions. As a way to test this hypothesis, HuT78 cells were plated in media containing no glucose, low glucose or high glucose. ST0702 was added and the cells were incubated for 5 h. An MTT assay was then carried out.

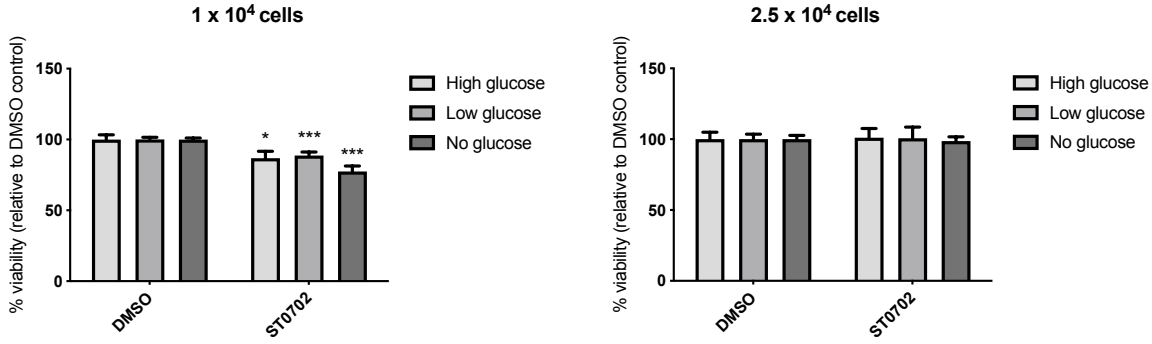

Figure 3-26:Results from glucose experiments on HuT78 cell line.
HuT78 cells were plated at 1 × 10^4 cells/well (left) or 2.5 × 10^4 cells/well of a 96-well plate (right). ST0702 or DMSO was added and the cells were incubated for 5 h. Following this MTT was carried out. Results for each assay are expressed as mean± SEM of three independent experiments.

When 1 × 10^4 cells were plated per well (of a 96-well plate), ST0702 showed greater efficacy in the presence of no glucose, compared to when cells were in glucose media (Figure 3.26). As the incubation time for these cells was only 5 h, the MTT is less an indicator of proliferation, and more so an indicator of metabolic activity in the cell. When 2.5 × 10^4 cells were plated per well, ST0702 showed no efficacy under any of the conditions.

Experiments were also carried out with PBMCs activated with aCD3/CD28, and very similar results were obtained to those seen in the HuT78 cells (Figure 3.27). ST0702 showed slightly greater antiproliferative activity in the presence of no glucose.

The results of these experiments were not overly conclusive, but they do indicate that perhaps metabolism could play an important role in the activity of ST0702. The short timeframe of the

experiments is the major contributor to the lack of a conclusive answer, as at a 5 hour timepoint no significant change in proliferation could be expected.

A similar study looking at the effects of glucose starvation on activated effector T cells, where the cells were generated via anti-CD3 and anti-CD28 antibody stimulation with IL-2 for 3 days, followed by acute glucose starvation for 5 h, showed that the rate of glycolysis decreased in CD8+ and CD4+ T cells as glucose concentration decreased, but the levels of OXPHOS were largely maintained during glucose-free conditions, leading to an increase in the OCR: ECAR ratio (228).

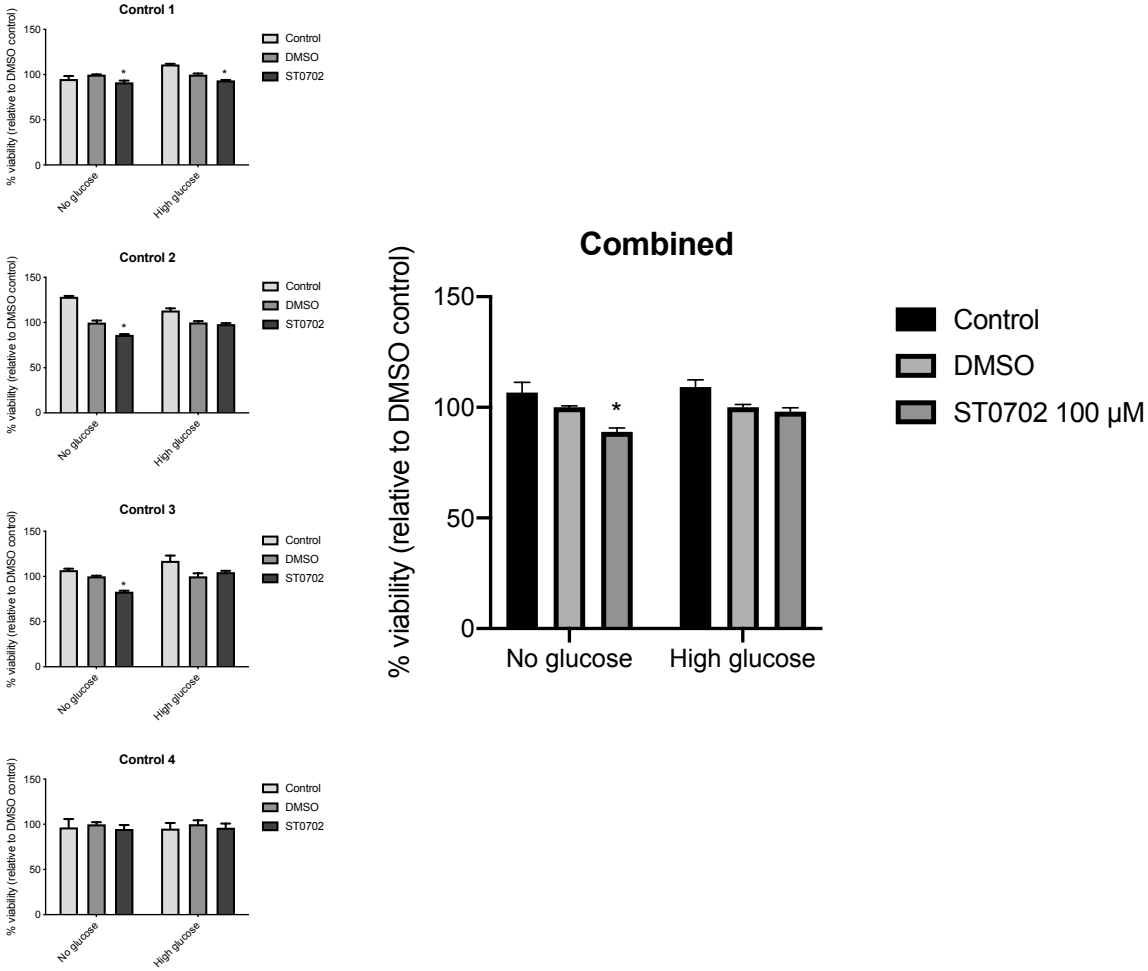

Figure 3-27: Results from glucose experiments on PBMCs activated with aCD3/CD28. PBMCs (5 × 10^5 cells/well in a 24-well plate) were seeded and stimulated with aCD3/CD28 beads for 72 h. They were then pre-treated with either DMSO or ST0702 100 µM for 30 min before being seeded in the presence of high (2 g/L) or no glucose medium and incubated for 5 h. The control cells received no treatment. MTT was then carried out. Data is expressed as mean± SEM of 4 donors, carried out in triplicate.

3.2.11 **Investigation into Effect of ST0702 on Metabolic Activity of the Cell**

Following on from the results of the T cell proliferation experiments, and in particular stemming from several discoveries about the effect of ST0702 on aspects of metabolism it was decided to investigate the metabolic profile of these cells, and the effect that the compound is having on the metabolic activity of the cells.

The first discovery was the effect of ST0702 (100 μM) on levels of AMPK, observed in the kinase array. ST0702 was seen to decrease levels of AMPK, which was very interesting, especially when considered with respect to metformin, a compound that has been investigated for effect in psoriasis and is a known activator of AMPK. Metformin has inhibitory action on Complex I of ETC and can therefore change the cellular ATP production via oxidative phosphorylation. Complex I inhibition by metformin activates AMPK. The increase in AMPK observed with metformin occurs because decreased Complex I activity leads to an overall reduction in ATP production by oxidative phosphorylation, thereby increasing the cellular AMP/ATP and ADP/ATP ratios. AMP or ADP binding to AMPK makes the kinase more susceptible to stimulatory phosphorylation by its upstream kinases and inhibits its dephosphorylation (245).

Metformin has been shown to inhibit the production of the pro-inflammatory cytokine IL-1β and increase levels of the anti-inflammatory cytokine IL-10. While the decrease in AMPK levels observed following treatment of T cell blasts with ST0702 (100 μM, Figure 3.6) might suggest that ST0702 would not have anti-psoriatic activity, it is worth noting that these effects have been proven to be independent of AMPK activation, and have been mimicked by the complex I inhibitor rotenone (245). Metformin has also been shown to inhibit HaCaT cell proliferation and this is thought to be linked to elevated levels of ROS production, which can induce tumour cell apoptosis (246).

As additional supporting evidence for a possible activity for ST0702 on cellular metabolism, ST0702 (100 μM) had a more pronounced effect on the inhibition of proliferation depending on the growth phases of the cells (as evidenced in the T cell blast experiments, Figures 3.20-3.25).

A number of experiments were carried out using a Seahorse XF Analyser. The Seahorse measures the oxygen consumption rate (OCR) and extracellular acidification rate (ECAR) of live cells in a multi-well plate. The OCR is an indicator of mitochondrial respiration, whilst the ECAR is largely the result of glycolysis.

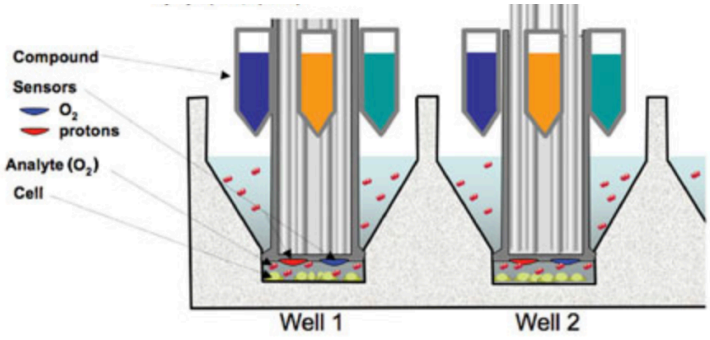

Figure 3-28: Diagram of sensors in seahorse apparatus.

3.2.11.1 *IL-2 Experiments using Seahorse XF Analyser*

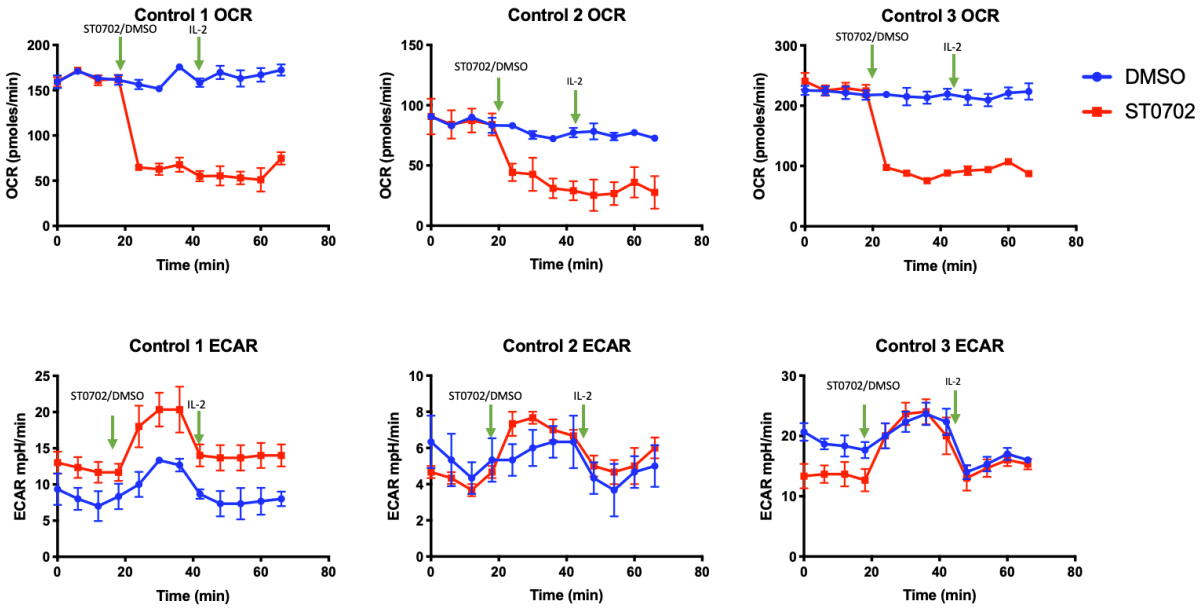

Figure 3-29: Seahorse experiments on activated PBMCs stimulated with IL-2.
PBMCs were plated in a 24 well plate at 5 ×10^5 cells/well. The cells were then activated by treating with aCD3/CD28 for 72 h. The cells were then counted and re-plated onto Seahorse XF24 plates at a density of 2.5 ×10^5 cells/well. Basal OCR readings were obtained and 100 µM ST0702 or DMSO was injected after 18 min. 20 ng/mL IL-2 was injected after 42 min. The OCR and ECAR was measured in triplicate for three donors and the results are expressed as mean ± SEM.

The first experiment carried out using the Seahorse XF Analyser was a simple experiment, which measured the change to the basal OCR of activated PBMCs following the addition of ST0702 (100 µM). A decrease in OCR was observed in all of the donors, and a corresponding increase in ECAR was observed in two of the three donors tested (Figure 3.29). Approximately

20 min after the addition of ST0702, IL-2 was added. IL-2 stimulates the rapid proliferation of the T cells, and the purpose of adding it was to see if this had an effect on the OCR. Interestingly, there was no difference in the OCR following the addition of IL-2. This was somewhat unexpected, as it is known that actively proliferating T cells usually switch to glycolysis, but perhaps the timeframe here wasn't long enough to see this switch occur. There was a slight increase observed in the ECAR following the addition of ST0702, but no increase was observed following IL-2 addition.

3.2.11.2 *Mitochondrial Stress measured using Seahorse XF Analyser*

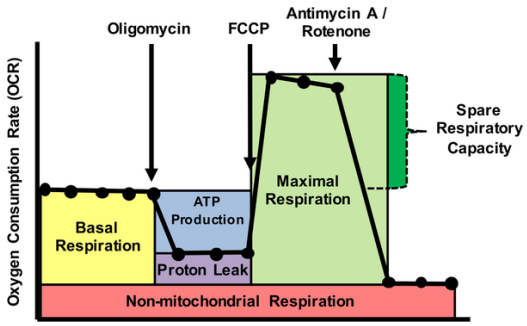

Compound	Target	Effect on OCR
Oligomycin	ATP synthase inhibitor	Decrease
FCCP	Mitochondrial uncoupler	Increase
Rotenone/Antimycin A	Complex I/III inhibitor	Decrease

Figure 3-30: Overview of Seahorse Mito-Stress test

The Mito Stress Test was also carried out using the Seahorse XF Analyser. This test can give an indication of mitochondrial function by providing information on basal respiration levels, ATP-dependent respiration, proton leakage and maximal respiration. From the results observed, it is clear that the mitochondrial respiration of the T cell blasts was compromised by the addition of 100 µM ST0702 (Figure 3.31).

Basal respiration is very dependent on the environment of the cells and can alter dramatically in response to ATP demand or the presence or absence of different substrates (247). It was seen to decrease following the addition of 100 µM ST0702. The addition of the ATP synthase inhibitor oligomycin and the subsequent decrease in respiration can allow for the determination of the levels of ATP-dependent respiration. Oligomycin shifts the entire ATP production to glycolysis. The coupling efficiency of the cells can be determined from the change in basal respiration rate on addition of oligomycin. In the experiments, the blasts treated with 100 µM ST0702 had a lower OCR following addition of oligomycin than the DMSO treated cells, indicating some level of mitochondrial dysfunction. Maximal respiratory capacity was

estimated by an FCCP -stimulated respiration and the observed decrease is a very strong indicator of potential mitochondrial dysfunction (247).

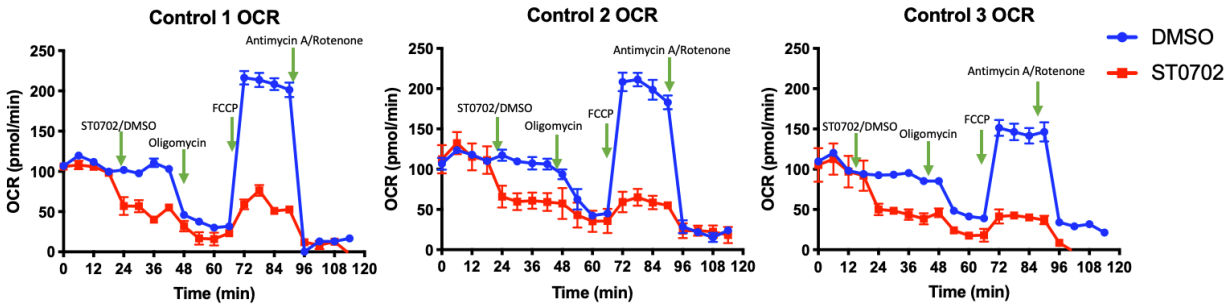

Figure 3-31: Mito-stress Seahorse experiments on T cell blasts.
PBMCs (5 × 10^5 cells/well in a 24-well plate) were seeded and stimulated with aCD3/CD28 beads for 72 h before adding two successive rounds of IL-2 (20 ng/ml) for 48 h. The cells were then counted and re-plated onto Seahorse XF24 plates at a density of 2.5 ×10^5 cells/well. Basal OCR readings were obtained and 100 µM ST0702 or DMSO was injected after 18 min. Oligomycin, FCCP, Antimycin A/Rotenone were injected sequentially. The OCR and ECAR was measured in triplicate for three donors and the results are expressed as mean ± SEM.

3.2.11.3 *Seahorse Metabolism: ST0702 Concentration Response*

The next experiment involved the testing of different concentrations of ST0702 (10, 25, 50 and 100 µM). Basal respiration rates of T cell blasts was measured, and the change in OCR following the addition of different concentrations of ST0702 was measured (Figure 3.32). Concentrations as low as 10 µM ST0702 were seen to decrease the OCR relative to the vehicle control (DMSO), with a good concentration dependent response observed, especially when the results from each of the three donors were combined. An increase in ECAR was also observed following the addition of ST0702, with the magnitude of the effect positively correlated with the concentration of ST0702 added.

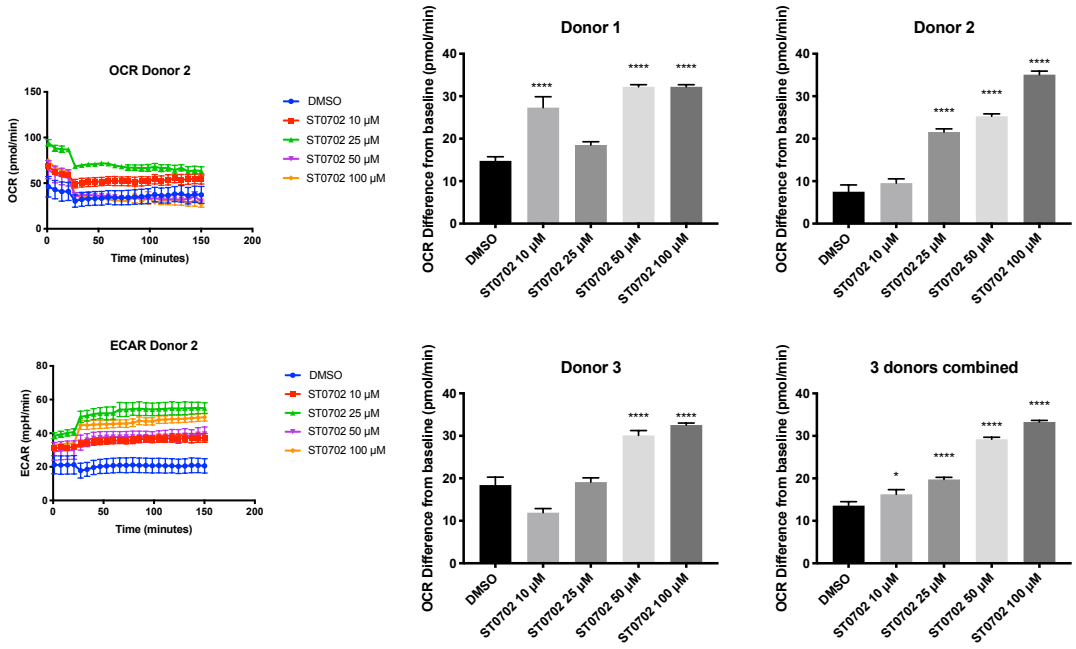

Figure 3-32: Seahorse experiment on T cell blasts: varying concentrations of ST0702. PBMCs (5 × 10^5 cells/well in a 24-well plate) were seeded and stimulated with aCD3/CD28 beads for 72 h before adding two successive rounds of IL-2 (20 ng/ml) for 48 h. The cells were then counted and re-plated onto Seahorse XF96 plates at a density of 2.5 ×10^5 cells/well. Basal OCR readings were obtained and compound or DMSO was injected after 24 min. The OCR and ECAR was measured in triplicate for three donors and the results are expressed as mean ± SEM.

3.2.11.4 *Seahorse experiments using HuT78 cells*

A similar experiment to that carried out in the T cell blasts in the previous section was carried out in the HuT78 cell line. Very similar results were observed for ST0702, with a decrease occurring in the OCR following the addition of 100, 50 and 25 µM ST0702 (Figure 3.33). ISAL was also tested, and mimicked, if not slightly exceeded the activity of ST0702, with slightly greater activity at 100, 50 and 25 µM. There was a sudden increase in ECAR following the addition of the compounds, but this returned to basal levels after several minutes, which differs from the T cell blasts, where following the rise in ECAR, the level remained steady. This was an unusual result, but the reduction in ECAR also occurred in the vehicle-treated cells (DMSO) so perhaps the rate of glycolysis reduced due to environmental factors in the media (substrate availability, pH, etc).

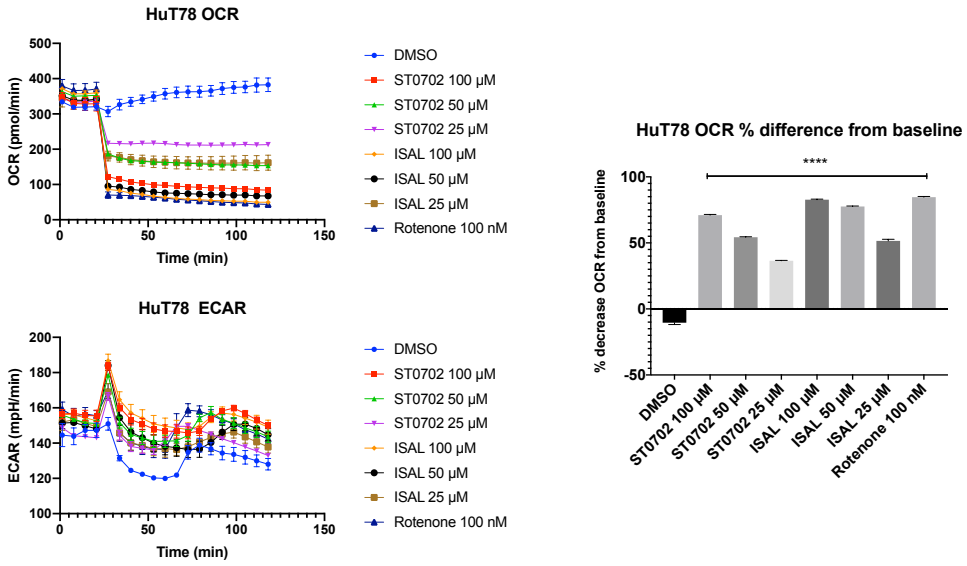

Figure 3-33: Seahorse results for compounds tested in HuT78 cells.
HuT78 cells were plated at a density of 1 ×10^5 cells/well. Basal OCR readings were obtained and compound or DMSO was injected after 24 min. The OCR and ECAR was measured in quadruplicate and the results are expressed as mean ± SEM.

3.2.11.5 *Seahorse experiments using HaCaT cells*

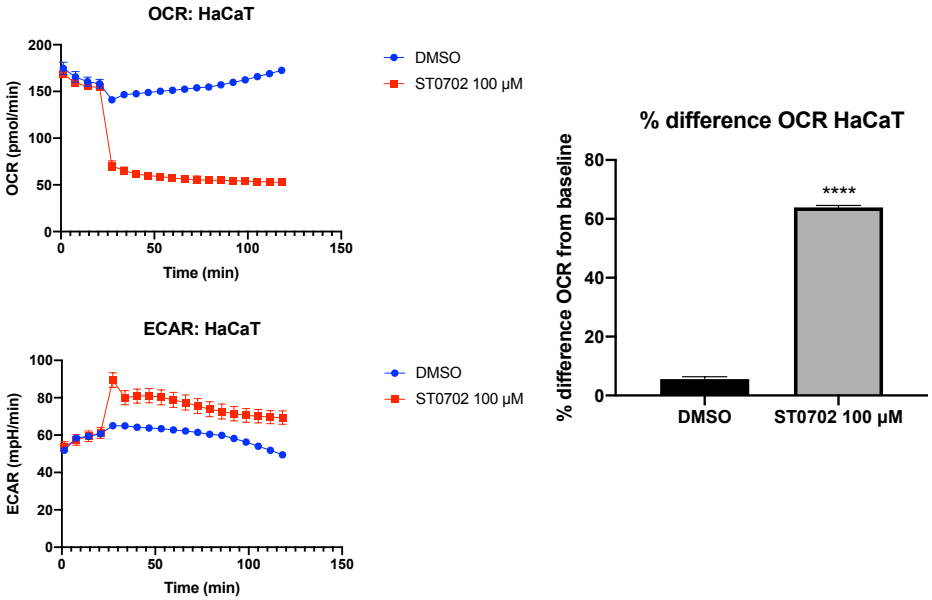

Figure 3-34: Seahorse results for compounds tested in HaCaT cells.
HaCaT cells were plated at a density of 1 ×10^4 cells/well and left to adhere for 48 h. Basal OCR readings were obtained and compound or DMSO was injected after 24 min. The OCR and ECAR was measured in quadruplicate and the results are expressed as mean ± SEM.

To verify if the effect of ST0702 on OXPHOS and glycolysis was specific to T cell metabolism the HaCaT keratinocyte cell line was tested (Figure 3.34). ST0702 was shown to decrease the OCR and increase the ECAR for these cells, with similar activity to that observed in the T cell blasts and the HuT78 cells.

3.2.11.6 *Alternative Viability Measure (Acid Phosphatase)*

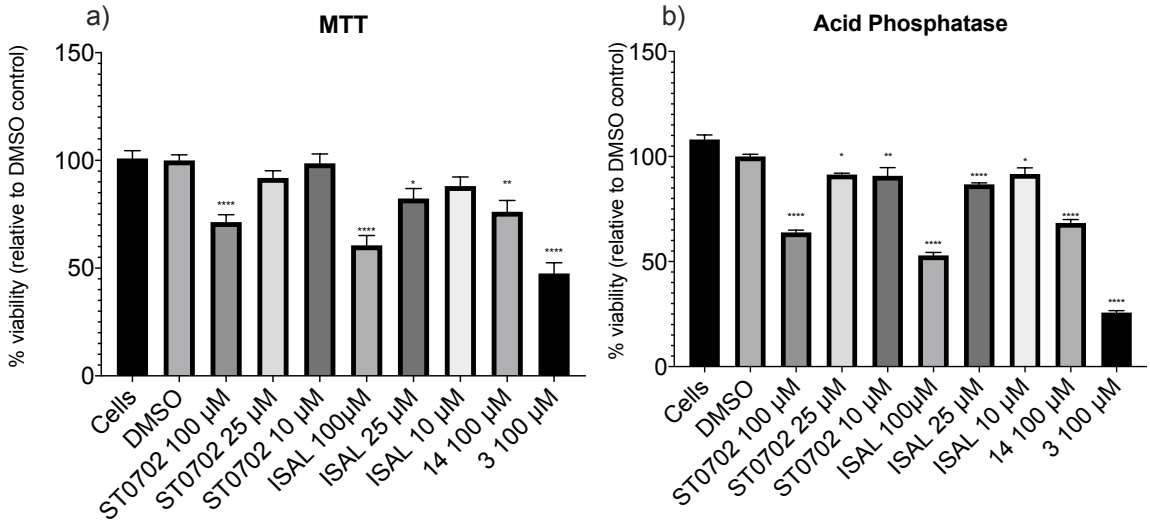

Figure 3-35: Results from a) MTT assay and b) Acid Phosphatase assay on HuT78 cells. HuT78 cells were plated at 1 × 10^4 cells per well of a 96-well plate. The cells were treated with 100 µM, 25 µM or 10 µM compound and incubated for 48 h. After this time, MTT and acid phosphatase assays were carried out. Results for each concentration are expressed as mean ± SEM of three experiments performed in triplicate.

With the discovery of the effect on ST0702 and related compounds on the OCR, it was necessary to consider the methods that were being used to determine the effect of these compounds. The primary viability assay that had been used was the MTT assay. The MTT is widely used to measure cell proliferation and to screen for anticancer drugs. It is based on the reduction of the tetrazolium salt, MTT, and it has been shown that cellular reduction of MTT is primarily a function of the mitochondria (248). Since it had been suggested that the compounds can affect the mitochondrial activity of the cells, there was a need for a method that examines proliferation that is not dependent on metabolic activity. The acid phosphatase assay was therefore used as an additional measure of antiproliferative activity. The results for the acid phosphatase assay mirrored that of the MTT assay, with even a slightly greater effect seen for some compounds (Figure 3.35). This serves to validate that the results of the MTT assays were due to the true antiproliferative effects of the compounds, and not simply the effect of the compounds on mitochondrial activity.

3.2.12 **Investigation into antiproliferative activity of Complex I inhibitor rotenone**

Rotenone is an organic pesticide that is a known complex I inhibitor and has been widely used to study the mitochondrial-induced oxidative stress, adaptive responsive pathways and signalling mechanisms. Rotenone has been shown to inhibit microtubule polymerisation and to arrest cell cycle at mitosis (249). Systemic administration of rotenone in experimental rats has been shown to induce degeneration of dopaminergic neurons and produces symptoms that are similar to those observed in Parkinson's disease. It has been suggested that microtubule depolymerisation by rotenone may cause the degeneration of dopaminergic neurons in the substantia nigra. The microtubule stabilising agent, paclitaxel provides protective effects against rotenone-induced toxicity whereas microtubule depolymerisation agents such as colchicine have similar effects to rotenone on dopaminergic neurons (250). Rotenone has been shown to inhibit the proliferation of HeLa and MCF-7 cells, and within its effective inhibitory concentration range it depolymerised microtubules of both cell types (249).

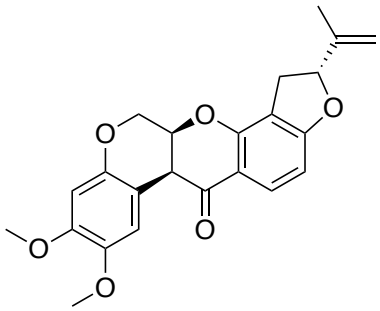

Figure 3-36: Structure of rotenone

3.2.12.1 *Antiproliferative effect of rotenone and oligomycin on T cell blasts*

The antiproliferative effect of the complex I inhibitor rotenone and the ATP synthase inhibitor oligomycin on T cell blasts was examined. Both rotenone (100 nM and 500 nM) and oligomycin (0.05 μM and 0.5 μM) caused an approximately 50% reduction in proliferation relative to the vehicle control. The fact that the effect was 50% indicates a cytostatic effect, whereby both compounds are not causing apoptosis, but rather the ETC inhibition is leading to a cessation of proliferation. However, rotenone has been shown to induce apoptosis, which is thought to be linked to its production of mitochondrial ROS (222).

Previous studies have shown that rotenone decreases the proliferation of naive CD8+ T cells after incubation with anti-CD3 and CD28 in a dose dependent manner and does not cause a decrease in initial cell survival (251). Additionally, treatment of murine splenic CD4+ T cells with rotenone has been shown to attenuate T cell activation potential upon anti-CD3 and anti-CD28 stimulation (252).

Oligomycin has also been shown to inhibit the proliferation of activated T cells (217), and appeared to have the most activity immediately following activation, and before the activated T cells made the switch to aerobic glycolysis.

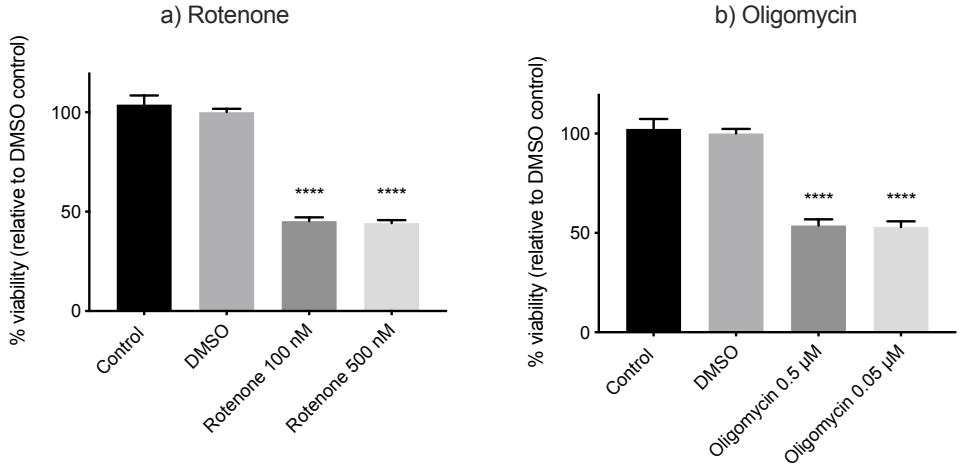

Figure 3-37: Results from MTT assay on T cell blasts testing a) rotenone and b) oligomycin. PBMCs were treated with anti-CD3/CD28 beads for 96 h and then with two consecutive IL-2 cycles for 48 h each. Rotenone or oligomycin were added for the last 24 h. The experiment was carried out in triplicate with four different donors. Data is expressed as mean ± SEM.

3.2.12.2 *STAT3 inhibitory activity of rotenone*

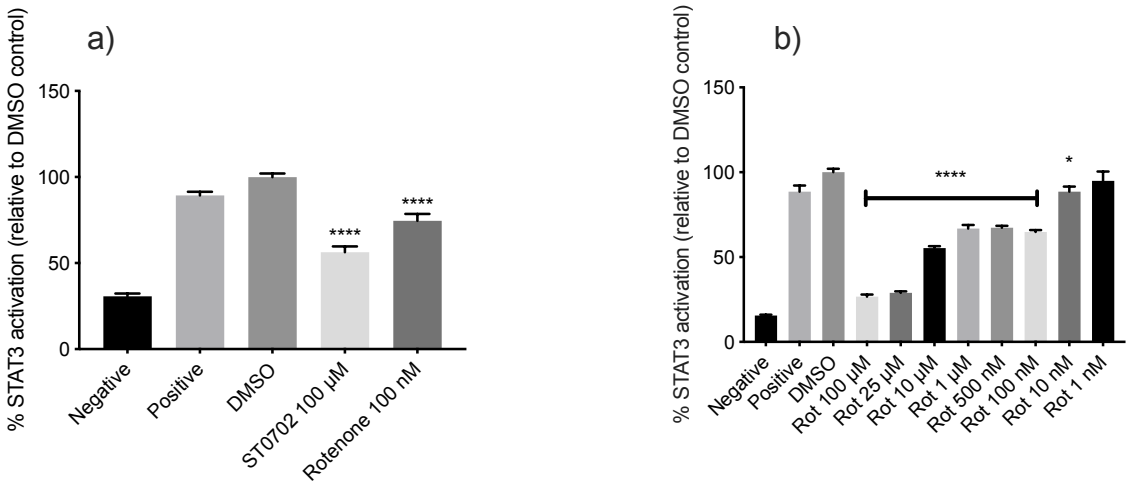

Figure 3-38: a) Inhibition of STAT3 activation in HEK-Blue IL-6 cells treated with rotenone and ST0702 and b) concentration response curve for inhibition of STAT3 activation in HEK-Blue IL-6 cells treated with rotenone.

HEK-Blue IL-6 cells were plated at 5 × 10^4 cells per well of a 96-well plate. Cells were treated with ST0702 (100 µM), rotenone (100nM) or DMSO (vehicle). After 30 min incubation, the cells were stimulated with 1 ng/mL IL-6. After 24 h Quantiblue Reagent was added and SEAP levels were determined. Data is expressed as mean ± SEM of three independent experiments.

To determine if the STAT3 inhibitory effects of 100 μM ST0702 could be attributable to ETC inhibition it was decided to investigate whether a Complex I inhibitor such as rotenone would cause inhibition of STAT3 activation. Rotenone was tested in the HEK-Blue STAT3 reporter assay and it was found to inhibit STAT3 activation at concentrations as low as 10 nM (Figure 3.38).

Recently, an experiment was carried out to determine whether rotenone induced oxidative stress can regulate mitochondrial STAT3 (253). Mitochondrial STAT3 (mSTAT3) is STAT3 that is present in the mitochondria and can regulate its function independent of transcription. mSTAT3 has been shown to confer a protective role during cellular stress, and targeting STAT3 has been shown to result in the dysregulation of mitochondrial activity, which is associated with excessive ROS production, reduced mitochondrial membrane potential and enhanced apoptosis (254, 255). mSTAT3 appears to be more dependent on phosphorylation of STAT3 on Ser727 (256). Ser727 phosphorylation is activated by the mitogen-activated protein kinase (MAPK) pathway (257). The study found that rotenone treatment enhanced phosphorylation of STAT3 on Ser727 and its mitochondrial localisation, and treatment with N-acetylcysteine (NAC), a ROS scavenger, decreased phosphorylation and mSTAT3 levels. This paper also noted that a decrease in the phosphorylation of STAT3 at Tyr705 was observed within 6 h of rotenone treatment, which aligns with the effects observed in this project. The paper reported a negative correlation between pSer727 and pTyr705 when HeLa or HEK-293 cells were treated with 0.5 μM rotenone. Reduced Ser727 phosphorylation of STAT3 has been associated with a concomitant increase in Tyr705 phosphorylation and cell proliferation of glioma cells (258). Several other studies have found STAT3 inhibitors that are able to inhibit OXPHOS by indirectly inhibiting complex I and II of the ETC via their action on mSTAT3 (256, 257).

In the HEK IL-6 reporter assay, it is measuring the activation of nuclear STAT3, which is activated by IL-6 and Tyr-705 phosphorylation, so the assay is giving no indication as to the effect that rotenone is having on mSTAT3 levels in the mitochondria of these cells.

3.2.12.3 *HuT78 and T cell Blasts MTT: Rotenone*

Treatment with rotenone (1 nM-10 μM) was shown to inhibit the proliferation of the constitutively activated T cell line, HuT78 (Figure 3.39). Rotenone (100 nM) was shown to have greater antiproliferative activity than ST0702. In these assays, ST0702 at 100 μM inhibited proliferation by around 30%, similar to results observed previously. Rotenone, when used at 100 nM caused a reduction in viability of almost 60%. At concentrations of 500 nM and higher, a plateau effect is observed, with antiproliferative activity not exceeding 75%.

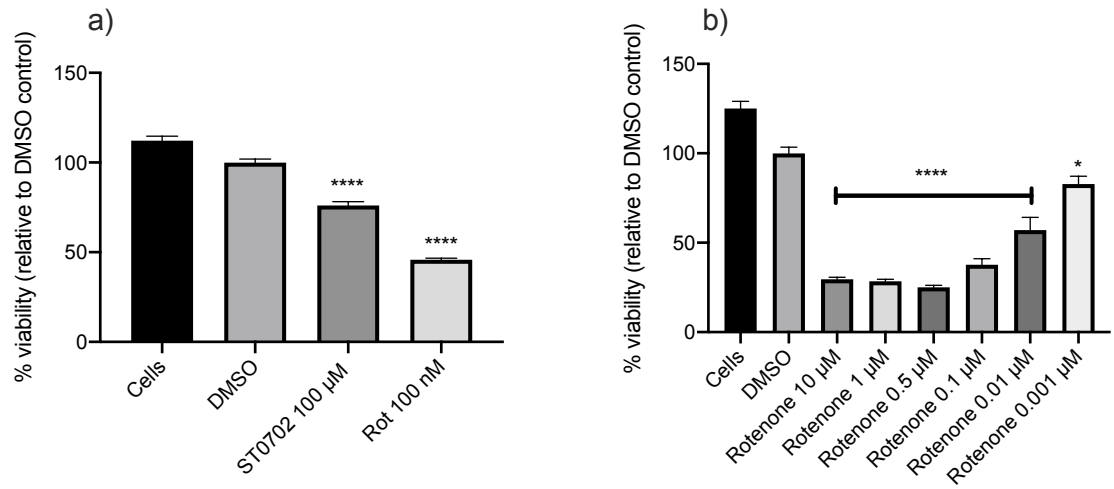

Figure 3-39: a) Antiproliferative effect of rotenone and ST0702 on HuT78 cells and b) concentration response curve for antiproliferative effect in HuT78 cells treated with rotenone. HuT78 cells were plated in 96 well plates at 1 × 10^4 cells per well of a 96-well plate. The cells were treated with inhibitors and incubated for 48 h. After this time, MTT was carried out. Results for each concentration are expressed as mean ± SEM of four independent experiments.

Experiments were carried out to examine whether the antiproliferative activity of rotenone on T cell blasts is dependent on the timepoint at which the rotenone was added (Figure 3.40). As described in Section 3.2.9, a number of experiments were carried out with PBMCs, in which the naïve T cells present had just been activated, or had been activated and stimulated with IL-2 to cause them to proliferate. The PBMCs were activated with aCD3/CD28 for 72 h, after which they were stimulated with IL-2 for 48 h, and some were then stimulated with another round of IL-2 for a further 48 h. The compounds were added at different stages of the expansion process. The different protocols were outlined previously in Figure 3.19. Whether the compound was added prior to the addition of IL-2 or 24 h post IL-2 stimulation appeared to make a difference as to the effectiveness of the compounds, with the compounds having activity at all points (except on non-activated or non-IL-2 stimulated cells) but appearing to have the greatest effect when added 24 h post the IL-2 stimulation (Protocols C and E). The effectiveness of rotenone did not depend on the time at which the compound was added, with 100 nM rotenone causing an approximate reduction of 50%. However, this lack of a differential effect could be due to the fact that rotenone is cytostatic, halting proliferation but not killing the cells, so the maximum achievable effect within this timeframe would be 50%, that is, one population doubling did not take place.

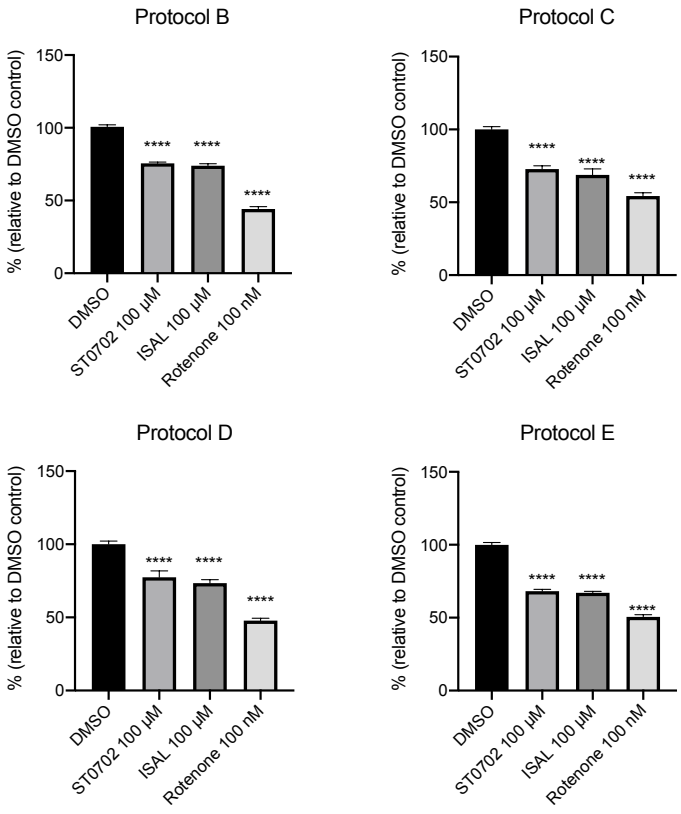

Figure 3-40: Antiproliferative activity of rotenone on PBMCs undergoing protocol B, C, D or E.

For protocols B and C, PBMCs (5 × 10^5 cells/well in a 24-well plate) were seeded and stimulated with aCD3/CD28 beads for 72 h before adding IL-2 (20 ng/ml) and being incubated for 48 h. MTT was then carried out. For Protocol B, the cells were pre-treated for 30 min prior to the addition of IL-2 and for Protocol C, the compounds were added for the last 24 h of treatment. For protocols D and E, PBMCs (5 × 10^5 cells/well in a 24-well plate) were seeded and stimulated with aCD3/CD28 beads for 72 h before adding two successive rounds of IL-2 (20 ng/ml) for 48 h. MTT was then carried out. For Protocol D, the cells were pre-treated for 30 min prior to the addition of the second round of IL-2 and for Protocol E, the compounds were added for the last 24 h of treatment. Results for each protocol is expressed as mean ± SEM of three different donors.

3.2.13 **Succinate, Pyruvate, Citrate and Aspartate Supplementation**

ST0702 (100 µM) has shown itself to be a STAT3 inhibitor, an inhibitor of cell proliferation and an inhibitor of the mitochondrial electron transport chain (ETC). In an attempt to link the effect of the compound on the ETC to its antiproliferative effects and STAT3 inhibition a number of rescue experiments were carried out with substrates for the ETC. The hypothesis

being explored was that the proliferation and STAT3 inhibitory effects of ST0702 were occurring as a result of the ETC inhibition. Were this the case, rescuing the inhibitory effects on the ETC should also reduce the antiproliferative effect and STAT3 inhibitory activity of the compound.

Inhibition of the mitochondrial ETC is known to suppress cell proliferation. Human cells in culture arrest upon inhibition of Complex I (259, 260) or III (261). Numerous reasons have been suggested for the ETC effect on proliferation, such as changes in ATP or ROS levels but the exact reason remains to be understood.

3.2.13.1 *Rescue experiments with succinate*

The first ETC substrate tested was succinate, which allows for the bypass of Complex I. Succinate is processed in Complex II of the ETC. It is an intermediate in the TCA cycle that can interact directly with the ETC, which enables a 'shortcut' route to ATP production via the ETC. Succinate is converted to fumarate in the TCA cycle by complex II (succinate dehydrogenase) of the ETC on the mitochondrial inner membrane. The remainder of the TCA cycle is driven by soluble mitochondrial enzymes, and results in the production of NADH which interacts with Complex I of the ETC. This drives the ETC sequentially from Complex I to Coenzyme Q, through to culmination at complex IV, missing Complex II. Succinate misses complex I and causes the ETC to run sequentially from Complex IV. Complex I of the ETC is particularly vulnerable to dysfunction, so in bypassing Complex I, succinate can provide a potential fuel source for dysfunctional mitochondria and produce ATP (262).

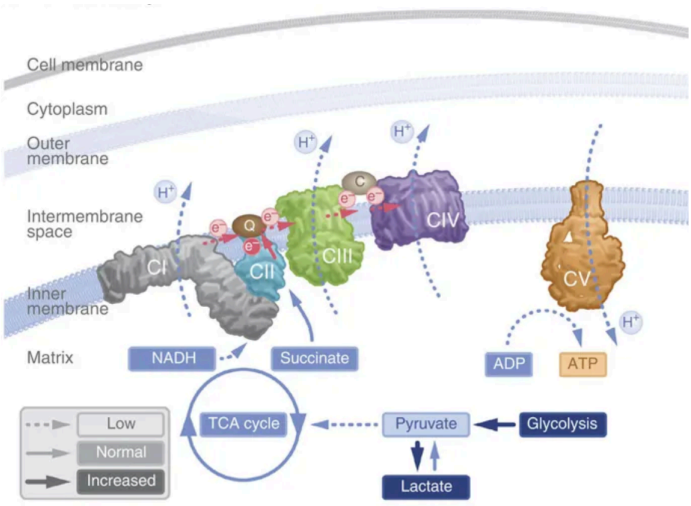

Figure 3-41: Occurrences within the ETC following Complex I inhibition (263).
Dysfunction in mitochondrial complex I reduces electron flow through the respiratory chain, shifts metabolism towards glycolysis, induces lactate accumulation and limits ATP production.

It was hypothesised that if ST0702 is an inhibitor of Complex I of the ETC then the supplementation of succinate should reverse its effects on proliferation. Succinate supplementation should allow for the production of ATP despite the inhibition of Complex I. Succinate is not cell membrane-permeable and exogenously given succinate has limited uptake into cells (263). Diethyl succinate was used as the source of succinate for these experiments, and this has been used as a cell permeable source of succinate by other researchers (264).

Rescue experiments were carried out with T cell blasts, HuT78 cells and HEK IL-6 cells (Figure 3.42). For the T cell blasts and the HuT78s, the supplementation of the media with succinate did not rescue the effects of ST0702 on proliferation, with the inhibition of proliferation observed with ST0702 being of the same magnitude as cells with no succinate supplementation. The effect of succinate addition to T cell blasts treated with ST0702 was also studied using the seahorse. The addition of succinate did not appear to have an effect on the OCR.

This suggests one of a number of scenarios, the first being that the effect of ST0702 on proliferation of HuT78 and T cell blasts is not caused by ETC inhibition at Complex I. If the compound was inhibiting Complex I and this was inhibiting proliferation then succinate addition would be expected to reduce the impact of this ETC inhibition on proliferation. Alternatively, ST0702 (100 μM) might be inhibiting other complexes on the ETC, such as Complex III, in which case succinate supplementation would not be expected to have any effect at rescuing the effect on proliferation.

Finally, that there could be an issue with the cell permeability of succinate and its poor uptake into T cell blasts. Diethyl succinate was used in these experiments, and papers have noted it to be the more cell permeable form but perhaps an investigation into the permeability of succinate might give different results. Cell permeable succinate prodrugs have been developed, and these might be more suitable for use in future experiments (263).

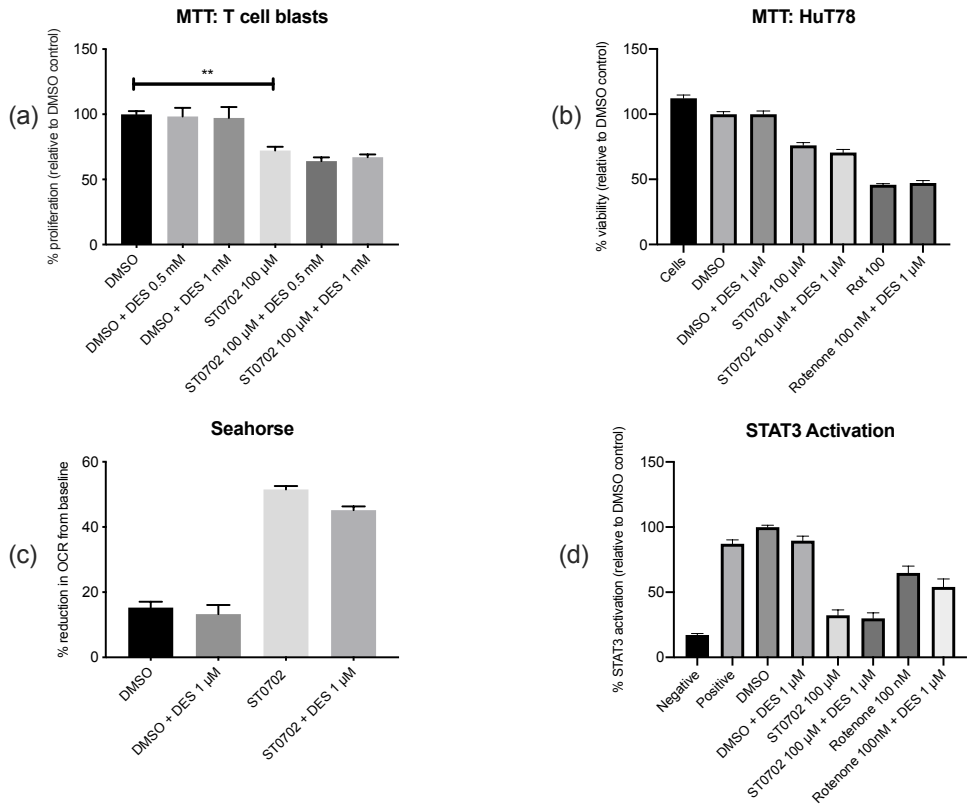

Figure 3-42: Effect of succinate supplementation on (a) proliferation of T cell blasts (b) proliferation of HuT78 cells (c) OCR and (d) STAT3 activation.

(a) PBMCs (5 × 10^5 cells/well) were seeded and stimulated with aCD3/CD28 beads for 72 h before adding two successive rounds of IL-2 (20 ng/ml) for 48 h. Cells were then treated with either DMSO or ST0702 100 µM in combination with 0.5 mM or 1 mM diethyl succinate (DES) for the last 24 h of stimulation. MTT was then carried out. Results are expressed as mean ± SEM for three different donors. (b) HuT78 cells were plated at 1 × 10^4 cells per well of a 96-well plate. The cells were then treated with either DMSO, ST0702 100 µM or rotenone 100 nM in combination with 1 mM diethyl succinate and incubated for 48 h. MTT was then carried out. (c) PBMCs were seeded and stimulated with aCD3/CD28 beads for 72 h before adding two successive rounds of IL-2 (20 ng/ml) for 48 h. The cells were then plated onto Seahorse XF96 plates at a density of 2.5 ×10^5 cells/well. Basal OCR readings were obtained and compound (DMSO or ST0702 100 µM) in combination with 1 mM diethyl succinate was injected after 24 min. The OCR was measured in triplicate for three donors and the results are expressed as the mean of % reduction in OCR from baseline ± SEM. (d) HEK-Blue IL-6 cells were plated at 5 × 10^4 cells per well of a 96-well plate. The cells were then treated with either DMSO, ST0702 100 µM or rotenone 100 nM in combination with 1 mM diethyl succinate. After 30 min incubation, the cells were stimulated with 1 ng/mL IL-6. After 24 h SEAP levels were determined. All results are expressed as mean ± SEM.

3.2.13.2 *Rescue experiments with pyruvate*

Upon Complex I inhibition, electrons from NADH cannot be transferred to molecular oxygen as an electron acceptor to form water and regenerate NAD+. A potential reason as to why the rescue effect of succinate on proliferation of HuT78 and T cell blasts was not observed could be because the NAD+/NADH ratio is still reduced, even though ATP is being produced and oxygen is being consumed.

Studies with the Complex I inhibitor metformin have shown that the choice of culture media can alter the sensitivity of the cell line to metformin, with evidence of cells cultured in RPMI being more sensitive to the antiproliferative effect of metformin than cells cultured in DMEM. An interesting difference in the two media is the presence of 1 mM pyruvate in DMEM, and its absence in RPMI, and cells cultured in DMEM without pyruvate exhibited increased sensitivity to metformin. This suggests a critical role of pyruvate as an environmental factor that can alter sensitivity to Complex I inhibitors (265).

In the presence of exogenous pyruvate, cells can regenerate NAD+ via the conversion of pyruvate to lactate. Therefore, when excess pyruvate is available in the environment, cells can utilize this pathway to maintain the NAD+/NADH ratio in the absence of Complex I activity.

Based on this hypothesis, the next experiment involved supplementing the cell growth media with pyruvate to investigate if the pyruvate could restore the NAD+/NADH ratio as measured by a reduction of the antiproliferative effect of the compound. The results of this experiment show that pyruvate supplementation does not appear to have any rescuing effect on the antiproliferative activity of rotenone on T cell blasts, implying that the imbalance in the NAD+/NADH ratio due to the inhibition of Complex I is not the cause of the antiproliferative effect (Figure 3.43).

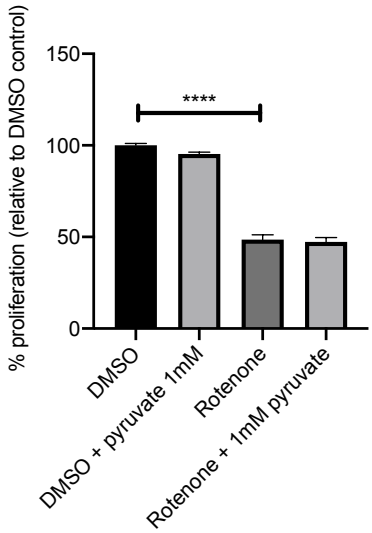

Figure 3-43: Antiproliferative Effect of rotenone in combination with pyruvate in T cell blasts. PBMCs (5 × 10^5 cells/well) were seeded and stimulated with aCD3/CD28 beads for 72 h before adding two successive rounds of IL-2 (20 ng/ml) for 48 h. Cells were then treated with either DMSO or rotenone 100 nM in combination with 1 mM pyruvate (as sodium pyruvate, stock: 100 mM in sterile H_2O) for the last 24 h of stimulation. MTT was then carried out. Data is presented as mean ± SEM of three donors.

3.2.13.3 *Rescue experiments with aspartate*

Supplementation with pyruvate is known to allow cells that are lacking in ETC function to proliferate. It has been shown that one of the key functions of the ETC for cell proliferation is to enable the synthesis of aspartate, a proteogenic amino acid that is a precursor in purine and pyrimidine synthesis (212). Complex I can support proliferation through NAD+ regeneration to maintain cellular NAD+/NADH balance and to allow aspartate synthesis (265). Supplementation with aspartate can also reverse the antiproliferative effects of ETC inhibition, and it has been suggested that pyruvate supplementation induces aspartate synthesis and that is the cause of the effect on proliferation. The addition of aspartate does not restore the cellular NAD+/NADH ratio, but rather the maintenance of the NAD+/NADH balance is required for proliferation in order to support de novo aspartate biosynthesis (212).

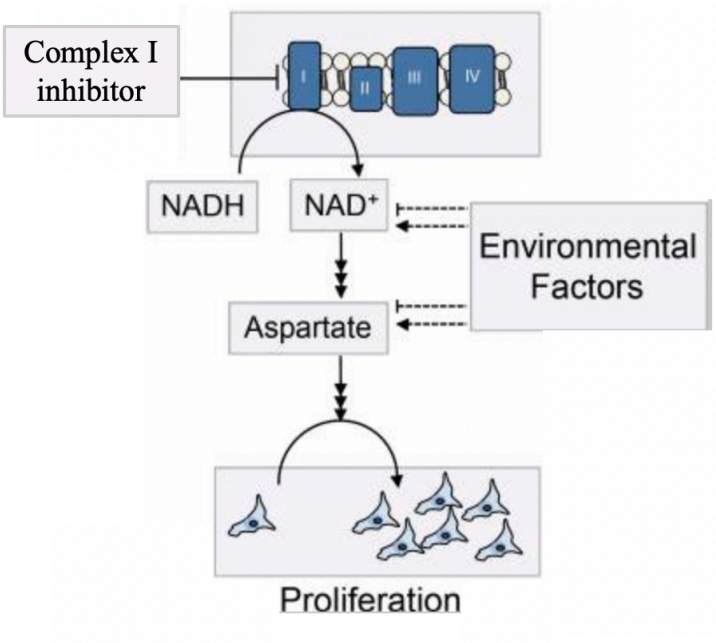

Figure 3-44: Complex I inhibitors can affect the NAD+/NADH balance and halt the synthesis of aspartate, thereby causing a reduction in proliferation. Modified from (265).

When T cell blasts were supplemented with aspartate there was a large reduction in the viability of the cells (Figure 3.44). This could be due to the fact that the source of aspartate being used was L-aspartic acid, in a solution that had been brought to pH 7.4 with 1M NaOH. However, the addition of the L-aspartic acid might still be affecting the pH of the cellular environment. As a result of the reduction in viability that occurred following the addition of aspartate it was difficult to ascertain whether the aspartate supplementation was having an effect on the antiproliferative activity of the compounds. For this reason, the data was presented in two ways; the first graph where the % values are expressed relative to the DMSO control (Figure 3.44a), and the second (adjusted) graph where the values are expressed relative to either the DMSO control, or the DMSO plus aspartate control, as appropriate (Figure 3.44b). With this adjusted graph it does appear like aspartate supplementation might be having a small 'rescuing' effect on the antiproliferative activity of ST0702, ISAL and rotenone, but this was not conclusive.

This reduction in cell viability following aspartate supplementation was not observed in HuT78 cells, and there was no change in antiproliferative activity of ST0702 when cells were treated in aspartate supplemented media. Similarly, aspartate supplementation did not reduce the STAT3 inhibitory effect of ST0702.

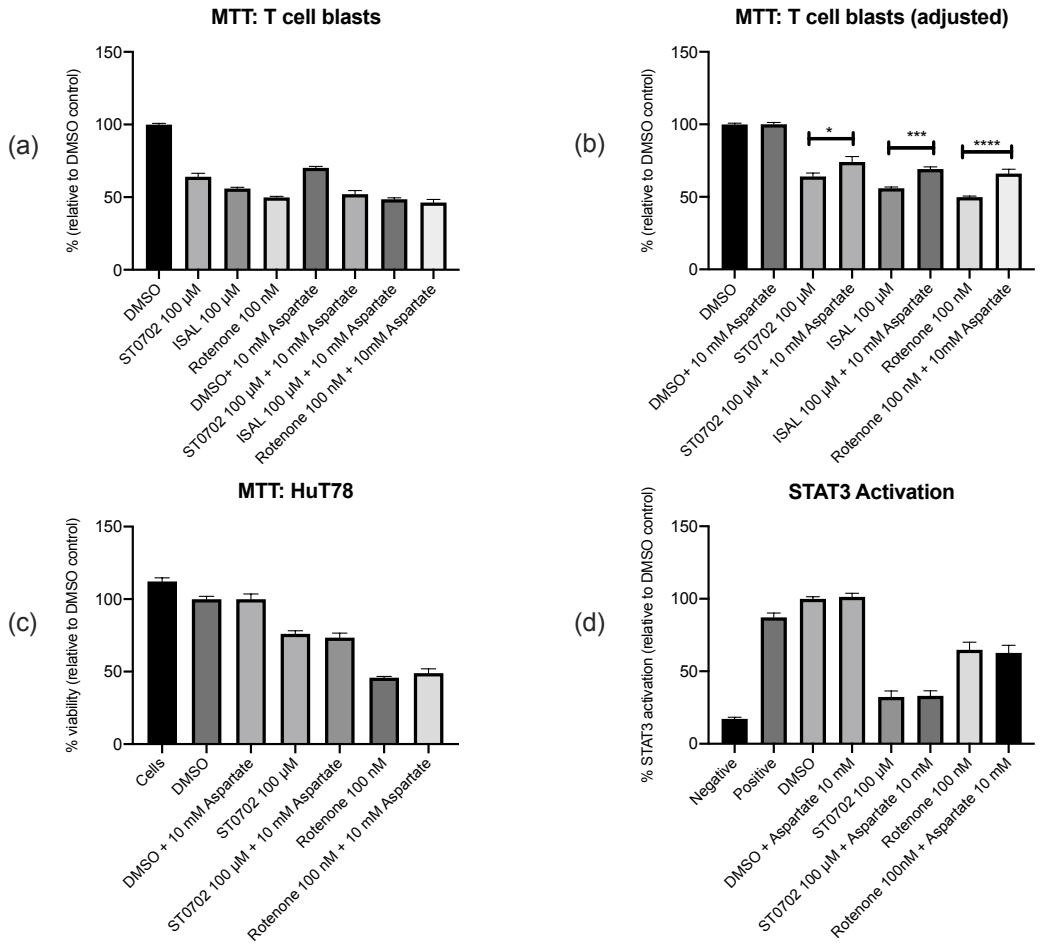

Figure 3-45: Effect of aspartate supplementation on (a) proliferation of T cell blasts (b) proliferation of T cell blasts (adjusted) (c) proliferation of HuT78 cells and (d) STAT3 activation.

(a) PBMCs (5 × 10^5 cells/well) were seeded and stimulated with aCD3/CD28 beads for 72 h before adding two successive rounds of IL-2 (20 ng/ml) for 48 h. Cells were then treated with either DMSO ST0702 100 µM, ISAL 100 µM or rotenone 100 nM in combination with 10 mM aspartate for the last 24 h of stimulation. MTT was then carried out. Results are expressed as mean ± SEM for three different donors. (b) The same results in (a), adjusted for the reduction in viability following treatment with aspartate.(c) HuT78 cells were plated at 1 × 10^4 cells per well of a 96-well plate. The cells were then treated with either DMSO ST0702 100 µM, ISAL 100 µM or rotenone 100 nM in combination with 10 mM aspartate and incubated for 48 h. MTT was then carried out. (d) HEK-Blue IL-6 cells were plated at 5 × 10^4 cells per well of a 96-well plate. Cells were then treated with either DMSO ST0702 100 µM, ISAL 100 µM or rotenone 100 nM in combination with 10 mM aspartate. After 30 min incubation, the cells were stimulated with 1 ng/mL IL-6. After 24 h SEAP levels were determined. All results are expressed as mean ± SEM.

3.2.13.4 *Rescue experiments with citrate*

Citrate is an intermediate in the TCA cycle. Citrate synthase catalyses the condensation of oxaloacetate with acetyl CoA to form citrate. Citrate then acts as a substrate for aconitase and is converted to aconitic acid. The TCA cycle ends with the regeneration of oxaloacetate.

Citrate is also a required carbon precursor for de novo fatty acid and membrane lipid synthesis. Fatty acids are synthesised in the cytoplasm from acetyl CoA. Acetyl CoA is generated from pyruvate by the action of pyruvate dehydrogenase and by β-oxidation of fatty acids in the mitochondria. For fatty acid biosynthesis, acetyl CoA has to be transported from the mitochondria to the cytoplasm. This transport is done via a shuttle system called the citrate shuttle. Oxaloacetate reacts with acetyl CoA to give citrate and then a tricarboxylate translocase transports citrate from the mitochondria to the cytosol. In the cytosol, citrate is cleaved back to oxaloacetate and acetyl CoA. This reaction is catalysed by ATP citrate lyase and requires the hydrolysis of one ATP molecule.

STAT3 is necessary for resting lymphocytes to initiate growth and proliferation. It is known that STAT3 is among the first signalling events activated in resting lymphocytes following growth factor stimulation. During this period, the inhibition of STAT3 blocks the expression of citrate synthase and reduces the level of intracellular citrate. The reduction in the levels of IC citrate affects the ability of cells to proliferate in response to extracellular growth factors. Exogenous addition of citrate could restore the fatty acid synthesis, cell growth and proliferation, suggesting that these effects were due to STAT3 dependent transcriptional regulation (266).

Since ST0702 is a known inhibitor of STAT3, and inhibition of STAT3 can lead to a reduction in the levels of intracellular citrate which can affect the ability of the cells to proliferate, experiments were designed to examine whether citrate supplementation would lessen or stop the antiproliferative effect of ST0702. As expected, citrate supplementation did not appear to affect the STAT3 inhibitory effect of ST0702 (Figure 3.46d), nor did it have any effect on oxidative phosphorylation, as measured using the Seahorse XF Analyser (Figure 3.46c). However, interestingly, in T cell blasts, citrate supplementation did cause a small decrease in the antiproliferative effect of ST0702 (Figure 3.46a), an indication that the effect of ST0702 on STAT3 and cellular metabolism and the antiproliferative effect of ST0702 are all somewhat linked.

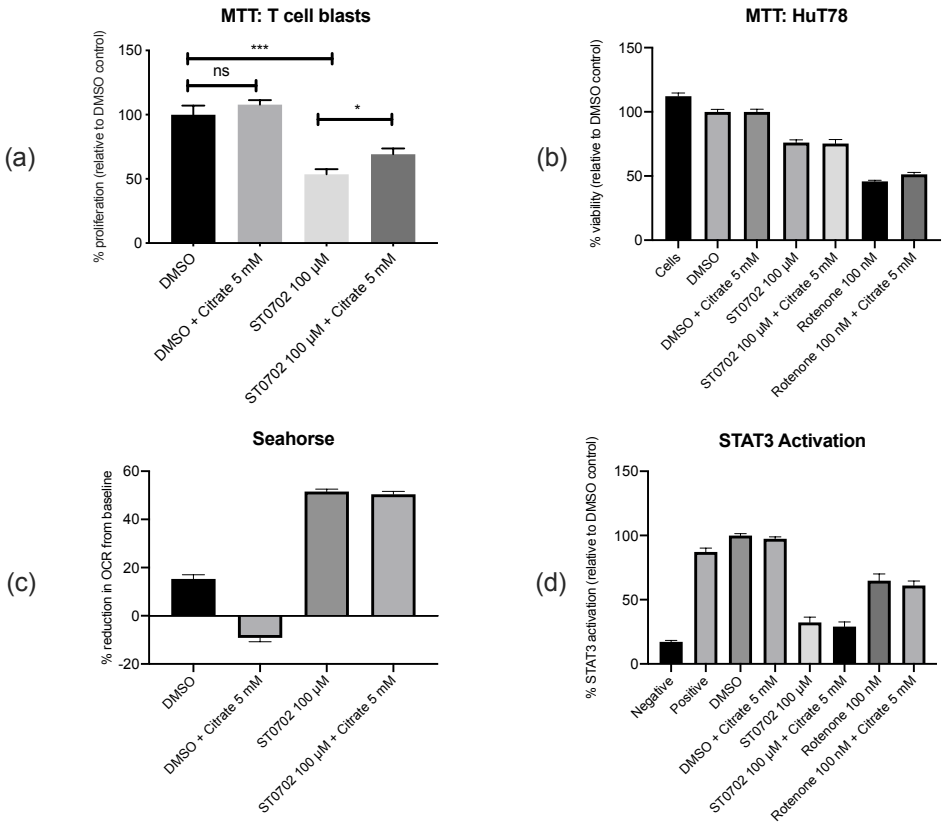

Figure 3-46: Effect of citrate supplementation on (a) proliferation of T cell blasts (b) proliferation of HuT78 cells (c) OCR and (d) STAT3 activation.

(a) PBMCs (5 × 10^5 cells/well) were seeded and stimulated with aCD3/CD28 beads for 72 h before adding two successive rounds of IL-2 (20 ng/ml) for 48 h. Cells were then treated with either DMSO or ST0702 100 µM in combination with 5 mM sodium citrate for the last 24 h of stimulation. MTT was then carried out. Results are expressed as mean ±SEM for three different donors. (b) HuT78 cells were plated at 1 × 10^4 cells per well of a 96-well plate. The cells were then treated with either DMSO, ST0702 100 µM or rotenone 100 nM in combination with 5 mM sodium citrate and incubated for 48 h. MTT was then carried out. (c) PBMCs were seeded and stimulated with aCD3/CD28 beads for 72 h before adding two successive rounds of IL-2 (20 ng/ml) for 48 h. The cells were then plated onto Seahorse XF96 plates at a density of 2.5 ×10^5 cells/well. Basal OCR readings were obtained and compound (DMSO or ST0702 100 µM) in combination with 5 mM sodium citrate was injected after 24 min. The OCR was measured in triplicate for three donors and the results are expressed as the mean of % reduction in OCR from baseline ± SEM. (d) HEK-Blue IL-6 cells were plated at 5 × 10^4 cells per well of a 96-well plate. The cells were then treated with either DMSO, ST0702 100 µM or rotenone 100 nM in combination with 5 mM sodium citrate. After 30 min incubation, the cells were stimulated with 1 ng/mL IL-6. After 24 h SEAP levels were determined. All results are expressed as mean ± SEM.

3.2.14 **Reactive Oxygen Species (ROS)**

3.2.14.1 *Effect of ST0702 on Mitochondrial ROS (mROS) production*

Experiments were carried out to determine whether ST0702 was having an effect on the production of mROS. These experiments were conducted using MitoSOX™, a mitochondrial superoxide indicator. The oxidation of MitoSOX™ by superoxide produces red fluorescence.

Two different experiments were carried out on PBMCs. In the first experiment PBMCs were pre-treated with compound for 30 min followed by stimulation with aCD3/CD28 beads. Following a 24 h incubation, the cells were stained with MitoSOX™. In both the ST0702 and rotenone treated cells, the levels of MitoSOX™ positive cells were higher than that of DMSO (Figure 3.47). These results were as expected for rotenone, which is a known inducer of mROS, whilst the fact that ST0702 acted in a similar way to rotenone was interesting. There was a slight, non-statistically significant increase in the levels of mROS production in cells activated with the beads. This could be linked to the fact that upon activation, the metabolism of immune cells, and specifically T cells, change, with naïve T cells relying heavily on OXPHOS whereas activated T cells switch to aerobic glycolysis. The fact that the change in levels was small could be because the T cells are not the predominant population in the PBMCs, so their activation does not have a large effect on overall mROS production.

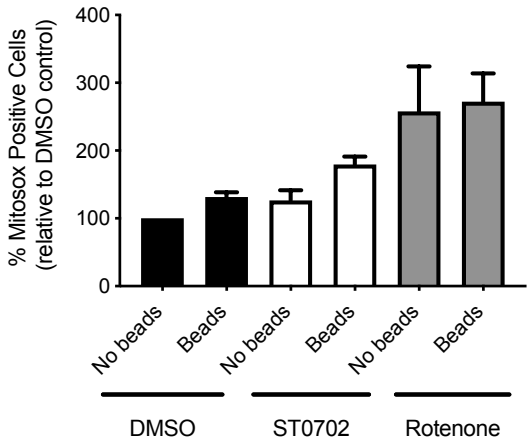

Figure 3-47: Levels of mROS in PBMCs ± aCD3/CD28.

PBMCs were plated in a 24 well plate at 5 × 10^5 cells/well. The cells were then pre-treated with compound (DMSO, 100 μM ST0702 or 100 nM rotenone) for 30 min, and following this aCD3/CD28 was added. The cells were incubated overnight. Next, 2.5 μM MitoSOX™ reagent was added and the cells were incubated for a further 30 min. The cells were then centrifuged, the supernatant was removed, and resuspended in PBS. The percentage of MitoSOX™ positive cells was determined using flow cytometry. Data is expressed as mean ± SEM of three independent donors.

The effects seen in this experiment were quite inconclusive so another experiment was completed to observe the effects of ST0702 on PBMCs that had been treated in such a way as to promote the expansion of the T cell population. In these experiments ST0702 (100 μM) was seen to a increase in levels of mROS relative to the DMSO control, and had the same effect as rotenone (100 nM) on mROS levels, however the increase was not statistically significant in the case of ST0702 (Figure 3.48).

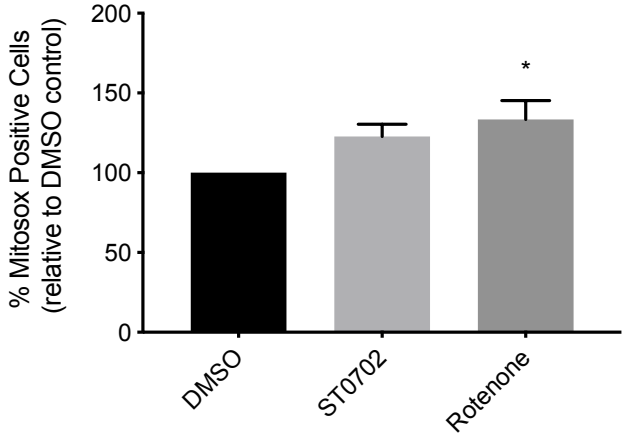

Figure 3-48: Levels of mROS in T cells treated with ST0702 or rotenone.
PBMCs were seeded and treated with aCD3/CD28 beads for 96 h, then treated with two cycles of IL-2 for 48 h each. DMSO, ST0702 100 μM or Rotenone 100 nM were added for the last 24 h of incubation. Cells were then incubated with MitoSOX™ for 30 min and analysed immediately. Graph represents average results from 4 different donors, expressed as percentage MitoSOX™+ cells relative to DMSO control.

The last experiment involved investigating the effect of the compounds on the HuT78 cells. The results for these experiments are presented as the percentage of MitoSOX+ cells, whereas in the PBMC and T cell experiments, the results were expressed as percentage MitoSOX+ cells relative to DMSO control. This was to account for the variation in the levels of mROS production for the different donors. Variation between donors was not an issue in the HuT78 cells, so the direct measure of MitoSOX+ cells could be used. Levels of mROS were greatly increased in HuT78 cells treated with ST0702, rotenone and ISAL, with ISAL having the greatest effect (Figure 3.49).

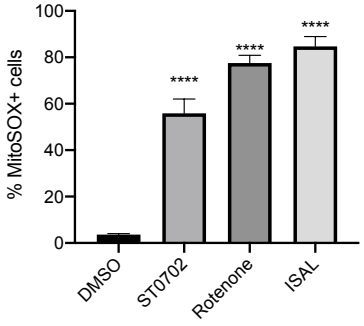

Figure 3-49: Levels of mROS in HuT78 cells treated with ST0702, ISAL or rotenone. HuT78 cells were seeded at 1 × 10^5 cells/well and treated with ST0702 100 μM, Rotenone 100 nM, ISAL 100 μM or DMSO (vehicle control) for 30 min. Cells were stained with MitoSOX and analysed by flow cytometry. Data is expressed as % MitoSOX positive cells and is the mean ± SEM of three independent experiments.

3.2.14.2 *Measurement of cellular ROS levels in HuT78 cells treated with compounds*

Levels of cellular ROS can arise from diverse intracellular sources including mitochondria, NOX, cytochrome P450, endoplasmic reticulum, peroxisomes and lysosomes (267). It is apparent from previous experiments that levels of mitochondrial ROS are higher in cells treated with ST0702 (100 μM), but it was not known if ST0702 could increase ROS production at other intracellular sites, or the extent of the contribution of mitochondrial ROS to total ROS levels. Levels of cellular ROS in HuT78 cells treated with both ST0702 and rotenone were measured and it was found that neither ST0702 nor rotenone treated cells appeared to cause an increase in cellular ROS levels (Figure 3.50).

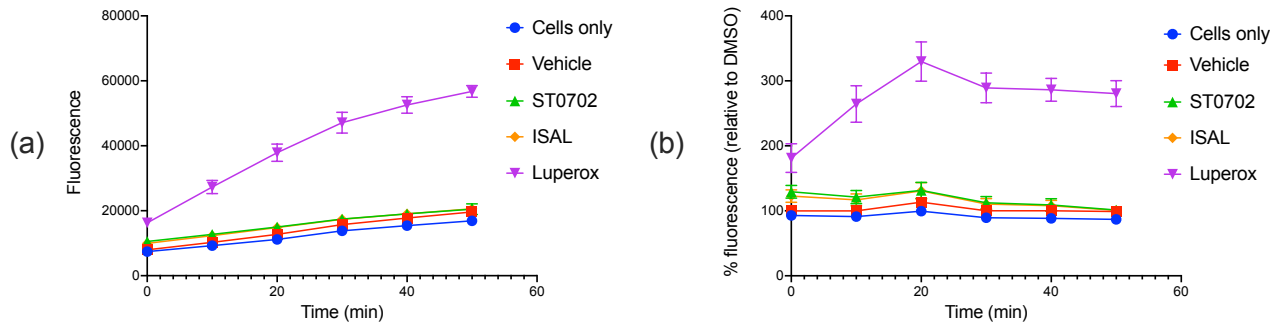

Figure 3-50: Cellular ROS levels in HuT78 cells treated with compounds.

HuT78 cells were plated at 1.5 × 10^4 cells/well and were incubated for 30 min with 25 μM DCFDA. The plate was then incubated in the dark for 30 min. Compounds were added (ST0702 and ISAL 100 μM). 100 μM Luperox was used as a positive control, and the vehicle was DMSO. A fluorescence reading was then taken every 10 min for 1 h. Results are expressed as mean ± SEM for each timepoint and is the average of three experiments. (a) shows total fluorescence readings, whilst (b) shows fluorescence readings expressed as percentage of the DMSO control.

3.2.15 **Rescue Experiments with ROS Scavengers**

Glutathione (GSH) is the most abundant low molecular weight thiol compound synthesised in cells and it is involved in the removal of ROS (268). GSH is an important hydrophilic antioxidant that protects against ROS. Removal of the radical forms can be done via non-enzymatic reduction with GSH (269). NAC is a precursor of L-cysteine that results in increased glutathione synthesis and it can act as a direct scavenger of ROS (270).

Experiments were carried out to determine if reducing the levels of cellular ROS by adding the ROS scavengers GSH and NAC would have any effect on the antiproliferative effect of rotenone. It was found that the inclusion of the ROS scavengers had no effect on the antiproliferative activity (Figure 3.51).

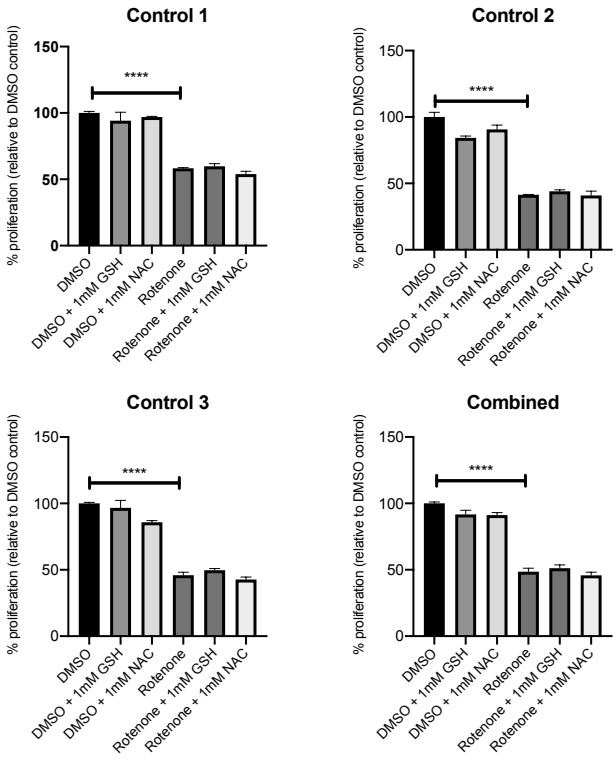

Figure 3-51: Antiproliferative effect of rotenone in combination with GSH or NAC in T cell blasts.

PBMCs (5×10^5 cells/well in a 24-well plate) were seeded and stimulated with aCD3/CD28 beads for 72 h before adding two successive rounds of IL-2 (20 ng/ml) for 48 h. Cells were then treated with either rotenone 100 nM or DMSO followed by either GSH 1 mM or NAC 1 mM for the last 24 h of stimulation. MTT was then carried out. Data is expressed as mean ± SEM.

3.2.16 **HSP90 Inhibition**

HSP90, a 90 kDa heat shock protein, is an ATP-dependent molecular chaperone that is essential for eukaryotic cells and is involved in many different cellular pathways (271). The role of molecular chaperones is to ensure changes that affect proteins, such as sudden increases in temperature (termed heat shock) are 'buffered' to guarantee proteostasis and maintain cellular homeostasis. Chaperones such as HSP90 interact with other proteins and help them to acquire a functionally active form, and then dissociate from the client protein once the final active structure is formed. HSP90 has several hundred protein clients, which are structurally and functionally diverse and include kinases, transcription factors, steroid hormone receptors and E3 ubiquitin ligases (272). Despite the name 'heat-shock' protein, most chaperones are ubiquitously expressed under normal conditions. For example, HSP90 comprises as much as 1-2% of total cellular protein content, and this amount increases about twofold under stress (273, 274). Among the chaperones, HSP90 is unique because it is not required for the

biogenesis of most polypeptides (275). Instead, it interacts with conformationally labile client proteins that have roles in growth control, cell survival and developmental processes (273).

In eukaryotes, HSP90 is the central component of a machinery that comprises a large number of cofactors, which bind reversibly to HSP90, thus establishing a flexible unit for the conformational control of many different cellular proteins (272).

There have been four isoforms of HSP90 identified, cytosolic HSP90α and HSP90β, mitochondrial TRAP1 (tumour necrosis factor-associated protein 1) and GRP94 (94 kDa glucose-related protein) in the endoplasmic reticulum. The two major isoforms of HSP90, HSP90α and HSP90β primarily reside in the cytoplasm and share an 85% homology (276, 277). HSP90β is the constitutive form, whereas HSP90α is induced in response to stress (278). HSP90 functions as a homodimer, and its dimerisation is necessary for its function (279). The HSP90 protomer consists of three distinct domains, the N-terminal domain (NTD) is involved in nucleotide binding and hydrolysis. Many small molecule inhibitors of HSP90 activity compete with ATP for binding to the nucleotide-binding pocket (271). The NTD is linked to the middle domain (MD) via a disordered region, containing basic and acidic residues, referred to as charged linker (CL). The function of this flexible linker is unknown as yet. The C-terminal domain (CTD) is responsible for constitutive dimerisation and contains an alternative ATP-binding site. All three domains, the NTD, the MD and the CTD provide interfaces for binding cochaperones and clients (271). The C-terminal domains are involved in dimerisation and dimer formation is independent of nucleotide binding and protein interactions. By contrast, dimerisation at the NTD is dependent on ATP binding, resulting in a conformational equilibrium ranging from a wide, open V-shaped orientation to an elongated orientation in which the NTDs dimerise and a gap remains between the two middle domains (280).

The function of HSP90 is regulated in a number of different ways, including transcriptional regulation, post-translational modifications (HSP90 and its cochaperones can be phosphorylated, SUMOylated, acetylated or S-nitrosylated), as well as regulation by co-chaperones. Clients first interact with HSP70 in a HSP40 mediated ATP hydrolysis-dependent process. HSP70 transfers the client onto HSP90 via an intermediate HSP70-client-HSP90 complex. Dissociation of HSP70 leads to the mature HSP90 client complex, which keeps the client in an inactive, but readily activatable state. The HSP90-client complex can dissociate upon client activation, or spontaneously, and the free client may re-enter the cycle through HSP70. The cochaperones regulate the chaperone cycle by stimulating or inhibiting HSP90's ATPase activity, acting as scaffolds or adaptors during client loading or stabilising the HSP90-client complex during different stages of the cycle (271). Co-chaperones are the most important regulators of HSP90. Some co-chaperones compete with each other for binding to HSP90,

whereas some can bind simultaneously or even synergistically (272). A comprehensive list of HSP90 interactors is maintained by the Picard laboratory (https://www.picard.ch/downloads).

HSP90 involvement has been suggested in many human diseases, such as cancer, neurodegenerative diseases and infectious diseases. In cancer, HSP90 plays an important role in the survival of cancer cells, since tumour cells seem to be in a 'stressed state', owing to the presence of mutant proteins and rapid proliferation. HSP machinery can be exploited by cancer cells to cope with proteotoxic stressors, such as the high mutation burden, hypoxia and acidosis that are often found in the tumour microenvironment. Cancer cells are also very dependent on HSP90 associated signalling pathways, such as HIF-1α and UHRF1, and numerous oncoproteins, tumour suppressors and proteins linked to tumour progression, invasiveness and metastatic potential are among recognised HSP90 clients (271, 272). HSP90 levels are markedly increased in tumours and high HSP90 expression is associated with a negative prognosis in breast cancer (273, 281), gastric cancer (282) and acute myeloid leukaemia (283). Cancer cells are generally more sensitive to HSP90 chemical inhibitors than normal somatic cells.

HSP90 inhibitors can act in a number of ways. There are inhibitors of the N-terminal ATP binding site, agents that bind to the C-terminal/middle domain, and inhibitors that target the co-chaperone/HSP90 interactions.

N-terminal inhibitors act by interfering with the binding of ATP to HSP90 and include natural compounds such as geldanamycin and radicicol which were shown to mimic the structure adopted by ATP in the N-terminal binding pocket of HSP90, leading to the selective inhibition of ATP binding and the depletion of HSP90 clients (280). Structure-activity relationship studies with geldanamycin led to the development of compounds with improved pharmacokinetic and pharmacodynamic properties compared to geldanamycin. In particular the modification of the 17-methoxy group led to active compounds such as 17-N-allylamino-17-demethoxygeldanamycin (17-AAG) that proved to be less toxic than the natural compound (284, 285).

Upon administration of N-terminal inhibitors there is a pro-survival heat shock response (HSR) induced which can be detrimental, as increased levels of heat shock proteins are observed. The currently proposed model for the mechanism of the HSR is that the binding of N-terminal HSP90 inhibitors releases the transcription factor heat shock factor-1 (HSF-1), which becomes phosphorylated, trimerises and translocates to the nucleus, leading to the overexpression of multiple heat shock proteins, such as HSP27, HSP40 and HSP70 (286). HSR is a prosurvival mechanism, so it can be a detrimental effect in anti-cancer therapy and is now known to be one of the most important causes of acquired resistance to HSP90 inhibitors (280). Silencing of

HSF1, HSP70 or HSP27 significantly increases cell sensitivity to HSP90 inhibition and induction of apoptosis in cancer cells (287).

C-terminal inhibitors act by binding to the second ATP binding site in the C-terminal domain of HSP90, and disrupt the interactions of HSP90 with both p23 and HSP70 co-chaperones. One such C-terminal inhibitor is the DNA gyrase inhibitor novobiocin, which binds to the CTD of HSP90 (288). It can induce the degradation of client protein substrates without induction of the HSR (289-291). Novobiocin exhibited an IC50 value of ~700 μM , making it significantly less potent than N-terminal inhibitors (geldanamycin and radicicol have IC50 values in the nanomolar range). For several years novobiocin was the only known inhibitor of the HSP90 C-terminal ATP-binding pocket but in recent years attempts have been made to identify more potent inhibitors.

There has been much interest in the development of HSP90 inhibitors for the treatment of cancer, since non-cancer cells appear to require a much smaller pool of HSP90 molecules than cancer cells so a sufficient therapeutic window exists. To date, there has only been moderate success, with no clear therapeutic effects. However, these trials did not look at patients with verified HSP90 dependent tumours, who would be expected to show greater response.

Several results of the project to date point to the potential effect of ST0702 on HSP90. Firstly, in the phosphokinase array, in the HuT78 cancer cell line (Figure 3.7) and the T cells blasts (Figure 3.5), the levels of GSK3a/b, AMPKa1, Akt, STAT3 and FAK were all decreased in the presence of ST0702. These are all known client proteins of HSP90.

The second piece of evidence came when examining results of immunoblotting for pSTAT3 and total STAT3 on the HuT78 cells. It was difficult to determine the effect of ST0702 on pSTAT3 levels as the levels were quite low, however it was noticed that in addition to a reduction in pSTAT3 levels in cells treated with ST0702, there was also increased degradation of total STAT3 in these cells (Figure 3.52). This was also observed in HuT78 cells that were treated with rotenone.

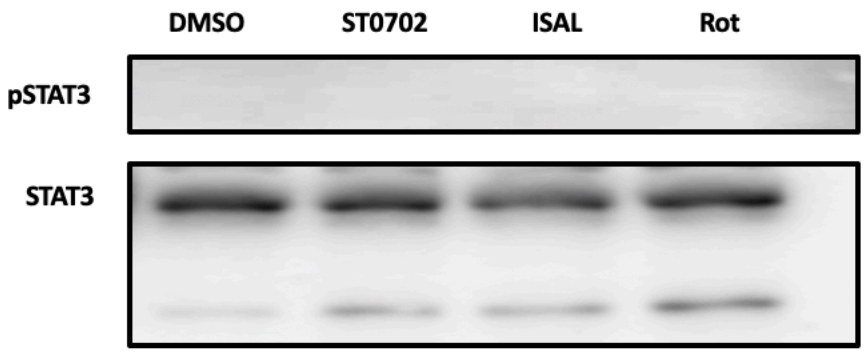

Figure 3-52: Results from pSTAT3 blot in HuT78 cells.
HuT78 cells were plated at 1 × 10^6 cells/well in a 24 well plate. The cells were pre-treated with DMSO or ST0702 100 μM for 30 min and were then stimulated with IL-6 for 30 min. Lysates were then prepared and western blotting was carried out.

Finally, compounds structurally related to deguelin, a rotenoid isolated from the African plant Mundulea sericea have been reported as HSP90 inhibitors with potent apoptotic and antiangiogenic effects on transformed cells and a variety of cancer cells. Mechanism studies showed that deguelin competes with ATP for binding to HSP90, which leads to a decrease in a number of HSP90 client proteins, including p53, CDK4, MAPK-1/2, Akt and HIF-1α (292). Deguelin binds to the C-terminal ATP-binding pocket of HSP90, thereby disrupting the function of HSP90 and causing the degradation of client proteins without affecting the expression of HSP70 (293). Deguelin is an derivative of rotenone, which is known to inhibit Complex I of the ETC, and has been extensively studied over the course of this project. ST0702 has been shown to mimic the effects of rotenone on the OCR in the Seahorse model.

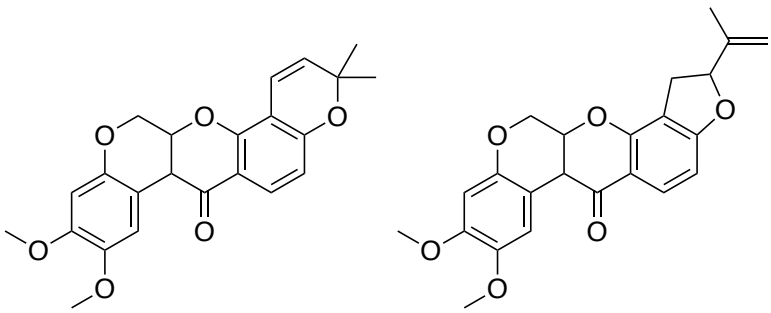

Deguelin Rotenone

Experiments were carried out with the N-terminal HSP90 inhibitor geldanamycin to investigate its effects on the proliferation of HuT78 cells and STAT3 inhibition in the HEK IL-6 cell line. For the assays, increasing concentrations of geldanamycin were used, ranging from 0.001 μM to 1 μM. Combinations of ST0702 and Geldanamycin were also tested, with the hypothesis being that were ST0702 and Geldanamycin acting on the same target, a synergistic effect may

not be observed when the two compounds are used in combination. From the results observed, it did not seem that the compounds were having a synergistic effect on HuT78 proliferation, with the IC50 for geldanamycin observed to be between 1-10 nM (Figure 3.54). For the inhibitory effect on the activation of STAT3, a very slight synergistic effect was observed, with the IC50 for geldanamycin between 10-100 nM (Figure 3.53a). Viability studies were also carried out in the HEK reporter cell line, the same cell line where the STAT3 inhibition was tested, and the loss in cell viability was no greater than 15% for the highest concentration of geldanamycin used, 1 μM (Figure 3.53b). The results from these assays suggest that geldanamycin has similar effects to ST0702 on STAT3 activation, which would be expected as STAT3 is a known client of HSP90 (294). The effect on the proliferation on the HuT78 cell line was also expected, as HSP90 inhibitors have been shown to inhibit proliferation of a variety of cancer cell lines.

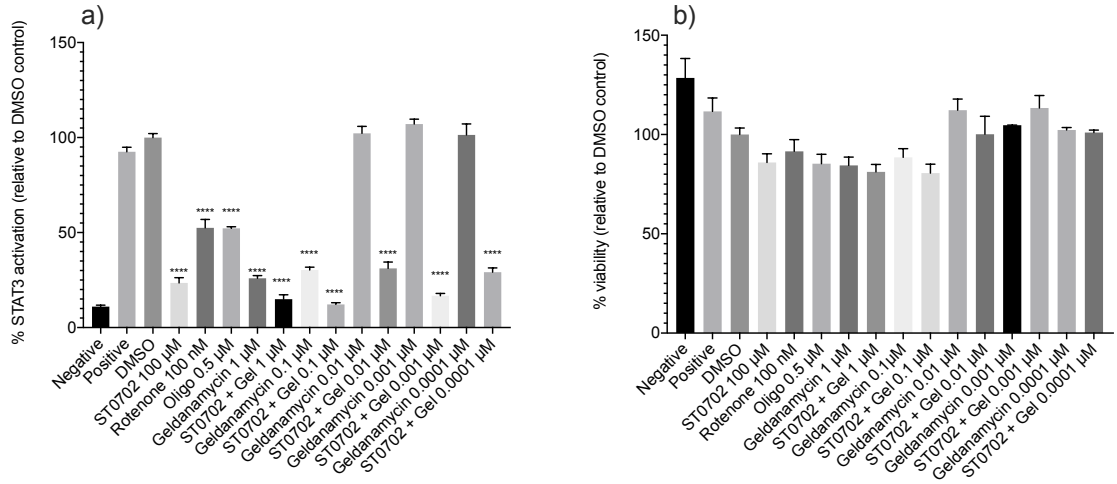

Figure 3-53: Results from HEK-Blue IL-6 cells treated with geldanamycin a) inhibitory effect on STAT3 activation and b) effect on viability measured using Alamar Blue assay.
HEK-Blue IL-6 cells were plated at 5 × 10^4 cells per well of a 96-well plate. Compound or DMSO was added. After 30 min incubation, the cells were stimulated with 1 ng/mL IL-6. After 24 h Quantiblue Reagent was added and SEAP levels were determined as an indicator of STAT3 activity. An Alamar Blue viability assay was also carried out. Data is expressed as mean +SEM of three independent experiments.

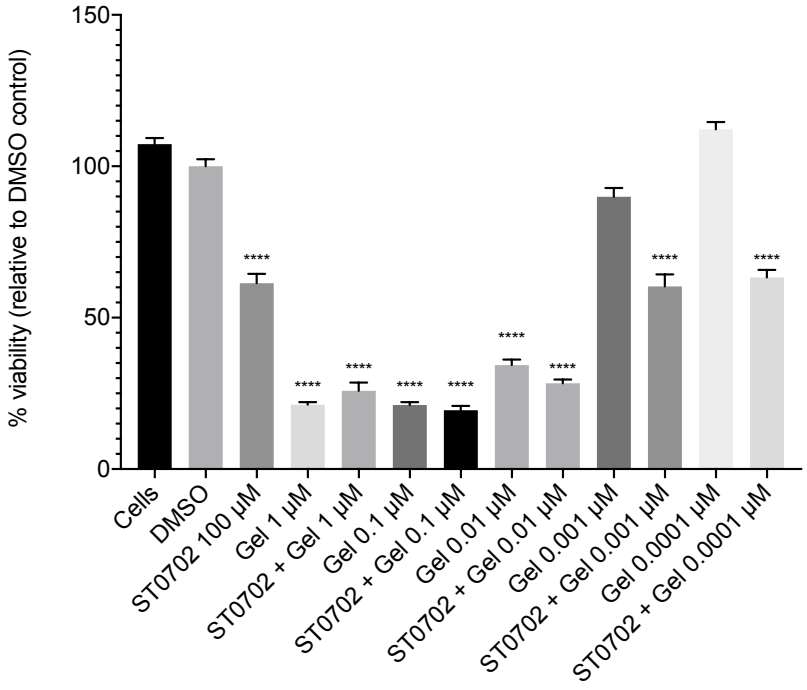

Figure 3-54: HuT78 proliferation experiments with geldanamycin.
HuT78 cells were plated in 96 well plates at 1 × 10^4 cells per well of a 96-well plate. The cells were treated with compounds and incubated for 48 h. After this time, MTT was carried out. Data is expressed as mean ± SEM of three independent experiments.

Immunoblotting was carried out to investigate the effect of ST0702 on various other HSP90 client proteins. The first protein examined was Akt. It had been observed in the protein kinase array that levels of pAkT were reduced in HuT78 cells treated with ST0702 100 µM so this was more of a confirmatory blot, but the same results were observed, that is, levels of pAkt were reduced when HuT78 cells were treated with 100 µM ST0702 (Figure 3.55).

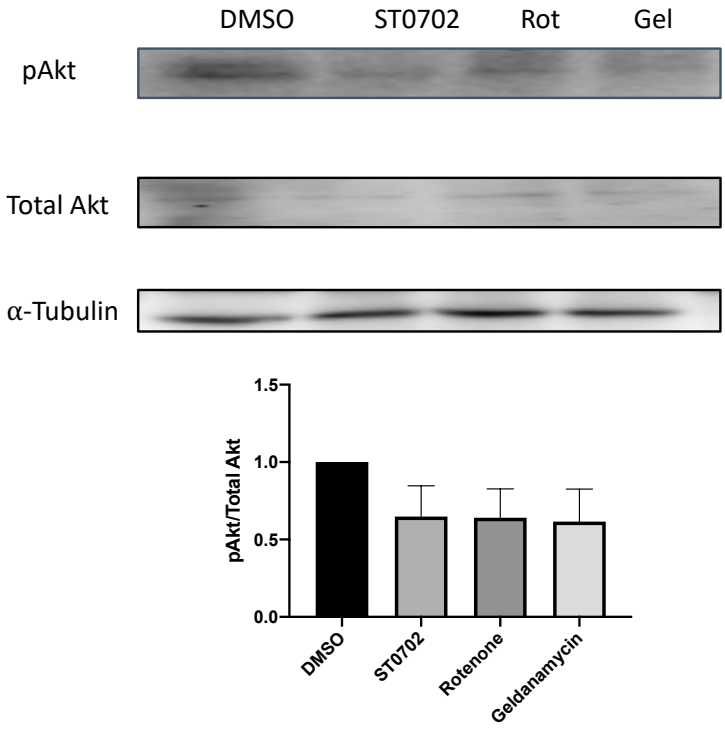

Figure 3-55: Results from pAkt blot with HuT78 cells.
HuT78 cells were plated at 1×10^6 cells/well in a 24 well plate. The cells were pre-treated with DMSO, ST0702 100 μM, rotenone 100 nM or geldanamycin 1 μM for 30 min and were then lysed. Immunoblotting for pAkT, total Akt and α-tubulin was then carried out on the lysates. Data is expressed as mean +SEM of three independent experiments.

The final protein investigated was HSP90 itself. There was no change observed in HSP90 levels following treatment with ST0702 100 μM, geldanamycin 1.5 mM or rotenone 100 nM (Figure 3.56). This could mean one of two things, the first being that ST0702 is not acting via HSP90 inhibition. The second is that ST0702 is not an N-terminal inhibitor of HSP90, but it could still be a C-terminal inhibitor. N-terminal inhibition of HSP90 induces the HSR so a rise in HSP90 levels following treatment with an N-terminal inhibitor would be expected. No change in HSP90 levels would be observed were the compound acting via C-terminal inhibition.

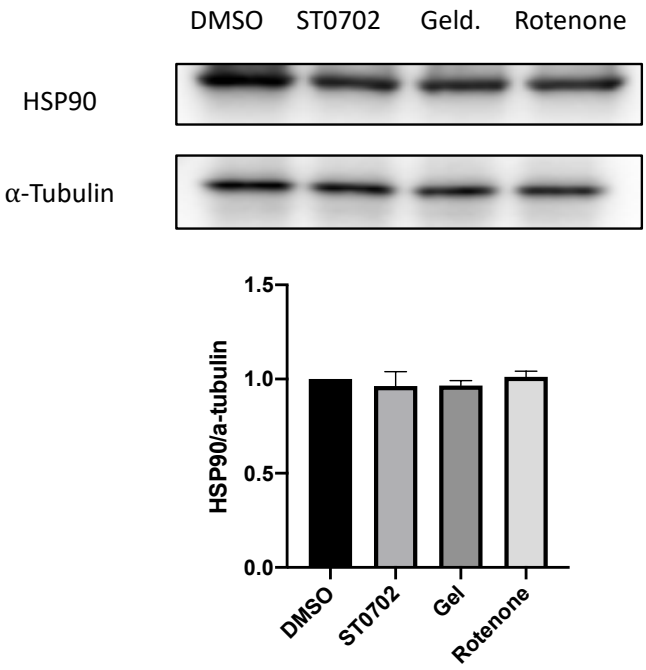

Figure 3-56: Results from HSP90 blot of HuT78 cells.
HuT78 cells were plated at 1 × 10^6 cells/well in a 24 well plate. The cells were pre-treated with DMSO, ST0702 100 μM, Rotenone 100 nM or Geldanamycin 1 μM for 30 min and were then lysed. Immunoblotting for HSP90 and α-tubulin was then carried out on the lysates. Data is expressed as mean +SEM of three independent experiments.

3.3 Chapter Conclusion

The objectives of the work carried out in this chapter were to elucidate the mechanism of action of ST0702 in the IMQ murine model of psoriasis, building on the conclusions drawn in the previous chapter that identified ST0702 as an inhibitor of T cell proliferation.

The first important finding from this chapter is that treatment of activated PBMCs and HuT78 cells with ST0702 (100 μM) can inhibit the phosphorylation of numerous proteins, many of which are important in IL-2 signalling. Levels of phosphorylated STAT3, STAT5, GSK-3 and Akt were all reduced, and these proteins are all known to be phosphorylated downstream of IL-2 binding to the IL-2R.

ST0702 was found to inhibit STAT3 signalling, and the antiproliferative effect on the HuT78 cell line and the STAT3 inhibitory effect were well correlated, which suggested that the inhibitory effect on STAT3 could be the cause of the antiproliferative effect. However, the lack of antiproliferative effect of the STAT3 inhibitor ruxolitinib on the HuT78 cells meant that STAT3 inhibition was unlikely to be cause of the antiproliferative effect on the T cells. The

mechanism by which the compound was causing STAT3 inhibition was investigated, to establish if the inhibition was occurring upstream of STAT3. ST0702 was found to not be a direct inhibitor of JAK1, JAK2 or JAK3. Additionally, Src inhibition does also not seem like a likely cause of the STAT3 inhibition, as the Src inhibitor PP2 did not cause a reduction in STAT3 activation in the same reporter assay that ST0702 was active in.

On foot of some clues regarding the potential effect of ST0702 on the metabolism of T cells, notably the reduction of phosphorylated AMPK levels in T cells following treatment with ST0702, and the fact that ST0702 had a more pronounced effect on the inhibition of proliferation depending on the growth phase of the T cell blasts, investigations were carried out into the effect of ST0702 on the metabolic activity of the T cells. The rate of glycolysis and OXPHOS in T cells treated with ST0702 were measured, and ST0702 was found to decrease the rate of OXPHOS, while also causing a slight increase in glycolysis. The effect of ST0702 on the ETC appeared similar to the effect of the Complex I inhibitor rotenone. Interestingly, rotenone also appeared to cause inhibition of STAT3 activation and reduced the proliferation of T cells.

Several attempts were made to link the effect of the compound on the ETC to its antiproliferative effects on T cells and STAT3 inhibition. The cells were supplemented with various substrates, but none seemed to rescue the effects of ST0702 on proliferation. This suggests that the ETC disruption caused by treatment with ST0702 is not directly relevant to its antiproliferative activity. Two possible reasons could be proposed for this, the first that activated T cells primarily produce ATP by aerobic glycolysis, so the effect of ST0702 on OXPHOS might not have as pronounced an effect as it would were the cells more dependent on OXPHOS. Secondly, although the production of ATP via OXPHOS is reduced following treatment with ST0702 the cells could potentially dip into their ATP stores, and this could be sufficient for proliferation to continue. Levels of mROS were also seen to increase in T cells treated with ST0702. Several inflammatory pathways that are implicated in psoriasis, such as JAK-STAT and MAPK, are known to be redox sensitive, and this could therefore be contributing to the mechanism of action.

Taking a closer look at the proteins that were affected by ST0702 treatment, and the observation that there was increased degradation of total STAT3 in HuT78 cells treated with ST0702 led to an investigation of the compound as a potential inhibitor of the molecular chaperone HSP90. The HSP90 inhibitor deguelin is structurally similar to rotenone, and since some of the effects of ST0702 were similar to that of rotenone it seemed plausible that ST0702 could be acting as a HSP90 inhibitor. The role of HSP90 inhibition in the pathogenesis of psoriasis is a relatively new area of investigation. Among the HSP90 client proteins are several members of the

JAK/STAT and MAPK pathway, both of which have been implicated in the pathogenesis of psoriasis. HSP90 also chaperones antigenic peptides that are taken up by the APC to be presented by MHC class I molecules (295). There is therefore a plausible role for HSP90 in the pathogenesis of psoriasis. The results of the studies that have been carried out look promising for determining a role for HSP90 inhibitors in the treatment of psoriasis. Firstly, HSP90 expression levels have been shown to be raised in keratinocytes and mast cells in patients with psoriasis (296). A study conducted with Debio 0932, an oral HSP90 inhibitor, showed that treatment with the inhibitor alleviated psoriasis in a murine xenograft transplantation model (297). The HSP90 inhibitor 17-AAG has been shown to alleviate the symptoms and lesions of IMQ-induced psoriasis in mouse studies and has been shown to have an effect on the Th1/Th2 and Th17/Treg immune imbalance that are considered to play a role in psoriasis pathogenesis (298). ST0702 was found to reduce the levels of several client proteins of HSP90, including STAT3 and Akt. Treatment with ST0702 was not found to affect levels of HSP90 itself, although the time at which measurement was made might not have been appropriate to detect its upregulation.

The work described in this chapter revealed that ST0702 has a selective antiproliferative effect on activated T cells, as demonstrated by an antiproliferative effect on T cell blasts and a malignant T cell line, and a lack of antiproliferative effect in the HaCaT cell line, the HEK reporter cell line and unstimulated PBMCs. Considerable efforts were spent on trying to elucidate the mechanism for this. Early findings that ST0702 inhibits IL-2 signalling were significant because they identified a role for STAT3 in the effect. In the phosphokinase array other proteins that were apparently unrelated to IL-2 signalling were shown to be affected. These were later collectively identified as HSP90 client proteins. It is known that STAT3 itself is a HSP90 client and the HSP90 inhibitor geldanamycin was shown to be an inhibitor in the STAT3 reporter assay. Other indirect evidence pointed towards HSP90 inhibition as an explanation for the effects of ST0702, for example the overlapping activity profile of ST0702 and rotenone and the latter's relationship with deguelin. Finally, in work completed in the Gilmer lab shortly after the completion of the experimental work described here, in cell free experiments ST0702 was shown to interact with HSP90 at the C-terminal preventing cyclophilin binding. It had no effect on geldanamycin binding at the N-terminal.

Chapter 4: Investigation into the potential use of developed compounds for the treatment of CTCL

4.1 Introduction

From the work outlined in the previous chapters it was known that ST0702 affects the proliferation of T cells. The exact mechanism of action remained elusive, but it was known that ST0702 inhibits STAT3 signalling, inhibits OXPHOS, potentially acts as an inhibitor of HSP90 (either directly or indirectly) and has an antiproliferative effect on T cell blasts and a malignant T cell line. ST0702 appeared to have a somewhat selective effect on malignant cells, as demonstrated by a lack of antiproliferative effect when tested on the non-malignant unstimulated PBMCs, HEK IL-6 reporter cells and HaCaT keratinocyte cells.

The HuT78 cell line was derived from a patient with Sézary syndrome (SS), a form of CTCL. It was decided to investigate the potential of these compounds as pharmacological treatments for CTCL, and in particular, as skin-directed treatment for mycosis fungoides (MF), the most common manifestation of CTCL. In addition to the antiproliferative effect on the HuT78 cell line, signalling pathways that have been implicated in the mechanism of action of ST0702 on T cell proliferation, notably HSP90 chaperoning, STAT3 overexpression, IL-2 signalling and ETC disruption have all been implicated in the pathogenesis of MF. This evidence suggested a potential role for ST0702 or related compounds in the treatment of MF.

CTCLs have been discussed in the introductory chapter, but a more detailed investigation into the molecular signalling pathways involved in the disease pathogenesis will also be discussed. Using cell lines derived from MF patients the potential of ST0702 and related compounds as antiproliferative agents in MF was assessed.

4.1.1 Molecular Pathogenesis of Cutaneous Lymphomas

CTCL is a class of non-Hodgkin lymphoma that is characterised by abnormal accumulation of malignant T cells in the skin, which can potentially result in the development of plaques, rashes and tumours. The most common presentation of CTCL is Mycosis Fungoides (MF), and in rare cases the disease can develop into Sézary syndrome (SS), which can be considered a leukaemic form of MF.

The skin-homing behaviour of the malignant T cell in MF/SS arises from the balance between appropriate skin responses and dysregulated responses, however the exact trigger for this constitutive activation remains unknown (35). CTCL has been thought to result from antigenic stimulation in genetically susceptible individuals that leads to uncontrolled clonal expansion

and the accumulation of T cell helper memory cells in the skin. No pathognomonic chromosomal abnormality is known for CTCL, but there is significant genetic instability observed (299, 300). In a study of the genomic profile of 41 skin biopsies from tumour stage MF, 76% of cases showed genomic aberrations (301). Deficient expression or function of negative regulators, including SOCS3 and protein tyrosine phosphatases such as SHP-1 have been implicated in the dysregulation of the JAK-STAT pathway and interleukin-independent proliferation of malignant T cells (302-304). Whole genome sequencing studies of MF/SS have revealed somatic mutations in genes involved in TCR/NF-κB signalling, Th2 differentiation, cell survival and fate, epigenetic regulation, homologous recombination and cell-cycle control (305).

A number of extrinsic triggers have been identified as potential triggers for CTCL including immunosuppression, hydrochlorothiazide diuretics, and several bacterial and viral infections (306). The role of infections in disease progression has been recognised in several studies. Staphylococcus aureus (SA), a common pathogen found on the skin, is thought to promote malignant inflammation, with the CD4+ T cell response to SA potentially enhancing neoplastic progression of CTCL (307). A recent study has shown that antibiotic treatment of CTCL can inhibit the disease activity and lymphocyte proliferation in lesional skin and this effect was attributed to the eradication of SA and hence the inhibition of the SA mediated responses of bystander T cells (308).

4.1.2 **Sézary Syndrome Versus Mycosis Fungoides: Single Disease Spectrum?**

In the past, SS had been considered an aggressive leukaemic variant of MF and the two diseases were thought to be points on the same disease spectrum. However, the discovery of the existence of distinct memory T cell populations led to the revelation that MF and SS arise from functionally and phenotypically different T cell subsets. In healthy skin, skin resident effector memory CD4+ helper T cells (T_{EM}) respond to skin injury. When inflammation occurs, APCs recruit memory T cells (T_{CM}) to the skin (309). T_{CM} are characterised by L-selectin (CD62L) and CCR7 (both lymph-node homing receptors) expression, and are lymph-node homing circulating cells. T_{EM} in the skin express skin-homing addressins, such as CLA, a skin homing signal receptor, and CCR4, which binds to skin-manufactured chemokines. They do not express CCR7 (310).

It has been shown that neoplastic cells in SS patients expressed a $CCR7^{+}$/L-$selectin^{+}$ T_{CM} immunophenotype, while neoplastic cells in MF patients demonstrated a CLA+/CCR4+ T_{EM} phenotype (311). This has been further demonstrated by the fact that low-dose alemtuzumab effectively treated patients with leukaemic CTCL/SS but not MF patients. Alemtuzumab

targeted circulating T_{CM} cells in peripheral blood and skin but not the skin resident, non-circulating T_{EM} (138). This can be taken as an explanation as to why CTCL does not always progress from early to late stage disease in a stepwise manner and why SS has a worse prognosis than leukaemic MF (312).

Additionally, it has been shown that the microRNA (miRNA) expression profile differs between erythrodermic MF and SS (313). miRNAs are short, non-coding RNA molecules which function in RNA silencing and the post-transcriptional regulation of gene expression. Several miRNAs have been found to be differentially expressed in CTCL compared with normal skin, and they have been proposed as diagnostic markers to distinguish CTCL from more benign skin conditions (314). One miRNA of interest is miR-155, which is STAT5 regulated. The expression of miR-155 is higher in SS compared to MF, and expression levels increases with MF stage (313).

4.1.3 T cells in CTCL

The malignant T cells in both MF and SS typically exhibit the phenotype of mature CD4+ memory cells (114, 315). In addition to the malignant cells, the cutaneous lesions also contain a large amount of non-malignant inflammatory cells. In early stage MF the infiltrate primarily consists of non-malignant Th1 cells and CD8+ T cells, which appear to control the malignant T cells by the secretion of cytokines such as IFN-α and IFN-γ and cytotoxicity directed against malignant T cells expressing tumour-associated antigens (316). It has been shown that the number of circulating CD8+ T cells is correlated with a better patient outcome (317), and reduced numbers of CD8+ T cells in a biopsied CTCL lesion is related to a lack of complete response to therapy (318). As the disease progresses, the malignant T cells accumulate and there is a decrease in the number of non-malignant immune cells. More advanced cutaneous lesions are composed almost entirely of malignant cells (316). As the disease advances there is a stage-dependent decrease in the number and function of activated CD8+ T cells and NK cells resulting in the suppression of the host's immune system. There is a shift to Th2 cytokines (IL-4, IL-5, IL-10 and IL-13) (319). As a result CTCL patients with advanced disease often develop severe immunodeficiency and frequently die of infections rather than due to the tumour burden (320).

A case has been put forward that CTCL is a malignant proliferation of Tregs, with a number of studies showing that MF lesions contain FOXP3+ infiltrating non-malignant T cells (321). These Tregs are highly immunosuppressive regulatory T cells, so could explain the immunodeficiency that arises in advanced stages of the disease. Tregs can induce immunosuppression by influencing CD4+ and CD8+ T cells, NK cells and APCs. They can

target T cells by secreting the immunosuppressive cytokines IL-10 and TGF-β, by cytolysis and by causing IL-2 deprivation and they can modulate the function of APCs by causing decreased co-stimulation or decreased antigen presentation (322).

In addition to being a lymphoma, MF may also be considered an inflammatory skin disease involving early stages of clonal and reactive cells that have the capacity to produce cytokines. For example there is increased production of IL-4 and IL-5 in advanced stages of the disease as it shifts to a Th2 response (114). It has been proposed that the pathogenesis of CTCL largely depends on the apoptosis resistance of malignant T cells rather than the increased proliferation (323).

4.1.4 **Signalling Pathways in CTCL**

There has been recent evidence that disturbances in particular metabolic signalling pathways, such as RAS-MAPK, TCR-PLCG1-NFAT and JAK-STAT, can play a role in the pathogenesis of CTCL (237). Both MF and SS are considered Th2 diseases. Both the tumour cells and the tumour microenvironment can promote Th2 differentiation. This is beneficial for the tumour cells because a Th1 environment would increase anti-tumour responses (324).

The cytokine imbalance, characterised by increased Th2 and decreased Th1 cytokine production, which is initiated and perpetuated by a clone of Th2 cells has important therapeutic implications. Attempts to readjust this cytokine imbalance through the exogenous administration of Th1-type cytokines have shown potential in the treatment of CTCL. IFN-α is a Th1 cytokine produced by T cells and macrophages, and treatment with IFN- α2a demonstrated a 64% overall response rate and 27% complete response rate when used to treat different stages of CTCL (325). IFN-α can activate CD8+ T cells and NK cells and suppresses Th2 cytokine production from malignant T cells. IFN-γ has also demonstrated significant clinical responses in CTCL patients (326).

In early CTCL stages, where the disease presents with erythematous scaly patches and plaques, STAT4 appears to be overexpressed (327). STAT4 activity is required for Th1 differentiation and is induced by the cytokine IL-12, which signals through the receptors JAK2 and TYK2. STAT4 activation is lost at later clinical stages, when the disease acquires predominantly Th2 phenotype.

Upregulation of STAT5 signalling has also been shown to occur in the early stages of CTCL. STAT5 can be activated by IL-2, IL-7 and IL-15 signalling (early stage) or via JAK1 and JAK3 signalling, which are constitutively active in malignant cells (327). STAT5 is involved in the transcription of anti-apoptotic proteins (bcl-2 and bcl-x), cell cycle genes (Cyclin D and c-myc)

and IL-4, which all work to promote carcinogenesis. Inhibition of this protein signalling in CTCL inhibits proliferation (327).

The state of activation of the malignant T cell in MF/SS is evidenced by the constitutive phosphorylation of STAT3. Constitutive expression of STAT3 has been consistently observed in advanced stages of CTCL (328). Cytokines that signal through receptors containing the common cytokine receptor γ chain have been shown to be vital for the ex vivo survival and proliferation of malignant T cells (329). This family of receptors include IL-2, IL-4, IL-7, IL-9, IL-15 and IL-21. The activation of these receptors activates the JAK3/STAT3 pathway. STAT3 can also be activated by intracellular tyrosine kinases such as Src and abl. STAT3 upregulation often signals the progression from indolent to more aggressive disease states. Constitutively activated STAT3 can increase survival and resistance to apoptosis in malignant T cells, promote Th2 and Th17 phenotypes in advanced disease and induces the expression of miR-21 oncogenic micro-RNA (327). Activated STAT3 has been detected in a large proportion of patients with advanced CTCL and STAT3 has been proposed as a molecular target for therapeutic interventions in CTCL. Treatment with a STAT3 inhibitor (ruxolitinib) has been shown to inhibit CTCL cell proliferation and JAK/STAT activity in CTCL cell lines (MyLa, HuT-78 and HH cells) (237). STAT3/5 dependent overexpression of IL-9 has been identified as a potential target for therapy development in MF, with IL-9 overexpression observed in lesional skin and IL-9 depleted mice exhibiting a reduction in tumour growth (330).

CTCL patients have been shown to express high levels of the IL-2 high affinity receptor and undergo antigen independent activation (328). In healthy individuals peripheral blood T cells do not express IL-2 high-affinity receptors. In contrast to MF cells, resting T cells only express IL-2Rα and undergo IL-2 dependent proliferation following antigen receptor stimulation. STAT3 can bind to the promoter of the IL-2Rα gene, and STAT3 deficient T cells from transgene animals showed a decreased IL-2Rα expression in response to antigen and IL-2. CTCL tumour cell lines usually express high levels of IL-2Rα and it has been shown that the STAT3 inhibitor, AG490, causes a decrease in the expression of IL-2Rα and IL-2 sensitivity. This suggests a role for STAT3 in the aberrant expression of IL-2Rα in CTCL (331). Genomic analysis has also revealed recurrent deletions of genes involved in the JAK-STAT pathway, such as the negative-feedback JAK/STAT inhibitor, SOCS1 (332).

Deregulated JAK/STAT signalling is involved in many types of cancer. Activated STAT3 has been detected in a large proportion of patients with advanced CTCL. Treatment with a JAK3 inhibitor (ruxolitinib) has been shown to inhibit CTCL cell proliferation and JAK/STAT activity in CTCL cell lines (MyLa, HuT-78 and HH cells) (237). HuT-78 cells have a JAK 3

mutation, and although there is no JAK3 mutation in HH or MyLa cells, they have been shown to be sensitive to ruxolitinib and tofacitinib (333).

Constitutive activation of the NF-κB signalling pathway has been shown to occur in CTCL, likely caused by several mutations, such as the recurrent point mutation (Thr377Ile) of TNFRSF1B found in 18% of MF cases. NF-κB can regulate the gene expression of TNF-α, IL-2, IL-6, TGF-β and IFN-β. NF-κB is usually sequestered into the cytoplasm by IκB, and can translocate to the nucleus only following the degradation of IκB. Recurrent deletions of C-terminus of NF-κB leads to proteosomal cleavage of IκB causing constitutive activation (305, 323).

4.1.5 **HDAC inhibitors, HSP90 and CTCL**

Histone deacetylases are enzymes that can affect cellular signalling and gene expression via the removal of acetyl groups attached to lysine residues in histones and non-histone proteins. This can lead to decreased DNA accessibility and gene silencing. Their functional counterpart, the histone aectyltransferases (HATs) catalyse the addition of acetyl groups to histones, leading to euchromatin structure and increased gene transcription (143). HDACs are frequently dysregulated in tumours and contribute to a loss of cell cycle control, differentiation and apoptosis. The HDAC inhibitors (HDACi) vorinostat and romidepsin are both FDA approved for the treatment of CTCL. The exact mechanism of HDACis in CTCL is not known, but it has been shown that the HDACi vorinostat can monitor the signalling of the T cell receptor, MAPK and JAK-STAT pathways (334). HSP90 has been shown to be downregulated following vorinostat treatment. The MyLa and HH cells were both sensitive to the effects of the HSP90 inhibitor 17-AAG, with the IC50 for proliferation/viability in the nanomolar range. Co-administration of vorinostat and 17-AAG resulted in an antagonistic interaction, which could be explained by the fact that vorinostat inhibits HSP90 (334). HDACs are known to promote the acetylation of HSP90, leading to the binding and stabilisation of HSP90 client proteins, and the inhibition of histone deacetylase 6 has been shown to disrupt the chaperone function of HSP90, resulting in the ubiquitination and degradation of the client proteins (335, 336). It has been demonstrated with romidepsin that treatment of cells results in the reduction of a number of client proteins of HSP90, notably p53, Raf-1 and ErbB, and that the inhibition of the binding of these target proteins was associated with acetylation of HSP90 (337). The ability of HDACis to modulate HSP90 function requires further investigation, as it has not been determined whether it is the HSP90 modulation, or the direct effect that the HDACis are having on the transcription of the client proteins themselves that is the dominant mechanism responsible for the observed pharmacological effect in CTCL (336).

4.1.6 Cellular metabolism and ROS in CTCL

Quiescent and memory lymphocytes mainly rely on oxidative phosphorylation to meet their energy needs but upon activation switch to aerobic glycolysis. An important mediator of anabolic pathways in activated cells is mTOR. The IL-2 and co-stimulatory CD28 signalling in activated T cells induce a switch to glycolysis with the activation of the PI3K pathway and downstream Akt. The activated Akt can then induce the mTOR pathway and increases utilisation of glucose and amino acids to support and activate T cell proliferation (338).

The mTOR pathway regulates protein synthesis and metabolism. The mTOR inhibitor rapamycin has been shown to reduce the proliferation of the CTCL cell lines HH, HuT78 and MyLa (339, 340). Rapamycin was shown to inhibit tumour growth and decrease the rate of aerobic glycolysis in a mouse model of CTCL, and it is thought that the inhibition of mTOR signalling alters the metabolic phenotype of lymphoma cells by reducing glycolytic state and thus counteracting the Warburg effect (339).

Mucin 1 (MUC1) is a heterodimeric protein that regulates critical pathways of oncogenesis, including those involved with cell proliferation, self-renewal, tissue invasion and apoptosis. MUC1 protects against ROS-mediated cell death due to hypoxic or stress-induced injury. It is aberrantly expressed in epithelial tumours and a number of haematological malignancies. MUC1 is overexpressed in T cell lines, and exposure of CTCL to a MUC1 inhibitor was associated with a downregulation of TP53-inducible glycolysis and apoptosis regulator (TIGAR), depletion of NADPH and GSH, and an increase in ROS levels, promoting oxidative stress-induced late apoptosis/necrosis (341).

In CTCL, ROS have been identified as a critical link between cellular metabolism and invasive properties (342). The highly invasive state of malignant B and T cells shows a reprogrammed metabolic profile with increased glycolysis and decreased OXPHOS. This highly invasive state also shows redox-mediated activation of HIF-1α, which is necessary for in vitro migration and in vivo dissemination of malignant cells (342). Interestingly, HIF-1α is a known client protein of HSP90, and HIF-1α activation is inhibited in the presence of geldanamycin (343).

HIF-1α has shown itself to be critical for resistance against mitochondrial Complex I dysfunction. Treatment of HIF-1α knockout cells with the biguanide phenformin, a known Complex I inhibitor, led to increased cell death compared to wild-type cells (344). It has also been shown that mROS-mediated activation of HIF-1α signalling is the critical driver of metabolic reprogramming during the dysfunction of mitochondrial Complex I in malignant cells (344).

4.1.7 Overview of CTCL Cell Lines

The objective of this chapter was to assess the potential of ST0702 and related compounds as antiproliferative agents in MF, so cell lines that were representative of CTCL and could be used to test the activity of the compounds were identified. A number of different cell lines representing different types of CTCL were available. Human T Cell Lymphotropic Virus Type 1 (HTLV-1) is a virus that has been implicated in Adult T cell Leukaemia/Lymphoma (ATLL), a recognised variant of CTCL. Most CTCL variants are not caused by viruses. ATLL can have a variety of presentations, some not unlike the classical symptoms of MF, which can lead to a misdiagnosis of MF. An example of such a misdiagnosis arose with the cell lines, HuT102 and MJ. The cells were obtained from a 28 year old African-American male, and a 50 year old Caucasian male, respectively, and both were diagnosed with 'advanced Mycosis Fungoides'. The cell lines were later found to have the HTLV-1 virus, and likely represented ATLL, not MF (345).

The malignant cells in MF have a mature CD4+ T-helper phenotype (346). Despite the malignant nature of MF cells, they do not grow well in vitro, making the establishment of cell lines quite difficult. The cell lines utilised in this project were the MyLa cells, which represent advanced extensive MF skin disease, HH cells which represent aggressive leukaemic MF and HuT78 cells which represent SS. MyLa, HH and HuT78 cells have all been shown to be HTLV-1 negative (345). These cells all demonstrate significant and ongoing genomic instability. There are no known cell lines that represent early stage MF (345).

These cell types were chosen based on availability, and also because they have been shown to represent different clinical CTCL cases. In a recent study of 9 HTLV-1$^-$ CTCL cell lines, MyLa, Mac2a, PB2B, HH, H9, HuT78, SZ4, Sez4 and SeAx it was found that these cell lines represent six clinical CTCL cases: 1) MyLa, 2) Mac2A/PB2B, 3) HH, 4) HuT78/H9, 5) SeAx and 6) Sez4/SZ4 (345).

The different cell lines have been shown to differ in their sensitivity to therapies. Three commonly used therapies in CTCL are romidepsin, vorinostat and bexarotene. Romidepsin and vorinostat are histone deacetylase inhibitors, whilst bexarotene is an antineoplastic retinoid. HuT78, HH and MyLa cell lines were treated with these compounds to test their sensitivity to these therapies. HuT78 were shown to be responsive to romidepsin and vorinostat. HH were responsive to romidepsin and bexarotene, whilst MyLa were only responsive to romidepsin (345).

4.2 Results and Discussion

To get an indication as to the ability of the compounds to work as skin-directed therapy for the treatment of MF a number of experiments were designed. The experiments were designed to investigate the potential of the compounds in MF, rather than to produce any new mechanistic insights.

4.2.1 Investigation into the activity of the compounds on MyLa cells

The MyLa cell lines were purchased from the ECACC. The product literature stated that MyLa CD4+ cells (referred to in the literature as My-La, marker chromosome) were established from a plaque biopsy of an 82 year old Caucasian male with mycosis fungoides stage II. The product literature advised that the My-La cells were strictly dependent on IL-2 and IL-4 being present in the culture medium. The MyLa cells purchased originated in the Kaltoft laboratory.

The MyLa cells previously described by the Kaltoft lab (347) were obtained from an 82 year old Caucasian man with MF. Most T cells obtained were CD4+ and only a few had a CD8 antigen. Lymphocytes from the skin biopsy proliferated vigorously, and the cell line was termed My-La, 46, XY. These cells underwent 40-50 cell population doublings, and then entered a crisis lasting 2-3 weeks, in which no proliferation occurred. Following this, there was continuous growth of a cell strain called My-La, 46, XY,-18,+i(18q). Cell numbers of this cell line doubled more than 150 times, so this cell line was considered continuous. The My-La, 46, XY was considered a finite cell line. While attempting to repeat the production of the My-La, 46, XY,-18,+i(18q) from the My-La, 46, XY cell line, occasionally a different cell strain, termed the My-La marker chromosomes appeared. There have been more than 125 cell population doublings of this cell strain so it is considered continuous.

The Kaltoft lab found that the My-La, 46, XY cell line required both IL-2 and IL-4 to proliferate. When either IL-2 or IL-4 was eliminated from the culture media, the My-La, 46, XY cell line did not develop into a continuous cell line. The continuous cell line, My-La, 46, XY,-18,+i(18q) was also dependent on IL-2 and IL-4 supply, whereas My-La marker chromosomes only required IL-2 for growth.

The MyLa CD4+ cell line used in this project required IL-2 and IL-4 to grow, however the company also stated that it is referred to in the literature as My-La, marker chromosome, which Kaltoft describes as only requiring IL-2 to grow. On contacting the company for clarification, all that was confirmed was that the MyLa CD4+ are non-malignant cells, taken from a non-malignant homing T cell line from a patient with MF.

The confusion over the classification of these MyLa cells persisted as more research was carried out, with many publications simply stating that MyLa cells were used, without specifying further. For example, a publication using MyLa cells to establish a mouse xenograft model for MF states that MyLa cells were used, and references the Kaltoft paper as the source (346). However, that paper also states that the MyLa cells grow independently of externally added cytokines, which is not a feature of any of the continuous cell lines identified by Kaltoft.

Another paper (307) documented the isolation of malignant T cell lines from blood, the malignant MyLa 1929, the MyLa 2039 and MyLa 2059 subline, which were established from the plaque biopsy of an MF patient. The non-malignant T cell lines, MyLa 1928, 1850, 2355, 1855 and 3241 were also documented in this paper. The non-malignant cell lines were all CD2+, CD3+, CD4+ and CD8-. The malignant cell lines were CD2+, CD3-, CD4- and CD8-, except MyLa 1929 which was CD2+, CD3+, CD4- and CD8+. This paper noted how the molecular and functional features of non-malignant T cells were different than malignant T cells. The non-malignant T cells did not have constitutive JAK3/STAT3 activity or spontaneous production of cytokines, and they stopped proliferating and underwent apoptosis following cytokine starvation. They were therefore grown in media supplemented with IL-2 and IL-4 (307).

The malignant MyLa 2000 and MyLa 3675, and the non-malignant MyLa 1885 and MyLa 1928 were obtained from a plaque biopsy of a single patient with MF. The MyLa 2000 were grown in conditional media without any cytokine supplementation, whereas the MyLa 3675 were grown in media supplemented with IL-2. Again, these non-malignant cell lines were grown in media supplemented with IL-2 and IL-4 (348).

The first set of experiments conducted with the MyLa cell line studied the effect of ST0702 and ISAL on the proliferation of the MyLa cell line. It can be seen that the compounds did not have a large effect on the proliferation of the cell line, with ST0702 causing an approximately 15% decrease in viability/proliferation and ISAL only causing about a 10% decrease (Figure 4.1). Acid phosphatase was also used as a measure of viability, as there was a need for a method that examines viability that was not dependent on metabolic activity, as it has been shown that the compounds can affect the mitochondrial activity of the cells. The results for the acid phosphatase assay mirrored those observed in the MTT.

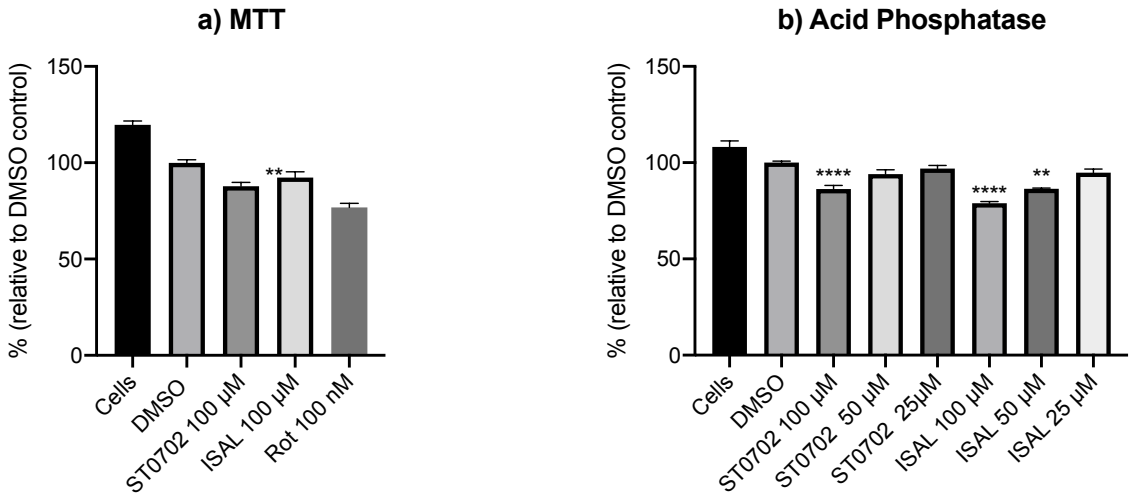

Figure 4-1: Proliferation Results from MyLa cells treated with ST0702 or ISAL.
MyLa cells were plated at 1 × 10^4 cells per well of a 96-well plate. The cells were treated with 100, 50 or 25 µM compound and incubated for 48 h. After this time, MTT (a) or Acid Phosphatase (b) was carried out. Results for each concentration are expressed as mean ± SEM of three experiments performed in triplicate.

Further experiments carried out on the MyLa cells tested the effects of the compounds on cells that were grown in the presence or absence of cytokine supplementation. Due to the confusion surrounding the malignancy of these cells, and the confirmation from the original source that they were non-malignant, it was decided to test if the cells were more or less sensitive to the effect of the compounds when grown in media lacking cytokine supplementation. The cells were found to grow in media without IL-2 and IL-4 supplementation, however this was not tested beyond 10 population doublings, so perhaps this was not enough time for the cells to enter a crisis in which they do not proliferate. Three conditions were investigated, the first where cells were grown in media without any cytokine supplementation and tested with the compound, the second where the cells were stimulated with the relevant cytokines at the time of treatment with the compounds, and the third where the cells were grown and kept in cytokine-supplemented media at all times. The third condition was the one that followed the manufacturer's protocol most closely.

The cells appeared to be almost equally responsive to the antiproliferative effect of ST0702 when tested in cells without cytokine supplementation as when tested with cells in receipt of cytokine supplementation (Figure 4.2). Interestingly, the cells that were stimulated with IL-2 and IL-4 at the time of treatment with the compounds were the least responsive.

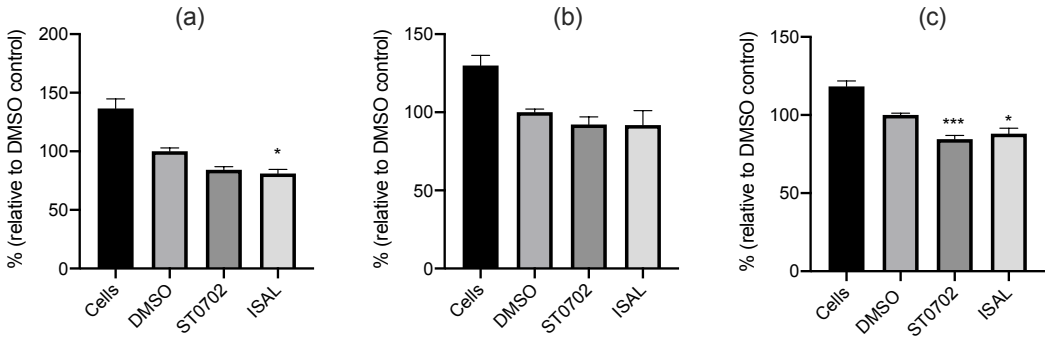

Figure 4-2: Proliferation Results from MyLa grown with/without cytokine supplementation. MyLa cells were plated at 1 × 10^4 cells per well of a 96-well plate. For experiment (a), the MyLa cells were grown in media without supplementation of IL-2 and IL-4, for experiment (b) the cells were grown in media without IL-2 and IL-4 supplementation but IL-2 and IL-4 were added at the time of treatment with compound, and for experiment (c) the cells were grown and treated in media supplemented with IL-2 and IL-4. For all experiments the cells were treated with 100 μM compound and incubated for 48 h. After this time, MTT or Acid Phosphatase was carried out. Results for each concentration are expressed as mean ± SEM of three experiments performed in triplicate.

The antiproliferative effect of the compounds in these cells was modest when compared to the effect observed in the HuT78 cell line, another CTCL cell line. In the HuT78 cells, treatment with 100 μM ST0702 caused a reduction in proliferation of approximately 40% (Figure 2.24), whereas in the MyLa, treatment with the same concentration of ST0702 saw only a 15% reduction in proliferation.

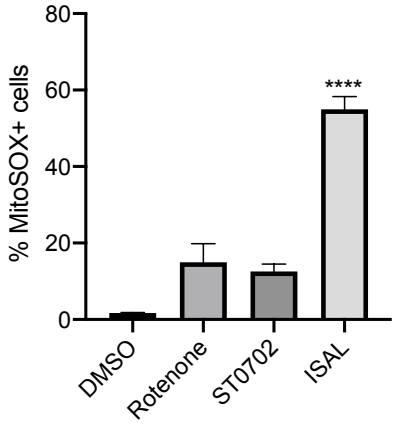

Figure 4-3: mROS Production in MyLa following treatment with rotenone, ST0702 or ISAL. MyLa cells were seeded at 1 × 10^5 cells/well and treated with ST0702 100 μM, rotenone 100 nM, ISAL 100 μM or DMSO for 30 min. Cells were then stained with MitoSOX and analysed by flow cytometry. Data is presented as mean ± SEM of three independent experiments.

The final experiment carried out on the MyLa cells was to examine the production of mROS by cells following treatment with compounds. It was clear that while ST0702 had a modest effect on the production of mROS, ISAL had a profound effect, with levels much higher than that of the Complex I inhibitor rotenone (included here as expected to raise mROS levels) (Figure 4.3). Inhibitors of the ETC would be expected to cause an increase in ROS production, but up to this point there has been no evidence of a difference in the levels of activity of ST0702 and ISAL.

4.2.2 **Investigation into the activity of the compounds on HH cells**

HH are a CTCL cell line derived from the peripheral blood of a 61 year old Caucasian male who had tumour stage (IIB) MF with lymph node disease and later progressed to leukaemic MF with spleen involvement (349). The line was established from blood taken after extensive chemotherapy and the immunophenotype of the cultured cells was CD2+, CD3+, CD4+, CD5+, CD8-, DR+ and CD25- (Tac, IL-2 receptor α-chain). HH cells lack a detectable IL-2 receptor α-chain, but they do show increased proliferation in response to exogenous IL-2, most likely due to the presence of the IL-2 receptor β-chain (349). Studies carried out recently have shown that whilst HH cells were thought to represent aggressive leukaemic MF, they more specifically represent $CD30^+$ MF (345). MF is not considered to fall under the classification of CD30+ lymphoproliferative disorders, but there can be overlap between MF and the CD30+ lymphoproliferative disorders, and they often co-exist in the same patient. CD30 expression has been detected across all stages in MF, but there were significantly more CD30+ patients with late-stage MF than early-stage MF (350).

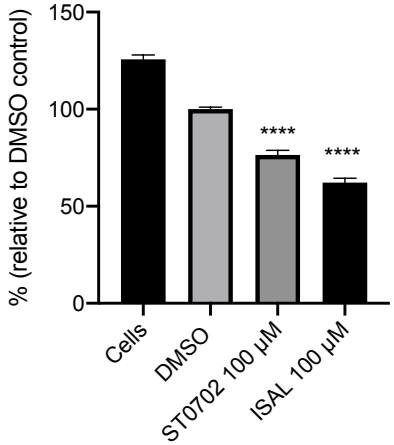

Figure 4-4: Proliferation Results from HH treated with ST0702 or ISAL.
HH cells were seeded at 1 ×10^4 in a 96-well plate and treated with compounds for 48 h before carrying out an MTT assay. Results are averaged from three independent experiments and are expressed as mean ± SEM.

Treatment with ST0702 caused a decrease in proliferation of HH cells, with statistically significant inhibition of about 25% observed (Figure 4.4). ISAL had a more pronounced effect, with inhibition of approximately 35%. The HH cells were more responsive to the antiproliferative effect of ST0702 and ISAL than the MyLa cells. The effect of the DMSO vehicle control on the HH cells was quite significant, and was consistently observed in all experiments carried out with these cells. DMSO was used at a concentration of 0.5% v/v, the same concentration that was used in the HuT78 proliferation experiments. The exact cause for the increased sensitivity of these cells was not determined.

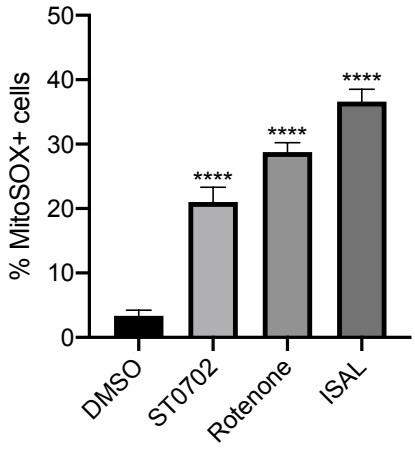

Figure 4-5: mROS production in HH following treatment with rotenone, ST0702 or ISAL. HH cells were seeded at 1 × 10^5 cells/well and treated with Rotenone 100 nM, ST0702 100 μM, ISAL 100 μM or DMSO for 30 min. Cells were then stained with MitoSOX and analysed by flow cytometry. Data is expressed as mean ± SEM of three independent experiments.

Treatment of the HH cells with the compounds also led to an increased production of mROS, with ST0702 causing an increase in levels of mROS similar to that of rotenone (Figure 4.5). Again, ISAL had the greatest effect, producing more mROS than rotenone. This result echoes what was observed when mROS levels were measured in MyLa, and suggests that ISAL might have an advantage over ST0702 at driving the production of mROS in the CTCL cell lines.

The HH cells were tested in the Seahorse XF Analyser to measure the changes in OCR and ECAR in these cells following treatment with ST0702 or ISAL. Similarly to when the proliferation of the HH cells was measured using MTT, the vehicle (DMSO) effect was quite large here, and cells treated with vehicle had a large increase in OCR (Figure 4.6). A review of the literature has not led to the discovery of the potential explanation for this effect, so more studies would be needed to draw a conclusion from these results.

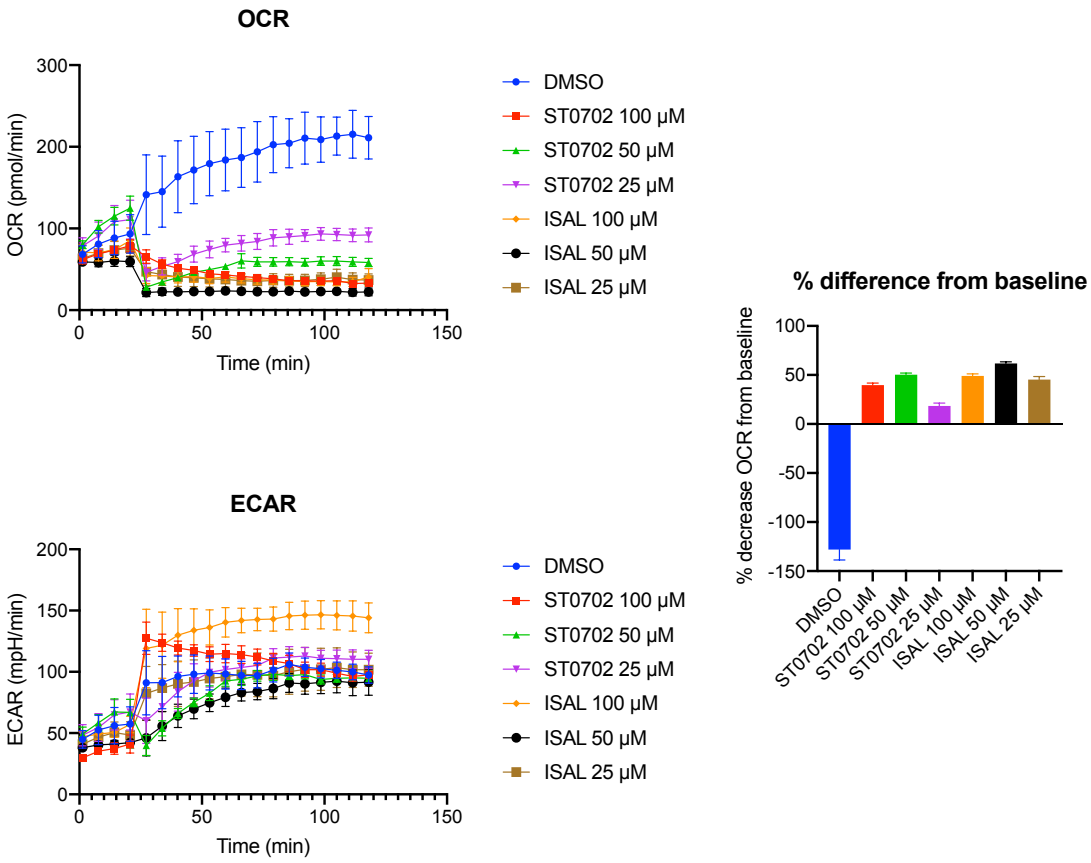

Figure 4-6: Seahorse results in HH Cells.

HH cells were plated at a density of 1 ×10^5 cells/well. Basal OCR readings were obtained and compound or DMSO was injected after 24 min. The OCR and ECAR was measured in quadruplicate and the results are expressed as mean ± SEM.

4.2.3 Testing Chapter 2 Compounds on HH and MyLa Cell Lines

The broad panel of isosorbide and isomannide compounds that were characterised on HuT78 cells as described in Chapter 2 were assessed for antiproliferative activity in the MF relevant cell lines to investigate first of all if the effect on these cell lines correlated with the effect in HuT78 cells and therefore the effects might have common mechanistic origin, and also to see if less active compounds in that model might be nonetheless active in the CTCL cell lines.

As presented in Figures 4.7 and 4.8 the majority of the isosorbide and isomannide compounds described in Chapter 2 failed to exert significant antiproliferative effects in either the HH or the MyLa cell lines. This was consistent with the lack of antiproliferative activity of these compounds in the HuT78 cell line. Four compounds, **10**, **11e**, **19f** and **19g** showed activity in the HH cells, but none of these were as effective as ST0702.

The only additional compound that showed antiproliferative activity in the MyLa and HH cell lines was **3**. This compound had been tested in the Aldara model, so its in vivo efficacy was known.

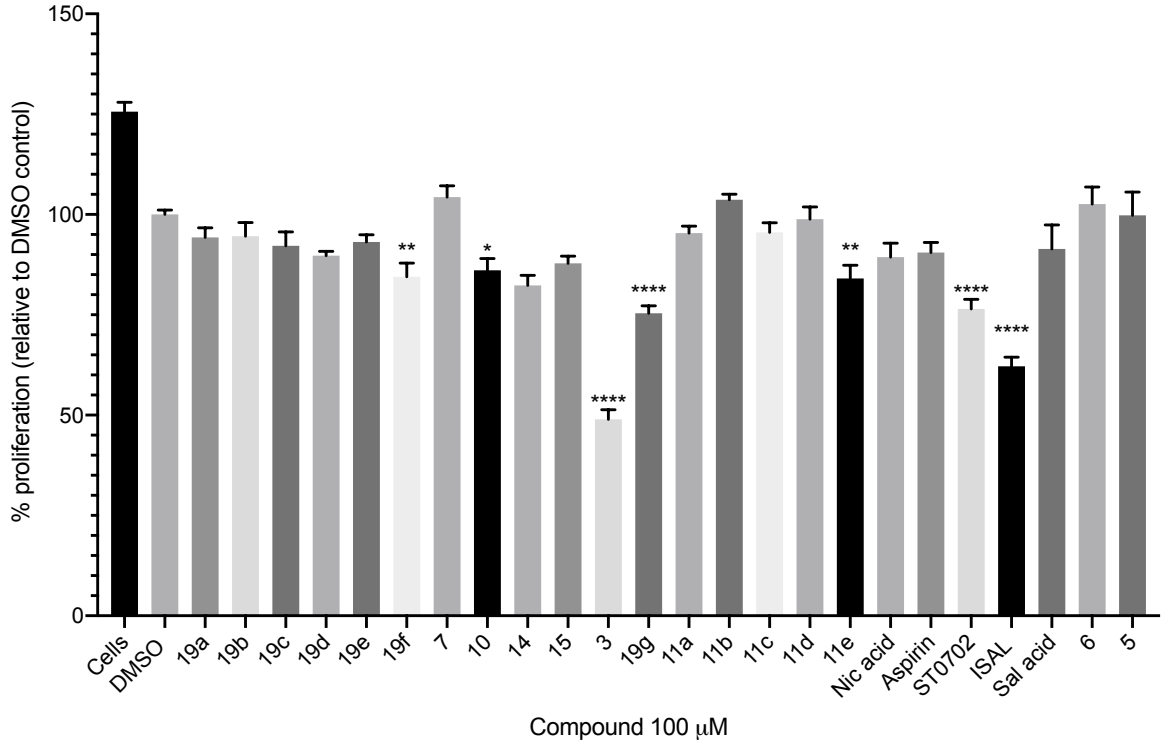

Figure 4-7: Antiproliferative effect of chapter 2 compounds on HH cells.
HH cells were seeded at 1 × 10^4 in a 96-well plate and treated with compounds for 48 h before carrying out an MTT assay. Results are averaged from three independent experiments and are expressed as mean ± SEM.

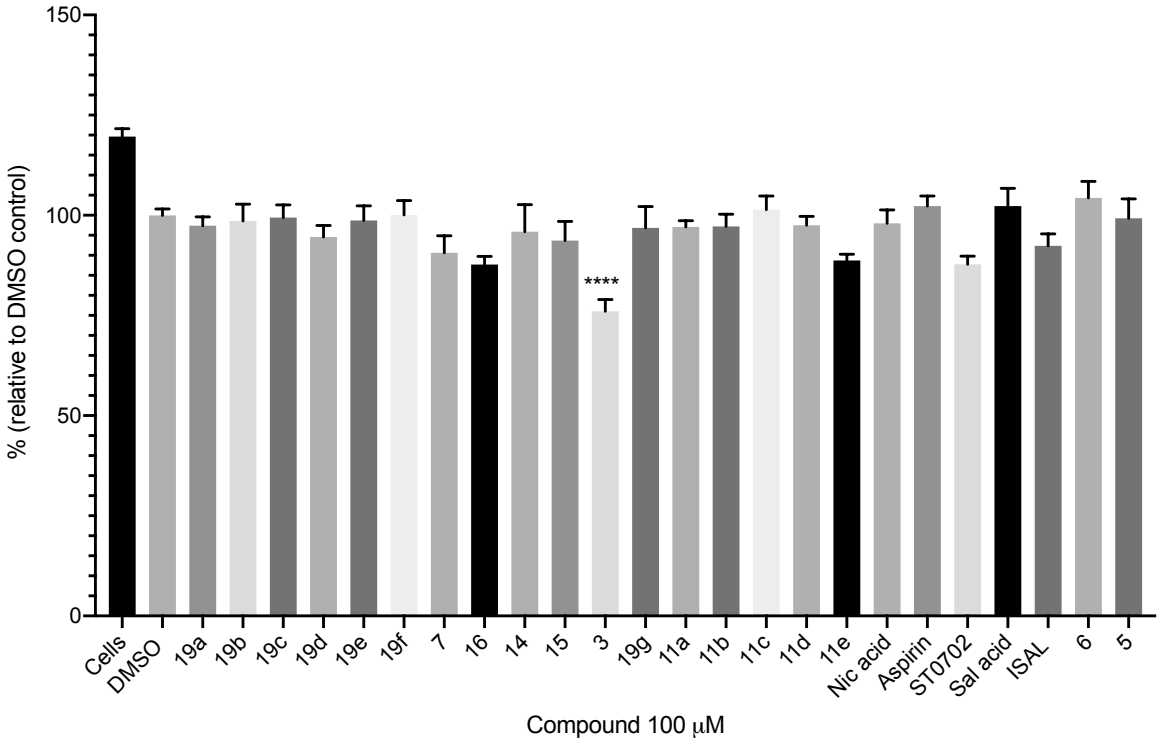

Figure 4-8: Antiproliferative effect of chapter 2 compounds on MyLa cells
MyLa cells were plated at 1 × 10^4 cells per well of a 96-well plate. The cells were treated with 100 μM compound and incubated for 48 h. After this time, MTT was carried out. Results are expressed as mean ± SEM of three experiments performed in triplicate.

4.3 Conclusion

ST0702 and ISAL exert antiproliferative activity on a number of T cell lines representing various manifestations and disease stages of CTCL. The compounds had previously been shown to have antiproliferative activity on the HuT78 cells, which were isolated from a patient with Sézary syndrome. The aim of this chapter was to determine whether ST0702 or related compounds might have the potential to be effective pharmacological agents for skin-directed therapy for the most common manifestation of CTCL, MF. Two cell lines that were derived from MF patients were used to test the efficacy of the compounds, the HH and MyLa cell lines. The compounds had the largest antiproliferative effects on the HH cell line, which was established from a patient with leukaemic MF. The compounds had a lesser effect on the MyLa cells, which were isolated from the plaque of a patient with MF. It may be significant that the MyLa cell line used in this project were probably non-malignant. This could be a potential reason for the lack of effect observed, with the compounds possibly only acting on actively proliferating, malignant cells. It was not possible to develop or source a malignant MyLa line

as the few laboratories that had previously reported them were sadly unwilling to provide them or were commercially constrained.

ST0702 is being considered as a topical agent, so would only be considered for skin-directed therapy, making it more suitable for the treatment of early stage MF. Unfortunately, there is no cutaneous non-tumorigenic T cell line available so in vitro investigations to prove the tumour specificity of the effects could not be carried out. There are several differences between early stage and late stage MF, with the disease acquiring a more Th2 phenotype and having reduced numbers of CD8+ T cells with advancing stages (316, 317). Therefore the results observed in the MyLa might not be directly correlated to antiproliferative activity in early stage MF.

The inhibitory effect of ST0702 and ISAL on STAT3 activation may have contributed to their antiproliferative effects on the CTCL cell lines. The JAK1/2 inhibitor ruxolitinib has been shown to decrease the proliferation of HuT78, HH and MyLa cells (malignancy not stated), with IC50 values of 24, 21, and 14 μM respectively (237).

The fact that the compounds cause an increase in mROS levels in the CTCL lines may be significant with respect to their anti-proliferative activity. The elimination of tumour cells through the induction of apoptosis represents a principal goal in cancer treatment, and resistance to particular therapies can frequently be explained by a deficiency in apoptosis. In CTCL, the activation of the extrinsic caspase cascade plays a role in controlling apoptosis, and apoptosis resistance is associated with reduced expression of the death receptor CD95/FAS and activation of the pro-survival transcription factors NF-κB and STAT3 (351).

There have been an increasing number of studies in recent years looking at the role of ROS in apoptosis regulation in cancer cells. A derivative of indirubin, a major component of a traditional Chinese medicine remedy and used to treat leukaemia, has been shown to reduce viability and induce apoptosis of HuT78, HH and MyLa cells (351). This derivative has been shown to enhance levels of ROS, indeed, when the ROS scavengers tocopherol and N-acetylcysteine were added, the effect of the derivative on cell proliferation was strongly diminished and the induction of apoptosis was completely prevented.

Although tumours are widely believed to rely predominantly on aerobic glycolysis, certain tumour types may reprogram towards oxidative phosphorylation to meet their energy production needs (254). The inhibition of STAT3 has been shown to inhibit OXPHOS, likely due to the inhibition of the activity of mSTAT3. mSTAT3 increases ETC activity, and cells which are deficient in mSTAT3 have reduced ATP production (352). OPB-111077, a small molecule STAT3 inhibitor has also been shown to inhibit OXPHOS. A phase I trial looking at its efficacy in patients with advanced cancers found only modest activity when used as

monotherapy, but clinical trials are now being carried out to examine its efficacy when combined with other pharmacological agents and in drug-resistant oncogene-addicted tumours (353, 354).

To conclude, ST0702 and ISAL (100 μM) appear to have a modest but statistically significant effect on the proliferation of MF cell lines, HH and MyLa. The fact that ST0702 and ISAL act as both disruptors of OXPHOS and as STAT3 inhibitors may be increasing their activity in the CTCL cell lines, and the increased mROS levels in MF cell lines treated with ISAL and ST0702 could also be contributing to the effect. However, the magnitude of antiproliferative effect of ST0702 and ISAL on MF cell lines was not considered to be decisively large, and therefore the final phase of the research project, described in Chapter 5 was an attempt to design new more potent inhibitors of proliferation in CTCL, especially in the MyLa and HH cell lines.

Chapter 5: Identification of a Potential Lead Compound for MF Therapy

5.1 Introduction

As described earlier, ST0702 and related compounds have demonstrated antiproliferative activity in various CTCL cell lines. The aim of this chapter is to describe studies that were carried out towards the identification of new substances with potential clinical utility for the skin-directed treatment of MF that have greater activity than ST0702. Neither ST0702 nor ISAL had demonstrated antiproliferative activity in MyLa cells, and their effect on proliferation of HH cells was modest. The other known compounds, the isomannide and isosorbide analogues described in Chapter 2, also had limited antiproliferative efficacy in the HH and MyLa cell lines. Our strategy was to broadly screen compounds across the isosorbide library to understand structural features leading to MyLa proliferation inhibition and to use this information in the design of new substances with interesting efficacy and selectivity on MyLa viability. We were successful in designing a compound series with interesting activity features.

5.1.1 Library of Compounds tested

To assist in the optimisation of compounds, a broad library of isosorbide-based esters was identified and investigated. The initial screening compounds were available in the lab, having been synthesised by previous researchers in the Gilmer group. The library also contained a number of compounds that had been synthesised throughout this project, but had not yet been tested in biological assays. The compounds all contained an isosorbide scaffold, with different substituents on the 2- and 5-positions. Some compounds were chosen based on their similarity to ST0702, such as isosorbide-2 aspirinate-5-*o*-toluate (**27**), which differs from ST0702 because of the toluate ester in the 5-position, as opposed to the nicotinate ester in ST0702.

It had been ascertained from previous work that for optimal inhibitory activity on the proliferation of CTCL cells the isosorbide group should have an aryl group on both position 5 and position 2. Examples of this include ST0702 itself, ISAL, **14** and **3**, which were the lead compounds from the first set of compounds based on STAT3 activation and HuT78 proliferation. It was desirable to investigate as far as possible within the current compound set the positional substitution effects on proliferation inhibition.

A number of legacy compounds from the Gilmer lab contained a carbamate ester at position 2. Carbamates are esters of carbamic acid. These carbamates had been previously investigated as potential butyryl cholinesterase inhibitors (355-358). Structurally, the carbamate functionality is related to amide-ester hybrid features, and the group displays good chemical and proteolytic

stabilities (359). Carbamates have been used as peptide-bond surrogates, mainly due to their chemical stability and capacity to permeate cell membranes. Carbamates are also able to modulate inter- and intramolecular interactions with the target enzyme or receptors. The carbamate functionality imposes a certain degree of conformational restriction due to the delocalisation of nonbonded electrons on nitrogen into the carboxyl moiety. The carbamate functional group can also participate in hydrogen bonding through the carboxyl group and the backbone NH. Substitution of the O and N-terminals of a carbamate can allow for the modulation of biological properties and improvement in stability and pharmacokinetic properties (359).

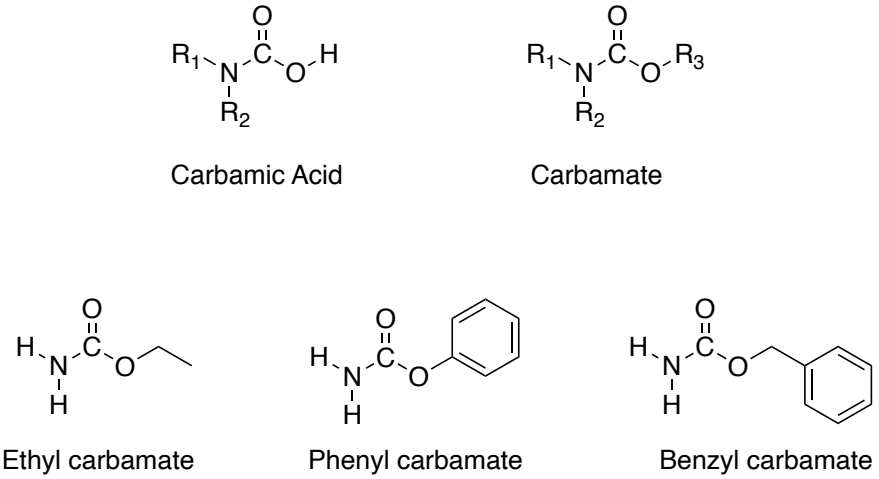

Figure 5-1: Examples of different carbamates.

A full list of the compounds tested, and their chemical structures, can be found in Figure A3 of the Appendix. The library of compounds were tested as inhibitors of proliferation of MF CTCL cell lines (MyLa, HH) and of leukaemic CTCL cell lines (HuT78), as STAT3 inhibitors, and as inhibitors of oxidative phosphorylation.

5.2 Results and Discussion

5.2.1 Library Screening for antiproliferative effect on CTCL cell lines

The first set of experiments carried out assessed the inhibitory effects of the compound set at 100 μM on the MyLa cell line. The cells were incubated with the compounds for 48 h, after which time the antiproliferative activity was measured. A number of compounds showed good inhibitory effect in the first screen (Figure 5.2). The most effective compound was **36**, isosorbide-2-aspirinate-5-(3-chloromethyl) benzoate, followed by **48**, isosorbide-2-aspirinate-5-(6-chloronicotinate), both with anti-proliferative effects greater than 50%. Compounds **41**, **37**, **38**, **31**, **26** and **33** all caused reductions of between 30 and 45%. Aside from the carbamates, these compounds all had a substituted aryl group attached at position 2 and position 5 of an

isosorbide skeleton, which confirmed that the SAR inferred from the first set of compounds screened was correct.

Compounds unsubstituted at position 2 or 5- showed greatly reduced inhibition of proliferation in the MyLa cells. Compounds **23** (isosorbide-5-salicylate), **24** (isosorbide-5-aspirinate), **40** (isosorbide-2-ethylcarbamate), **53** (isosorbide-2-*m*-methoxybenzoate), **54** (isosorbide-2-*p*-methoxybenzoate) and **42** (isosorbide-2-phenylcarbamate) all had no antiproliferative effect in the MyLa cells.

Several compounds bearing a nitrate ester group (-ONO_2) on position 5 of the isosorbide group were also found to be inactive. Compounds **25**, **12**, **9e**, **49**, **50** and **51** all contained a nitrate ester group on position 5 and all were demonstrated to be inactive. Another interesting and consistent observation was the lack of effect of the isonicotinate ester compounds, as evidenced by compounds **4** (isosorbide-2-aspirinate-5-isonicotinate), **15** (isosorbide-2-benzoate-5-isonicotinate) and **52** (isosorbide-2-salicylate-5-isonicotinate).

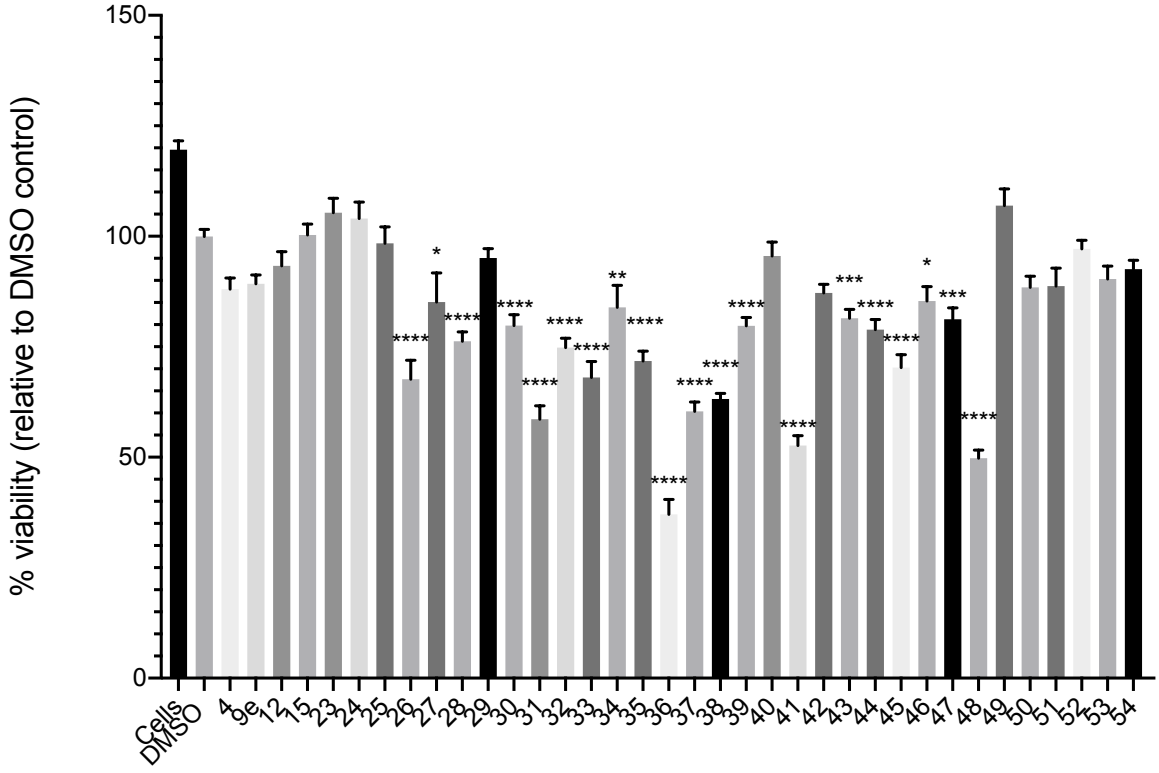

Figure 5-2: Antiproliferative activity of library of compounds tested at 100 μM on MyLa cells. MyLa cells were plated at 1 × 10^4 cells per well of a 96-well plate. The cells were treated with compound and incubated for 48 h. After this time, MTT was carried out. Results for each concentration are expressed as mean ± SEM of three experiments performed in triplicate.

This panel were also screened for effects on the HH cell line, and the results are shown in Figure 5.3. In general, the compounds were more effective on HH cells than the MyLa cell line. Compounds **36**, **41**, **48** and **27** all exhibited >50% inhibition. Interestingly the compounds that showed highest antiproliferative activity in the MyLa experiments also had effect in the HH cells, with the exception of **37** (isosorbide-2-aspirinate-5-biphenyl ester) which was highly antiproliferative in the MyLa, but had a very small effect on the proliferation of HH cells.

Once again bearing an unsubstituted hydroxy or a nitrate ester group in the 5 position of the isosorbide ring led to reduced activity (5-OH: Compounds **23**, **24**, **40**, **42**, **53**, **54**. 5-ONO_2: Compounds **44**, **47**, **12**, **9e**, **49**, **50**). Also, the 5-isonicotinates (**4**, **52** and **15**) were less active.

In both the HH and the MyLa cells, there was a significant effect of DMSO on cell viability compared to cells that received no treatment. The vehicle control was cells treated with 0.5% DMSO (1 µL in a 200 µL well of a 96 well plate). A similar DMSO level was used in the HuT78 experiments, but the effect was not as large. The reasons for this effect are not known but it needs to be considered in reviewing the experimental results.

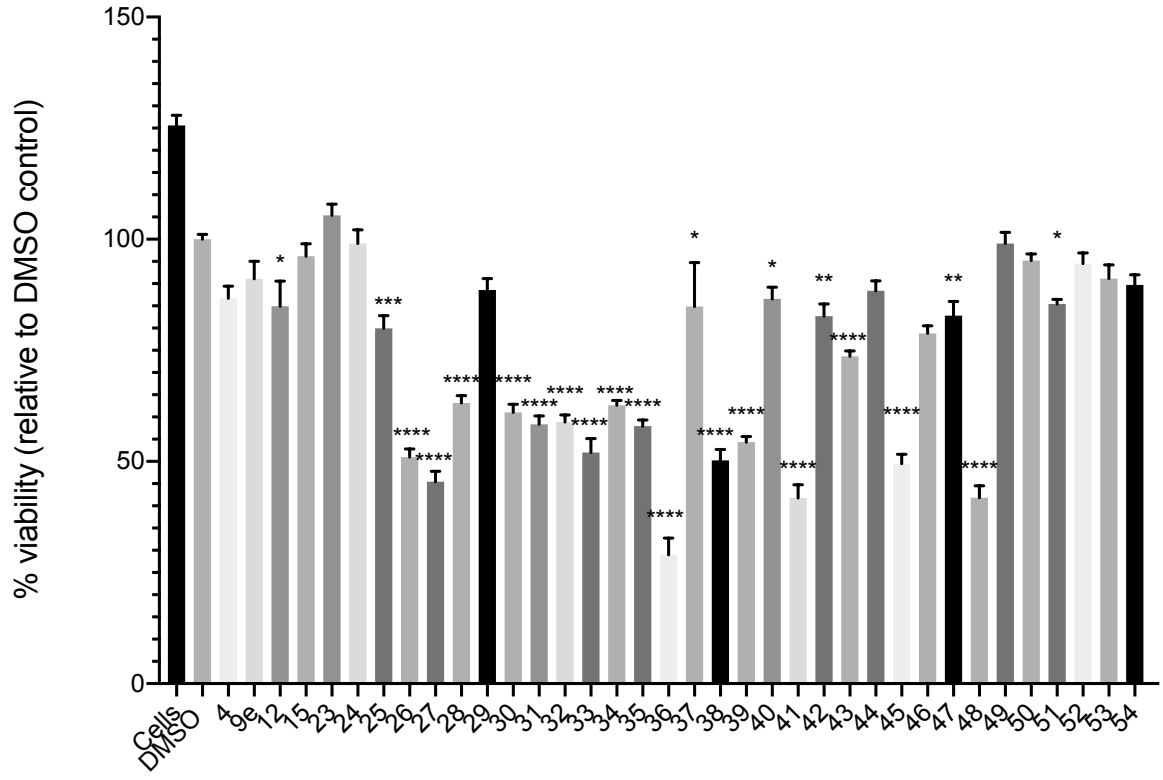

Figure 5-3: Antiproliferative activity of broad library of compounds tested at 100 µM on HH cells.

HH cells were plated at 1 × 10^4 cells per well of a 96-well plate. The cells were treated with compound and incubated for 48 h. After this time, MTT was carried out. Results for each concentration are expressed as mean ± SEM of three experiments performed in triplicate.

The inhibitory effect of the compounds on cell viability in the two CTCL cell lines was plotted (Figure 5.4). The most efficacious compounds in both assays were identified. These compounds are presented in Figure 5.5.

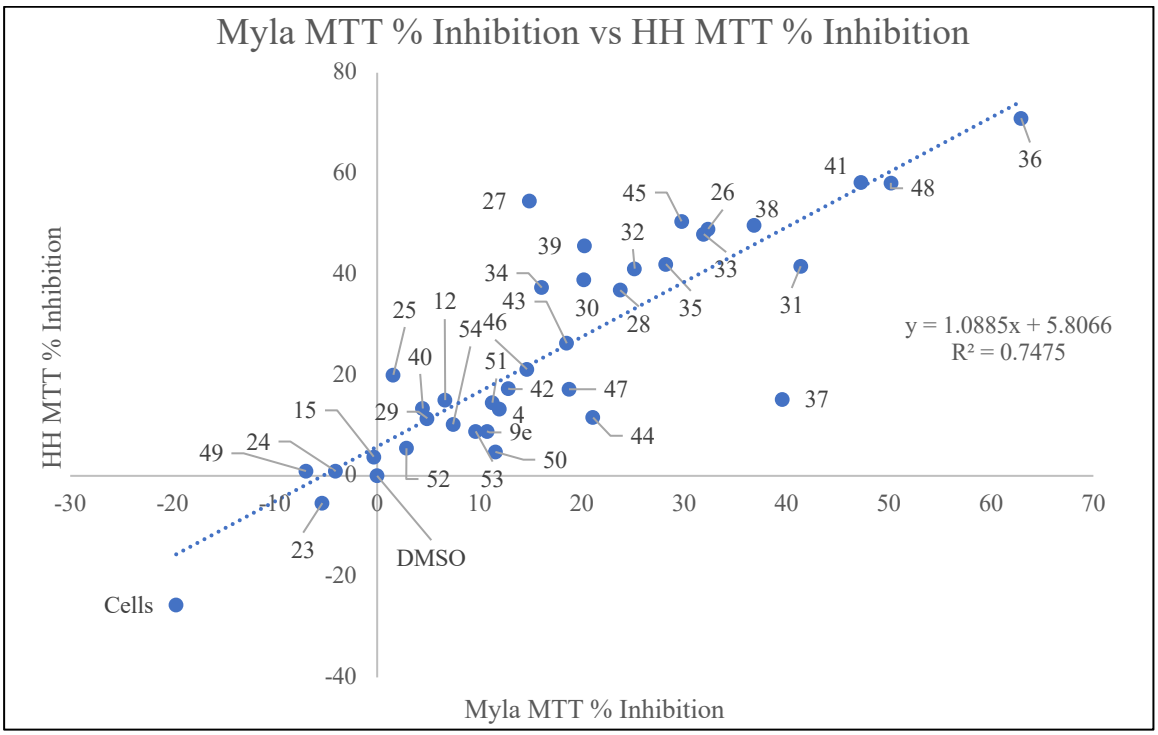

Figure 5-4: Correlation curve of MyLa MTT % inhibition vs HH MTT % inhibition. MyLa % reduction in proliferation was measured using MTT and the results presented in Figure 5.2. HH % reduction in proliferation was measured using MTT and the results presented in Figure 5.3.

The compounds with carbamate functional groups, **48**, **41** and **45** were considered less promising candidates for application in skin treatment because of their likely stability in skin, indeed some of these are already established as potent inhibitors of serum cholinesterase. This means that there is a possibility that these intact compounds could penetrate the skin, and potentially exert systemic effects. Compounds **36** and **31** both contain a chlorine atom, which was considered undesirable since it is mainly an xenobiotic atom. Chlorine drugs are known but these have undergone extensive toxicity testing. Compound **36**, exerted antiproliferative effect on both the HH and the MyLa cells above 50%, suggestive of a cytotoxic effect rather than a cytostatic effect. Compound **38** is a biphenyl diester, that again looked unfavourable for application in medicine compared with some of the other compounds in the MyLa hits, particularly with the potential for biphenyl to cause carcinogenicity in humans (360). The two most promising compounds to arise out of this study were **33**, isosorbide-2-aspirinate-5-*p*-methoxybenzoate, and **26**, isosorbide-2-aspirinate-5-*m*-toluate.

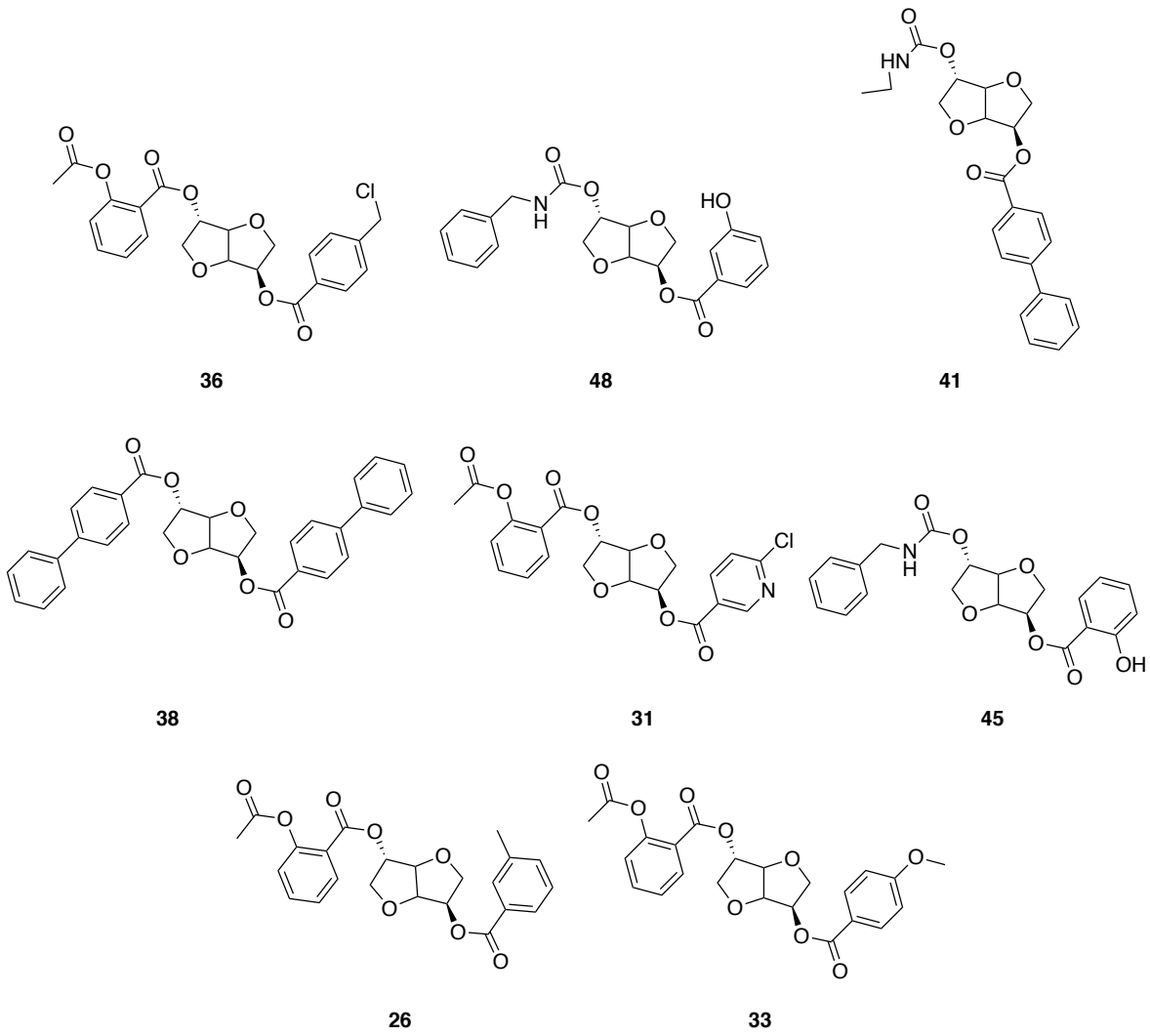

Figure 5-5: Compounds with greatest antiproliferative activity of HH and MyLa cells.

5.2.2 **Library screening for antiproliferative effect on HuT78 cells**

We next measured the compound effect on proliferation of the HuT78 cell line used in previous studies described in this thesis. The HuT78 cell line is perhaps a little less relevant than the MyLa and HH which are both specifically MF cell lines, because HuT78 cells were derived from a patient with SS, an aggressive leukaemic variant of MF.

This screen revealed several isosorbide esters in the Gilmer collection with significantly greater activity than ST0702 which up to that point in the work had been regarded as the lead because of its activity. Under the experimental conditions, it had been shown that ST0702 (100 μM) caused a reduction in viability in the HuT78 cells of around 40% (Figure 2.24). A number of the compounds tested here, such as **31** (63% reduction), **33** (70% reduction), **35** (60% reduction), **36** (81% reduction), **37** (67% reduction), **38** (55% reduction), **41** (66% reduction), **45** (66% reduction) and **48** (76% reduction) had inhibitory activity greater than 60% (Figure

5.6). The majority of these compounds (**31**, **33**, **35**, **36**, **37**, **38**) had aryl esters at the 2 and 5 position. Three of the hits had carbamate functional groups attached at position 2 of the isosorbide ring (**41**, **45** and **48**).

As before, compounds bearing an unsubstituted 5-hydroxy or a nitrate ester group exhibited little or no activity. Compounds with isonicotinate groups also had no activity, so it can be proposed that the presence of a hydroxy, nitrate ester or isonicotinate group at position 5 of the isosorbide ring does not confer activity.

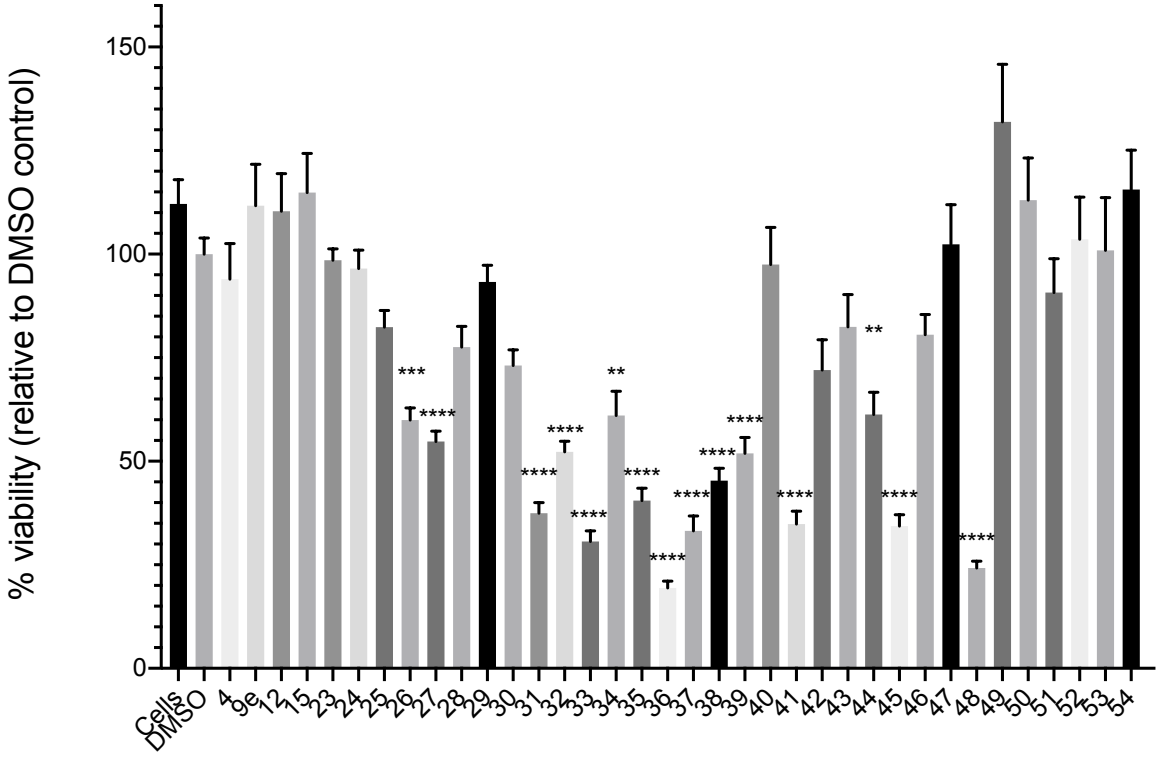

Figure 5-6: Antiproliferative activity of library of compounds tested at 100 μM on HuT78 cells. HuT78 cells were plated at 1 × 10^4 cells per well of a 96-well plate. The cells were treated with compound and incubated for 48 h. After this time, MTT was carried out. Results for each concentration are expressed as mean ± SEM of three experiments performed in triplicate.

5.2.3 **Library screening for inhibition of STAT3 activity in the IL-6 reporter**

The library was next screened in the HEK-Blue IL-6 reporter described earlier (Section 3.2.4). A number of compounds emerged from this screen with interesting levels of STAT3 inhibitory activity, including **36** (85% reduction), **32** (84% reduction), **48** (82% reduction), and **26**, **27**, **39**, **41**, **45** and **33**, all of which had reductions of between 70 and 80% (Figure 5.7). Again this screen produced a breakthrough in the STAT3 inhibitory ceiling up to that point.

Among the interesting compounds and potential candidates, **26** and **27**, the *m*- and *o*- toluates, exhibited a very similar effect in this assay suggesting tolerance for position of substitution. The analogous compounds **32** and **33**, the *o*- and *p*- anisates also differ only in the substitution pattern of the methoxy group on the aromatic ring. These presented similar inhibitory effect in this assay.

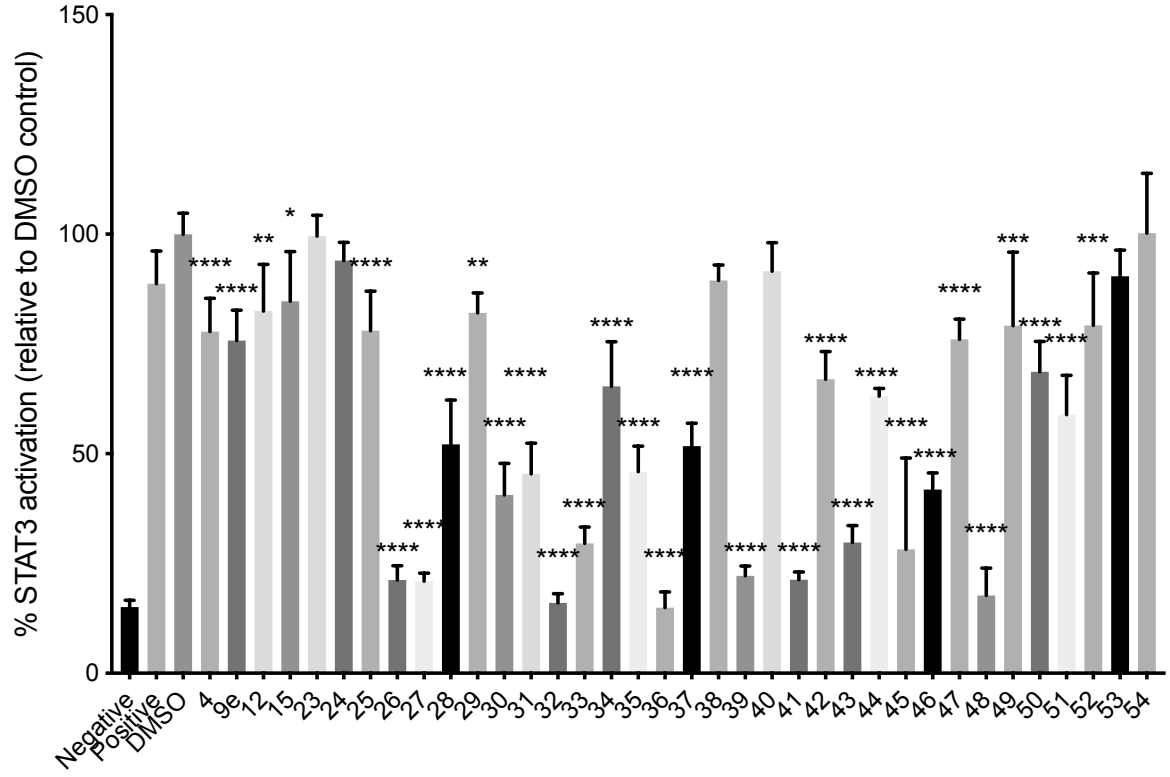

Figure 5-7: STAT3 inhibitory activity of broad library of compounds tested at 100 μM. HEK-Blue IL-6 cells were plated at 5 × 10^4 cells per well of a 96-well plate. Cells were treated with 100 μM compound or DMSO vehicle. After 30 min incubation, the cells were stimulated with 1 ng/mL IL-6. After 24 h Quantiblue Reagent was added and SEAP levels were determined. Data is expressed as mean ± SEM of three experiments performed in triplicate.

Another interesting finding was that active compounds such as **26**, **27**, **32** and **33** did not possess an aspirin ester. However **39**, which had a salicylate ester at both position 2 and 5, did inhibit STAT3 activation to a large degree. Three compounds, **41**, **45** and **48** that contained carbamate functional groups at the 2-position had large inhibitory effects on STAT3 activation.

Further insight into the SAR requirements for these effects can be gleaned from reviewing inactive compounds in the assay. Compounds **23** (isosorbide-5-salicylate), **24** (isosorbide-5-aspirinate), **40** (isosorbide-2-ethylcarbamate), **53** (isosorbide-2-*m*-methoxybenzoate) and **54** (isosorbide-2-*p*-methoxybenzoate) all had no effect on STAT3 inhibition. These compounds are all unsubstituted at the 2- or 5- position. The only other compound in the library with an

unsubstituted isosorbide hydroxyl group was **42** (isosorbide-2-phenylcarbamate). This had a modest effect on STAT3 activation, but overall it can be concluded that diaryl substitution is a requirement for activity.

The compounds were next screened for activity at 25 μM (Figure 5.8). Of the most effective compounds, only three compounds, **48**, **41** and **33** exhibited inhibitory activity greater than 40% at 25 μM.

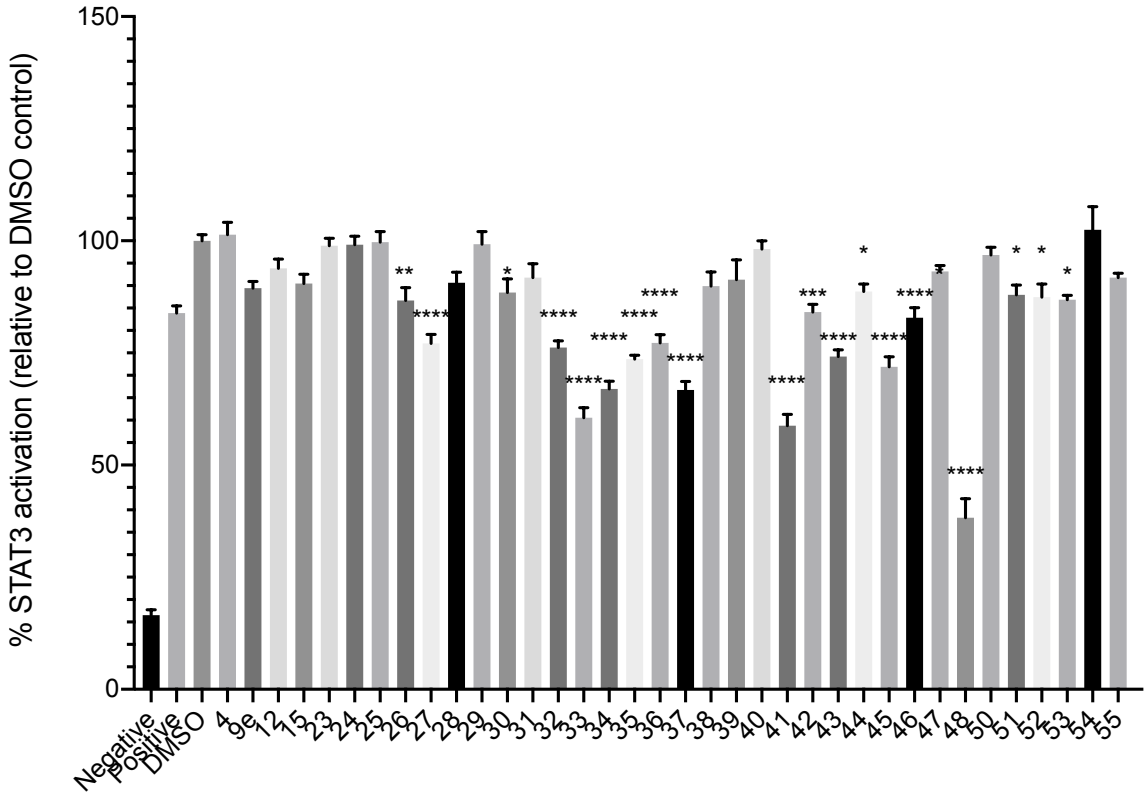

Figure 5-8: STAT3 inhibitory activity of broad library of compounds tested at 25 μM. HEK-Blue IL-6 cells were plated at 5 × 10^4 cells per well of a 96-well plate. The cells were treated with compound and after 30 min incubation, the cells were stimulated with 1 ng/mL IL-6. After 24 h Quantiblue Reagent was added and SEAP levels were determined. Data is expressed as mean ± SEM of three experiments performed in triplicate.

The correlation between the effect of the compounds on STAT3 activation and the anti-proliferative effect on HuT78 cells was examined (Figure 5.9). The coefficient of determination was 0.5883. A number of interesting compounds, such as **38**, had an anti-proliferative effect on HuT78 but did not inhibit STAT3. Compound **43**, also had a small anti-proliferative effect on HuT78, considering its inhibitory effect on STAT3 activation (70%). From the correlation curve it can be seen that the best compounds in the STAT3 and HuT78 MTT assay combined were **36**, **48**, **41**, **45**, **33**, **32**, **39**, **27**, **35** and **37**. The structures for compounds **36**, **48**, **41**, **45** and

33 are outlined in Figure 5.5. The structures for compounds **32**, **39**, **27**, **35** and **37** are given in Figure 5.10.

There is a consistent pattern through the series with respect to inhibition of cell proliferation across multiple cell lines and STAT3. Compounds **36**, **48**, **41** and **33** all appear to have a significant effect on MyLa, HH and HuT78 proliferation and cause a reduction in STAT3 activation. Compounds **41** and **48** have already been ruled out due to the stability of the carbamate group, and resistance to esterase activity. Compound **36** has also been ruled out due to the potential toxicity of the chloro-group. Compound **33** was identified as a substance of interest because of its activity in multiple measures and its potentially safe esterase mediated metabolites, including aspirin, salicylic acid and *p*-anisic acid, a substance used in various food and cosmetic applications.

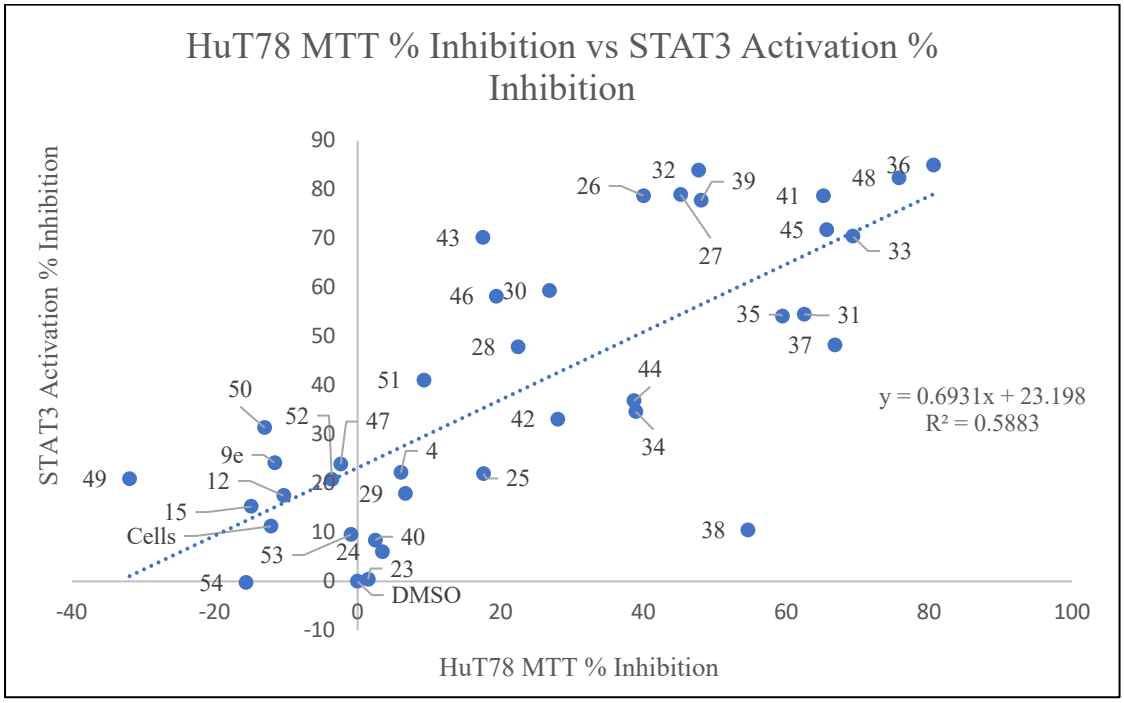

Figure 5-9: Correlation curve of HuT78 MTT % inhibition vs STAT3 activation.
HuT78 % reduction in proliferation was measured using MTT and the results presented in Figure 5.6. STAT3 % inhibition was measured using HEK-Blue IL-6 reporter cell lines and the results were presented in Figure 5.7.

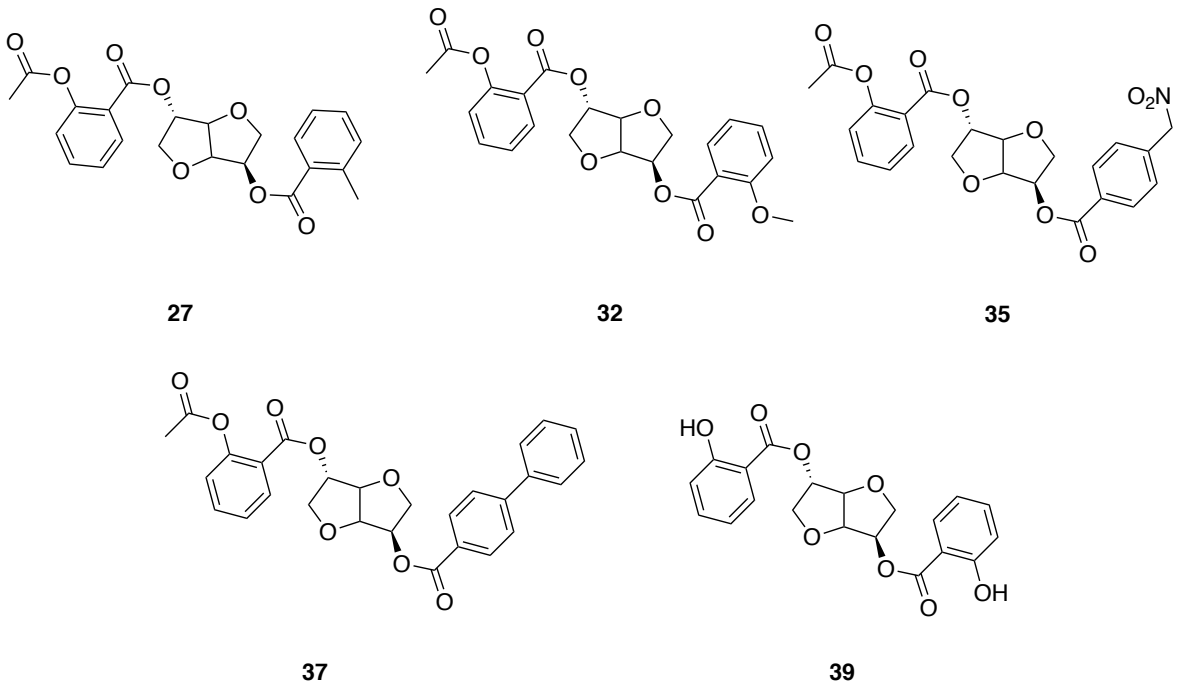

Figure 5-10: Selection of compounds with greatest antiproliferative activity on HuT78 cells and STAT3 inhibitory activity.

5.2.4 **Effect of hits from CTCL inhibitors studies on OCR and role of OXPHOS**

The effect of hit compounds on oxidative phosphorylation in HuT78 cells was measured (Figure 5.11). Compounds were selected for evaluation based on their antiproliferative effect on the HH and MyLa cell lines. The biggest effect was observed with ST0702 and its analogue **26** which is a 2-aspirinate with a *m*-toluate ester in the 5-position. The toluate ester **26** had previously been shown to possess good antiproliferative activity in the all CTCL cell lines and STAT3 inhibitory activity. Compound **33**, which had become a kind of lead at this stage because its inhibitory properties on CTCL cell lines and STAT3 reporter, did have small effect on the OCR. Compound **32** was also tested, as it is very similar structurally to **33**, differing only in the substitution pattern of the methoxy group on the benzoate ring at position-5. In compound **32**, the methoxy is in the ortho position, whilst in **33**, it is para. The two compounds have demonstrated very similar activity in all previous assays, with **33** appearing just slightly more effective in the HH and MyLa cells. Similar results are observed here, in that the magnitude of effect for both compounds is similar, but compound **32** had slightly greater effects on OCR in the HuT78 cells. Interestingly, the carbamate compounds tested, **41** and **48**, which had been so effective at inhibiting proliferation in the CTCL cell lines, had no effect on OXPHOS. This indicates a requirement for ester functionality for the OCR inhibitory effect and also that the CTCL inhibitory effect of these compounds is unlikely to be due to the suppression of OCR. At this stage of the project it was not possible to tell if the OCR effect of

ST0702 and **33** was causative in the CTCL inhibitory effect. The structures for compounds **26**, **33**, **38**, **41** and **48** are outlined in Figure 5.5, whilst the structure for **32** is outlined in Figure 5.10.

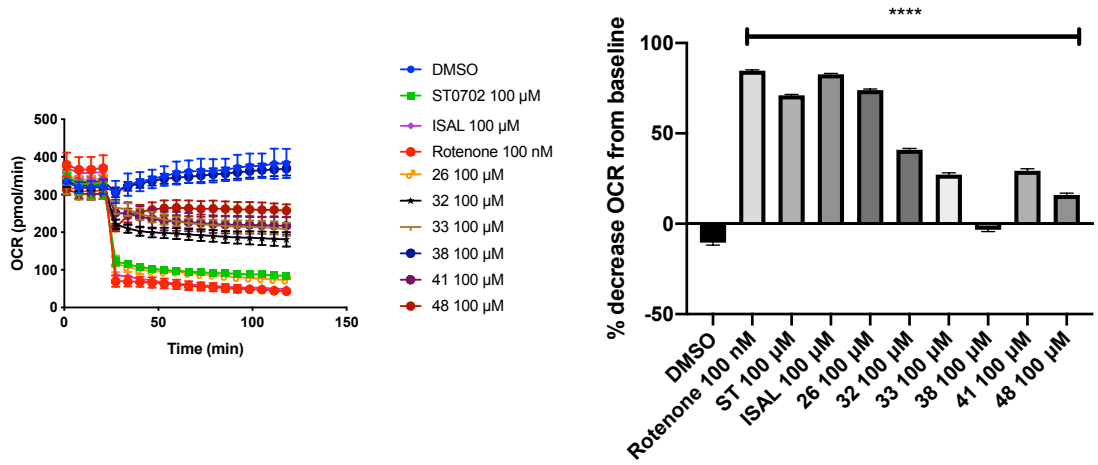

Figure 5-11: Inhibitory effect of compounds on OCR levels in HuT78 cells measured using Seahorse XF Analyser.

HuT78 cells were plated at a density of 1 ×10^5 cells/well. Basal OCR readings were obtained and compound or DMSO was injected after 24 min. The OCR was measured in quadruplicate and the results are expressed as mean ± SEM.

5.2.5 Design and synthesis of analogues of 33: Dianisates and Anisate Nicotinates

Compound **33** had been identified as the most interesting of the compounds from the broad compound library. It had an aspirinate group at the -2 position and a para-methoxybenzoate group at the -5 position, rather than the nicotinate group that is present in ST0702.

Assay	% inhibition ± SEM
MyLa MTT	31.92 ± 3.58
HuT78 MTT	69.36 ± 2.56
STAT3	70.42 ± 1.53
HH MTT	47.97 ± 3.16
HaCaT MTT	53.5 ± 9.32

*Figure 5-12: Effects of compound **33** (100 µM) in various biological assays*

Based on the results of compound **33**, and in particular its effects on the HH and MyLa cells, it was decided to synthesise a new library of compounds with a similar structure to **33**. The importance of the aspirinate group at position 2 of the isosorbide group had not been fully investigated, as the majority of the compounds tested in Library 2 had the aspirinate group in

position 2. Since the methoxy-benzoate group seemed to confer activity at the 5-position, it was decided to assess the effect of methoxy substitution in position 2 while retaining the 5-anisate ester, in other words it was decided to produce and test symmetrical and unsymmetrical 2,5-dianisates.

5.2.5.1 *Synthesis of 2, 5-isosorbide-dianisate compounds*

For the first set of compounds the methoxy benzoate group at position 5 was retained, but the aspirinate group in position-2 of compound **33** was replaced with an anisate group. The substitution position of the methoxy substituent on the ring was varied, as the results from the library screening had also highlighted that different substitution patterns on the aromatic rings could influence properties. In all, nine possible dianisate compounds were prepared. They were synthesised from isosorbide in either a one or a three-step sequence. These compounds will be referred to as the dianisate compounds, as they have a methoxybenzoate (anisate) ester at both position 2 and position 5 of the isosorbide ring.

Symmetrical dianisates (2,5-) could be synthesised directly from isosorbide (**55**) in a one-step reaction involving a reaction with two equivalents of 2,3 or 4- methoxybenzoyl chloride in the presence of tertiary base (Figure 5.13). These reactions proceeded smoothly, with percentage yields of approximately 90%, and, the final compounds were characterised using ^{1}H NMR, ^{13}C NMR and HRMS (high resolution mass spectroscopy).

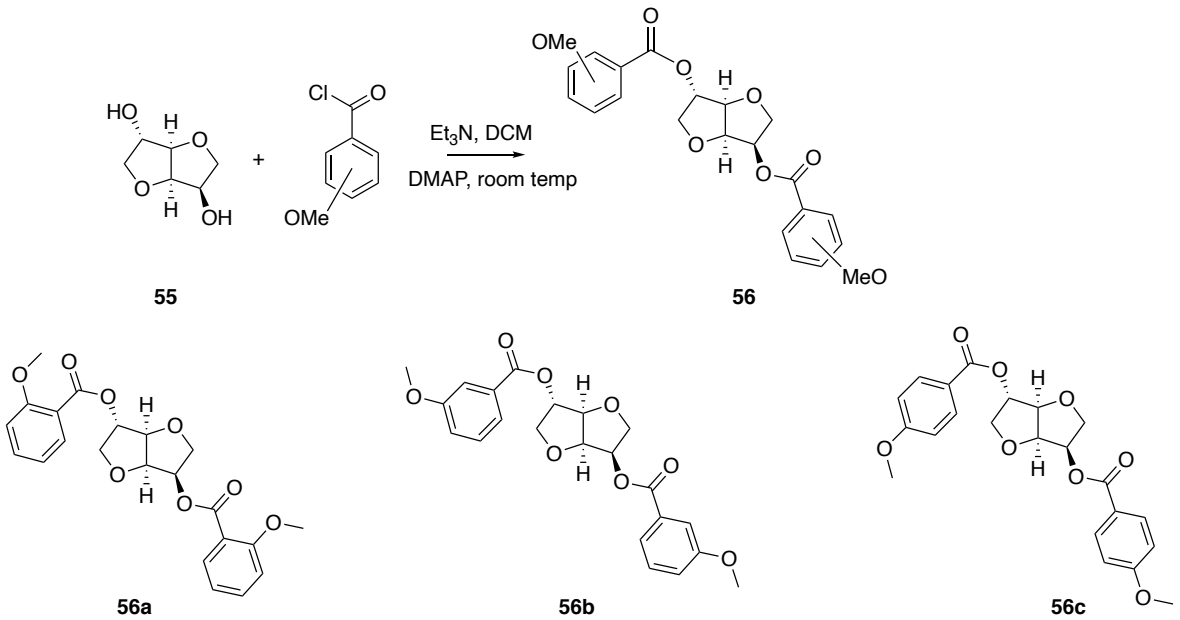

*Figure 5-13: Synthesis of symmetrical dianisates (**56**) from isosorbide (**55**) via a 1-step sequence.*

Unsymmetrically substituted dianisates were prepared by making first the anisate ester of ISMN (**57** below in Figure 5.14). The nitrate ester group at position 5 was then removed reductively, allowing it to be esterified with either *o*, *m* or *p*- methoxybenzoyl chloride.

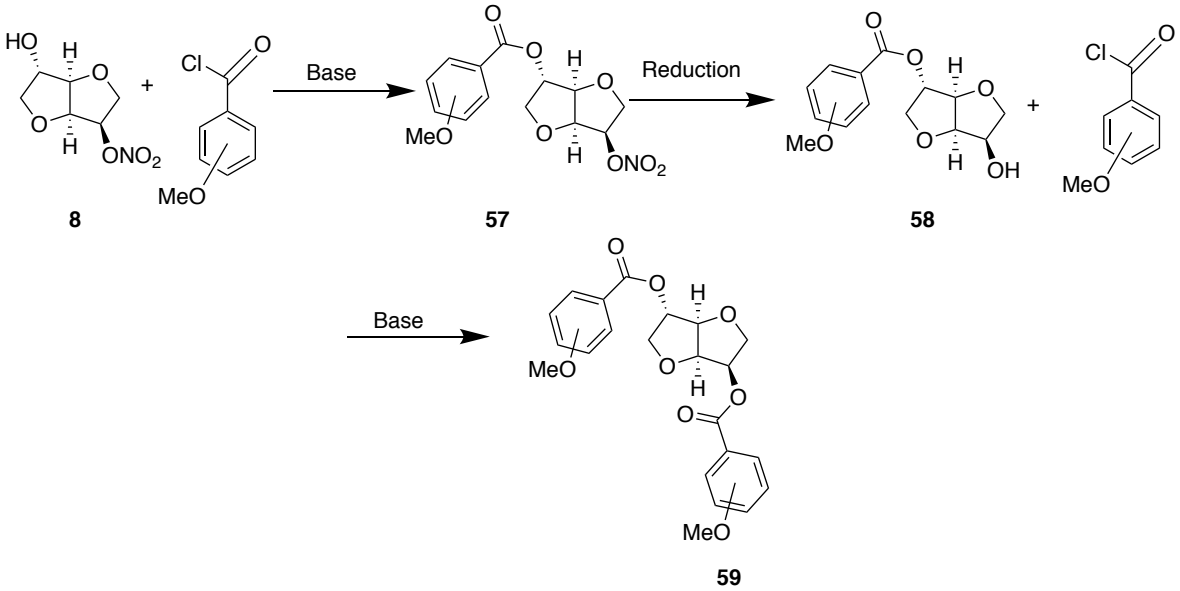

*Figure 5-14: Synthesis of unsymmetrical dianisates (**59**) from ISMN (**8**) via a 3-step sequence.*

The first reaction involves the esterification of the free hydroxyl group on the 2 position of the isosorbide ring with methoxybenzoyl chloride. In contrast to isosorbide, in ISMN, the 5 position is protected by the presence of the nitrate ester. Three different methoxybenzoyl chlorides are used, one with an ortho substitution, another with meta and the final having a para substitution pattern. The reactions were carried out under basic conditions and proceeded quickly at room temperature. DMAP was added as it had been found to speed up time to reaction completion. It is an electron rich pyridine that has been shown to provide superior levels of catalytic turnover for the acylation of sterically hindered alcohols. Yields of greater than 90% were obtained for these reactions and products were characterised using ^{1}H NMR.

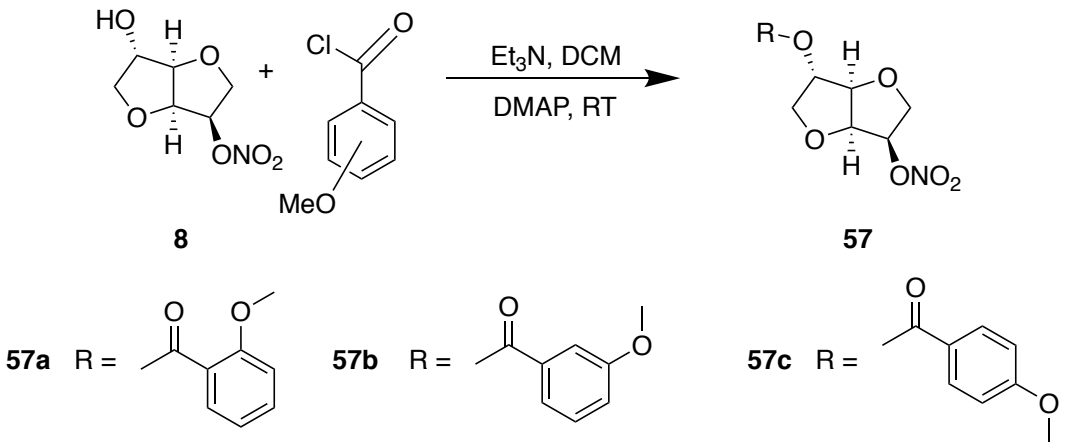

*Figure 5-15:Esterification of ISMN (**8**) with the appropriate methoxybenzoyl chlorides.*

The second reaction involved the reduction of the nitrate ester group using catalytic hydrogenation. Palladium on carbon (Pd/C) was used as the catalyst. The palladium metal is supported on activated carbon to maximise its surface area and activity. The nitrate ester is reduced to a hydroxyl group, which is then free to be esterified with the relevant acyl chloride in the next reaction. These reductions proceeded smoothly, with products generated at yields of greater than 80%.

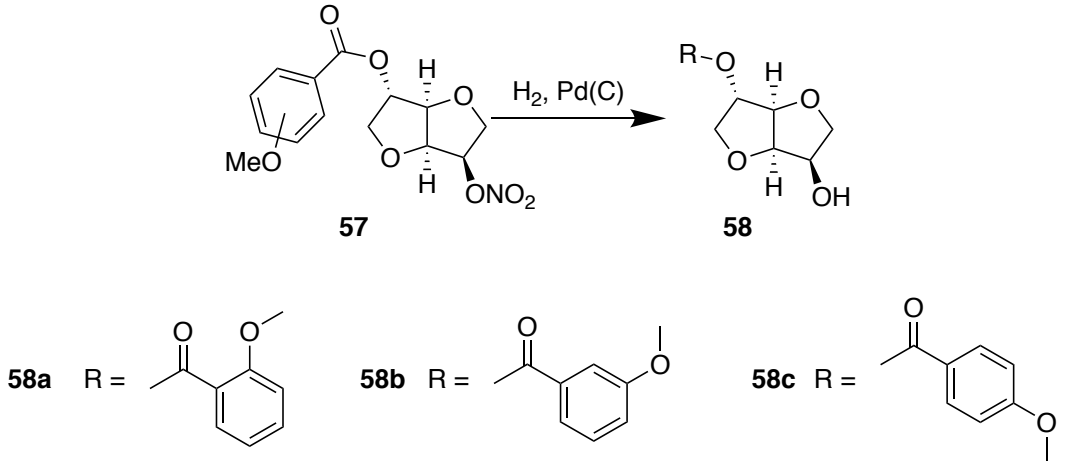

*Figure 5-16: Reduction of nitrate esters on C-2 esterified isosorbide compounds (**57**) using H_2, Pd/C.*

The final reaction involved the esterification of the available hydroxyl group at position 5 of the isosorbide ester. The synthesis was achieved by the reaction of methoxybenzoyl chlorides with a free -OH group at position-5 of the isosorbide ester in the presence of the tertiary amine, triethylamine and DMAP to produce the corresponding unsymmetrical dimethoxybenzoyl ester isosorbide derivatives (**59**). Product yields of greater than 80% were obtained for all these compounds, with the exception of **59d** (77% yield). The final compounds were characterised using ^{1}H NMR, ^{13}C NMR and HRMS.

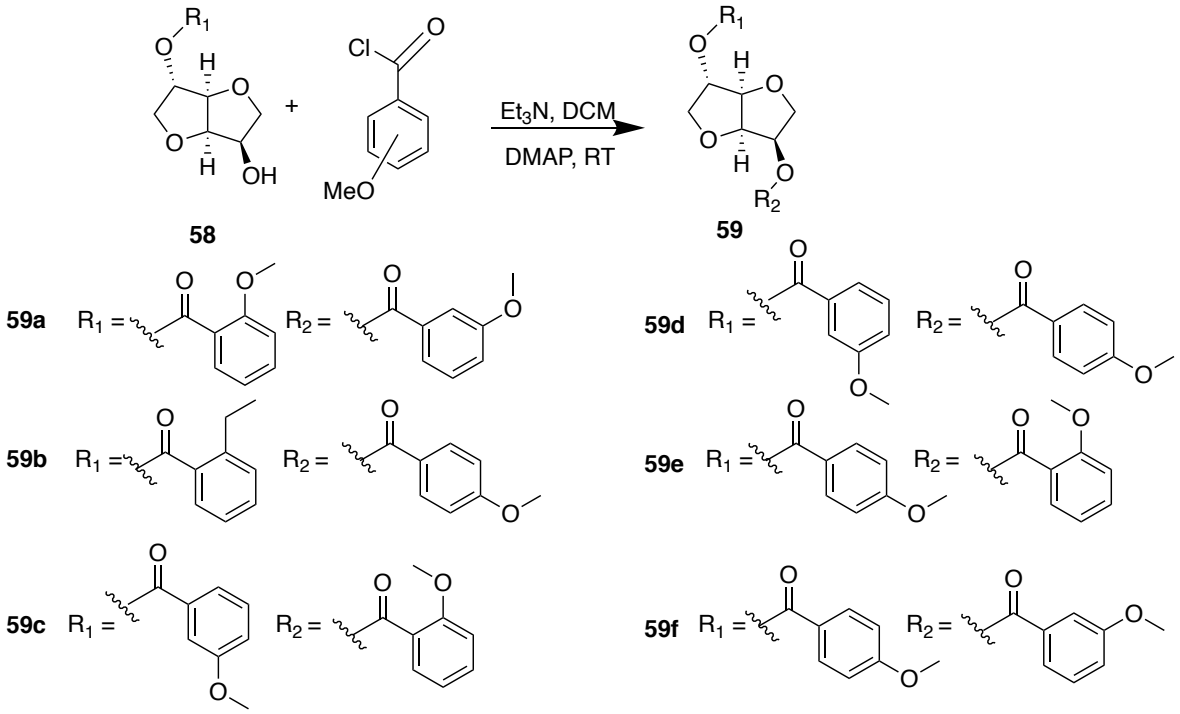

Figure 5-17: Esterification of isosorbide C5 with methoxybenzoyl chlorides.

5.2.5.2 *Synthesis of 2-anisate-5-nicotinate compounds*

Following the completion of this series it was decided to also investigate the effect of introducing a methoxy benzoate group at the 2-position but retaining the nicotinate ester at the 5-position. The 5-nicotinate is a feature of ST0702 and ISAL. The substitution position of the methoxy group on the 2-aryl substituent was varied. This produced three final test compounds; isosorbide-2-*o*-methoxybenzoate-5-nicotinate, isosorbide-2-*m*-methoxybenzoate-5-nicotinate and isosorbide-2-*p*-methoxybenzoate-5-nicotinate. These compounds will be referred to as the anisate nicotinate compounds, as they have a methoxybenzoate (anisate) ester at position 2 and a nicotinate ester position 5 of the isosorbide ring.

These compounds were synthesised in a three step sequence starting from ISMN, with esterification at the 2-position with anisoyl-chlorides, followed by reduction of the nitrate ester group to a hydroxyl group by hydrogenation. The free hydroxyl group was then esterified using nicotinoyl chloride. The reaction scheme is outlined in Figure 5.18. The first two steps of the reaction are the same as those outlined in Figure 5.15 and 5.16.

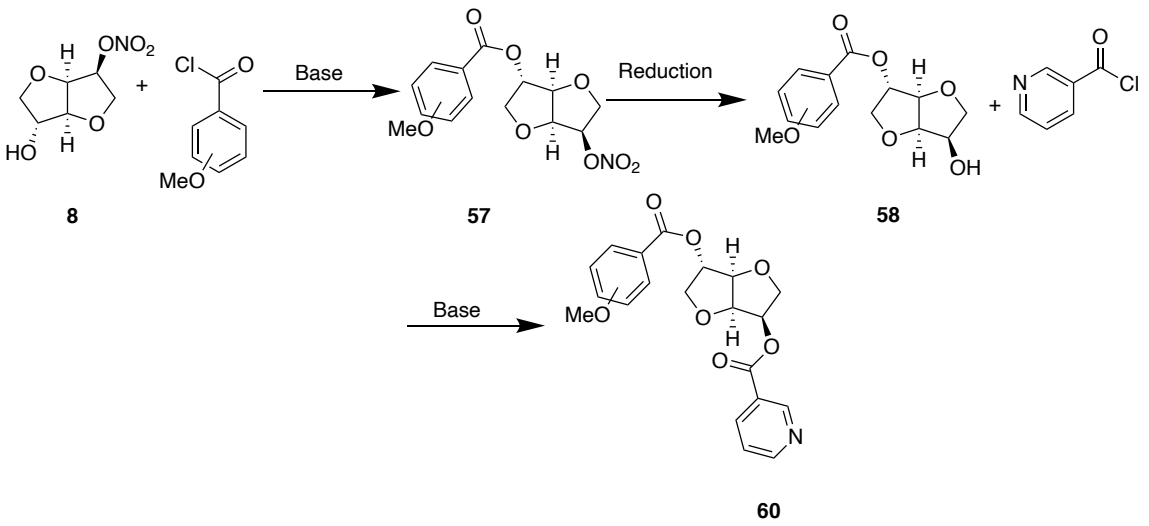

*Figure 5-18: General reaction scheme for synthesis of isosorbide-2-(o,m,p)-anisate-5-nicotinates (**60**) from ISMN (**8**).*

The final step of this reaction involves the introduction of the nicotinate functional group onto the available hydroxyl group at position 5 of the isosorbide esters as shown in Figure 5.19. The synthesis was achieved by the reaction of nicotinoyl chloride with the free -OH group at position-5 of the isosorbide ester in the presence of the tertiary amine, triethylamine and DMAP to produce the corresponding isosorbide-2-methoxybenzoate-5-nicotinate compounds, with varying substitution patterns of the methoxy group on the aromatic ring.

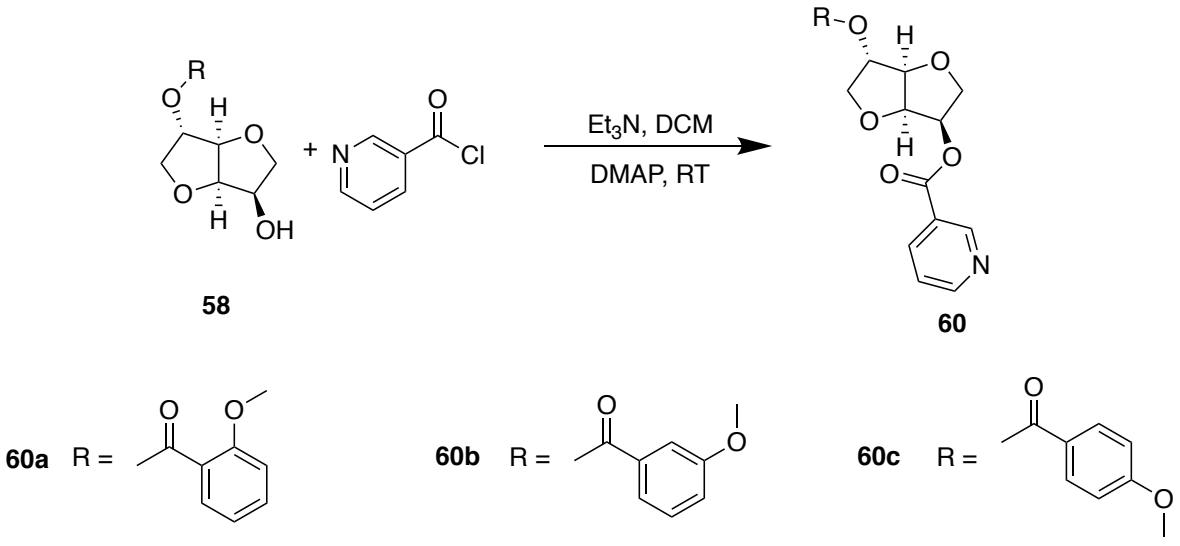

*Figure 5-19: Esterification of isosorbide-2-methoxybenzoate (**58**) with nicotinoyl chloride.*

This final reaction, where the monosubstituted isosorbide is reacted with nicotinoyl chloride did pose some degree of difficulty. The addition of the nicotinate ester group is always quite

slow, and requires many more equivalents of nicotinoyl chloride to be used than would be expected. It is also quite difficult to determine when the reaction has gone to completion, because the nicotinate product has similar Rf to the starting material from which it is derived. Freshly prepared vanillin stain can be used to discriminate between the starting material and product but the reaction needs to go as far as possible to completion since the purification/separation on silica gel is challenging. The percentage yields obtained for the products of these reactions ranged from 45 to 66%. The final compounds were characterised using ^{1}H NMR, ^{13}C NMR and HRMS.

5.2.6 **Antiproliferative activity of dianisates and anisate-nicotinates on MyLa cells**

The inhibitory effect of the compounds on MyLa cell proliferation was determined following incubation at 100 μM for 48 h. As has been seen in our previous studies, the DMSO effect on MyLa cells was again quite large. The compounds **59b**, **59e**, **60a** and **60b** all had antiproliferative activity of greater than 40% compared to the DMSO vehicle control. This was higher than the antiproliferative effect observed for **33**. Interestingly, the dianisate compounds with the symmetrically substituted dianisates i.e. **56a**, **56b** and **56c,** demonstrated no antiproliferative activity.

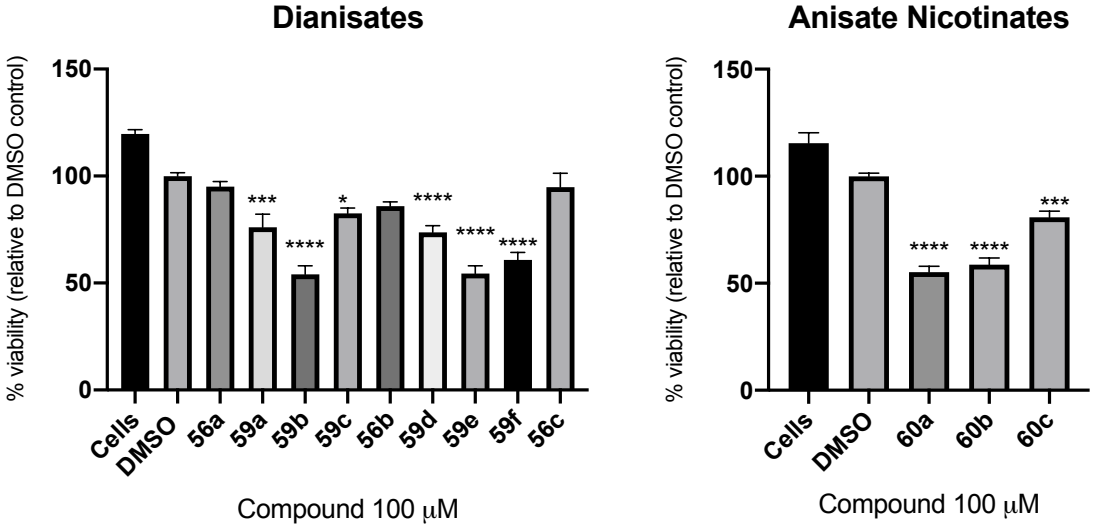

Figure 5-20: Antiproliferative activity of dianisates and anisates tested at 100 μM on MyLa cells.

MyLa cells were plated at 1 × 10^{4} cells per well of a 96-well plate. The cells were treated with compound and incubated for 48 h. After this time, MTT was carried out. Results for each concentration are expressed as mean ± SEM of three experiments performed in triplicate.

The compounds were then tested at 100, 50 and 25 μM. The **59b** substituted compound emerged as interesting with significant effects over the entire concentration range suggesting

that the inhibitory effect had already plateaued at 25 µM. **59b** was the most potent inhibitor of MyLa proliferation that we were able to identify and its properties justified its design and synthesis. The anisate-nicotinate compounds tested showed modest inhibitory properties in general with some notable effects with **60a**. The common 2-*o*-OMe was noted in the two compounds. The compound **19g** has the same structure as **60a**, the only difference being that **19g** has an isomannide group, whereas **60a** has an isosorbide. **19g** had no antiproliferative activity when tested the MyLa cells (Figure 4.8), again signifying that the presence of the isosorbide group confers greater activity.

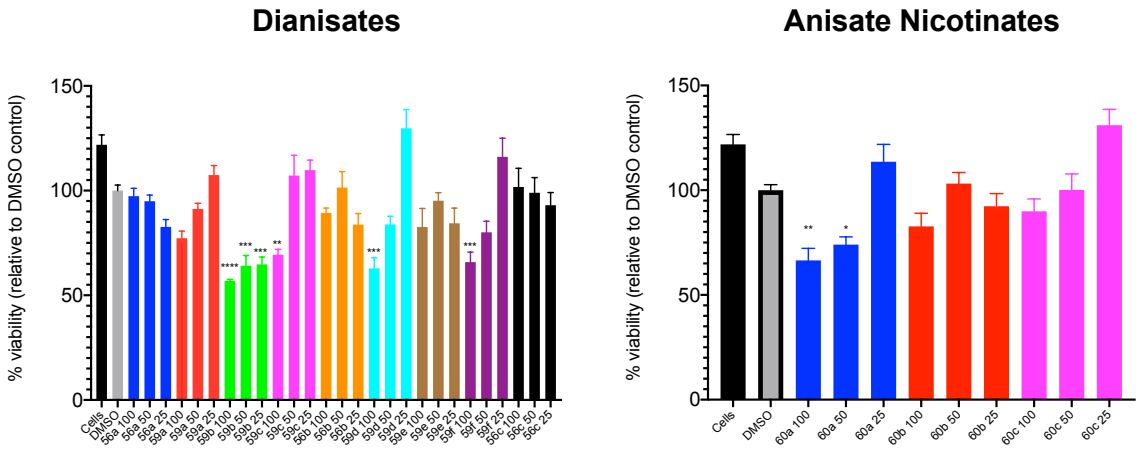

Figure 5-21: Antiproliferative activity of dianisates and anisates at 100, 50 and 25 µM on MyLa cells.

MyLa cells were plated at 1 × 10^4 cells per well of a 96-well plate. The cells were treated with compound and incubated for 48 h. After this time, MTT was carried out. Results for each concentration are expressed as mean ± SEM of three experiments performed in triplicate.

5.2.7 Antiproliferative effect of dianisates and anisates on HH cells

The anisate and anisate nicotinate compounds were next tested in the HH cell line. The most effective compounds in this cell line were **59f**, **60b** and **60a** with proliferation inhibition of greater than 50% (**60a** and **60b** both inhibiting HH proliferation by approximately 60%). The compounds were tested at 100, 25 and 10 µM. None of the dianisate compounds had statistically significant effects on proliferation in HH when assessed at 25 or 10 µM. The compound **60b** did have statistically significant effects at 25 and 10 µM, but the magnitude of effect at these concentrations was quite small.

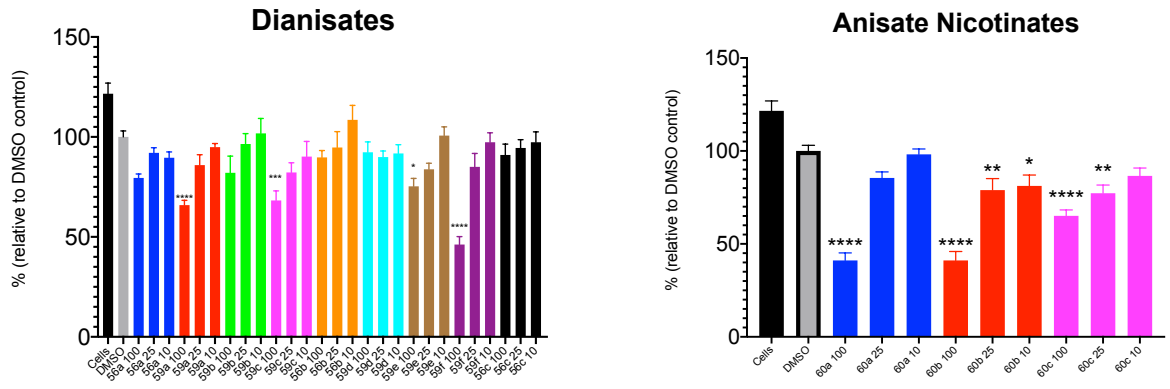

Figure 5-22: Antiproliferative activity of anisates and dianisates at 100, 25 and 10 μM on HH cells.

HH cells were plated at 1 × 10^4 cells per well of a 96-well plate. The cells were treated with compound and incubated for 48 h. After this time, MTT was carried out. Results for each concentration are expressed as mean ± SEM of three experiments performed in triplicate.

When the results for the percentage inhibition of the compounds in the MyLa cells are correlated with the percentage inhibition of the compounds in the HH cells, the most effective compounds at inhibiting the proliferation of MF cell lines can be easily identified. These were **60b**, **60a** and **59f**. Compound **59b**, which had shown good antiproliferative activity at 25 μM in the MyLa cell line, had limited effect on proliferation of the HH cells.

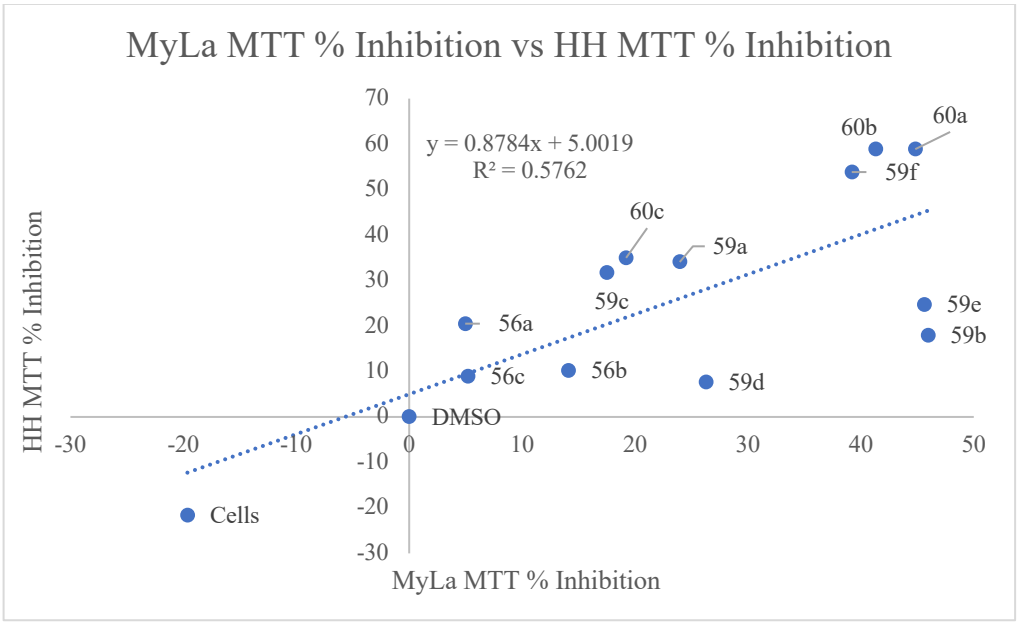

Figure 5-23: Correlation curve of MyLa MTT% inhibition vs HH MTT % inhibition.

MyLa % reduction in proliferation was measured using MTT and the results presented in Figure 5.20. HH % reduction in proliferation was measured using MTT and the results presented in Figure 5.22.

5.2.8 **Antiproliferative effect on HuT78 cells**

The anisate compounds were tested in the HuT78 cell line at 100 μM (Figure 5.24). When these cells were treated with 100 μM ST0702 there was a 37% reduction in cell proliferation, measured using MTT (Figure 2.24). Compound **33**, the structure of which these compounds were based on, had a 70% reduction in proliferation when tested at 100 μM in HuT78 cells (Figure 5.6).

The most active compounds observed in the new compound library were **60a** (77% inhibition), **60b** (72% inhibition) and **59f** (72% inhibition) which all showed greater efficacy than **33**. Of note, all of the new compounds demonstrated greater activity than ST0702 at inhibiting HuT78 proliferation. Also, **60a** (77% inhibition) demonstrated much greater activity than the corresponding isomannide-based compound **19g**, which caused a 30% inhibition when tested in the HuT78 cells (Figure 2.47).

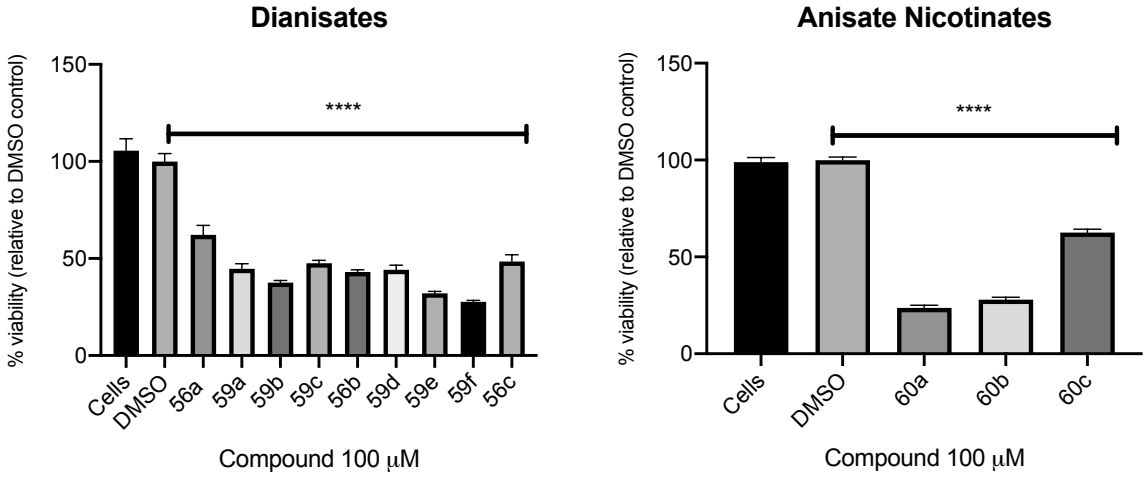

Figure 5-24: Antiproliferative effect of dianisates and anisate nicotinates (100 μM) on HuT78 cells.

HuT78 cells were plated at 1 × 10^4 cells/well. Compounds were added and the cells were incubated for 48 h. Following this incubation, MTT was carried out. The experiments were carried out in triplicate and data is presented as mean ± SEM.

Additionally, to check that it was the intact compound that was having the effect, the precursors and potential metabolites of the compounds were also tested for efficacy in the model. The anisic acids were tested themselves and had no effect on cell viability. The monosubstituted anisate compounds (**58a, 58b** and **58c**, structures shown in Figure 5.16) were also tested. One of these compounds, 2-*o*-anisate-5-OH (**58a**) had very interesting effects, with a reduction in proliferation of almost 80%.

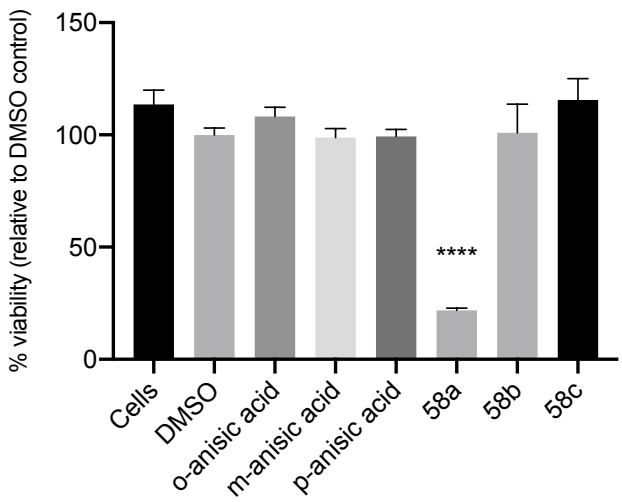

Figure 5-25: Antiproliferative activity of 100 μM anisic acids and isosorbide-2-(o,m,p)-anisate-5-hydroxyl compounds on HuT78 cells.
HuT78 cells were plated at 1 × 10^4 cells/well. Compounds were added and the cells were incubated for 48 h. Following this incubation, MTT was carried out. The experiments were carried out in triplicate and data is presented as mean ± SEM.

The compounds were tested at different concentrations to get an indication of approximate IC_{50} values. Both panels in general produced a concentration dependent effect on cell proliferation. In the cytostatic context, where compound mechanism leads to a reduction in proliferation, this format of assay can't be used to determine the IC_{50}, since it is not possible to say how many of the surviving cells were present at the start of the experiment. In this assay format, considering the mechanism of action, we are estimating total viability and its reduction, which reflects rather than directly equates to inhibition of proliferation. Several dianisates had estimated IC_{50} values for viability inhibition of around 50 μM. Some of the anisate-nicotinates appeared to induced apoptosis because of their dramatic effect on viability at 100 μM. One of these, the 2-*o*-anisate (**60a**) produced viability inhibition values in excess of 50% at 50 μM.

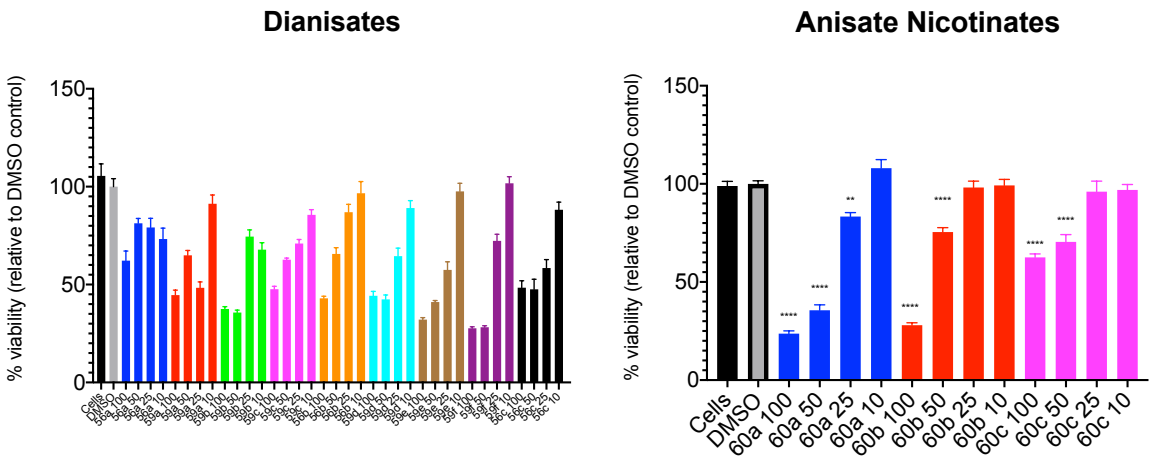

Figure 5-26: Antiproliferative effect of dianisates and anisate nicotinates (100, 50, 25, 10 μM) on HuT78 cells.

HuT78 cells were plated at 1 × 10^4 cells/well. Compounds were added and the cells were incubated for 48 h. Following this incubation, MTT was carried out. The experiments were carried out in triplicate and data is presented as mean ± SEM.

5.2.9 Inhibition of STAT3 Activation by anisate esters in the IL-6 reporter assay

The next step was to check the effect of the anisate esters on STAT3 activation in the reporter assay. (HEK-Blue IL-6 reporter cell line). ST0702 has been shown to inhibit STAT3 activation by approximately 40-50% (Figure 3.12). Compound **33** inhibited STAT3 activation by 70% (Figure 5.27).

The anisates and dianisates were very effective at inhibiting STAT3, with **59a** (83% inhibition) and **59c** (81% inhibition) the most active compounds. However there was a rapid fall off in activity with most compounds in the dianisate series, apart from **56c** which showed significant inhibitory activity at 25 μM.

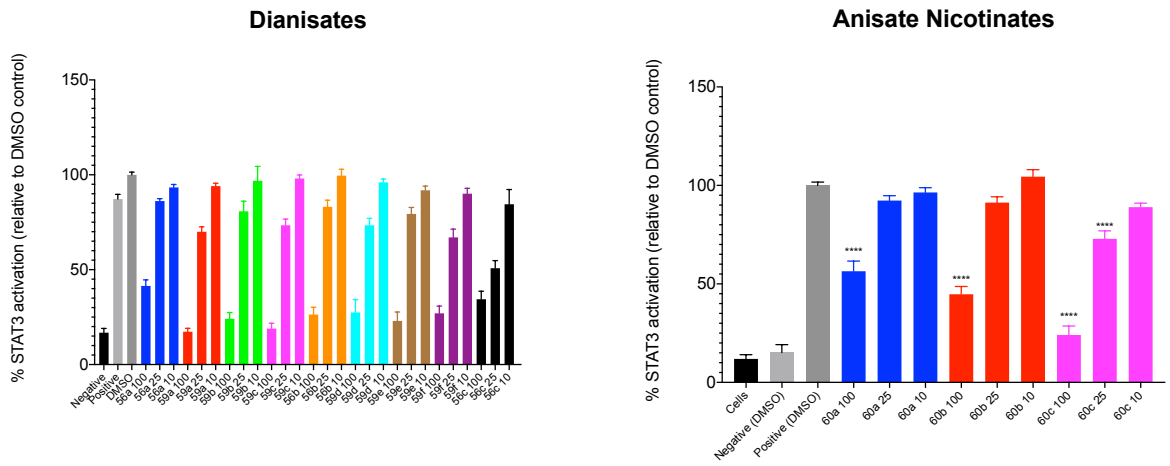

Figure 5-27: STAT3 inhibitory activity of dianisates and anisate nicotinates at 100, 25 and 10 μM.

HEK-Blue IL-6 cells were plated at 5 × 10^4 cells per well of a 96-well plate. Compounds or vehicle (DMSO) were added. After 30 min incubation, the cells were stimulated with 1 ng/mL IL-6. After 24 h Quantiblue Reagent was added and SEAP levels were determined. Data is expressed as mean ± SEM of three experiments performed in triplicate.

Once again, the potential metabolites and precursors to the compounds were tested, and neither the anisic acids nor the 2-anisate-5-OH compounds (**58**) caused a reduction in STAT3 activation (Figure 5.28). Interestingly, 2-*o*-anisate-5-OH, which had a large effect on HuT78 proliferation, did not inhibit STAT3 activity demonstrating that its anti-proliferative activity is not related to STAT3 inhibition.

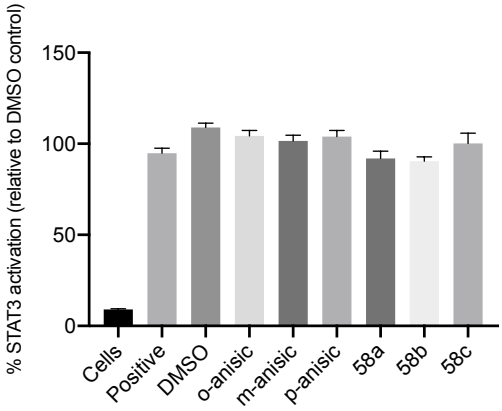

Figure 5-28: STAT3 inhibitory activity of anisic acids and isosorbide-2-(o,m,p)-anisate-5-hydroxyl compounds tested at 100 μM.

HEK-Blue IL-6 cells were plated at 5 × 10^4 cells per well of a 96-well plate. Compound or vehicle control (DMSO) was added. After 30 min incubation, the cells were stimulated with 1 ng/mL IL-6. After 24 h Quantiblue Reagent was added and SEAP levels were determined. Data is expressed as mean ± SEM of three experiments performed in triplicate.

Similar to the correlations examined in chapter 4, the relationship between the ability of the compounds to inhibit the proliferation of HuT78 cells and their ability to inhibit the activation of STAT3 was investigated. It was found that there was a strong correlation between the anti-proliferative effect and the STAT3 inhibitory effect of the dianisates (Figure 5.29). This correlation was not as strong for the anisate nicotinates, as can be seen from the coefficient of determination (r^2). For the dianisates the correlation was 0.89, for the anisate nicotinates the correlation was 0.48, and when the two sets of compounds were combined the correlation was 0.53. This may indicate that in the dianisate panel, effects on cell viability are caused by or strongly related to in some way, inhibition of STAT3, and that for the anisate nicotinate compounds there are other factors involved.

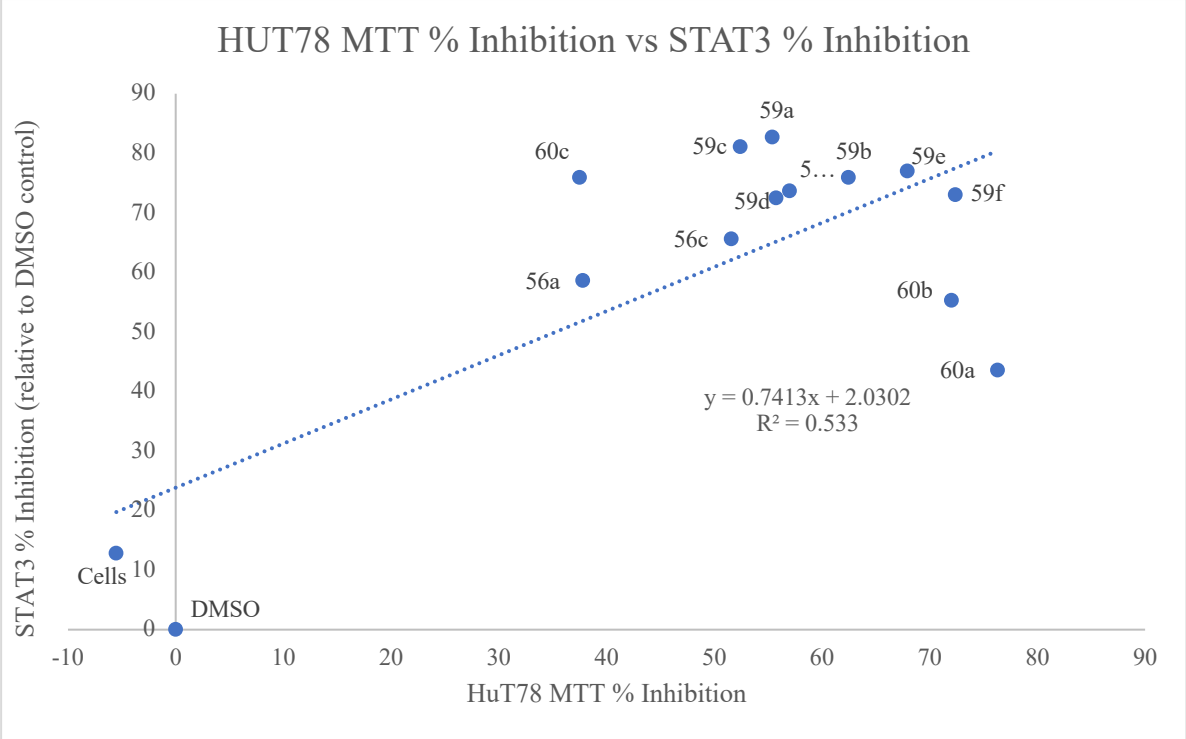

Figure 5-29: Correlation curves for HuT78 % reduction in proliferation versus STAT3 % inhibition for dianisates and anisate nicotinates tested at 100 µM.
HuT78 % reduction in proliferation was measured using MTT and the results presented in Figure 5.24. STAT3 % inhibition was measured using HEK-Blue IL-6 reporter cell lines and the results were presented in Figure 5.27.

5.2.10 **Viability of HEK IL-6 Cells under STAT3 reporter assay conditions**

The effect of test compounds on HEK viability was investigated in order to rule out a contribution from reduced viability to the apparent reporter inhibition. Data from initial experiments with the reporter cell line treated with test compounds and evaluated by MTT was

highly variable. MTT requires the cell supernatant to be removed and this was not possible with the HEK cells as removing the supernatant caused some disruption of the cells as they are loosely adherent. This was the assigned cause to the large variation in results in the MTT experiments. It was decided to use the comparable Alamar Blue assay to investigate the viability of the reporter cells. It can be seen from Figure 5.30 that many of the compounds do not appear to be killing HEKs to a significant extent. The compounds having the largest effect on viability were **60c** (30% decrease), **59c** (27% decrease), and **59f** (23% decrease).

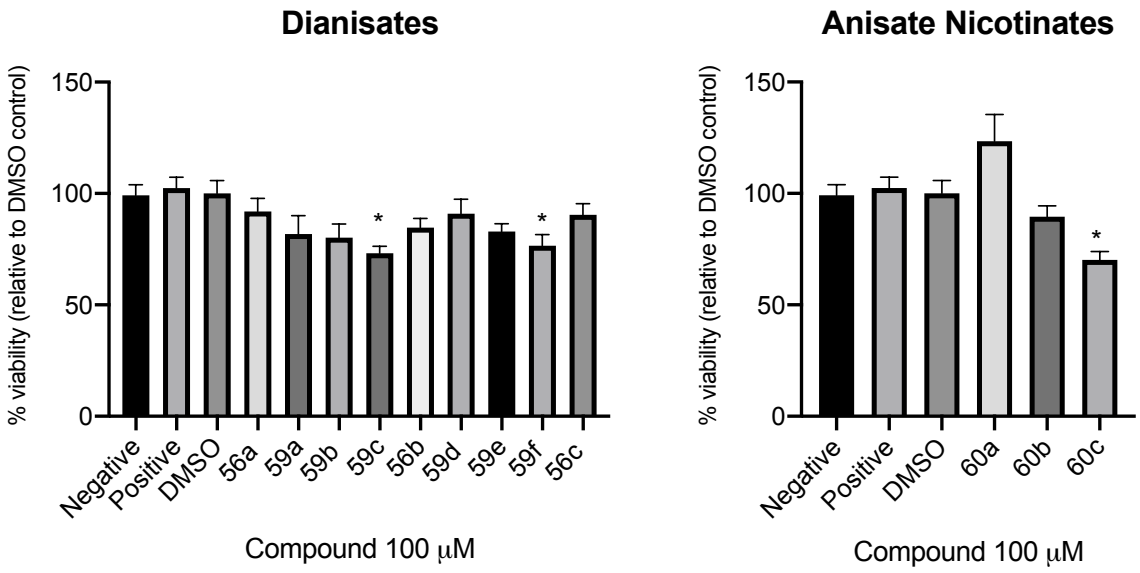

Figure 5-30: Effect of anisate esters (100 μM) on viability of HEK-Blue IL-6 cells.
HEK-Blue IL-6 cells were plated at 5 × 10^4 cells per well of a 96-well plate. Compound or DMSO was added. After 30 min incubation, the cells were stimulated with 1 ng/mL IL-6. After 24 h Alamar Blue was added and viability was determined using a spectrophotometer. Data is expressed as mean ± SEM of three experiments performed in triplicate.

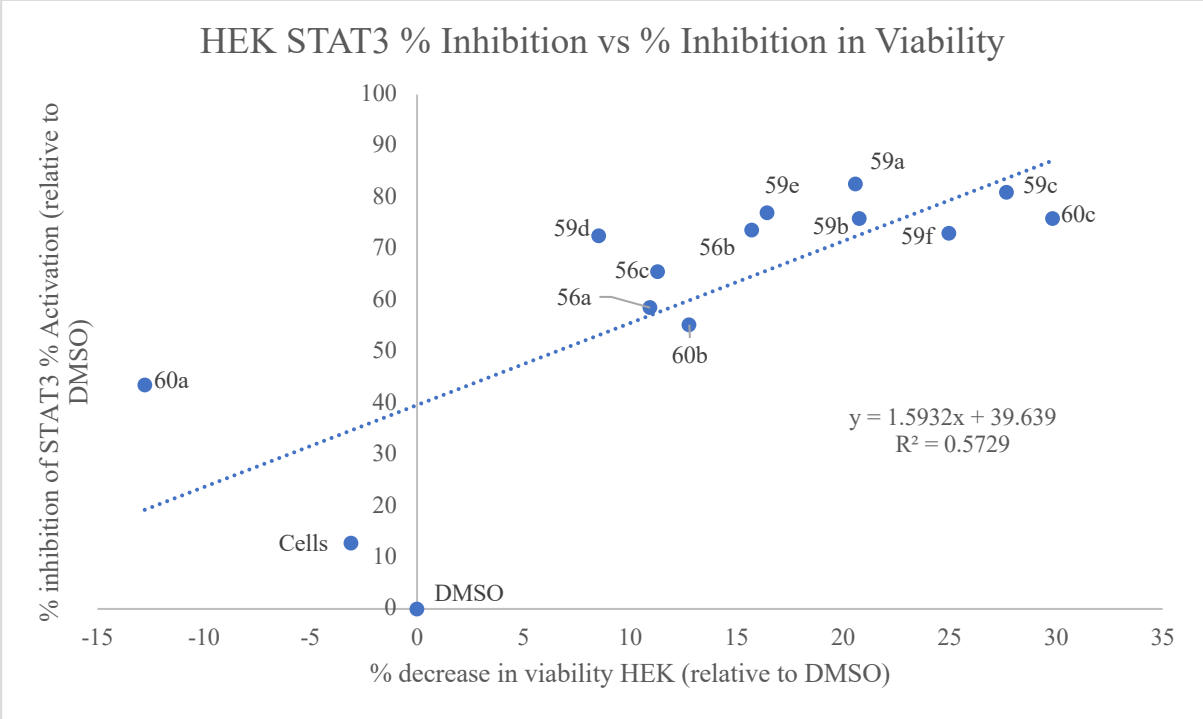

Figure 5-31:Correlation curve of STAT3 inhibitory activity and decrease in % viability of HEKs for dianisates and anisate nicotinates tested at 100 μM.
STAT3 % inhibition was measured using HEK-Blue IL-6 reporter cell lines and the results were presented in Figure 5.27. Viability of HEK IL-6 was measured using Alamar Blue and the results are presented in Figure 5.30.

The correlation between STAT3 inhibition and viability indicates that about 57% of the variation is explained by the model. This indicates that the effect on STAT3 activation by at least some of the compounds cannot be directly attributed to a reduction in cell viability. This becomes especially evident when individual compounds are studied, such as **60a**, where STAT3 activation is inhibited by 44%, but there is no decrease in cell viability observed. Another interesting compound is **59a**, which had the largest inhibitory effect on STAT3 (83%), but only a 20% reduction in cell viability. It is also worth noting that although the effects seem somewhat correlated the scale of the effects differ, with the reduction in STAT3 activation varying from 43% to 83%, whilst the largest effect seen on cell viability was 30%. We concluded that the STAT3 inhibitory data are reliable and not significantly influenced by viability effects. Additionally, the lack of antiproliferative effect of the majority of the compounds on these HEK cells is suggestive of a selective antiproliferative effect on malignant cells. We were interested to test the potential selective viability effect on another cell line relevant to potential clinical applications of the compounds.

5.2.11 **Effect of Dianisate and Anisate Nicotinates on the proliferation of the HaCaT cell line**

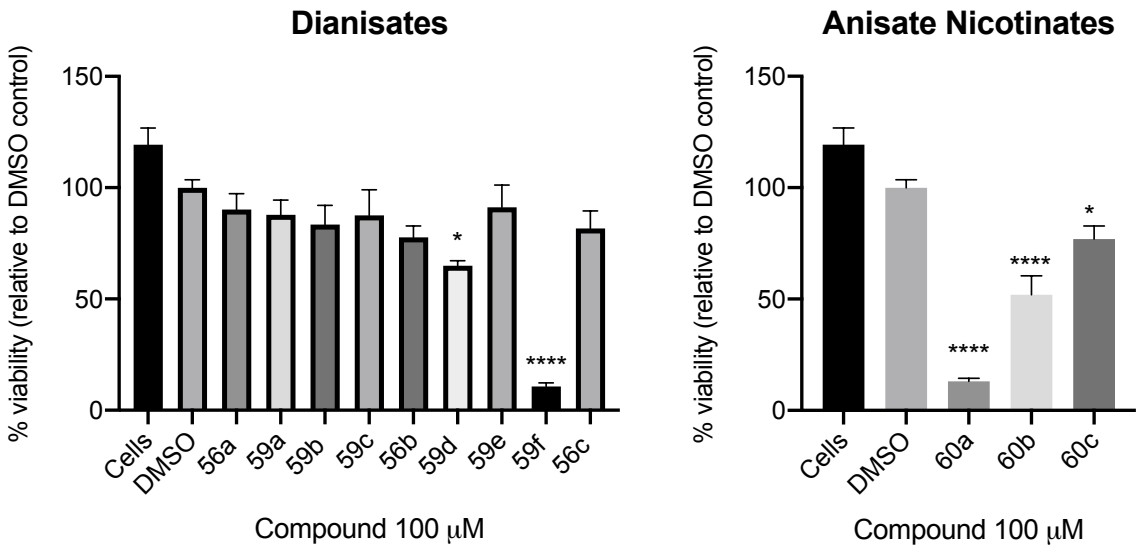

Figure 5-32: Antiproliferative effect of dianisates and anisate nicotinates in HaCaT cells. Cells were plated at 1 × 10^4 cells per well of a 96-well plate and left to adhere for 24 h. The compounds were then added and the plate was incubated for 48 h. Following this MTT was carried out.

The compounds were tested for their effect on the viability of the immortalised but normal keratinocyte cell line HaCaT at 100 μM. In the majority of cases compounds that had previously been shown to exert significant effects on malignant cell viability had little effect on HaCaT proliferation. Several compounds did exert a significant effect on viability. These included **59f**, which reduced proliferation of the HuT78 cell line and had additional effects on viability in the HEK-Blue IL-6 cells. Compound **60a** also exerted marked effects on the keratinocyte cell line viability. The very high antiproliferative effect of these substances was suggestive of a cytotoxic as opposed to a cytostatic effect.

The role of keratinocytes in the pathogenesis of CTCL is somewhat unclear, but malignant T cells have been shown to strongly impact skin structure, through effects on keratinocyte activation and proliferation, as observed in an organotypic skin model and a xenograft CTCL model (361, 362). Malignant T cells and their supernantants triggered JAK and MAPK activation in keratinocytes, downregulation of differentiation markers such as keratin 10 and involucrin, epidermal hyperproliferation, disorganised keratinocyte stratification and decreased barrier formation, this mimicking many features seen in CTCL lesions (361). In the experiments, HaCaT cells without malignant T cells showed normal stratification and differentiation, with an average of four cell layers. When the malignant MyLa 2059 cells or

supernatant from MyLa 2059 were added, the epithelial stratification was disrupted, with a combination of epithelial hyperplasia and hyperproliferation with an average of 15 cell layers (361).

5.2.12 **Measurement of levels of apoptosis in HuT78 cells**

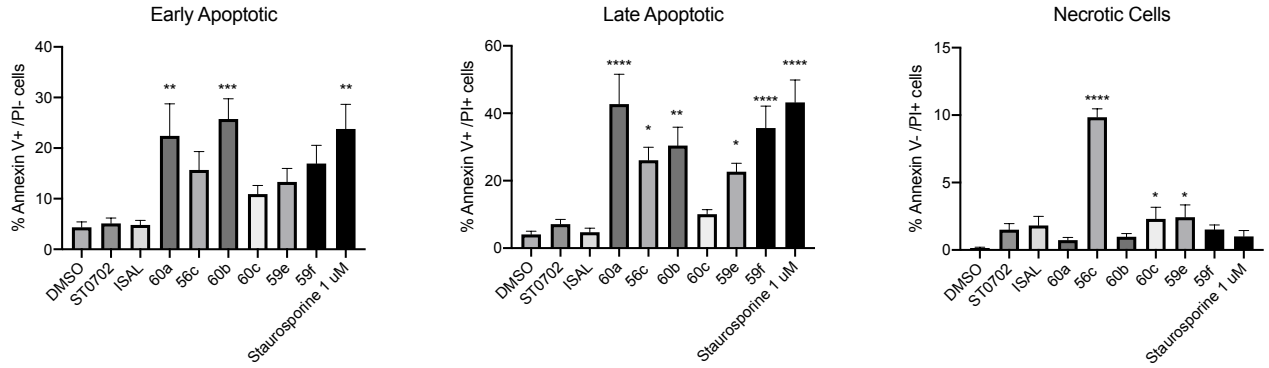

Figure 5-33: Levels of apoptosis in HuT78 cells treated with 100 μM anisate esters. HuT78 were plated at 1 × 10^4 cells/well and treated with compound for 48 h. After 48 h the cells were stained with Annexin V and PI. The samples were analysed by flow cytometry.

The levels of apoptotic and necrotic cells following treatment with lead compounds was measured, in order to profile relative cytotoxic/cytostatic contributions to cell viability inhibition that had been observed in the earlier assays. ST0702 and ISAL had similar levels of apoptosis to the DMSO vehicle control. All of the anisates and anisate nicotinates were more apoptotic than ST0702 or ISAL. Compound **60c** appeared to cause the most necrosis, and levels were much greater than observed with any of the other compounds. The most pro-apoptotic compounds were **60a** and **60b**, whilst **60c** and **59e** did not cause much apoptosis. Considering the marked effects of these compounds on proliferation on a range of CTCL cell lines, and their selectivity, the overall profile of these compounds could be described as cytostatic but selective. This was considered a fruitful outcome of the project – identification of chemotypes related to ST0702 able to selectively induce cytostatic effects in CTCL cell lines.

5.3 Discussion and Conclusion

The objective of the work carried out in this chapter was to identify or design a substance type for the skin-directed treatment of MF. Building on the knowledge of the work described in previous chapters there was some knowledge of SAR, and the functional group requirements for evoking the biological effect of interest, selective inhibition of T cell proliferation. The initial screening of a broad library of isosorbide-based ester compounds from the Gilmer lab

for antiproliferative activity in MF cell lines produced interesting and useful data that enriched the knowledge of SAR. Compound **33** emerged from this work as an interesting lead, possessing good antiproliferative effect, potential for innocuous metabolites in skin and later, lack of effect on the electron transport chain in the Seahorse model. When tested at 100 μM, it was an inhibitor of MyLa, HH and HuT78 proliferation, as well as inhibiting the activation of STAT3.

A panel of dianisate and anisate nicotinate compounds was synthesised. The compounds that were the largest inhibitors of proliferation of HuT78, HH and MyLa were **60a**, **60b** and **59f**. These compounds were all very toxic in the HaCaT keratinocyte cell line with evidence of apoptosis in cytometry experiments with PI/Annexin staining. The most interesting compound identified in this thesis is arguably **59b**. It appears not to be cytotoxic from its inhibitory ceiling on viability, it has little effect on viability on HaCaTs or HEKs but has significant antiproliferative effect on the MyLa cells at concentrations as low as 10 μM. However it was not as effective in assays studying viability of the HH cell line, another MF cell line that may however be characteristic of a different stage of disease than MyLa. Figure 5.34 below presents key summary data for the compound panel described first in this chapter.

	% Inhibition					
Compound (100 μM)	**HuT78 proliferation**	**HH proliferation**	**MyLa proliferation**	**STAT3 activation**	**HEK-IL-6 viability**	**HaCaT proliferation**
56a	38	21	5	59	8	10
59a	56	34	24	83	19	13
59b	63	18	46	76	20	17
59c	53	32	18	86	27	13
56b	58	11	14	80	15	23
59d	56	8	27	85	10	35
59e	68	25	45	85	17	9
59f	73	55	40	74	24	90
56c	52	10	5	73	10	19
60a	77	59	45	44	(+23)	87
60b	73	59	42	56	11	50
60c	38	35	20	76	30	23

Figure 5-34: Key summary data for the dianisate and anisate nicotinate compounds.

5.4 Future Work

The work described in this chapter opens up new avenues for compound design towards the target profile. Diaryl esters of isosorbide that are appropriately substituted can exhibit significant inhibitory effects towards a range of malignant cell lines including those

representative of CTCL diseases. The effect on T cells remains to be biochemically/mechanistically characterised but it appears to be mainly cytostatic. This is consistent with the work in the earlier chapters classifying the effects of ISAL and ST0702.

The objective of cancer therapy is to selectively kill cancer cells. This has transpired to be a remarkably difficult thing to achieve in practice, partly because of the similarity between normal cells and cancer cells, but also due to the various mechanisms of resistance of cancer cells. Cancer cells can acquire resistance-conferring genetic mutations, and their plasticity, that is, their ability to reversibly convert to a phenotype that is independent of the drug targeted pathway, can confer drug resistance to the cancer cells. Even with the most effective cancer therapies that lead to partial or complete response, small populations of cancer cells often survive drug treatment. These cells, often referred to as minimal residual disease, can drive cancer relapse if treatment is discontinued (363).

In this work I have shown that ST0702/ISAL which exerts an anti-inflammatory effect in the murine model of psoriasis, may do so through inhibition of T cell function and proliferation. The compounds were shown to reduce the viability of multiple cell lines from CTCL patients but to have lesser effects on normal PBMCs, keratinocytes and HEK293 cells. The selective effect on proliferation appears to be cytostatic resulting in low levels of apoptosis. A mechanistic explanation for the effect is provided by the observations in the phosphokinase array of interference in multiple aspects of IL-2 signalling pathways including STAT3/5, Akt and GSK. We were able to propose a mechanism for this having excluded inhibition of JAK1/2/3 and separate parallel or independent effects on cellular ATP synthesis.

The JAK-STAT, Ras-MAPK and mTOR pathways are all known to be involved in driving the development and progression of CTCL. There is evidence for the inhibitory effects of ST0702 and ISAL on phosphorylation of proteins that play signalling roles in these pathways, and these include proteins that are known HSP90 clients. A plausible explanation of inhibition of HSP90 has recently received preliminary experimental support in the Gilmer lab in vitro using HSP90 protein. The effect of ST0702 and the anisate compounds on these pathways needs to be verified, and the potential link to HSP90 inhibition studied further.

Overall, the new data therefore indicates, and the general finding of the project if this is true, that selective cytostatic effects can be achieved in CTCL cell lines, possibly leading to a therapeutic effect through inhibition of HSP90 via its clients. At this stage it is not clear which of the HSP90 clients that is affected by the isosorbide compounds is responsible for the viability effects. The interesting correlations observed between STAT3 inhibition and CTCL cell line proliferation in the isosorbide series is probably not causative because of the finding that ruxolitinib affects one but not the other. There is rich potential for interesting and fruitful future

work in this area. Having begun the investigations through observation of the effects of ST0702/ISAL in the Aldara™ model, and attributed these effects to T cell inhibition, it would be most interesting now to repeat the Aldara™ model with analogues not directly related chemically to the original series but mechanistically similar. An example of this could be the anisates or anisate nicotinates described in Chapter 5 which don't possess an aspirin or salicylate group, but which are nonetheless potent and selective inhibitors of T cell proliferation through cytotoxic and cytostatic effects that are more or less selective for malignant cells or normal keratinocytes. The anisates represent a key outcome of the work being a result of careful scrutiny of the activity profile of a large family of isosorbide compounds synthesised in this work or belonging to the Gilmer lab.

Future studies leading on from this project will likely involve the establishment of an in vivo model of CTCL and one or more of the anisate compounds being tested alongside ISAL in the model to assess the potential of these compounds as pharmacological agents for the treatment of CTCL. The establishment of an in vivo model of CTCL may pose challenges, with many studies carried out over the last few years to develop mouse xenograft models having involved only a small number of animals and have experienced a highly variable rate of engraftment that appeared to depend on both mouse strain and the cell line being used. As discussed earlier in this chapter, there are very few CTCL lines available and most of them have been derived from blood samples of patients with CTCL. More recent studies have used an intrahepatic xenograft model of CTCL in adult immunodeficient mice, which was particularly interesting because most previous studies choose the subcutaneous site for grafting, even though most of the cells are derived from blood circulating tumour T cells (364). This was found to be a useful model for in vivo screening of therapeutic models and could potentially be used in future studies to advance this project.

Chapter 6: Materials and Methods

6.1 Statistical Analysis

Analysis of results was carried out using GraphPad Prism 8 for Mac (GraphPad software, USA). Where two groups of results were being compared, the student's t-test was used. Results for more than three groups were analysed using one way ANOVA. Dunnett's multiple comparisons method was used as a follow-up test to the ANOVA to compare every mean to the control mean. Histograms are presented as the mean ± SEM and statistical significance was judged as a *p* value < 0.05. *P < 0.05, ** P < 0.01, *** P < 0.001 and **** P < 0.001. Linear regression analysis was used for correlations with r^2 quoted and graphs were plotted in Microsoft® Excel.

6.2 Biology

6.2.1 Compounds

Commercial compounds being tested were obtained from Sigma. Other compounds were synthesised as outlined in Chapters 2 and 5. The compounds were maintained as 100 mM or 10 mM stocks in dimethyl sulfoxide (DMSO) and stored at 4°C. For biological assays the compounds were diluted to the appropriate concentration with medium. Final DMSO concentrations were usually 0.5%, but did not exceed 1%, unless otherwise stated.

6.2.2 Cell Culture

The following cell lines were used for the experiments in this thesis:

- THP1-Blue NF-κB Cells, a reporter cell line for NF-κB activity
- Human HuT78 lymphoblast T cell line
- HEK-Blue IL-6, a reporter cell line for STAT3 activity
- HaCaT, a keratinocyte cell line
- Human HH lymphoblast T cell line
- Human MyLa lymphoblast T cell line

6.2.3 Culture of THP1-Blue NF-κB Cells

The THP1-Blue NF-κB cells (Invivogen, Toulouse, France) were derived from the human THP-1 monocyte cell line by stable integration of an NF-κB-inducible SEAP reporter construct. THP1-Blue NF-κB cells express a secreted embryonic alkaline phosphatase (SEAP)

reporter gene driven by an IFN-β minimal promoter fused to five copies of the NF-κB consensus transcriptional response element and three copies of the c-Rel binding site. As a result, THP1-Blue NF-κB cells allow the monitoring of NF-κB activation by determining the activity of SEAP. The cells were cultured in RPMI supplemented with 10% heat inactivated FBS, 2 mM L-glutamine, 100 µg/mL Normocin and 100 U/mL Penicillin/Streptomycin (PenStrep) in a humidified atmosphere at 37°C and 5% CO_2. The cells were kept in T25 cm^2 flasks and cell density was monitored using a haemocytometer. Cell concentration was maintained between 5×10^5 to 2×10^6 cells/mL. Fresh medium was added every 2–3 days.

6.2.4 Culture of HuT78 Cells

The human HuT78 cell line (American Type Culture Collection (ATCC), Manassas, VA, USA) was established from the peripheral blood of a 53 year old white male with Sézary syndrome and has a mature helper T cell phenotype. HuT78 cells were cultured in RPMI supplemented with 10% FBS, 2 mM L-glutamine and 50 U/mL Penicillin/Streptomycin (PenStrep) in a humidified atmosphere at 37°C and 5% CO_2. The cells were kept in T25 cm^2 flasks and cell density was monitored using a haemocytometer. Cell concentration was maintained between 2×10^5 to 1×10^6 cells/mL. Fresh medium was added every 2–3 days.

6.2.5 Culture of HEK-Blue IL-6 Cells

The HEK-Blue IL-6 Cells (Invivogen, Toulouse, France) were generated by stably introducing the human IL-6R gene into HEK293 cells. The cells were then further transfected with a reporter gene expressing SEAP under the control of an IFNβ minimal promoter fused to four STAT3 binding sites. The cells were cultured in DMEM supplemented with 4.5g/L glucose, 10% FBS, 2 mM L-glutamine and 50 U/mL Penicillin/Streptomycin (PenStrep) in a humidified atmosphere at 37°C and 5% CO_2. The cells were kept in T75 cm^2 flasks and the growth did not exceed 80% confluency. The growth medium was changed twice weekly.

6.2.6 Culture of HaCaT Cells

The HaCaT cell line (CLS, Eppelheim, Germany) is derived from a spontaneously transformed aneuploid immortal keratinocyte cell line from adult human skin. The cells were cultured in DMEM supplemented with 10% FBS, 2mM L-glutamine and 50 U/mL Penicillin/Streptomycin (PenStrep) in a humidified atmosphere at 37°C and 5% CO_2. The cells were kept in T25 cm^2 flasks and the growth did not exceed 80% confluency. The cells were split twice weekly using TrypLE Express (Gibco, Billings, MT, USA) according to

manufacturer's instructions to detach the cells. Cells were plated and left for 24 h to adhere before any experiments were conducted.

6.2.7 Culture of HH Cells

The human HH cell line (American Type Culture Collection (ATCC), Manassas, VA, USA) was established from the peripheral blood of a 61 year old Caucasian male with cutaneous T cell lymphoma. HH cells were cultured in RPMI supplemented with 10% FBS, 2 mM L-glutamine and 50 U/mL Penicillin/Streptomycin (PenStrep) in a humidified atmosphere at 37°C and 5% CO_2. The cells were kept in T25 cm^2 flasks and cell density was monitored using a haemocytometer. Cell concentration was maintained between 2×10^5 to 1×10^6 cells/mL. Fresh medium was added every 2–3 days.

6.2.8 Culture of MyLa Cells

The human MyLa CD4+ cell line (European Collection of Authenticated Cell Cultures (ECACC), Salisbury, UK) was established from a plaque biopsy of an 82 year old male with mycosis fungoides stage II by inclusion of IL-2 and IL-4 in the culture medium. MyLa cells were cultured in RPMI supplemented with 10% FBS, 10 U/mL IL-2, 10 U/mL IL-4, 2 mM L-glutamine and 50 U/mL Penicillin/Streptomycin (PenStrep) in a humidified atmosphere at 37°C and 5% CO_2. The cells were kept in T25 cm^2 flasks and cell density was monitored using a haemocytometer. Cell concentration was maintained between 3×10^5 to 9×10^5 cells/mL. Fresh medium was added every 2–3 days.

6.2.9 Isolation and Culture of PBMCs

Peripheral blood mononuclear cells (PBMCs) were isolated from buffy coats obtained from the Irish Blood Transfusion Service at St James' Hospital. Cells were isolated by density gradient separation using Lymphoprep (STEMCELL Technologies, Cambridge, UK) according to manufacturer's instructions. Once isolated, PBMCs were either frozen down for future use or cultured in RPMI supplemented with 10% FBS, 2mM L-glutamine and 50 U/mL Penicillin/Streptomycin (PenStrep) in a humidified atmosphere at 37°C and 5% CO_2.

6.2.10 Cell Counting

Cell concentrations were determined using a bright line haemocytometer in conjunction with the exclusion dye 0.4% Trypan blue to exclude non-viable cells. 10 µL of medium containing cells were diluted in 90 µL trypan blue and mixed well. The mixed cell suspension was injected

into the haemocytometer underneath the coverslip. The volume of fluid under each 4×4 counting chamber was 0.1 mm^3. The number of cells was calculated as: Average/mm^3 × 10 (dilution factor in trypan blue) × 10^4.

6.2.11 Cryopreservation and Revival of Cells

Cells were maintained in a T75 flask. To freeze stocks, a cell pellet was obtained and the supernatant removed. The cells were then resuspended in 5 mL 100% FBS. To this, 5 mL of FBS containing 20% DMSO was then added dropwise to give a final concentration of 10% DMSO in FBS. 1 mL of this suspension was pipetted into sterile cryovials, which were then placed inside a freezing container (Mr Frosty, Thermo Fisher Scientific, Waltham, MA, USA) in a -80°C freezer for 24 h and then transferred to liquid nitrogen for longer term storage.

To revive a cell stock, the cryovial was removed from the liquid nitrogen tank. The cells were thawed by adding warmed media slowly. This was then transferred to a falcon tube and centrifuged at the appropriate rpm and time (depending on the cell type). Once the supernatant was removed the cells were resuspended in medium and transferred to a T25 cm^2 cell culture flask in a volume of 5 mL medium.

6.2.12 Preparation of T cell blasts

PBMCs (5 ×10^5 cells/mL) were seeded and stimulated with aCD3/CD28 beads for 72 h before adding two successive rounds of IL-2 (20 ng/mL) for 48 h. For T cell expansion, PBMCs were seeded at 5 × 10^5 cells/well in a 24-well plate and stimulated with anti CD3/ anti CD28 beads (Dynabeads, Gibco, Waltham, MA, USA) for 96 h. After this time, cells were spun down, 250 µL of spent media was removed and 500 µL fresh media were added, and cells were reseeded in the wells and treated with 20 ng/mL IL-2 for 48 h. This procedure was repeated again and cells treated for another 48 h with IL-2.

6.2.13 MTT Assay

Cell viability was measured using the 3-[4,5-dimethylthiazol-2-yl]-2,5-diphenyltetrazolium bromide (MTT, Sigma, St Louis, MO, USA) assay. For non-adherent cells, the compounds to be tested were first diluted in medium to the appropriate concentration. Cells were plated in flat-bottom 96-well plate and treated with compounds. The vehicle control wells were treated with 0.5% DMSO. When the treated cells were ready to be assayed (incubation times varied), 10 µL of 5 mg/mL MTT in PBS was added to each well of a U-bottom 96 well plate. The cells (in medium) were then mixed to homogenise and added to the U-bottomed 96-well plate on

top of the MTT reagent. The plate was then incubated for 30 min–2 h 30 min (depending on the cell type) at 37°C and 5% CO_2. After this time, the plate was centrifuged at 1300 rpm and the medium was gently aspirated. The formazan crystals were dissolved in 100 µL DMSO. The plates were shaken for 10 min to dissolve the formazan crystals and then read on a $VERSA_{max}$ Microplate Reader at a wavelength of 570 nm and 630 nm. The reading at 630 nm was subtracted from the reading at 570 nm. A similar procedure was followed for the MTT for the adherent cells, the difference being that the MTT reagent was added directly to the wells of the flat-bottomed plate, that is, no transfer of cells into the U-bottom plate took place.

6.2.14 **Acid Phosphatase Assay**

Cells were plated in flat-bottomed 96 well plates and treated with compound. When the treated cells were ready to be assayed (incubation times varied), the culture medium was removed using a multichannel pipettor. For non-adherent cells, the cells and supernatant were transferred to U-bottomed 96 well plates which were then centrifuged at 1300 rpm for 5 min, allowing the culture medium to then be removed. To each well, 100 µL of buffer containing 0. 1 M sodium acetate (pH 5.5), 0.1% Triton X and 5 mM phosphatase substrate (pNPP, Sigma, St Louis, MO, USA) was added. In the case of non-adherent cells, the cells were resuspended in the buffer and were then placed in an incubator (37°C and 5% CO_2) for 30 min-2 h 30, depending on the cell type and the cell density in the well. The plates are then removed from the incubator and 50 µL 1 M NaOH was added to each well. Absorbance was then read using a $VERSA_{max}$ Microplate Reader at a wavelength of 405 nm, correcting at 630 nm.

6.2.15 **Alamar Blue Assay**

Cells were plated in flat-bottomed 96 well plates and treated with compound. When the treated cells were ready to be assayed (incubation times varied), 20 µL of alamarBlue™ Cell Viability Reagent (Thermo Fisher Scientific, Waltham, MA, USA) was added directly to the wells. The plate was then placed in an incubator (37°C and 5% CO_2) for 1- 4 h, depending on the cell type and the cell density in the well. Absorbance was then read using a $VERSA_{max}$ Microplate Reader at a wavelength of 570 nm, correcting at 630 nm.

6.2.16 **NF-κB Activation Assay**

THP1-Blue™ NF-κB cells allow the monitoring of NF-κB activation by determining the activity of SEAP. Levels of NF-κB-induced SEAP can be readily monitored using QUANTI-Blue™ (Invivogen, Toulouse, France). THP1-Blue NF-κB cells were plated at 1×10^5 cells/mL in a flat-bottomed 96 well plate. They were preincubated with ST0702 for 30 min, and then

stimulated with 100 ng/mL TNF-alpha. Cells were incubated at 37°C and 5% CO_2 for 24 h. Following this incubation, 20 µL of cell supernatant were transferred into a fresh flat-bottom 96-well plate and 180 µL of QUANTI-Blue were added per well. After a 20 min incubation, colour was measured by reading in a $VERSA_{max}$ Microplate Reader at a wavelength of 630 nm.

6.2.17 Flow Cytometric Analysis of Cell Apoptosis

Flow cytometry was used to investigate the presence of apoptotic cells using Annexin V and Propidium Iodide (PI) staining (FITC Annexin V Apoptosis Detection Kit, BD Biosciences, San Jose, CA, USA). The assay measures the binding of fluorescently labelled Annexin V to the phospholipid phosphatidylserine, which is located on the inner side of the cell membrane in healthy cells but flips to the external side in early phases of apoptosis. PI is excluded from cells that have intact and functional membranes, but dead cells cannot exclude this dye and it binds to their DNA. Combining staining for phosphatidylserine with Annexin V and PI allows detection of early apoptosis (Annexin V^+/PI), late apoptosis (Annexin V^+/PI^+) and cell death (Annexin V^-/PI^+).

For this assay, HuT78 cells were plated at a concentration of 1×10^4 cells/well, treated with compounds as appropriate and incubated at 37°C for 24, 48 or 72 h. The cells were spun down and resuspended in 100 µL binding buffer. Fluorescently-labelled Annexin V (2 µL) was added to the cells and the samples were vortexed and incubated at room temperature in the dark for 5 min. After incubation, PI (2 µL) was added to the samples, followed by 400 µL of Annexin V binding buffer. Flow cytometric analysis was then carried out testing a minimum of 10,000 events per sample in a FACSCantoII (BD Biosciences, San Jose, CA, USA). The data were analysed using FACSDIVA software.

6.2.18 BCA Protein Assay: Calculation of Protein Concentration of Lysates

The BCA Protein Assay is a detergent compatible formulation based on bicinchoninic acid (BCA) for the colorimetric detection of total protein (BCA Protein Assay Kit, Thermo Fisher Scientific, Waltham, MA, USA). The method combines the reduction of Cu^{2+} to Cu^{1+} by protein in an alkaline medium (the Biuret reaction) with the highly sensitive and selective colorimetric detection of the Cu^{2+} cation using a unique reagent containing bicinchoninic acid. 50 parts of BCA reagent A (Na_2CO_3, $NaHCO_3$, bicinchoninic acid, sodium tartrate in 0.1 M NaOH) were added to 1 part BCA reagent B (4% $CuSO_4$). 200 µL of this solution was added to 1 µL of protein lysate in a 96 well plate. For comparison, 10 µL of several concentrations of bovine serum albumin (BSA) standards were added to 200 µL of the BCA mix. The solutions were incubated at 37°C for 1 h followed by reading in a $VERSA_{max}$ Microplate Reader at a wavelength of 570 nm.

6.2.19 **Proteome Profiler Array: Human Phospho-Kinase Array Kit**

The Human Phospho-Kinase Array kit (Cat No: ARY003B, R&D Systems, Minneapolis, MN, USA) was used as outlined in the protocol.

For the experiment using PBMCs, the PBMCs were seeded at 1×10^6 cells/mL and activated with 10 μg/mL PHA over a 72 h period. They were then serum-starved (1% serum) for 4 h, and for the last 30 min of this incubation they were treated with either 100 μM ST0702 or DMSO control. 20 ng/mL IL-2 was then added and after 15 min the cells were placed on ice. The cells were spun down at 4°C, the supernatant was removed and the pellet was lysed following manufacturer's instructions. The protein amount was quantified using the BCA assay and 500 μg of protein was used for the assay. The protocol was then followed as outlined in the manual. The images were obtained after a 20 min exposure time.

For the experiment using HuT78 cells, the HuT78 cells were seeded in T25 flasks at a density of 1×10^6 cells/mL and either 100 μM ST0702 or DMSO control was added. The cells were incubated for 30 min. Following this the cells were placed on ice. The cells were centrifuged at 1300 rpm for 5 min, the supernatant was removed, the cells were washed in PBS, and the pellet was lysed following the protocol outlined in the kit. The protein amount was quantified using the BCA assay and 500 μg of protein was used for the assay. The protocol was then followed as outlined in the manual. The images were obtained after a 20 min exposure time.

6.2.20 **HEK IL-6 Blue Reporter Assay**

HEK-Blue™ IL-6 cells allow for the monitoring of the effects of different compounds on the activation of the STAT3 pathway. These cells were generated by stable transfection of HEK293 cells with the human IL-6 receptor (IL-6R) gene and a STAT3-inducible SEAP reporter gene. Upon IL-6 stimulation, HEK-Blue™ IL-6 cells trigger the activation of STAT3 and the subsequent secretion of SEAP. Levels of STAT3-induced SEAP can be readily monitored using QUANTI-Blue™ (Invivogen, Toulouse, France).

For this assay, cells were seeded at 5×10^4 cells/well in a flat-bottom 96-well plate in assay media (the same as culture media but with heat-inactivated FBS). Compounds were then added in 20 μL and cells treated for 30 min before the addition of IL-6 at 1 ng/ml. Cells were incubated at 37°C and 5% CO_2 for 24 h. Following this incubation, 10 μL of cell supernatant were transferred into a fresh flat-bottom 96-well plate and 90 μL of QUANTI-Blue were added per well. After a 20 min incubation, colour was measured by reading in a $VERSA_{max}$ Microplate Reader at a wavelength of 630 nm.

6.2.21 **IL-2 ELISA**

IL-2 produced by HuT78 cells was detected by ELISA (Peprotech, Rocky Hill, NJ, USA) according to manufacturer's instructions. HuT78 cells were plated in a 24 well plate at 1×10^6 cells/well. DMSO, 100 μM ST0702 or 5 μM Go6976 was added to the cells. Following 30 min incubation PMA 10 ng/mL was added and the cells were incubated overnight. The amount of IL-2 in the supernatant was then measured.

6.2.22 **Human Skin Microsomes**

Human skin S9 fractions were purchased (Sekisui-Xenotech H0610.E59 Lot No. 1710144). 0.125 mL of the human skin S9 fraction 4 mg/mL protein was diluted to a concentration of 0.5 mg/mL in phosphate buffered saline pH 7.4, 1.0 mM EDTA and 3.0 mM magnesium chloride) The microsomes were incubated with 100 μM ST0702 at 37˚C. At stated timepoints over a 24 h period, a quantity of the microsomal solution was removed and quenched with acetonitrile. This was then centrifuged and the concentration of ST0702 and its metabolites were analysed using HPLC. The formation of products was monitored by HPLC with photodiode array detection. Peak areas were calculated at the 235 nm wavelength. The solvent system consisted of A = 0.1% formic acid in water and B = 0.1% formic acid in acetonitrile and a gradient method was run. Products and standards were chromatographically separated on a Thermo Scientific BDS Hypersil C18 column 5 μm, 250 mm × 4.6 mm, at a flow rate of 1 mL/min and a temperature of 25°C. ST0702 eluted after approximately 17 min.

6.2.23 **Mouse Skin Microsome**

CD1 mouse skin microsomes were purchased (Xenotech M1000.E/ Lot No. 1110115). The CD1 mouse skin microsomes were diluted to a concentration of 0.5 mg/mL in PBS pH 7.4, 1.0 mM EDTA and 3.0 mM magnesium chloride. The microsomes were incubated with 100 μM ST0702 at 37˚C. At stated timepoints over a 24 h period, a quantity of the microsomal solution was removed and quenched with acetonitrile. This was then centrifuged and the concentration of ST0702 and its metabolites were analysed using HPLC. The HPLC method used was the same as outlined for the human skin study.

6.2.24 **Seahorse Protocol**

PBMCs (5×10^5 cells/mL) were seeded and stimulated with aCD3/CD28 beads for 72 h before adding two successive rounds of IL-2 (20 ng/mL) for 48 h. For T cell expansion, PBMCs were seeded at 5×10^5 cells/well in a 24-well plate and stimulated with anti CD3/ anti CD28 beads

(Dynabeads, Gibco, Waltham, MA, USA) for 96 h. After this time, cells were spun down, 250 µL of spent media was removed and 500 µL fresh media were added, and cells were reseeded in the wells and treated with 20 ng/mL IL-2 for 48 h. This procedure was repeated again and cells treated for another 48 h with IL-2. The cells were then seeded at 2.5×10^5 cells/well onto Agilent Seahorse XF96 Cell Culture plate (Agilent, Santa Clara, CA, USA). The cells were seeded in 50 µL Seahorse XF DMEM Medium, pH 7.4 (Agilent, Santa Clara, CA, USA), with 25 mM glucose, 1 mM sodium pyruvate and 2 mM L-glutamine.

To prepare the Seahorse XF96 Cell Culture plate, two days before the assay, the plate was coated with 10 µL poly-lysine and incubated in a non-CO_2 incubator overnight. The following day, the poly-lysine was removed from the plate and washed with 200 µL sterile water. The plate was then left to airdry overnight, and on the day of the assay the cells were seeded on this plate.

The day before the assay was run, 20 mL Seahorse XF Calibrant was placed in a 50 mL falcon tube, and the tube was placed in a non-CO_2 incubator overnight. The Extracellular Flux Assay kit (Agilent, Santa Clara, CA, USA) was opened and each well of the utility plate was filled with 200 µL sterile water. The sensor cartridge was then lowered onto the utility plate, and the assembled sensor cartridge and utility plate was placed in a non-CO_2 incubator overnight. On the day of the assay the water is discarded from the utility plate and each well of the utility plate is filled with 200 µL of the pre-warmed XF Calibrant. The sensor cartridge is then lowered onto the utility plate and placed in a non-CO_2 37°C incubator for 45-60 min prior to loading the injection ports of the sensor cartridge.

On the day of the assay, the cell plate (with the cells plated at 2.5×10^5 cells/50 µL/well) was centrifuged at 1200 rpm with the brake off. Once it reached the desired speed, the centrifuge was stopped. Once this was finished, the plate was turned 180° and the centrifugation was repeated. This ensures that cells are stuck down at all sides of the well.

Following the centrifugation, 150 µL seahorse media was added on top of the cells. The plate was then placed in a non-CO_2 incubator for at least 30 min.

The compounds for injection were diluted in seahorse media and added to the appropriate injection ports of the sensor cartridge. Each injection is 25 µL. The calibration plate was then placed in a non-CO_2 incubator for 10 min.

The protocol was set up on the Seahorse XF96 Analyzer. The first step involved the sensor cartridge calibration, whereby the sensor cartridge and utility plate are placed into the Analyzer. When the calibration was complete, the tray of the Analyzer opened, the utility plate was

removed and replaced with the cell plate. After completing equilibration, baseline measurements were then taken (as outlined in protocol). Injections were made at the times specified in the protocols and readings are taken every 6 min (3 min mix, 3 min measure). Each condition was performed in quadruplicate.

6.2.25 **Preparation of Cellular Protein Extracts**

Cellular protein extracts were prepared by washing cells twice with ice cold PBS followed by incubation at 4 ˚C for 30 min in cell lysis buffer composed of RIPA Buffer (50 mM Tris HCl pH 8, 150 mM NaCl, 1% NP-40, 0.5% sodium deoxycholate and 0.1% SDS) supplemented with freshly added protease inhibitor cocktail (Sigma, P8340, 1 in 500 dilution), 1 mM sodium orthovanadate and 1 mM phenylmethylsulfonyl fluoride (PMSF).

Following incubation, nuclear and cellular debris were removed by microcentrifugation at 13000 rpm for 10 min at 4 ˚C. The supernatant was carefully removed, taking care not to disturb the pellet of debris, and added to a clean Eppendorf tube. It was then prepared for sodium dodecyl-sulfate polyacrylamide gel electrophoresis (SDS-PAGE) or stored at -20 ˚C. The lysate was prepared to be loaded onto the gel by first adding Western blot loading buffer (stock was 5X, used at 1X) and then boiling for 10 min.

This protocol was used to prepare protein extracts from HuT78 cells (24 well plate at 1×10^6 cells/well) and HEK-Blue IL-6 reporter cells (6 well plate at 2×10^5 cells per well and incubated for 48 h).

6.2.26 **Western Blotting**

To make up the gel the electrophoresis plates were firstly rinsed with ethanol. Rubber gaskets were attached to notched plates and the plain glass plate was added and fastened using green clips on each side. The 10% acrylamide resolving gel and the stacking gel were made up using the following components outlined in Table 6.1.

Component	Resolving Gel	Stacking Gel
Distilled H_2O	7.9 mL	4.6 mL
30% acrylamide	6.7 mL	1 mL
1.5 M Tris HCl (pH 8.8)	5.0 mL	
1.0 M Tris HCl (pH 6.8)		750 µL
10% SDS	200 µL	30 µL
10% APS	200 µL	60 µL
TEMED	8 µL	12 µL

Figure 6-1: Components of resolving and stacking gel used in Western blots.

The resolving gel was poured between the glass plates up to the 1 cm mark and overlaid with 1 mL of isopropanol. This was allowed to set for approximately 40 min at room temperature, the isopropanol was removed and the top of the gel was washed with water. The stacking gel was then added along with the combs and allowed to set for 8 minutes.

The gels were placed in the electrophoresis rig, which was filled with 1X SDS-PGE running buffer (5X running buffer: 15.1 g TRIZMA base, 94 g Glycine, 50 mL of 10% w/v SDS, made up to 1 L with distilled water). 10 µL sample was loaded into each well and a molecular weight marker (1.5 µL) (PageRuler Plus Prestained Protein Ladder, Thermo Fisher Scientific, Rockford, IL) is used for each gel. The gel was run at 80 mA until the samples were through the stacking gel, and then the voltage was increased to 110 mA.

The proteins on the gel were transferred to a polyvinylidene fluoride (PVDF) membrane using a semi-dry transfer method. The gels were allowed to transfer for 1 h 15 min at 100 mA per gel in 1X transfer buffer (1X Transfer Buffer: 5.8 g TRIS, 2.9 g Glycine, 4 mL 10% SDS, 200 mL MeOH, made up to 1 L in ddH2O).

Once transferred, the membrane was incubated in 5% BSA in tris-buffered saline with tween-20 (TBS-T) with gentle shaking for 1 h to block non-specific binding sites. The primary antibody was prepared in 5% BSA in TBS-T. The membrane was incubated with the primary antibody at 4 ˚C overnight with gentle shaking. Following incubation with the primary antibody, the membrane was washed three times for 5 min (each wash) in TBS-T. The membrane was then incubated for 1-2 h with the relevant horseradish peroxidase (HRP) conjugated secondary antibody with gentle shaking at room temperature. This is followed by three 5 min washes.

The HRP development solution (6 mL of 100 mM Tris-HCl (pH 8.5), 3.6 µL of 30% H_2O_2, 30 µL of 250 mM luminol and 133 µL 90 mM 4-iodophenylboronic acid) was freshly made up

and added to the membrane for 60 sec before bringing the membrane to the Geldock. Following imaging the membrane was washed three times in TBS-T and re-probed with α-tubulin to act as a loading control. The densitometry of the bands were quantified using Lab Image software.

6.2.27 **Cellular ROS**

Cellular ROS levels can be measured in live cells by a technique that converts 2',7'-dichlorofluorescin diacetate (DCFDA) which is oxidised to a fluorescence dye 2',7'-dichlorofluorescein (DCF). HuT78 cells were plated in a 96 well plate at 1.5×10^4 cells/well. The cells were plated in phenol-red free DMEM. The plate was then centrifuged at 1300 rpm for 5 min. The supernatant was aspirated off and the cells were resuspended in media containing 25 μM DCFDA. The plate was then incubated in the dark for 30 min. Following this, the plate was centrifuged at 1300 rpm for 5 min, the supernatant was removed and the cells were resuspended in media containing the compounds to be tested. Luperox- TBH 70 X (458139, Sigma Aldrich) (100 μM) was used as the positive control. The plate was shaken for 5 min and a fluorescence reading was then taken every 5 min for 1 h (excitation: 485 nm, emission 520 nm).

6.2.28 **MitoSOX Flow Cytometry**

MitoSOX (MitoSOX™ Red Mitochondrial Superoxide Indicator, Thermo Fisher Scientific, Waltham, MA, USA) is a red mitochondrial superoxide indicator. It is used to measure levels of mitochondrial ROS in live cells. The MitoSOX reagent is live cell permeant and rapidly and selectively targets the mitochondria. Once in the mitochondria, MitoSOX is oxidised by superoxide and exhibits red fluorescence.

HuT78, HH or MyLa cells were plated at 1×10^5 cells/well in 96 well plate. For the PBMCs, they were expanded into T cell blasts as per protocol (section 6.1.12) and on Day 7, the final volume of cells in the well was 1 mL. The cells were then treated with compound for 30 min. Following this, the cells were transferred to flow tubes and 2.5 μM MitoSOX reagent was added (stock: 5 mM). The cells were then incubated for a further 30 min, then centrifuged at 1300 rpm for 5 min. The supernatant was removed and the cells were resuspended in PBS (200 μL).

Flow cytometric analysis was then carried out testing a minimum of 10,000 events per sample in a FACSCantoII (BD Biosciences, San Jose, CA, USA). The data were analysed using FACSDIVA software.

6.3 Chemistry

6.3.1 General methods

All chemicals and starting materials were commercially purchased and used as provided except where stated. All reactions were monitored by TLC (visualisation using UV light, ammonium molybdate/ceric sulfate solution or vanillin) and/or HPLC. ^{1}H and ^{13}C nuclear magnetic resonance (NMR) spectra were recorded at 27°C on an Agilent 400 spectrometer (400 MHz, ^{1}H; 101 MHz, ^{13}C). Coupling constants are reported in Hertz. For ^{1}H-NMR assignments, chemical shifts are reported: shift value (description of absorption, coupling constant(s) where applicable, number of protons). Mass spectrometry was performed by School of Chemistry, TCD. Samples were introduced by electrospray ionisation (ESI) in the positive ion mode or in the negative ion mode. The HPLC system used consisted of an Alliance HPLC with a Waters 2695 Separations module system and Waters 2996 photodiode array detector (Waters, Santry, Ireland). Empower® software was used for system control, data acquisition and processing.

6.3.2 Synthesis

Isosorbide 2-acetate-5-mononitrate (9a)

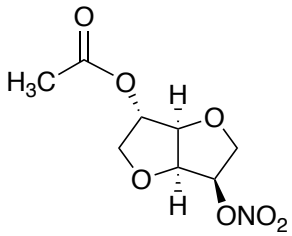

Isosorbide mononitrate (mol. wt. 191.139 g/mol, 10 mmol, 1.91 g) was dissolved in dichloromethane (50 mL) in a 100 mL round bottomed flask. Triethylamine (mol. wt. 101.19 g/mol, d. 0.7255 g/mL, 11 mmol, 1.52 mL), 4-Dimethylaminopyridine (mol. wt. 122.17 g/mol, 2 mmol, 0.244 g), and acetic anhydride (mol. wt. 102.09 g/mol, d. 1.08 g/mL, 11 mmol, 1.04 mL) were added to the flask. The reaction mixture was stirred for 3 h. The reaction was monitored by TLC (1:1 hexane: ethyl acetate) to observe the disappearance of the ISMN. Once complete, the mixture was washed with 1 M HCl (50 mL), saturated sodium bicarbonate solution (50 mL), saturated brine solution (50 mL) and dried with anhydrous sodium sulfate (1 g). Evaporation of the dichloromethane and crystallisation using diethyl ether yielded a white powder (2.133 g, 91.54 %) mol. wt. 233.18 g/mol. **^{1}H NMR** (400 MHz, CHLOROFORM-d) **δ ppm:** 2.06 (s, 3 H, CH_3) 3.89 (dd, J=11.20, 5.81 Hz, 1 H, Is-H4) 3.94 - 4.05 (m, 3 H, Is-H1/6) 4.47 (d, J=4.98 Hz, 1 H, Is-H1) 4.96 (t, J=5.18 Hz, 1 H, Is-H3) 5.16 - 5.23 (m, 1 H, Is-H5) 5.33 (td, J=5.29, 3.11 Hz, 1 H, Is-H2)

Isosorbide 2-acetate (10a)

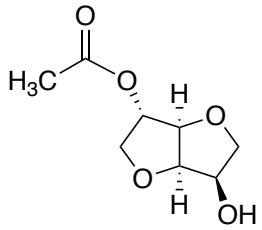

Isosorbide 2-acetate-5-mononitrate (mol. wt. 233.18 g/mol, 9.14 mmol, 2.133 g) was dissolved in ethyl acetate (30 mL) in a 100 mL round bottomed flask. A spatula tip full of 10 % palladium on activated carbon was added to the solution. Air was expelled from the flask and the mixture was kept under an atmosphere of hydrogen gas. The mixture was stirred for 24 h. The reaction was monitored by TLC (1:1 hexane: ethyl acetate) to observe the disappearance of the Isosorbide 2-acetate-5-mononitrate. Once complete, the reaction mixture was filtered through a fritted glass funnel to remove the catalyst. The solvent was evaporated under vacuum and crystallised using diethyl ether to give a white powder (mol. wt. 188.18 g/mol, 1.55 g, 90 %) **^{1}H NMR** (400 MHz, CHLOROFORM-d) **δ ppm:** 2.10 (s, 3 H, CH_3) 2.58 (d, J=7.46 Hz, 1 H, OH) 3.58 (dd, J=9.54, 5.81 Hz, 1 H, Is-H4) 3.90 (dd, J=9.54, 6.22 Hz, 1 H, Is-H6) 3.99 – 4.07 (m, 2 H, Is-H1/6) 4.32 (dd, J=7.26, 5.60 Hz, 1 H, Is-H1) 4.49 (d, J=4.15 Hz, 1 H, Is-H5) 4.64 (t, J=4.98 Hz, 1 H, Is-H3) 5.19 – 5.26 (m, 1 H, Is-H2)

Isosorbide 2-acetate-5-nicotinate (11a)

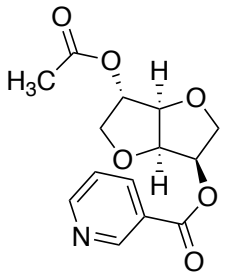

Isosorbide 2-acetate (mol. wt. 188.18 g/mol, 2.65 mmol, 0.500 g) was dissolved in dichloromethane (30 mL) in a 100 mL round bottomed flask. Triethylamine (mol. wt. 101.19 g/mol, d. 0.7255 g/mL, 5.8 mmol, 0.810 mL), 4-Dimethylaminopyridine (mol. wt. 122.17 g/mol, 0.53 mmol, 0.065 g), and nicotinoyl chloride hydrochloride (mol. wt. 178.02 g/mol, 2.915 mmol, 0.52 g) were added to the flask. The reaction mixture was stirred for 24 h. The reaction was monitored by TLC (1:1 hexane: ethyl acetate) to observe the disappearance of the starting material. After 24 h, additional triethylamine (mol. wt. 101.19 g/mol, d. 0.7255 g/mL, 2.9 mmol, 0.405 mL), DMAP (mol. wt. 122.17 g/mol, 0.53 mmol, 0.065 g), and nicotinoyl chloride hydrochloride (mol. wt. 178.02 g/mol, 1.46 mmol, 0.260 g) were added to ensure completion of the reaction. Once complete, the dichloromethane was removed under vacuum.

The crude product was then dissolved in DCM and purified by column chromatography, using hexane and ethyl acetate (1:1) as eluent. Once the solvent was evaporated off, the mixture was recrystallized with diethyl ether to yield a white crystalline powder (0.500 g, 64 %) mol. wt. 293.28 g/mol. **^{1}H NMR** (400 MHz, CHLOROFORM-d) **δ ppm:** 2.07 (s, 3 H, CH_3) 3.90 – 4.06 (m, 4 H, Is-H1/H6) 4.53 (d, *J*=4.88 Hz, 1 H, Is-H3) 4.98 (t, *J*=5.19 Hz, 1 H, Is-H4) 5.22 (d, *J*=3.05 Hz, 1 H, Is-H2) 5.41 (q, *J*=5.29 Hz, 1 H, Is-H5) 7.41 (dd, *J*=7.94, 4.88 Hz, 1 H, Nic-H5) 8.31 (dt, *J*=7.94, 1.83 Hz, 1 H, Nic-H4) 8.79 (dd, *J*=4.58, 1.53 Hz, 1 H, Nic-H6) 9.24 (d, *J*=1.83 Hz, 1 H, Nic-H2). **^{13}C NMR ppm ($CDCl_3$):** 20.53, 43.89, 70.29, 73.08, 74.48, 76.36, 76.68, 77.55, 80.57, 85.76, 123.00, 125.08, 136.81, 150.60, 153.36, 164.21, 169.65. **HRMS (ESI)** calculated for $C_{14}H_{15}NNaO_6$ [M^++Na] 316.079158: found 316.0804.

Isosorbide 2-propionate-5-mononitrate (9b)

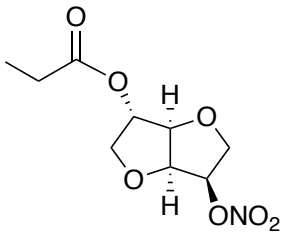

Isosorbide mononitrate (mol. wt. 191.139 g/mol, 10 mmol, 1.91 g) was dissolved in dichloromethane (50 mL) in a 100 mL round bottomed flask. Triethylamine (mol. wt. 101.19 g/mol, d. 0.7255 g/mL, 11 mmol, 1.52 mL), 4-Dimethylaminopyridine (mol. wt. 122.17 g/mol, 5 mmol, 0.61 g), and propionyl chloride (mol. wt. 92.522 g/mol, d. 1.065 g/mL, 11 mmol, 0.956 mL) were added to the flask. The reaction mixture was stirred for 4 h. The reaction was monitored by TLC (1:1 hexane: ethyl acetate) to observe the disappearance of the ISMN. Once complete, the mixture was washed with 1 M HCl (50 mL), saturated sodium bicarbonate solution (50 mL), saturated brine solution (50 mL) and dried with anhydrous sodium sulfate (1 g). Evaporation of the dichloromethane and crystallisation using diethyl ether yielded a white powder (2.1 g, 85 %) mol. wt. 247.20 g/mol. **^{1}H NMR** (400 MHz, CHLOROFORM-d) **δ ppm**: 1.07 – 1.20 (m, 3 H, CH_3) 2.35 (q, J=7.60 Hz, 2 H, CH_2) 3.86 – 3.94 (m, 1 H, Is-H4) 3.99 – 4.07 (m, 3 H, Is-H1/6) 4.48 (d, J=4.98 Hz, 1 H, Is-H1) 4.98 (t, J=5.18 Hz, 1 H, Is-H3) 5.18 – 5.25 (m, 1 H, Is-H5) 5.35 (td, J=5.60, 2.90 Hz, 1 H, Is-H2)

Isosorbide 2-propionate (10b)

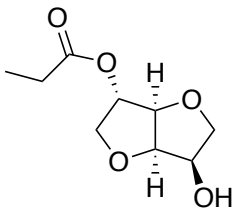

Isosorbide 2-propionate-5-mononitrate (mol. wt. 247.20 g/mol, 5 mmol, 1.25 g) was dissolved in ethyl acetate (30 mL) in a 100 mL round bottomed flask. A spatula tip full of 10 % palladium on activated carbon was added to the solution. Air was expelled from the flask and the mixture was kept under an atmosphere of hydrogen gas. The mixture was stirred for 6 h. The reaction was monitored by TLC (1:1 hexane: ethyl acetate) to observe the disappearance of the Isosorbide 2-propionate-5-mononitrate. Once complete, the reaction mixture was filtered through a fritted glass funnel to remove the catalyst. The solvent was evaporated under vacuum and crystallised using diethyl ether to give a white powder (0.95g, 93 %) mol. wt. 202.21 g/mol. **^{1}H NMR** (400 MHz, CHLOROFORM-d) **δ ppm:** 1.07 – 1.20 (m, 3 H, CH_3) 2.09 (s, 2 H, OH) 2.30 – 2.40 (m, 2 H, CH_2) 3.58 (dd, J=9.54, 5.81 Hz, 1 H, Is-H4) 3.87 – 3.95 (m, 1 H, Is-H6) 3.99 – 4.06 (m, 2 H, Is-H1/H6) 4.28 – 4.36 (m, 1 H, Is-H1) 4.48 (dd, J=4.56, 0.83 Hz, 1 H, Is-H5) 4.60 – 4.66 (m, 1 H, Is-H3) 5.16 – 5.27 (m, 1 H, Is-H2)

Isosorbide 2-propionate-5-nicotinate (11b)

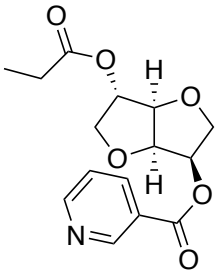

Isosorbide 2-propionate (mol. wt. 202.21g/mol, 2.23 mmol, 0.450 g) was dissolved in dichloromethane (30 mL) in a 100 mL round bottomed flask. Triethylamine (mol. wt. 101.19 g/mol, d. 0.7255 g/mL, 4.9 mmol, 0.680 mL), 4-Dimethylaminopyridine (mol. wt. 122.17 g/mol, 0.223 mmol, 0.027 g), and nicotinoyl chloride hydrochloride (mol. wt. 178.02 g/mol, 2.453 mmol, 0.436 g) were added to the flask. The reaction mixture was stirred for 24 h. The reaction was monitored by TLC (1:1 hexane: ethyl acetate) to observe the disappearance of the starting material. After 24 h, additional triethylamine (mol. wt. 101.19 g/mol, d. 0.7255 g/mL, 2.45 mmol, 0.340 mL), DMAP (mol. wt. 122.17 g/mol, 0.223 mmol, 0.027 g), and nicotinoyl chloride hydrochloride (mol. wt. 178.02 g/mol, 1.227 mmol, 0.218 g) were added to ensure completion of the reaction. Once complete, the dichloromethane was removed under vacuum. The crude product was then dissolved in DCM and purified by column chromatography, using hexane and ethyl acetate (1:1) as eluent. Once the solvent was evaporated off, the mixture was recrystallized with diethyl ether to yield a white crystalline powder (0.51 g, 74.5 %) mol. wt. 307.30 g/mol. **^{1}H NMR** (400 MHz, CHLOROFORM-d) **δ ppm:** 1.14 (t, *J*=7.32 Hz, 3 H, CH_3) 2.35 (q, *J*=7.53 Hz, 2 H, CH_2) 3.92 – 4.09 (m, 4 H, Is-H1/6) 4.54 (d, *J*=4.88 Hz, 1 H, Is-H3) 4.99 (t, *J*=4.88 Hz, 1 H, Is-H4) 5.25 (d, *J*=3.66 Hz, 1 H, Is-H2) 5.42 (q, *J*=5.09 Hz, 1 H, Is-H5)

7.42 (dd, *J*=7.94, 4.88 Hz, 1 H, Nic-H5) 8.33 (dt, *J*=8.09, 2.06 Hz, 1 H, Nic-H4) 8.81 (dd, *J*=4.58, 1.53 Hz, 1 H, Nic-H6) 9.25 (s, 1 H, Nic-H2). **^{13}C NMR ppm ($CDCl_3$):** 8.62, 20.33, 27.13, 70.28, 73.21, 74.56, 76.37, 76.69, 77.39, 80.60, 85.85, 112.10, 123.05, 136.89, 150.62, 153.36, 164.26, 173.15.

Isosorbide 2-butyrate-5-mononitrate (9c)

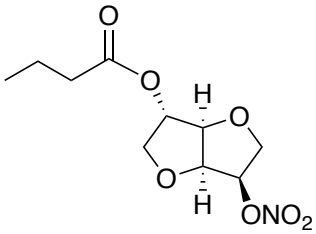

Isosorbide mononitrate (mol. wt. 191.139 g/mol, 10 mmol, 1.91 g) was dissolved in dichloromethane (50 mL) in a 100 mL round bottomed flask. Triethylamine (mol. wt. 101.19 g/mol, d. 0.7255 g/mL, 11 mmol, 1.52 mL), 4-Dimethylaminopyridine (mol. wt. 122.17 g/mol, 5 mmol, 0.61 g), and butyrl chloride (mol. wt. 106.55 g/mol, d. 1.026 g/mL, 11 mmol, 1.14 mL) were added to the flask. The reaction mixture was stirred for 4 h. The reaction was monitored by TLC (1:1 hexane:ethyl acetate) to observe the disappearance of the ISMN. Once complete, the mixture was washed with 1 M HCl (50 mL), saturated sodium bicarbonate solution (50 mL), saturated brine solution (50 mL) and dried with anhydrous sodium sulfate (1 g). Evaporation of the dichloromethane yielded a yellow oil (2.359 g, 90 %) mol. wt. 261.23 g/mol. **^{1}H NMR** (400 MHz, CHLOROFORM-d) **δ ppm:** 0.95 (t, J=7.46 Hz, 3 H, CH_3) 1.58 - 1.71 (m, 2 H, CH_2) 2.31 (t, J=7.46 Hz, 2 H, CH_2) 3.86 - 3.95 (m, 1 H, Is-H4) 3.99 - 4.06 (m, 3 H, Is-H1/6) 4.48 (d, J=4.98 Hz, 1 H, Is-H1) 4.98 (t, J=5.39 Hz, 1 H, Is-H3) 5.23 (s, 1 H, Is-H5) 5.36 (td, J=5.60, 2.90 Hz, 1 H, IsH2)

Isosorbide 2-butyrate (10c)

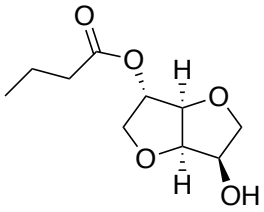

Isosorbide 2-butyrate-5-mononitrate (mol. wt. 261.23 g/mol, 8.7 mmol, 2.28 g) was dissolved in acetic acid (20 mL) in a 100 mL round bottomed flask. Zinc powder (mol. wt. 65 g/mol, 87 mmol, 5.695 g) was added to the flask. The mixture was stirred for 6 h. The reaction was monitored by TLC (1:1 hexane: ethyl acetate) to observe the disappearance of the Isosorbide 2-butyrate-5-mononitrate. Once complete, the reaction mixture was filtered through cotton

wool to remove the catalyst. Ethyl acetate was then added to the reaction mixture and following this the mixture was washed with 1 M HCl (50 mL), saturated sodium bicarbonate solution (50 mL), saturated brine solution (50 mL) and dried with anhydrous sodium sulfate (1 g). Evaporation of the ethyl acetate yielded a white powder (1.13 g, 60 %) mol. wt. 216.23 g/mol. **^{1}H NMR** (400 MHz, CHLOROFORM-d) **δ ppm:** 0.87 - 0.97 (m, 3 H, CH_3) 1.64 (sxt, J=7.38 Hz, 2 H, CH_2) 2.07 (s, 1 H, OH) 2.25 - 2.32 (m, 2 H, CH_2) 3.55 (dd, J=9.54, 5.81 Hz, 1 H, Is-H4) 3.87 (dd, J=9.33, 6.01 Hz, 1 H, Is-H6) 4.00 (d, J=2.49 Hz, 2 H, Is-H1/6) 4.29 (q, J=5.81 Hz, 1 H, Is-H1) 4.44 - 4.47 (m, 1 H, Is-H5) 4.61 (t, J=4.77 Hz, 1 H, Is-H3) 5.21 (s, 1 H, Is-H2).

Isosorbide 2-butyrate-5-nicotinate (11c)

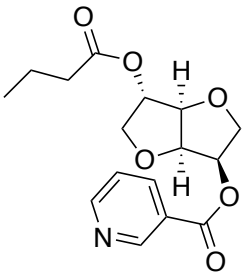

Isosorbide 2-butyrate (mol. wt. 216.23 g/mol, 2.31 mmol, 0.500 g) was dissolved in dichloromethane (30 mL) in a 100 mL round bottomed flask. Triethylamine (mol. wt. 101.19 g/mol, d. 0.7255 g/mL, 5.08 mmol, 0.706 mL), 4-Dimethylaminopyridine (mol. wt. 122.17 g/mol, 0.231 mmol, 0.03 g), and nicotinoyl chloride hydrochloride (mol. wt. 178.02 g/mol, 2.541 mmol, 0.453 g) were added to the flask. The reaction mixture was stirred for 24 h. The reaction was monitored by TLC (1:1 hexane: ethyl acetate) to observe the disappearance of the starting material. After 24 h, additional triethylamine (mol. wt. 101.19 g/mol, d. 0.7255 g/mL, 2.54 mmol, 0.353 mL), DMAP (mol. wt. 122.17 g/mol, 0.231 mmol, 0.030 g), and nicotinoyl chloride hydrochloride (mol. wt. 178.02 g/mol, 1.27 mmol, 0.227 g) were added to ensure completion of the reaction. Once complete, the mixture was washed with 1 M HCl (50 mL), saturated sodium bicarbonate solution (50 mL), saturated brine solution (50 mL) and dried with anhydrous sodium sulfate (1 g). Evaporation of the dichloromethane and crystallisation using diethyl ether yielded a white powder (0.5 g, 67.3 %) mol. wt. 321.33 g/mol. **^{1}H NMR** (400 MHz, CHLOROFORM-d) **δ ppm:** 0.75 - 0.87 (m, 3 H, CH_3) 1.53 (sxtd, *J*=7.45, 7.45, 7.45, 7.45, 7.45, 1.83 Hz, 2 H, CH_2) 2.20 (td, *J*=7.32, 1.83 Hz, 2 H, CH_2) 3.78 - 3.98 (m, 4 H, Is-H1/H6) 4.44 (d, *J*=4.27 Hz, 1 H, Is- H3) 4.82 - 4.92 (m, 1 H, Is-H4) 5.14 (br. s., 1 H, Is-H2) 5.25 - 5.38 (m, 1 H, Is-H5) 7.27 - 7.38 (m, 1 H, Nic-H5) 8.14 - 8.26 (m, 1 H, Nic-H4) 8.64 - 8.76 (m, 1 H, Nic-H6) 9.14 (br. s., 1 H, Nic-H2). **^{13}C NMR ppm ($CDCl_3$):** 13.22, 17.98, 35.63, 70.27, 73.21, 74.54, 76.37, 76.68, 77.30, 80.58, 85.84, 123.03, 136.84, 150.61, 153.36, 164.25, 172.30. **HRMS (ESI)** calculated for $C_{16}H_{19}NNaO_6$ [M^++Na] 344.110458: found 344.1100.

Isosorbide 2-valeroate-5-mononitrate (9d)

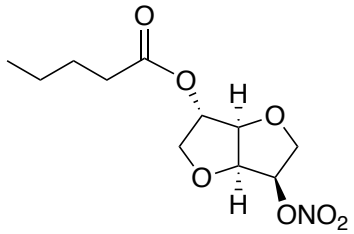

Isosorbide mononitrate (mol. wt. 191.139 g/mol, 10 mmol, 1.91 g) was dissolved in dichloromethane (50 mL) in a 100 mL round bottomed flask. Triethylamine (mol. wt. 101.19 g/mol, d. 0.7255 g/mL, 11 mmol, 1.52 mL), 4-Dimethylaminopyridine (mol. wt. 122.17 g/mol, 5 mmol, 0.61 g), and valeroyl chloride (mol. wt. 120.58 g/mol, d. 1.016 g/mL, 11 mmol, 1.305 mL) were added to the flask. The reaction mixture was stirred for 12 h. The reaction was monitored by TLC (1:1 hexane: ethyl acetate) to observe the disappearance of the ISMN. Once complete, the mixture was washed with 1 M HCl (50 mL), saturated sodium bicarbonate solution (50 mL), saturated brine solution (50 mL) and dried with anhydrous sodium sulfate (1 g). Evaporation of the dichloromethane yielded a yellow oil (2.39 g, 87 %) mol. wt. 275.26 g/mol. **^{1}H NMR** (400 MHz, CHLOROFORM-d) **δ ppm:** 0.84 - 0.91 (m, 3 H, CH_3) 1.32 (dd, J=14.93, 7.46 Hz, 2 H, CH_2) 1.51 - 1.65 (m, 2 H, CH_2) 2.31 (t, J=7.46 Hz, 2 H, CH_2) 3.56 (dd, J=9.54, 6.22 Hz, 1 H, Is-H4) 3.87 (dd, J=9.54, 6.22 Hz, 1 H, Is-H6) 4.00 (d, J=2.07 Hz, 2 H, Is-H1/6) 4.30 (q, J=5.81 Hz, 1 H, Is-H1) 4.45 (d, J=4.56 Hz, 1 H, Is-H3) 4.61 (t, J=4.98 Hz, 1 H, Is-H5) 5.21 (s, 1 H, Is-H2)

Isosorbide-2-valeroate (10d)

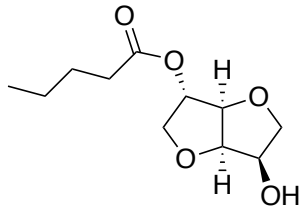

Isosorbide 2-valeroate-5-mononitrate (mol. wt. 275.26 g/mol, 8.7 mmol, 2.39 g) was dissolved in acetic acid (20 mL) in a 100 mL round bottomed flask. Zinc powder (mol. wt. 65 g/mol, 87 mmol, 5.643 g) was added to the flask. The mixture was stirred for 6 h. The reaction was monitored by TLC (1:1 hexane: ethyl acetate) to observe the disappearance of the Isosorbide 2-valeroate-5-mononitrate. Once complete, the reaction mixture was filtered through cotton wool to remove the catalyst. Ethyl acetate was then added to the reaction mixture and following this the mixture was washed with 1 M HCl (50 mL), saturated sodium bicarbonate solution (50 mL), saturated brine solution (50 mL) and dried with anhydrous sodium sulfate (1 g). Evaporation of the ethyl acetate yielded a white powder (1.50 g, 75 %) mol. wt. 230.26 g/mol.

^{1}H NMR (400 MHz, CHLOROFORM-d) **δ ppm:** 0.87 - 0.95 (m, 3 H, CH_3) 1.29 - 1.39 (m, 2 H, CH_2) 1.55 - 1.65 (m, 2 H, CH_2) 2.32 (t, J=7.67 Hz, 2 H, CH_2) 3.86 - 3.94 (m, 1 H, Is-H4) 3.97 - 4.06 (m, 3 H, Is-H1/6) 4.47 (d, J=4.98 Hz, 1 H, Is-H1) 4.98 (t, J=5.18 Hz, 1 H, Is-H3) 5.22 (s, 1 H, Is-H5) 5.35 (td, J=5.60, 2.90 Hz, 1 H, Is-H2)

Isosorbide 2-valeroate-5-nicotinate (11d)

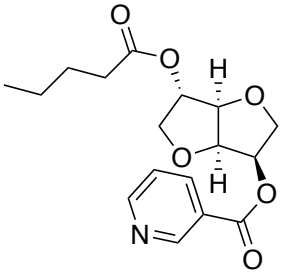

Isosorbide 2-valeroate (mol. wt. 230.26 g/mol, 4.34 mmol, 1 g) was dissolved in dichloromethane (50 mL) in a 100 mL round bottomed flask. Triethylamine (mol. wt. 101.19 g/mol, d. 0.7255 g/mL, 18.24 mmol, 2.53 mL) and nicotinoyl chloride hydrochloride (mol. wt. 178.02 g/mol, 9.548 mmol, 1.7 g) were added to the flask. The reaction mixture was stirred at room temperature for 24 h. The reaction was monitored by TLC (1:1 hexane: ethyl acetate) to observe the disappearance of the starting material. Once complete, the mixture was washed with 1 M HCl (50 mL), saturated sodium bicarbonate solution (50 mL), saturated brine solution (50 mL) and dried with anhydrous sodium sulfate (1 g). The crude product was then dissolved in DCM and purified by column chromatography, using hexane and ethyl acetate (1:1) as eluent. Once the solvent was evaporated off, the mixture was recrystallized with diethyl ether to yield a white crystalline powder (0.3 g, 22%) mol. wt. 321.33 g/mol. **^{1}H NMR** (400 MHz, CHLOROFORM-d) **δ ppm:** 0.91 (t, *J*=7.32 Hz, 3 H, CH_3) 1.27 - 1.40 (m, 2 H, CH_2) 1.60 (quin, *J*=7.63 Hz, 2 H, CH_2) 2.32 (t, *J*=7.32 Hz, 2 H, CH_2) 3.89 - 4.12 (m, 4 H, Is-H1/6) 4.54 (d, *J*=4.88 Hz, 1 H, IS-H3) 4.98 (t, *J*=5.19 Hz, 1 H, Is-H4) 5.25 (d, *J*=3.05 Hz, 1 H, Is-H2) 5.42 (q, *J*=5.49 Hz, 1 H, H5) 7.36 - 7.45 (m, 1 H, Nic-H5) 8.33 (dd, *J*=7.94, 1.83 Hz, 1 H, Nic-H4) 8.76 - 8.85 (m, 1 H, Nic-H6) 9.19 - 9.29 (m, 1 H, Nic-H2). **^{13}C NMR ppm ($CDCl_3$):** 13.32, 21.84, 26.55, 33.52, 70.28, 73.22, 74.58, 76.36, 76.68, 77.31, 80.59, 85.85, 123.07, 136.95, 150.53, 153.27, 164.22, 172.50. **HRMS (ESI)** calculated for $C_{17}H_{21}NNaO_6$ [M^++Na] 358.126108: found 358.1254.

Isosorbide 2-benzoate-5-mononitrate (9e)

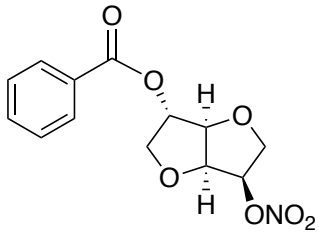

Isosorbide mononitrate (mol. wt. 191.139 g/mol, 10 mmol, 1.91 g) was dissolved in dichloromethane (50 mL) in a 100 mL round bottomed flask. Triethylamine (mol. wt. 101.19 g/mol, d. 0.7255 g/mL, 11 mmol, 1.52 mL), 4-Dimethylaminopyridine (mol. wt. 122.17 g/mol, 5 mmol, 0.61 g), and benzoyl chloride (mol. wt. 140.57 g/mol, d. 1.211 g/mL, 11 mmol, 1.74 mL) were added to the flask. The reaction mixture was stirred at room temperature for 12 h. The reaction was monitored by TLC (1:1 hexane: ethyl acetate) to observe the disappearance of the ISMN. Once complete, the mixture was washed with 1 M HCl (50 mL), saturated sodium bicarbonate solution (50 mL), saturated brine solution (50 mL) and dried with anhydrous sodium sulfate (1 g). Evaporation of the dichloromethane and crystallisation with diethyl ether yielded a white powder (2.5 g, 84.7%) mol. wt. 295.25 g/mol. **^{1}H NMR** (400 MHz, CHLOROFORM-d) **δ ppm:** 3.90 - 4.01 (m, 1 H, Is-H4) 4.03 - 4.15 (m, 2 H, Is-H1/6) 4.16 - 4.23 (m, 1 H, Is-H6) 4.65 (d, J=4.98 Hz, 1 H, Is-H1) 5.08 (t, J=5.18 Hz, 1 H, Is-H3) 5.40 (td, J=5.39, 2.90 Hz, 1 H, Is-H5) 5.49 (d, J=2.90 Hz, 1 H, Is-H2) 7.42 - 7.52 (m, 2 H, Ar-H2/4) 7.54 - 7.66 (m, 1 H, Ar-H3) 7.99 - 8.08 (m, 2 H, Ar-H1/5) **^{13}C NMR** (101 MHz, CHLOROFORM-*d*) **δ ppm** 69.32, 73.67, 76.73, 77.05, 77.36, 77.88, 81.33, 81.62, 86.78, 128.51, 129.34, 129.79, 133.53, 165.55.

Isosorbide-2-benzoate (10e)

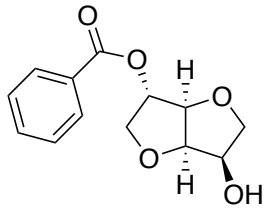

Isosorbide 2-benzoate-5-mononitrate (mol. wt. 295.25 g/mol, 8.47 mmol, 2.5 g) was dissolved in ethyl acetate (20 mL) in a 100 mL round bottomed flask. A spatula tip full of 10 % palladium on activated carbon was added to the solution. Air was expelled from the flask and the mixture was kept under an atmosphere of hydrogen gas. The mixture was stirred for 12 h. The reaction was monitored by TLC (1:1 hexane: ethyl acetate) to observe the disappearance of the Isosorbide 2-benzoate-5-mononitrate. Once complete, the reaction mixture was filtered through a fritted glass funnel to remove the catalyst. The solvent was evaporated under vacuum and

crystallised using diethyl ether to give a white powder (1.92 g, 90.5%) mol. wt. 250.25 g/mol. **^{1}H NMR** (400 MHz, CHLOROFORM-d) **δ ppm:** 2.63 (d, J=6.63 Hz, 1 H, OH) 3.63 (dd, J=9.54, 5.81 Hz, 1 H, Is-H4) 3.95 (dd, J=9.54, 5.81 Hz, 1 H, Is-H6) 4.13 (dd, J=10.57, 3.52 Hz, 1 H, Is-H6) 4.21 (d, J=10.78 Hz, 1 H, Is-H1) 4.37 (t, J=5.39 Hz, 1 H, Is-H1) 4.65 (d, J=4.56 Hz, 1 H, Is-H3) 4.71 - 4.78 (m, 1 H, Is-H5) 5.49 (d, J=3.32 Hz, 1 H, Is-H2) 7.40 - 7.53 (m, 2 H, Ar-H2/4) 7.57 - 7.63 (m, 1 H, Ar-H3) 8.04 (dd, J=8.29, 1.24 Hz, 2 H, Ar-H1/5).

Isosorbide 2-benzoate-5-nicotinate (11e)

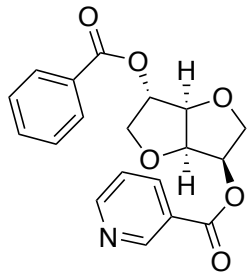

Isosorbide 2-benzoate (mol. wt. 250.25 g/mol, 6.4 mmol, 1.6 g) was dissolved in dichloromethane (50 mL) in a 100 mL round bottomed flask. Triethylamine (mol. wt. 101.19 g/mol, d. 0.7255 g/mL, 14.08 mmol, 1.95 mL), 4-Dimethylaminopyridine (mol. wt. 122.17 g/mol, 0.64 mmol, 0.078 g) and nicotinoyl chloride hydrochloride (mol. wt. 178.02 g/mol, 7.04 mmol, 1.254 g) were added to the flask. The reaction mixture was stirred at room temperature for 24 h. The reaction was monitored by TLC (1:1 hexane: ethyl acetate) to observe the disappearance of the starting material. After 24 h, additional triethylamine (mol. wt. 101.19 g/mol, d. 0.7255 g/mL, 7.04 mmol, 0.975 mL), DMAP (mol. wt. 122.17 g/mol, 0.64 mmol, 0.078 g), and nicotinoyl chloride hydrochloride (mol. wt. 178.02 g/mol, 3.52 mmol, 0.627 g) were added to ensure completion of the reaction. Once complete, the mixture was washed with 1 M HCl (50 mL), saturated sodium bicarbonate solution (50 mL), saturated brine solution (50 mL) and dried with anhydrous sodium sulfate (1 g). The crude product was then dissolved in DCM and purified by column chromatography, using hexane and ethyl acetate (1:1) as eluent. Once the solvent was evaporated off, the mixture was recrystallized with diethyl ether to yield a white crystalline powder (1.2 g, 52.8 %) mol. wt. 355.35 g/mol. **^{1}H NMR** (400 MHz, CHLOROFORM-d) **δ ppm:** 4.01 - 4.19 (m, 4 H, Is-H1/6) 4.70 (d, J=4.88 Hz, 1 H, H3) 5.09 (t, J=5.19 Hz, 1 H, Is-H4) 5.42 - 5.53 (m, 2 H, Is-H2/5) 7.40 - 7.50 (m, 3 H, A-H2/5, Nic-H5) 7.54 - 7.65 (m, 1 H, Ar-H3) 7.98 - 8.07 (m, 2 H, Ar-H1/5) 8.35 (dt, J=7.94, 1.83 Hz, 1 H,Nic-H4) 8.82 (d, J=3.66 Hz, 1 H, Nic-H6) 9.28 (s, 1 H, Nic-H2). **^{13}C NMR ppm ($CDCl_3$):** 70.33, 73.17, 74.64, 76.36, 76.68, 77.99, 80.70, 85.91, 123.07, 128.12, 129.05, 129.40, 133.10, 136.91, 150.62, 153.37, 164.31, 165.22. **HRMS (ESI)** calculated for $C_{19}H_{17}NNaO_6$ [M^++Na] 378.09408: found 378.0932.

Isosorbide-2-benzoate-5-isonicotinate (15)

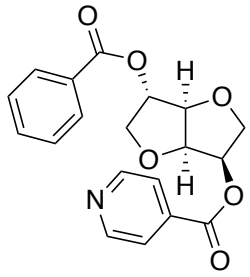

Isosorbide-2-benzoate (mol. wt. 250.25 g/mol, 0.8 mmol, 0.2 g) was dissolved in dichloromethane (30 mL) in a 100 mL round bottomed flask. Triethylamine (mol. wt. 101.19 g/mol, d. 0.7255 g/mL, 2.64 mmol, 0.366 mL), 4-Dimethylaminopyridine (mol. wt. 122.17 g/mol, 0.08 mmol, 0.01 g) and isonicotinoyl chloride hydrochloride (mol. wt. 178.02 g/mol, 0.88 mmol, 0.157 g) were added to the flask. The reaction mixture was stirred at room temperature for 24 h. The reaction was monitored by TLC (1:1 hexane: ethyl acetate) to observe the disappearance of the starting material. After 24 h, additional triethylamine (mol. wt. 101.19 g/mol, d. 0.7255 g/mL, 2.64 mmol, 0.366 mL), DMAP (mol. wt. 122.17 g/mol, 0.08 mmol, 0.010 g), and isonicotinoyl chloride hydrochloride (mol. wt. 178.02 g/mol, 0.88 mmol, 0.157 g) were added to ensure completion of the reaction. Once complete, the mixture was washed with 1 M HCl (50 mL), saturated sodium bicarbonate solution (50 mL), saturated brine solution (50 mL) and dried with anhydrous sodium sulfate (1 g). The crude product was then dissolved in DCM and purified by column chromatography, using hexane and ethyl acetate (1:1) as eluent. Once the solvent was evaporated off, the mixture was recrystallized with diethyl ether to yield a white crystalline powder (0.12 g, 42.2 %) mol. wt. 355.35 g/mol. **^{1}H NMR** (400 MHz, CHLOROFORM-d) **δ ppm:** 4.04 - 4.16 (m, 4 H, Is-H1/6) 4.66 - 4.77 (m, 1 H, Is-H3) 5.08 (t, J=4.98 Hz, 1 H, Is-H4) 5.41 - 5.53 (m, 2 H, Is-H2/5) 7.45 (t, J=7.67 Hz, 2 H, Ar-H2/5) 7.59 (t, J=7.46 Hz, 1 H, Ar-H3) 7.90 (d, J=5.81 Hz, 2 H, Nic-H3/5) 7.97 - 8.09 (m, 2 H, Ar-H1/5) 8.83 (d, J=4.56 Hz, 2 H, Nic-H2/6). **^{13}C NMR** (101 MHz, CHLOROFORM-*d*) **δ ppm** 73.55, 75.39, 76.73, 77.03, 77.36, 78.28, 81.02, 86.29, 128.51, 129.77, 133.49. **HRMS (ESI)** calculated for $C_{19}H_{18}NO_6$ [M^++H] 356.112864: found 356.112982.

Isosorbide-2-nicotinate-5-benzoate (14)

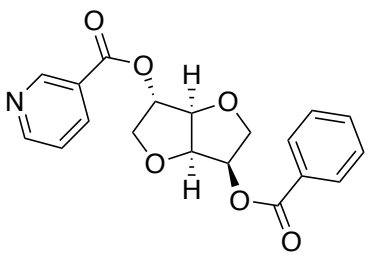

Isosorbide mononitrate (mol. wt. 191.139 g/mol, 10 mmol, 1.91 g) was dissolved in dichloromethane (50 mL) in a 100 mL round bottomed flask. Triethylamine (mol. wt. 101.19 g/mol, d. 0.7255 g/mL, 22 mmol, 3.05 mL), 4-Dimethylaminopyridine (mol. wt. 122.17 g/mol, 1 mmol, 0.12 g), and nicotinoyl chloride hydrochloride (mol. wt. 178.02 g/mol, 11 mmol, 1. 96 g) were added to the flask. The reaction mixture was stirred at room temperature for 16 h. The reaction was monitored by TLC (1:1 hexane: ethyl acetate) to observe the disappearance of the ISMN. After 16 h, additional nicotinoyl chloride hydrochloride (5.5 mmol, 0.98 g) and trimethylamine (11 mmol, 1.525 mL) was added and the reaction proceeded for a further hour. Once complete the product was purified using column chromatography, using hexane and ethyl acetate (1:1) as the eluent. Once the solvent was evaporated off, the mixture was recrystallized with diethyl ether to yield a white crystalline powder (2.14g, 72.3% mol.wt. 296.24 g/mol). Isosorbide 2-nicotinate-5-mononitrate (mol. wt. 296.24 g/mol, 1.35 mmol, 0.4 g) was dissolved in ethyl acetate (10 mL) in a 50 mL round bottomed flask. A spatula tip full of 10 % palladium on activated carbon was added to the solution. Air was expelled from the flask and the mixture was kept under an atmosphere of hydrogen gas. The mixture was stirred for 10 h. The reaction was monitored by TLC (3:1 ethyl acetate: hexane) to observe the disappearance of the Isosorbide 2-nicotinate-5-mononitrate. The reaction was stopped prior to completion as cleavage of the nicotinate ester group occurred as the reaction proceeded. The reaction mixture was filtered through a fritted glass funnel to remove the catalyst. The solvent was evaporated under vacuum. The product was purified using column chromatography, using a gradient dichloromethane and MeOH solvent system. Once the solvent was evaporated off, the product was recrystallized with diethyl ether to yield a white solid (0.15 g, 44.2 % mol.wt. 251.24 g/mol). Isosorbide 2-nicotinate-5-hydroxide (mol. wt. 251.24 g/mol, 0.398 mmol, 0.1 g) was dissolved in 20 mL dichloromethane. Triethylamine (mol. wt. 101.19 g/mol, d. 0.7255 g/mL, 0.438 mmol, 0.048 mL), 4-Dimethylaminopyridine (mol. wt. 122.17 g/mol, 0.199 mmol, 0.019 g) and benzoyl chloride (mol. wt. 140.57 g/mol, 0.438 mmol, 0.041 g) were added to the flask. The reaction mixture was stirred at room temperature for 2 h. The reaction was monitored by TLC (1:1 hexane: ethyl acetate) to observe the disappearance of the starting material. The product was purified using column chromatography, using hexane and ethyl acetate (1:1) as the eluent. Once the solvent was evaporated off, the product was recrystallized with diethyl ether to yield a white solid (0.04 g, 28.2% mol.wt. 355.35 g/mol). **^{1}H NMR** (400 MHz, CHLOROFORM-d) **δ ppm:** 4.02 - 4.16 (m, 4 H, Is-H1/6) 4.71 (d, *J*=4.40 Hz, 1 H, Is-H3) 5.09 (t, *J*=5.14 Hz, 1 H, Is-H4) 5.45 (q, *J*=5.87 Hz, 1 H, Is-H2) 5.52 (d, *J*=3.42 Hz, 1 H, Is-H5) 7.37 - 7.52 (m, 3 H, Ar-H2/4, Nic-H5) 7.55 - 7.64 (m, 1 H, Ar-H3) 8.05 - 8.13 (m, 2 H, Ar-H1/5) 8.30 (dd, *J*=7.83, 1.96 Hz, 1 H, Nic-H4) 8.81 (d, *J*=1.00 Hz, 1 H, Nic-H6) 9.22 (br. s., 1 H, Nic-H2). **^{13}C NMR** (101 MHz, CHLOROFORM-*d*) **δ ppm** 70.91, 73.39, 74.41, 76.73, 77.05,

77.36, 79.02, 81.24, 86.08, 123.46, 128.51, 129.81, 133.37, 137.34, 150.89, 153.71, 165.93. **HRMS (ESI)** calculated for $C_{19}H_{17}NNaO_6$ [M^++Na] 378.09408: found 378.095189

Isosorbide-2-benzyloxybenzoate-5-nitrate (20)

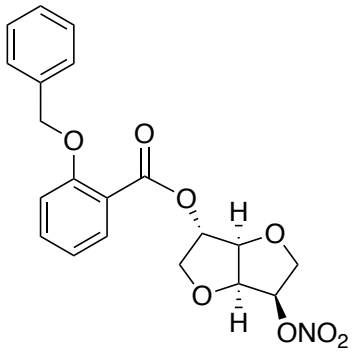

Isosorbide mononitrate (mol. wt. 191.139 g/mol, 10 mmol, 0.637 g) was dissolved in dichloromethane (20 mL) in a 50 mL round bottomed flask. 2-benzyloxybenzoic acid (mol.wt. 228.24 g/mol, 11 mmol, 0.837 g), 4-Dimethylaminopyridine (mol. wt. 122.17 g/mol, 11 mmol, 0.447 g), and N,N'-Dicyclohexylcarbodiimide (mol. wt. 206.33 g/mol, 11 mmol, 0.756 g) were added to the flask. The reaction mixture was stirred for 1 h at 30°C. The reaction was monitored by TLC (2:1 hexane: ethyl acetate) to observe the disappearance of the ISMN. Once complete, the mixture was filtered and washed with 1 M HCl (50 mL), saturated sodium bicarbonate solution (50 mL), saturated brine solution (50 mL) and dried with anhydrous sodium sulfate (1 g). The reaction was then purified using column chromatography (hexane: ethyl acetate 3:1). The resultant product, isosorbide-2-benzyloxybenzoate-5-nitrate, was a white solid (0.355 g, 26.5%, mol.wt. 401.37 g/mol). **^{1}H NMR** (400 MHz, CHLOROFORM-d) **δ ppm:** 3.83 (dd, J=11.20, 5.81 Hz, 1 H, Is-H4) 3.96 - 4.05 (m, 2 H, Is-H1/H6) 4.07 - 4.13 (m, 1 H, Is-H6) 4.39 (d, J=4.98 Hz, 1 H, Is-H1) 4.59 (t, J=5.18 Hz, 1 H, Is-H3) 5.10 - 5.13 (m, 2 H, -CH_2) 5.21 (td, J=5.60, 2.90 Hz, 1 H, Is-H5) 5.44 (d, J=2.90 Hz, 1 H, Is-H2) 6.98 - 7.05 (m, 2 H, Sal-H3, Ar-H3) 7.35 - 7.44 (m, 3 H, Ar-H1/5, Sal-H6) 7.45 - 7.50 (m, 3 H, Ar-H2/4, Sal-H5) 7.81 (dd, J=7.67, 1.87 Hz, 1 H, Sal-H6). **^{13}C NMR** (101 MHz, CHLOROFORM-*d*) **δ ppm** 69.16, 70.68, 73.55, 76.73, 77.05, 77.36, 77.65, 81.36, 86.72, 120.57, 127.79, 128.15, 128.66, 132.03, 133.98.

Isosorbide-2-benzyloxybenzoate (21)

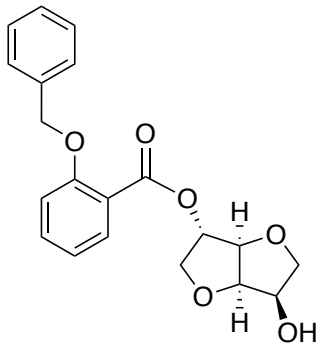

Isosorbide-2-benzyloxybenzoate-5-nitrate (mol. wt. 401.37 g/mol, 7.77 mmol, 3.12 g) was dissolved in acetic acid (20 mL) in a 100 mL round bottomed flask. Zinc powder (mol. wt. 65 g/mol, 95 mmol, 6.2 g) was added to the flask. The mixture was stirred for 5 h. The reaction was monitored by TLC (1:1 hexane: ethyl acetate) to observe the disappearance of the Isosorbide 2-benzyloxybenzoate-5-mononitrate. Once complete, the reaction mixture was filtered through cotton wool to remove the catalyst. Ethyl acetate was then added to the reaction mixture and following this the mixture was washed with 1 M HCl (50 mL), saturated sodium bicarbonate solution (50 mL), saturated brine solution (50 mL) and dried with anhydrous sodium sulfate (1 g). Evaporation of the ethyl acetate yielded a white powder (2.21 g, 80 %) mol. wt. 356.37 g/mol. **^{1}H NMR** (400 MHz, CHLOROFORM-*d*) **δ ppm** 2.60 (br. s, 1 H, -OH) 3.56 (dd, *J*=9.54, 6.11 Hz, 1 H, Is-H4) 3.86 (dd, *J*=9.29, 5.87 Hz, 1 H, Is-H6) 4.04 (dd, *J*=10.51, 3.67 Hz, 1 H, Is-H1) 4.13 (d, *J*=10.76 Hz, 1 H, Is-H1) 4.19 (q, *J*=5.87 Hz, 1 H, IS-H5) 4.31 (t, *J*=4.89 Hz, 1 H, Is-H3) 4.42 (d, *J*=4.40 Hz, 1 H, Is-H6) 5.13 (s, 2 H, -CH_2) 5.46 (d, *J*=2.93 Hz, 1 H, Is-H2) 6.98 - 7.07 (m, 2 H, Sal-H3, Ar-H3) 7.32 - 7.45 (m, 3 H, Ar-H1/5, Sal-H6) 7.46 - 7.53 (m, 3 H, Ar-H2/4, Sal-H5) 7.83 (dd, *J*=7.58, 1.71 Hz, 1 H, Sal-H6). **^{13}C NMR** (101 MHz, CHLOROFORM-*d*) δ **ppm** 70.68, 72.36, 73.62, 76.73, 77.05, 77.38, 78.67, 81.92, 85.71, 113.37, 120.55, 127.70, 128.17, 128.64, 132.05, 133.96, 136.45, 158.35.

Isosorbide-2-benzyloxybenzoate-5-nicotinate (22)

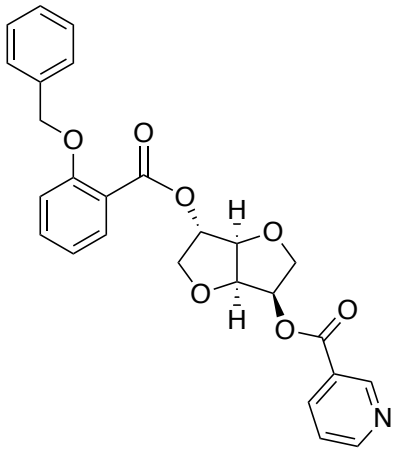

Isosorbide-2-benzyloxybenzoate-5- OH (mol. wt. 356.37 g/mol, 5.69 mmol, 2.03 g) was dissolved in dry dichloromethane (20 mL) in a 100 mL round bottomed flask. Triethylamine (mol. wt. 101.19 g/mol, d. 0.7255 g/mL, 22.76 mmol, 3.17 mL), 4-Dimethylaminopyridine (mol. wt. 122.17 g/mol, 2.845 mmol, 0.347 g), and nicotinoyl chloride hydrochloride (mol. wt. 178.02 g/mol, 34.14 mmol, 6.08 g) were added to the flask. The reaction mixture was stirred for 24 h. The reaction was monitored by TLC (1:2 hexane: ethyl acetate) to observe the disappearance of the isosorbide-2-(2-benzyloxybenzoate). Once complete, the mixture was washed with 1 M HCl (50 mL), saturated sodium bicarbonate solution (50 mL), saturated brine solution (50 mL) and dried with anhydrous sodium sulfate (1 g). Evaporation of the dichloromethane and crystallisation using diethyl ether yielded a white powder (1.38 g, 52.4 %) mol. wt. 461.47 g/mol. **^{1}H NMR** (400 MHz, CHLOROFORM-*d*) **δ ppm** 4.01 (d, *J*=5.38 Hz, 2 H, Is-H1/6) 4.05 (d, *J*=2.45 Hz, 2 H, Is-H1/6) 4.48 (d, *J*=4.89 Hz, 1 H, Is-H4) 4.70 (t, *J*=5.14 Hz, 1 H, Is-H3) 5.14 (s, 2 H, -CH_2) 5.33 (q, *J*=5.38 Hz, 1 H, Is-H5) 5.47 (s, 1 H, Is-H2) 6.96 - 7.08 (m, 2 H, Sal-H3, Ar-H3) 7.30 - 7.38 (m, 1 H, Nic-H5) 7.39 - 7.52 (m, 6 H, Ar-H1/2/3/4, Sal-H5/6) 7.82 (dd, *J*=7.58, 1.71 Hz, 1 H, Sal-H6) 8.38 (dt, *J*=8.19, 1.77 Hz, 1 H, Nic-H4) 8.83 (br. s., 1 H, Nic-H6) 9.29 (br. s., 1 H, Nic-H2). **^{13}C NMR** (101 MHz, CHLOROFORM-*d*) **δ ppm** 70.55, 70.66, 73.53, 75.06, 76.73, 77.03, 77.36, 78.15, 80.91, 86.24, 123.62, 127.63, 128.11, 128.66, 132.03, 133.94, 136.49, 137.68, 153.20, 158.37.

Isosorbide-2-salicylate-5-nicotinate (ISAL, 2)

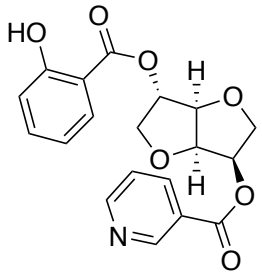

Method 1: Isosorbide-2-benzyloxybenzoate-5-nicotinate (mol. wt. 461.47 g/mol, 2.69 mmol, 1.24 g) was dissolved in acetic acid (15 mL) in a 100 mL round bottomed flask. Hydrobromic acid (80.91 g/mol, 1.49 g/cm³, 276 mM, 15 mL) was added dropwise to the flask. The reaction was stirred for 90 min. The reaction was monitored by TLC (1:2 hexane: ethyl acetate) to observe the disappearance of the isosorbide-2-(2-benzyloxybenzoate)-5-nicotinate. Once complete, the reaction mixture was washed with ethyl acetate (50 mL) and water (50 mL), followed by saturated sodium bicarbonate solution (50 mL), saturated brine solution (50 mL) and then was dried with anhydrous sodium sulfate (1 g). After the ethyl acetate had been evaporated, the product was purified by column chromatography, using hexane and ethyl acetate (3:1) as eluent, which gave a white solid (0.849 g, 85 %) mol. wt. 371.35 g/mol.

Method 2: 25 mg ST0702 was incubated with 10% FBS, 1% DMSO and water. The disappearance of the ST0702 and the appearance of isosorbide-2-salicylate-5-nicotinate was monitored using HPLC, with the retention times of the two compounds being known. For the first hour the mixture was not incubated so as to assess the speed at which metabolism was occurring. After one h the mixture was incubated. After a total time of 5 h and 30 min the ST0702 was seen to have all been metabolised and the mixture was added to a separating funnel with 100 mL DCM to quench the reaction. The isosorbide-2-salicylate-5-nicotinate partitioned into the DCM layer. The water/FBS mixture was washed a number of times with DCM. All the DCM was collected and washed first with deionised water, then sodium bicarbonate, then water and was dried using anhydrous sodium sulfate. The DCM was evaporated off and an NMR was completed, which showed some small impurities. It is likely that the compound isosorbide-2-salicylate-5-nicotinate was further metabolised. Flash column chromatography was carried out to remove impurities, and another NMR was carried out. 4.3mg of pure isosorbide-2-salicylate-5-nicotinate was isolated.

^{1}H NMR (400 MHz, CHLOROFORM-*d*) **δ ppm** 4.03 - 4.23 (m, 4 H, Is-H1/H6) 4.63 - 4.77 (m, 1 H, Is-H3) 5.03 - 5.19 (m, 1 H, Is-H4) 5.47 (q, *J*=5.87 Hz, 1 H, Is-H2) 5.52 (s, 1 H, Is-H5) 6.89 (t, *J*=6.85 Hz, 1 H, Sal-H5) 6.94 - 7.08 (m, 1 H, Sal-H3) 7.38 - 7.56 (m, 2 H, Sal-H4, Nic-H5) 7.81 (d, *J*=1.96 Hz, 1 H, Sal-H6) 8.33 - 8.44 (m, 1 H, Nic-H4) 8.84 (br. s., 1 H, Nic-H6)

9.30 (br. s., 1 H, Nic-H2) 10.53 (s, 1 H, -OH) **^{13}C NMR** (101 MHz, CHLOROFORM-*d*) **δ ppm** 70.45, 72.87, 74.58, 76.37, 76.68, 78.35, 80.74, 85.79, 111.39, 117.41 118.98, 129.60, 135.97, 137.20, 150.36, 153.12, 168.87. **HRMS (ESI)** calculated for $C_{19}H_{18}NO_7$ [M^++H] 372.107778: found 372.108083.

Isosorbide-2-salicylate (6)

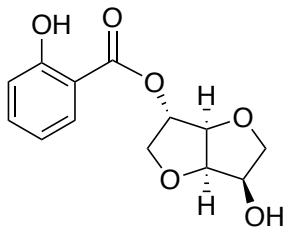

Isosorbide-2-benzyloxybenzoate-5-nitrate (0.15 g, mol. wt. 401.37 g/mol, 0.373 mmoles) was then dissolved in 20 mL ethyl acetate. 0.1 g of 10 % palladium on activated carbon was added to the solution. Air was expelled from the flask and the mixture was kept under an atmosphere of hydrogen gas. The mixture was stirred for 24 h. The reaction was monitored by TLC (1:1 hexane: ethyl acetate) to observe the disappearance of the isosorbide-2-benzyloxybenzoate-5-nitrate. Once complete, the reaction mixture was filtered through a fritted glass funnel to remove the catalyst. The solvent was evaporated under vacuum and purified using column chromatography crystallised using diethyl ether to give a white powder (0.065 g, 65%, mol.wt. 266.25 g/mol). **^{1}H NMR** (400 MHz, CHLOROFORM-*d*) **δ ppm** 3.65 (dd, *J*=9.78, 5.87 Hz, 1 H, Is-H4) 3.93 - 3.98 (m, 1 H, Is-H6) 4.11 - 4.17 (m, 1 H, Is-H1) 4.22 (d, *J*=10.76 Hz, 1 H, Is-H1) 4.33 - 4.41 (m, 1 H, Is-H1) 4.66 (d, *J*=3.91 Hz, 1 H, Is-H3) 4.74 (t, *J*=5.00 Hz, 1 H, Is-H5) 5.51 (d, *J*=2.93 Hz, 1 H, Is-H2) 6.90 (t, *J*=8.80 Hz, 1 H, Sal-H5) 7.01 (d, *J*=9.78 Hz, 1 H, Sal-H3) 7.49 (t, *J*=7.90 Hz, 1 H, Sal-H4) 7.82 (d, *J*=9.78 Hz, 1 H, Sal-H6) 10.54 (s, 1 H, -OH).**^{13}C NMR** (101 MHz, CHLOROFORM-*d*) **δ ppm** 72.34, 73.71, 76.71, 77.03, 77.23, 77.36, 82.14, 85.62, 129.92, 136.33, 161.94

Isomannide 2-acetate (18a)

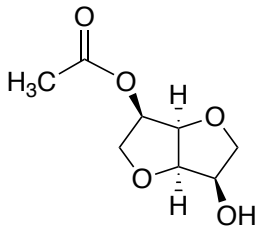

Isomannide (mol. wt. 146.14 g/mol, 6.84 mmol, 1 g) was dissolved in DCM (50 mL). Acetic anhydride (mol. wt. 102.09 g/mol, d 1.08 g/mL, 6.84 mmol, 0.698 g, 0.647 mL), triethylamine (mol. wt. 101.19 g/mol, d 0.726 g/mL, 7.52 mmol, 0.761 g, 1.042 mL) and DMAP (mol. wt.

122.17 g/mol, 1.368 mmol, 0.167 g) were added to the reaction vessel and the mixture was stirred for 4 h. The reaction progress was monitored by TLC (1:1, ethyl acetate: hexane) to observe the formation of mono-substituted and/or di-substituted products. Purification by column chromatography, using hexane and ethyl acetate (1: 2) as eluent, gave an oil residue (0.59 g, 46 %). Mol. wt. 188.19 g/mol. **^{1}H NMR** (400 MHz, CHLOROFORM-d) **δ ppm:** 2.14 (s, 3 H, CH_3), 3.61 (dd, J=9.12, 7.05 Hz, 1 H, IsH-6'), 3.85 (dd, J=9.54, 6.63 Hz, 1 H, IsH-1'), 3.99 (dd, J=9.33, 6.43 Hz, 1 H, IsH-6), 4.13 (dd, J=9.54, 6.22 Hz, 1 H, IsH-1), 4.27 - 4.36 (m, 1 H, IsH-5), 4.50 (t, J=5.39 Hz, 1 H, IsH-4), 4.70 (t, J=5.18 Hz, 1 H, IsH-3), 5.13 - 5.19 (m, 1 H, IsH-2).

Isomannide 2-acetate 5-nicotinate (19a)

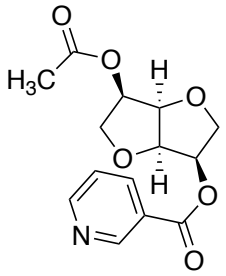

Isomannide 2-acetate (mol. wt. 188.19 g/mol, 3.135 mmol, 0.59 g) was dissolved in DCM (30 mL). Nicotinoyl chloride (mol. wt. 178.02 g/mol, 6.897 mmol, 1.228 g), triethylamine (mol. wt. 101.19 g/mol, d 0.726 g/mL, 10.35 mmol, 1.047 g, 1.434 mL) and DMAP (mol. wt. 122.17 g/mol, 1.568 mmol, 0.192 g) were added to the reaction vessel and the mixture was stirred overnight. The reaction progress was monitored by TLC (2:1, ethyl acetate: hexane) to observe the disappearance of the starting materials. Nicotinoyl chloride (mol. wt. 178.02 g/mol, 1.724 mmol, 0.307 g) and triethylamine (mol. wt. 101.19 g/mol, d 0.726 g/mL, 3.45 mmol, 0.349 g, 0.478 mL) were added to the reaction vessel and the mixture was stirred overnight. Purification by column chromatography, using hexane and ethyl acetate (1: 2) as eluent, gave a white solid (0.283 g, 31 %). Mol. wt. 293.27 g/mol. **^{1}H NMR** (400 MHz, CHLOROFORM-d) **δ ppm**: 2.12 - 2.23 (m, 4 H, CH_3), 3.82 (dd, J=9.12, 7.46 Hz, 1 H, IsH-1'), 4.03 - 4.10 (m, 2 H, IsH-1, IsH-6), 4.13 - 4.18 (m, 1 H, IsH-6'), 4.73 - 4.78 (m, 1 H, IsH-3), 4.87 (t, J=5.39 Hz, 1 H, IsH-4), 5.12 (td, J=6.84, 5.39 Hz, 1 H, IsH-2), 5.38 (q, J=5.81 Hz, 1 H, IsH-5), 7.42 (ddd, J=7.88, 4.98, 0.83 Hz, 1 H, ArH-4), 8.35 (dt, J=7.88, 2.07 Hz, 1 H, ArH-3), 8.81 (dd, J=4.98, 1.66 Hz, 1 H, ArH-5), 9.28 (d, J=1.66 Hz, 1 H, ArH-1). **^{13}C NMR** (101 MHz, CHLOROFORM-d) **δ ppm:** 20.63 (CH_3), 70.18 (IsC-1), 70.90 (IsC-6), 73.49 (IsC-2), 74.63 (IsC-5), 80.42 (IsC-3), 80.57 (IsC-4), 123.33 (ArC-4), 125.21 (ArC-2), 137.22 (ArC-3), 151.02 (ArC-1), 153.74 (ArC-5), 164.63 (-O<u>C</u>(O)Ar), 170.33 (-O<u>C</u>(O)CH_3). **HRMS (ESI)** calculated for $C_{14}H_{15}NO_6$ [M+H] 293.27: found, 293.2846.

Isomannide 2-propionate (18b)

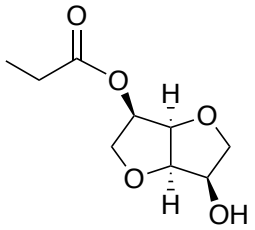

Isomannide (mol. wt. 146.14 g/mol, 6.84 mmol, 1 g) was dissolved in DCM (50 mL). Propionyl chloride (mol. wt. 92.524 g/mol, d 1.065 g/mL, 6.84 mmol, 0.633 g, 0.594 mL) and triethylamine (mol. wt. 101.19 g/mol, d 0.726 g/mL, 7.52 mmol, 0.761 g, 1.042 mL) were added to the reaction vessel and the mixture was stirred overnight at 0°C. The reaction progress was monitored by TLC (1:1, ethyl acetate: hexane) to observe the formation of mono-substituted and/or di-substituted products. Purification by column chromatography, using hexane and ethyl acetate (1: 1.5) as eluent, gave an oil residue (0.569 g, 41 %). Mol. wt. 202.16 g/mol. **^{1}H NMR** (400 MHz, CHLOROFORM-d) **δ ppm:** 1.13 - 1.20 (m, 3 H, CH_3), 2.35 - 2.46 (m, 2 H, CH_2), 3.58 (dd, J=9.12, 7.05 Hz, 1 H, IsH-6'), 3.85 (dd, J=9.33, 6.43 Hz, 1 H, IsH-1'), 3.97 (dd, J=9.33, 6.43 Hz, 1 H, IsH-6), 4.07 - 4.12 (m, 1 H, IsH-1), 4.25 - 4.34 (m, 1 H, IsH-5), 4.49 (t, J=5.18 Hz, 1 H, IsH-4), 4.70 (t, J=5.18 Hz, 1 H, IsH-3), 5.16 (q, J=5.94 Hz, 1 H, IsH-2).

Isomannide 2-propionate 5-nicotinate (19b)

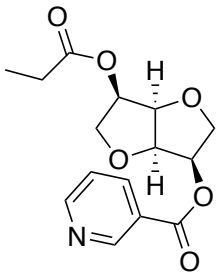

Isomannide 2-propionate (mol. wt. 202.16 g/mol, 2.72 mmol, 0.55 g) was dissolved in DCM (30 mL). Nicotinoyl chloride (mol. wt. 178.02 g/mol, 5.99 mmol, 1.066 g), triethylamine (mol. wt. 101.19 g/mol, d 0.726 g/mL, 8.98 mmol, 0.909 g, 1.245 mL) and DMAP (mol. wt. 122.17 g/mol, 1.36 mmol, 0.166 g) were added to the reaction vessel and the mixture was stirred overnight. The reaction progress was monitored by TLC (3:1, ethyl acetate: hexane) to observe the disappearance of the starting materials. The reaction mixture was washed with 1 M HCl (50 mL), $NaHCO_3$ (50 mL), water (50 mL), saturated brine solution (50 mL) and dried with anhydrous sodium sulfate. The reaction mixture was evaporated to dryness to give an oil residue (0.769 g, 92 %). Mol. wt. 307.30 g/mol. **^{1}H NMR** (400 MHz, CHLOROFORM-d) **δ ppm:** 1.15 - 1.21 (m, 3 H, CH_3), 2.44 (qd, J=7.53, 1.45 Hz, 2 H, CH_2), 3.81 (dd, J=9.12, 7.05

Hz, 1 H, IsH-1'), 4.01 - 4.07 (m, 2 H, IsH-1, IsH-6), 4.10 - 4.16 (m, 1 H, IsH-6'), 4.75 (t, J=5.39 Hz, 1 H, IsH-3), 4.86 (t, J=5.39 Hz, 1 H, IsH-4), 5.09 - 5.15 (m, 1 H, IsH-2), 5.37 (q, J=5.94 Hz, 1 H, IsH-5), 7.41 (dd, J=7.88, 4.98 Hz, 1 H, ArH-4), 8.34 (dt, J=7.88, 1.87 Hz, 1 H, ArH-3), 8.80 (d, J=4.98 Hz, 1 H, ArH-5), 9.27 (s, 1 H, ArH-1). **^{13}C NMR** (101 MHz, CHLOROFORM-d) **δ ppm:** 9.01 (CH_3), 27.18 (-CH_2CH_3), 70.32 (IsC-1), 70.79 (IsC-6), 73.33 (IsC-2), 74.62 (IsC-5), 80.44 (IsC-3), 80.54 (IsC-4), 123.32 (ArC-4), 125.22 (ArC-2), 137.20 (ArC-3), 151.01 (ArC-1), 153.73 (ArC-5), 164.63 (-O<u>C</u>(O)Ar), 173.83 (-O<u>C</u>(O)CH_2CH_3). **HRMS (ESI)** calculated for $C_{15}H_{17}NO_6$ [M+H] 307.30: found, 307.2146.

Isomannide 2-butyrate (18c)

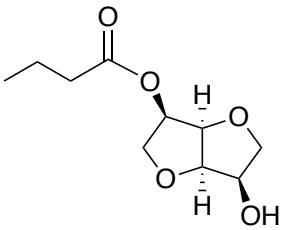

Isomannide (mol. wt. 146.14 g/mol, 6.84 mmol, 1 g) was dissolved in DCM (50 mL). Butyryl chloride (mol. wt. 106.55 g/mol, d 1.03 g/mL, 6.84 mmol, 0.728 g, 0.708 mL) and triethylamine (mol. wt. 101.19 g/mol, d 0.726 g/mL, 7.52 mmol, 0.761 g, 1.042 mL) were added to the reaction vessel and the mixture was stirred overnight at 0°C. The reaction progress was monitored by TLC (2:1, ethyl acetate: hexane) to observe the formation of mono-substituted and/or di-substituted products. Purification by column chromatography, using hexane and ethyl acetate (1: 2) as eluent, gave an oil residue (0.692 g, 47 %). Mol. wt. 216.19 g/mol. **^{1}H NMR** (400 MHz, CHLOROFORM-d) **δ ppm:** 0.94 (t, J=7.46 Hz, 3 H, CH_3), 1.66 (sxt, J=7.38 Hz, 2 H, CH_3-<u>CH_2</u>-CH_2), 2.29 - 2.39 (m, 2 H, CH_2), 3.55 (dd, J=9.12, 7.05 Hz, 1 H, IsH-6'), 3.82 (dd, J=9.54, 6.63 Hz, 1 H, IsH-1'), 3.95 (dd, J=9.12, 6.22 Hz, 1 H, IsH-6), 4.08 (dd, J=9.33, 6.43 Hz, 1 H, IsH-1), 4.27 (q, J=6.22 Hz, 1 H, IsH-5), 4.46 (t, J=5.18 Hz, 1 H, IsH-4), 4.68 (t, J=5.18 Hz, 1 H, IsH-3), 5.13 (q, J=6.22 Hz, 1 H, IsH-2).

Isomannide 2-butyrate 5-nicotinate (19c)

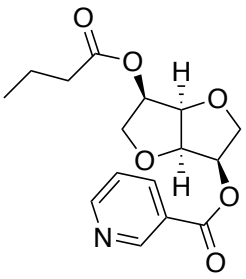

Isomannide 2-butyrate (mol. wt. 216.19 g/mol, 3.2 mmol, 0.692 g) was dissolved in DCM (30 mL). Nicotinoyl chloride (mol. wt. 178.02 g/mol, 7.04 mmol, 1.253 g), triethylamine (mol. wt. 101.19 g/mol, d 0.726 g/mL, 10.56 mmol, 1.069 g, 1.464 mL) and DMAP (mol. wt. 122.17 g/mol, 1.6 mmol, 0.195 g) were added to the reaction vessel and the mixture was stirred overnight. The reaction progress was monitored by TLC (2:1, ethyl acetate: hexane) to observe the disappearance of the starting materials. Nicotinoyl chloride (mol. wt. 178.02 g/mol, 1.76 mmol, 0.314 g) and triethylamine (mol. wt. 101.19 g/mol, d 0.726 g/mL, 3.52 mmol, 0.356 g, 0.488 mL) were added to the reaction vessel and the mixture was stirred overnight. The reaction mixture was washed with 1 M HCl (50 mL), $NaHCO_3$ (50 mL), water (50 mL), saturated brine solution (50 mL) and dried with anhydrous sodium sulfate. The reaction mixture was evaporated to dryness to give an oil residue (0.51 g, 50 %). Mol. wt. 321.33 g/mol. **^{1}H NMR** (400 MHz, CHLOROFORM-d) **δ ppm:** 0.96 - 1.01 (m, 3 H, CH_3), 1.69 - 1.73 (m, 2 H, CH_3-$\underline{CH_2}$-CH_2), 2.37 - 2.42 (m, 2 H, CH_2), 3.81 (dd, J=9.12, 7.05 Hz, 1 H, IsH-1'), 4.01 - 4.07 (m, 2 H, IsH-1, IsH-6), 4.12 - 4.17 (m, 1 H, IsH-6'), 4.76 (t, J=5.39 Hz, 1 H, IsH-3), 4.86 (t, J=5.39 Hz, 1 H, IsH-4), 5.09 - 5.15 (m, 1 H, IsH-2), 5.37 (q, J=5.94 Hz, 1 H, IsH-5), 7.42 (dd, J=7.88, 4.98 Hz, 1 H, ArH-4), 8.34 (dt, J=7.88, 1.87 Hz, 1 H, ArH-3), 8.78 - 8.84 (m, 1 H, ArH-5), 9.28 (s, 1 H, ArH-1). **^{13}C NMR** (101 MHz, CHLOROFORM-d) **δ ppm:** 13.58 (CH_3), 18.36 (-CH_3-$\underline{CH_2}$-CH_2), 35.76 (CH_2), 70.35 (IsC-1), 70.76 (IsC-6), 73.27 (IsC-2), 74.63 (IsC-5), 80.44 (IsC-3), 80.53 (IsC-4), 123.33 (ArC-4), 125.21 (ArC-2), 137.24 (ArC-3), 151.00 (ArC-1), 153.71 (ArC-5), 164.63 (-O$\underline{C}$(O)Ar), 173.01 (-O$\underline{C}$(O)$CH_2CH_2CH_3$). **HRMS (ESI)** calculated for $C_{16}H_{19}NO_6$ [M+H] 321.33: found, 321.2502.

Isomannide 2-valeroate (18d)

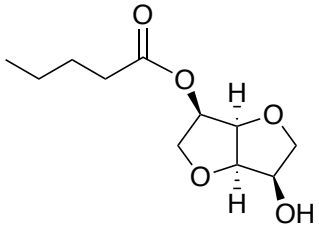

Isomannide (mol. wt. 146.14 g/mol, 6.84 mmol, 1 g) was dissolved in DCM (50 mL). Valeroyl chloride (mol. wt. 120.55 g/mol, d 0.995 g/mL, 6.84 mmol, 0.825 g, 0.829 mL) and triethylamine (mol. wt. 101.19 g/mol, d 0.726 g/mL, 7.52 mmol, 0.761 g, 1.042 mL) were added to the reaction vessel and the mixture was stirred overnight at 0°C. The reaction progress was monitored by TLC (2:1, ethyl acetate: hexane) to observe the formation of mono-substituted and/or di-substituted products. Purification by column chromatography, using hexane and ethyl acetate (1: 2) as eluent, gave an oil residue (0.85 g, 54 %). Mol. wt. 230.19 g/mol. **^{1}H NMR** (400 MHz, CHLOROFORM-d) **δ ppm:** 0.92 (t, J=7.46 Hz, 3 H, CH_3), 1.37

(dq, J=14.88, 7.34 Hz, 2 H, CH_3-$\underline{CH_2}$-CH_2), 1.58 - 1.68 (m, 2 H, CH_2-$\underline{CH_2}$-CH_2), 2.39 (td, J=7.57, 1.45 Hz, 2 H, CH_2), 3.58 (dd, J=9.12, 7.05 Hz, 1 H, IsH-6'), 3.84 (dd, J=9.33, 6.43 Hz, 1 H, IsH-1'), 3.97 (dd, J=9.12, 6.22 Hz, 1 H, IsH-6), 4.11 (dd, J=9.54, 6.22 Hz, 1 H, IsH-1), 4.30 (q, J=6.22 Hz, 1 H, IsH-5), 4.49 (t, J=5.18 Hz, 1 H, IsH-4), 4.70 (t, J=5.18 Hz, 1 H, IsH-3), 5.12 - 5.19 (m, 1 H, IsH-2).

Isomannide 2-valeroate 5-nicotinate (19d)

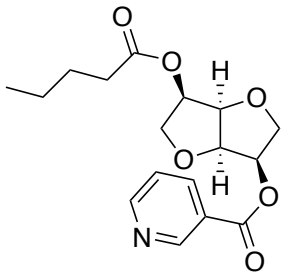

Isomannide 2-valeroate (mol. wt. 230.19 g/mol, 3.693 mmol, 0.85 g) was dissolved in DCM (30 mL). Nicotinoyl chloride (mol. wt. 178.02 g/mol, 8.124 mmol, 1.446 g), triethylamine (mol. wt. 101.19 g/mol, d 0.726 g/mL, 12.19 mmol, 1.233 g, 1.689 mL) and DMAP (mol. wt. 122.17 g/mol, 1.846 mmol, 0.226 g) were added to the reaction vessel and the mixture was stirred overnight. The reaction progress was monitored by TLC (2:1, ethyl acetate: hexane) to observe the disappearance of the starting materials. Nicotinoyl chloride (mol. wt. 178.02 g/mol, 2.03 mmol, 0.362 g) and triethylamine (mol. wt. 101.19 g/mol, d 0.726 g/mL, 4.06 mmol, 0.411 g, 0.563 mL) were added to the reaction vessel and the mixture was stirred overnight. The reaction mixture was washed with 1 M HCl (50 mL), $NaHCO_3$ (50 mL), water (50 mL), saturated brine solution (50 mL) and dried with anhydrous sodium sulfate. The reaction mixture was evaporated to dryness to give an oil residue (0.93 g, 75 %). Mol. wt. 335.35 g/mol. **^{1}H NMR** (400 MHz, CHLOROFORM-d) **δ ppm:** 0.89 - 0.98 (m, 3 H, CH_3), 1.38 (dq, J=14.93, 7.46 Hz, 2 H, CH_3-$\underline{CH_2}$-CH_2), 1.60 - 1.69 (m, 2 H, CH_2-$\underline{CH_2}$-CH_2), 2.37 - 2.47 (m, 2 H, CH_2), 3.81 (dd, J=9.12, 7.05 Hz, 1 H, IsH-1'), 4.04 (m, J=9.54, 6.22, 4.56 Hz, 2 H, IsH-1, IsH-6), 4.11 - 4.17 (m, 1 H, IsH-6'), 4.73 - 4.78 (m, 1 H, IsH-3), 4.86 (t, J=5.39 Hz, 1 H, IsH-4), 5.12 (td, J=6.84, 5.39 Hz, 1 H, IsH-2), 5.37 (q, J=5.81 Hz, 1 H, IsH-5), 7.38 - 7.45 (m, 1 H, ArH-4), 8.34 (dt, J=7.88, 2.07 Hz, 1 H, ArH-3), 8.81 (dd, J=4.77, 1.87 Hz, 1 H, ArH-5), 9.28 (d, J=1.24 Hz, 1 H, ArH-1). **^{13}C NMR** (101 MHz, CHLOROFORM-d) **δ ppm:** 13.66 (CH_3), 22.16 (-CH_3-$\underline{CH_2}$-CH_2), 26.89 (-CH_2-$\underline{CH_2}$-CH_2), 33.60 (CH_2), 70.35 (IsC-1), 70.76 (IsC-6), 73.28 (IsC-2), 74.63 (IsC-5), 80.44 (IsC-3), 80.53 (IsC-4), 123.32 (ArC-4), 125.42 (ArC-2), 137.22 (ArC-3), 151.01 (ArC-1), 153.72 (ArC-5), 164.63 (-O$\underline{C}$(O)Ar), 173.18 (-O$\underline{C}$(O)$CH_2CH_2CH_2CH_3$). **HRMS (ESI)** calculated for $C_{17}H_{21}NO_6$ [M+H] 335.35: found, 335.2354.

Isomannide 2-benzoate (18e)

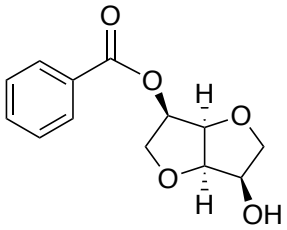

Isomannide (mol. wt. 146.14 g/mol, 6.84 mmol, 1 g) was dissolved in DCM (50 mL). Benzoyl chloride (mol. wt. 140.57 g/mol, d 1.21 g/mL, 6.84 mmol, 0.9615 g, 0.795 mL) and triethylamine (mol. wt. 101.19 g/mol, d 0.726 g/mL, 7.52 mmol, 0.761 g, 1.042 mL) were added to the reaction vessel and the mixture was stirred overnight at 0°C. The reaction progress was monitored by TLC (1:1, ethyl acetate: hexane) to observe the formation of mono-substituted and/or di-substituted products. The reaction mixture was washed with 1 M HCl (50 mL), $NaHCO_3$ (50 mL), water (50 mL), saturated brine solution (50 mL) and dried with anhydrous sodium sulfate. Purification by column chromatography, using hexane and ethyl acetate (1: 1.5) as eluent, gave a white solid (0.67 g, 39 %). Mol. wt. 250.21 g/mol. **^{1}H NMR** (400 MHz, CHLOROFORM-d) **δ ppm:** 3.63 (dd, J=9.12, 7.05 Hz, 1 H, IsH-6'), 3.99 (dd, J=9.12, 6.22 Hz, 1 H, IsH-1'), 4.05 (dd, J=9.74, 6.01 Hz, 1 H, IsH-6), 4.23 (dd, J=9.74, 6.01 Hz, 1 H, IsH-1), 4.30 - 4.37 (m, 1 H, IsH-5), 4.56 (t, J=5.18 Hz, 1 H, IsH-4), 4.85 (t, J=5.18 Hz, 1 H, IsH-3), 5.41 (q, J=5.81 Hz, 1 H, IsH-2), 7.44 - 7.49 (m, 2 H, ArH-meta), 7.56 - 7.61 (m, 1 H, ArH-para) 8.06 - 8.12 (m, 2 H, ArH-ortho).). **^{13}C NMR** (101 MHz, CHLOROFORM-d) **δ ppm:** 71.17 (IsC-1), 72.23 (IsC-6), 73.91 (IsC-2), 74.51 (IsC-5), 80.74 (IsC-3), 81.64 (IsC-4), 128.44 (2 C, ArC-Benz), 129.80 (2 C, ArC-Benz), 130.1 (1 C, ArC-Benz), 133.31 (ArC-Benz), 165.91 (-O<u>C</u>(O)Ar).

Isomannide 2-benzoate 5-nicotinate (19e)

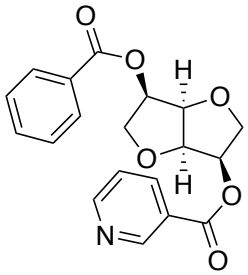

Isomannide 2-benzoate (mol. wt. 250.21 g/mol, 1.998 mmol, 0.5 g) was dissolved in DCM (30 mL). Nicotinoyl chloride (mol. wt. 178.02 g/mol, 4.396 mmol, 0.783 g), triethylamine (mol. wt. 101.19 g/mol, d 0.726 g/mL, 6.593 mmol, 0.667 g, 0.914 mL) and DMAP (mol. wt. 122.17 g/mol, 0.999 mmol, 0.122 g) were added to the reaction vessel and the mixture was stirred for 5 h. The reaction progress was monitored by TLC (3:1, ethyl acetate: hexane) to observe the

disappearance of the starting materials. Nicotinoyl chloride (mol. wt. 178.02 g/mol, 1.099 mmol, 0.196 g) and triethylamine (mol. wt. 101.19 g/mol, d 0.726 g/mL, 2.198 mmol, 0.222 g, 0.305 mL) were added to the reaction vessel and the mixture was stirred over the weekend. The reaction mixture was washed with 1 M HCl (50 mL), $NaHCO_3$ (50 mL), water (50 mL), saturated brine solution (50 mL) and dried with anhydrous sodium sulfate. The reaction mixture was evaporated to dryness to give a white solid (0.596 g, 84 %). Mol. wt. 355.34 g/mol. **^{1}H NMR** (400 MHz, CHLOROFORM-d) **δ ppm:** 3.99 - 4.09 (m, 2 H, IsH-1', IsH-6'), 4.13 - 4.20 (m, 2 H, IsH-1, IsH-6), 4.89 - 4.94 (m, 2 H, IsH-3, IsH-4), 5.34 - 5.42 (m, 2 H, IsH-2, IsH-5), 7.40 - 7.50 (m, 3 H, ArH-Benz), 7.58 - 7.63 (m, 1 H, ArH-4), 8.07 - 8.15 (m, 2 H, ArH-Benz) 8.36 (dt, J=7.88, 2.07 Hz, 1 H, ArH-3), 8.82 (dd, J=4.98, 1.66 Hz, 1 H, ArH-5), 9.30 (d, J=1.66 Hz, 1 H, ArH-1). **^{13}C NMR** (101 MHz, CHLOROFORM-d) **δ ppm:** 70.68 (IsC-1), 70.70 (IsC-6), 74.04 (IsC-2), 74.60 (IsC-5), 80.58 (IsC-3), 80.74 (IsC-4), 123.35 (ArC-4), 125.43 (ArC-2), 128.46 (2 C, ArC-Benz), 129.82 (2 C, ArC-Benz), 130.1 (1 C, ArC-Benz), 133.34 (ArC-Benz), 137.25 (ArC-3), 151.06 (ArC-1), 153.77 (ArC-5), 165.93 (-O<u>C</u>(O)Ar), 173.29 (-O<u>C</u>(O)Ar). **HRMS (ESI)** calculated for $C_{19}H_{17}NO_6$ [M+H] 355.34: found, 355.2158.

Isomannide 2-aspirinate (18f)

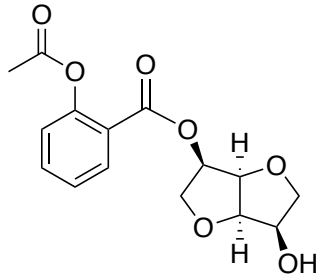

Isomannide (mol. wt. 146.14 g/mol, 3.42 mmol, 0.5 g) was dissolved in DCM (20 mL). *O*-acetylsalicyloyl chloride (mol. wt. 198.61 g/mol, 3.42 mmol, 0.679 g) and triethylamine (mol. wt. 101.19 g/mol, d 0.726 g/mL, 3.76 mmol, 0.38 g, 0.52 mL) were added to the reaction vessel and the mixture was stirred for 3 h at 0°C. The reaction progress was monitored by TLC (2:1, ethyl acetate: hexane) to observe the formation of mono-substituted and/or di-substituted products. Purification by column chromatography, using hexane and ethyl acetate (1: 2) as eluent, gave a white solid (0.43 g, 41 %). Mol. wt. 308.25 g/mol. **^{1}H NMR** (400 MHz, CHLOROFORM-d) **δ ppm:** 2.37 (s, 3 H, CH_3), 3.63 (dd, J=9.12, 7.05 Hz, 1 H, IsH-6'), 3.93 - 4.01 (m, 2 H, IsH-1', IsH-6), 4.21 (dd, J=9.54, 6.22 Hz, 1 H, IsH-1), 4.30 - 4.37 (m, 1 H, IsH-5), 4.54 (t, J=5.18 Hz, 1 H, IsH-4), 4.79 (t, J=5.18 Hz, 1 H, IsH-3), 5.33 - 5.39 (m, 1 H, IsH-2), 7.10 - 7.15 (m, 1 H, ArH-para), 7.31 - 7.37 (m, 1 H, ArH-meta) 7.59 (td, J=7.67, 1.66 Hz, 1 H, ArH-meta), 8.09 (dd, J=7.88, 1.66 Hz, 1 H, ArH-ortho).

Isomannide 2-aspirinate 5-nicotinate (19f)

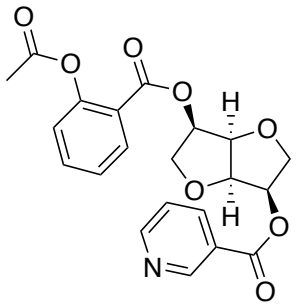

Isomannide 2-aspirinate (mol. wt. 308.25 g/mol, 1.43 mmol, 0.44 g) was dissolved in DCM (20 mL). Nicotinoyl chloride (mol. wt. 178.02 g/mol, 3.146 mmol, 0.56 g), triethylamine (mol. wt. 101.19 g/mol, d 0.726 g/mL, 4.719 mmol, 0.478 g, 0.655 mL) and DMAP (mol. wt. 122.17 g/mol, 0.715 mmol, 0.088 g) were added to the reaction vessel and the mixture was stirred over the weekend. The reaction progress was monitored by TLC (4:1, ethyl acetate: hexane) to observe the disappearance of the starting materials. Nicotinoyl chloride (mol. wt. 178.02 g/mol, 1.572 mmol, 0.28 g) and triethylamine (mol. wt. 101.19 g/mol, d 0.726 g/mL, 3.146 mmol, 0.318 g, 0.436 mL) were added to the reaction vessel and the mixture was stirred overnight. The reaction mixture was washed with 1 M HCl (50 mL), $NaHCO_3$ (50 mL), water (50 mL), saturated brine solution (50 mL) and dried with anhydrous sodium sulfate. Purification by column chromatography, using hexane and ethyl acetate (1: 3) as eluent, gave a white foamy solid (0.4 g, 68 %). Mol. wt. 413.38 g/mol. **^{1}H NMR** (400 MHz, CHLOROFORM-d) **δ ppm:** 2.38 (s, 3 H, CH_3), 3.95 (dd, J=9.33, 6.84 Hz, 1 H, IsH-1'), 4.06 (dd, J=9.54, 6.63 Hz, 1 H, IsH-6'), 4.14 (dd, J=14.93, 9.54, 6.22 Hz, 2 H, IsH-1, IsH-6), 4.88 (dt, J=14.31, 5.08 Hz, 2 H, IsH-3, IsH-4), 5.31 - 5.41 (m, 2 H, IsH-2, IsH-5), 7.13 (dd, J=8.09, 1.04 Hz, 1 H, ArH-Asp), 7.35 (td, J=7.67, 1.24 Hz, 1 H, ArH-Asp), 7.42 (ddd, J=7.88, 4.98, 0.83 Hz, 1 H, ArH-4), 7.60 (td, J=7.67, 1.66 Hz, 1 H, ArH-Asp), 8.11 (dd, J=7.88, 1.66 Hz, 1 H, ArH-Asp) 8.35 (dt, J=7.88, 2.07 Hz, 1 H, ArH-3), 8.82 (dd, J=4.98, 1.66 Hz, 1 H, ArH-5), 9.28 (dd, J=2.07, 0.83 Hz, 1 H, ArH-1). **^{13}C NMR** (101 MHz, CHLOROFORM-d) **δ ppm:** 20.99 (CH_3), 70.52 (IsC-1), 70.56 (IsC-6), 74.11 (IsC-2), 74.56 (IsC-5), 80.54 (IsC-3), 80.71 (IsC-4), 123.1 (ArC-Asp), 123.93 (ArC-4), 124.4 (ArC-Asp), 125.4 (ArC-Asp), 125.81 (ArC-2), 130.3 (ArC-Asp), 132.02 (ArC-Asp), 137.22 (ArC-3), 150.78 (Ar<u>C</u>-OC(O)CH_3), 150.99 (ArC-1), 153.74 (ArC-5), 164.87 (-O<u>C</u>(O)Ar), 169.01 (-O<u>C</u>(O)CH_3), 173.49 (-O<u>C</u>(O)Ar). **HRMS (ESI)** calculated for C-$_{21}H_{19}NO_6$ [M+H] 413.38: found, 413.3038.

Isomannide-2-methoxybenzoate (18g)

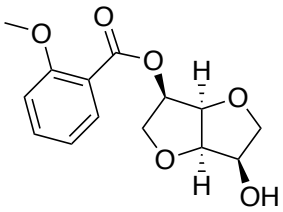

Isomannide (mol. wt. 146.14 g/mol, 3.42 mmol, 0.5g) was dissolved in 20 mL dry dichloromethane. *O*-methoxybenzoyl chloride (mol. wt. 170.59 g/mol, d. 1.146 g/mL, 3.42 mmol, 0.51 mL) and trimethylamine (mol. wt. 101.19 g/mol, d 0.726 g/mL, 3.76 mmol, 0.521 mL). The reaction was kept on ice and stirred for 18 h. The reaction progress was monitored by TLC (2:1, ethyl acetate: hexane). The crude product was then separated using column chromatography with 2:1, ethyl acetate: hexane as the solvent system. The product was obtained as a white solid (0.20g, 20.87%, mol.wt. 280.09 g/mol). The low yield can be attributed to the formation of isomannide-2,5-dimethoxybenzoate. **^{1}H NMR** (400 MHz, CHLOROFORM-d) **δ ppm:** 2.69 (d, J=8.71 Hz, 1 H, -OH) 3.66 (dd, J=9.33, 6.84 Hz, 1 H, Is-H4) 3.91 (s, 3 H, -CH_3) 3.97 - 4.05 (m, 2 H, Is-H6) 4.22 (dd, J=9.54, 6.22 Hz, 1 H, Is-H1) 4.26 - 4.38 (m, 1 H, Is-H1) 4.55 (t, J=5.39 Hz, 1 H, Is-H5) 4.83 (t, J=5.18 Hz, 1 H, Is-H3) 5.38 (q, J=6.08 Hz, 1 H, Is-H2) 6.91 - 7.04 (m, 2 H, ArH4/5) 7.49 (td, J=7.88, 1.66 Hz, 1 H, Ar-H3) 7.88 (dd, J=8.09, 1.87 Hz, 1 H, Ar-H6).

Isomannide-2-methoxybenzoate-5-nicotinate (19g)

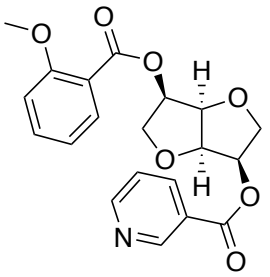

Isomannide-2-methoxybenzoate (mol.wt. 280.09 g/mol, 0.35 mmol, 0.1g) was dissolved in 20 mL dry dichloromethane. Nicotinoyl chloride (mol. wt. 178.02 g/mol, 0.77 mmol, 0.14 g), triethylamine (mol. wt. 101.19 g/mol, d 0.726 g/mL, 1.155 mmol, 0.163 mL) and 4-Dimethylaminopyridine (mol. wt. 122.17 g/mol, 0.175 mmol, 0.022 g) were added to the reaction vessel and the mixture was stirred for 4 h. The reaction progress was monitored using TLC (2:1 ethyl acetate: hexane). After 4 h additional nicotinoyl chloride (mol. wt. 178.02 g/mol, 0.77 mmol, 0.14 g), trimethylamine (mol. wt. 101.19 g/mol, d 0.726 g/mL, 1.155 mmol, 0.163 mL) and 4-Dimethylaminopyridine (mol. wt. 122.17 g/mol, 0.175 mmol, 0.022 g) was added to the reaction mixture. The reaction was stirred for 48 h. Once the starting material was

no longer visible on the TLC the reaction mixture was washed with 1 M HCl (50 mL), $NaHCO_3$ (50 mL), water (50 mL), saturated brine solution (50 mL) and dried with anhydrous sodium sulfate. The final product was an off-white solid (0.06g, 43.8%, mol. wt. 385.12 g/mol). **^{1}H NMR** (400 MHz, CHLOROFORM-d) **δ ppm:** 3.90 - 3.94 (m, 3 H) 3.94 - 3.99 (m, 1 H) 4.06 - 4.11 (m, 1 H) 4.17 (dd, J=9.54, 6.22 Hz, 2 H) 4.91 (quin, J=4.98 Hz, 2 H) 5.27 - 5.44 (m, 2 H) 6.92 - 7.07 (m, 2 H) 7.32 - 7.46 (m, 1 H) 7.46 - 7.55 (m, 1 H) 7.91 (dd, J=7.88, 1.66 Hz, 1 H) 8.35 (dt, J=7.98, 2.02 Hz, 1 H) 8.81 (dd, J=4.77, 1.87 Hz, 1 H) 9.28 (dd, J=2.07, 0.83 Hz, 1 H). **^{13}C NMR** (101 MHz, CHLOROFORM-*d*) **δ ppm** 56.02, 70.70, 70.75, 73.75, 74.81, 76.73, 77.03, 77.36, 80.59 80.68, 112.10, 120.19, 123.57, 132.03, 134.11, 137.68, 150.69, 153.33, 164.56, 165.15.

Isosorbide-2-(2-methoxybenzoate)-5-nitrate (57a)

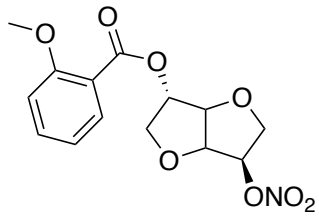

Isosorbide mononitrate (mol. wt. 191.139 g/mol, 1.046 mmol, 0.2 g) was dissolved in dry dichloromethane (10 mL) in a 50 mL round bottomed flask. Triethylamine (mol. wt. 101.19 g/mol, d. 0.7255 g/mL, 1.151 mmol, 0.160 mL), 4-Dimethylaminopyridine (mol. wt. 122.17 g/mol, 0.523 mmol, 0.064 g), and *o*-methoxybenzoyl chloride (mol. wt. 170.59 g/mol, d. 1.146 g/mL, 1.151 mmol, 0.171 mL) were added to the flask. The reaction mixture was stirred for 3 h. The reaction was monitored by TLC (1:1 hexane: ethyl acetate) to observe the disappearance of the ISMN. Once complete, the mixture was washed with 1 M HCl (50 mL), saturated sodium bicarbonate solution (50 mL), saturated brine solution (50 mL) and dried with anhydrous sodium sulfate (1 g). Evaporation of the dichloromethane and crystallisation using diethyl ether yielded a white powder (0.311 g, 91.5 %) mol. wt. 325.27 g/mol.**^{1}H NMR** (400 MHz, CHLOROFORM-d) **δ ppm**: 3.91 (s, 3 H, -CH_3) 3.95 (dd, *J*=11.20, 5.81 Hz, 1 H, Is-H4) 4.04 - 4.14 (m, 2 H, Is-H1/H6) 4.16 - 4.21 (m, 1 H, Is-H6) 4.64 (d, *J*=4.56 Hz, 1 H, Is-H1) 5.05 (t, *J*=5.18 Hz, 1 H, Is-H3) 5.39 (td, *J*=5.49, 3.11 Hz, 1 H, Is-H5) 5.47 (d, *J*=2.90 Hz, 1 H, Is-H2) 6.92 - 7.03 (m, 2 H, Ar-H4/5) 7.45 - 7.55 (m, 1 H, Ar-H3) 7.78 (dd, *J*=7.88, 1.66 Hz, 1 H, Ar-H6). **^{13}C NMR** (101 MHz, CHLOROFORM-*d*) **δ ppm** 55.96, 69.20, 73.71, 76.98, 77.30, 77.56, 81.33, 81.52, 86.75, 112.09, 120.10, 131.69, 134.11, 214.66.

Isosorbide-2-(2-methoxybenzoate) (58a)

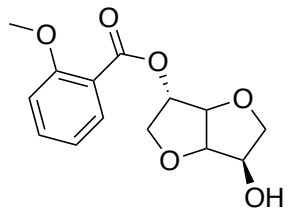

Isosorbide-2-(2-methoxybenzoate)-5-nitrate (mol. wt. 325.27 g/mol, 3.07 mmol, 1g) was dissolved in ethyl acetate (20 mL) in a 100 mL round-bottomed flask. Palladium on activated carbon (Pd/C) (mol. wt. 106.42 g/mol, 14.10 mmol, 1.5 g) was added to the flask. Air was expelled from the flask and the mixture was kept under an atmosphere of hydrogen gas. The mixture was stirred for 24 h. The reaction was monitored by TLC (1:1 hexane: ethyl acetate) to observe the disappearance of the Isosorbide-2-(2-methoxybenzoate)-5-nitrate. Once complete, the reaction mixture was filtered through Celite powder to remove the catalyst. Evaporation of the ethyl acetate yielded a white powder (0.70 g, 81.39 %) mol. wt. 280.09 g/mol. **^{1}H NMR** (400 MHz, CHLOROFORM-*d*) **δ ppm** 2.48 (br. s., 1 H, -OH) 3.61 (br. s., 1 H, Is-H4) 3.90 (br. s., 4 H, -CH_3/Is-H6) 4.15 (d, *J*=22.81 Hz, 2 H, Is-H1/6) 4.34 (br. s., 1 H, Is-H1) 4.68 (d, *J*=21.98 Hz, 1 H, Is-H3/5) 5.46 (br. s., 1 H, Is-H2) 6.98 (br. s., 2 H, Ar-H4/5) 7.50 (br. s., 1 H, Ar-H3) 7.78 (br. s., 1 H, Ar-H6).

Isosorbide-2-(3-methoxybenzoate)-5-nitrate (57b)

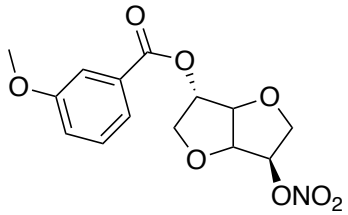

Isosorbide mononitrate (mol. wt. 191.139 g/mol, 5 mmol, 0.955 g) was dissolved in dry dichloromethane (20 mL) in a 100 mL round bottomed flask. Triethylamine (mol. wt. 101.19 g/mol, d. 0.7255 g/mL, 5.5 mmol, 0.763 mL), 4-Dimethylaminopyridine (mol. wt. 122.17 g/mol, 2.5 mmol, 0.305 g), and *m*-methoxybenzoyl chloride (mol. wt. 170.59 g/mol, d. 1.214 g/mL, 5.5 mmol, 0.773 mL) were added to the flask. The reaction mixture was stirred for 1.5 h. The reaction was monitored by TLC (1:1 hexane: ethyl acetate) to observe the disappearance of the ISMN. Once complete, the mixture was washed with 1 M HCl (50 mL), saturated sodium bicarbonate solution (50 mL), saturated brine solution (50 mL) and dried with anhydrous sodium sulfate (1 g). Evaporation of the dichloromethane and crystallisation using diethyl ether yielded a white powder (1.44 g, 88.9 %) mol. wt. 325.27 g/mol. ^{1}H NMR (400 MHz, CHLOROFORM-*d*) δ ppm 3.84 - 3.91 (m, 3 H, -CH_3) 3.95 (dd, *J*=11.20, 5.81 Hz, 1 H, Is-H4)

4.05 - 4.16 (m, 2 H, Is-H1/6) 4.16 - 4.22 (m, 1 H, Is-H6) 4.64 (d, *J*=4.98 Hz, 1 H, Is-H1) 5.08 (t, *J*=5.18 Hz, 1 H, Is-H3) 5.40 (td, *J*=5.49, 3.11 Hz, 1 H, Is-H5) 5.48 (d, *J*=3.32 Hz, 1 H, Is-H2) 7.13 (dd, *J*=8.29, 2.49 Hz, 1 H, Ar-H4) 7.36 (t, *J*=7.88 Hz, 1 H, Ar-H5) 7.54 (s, 1 H, Ar-H2) 7.62 (d, *J*=7.46 Hz, 1 H, Ar-H6).

Isosorbide-2-(3-methoxybenzoate) (58b)

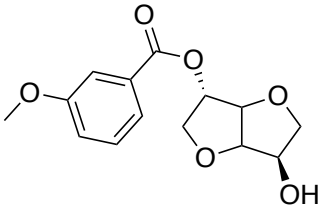

Isosorbide-2-(3-methoxybenzoate)-5-nitrate (mol. wt. 325.27 g/mol, 3.07 mmol, 1g) was dissolved in ethyl acetate (20 mL) in a 100 mL round-bottomed flask. Palladium on activated carbon (Pd/C) (mol. wt. 106.42 g/mol, 14.10 mmol, 1.5 g) was added to the flask. Air was expelled from the flask and the mixture was kept under an atmosphere of hydrogen gas. The mixture was stirred for 48 h. The reaction was monitored by TLC (1:1 hexane: ethyl acetate) to observe the disappearance of the Isosorbide-2-(3-methoxybenzoate)-5-nitrate. Once complete, the reaction mixture was filtered through Celite powder to remove the catalyst. Evaporation of the ethyl acetate yielded a white powder (0.73 g, 84.8%) mol. wt. 280.09 g/mol. **^{1}H NMR** (400 MHz, CHLOROFORM-*d*) **δ ppm** 2.63 (br. s., 1 H, -OH) 3.63 (dd, *J*=9.33, 6.01 Hz, 1 H, is-H4) 3.86 (s, 3 H, -CH_3) 3.95 (dd, *J*=9.33, 6.01 Hz, 1 H, Is-H6) 4.13 (dd, *J*=10.78, 3.32 Hz, 1 H, Is-H6) 4.20 (d, *J*=10.78 Hz, 1 H, Is-H1) 4.37 (d, *J*=5.39 Hz, 1 H, Is-H1) 4.65 (d, *J*=4.56 Hz, 1 H, Is-H5) 4.70 - 4.77 (m, 1 H, Is-H3) 5.48 (d, *J*=3.32 Hz, 1 H, Is-H2) 7.14 (dd, *J*=8.29, 2.49 Hz, 1 H, Ar-H4) 7.37 (t, *J*=7.88 Hz, 1 H, Ar-H5) 7.55 (s, 1 H, Ar-H2) 7.63 (d, *J*=7.46 Hz, 1 H, Ar-H6).

Isosorbide-2-(4-methoxybenzoate)-5-nitrate (57c)

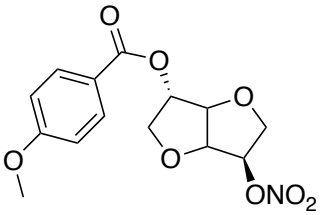

Isosorbide mononitrate (mol. wt. 191.139 g/mol, 5 mmol, 0.955 g) was dissolved in dry dichloromethane (20 mL) in a 100 mL round bottomed flask. Triethylamine (mol. wt. 101.19 g/mol, d. 0.7255 g/mL, 5.5 mmol, 0.763 mL), 4-Dimethylaminopyridine (mol. wt. 122.17 g/mol, 2.5 mmol, 0.305 g), and *p*-methoxybenzoyl chloride (mol. wt. 170.59 g/mol, 5.5 mmol, 0.938 g) were added to the flask. The reaction mixture was stirred for 6 h. The reaction was

monitored by TLC (1:1 hexane: ethyl acetate) to observe the disappearance of the ISMN. Once complete, the mixture was washed with 1 M HCl (50 mL), saturated sodium bicarbonate solution (50 mL), saturated brine solution (50 mL) and dried with anhydrous sodium sulfate (1 g). Evaporation of the dichloromethane and crystallisation using diethyl ether yielded a white powder (1.50 g, 92.5 %) mol. wt. 325.27 g/mol. ^{1}H **NMR** (400 MHz, CHLOROFORM-*d*) **δ ppm** 3.88 (br. s., 3 H, -CH_3) 3.94 (dd, *J*=11.40, 5.60 Hz, 1 H, Is-H4) 4.04 - 4.14 (m, 2 H, Is-H1/6) 4.14 - 4.21 (m, 1 H, Is-H6) 4.63 (d, *J*=4.98 Hz, 1 H, Is-H1) 5.07 (t, *J*=5.18 Hz, 1 H, Is-H3) 5.40 (td, *J*=5.49, 2.70 Hz, 1 H, Is-H5) 5.46 (d, *J*=2.90 Hz, 1 H, Is-H2) 6.92 (m, *J*=8.71 Hz, 2 H, Ar-H3/5) 7.98 (m, *J*=8.71 Hz, 2 H, Ar-H2/6)

Isosorbide-2-(4-methoxybenzoate) (58c)

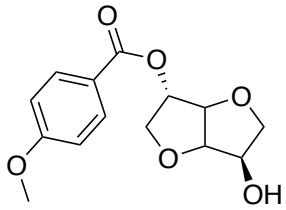

Isosorbide-2-(4-methoxybenzoate)-5-nitrate (mol. wt. 325.08 g/mol, 3.07 mmol, 1g) was dissolved in ethyl acetate (20 mL) in a 100 mL round-bottomed flask. Palladium on activated carbon (Pd/C) (mol. wt. 106.42 g/mol, 14.10 mmol, 1.5 g) was added to the flask. Air was expelled from the flask and the mixture was kept under an atmosphere of hydrogen gas. The mixture was stirred for 24 h. The reaction was monitored by TLC (1:1 hexane: ethyl acetate) to observe the disappearance of the Isosorbide-2-(4-methoxybenzoate)-5-nitrate. Once complete, the reaction mixture was filtered through Celite powder to remove the catalyst. Evaporation of the ethyl acetate yielded a white powder (0.81 g, 94.19 %) mol. wt. 280.09 g/mol. **^{1}H NMR** (400 MHz, CHLOROFORM-*d*) **δ ppm** 2.62 (br. s., 1 H, -OH) 3.62 (dd, *J*=9.12, 6.22 Hz, 1 H, Is-H4) 3.81 - 4.00 (m, 4 H -CH_3, Is-H6) 4.07 - 4.23 (m, 2 H, Is-H1/6) 4.36 (d, *J*=5.39 Hz, 1 H, Is-H1) 4.63 (d, *J*=4.15 Hz, 1 H, Is-H5) 4.72 (t, *J*=4.56 Hz, 1 H, Is-H3) 5.46 (br. s., 1 H, Is-H2) 6.93 (m, *J*=8.71 Hz, 2 H, Is-H3/5) 7.99 (m, *J*=8.71 Hz, 2 H, Is-H2/6)

Isosorbide-2,5-di-*o*-methoxybenzoate (56a)

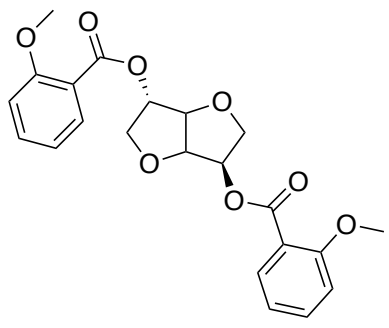

Isosorbide (mol. wt. 146.14 g/mol, 6.85 mmol, 1.0 g) was dissolved in dry dichloromethane (20 mL) in a 100 mL round bottomed flask. Triethylamine (mol. wt. 101.19 g/mol, d. 0.7255 g/mL, 21.23 mmol, 2.962 mL), 4-Dimethylaminopyridine (mol. wt. 122.17 g/mol, 3.43 mmol, 0.418 g), and *o*-methoxybenzoyl chloride (mol. wt. 170.59 g/mol, d. 1.146 g/mL, 14.38 mmol, 2.14 mL) were added to the flask. The reaction mixture was stirred for 3 h. The reaction was monitored by TLC (1:1 hexane: ethyl acetate) to observe the disappearance of the isosorbide. Once complete, the mixture was washed with 1 M HCl (50 mL), saturated sodium bicarbonate solution (50 mL), saturated brine solution (50 mL) and dried with anhydrous sodium sulfate (1 g). Evaporation of the dichloromethane and crystallisation using diethyl ether yielded a white powder (2.64 g, 93.0 %) mol. wt. 414.4 g/mol. **^{1}H NMR** (400 MHz, CHLOROFORM-*d*) **δ ppm** 3.92 (s, 3 H -CH_3) 3.91 (s, 3 H-CH_3) 3.98 (m, *J*=9.70, 5.60 Hz, 1 H, Is-H6) 4.06 - 4.22 (m, 3 H, Is-H1/6) 4.70 (d, *J*=4.56 Hz, 1 H, Is-H4) 5.03 (t, *J*=4.98 Hz, 1 H, Is-H3) 5.40 (q, *J*=5.53 Hz, 1 H, Is-H5) 5.47 (d, *J*=3.32 Hz, 1 H, Is-H2) 6.92 - 7.04 (m, 4 H, Ar-H4/5) 7.50 (t, *J*=7.88 Hz, 2 H, Ar-H3) 7.79 (d, *J*=7.88 Hz, 1 H, Ar-H6) 7.89 (d, *J*=8.09 Hz, 1 H, Ar-H6). **^{13}C NMR** (101 MHz, CHLOROFORM-*d*) **δ ppm** 55.97, 70.60, 74.22, 76.99, 81.01, 86.14, 112.05, 120.10, 131.97, 133.94. **HRMS (ESI)** calculated for $C_{22}H_{22}NaO_8$ [M^++Na] 437.120688: found 437.1205.

Isosorbide-2,5-di-*m*-methoxybenzoate (56b)

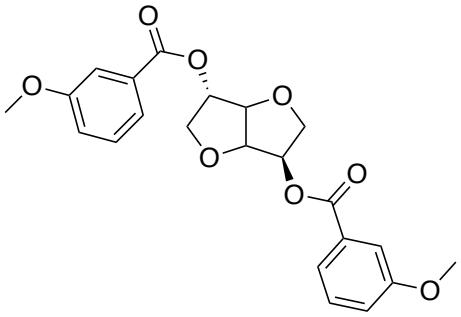

Isosorbide (mol. wt. 146.14 g/mol, 6.85 mmol, 1.0 g) was dissolved in dry dichloromethane (20 mL) in a 100 mL round bottomed flask. Triethylamine (mol. wt. 101.19 g/mol, d. 0.7255 g/mL, 21.23 mmol, 2.962 mL), 4-Dimethylaminopyridine (mol. wt. 122.17 g/mol, 3.43 mmol, 0.418 g), and *m*-methoxybenzoyl chloride (mol. wt. 170.59 g/mol, d. 1.214 g/mL, 14.38 mmol, 2.018 mL) were added to the flask. The reaction mixture was stirred for 1.5 h. The reaction was monitored by TLC (1:1 hexane: ethyl acetate) to observe the disappearance of the isosorbide. Once complete, the mixture was washed with 1 M HCl (50 mL), saturated sodium bicarbonate solution (50 mL), saturated brine solution (50 mL) and dried with anhydrous sodium sulfate (1 g). Evaporation of the dichloromethane and crystallisation using diethyl ether yielded a white powder (2.54 g, 89.5 %) mol. wt. 414.4 g/mol. **^{1}H NMR** (400 MHz, CHLOROFORM-*d*) **δ**

ppm 3.87 (s, 3 H, -CH_3) 3.86 (s, 3 H, -CH_3) 4.02 - 4.17 (m, 4 H, Is-H1/H6) 4.69 (d, *J*=4.56 Hz, 1 H, Is-H4)5.08 (t, *J*=5.18 Hz, 1 H, Is-H3) 5.43 (q, *J*=5.39 Hz, 1 H, Is-H5) 5.49 (d, *J*=2.90 Hz, 1 H, Is-H2) 7.08 - 7.17 (m, 2 H, Ar-H4) 7.31 - 7.42 (m, 2 H, Ar-H5) 7.54 - 7.65 (m, 3 H, Ar-H2/6) 7.66 - 7.72 (m, 1 H, Ar-H6). **^{13}C NMR** (101 MHz, CHLOROFORM-*d*) **δ ppm** 55.46, 70.76, 73.46, 76.99, 81.13, 86.17, 114.19, 119.74, 122.13, 129.49. **HRMS (ESI)** calculated for $C_{22}H_{22}NaO_8$ [M^++Na] 437.120688: found 437.1211.

Isosorbide-2,5-di-*p*-methoxybenzoate (56c)

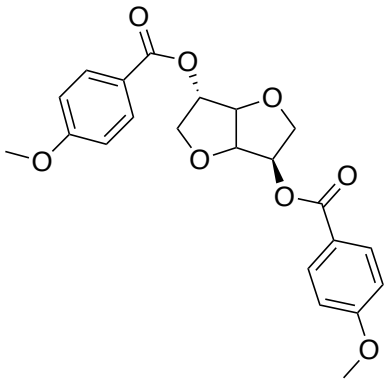

Isosorbide (mol. wt. 146.14 g/mol, 6.85 mmol, 1.0 g) was dissolved in dry dichloromethane (20 mL) in a 100 mL round bottomed flask. Triethylamine (mol. wt. 101.19 g/mol, d. 0.7255 g/mL, 21.23 mmol, 2.962 mL), 4-Dimethylaminopyridine (mol. wt. 122.17 g/mol, 3.43 mmol, 0.418 g), and *p*-methoxybenzoyl chloride (mol. wt. 170.59 g/mol, 14.38 mmol, 2.44 g) were added to the flask. The reaction mixture was stirred for 2 h. The reaction was monitored by TLC (1:1 hexane: ethyl acetate) to observe the disappearance of the isosorbide. Once complete, the mixture was washed with 1 M HCl (50 mL), saturated sodium bicarbonate solution (50 mL), saturated brine solution (50 mL) and dried with anhydrous sodium sulfate (1 g). Evaporation of the dichloromethane and crystallisation using diethyl ether yielded a white powder (2.60 g, 91.5 %) mol. wt. 414.4 g/mol. **^{1}H NMR** (400 MHz, CHLOROFORM-*d*) **δ ppm** 3.83 (s, 3 H, -CH_3) 3.87 (s, 3 H, -CH_3) 3.99 - 4.18 (m, 4 H, Is-H1/6) 4.68 (d, *J*=4.56 Hz, 1 H, Is-H4) 5.05 (t, *J*=4.98 Hz, 1 H, Is-H3) 5.40 (q, *J*=5.39 Hz, 1 H, Is-H5) 5.47 (d, *J*=2.90 Hz, 1 H, Is-H2) 6.93 (t, *J*=9.12 Hz, 4 H, Ar-H3/5) 7.98 (d, *J*=8.71 Hz, 2 H, Ar-H2/6) 8.05 (d, *J*=9.12 Hz, 2 H, Ar-H2/6). **^{13}C NMR** (101 MHz, CHLOROFORM-*d*) **δ ppm** 55.44, 73.58, 76.67, 81.17, 86.19, 113.67, 131.84, 165.66. **HRMS (ESI)** calculated for $C_{22}H_{22}NaO_8$ [M^++Na] 437.120688: found 437.121069.

Isosorbide-2-(*o*-methoxybenzoate)-5-(*m*-methoxybenzoate) (59a)

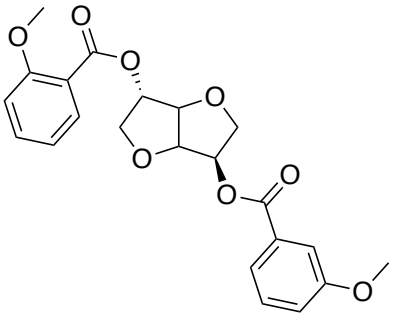

Isosorbide-2-(2-methoxybenzoate) (mol. wt. 280.09 g/mol, 1.07 mmol, .30 g) was dissolved in dry dichloromethane (10 mL) in a 50 mL round bottomed flask. Triethylamine (mol. wt. 101.19 g/mol, d. 0.7255 g/mL, 5.36 mmol, .746 mL), 4-Dimethylaminopyridine (mol. wt. 122.17 g/mol, .535 mmol, 0.065 g), and *m*-methoxybenzoyl chloride (mol. wt. 170.59 g/mol, d. 1.214 g/mL, 1.18 mmol, 0.165 mL) were added to the flask. The reaction mixture was stirred for 3 h. The reaction was monitored by TLC (1:2 hexane: ethyl acetate) to observe the disappearance of the isosorbide-2-(2-methoxybenzoate). Once complete, the mixture was washed with 1 M HCl (50 mL), saturated sodium bicarbonate solution (50 mL), saturated brine solution (50 mL) and dried with anhydrous sodium sulfate (1 g). Evaporation of the dichloromethane and crystallisation using diethyl ether yielded a white powder (0.407 g, 91.7 %) mol. wt. 414.4 g/mol. **^{1}H NMR** (400 MHz, CHLOROFORM-*d*) **δ ppm** 3.86 (s, 3 H, -CH_3) 3.93 (s, 3 H, -CH_3) 4.00 (m, *J*=10.00, 5.40 Hz, 1 H, Is-H6) 4.05 - 4.23 (m, 3 H, Is-H1/6) 4.70 (d, *J*=4.56 Hz, 1 H, Is-H4) 5.06 (t, *J*=5.18 Hz, 1 H, Is-H3) 5.41 (q, *J*=5.39 Hz, 1 H, Is-H5) 5.48 (d, *J*=3.32 Hz, 1 H, Is-H2) 6.96 - 7.05 (m, 2 H, Ar-o-H4/5) 7.13 (dd, *J*=6.20, 2.90 Hz, 1 H, Ar-m-H4) 7.36 (t, *J*=7.88 Hz, 1 H, Ar-m-H5) 7.46 - 7.57 (m, 2 H, Ar-o-H3/Ar-m-H2) 7.63 (d, *J*=7.88 Hz, 1 H, Ar-m-H6) 7.89 (dd, *J*=7.88, 1.66 Hz, 1 H, Ar-o-H6). **^{13}C NMR** (101 MHz, CHLOROFORM-*d*) **δ ppm** 56.29, 71.01, 73.73, 74.51, 77.64, 79.05, 81.37, 112.40, 114.51, 120.47 122.47, 129.79, 132.28, 134.30. **HRMS (ESI)** calculated for $C_{22}H_{22}NaO_8$ [M^++Na] 437.120688: found 437.1216.

Isosorbide-2-(*o*-methoxybenzoate)-5-(*p*-methoxybenzoate) (59b)

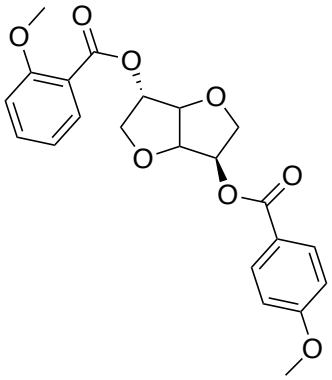

Isosorbide-2-(2-methoxybenzoate) (mol. wt. 280.09 g/mol, 1.07 mmol, .30 g) was dissolved in dry dichloromethane (10 mL) in a 50 mL round bottomed flask. Triethylamine (mol. wt. 101.19 g/mol, d. 0.7255 g/mL, 5.36 mmol, .746 mL), 4-Dimethylaminopyridine (mol. wt. 122.17 g/mol, .535 mmol, 0.065 g), and *p*-methoxybenzoyl chloride (mol. wt. 170.59 g/mol, 1.18 mmol, 0.201 g) were added to the flask. The reaction mixture was stirred for 3 h. The reaction was monitored by TLC (1:2 hexane: ethyl acetate) to observe the disappearance of the isosorbide-2-(2-methoxybenzoate). Once complete, the mixture was washed with 1 M HCl (50 mL), saturated sodium bicarbonate solution (50 mL), saturated brine solution (50 mL) and dried with anhydrous sodium sulfate (1 g). Evaporation of the dichloromethane and crystallisation using diethyl ether yielded a white powder (0.421 g, 94.9 %) mol. wt. 414.4 g/mol.**^{1}H NMR** (400 MHz, CHLOROFORM-*d*) **δ ppm** 3.88 (s, 3 H, -CH_3) 3.90 (s, 3 H, CH_3) 3.97 - 4.17 (m, 4 H, Is-H1/6) 4.69 (d, *J*=4.56 Hz, 1 H, Is-H4) 5.02 (t, *J*=4.98 Hz, 1 H, Is-H3) 5.40 (q, *J*=5.39 Hz, 1 H, Is-H5) 5.48 (d, *J*=2.90 Hz, 1 H, Is-H2) 6.90 - 7.02 (m, 4 H, Ar-p-H3/5, Ar-o-H4/5) 7.45 - 7.54 (m, 1 H, Ar-o-H3) 7.78 (dd, *J*=7.88, 2.07 Hz, 1 H, Ar-o-H6) 8.01 - 8.08 (m, 2 H, Ar-p-H2/6). **^{13}C NMR** (101 MHz, CHLOROFORM-*d*) **δ ppm** 55.43, 55.96, 74.22, 77.30, 81.17, 86.14, 112.06, 113.68, 120.09, 131.84, 133.99. **HRMS (ESI)** calculated for $C_{22}H_{22}NaO_8$ [M^++Na] 437.120688: found 437.1212.

Isosorbide-2-(*m*-methoxybenzoate)-5-(*o*-methoxybenzoate) (59c)

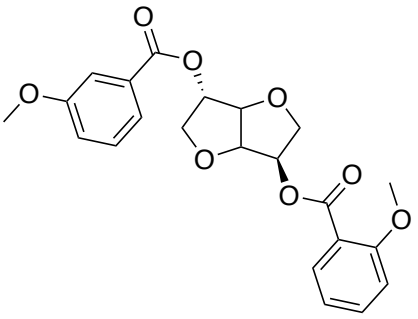

Isosorbide-2-(3-methoxybenzoate) (mol. wt. 280.09 g/mol, 1.07 mmol, .30 g) was dissolved in dry dichloromethane (10 mL) in a 50 mL round bottomed flask. Triethylamine (mol. wt. 101.19 g/mol, d. 0.7255 g/mL, 5.36 mmol, .746 mL), 4-Dimethylaminopyridine (mol. wt. 122.17 g/mol, .535 mmol, 0.065 g), and *o*-methoxybenzoyl chloride (mol. wt. 170.59 g/mol, d. 1.146 g/mL, 1.18 mmol, 0.176 mL) were added to the flask. The reaction mixture was stirred for 3 h. The reaction was monitored by TLC (1:2 hexane: ethyl acetate) to observe the disappearance of the isosorbide-2-(3-methoxybenzoate). Once complete, the mixture was washed with 1 M HCl (50 mL), saturated sodium bicarbonate solution (50 mL), saturated brine solution (50 mL) and dried with anhydrous sodium sulfate (1 g). Evaporation of the dichloromethane and crystallisation using diethyl ether yielded a white powder (0.387 g, 87.2 %) mol. wt. 414.4 g/mol. **^{1}H NMR** (400 MHz, CHLOROFORM-*d*) **δ ppm** 3.86 (s, 3 H-CH_3) 3.93 (s, 3 H, -CH_3) 3.96 - 4.04 (m, 1 H, Is-H6) 4.06 - 4.15 (m, 2 H, Is-H1) 4.16 - 4.23 (m, 1 H, Is-H1) 4.70 (d, *J*=4.56 Hz, 1 H, Is-H4) 5.06 (t, *J*=5.18 Hz, 1 H, is-H3) 5.41 (q, *J*=5.39 Hz, 1 H, Is-H5) 5.48 (d, *J*=3.32 Hz, 1 H, Is-H2) 6.95 - 7.05 (m, 2 H, Ar-o-H4/5) 7.13 (dd, *J*=6.22, 2.49 Hz, 1 H, Ar-m-H4) 7.36 (t, *J*=7.90 Hz, 1 H, Ar-m-H5) 7.47 - 7.57 (m, 2 H, Ar-o-H3, Ar-m-H2) 7.63 (dd, *J*=7.88, 1.00 Hz, 1 H, Ar-m-H6) 7.89 (dd, *J*=7.88, 1.66 Hz, 1 H, Ar-o-H6). **^{13}C NMR** (101 MHz, CHLOROFORM-*d*) **δ ppm** 55.94, 73.39, 74.17, 77.30, 78.71, 112.06, 114.17, 120.13, 122.13, 129.45, 131.94, 133.96. **HRMS (ESI)** calculated for $C_{22}H_{22}NaO_8$ [M^++Na] 437.120688: found 437.1213.

Isosorbide-2-(*m*-methoxybenzoate)-5-(*p*-methoxybenzoate) (59d)

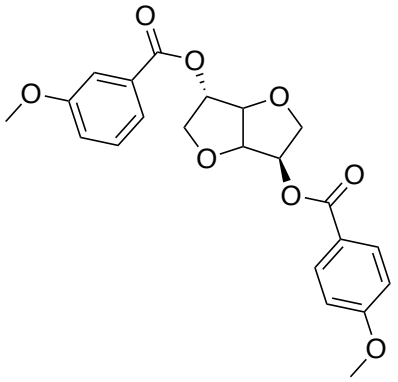

Isosorbide-2-(3-methoxybenzoate) (mol. wt. 280.09 g/mol, 1.07 mmol, .30 g) was dissolved in dry dichloromethane (10 mL) in a 50 mL round bottomed flask. Triethylamine (mol. wt. 101.19 g/mol, d. 0.7255 g/mL, 5.36 mmol, .746 mL), 4-Dimethylaminopyridine (mol. wt. 122.17 g/mol, .535 mmol, 0.065 g), and *p*-methoxybenzoyl chloride (mol. wt. 170.59 g/mol, 1.18 mmol, 0.176 mL) were added to the flask. The reaction mixture was stirred for 3 h. The reaction was monitored by TLC (1:2 hexane: ethyl acetate) to observe the disappearance of the isosorbide-2-(3-methoxybenzoate). Once complete, the mixture was washed with 1 M HCl (50

mL), saturated sodium bicarbonate solution (50 mL), saturated brine solution (50 mL) and dried with anhydrous sodium sulfate (1 g). Evaporation of the dichloromethane and crystallisation using diethyl ether yielded a white powder (0.345 g, 77.8 %) mol. wt. 414.4 g/mol. **^{1}H NMR** (400 MHz, CHLOROFORM-*d*) **δ ppm** 3.88 (d, *J*=10.80 Hz, 6 H-CH_3) 3.99 - 4.18 (m, 4 H, Is-H1/6) 4.69 (d, *J*=4.56 Hz, 1 H, Is-H4) 5.06 (t, *J*=4.98 Hz, 1 H, Is-H3) 5.41 (q, *J*=5.39 Hz, 1 H, Is-H5) 5.49 (d, *J*=3.32 Hz, 1 H, Is-H2) 6.95 (dd, *J*=8.71, 1.00 Hz, 2 H, Ar-p-H3/5) 7.13 (dd, *J*=5.81, 2.49 Hz, 1 H, Ar-m-H4) 7.35 (t, *J*=8.09 Hz, 1 H, Ar-m-H5) 7.54 (dd, *J*=2.49, 1.66 Hz, 1 H, Ar-m-H2) 7.62 (d, *J*=7.70 Hz, 1 H, Ar-m-H6) 8.05 (dd, *J*=8.71, 1.00 Hz, 2 H, Ar-p-H2/6). **^{13}C NMR** (101 MHz, CHLOROFORM-*d*) **δ ppm** 55.46, 70.75, 74.21, 76.68, 78.61, 81.21, 86.13, 113.73, 114.19, 119.86, 122.14, 129.47, 131.85. **HRMS (ESI)** calculated for $C_{22}H_{22}NaO_8$ [M^++Na] 437.120688: found 437.121175.

Isosorbide-2-(*p*-methoxybenzoate)-5-(*o*-methoxybenzoate) (59e)

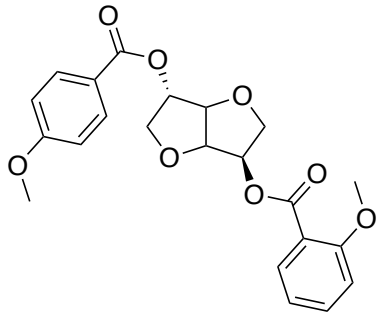

Isosorbide-2-(4-methoxybenzoate) (mol. wt. 280.09 g/mol, 1.07 mmol, .30 g) was dissolved in dry dichloromethane (10 mL) in a 50 mL round bottomed flask. Triethylamine (mol. wt. 101.19 g/mol, d. 0.7255 g/mL, 5.36 mmol, .746 mL), 4-Dimethylaminopyridine (mol. wt. 122.17 g/mol, .535 mmol, 0.065 g), and *o*-methoxybenzoyl chloride (mol. wt. 170.59 g/mol, d. 1.146 g/mL, 1.18 mmol, 0.176 mL) were added to the flask. The reaction mixture was stirred for 3 h. The reaction was monitored by TLC (1:2 hexane: ethyl acetate) to observe the disappearance of the isosorbide-2-(4-methoxybenzoate). Once complete, the mixture was washed with 1 M HCl (50 mL), saturated sodium bicarbonate solution (50 mL), saturated brine solution (50 mL) and dried with anhydrous sodium sulfate (1 g). Evaporation of the dichloromethane and crystallisation using diethyl ether yielded a white powder (0.392 g, 88.4 %) mol. wt. 414.4 g/mol. **^{1}H NMR** (400 MHz, CHLOROFORM-*d*) **δ ppm** 3.90 (s, 3 H, -CH_3) 3.88 (s, 3 H, -CH_3) 3.97 - 4.17 (m, 4 H, Is-H1/6) 4.69 (d, *J*=4.56 Hz, 1 H, Is-H4) 5.02 (t, *J*=4.98 Hz, 1 H, is-H3) 5.40 (q, *J*=5.39 Hz, 1 H, Is-H5) 5.48 (d, *J*=2.90 Hz, 1 H, Is-H2) 6.90 - 7.02 (m, 4 H, Ar-o-H4/5, Ar-p-H3/5) 7.45 - 7.54 (m, 1 H, Ar-o-H3) 7.78 (dd, *J*=7.88, 2.07 Hz, 1 H, Ar-o-H6) 8.05 (d, *J*=8.71 Hz, 2 H, Ar-p-H2/6). **^{13}C NMR** (101 MHz, CHLOROFORM-*d*) **δ ppm** 55.97, 56.68,

77.32, 81.02, 113.69, 120.15, 131.82, 133.89. **HRMS (ESI)** calculated for $C_{22}H_{22}NaO_8$ [M^++Na] 437.120688: found 437.120911.

Isosorbide-2-(*p*-methoxybenzoate)-5-(*m*-methoxybenzoate) (59f)

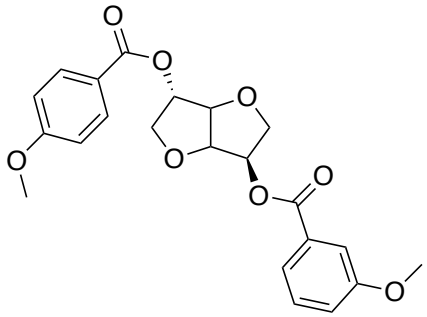

Isosorbide-2-(4-methoxybenzoate) (mol. wt. 280.09 g/mol, 1.07 mmol, .30 g) was dissolved in dry dichloromethane (10 mL) in a 50 mL round bottomed flask. Triethylamine (mol. wt. 101.19 g/mol, d. 0.7255 g/mL, 5.36 mmol, .746 mL), 4-Dimethylaminopyridine (mol. wt. 122.17 g/mol, .535 mmol, 0.065 g), and *m*-methoxybenzoyl chloride (mol. wt. 170.59 g/mol, d. 1.214 g/mL, 1.18 mmol, 0.166 mL) were added to the flask. The reaction mixture was stirred for 3 h. The reaction was monitored by TLC (1:2 hexane: ethyl acetate) to observe the disappearance of the isosorbide-2-(4-methoxybenzoate). Once complete, the mixture was washed with 1 M HCl (50 mL), saturated sodium bicarbonate solution (50 mL), saturated brine solution (50 mL) and dried with anhydrous sodium sulfate (1 g). Evaporation of the dichloromethane and crystallisation using diethyl ether yielded a white powder (0.365 g, 82.3 %) mol. wt. 414.4 g/mol. **^{1}H NMR** (400 MHz, CHLOROFORM-*d*) **δ ppm** 3.80 - 3.91 (m, 6 H, -CH_3) 4.01 - 4.16 (m, 4 H, Is-H1/6) 4.68 (d, *J*=4.56 Hz, 1 H, Is-H4) 5.07 (t, *J*=4.98 Hz, 1 H, Is-H3) 5.42 (q, *J*=5.39 Hz, 1 H, Is-H5) 5.47 (d, *J*=2.49 Hz, 1 H, Is-H2) 6.92 (d, *J*=9.12 Hz, 2 H, Ar-p-H3/5) 7.14 (dd, *J*=8.29, 2.90 Hz, 1 H, Ar-m-H4) 7.37 (t, *J*=7.88 Hz, 1 H, Ar-m-H5) 7.61 (s, 1 H, Ar-m-H2) 7.69 (d, *J*=7.46 Hz, 1 H, Ar-m-H6) 7.98 (d, *J*=8.71 Hz, 2 H, Ar-p-H2/6). **^{13}C NMR** (101 MHz, CHLOROFORM-*d*) **δ ppm** 55.45, 70.72, 73.56, 74.61, 76.67, 78.15, 81.11, 86.24, 113.68, 119.73, 122.14, 129.48, 131.81, 159.59, 165.29, 165.84, 214.31. **HRMS (ESI)** calculated for $C_{22}H_{22}NaO_8$ [M^++Na] 437.120688: found 437.1207.

Isosorbide-2-(*o*-methoxybenzoate)-5-nicotinate (60a)

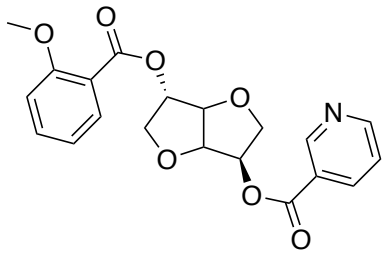

Isosorbide-2-(2-methoxybenzoate) (mol. wt. 280.09 g/mol, 1.07 mmol, .30 g) was dissolved in dry dichloromethane (10 mL) in a 50 mL round bottomed flask. Triethylamine (mol. wt. 101.19 g/mol, d. 0.7255 g/mL, 8.56 mmol, 1.556 mL), 4-Dimethylaminopyridine (mol. wt. 122.17 g/mol, .535 mmol, 0.065 g), and nicotinoyl chloride hydrochloride (mol. wt. 178.02 g/mol, 4.28 mmol, 0.999 g) were added to the flask. The reaction mixture was stirred for 24 h. The reaction was monitored by TLC (1:3 hexane: ethyl acetate) to observe the disappearance of the isosorbide-2-(2-methoxybenzoate). Once complete, the mixture was washed with 1 M HCl (50 mL), saturated sodium bicarbonate solution (50 mL), saturated brine solution (50 mL) and dried with anhydrous sodium sulfate (1 g). Evaporation of the dichloromethane and crystallisation using diethyl ether yielded a white powder (0.187 g, 45.4 %) mol. wt. 385.37 g/mol. **^{1}H NMR** (400 MHz, CHLOROFORM-*d*) **δ ppm** 3.90 (s, 3 H, -CH_3) 4.02 - 4.15 (m, 4 H, Is-H1/6) 4.69 (d, *J*=4.56 Hz, 1 H, Is-H4) 5.05 (t, *J*=5.18 Hz, 1 H, Is-H3) 5.45 (q, *J*=5.39 Hz, 1 H, Is-H5) 5.49 (s, 1 H, Is-H2) 6.92 - 7.03 (m, 2 H, Ar-H4/5) 7.43 (dd, *J*=7.88, 4.98 Hz, 1 H, Nic-H5) 7.46 - 7.54 (m, 1 H, Ar-H3) 7.78 (dd, *J*=7.88, 1.66 Hz, 1 H, Ar-H6) 8.34 (d, *J*=8.29 Hz, 1 H, Nic-H4) 8.82 (br. s., 1 H, Nic-H6) 9.28 (br. s., 1 H, Nic-H2). **HRMS (ESI)** calculated for $C_{20}H_{19}NNaO_7$ [M^++Na] 408.105373: found 408.105487.

Isosorbide-2-(*m*-methoxybenzoate)-5-nicotinate (60b)

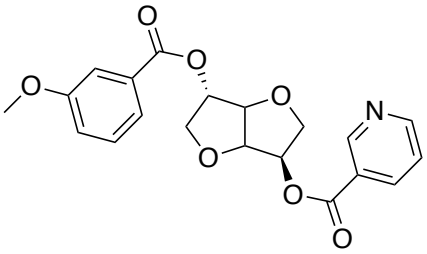

Isosorbide-2-(3-methoxybenzoate) (mol. wt. 280.09 g/mol, 1.07 mmol, .30 g) was dissolved in dry dichloromethane (10 mL) in a 50 mL round bottomed flask. Triethylamine (mol. wt. 101.19 g/mol, d. 0.7255 g/mL, 8.56 mmol, 1.556 mL), 4-Dimethylaminopyridine (mol. wt. 122.17 g/mol, .535 mmol, 0.065 g), and nicotinoyl chloride hydrochloride (mol. wt. 178.02 g/mol, 4.28 mmol, 0.999 g) were added to the flask. The reaction mixture was stirred for 24 h. The reaction was monitored by TLC (1:2 hexane: ethyl acetate) to observe the disappearance of the isosorbide-2-(3-methoxybenzoate). Once complete, the mixture was washed with 1 M HCl (50 mL), saturated sodium bicarbonate solution (50 mL), saturated brine solution (50 mL) and dried with anhydrous sodium sulfate (1 g). Evaporation of the dichloromethane and crystallisation using diethyl ether yielded a white powder (0.256 g, 62.1 %) mol. wt. 385.37 g/mol. **^{1}H NMR** (400 MHz, CHLOROFORM-*d*) **δ ppm** 3.84 (s, 3 H, -CH_3) 4.03 - 4.16 (m, 4 H, Is-H1/6) 4.69 (d, *J*=4.56 Hz, 1 H, Is-H4) 5.08 (t, *J*=5.18 Hz, 1 H, Is-H3) 5.45 (q, *J*=5.40 Hz, 1 H, Is-H5) 5.49

(s, 1 H, Is-H2) 7.12 (dd, *J*=8.30, 2.49 Hz, 1 H, Ar-H4) 7.34 (t, *J*=7.88 Hz, 1 H, Ar-H5) 7.43 (dd, *J*=7.88, 4.98 Hz, 1 H, Nic-H5) 7.53 (t, *J*=2.50 Hz, 1 H, Ar-H2) 7.61 (d, *J*=7.88 Hz, 1 H, Ar-H6) 8.35 (d, *J*=7.90 Hz, 1 H, Nic-H4) 8.82 (br. s., 1 H, Nic-H6) 9.28 (br. s., 1 H, Nic-H2). **^{13}C NMR** (101 MHz, CHLOROFORM-*d*) **δ ppm** 55.52, 70.59, 73.55, 75.44, 76.71, 77.03, 77.23, 77.34, 78.37, 80.97, 86.29, 114.32, 119.88, 122.16, 129.54, 130.66. **HRMS (ESI)** calculated for $C_{20}H_{19}NNaO_7$ [M^++Na] 408.105373: found 408.1061.

Isosorbide-2-(*p*-methoxybenzoate)-5-nicotinate (60c)

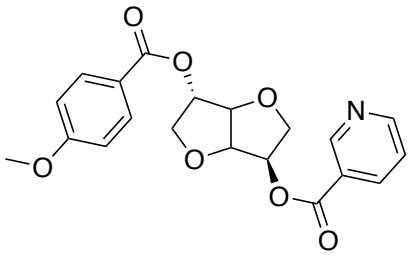

Isosorbide-2-(4-methoxybenzoate) (mol. wt. 280.09 g/mol, 1.07 mmol, .30 g) was dissolved in dry dichloromethane (10 mL) in a 50 mL round bottomed flask. Triethylamine (mol. wt. 101.19 g/mol, d. 0.7255 g/mL, 8.56 mmol, 1.556 mL), 4-Dimethylaminopyridine (mol. wt. 122.17 g/mol, .535 mmol, 0.065 g), and nicotinoyl chloride hydrochloride (mol. wt. 178.02 g/mol, 4.28 mmol, 0.999 g) were added to the flask. The reaction mixture was stirred for 24 h. The reaction was monitored by TLC (1:2 hexane: ethyl acetate) to observe the disappearance of the isosorbide-2-(4-methoxybenzoate). Once complete, the mixture was washed with 1 M HCl (50 mL), saturated sodium bicarbonate solution (50 mL), saturated brine solution (50 mL) and dried with anhydrous sodium sulfate (1 g). Evaporation of the dichloromethane and crystallisation using diethyl ether yielded a white powder (0.256 g, 66.7 %) mol. wt. 385.37 g/mol. **^{1}H NMR** (400 MHz, CHLOROFORM-*d*) **δ ppm** 3.87 (s, 3 H, -CH_3) 4.02 - 4.16 (m, 4 H, Is-H1/6) 4.69 (d, *J*=4.56 Hz, 1 H, Is-H4) 5.07 (t, *J*=5.18 Hz, 1 H, Is-H3) 5.43 - 5.47 (m, 1 H, Is-H5) 5.48 (s, 1 H, Is-H2) 6.92 (d, *J*=9.12 Hz, 2 H, Ar-H3/5) 7.44 (dd, *J*=7.88, 4.98 Hz, 1 H, Nic-H5) 7.98 (d, *J*=9.12 Hz, 2 H, Ar-H2/6) 8.36 (d, *J*=8.10 Hz, 1 H, Nic-H4) 8.82 (s, 1 H, Nic-H6) 9.29 (br. s., 1 H, Nic-H2). **^{13}C NMR** (101 MHz, CHLOROFORM-*d*) **δ ppm** 69.16, 70.68, 73.55, 76.73, 77.05, 77.36, 77.65, 81.36, 86.72, 120.57, 127.79, 128.15, 128.66, 132.03, 133.98. **HRMS (ESI)** calculated for $C_{20}H_{19}NNaO_7$ [M^++Na] 408.105373: found 408.106098.

References

1. Sabat R, Wolk K, Loyal L, Döcke W-D, Ghoreschi K. T cell pathology in skin inflammation. Seminars in Immunopathology. 2019;41(3):359-77.
2. Kabashima K, Honda T, Ginhoux F, Egawa G. The immunological anatomy of the skin. Nature Reviews Immunology. 2019;19(1):19-30.
3. Richmond JM, Harris JE. Immunology and Skin in Health and Disease. Cold Spring Harbor Perspectives in Medicine. 2014;4(12):a015339.
4. Matsui T, Amagai M. Dissecting the formation, structure and barrier function of the stratum corneum. Int Immunol. 2015;27(6):269-80.
5. Nguyen AV, Soulika AM. The Dynamics of the Skin's Immune System. International journal of molecular sciences. 2019;20(8):1811.
6. Wong R, Geyer S, Weninger W, Guimberteau J-C, Wong JK. The dynamic anatomy and patterning of skin. Experimental Dermatology. 2016;25(2):92-8.
7. Pasparakis M, Haase I, Nestle FO. Mechanisms regulating skin immunity and inflammation. Nature reviews Immunology. 2014;14(5):289-301.
8. Ho AW, Kupper TS. T cells and the skin: from protective immunity to inflammatory skin disorders. Nature Reviews Immunology. 2019;19(8):490-502.
9. Wang A, Bai Y. Dendritic cells: The driver of psoriasis. J Dermatol. 2020;47(2):104-13.
10. Toebak MJ, Gibbs S, Bruynzeel DP, Scheper RJ, Rustemeyer T. Dendritic cells: biology of the skin. Contact Dermatitis. 2009;60(1):2-20.
11. Conrad C, Meller S, Gilliet M. Plasmacytoid dendritic cells in the skin: To sense or not to sense nucleic acids. Semin Immunol. 2009;21(3):101-9.
12. Italiani P, Boraschi D. From Monocytes to M1/M2 Macrophages: Phenotypical vs. Functional Differentiation. Frontiers in immunology. 2014;5:514.
13. Sieweke MH, Allen JE. Beyond stem cells: self-renewal of differentiated macrophages. Science. 2013;342(6161):1242974.
14. Jenkins SJ, Ruckerl D, Cook PC, Jones LH, Finkelman FD, van Rooijen N, et al. Local macrophage proliferation, rather than recruitment from the blood, is a signature of TH2 inflammation. Science. 2011;332(6035):1284-8.
15. Krystel-Whittemore M, Dileepan KN, Wood JG. Mast Cell: A Multi-Functional Master Cell. Frontiers in immunology. 2016;6:620.
16. Mortaz E, Alipoor SD, Adcock IM, Mumby S, Koenderman L. Update on Neutrophil Function in Severe Inflammation. Frontiers in immunology. 2018;9(2171).
17. Leliefeld PHC, Koenderman L, Pillay J. How Neutrophils Shape Adaptive Immune Responses. Frontiers in immunology. 2015;6:471.
18. Clark RA, Chong B, Mirchandani N, Brinster NK, Yamanaka K, Dowgiert RK, et al. The vast majority of CLA+ T cells are resident in normal skin. Journal of immunology (Baltimore, Md : 1950). 2006;176(7):4431-9.
19. Alberts B, Johnson A, Lewis J. T Cells and MHC Proteins. Molecular Biology of the Cell 4th edition. New York: Garland Science; 2002.
20. Walsh SRA, Shear NH. Psoriasis and the new biologic agents: interrupting a T-AP dance. CMAJ. 2004;170(13):1933-41.
21. Josefowicz SZ, Lu LF, Rudensky AY. Regulatory T cells: mechanisms of differentiation and function. Annu Rev Immunol. 2012;30:531-64.
22. Breitfeld D, Ohl L, Kremmer E, Ellwart J, Sallusto F, Lipp M, et al. Follicular B helper T cells express CXC chemokine receptor 5, localize to B cell follicles, and support immunoglobulin production. J Exp Med. 2000;192(11):1545-52.
23. Schaerli P, Willimann K, Lang AB, Lipp M, Loetscher P, Moser B. CXC chemokine receptor 5 expression defines follicular homing T cells with B cell helper function. J Exp Med. 2000;192(11):1553-62.

24. Schlapbach C, Gehad A, Yang C, Watanabe R, Guenova E, Teague JE, et al. Human TH9 cells are skin-tropic and have autocrine and paracrine proinflammatory capacity. Science translational medicine. 2014;6(219):219ra8.
25. Clark RA, Schlapbach C. TH9 cells in skin disorders. Semin Immunopathol. 2017;39(1):47-54.
26. Lonsdorf AS, Hwang ST, Enk AH. Chemokine Receptors in T-Cell-Mediated Diseases of the Skin. Journal of Investigative Dermatology. 2009;129(11):2552-66.
27. Ahmed R, Bevan MJ, Reiner SL, Fearon DT. The precursors of memory: models and controversies. Nature reviews Immunology. 2009;9(9):662-8.
28. Watanabe R, Gehad A, Yang C, Scott LL, Teague JE, Schlapbach C, et al. Human skin is protected by four functionally and phenotypically discrete populations of resident and recirculating memory T cells. Science translational medicine. 2015;7(279):279ra39.
29. Gebhardt T, Wakim LM, Eidsmo L, Reading PC, Heath WR, Carbone FR. Memory T cells in nonlymphoid tissue that provide enhanced local immunity during infection with herpes simplex virus. Nat Immunol. 2009;10(5):524-30.
30. Egbuniwe IU, Karagiannis SN, Nestle FO, Lacy KE. Revisiting the role of B cells in skin immune surveillance. Trends in immunology. 2015;36(2):102-11.
31. Ponte P, Lopes MJP. Apparent safe use of single dose rituximab for recalcitrant atopic dermatitis in the first trimester of a twin pregnancy. Journal of the American Academy of Dermatology. 2010;63(2):355-6.
32. Dass S, Vital EM, Emery P. Development of psoriasis after B cell depletion with rituximab. Arthritis & Rheumatism. 2007;56(8):2715-8.
33. Mielke F, Schneider-Obermeyer J, Dörner T. Onset of psoriasis with psoriatic arthropathy during rituximab treatment of non-Hodgkin lymphoma. Annals of the Rheumatic Diseases. 2008;67(7):1056.
34. Robert C, Kupper TS. Inflammatory skin diseases, T cells, and immune surveillance. The New England journal of medicine. 1999;341(24):1817-28.
35. Kim EJ, Hess S, Richardson SK, Newton S, Showe LC, Benoit BM, et al. Immunopathogenesis and therapy of cutaneous T cell lymphoma. The Journal of clinical investigation. 2005;115(4):798-812.
36. Wong ITY, Tsuyuki RT, Cresswell-Melville A, Doiron P, Drucker AM. Guidelines for the management of atopic dermatitis (eczema) for pharmacists. Can Pharm J (Ott). 2017;150(5):285-97.
37. Odhiambo JA, Williams HC, Clayton TO, Robertson CF, Asher MI. Global variations in prevalence of eczema symptoms in children from ISAAC Phase Three. Journal of Allergy and Clinical Immunology. 2009;124(6):1251-8.e23.
38. Thomsen SF. Atopic dermatitis: natural history, diagnosis, and treatment. ISRN Allergy. 2014;2014:354250.
39. Williams HC. Clinical practice. Atopic dermatitis. The New England journal of medicine. 2005;352(22):2314-24.
40. Seegraber M, Srour J, Walter A, Knop M, Wollenberg A. Dupilumab for treatment of atopic dermatitis. Expert Rev Clin Pharmacol. 2018;11(5):467-74.
41. Siegfried EC, Hebert AA. Diagnosis of Atopic Dermatitis: Mimics, Overlaps, and Complications. J Clin Med. 2015;4(5):884-917.
42. Villasante Fricke AC, Miteva M. Epidemiology and burden of alopecia areata: a systematic review. Clin Cosmet Investig Dermatol. 2015;8:397-403.
43. Wang ECE, Christiano AM. The Changing Landscape of Alopecia Areata: The Translational Landscape. Adv Ther. 2017;34(7):1586-93.
44. Boehncke WH, Brembilla NC. Autoreactive T-Lymphocytes in Inflammatory Skin Diseases. Frontiers in immunology. 2019;10:1198.
45. Gilhar A, Etzioni A, Paus R. Alopecia areata. The New England journal of medicine. 2012;366(16):1515-25.

46. Barker CF, Billingham RE. Analysis of local anatomic factors that influence the survival times of pure epidermal and full-thickness skin homografts in guinea pigs. Ann Surg. 1972;176(5):597-604.
47. Reynolds AJ, Lawrence C, Cserhalmi-Friedman PB, Christiano AM, Jahoda CA. Trans-gender induction of hair follicles. Nature. 1999;402(6757):33-4.
48. Rajabi F, Drake LA, Senna MM, Rezaei N. Alopecia areata: a review of disease pathogenesis. British Journal of Dermatology. 2018;179(5):1033-48.
49. Gilhar A, Landau M, Assy B, Shalaginov R, Serafimovich S, Kalish RS. Mediation of Alopecia Areata by Cooperation Between CD4+ and CD8+ T Lymphocytes: Transfer to Human Scalp Explants on Prkdcscid Mice. Archives of dermatology. 2002;138(7):916-22.
50. Solimani F, Meier K, Ghoreschi K. Emerging Topical and Systemic JAK Inhibitors in Dermatology. Frontiers in immunology. 2019;10:2847.
51. Strazzulla LC, Wang EHC, Avila L, Lo Sicco K, Brinster N, Christiano AM, et al. Alopecia areata: Disease characteristics, clinical evaluation, and new perspectives on pathogenesis. Journal of the American Academy of Dermatology. 2018;78(1):1-12.
52. Boissy RE, Manga P. On the Etiology of Contact/Occupational Vitiligo. Pigment Cell Research. 2004;17(3):208-14.
53. Taïeb A, Picardo M. Vitiligo. New England Journal of Medicine. 2009;360(2):160-9.
54. Boniface K, Seneschal J, Picardo M, Taieb A. Vitiligo: Focus on Clinical Aspects, Immunopathogenesis, and Therapy. Clinical reviews in allergy & immunology. 2018;54(1):52-67.
55. Dell'Anna ML, Maresca V, Briganti S, Camera E, Falchi M, Picardo M. Mitochondrial impairment in peripheral blood mononuclear cells during the active phase of vitiligo. The Journal of investigative dermatology. 2001;117(4):908-13.
56. Badri AM, Todd PM, Garioch JJ, Gudgeon JE, Stewart DG, Goudie RB. An immunohistological study of cutaneous lymphocytes in vitiligo. J Pathol. 1993;170(2):149-55.
57. Wańkowicz-Kalińska A, van den Wijngaard RMJGJ, Tigges BJ, Westerhof W, Ogg GS, Cerundolo V, et al. Immunopolarization of CD4+ and CD8+ T Cells to Type-1–Like is Associated with Melanocyte Loss in Human Vitiligo. Laboratory Investigation. 2003;83(5):683-95.
58. Wang CQ, Cruz-Inigo AE, Fuentes-Duculan J, Moussai D, Gulati N, Sullivan-Whalen M, et al. Th17 cells and activated dendritic cells are increased in vitiligo lesions. PLoS One. 2011;6(4):e18907.
59. Bassiouny DA, Shaker O. Role of interleukin-17 in the pathogenesis of vitiligo. Clin Exp Dermatol. 2011;36(3):292-7.
60. Wu J, Zhou M, Wan Y, Xu A. CD8+ T cells from vitiligo perilesional margins induce autologous melanocyte apoptosis. Mol Med Rep. 2013;7(1):237-41.
61. Todd A, Anderson RJ, Groundwater PW, George SE. Current and potential new therapies for the treatment of psoriasis. The Pharmaceutical Journal. 2010;284:560-1.
62. Gudjonsson JE, Johnston A, Sigmundsdottir H, Valdimarsson H. Immunopathogenic mechanisms in psoriasis. Clinical and experimental immunology. 2004;135(1):1-8.
63. Novartis Ireland, Irish Skin Foundation, NUI Galway. The Burden of Psoriasis: Epidemiology, Quality of Life, Co-morbidities and Treatment Goals. 2015.
64. Feingold KR, Grunfeld C. Psoriasis: it's more than just the skin. Journal of lipid research. 2012;53(8):1427-9.
65. Raychaudhuri SK, Maverakis E, Raychaudhuri SP. Diagnosis and classification of psoriasis. Autoimmunity reviews. 2014;13(4-5):490-5.
66. Chalmers RJ, O'Sullivan T, Owen CM, Griffiths CE. A systematic review of treatments for guttate psoriasis. The British journal of dermatology. 2001;145(6):891-4.
67. Liang Y, Sarkar MK, Tsoi LC, Gudjonsson JE. Psoriasis: a mixed autoimmune and autoinflammatory disease. Current Opinion in Immunology. 2017;49(Supplement C):1-8.
68. Gisondi P, Di Mercurio M, Idolazzi L, Girolomoni G. Concept of Remission in Chronic Plaque Psoriasis. The Journal of rheumatology Supplement. 2015;93:57-60.

69. Schadler ED, Ortel B, Mehlis SL. Biologics for the primary care physician: Review and treatment of psoriasis. Disease-a-month : DM. 2019;65(3):51-90.
70. Fredriksson T, Pettersson U. Severe psoriasis--oral therapy with a new retinoid. Dermatologica. 1978;157(4):238-44.
71. Fleischer AB, Jr., Rapp SR, Reboussin DM, Vanarthos JC, Feldman SR. Patient measurement of psoriasis disease severity with a structured instrument. The Journal of investigative dermatology. 1994;102(6):967-9.
72. Gottlieb AB, Dann F. Comorbidities in Patients with Psoriasis. The American Journal of Medicine. 2009;122(12):1150.e1-.e9.
73. Veale DJ, Fearon U. The pathogenesis of psoriatic arthritis. The Lancet. 2018;391(10136):2273-84.
74. Chandran V. Genetics of Psoriasis and Psoriatic Arthritis. Indian J Dermatol. 55. India2010. p. 151-6.
75. Rahman P, Elder J. Genetic epidemiology of psoriasis and psoriatic arthritis. *Annals of the Rheumatic Diseases*. 2005;64(Suppl 2):ii37-ii9.
76. Elder JT, Nair RP, Guo SW, Henseler T, Christophers E, Voorhees JJ. The genetics of psoriasis. Archives of dermatology. 1994;130(2):216-24.
77. Nair RP, Duffin KC, Helms C, Ding J, Stuart PE, Goldgar D, et al. Genomewide Scan Reveals Association of Psoriasis with IL-23 and NF-κB Pathways. Nature genetics. 2009;41(2):199-204.
78. Murphy M, Kerr P, Grant-Kels JM. The histopathologic spectrum of psoriasis. Clinics in dermatology. 2007;25(6):524-8.
79. Salim N, Ahmad N, Musa SH, Hashim R, Tadros TF, Basri M. Nanoemulsion as a topical delivery system of antipsoriatic drugs. RSC Advances. 2016;6(8):6234-50.
80. Mayo Foundation for Medical Education and Research. How Psoriasis Develops 2020; (10 Aug 2018).
81. Hoffman MB, Hill D, Feldman SR. Current challenges and emerging drug delivery strategies for the treatment of psoriasis. Expert opinion on drug delivery. 2016;13(10):1461-73.
82. British Medical Association and Royal Pharmaceutical Society of Great Britain. Psoriasis: Treatment Summary. British National Formulary 71st Ed 2016.
83. Soleymani T, Hung T, Soung J. The role of vitamin D in psoriasis: a review. International journal of dermatology. 2015;54(4):383-92.
84. Sekhon S, Jeon C, Nakamura M, Afifi L, Yan D, Wu JJ, et al. Review of the mechanism of action of coal tar in psoriasis. The Journal of dermatological treatment. 2018;29(3):230-2.
85. Menter A, Griffiths CE. Current and future management of psoriasis. Lancet (London, England). 2007;370(9583):272-84.
86. Rapalli VK, Singhvi G, Dubey SK, Gupta G, Chellappan DK, Dua K. Emerging landscape in psoriasis management: From topical application to targeting biomolecules. Biomedicine & Pharmacotherapy. 2018;106:707-13.
87. Weinstein GD. Tazarotene gel: efficacy and safety in plaque psoriasis. Journal of the American Academy of Dermatology. 1997;37(2 Pt 3):S33-8.
88. Tang H, Lu JY, Zheng X, Yang Y, Reagan JD. The psoriasis drug monomethylfumarate is a potent nicotinic acid receptor agonist. Biochemical and biophysical research communications. 2008;375(4):562-5.
89. Krueger JG. The immunologic basis for the treatment of psoriasis with new biologic agents. Journal of the American Academy of Dermatology. 2002;46(1):1-23; quiz -6.
90. Rønholt K, Iversen L. Old and New Biological Therapies for Psoriasis. International journal of molecular sciences. 2017;18(11):2297.
91. Johnson-Huang LM, Lowes MA, Krueger JG. Putting together the psoriasis puzzle: an update on developing targeted therapies. Dis Model Mech. 2012;5(4):423-33.
92. Jenneck C, Novak N. The safety and efficacy of alefacept in the treatment of chronic plaque psoriasis. Therapeutics and clinical risk management. 2007;3(3):411-20.

93. Schmitt J, Zhang Z, Wozel G, Meurer M, Kirch W. Efficacy and tolerability of biologic and nonbiologic systemic treatments for moderate-to-severe psoriasis: meta-analysis of randomized controlled trials. The British journal of dermatology. 2008;159(3):513-26.
94. Fotiadou C, Lazaridou E, Sotiriou E, Ioannides D. Targeting IL-23 in psoriasis: current perspectives. Psoriasis (Auckl). 2018;8:1-5.
95. Nestle FO, Kaplan DH, Barker J. Psoriasis. New England Journal of Medicine. 2009;361(5):496-509.
96. Rafael A, Torres T. Topical therapy for psoriasis: a promising future. Focus on JAK and phosphodiesterase-4 inhibitors. European journal of dermatology : EJD. 2016;26(1):3-8.
97. Kofoed K, Skov L, Zachariae C. New drugs and treatment targets in psoriasis. Acta dermato-venereologica. 2015;95(2):133-9.
98. Wilks AF, Harpur AG, Kurban RR, Ralph SJ, Zurcher G, Ziemiecki A. Two novel protein-tyrosine kinases, each with a second phosphotransferase-related catalytic domain, define a new class of protein kinase. Mol Cell Biol. 1991;11(4):2057-65.
99. Hodge JA, Kawabata TT, Krishnaswami S, Clark JD, Telliez JB, Dowty ME, et al. The mechanism of action of tofacitinib - an oral Janus kinase inhibitor for the treatment of rheumatoid arthritis. Clinical and experimental rheumatology. 2016;34(2):318-28.
100. Schwartz DM, Kanno Y, Villarino A, Ward M, Gadina M, O'Shea JJ. JAK inhibition as a therapeutic strategy for immune and inflammatory diseases. Nature reviews Drug discovery. 2017;16(12):843-62.
101. Morales JK, Falanga YT, Depcrynski A, Fernando J, Ryan JJ. Mast cell homeostasis and the JAK–STAT pathway. Genes & Immunity. 2010;11(8):599-608.
102. David M, Gospodinov DK, Gheorghe N, Mateev GS, Rusinova MV, Hristakieva E, et al. Treatment of Plaque-Type Psoriasis With Oral CF101: Data from a Phase II/III Multicenter, Randomized, Controlled Trial. Journal of drugs in dermatology : JDD. 2016;15(8):931-8.
103. Mottok A, Steidl C. Biology of classical Hodgkin lymphoma: implications for prognosis and novel therapies. Blood. 2018;131(15):1654-65.
104. Groves FD, Linet MS, Travis LB, Devesa SS. Cancer surveillance series: non-Hodgkin's lymphoma incidence by histologic subtype in the United States from 1978 through 1995. J Natl Cancer Inst. 2000;92(15):1240-51.
105. Swerdlow S, Campo E, Harris N, Jaffe E, Pileri S, Stein H, et al. WHO Classification of Tumours of Haematopoietic and Lymphoid Tissues. 4 ed: Lyon: IARC Publications; 2008.
106. Matutes E. The 2017 WHO update on mature T- and natural killer (NK) cell neoplasms. International Journal of Laboratory Hematology. 2018;40(S1):97-103.
107. Willemze R, Hodak E, Zinzani PL, Specht L, Ladetto M. Primary cutaneous lymphomas: ESMO Clinical Practice Guidelines for diagnosis, treatment and follow-up. Ann Oncol. 2018;29(Suppl 4):iv30-iv40.
108. Criscione VD, Weinstock MA. Incidence of cutaneous T-cell lymphoma in the United States, 1973-2002. Archives of dermatology. 2007;143(7):854-9.
109. Imam MH, Shenoy PJ, Flowers CR, Phillips A, Lechowicz MJ. Incidence and survival patterns of cutaneous T-cell lymphomas in the United States. Leuk Lymphoma. 2013;54(4):752-9.
110. Lessin SR. Alibert lymphoma: renaming mycosis fungoides. Archives of dermatology. 145. United States 2009. p. 209-10.
111. Pulitzer M. Cutaneous T-cell Lymphoma. Clin Lab Med. 2017;37(3):527-46.
112. Hwang ST, Janik JE, Jaffe ES, Wilson WH. Mycosis fungoides and Sézary syndrome. The Lancet. 2008;371(9616):945-57.
113. Quaglino P, Pimpinelli N, Berti E, Calzavara-Pinton P, Alfonso Lombardo G, Rupoli S, et al. Time course, clinical pathways, and long-term hazards risk trends of disease progression in patients with classic mycosis fungoides: a multicenter, retrospective follow-up study from the Italian Group of Cutaneous Lymphomas. Cancer. 2012;118(23):5830-9.
114. Girardi M, Heald PW, Wilson LD. The Pathogenesis of Mycosis Fungoides. New England Journal of Medicine. 2004;350(19):1978-88.

115. Pérez C, Mondéjar R, García-Díaz N, Cereceda L, León A, Montes S, et al. Advanced-stage mycosis fungoides: role of the signal transducer and activator of transcription 3, nuclear factor-κB and nuclear factor of activated T cells pathways. The British journal of dermatology. 2020;182(1):147-55.
116. Willemze R, Cerroni L, Kempf W, Berti E, Facchetti F, Swerdlow SH, et al. The 2018 update of the WHO-EORTC classification for primary cutaneous lymphomas. Blood. 2019;133(16):1703-14.
117. Olsen E, Vonderheid E, Pimpinelli N, Willemze R, Kim Y, Knobler R, et al. Revisions to the staging and classification of mycosis fungoides and Sezary syndrome: a proposal of the International Society for Cutaneous Lymphomas (ISCL) and the cutaneous lymphoma task force of the European Organization of Research and Treatment of Cancer (EORTC). Blood. 2007;110(6):1713-22.
118. Hughes CF, Khot A, McCormack C, Lade S, Westerman DA, Twigger R, et al. Lack of durable disease control with chemotherapy for mycosis fungoides and Sezary syndrome: a comparative study of systemic therapy. Blood. 2015;125(1):71-81.
119. Akilov OE, Geskin L. Therapeutic advances in cutaneous T-cell lymphoma. Skin Therapy Lett. 2011;16(2):1-5.
120. Castellsague J, Kuiper JG, Pottegard A, Anveden Berglind I, Dedman D, Gutierrez L, et al. A cohort study on the risk of lymphoma and skin cancer in users of topical tacrolimus, pimecrolimus, and corticosteroids (Joint European Longitudinal Lymphoma and Skin Cancer Evaluation - JOELLE study). Clin Epidemiol. 2018;10:299-310.
121. Zackheim HS, Kashani-Sabet M, Amin S. Topical corticosteroids for mycosis fungoides. Experience in 79 patients. Archives of dermatology. 1998;134(8):949-54.
122. Kartan S, Shalabi D, O'Donnell M, Alpdogan SO, Sahu J, Shi W, et al. Response to Topical Corticosteroid Monotherapy in Mycosis Fungoides. Journal of the American Academy of Dermatology. 2020.
123. Geller S, Myskowski PL. Topical clobetasol propionate treatment and cutaneous adverse effects in patients with early-stage mycosis fungoides: an observational study. Cutis. 2020;105(5):E27-e32.
124. Lessin SR, Duvic M, Guitart J, Pandya AG, Strober BE, Olsen EA, et al. Topical chemotherapy in cutaneous T-cell lymphoma: positive results of a randomized, controlled, multicenter trial testing the efficacy and safety of a novel mechlorethamine, 0.02%, gel in mycosis fungoides. JAMA Dermatol. 2013;149(1):25-32.
125. Trautinger F, Eder J, Assaf C, Bagot M, Cozzio A, Dummer R, et al. European Organisation for Research and Treatment of Cancer consensus recommendations for the treatment of mycosis fungoides/Sezary syndrome - Update 2017. Eur J Cancer. 2017;77:57-74.
126. Alpdogan O, Kartan S, Johnson W, Sokol K, Porcu P. Systemic therapy of cutaneous T-cell lymphoma (CTCL). Chinese clinical oncology. 2019;8(1):10.
127. Heald P, Mehlmauer M, Martin AG, Crowley CA, Yocum RC, Reich SD. Topical bexarotene therapy for patients with refractory or persistent early-stage cutaneous T-cell lymphoma: results of the phase III clinical trial. Journal of the American Academy of Dermatology. 2003;49(5):801-15.
128. Breneman D, Duvic M, Kuzel T, Yocum R, Truglia J, Stevens VJ. Phase 1 and 2 trial of bexarotene gel for skin-directed treatment of patients with cutaneous T-cell lymphoma. Archives of dermatology. 2002;138(3):325-32.
129. Olsen EA, Hodak E, Anderson T, Carter JB, Henderson M, Cooper K, et al. Guidelines for phototherapy of mycosis fungoides and Sezary syndrome: A consensus statement of the United States Cutaneous Lymphoma Consortium. Journal of the American Academy of Dermatology. 2016;74(1):27-58.
130. Huber MA, Staib G, Pehamberger H, Scharffetter-Kochanek K. Management of refractory early-stage cutaneous T-cell lymphoma. Am J Clin Dermatol. 2006;7(3):155-69.

131. Deeths MJ, Chapman JT, Dellavalle RP, Zeng C, Aeling JL. Treatment of patch and plaque stage mycosis fungoides with imiquimod 5% cream. Journal of the American Academy of Dermatology. 2005;52(2):275-80.
132. Chong A, Loo WJ, Banney L, Grant JW, Norris PG. Imiquimod 5% cream in the treatment of mycosis fungoides--a pilot study. The Journal of dermatological treatment. 2004;15(2):118-9.
133. Dummer R, Urosevic M, Kempf W, Kazakov D, Burg G. Imiquimod induces complete clearance of a PUVA-resistant plaque in mycosis fungoides. Dermatology. 2003;207(1):116-8.
134. Rook AH, Gelfand JM, Wysocka M, Troxel AB, Benoit B, Surber C, et al. Topical resiquimod can induce disease regression and enhance T-cell effector functions in cutaneous T-cell lymphoma. Blood. 2015;126(12):1452-61.
135. Duvic M, Hymes K, Heald P, Breneman D, Martin AG, Myskowski P, et al. Bexarotene is effective and safe for treatment of refractory advanced-stage cutaneous T-cell lymphoma: multinational phase II-III trial results. J Clin Oncol. 2001;19(9):2456-71.
136. Duvic M, Martin AG, Kim Y, Olsen E, Wood GS, Crowley CA, et al. Phase 2 and 3 clinical trial of oral bexarotene (Targretin capsules) for the treatment of refractory or persistent early-stage cutaneous T-cell lymphoma. Archives of dermatology. 2001;137(5):581-93.
137. Devata S, Wilcox RA. Cutaneous T-Cell Lymphoma: A Review with a Focus on Targeted Agents. Am J Clin Dermatol. 2016;17(3):225-37.
138. Clark RA, Watanabe R, Teague JE, Schlapbach C, Tawa MC, Adams N, et al. Skin effector memory T cells do not recirculate and provide immune protection in alemtuzumab-treated CTCL patients. Science translational medicine. 2012;4(117):117ra7.
139. Lundin J, Hagberg H, Repp R, Cavallin-Stahl E, Freden S, Juliusson G, et al. Phase 2 study of alemtuzumab (anti-CD52 monoclonal antibody) in patients with advanced mycosis fungoides/Sezary syndrome. Blood. 2003;101(11):4267-72.
140. Perini GF, Pro B. Brentuximab Vedotin in CD30+ Lymphomas. Biol Ther. 2013;3:15-23.
141. Kim YH, Tavallaee M, Sundram U, Salva KA, Wood GS, Li S, et al. Phase II Investigator-Initiated Study of Brentuximab Vedotin in Mycosis Fungoides and Sezary Syndrome With Variable CD30 Expression Level: A Multi-Institution Collaborative Project. J Clin Oncol. 2015;33(32):3750-8.
142. Duvic M, Pinter-Brown LC, Foss FM, Sokol L, Jorgensen JL, Challagundla P, et al. Phase 1/2 study of mogamulizumab, a defucosylated anti-CCR4 antibody, in previously treated patients with cutaneous T-cell lymphoma. Blood. 2015;125(12):1883-9.
143. Lopez AT, Bates S, Geskin L. Current Status of HDAC Inhibitors in Cutaneous T-cell Lymphoma. Am J Clin Dermatol. 2018;19(6):805-19.
144. Whittaker SJ, Demierre MF, Kim EJ, Rook AH, Lerner A, Duvic M, et al. Final results from a multicenter, international, pivotal study of romidepsin in refractory cutaneous T-cell lymphoma. J Clin Oncol. 2010;28(29):4485-91.
145. Olsen EA, Kim YH, Kuzel TM, Pacheco TR, Foss FM, Parker S, et al. Phase IIb multicenter trial of vorinostat in patients with persistent, progressive, or treatment refractory cutaneous T-cell lymphoma. J Clin Oncol. 2007;25(21):3109-15.
146. Olsen E, Duvic M, Frankel A, Kim Y, Martin A, Vonderheid E, et al. Pivotal phase III trial of two dose levels of denileukin diftitox for the treatment of cutaneous T-cell lymphoma. J Clin Oncol. 2001;19(2):376-88.
147. Cope AC, Shen TY. The Stereochemistry of 1,4: 3,6-Dianhydrohexitol Derivatives1. Journal of the American Chemical Society. 1956;78(13):3177-82.
148. Jacquet F, Audinos R, Delmas M, Gaset A. Analytical techniques suitable for the study of the oxidation of a biomass-issued substrate: 4, 8-dihydroxy-2, 6-dioxabicyclo (3.3.0) octane (IR, 4S, 5R, 8R). Biomass. 1985;6(3):193-209.

149. Ledwidge MT, Ryan F, Kerins DM, O'Connell D, Cefali G, Harmon S, et al. In vivo impact of prodrug isosorbide-5-nicotinate-2-aspirinate on lipids and prostaglandin D2: is this a new immediate-release therapeutic option for niacin? Atherosclerosis. 2012;221(2):478-83.
150. Medina C, Harmon S, Inkielewicz I, Santos-Martinez MJ, Jones M, Cantwell P, et al. Differential inhibition of tumour cell-induced platelet aggregation by the nicotinate aspirin prodrug (ST0702) and aspirin. British journal of pharmacology. 2012;166(3):938-49.
151. Quilty F. Mechanistic Studies into the Effect of Deoxycholic Acid on Oesophageal Cancer Initiation and Progression [dissertation]. Dublin: Trinity College Dublin; 2015.
152. Madan RK, Levitt J. A review of toxicity from topical salicylic acid preparations. Journal of the American Academy of Dermatology. 2014;70(4):788-92.
153. Reiner Z, Catapano AL, De Backer G, Graham I, Taskinen MR, Wiklund O, et al. ESC/EAS Guidelines for the management of dyslipidaemias: the Task Force for the management of dyslipidaemias of the European Society of Cardiology (ESC) and the European Atherosclerosis Society (EAS). European heart journal. 2011;32(14):1769-818.
154. Hanson J, Gille A, Offermanns S. Role of HCA(2) (GPR109A) in nicotinic acid and fumaric acid ester-induced effects on the skin. Pharmacology & therapeutics. 2012;136(1):1-7.
155. Landray MJ, Haynes R, Hopewell JC, Parish S, Aung T, Tomson J, et al. Effects of extended-release niacin with laropiprant in high-risk patients. The New England journal of medicine. 2014;371(3):203-12.
156. Lloyd-Jones DM. Niacin and HDL cholesterol--time to face facts. The New England journal of medicine. 2014;371(3):271-3.
157. Gudjonsson JE, Johnston A, Dyson M, Valdimarsson H, Elder JT. Mouse models of psoriasis. The Journal of investigative dermatology. 2007;127(6):1292-308.
158. Lowe NJ, Breeding J, Kean C, Cohn ML. Psoriasiform dermatosis in a rhesus monkey. The Journal of investigative dermatology. 1981;76(2):141-3.
159. Jayo MJ, Zanolli MD, Jayo JM. Psoriatic plaques in Macaca fascicularis. Veterinary pathology. 1988;25(4):282-5.
160. Nestle FO, Nickoloff BJ. Animal models of psoriasis: a brief update. Journal of the European Academy of Dermatology and Venereology. 2006;20(s2):24-7.
161. van der Fits L, Mourits S, Voerman JS, Kant M, Boon L, Laman JD, et al. Imiquimod-induced psoriasis-like skin inflammation in mice is mediated via the IL-23/IL-17 axis. Journal of immunology (Baltimore, Md : 1950). 2009;182(9):5836-45.
162. Hawkes JE, Gudjonsson JE, Ward NL. The Snowballing Literature on Imiquimod-Induced Skin Inflammation in Mice: A Critical Appraisal. The Journal of investigative dermatology. 2017;137(3):546-9.
163. Grine L, Steeland S, Van Ryckeghem S, Ballegeer M, Lienenklaus S, Weiss S, et al. Topical imiquimod yields systemic effects due to unintended oral uptake. Scientific reports. 2016;6:20134.
164. Fukami T, Yokoi T. The Emerging Role of Human Esterases. Drug Metabolism and Pharmacokinetics. 2012;27(5):466-77.
165. Müller B, Kasper M, Surber C, Imanidis G. Permeation, metabolism and site of action concentration of nicotinic acid derivatives in human skin: Correlation with topical pharmacological effect. European Journal of Pharmaceutical Sciences. 2003;20(2):181-95.
166. Guzek DB, Kennedy AH, McNeill SC, Wakshull E, Potts RO. Transdermal drug transport and metabolism. I. Comparison of in vitro and in vivo results. Pharmaceutical research. 1989;6(1):33-9.
167. Rittirod T, Hatanaka T, Kagami N, Katayama K, Koizumi T. Simultaneous transport and metabolism of nicotinic acid derivatives in hairless mouse skin. Biol Pharm Bull. 1999;22(3):305-9.
168. Jia L, Liu X. The conduct of drug metabolism studies considered good practice (II): in vitro experiments. Current drug metabolism. 2007;8(8):822-9.
169. Goldminz AM, Au SC, Kim N, Gottlieb AB, Lizzul PF. NF-kappaB: an essential transcription factor in psoriasis. Journal of dermatological science. 2013;69(2):89-94.

170. Taniguchi K, Karin M. NF-κB, inflammation, immunity and cancer: coming of age. Nature Reviews Immunology. 2018;18(5):309-24.
171. Lizzul PF, Aphale A, Malaviya R, Sun Y, Masud S, Dombrovskiy V, et al. Differential Expression of Phosphorylated NF-κB/RelA in Normal and Psoriatic Epidermis and Downregulation of NF-κB in Response to Treatment with Etanercept. Journal of Investigative Dermatology. 2005;124(6):1275-83.
172. Georgescu SR, Tampa M, Caruntu C, Sarbu MI, Mitran CI, Mitran MI, et al. Advances in Understanding the Immunological Pathways in Psoriasis. International journal of molecular sciences. 2019;20(3):739.
173. Galimova E, Rätsep R, Traks T, Kingo K, Escott-Price V, Kõks S. Interleukin-10 family cytokines pathway: genetic variants and psoriasis. British Journal of Dermatology. 2017;176(6):1577-87.
174. Al-Balbeesi AO, Halwani M, Alanazi M, Elrobh M, Shaik JP, Khan AA, et al. Novel mutations in IL-10 promoter region -377 (C>T), -150 (C>A) and their association with psoriasis in the saudi population. Asian Pac J Cancer Prev. 2015;16(3):1247-50.
175. Sobhan MR, Farshchian M, Hoseinzadeh A, Ghasemibasir HR, Solgi G. Serum Levels of IL-10 and IL-22 Cytokines in Patients with Psoriasis. Iran J Immunol. 2016;13(4):317-23.
176. Colombo I, Sangiovanni E, Maggio R, Mattozzi C, Zava S, Corbett Y, et al. HaCaT Cells as a Reliable In Vitro Differentiation Model to Dissect the Inflammatory/Repair Response of Human Keratinocytes. Mediators of inflammation. 2017;2017:7435621.
177. Mosmann T. Rapid colorimetric assay for cellular growth and survival: application to proliferation and cytotoxicity assays. J Immunol Methods. 1983;65(1-2):55-63.
178. Tzeng TB, Fung HL. Pharmacokinetics of stereomeric 1,4:3,6-dianhydrohexitol mononitrates in rats. Pharmaceutical research. 1993;10(1):22-7.
179. Dillon GP, Gaynor JM, Khan D, Carolan CG, Ryder SA, Marquez JF, et al. Isosorbide-based cholinesterase inhibitors; replacement of 5-ester groups leading to increased stability. Bioorganic & medicinal chemistry. 2010;18(3):1045-53.
180. Liu J. Introduction to Nitrates. Nitrate Esters Chemistry and Technology. Singapore: Springer Singapore; 2019. p. 1-36.
181. Lipinski CA, Lombardo F, Dominy BW, Feeney PJ. Experimental and computational approaches to estimate solubility and permeability in drug discovery and development settings. Adv Drug Deliv Rev. 2001;46(1-3):3-26.
182. Wiedersberg S, Guy RH. Transdermal drug delivery: 30+ years of war and still fighting! Journal of Controlled Release. 2014;190:150-6.
183. Katare OP, Raza K, Singh B, Dogra S. Novel drug delivery systems in topical treatment of psoriasis: rigors and vigors. Indian journal of dermatology, venereology and leprology. 2010;76(6):612-21.
184. Sun L, Liu Z, Lin Z, Cun D, Tong HH, Yan R, et al. Comparison of normal versus imiquimod-induced psoriatic skin in mice for penetration of drugs and nanoparticles. Int J Nanomedicine. 2018;13:5625-35.
185. Lin YK, Yang SH, Chen CC, Kao HC, Fang JY. Using Imiquimod-Induced Psoriasis-Like Skin as a Model to Measure the Skin Penetration of Anti-Psoriatic Drugs. PLoS One. 2015;10(9):e0137890.
186. N'Da DD. Prodrug strategies for enhancing the percutaneous absorption of drugs. Molecules. 2014;19(12):20780-807.
187. Bos JD, Meinardi MM. The 500 Dalton rule for the skin penetration of chemical compounds and drugs. Exp Dermatol. 2000;9(3):165-9.
188. De Rie MA, Meinardi MM, Bos JD. Lack of efficacy of topical cyclosporin A in atopic dermatitis and allergic contact dermatitis. Acta dermato-venereologica. 1991;71(5):452-4.
189. Powles AV, Baker BS, McFadden J, Rutman AJ, Griffiths CE, Fry L, et al. Intralesional injection of cyclosporin in psoriasis. Lancet (London, England). 1988;1(8584):537.

190. Gazdar AF, Carney DN, Bunn PA, Russell EK, Jaffe ES, Schechter GP, et al. Mitogen requirements for the in vitro propagation of cutaneous T-cell lymphomas. Blood. 1980;55(3):409-17.
191. Cai Y, Fleming C, Yan J. New insights of T cells in the pathogenesis of psoriasis. Cell Mol Immunol. 2012;9(4):302-9.
192. Frohm M, Agerberth B, Ahangari G, Stahle-Backdahl M, Liden S, Wigzell H, et al. The expression of the gene coding for the antibacterial peptide LL-37 is induced in human keratinocytes during inflammatory disorders. The Journal of biological chemistry. 1997;272(24):15258-63.
193. Prinz JC. The role of T cells in psoriasis. Journal of the European Academy of Dermatology and Venereology : JEADV. 2003;17(3):257-70.
194. Ross SH, Cantrell DA. Signaling and Function of Interleukin-2 in T Lymphocytes. Annual Review of Immunology. 2018;36(1):411-33.
195. Gaffen SL, Liu KD. Overview of interleukin-2 function, production and clinical applications. Cytokine. 2004;28(3):109-23.
196. Fitch E, Harper E, Skorcheva I, Kurtz SE, Blauvelt A. Pathophysiology of psoriasis: recent advances on IL-23 and Th17 cytokines. Current rheumatology reports. 2007;9(6):461-7.
197. Di Cesare A, Di Meglio P, Nestle FO. The IL-23/Th17 Axis in the Immunopathogenesis of Psoriasis. Journal of Investigative Dermatology. 2009;129(6):1339-50.
198. Johansen C, Usher PA, Kjellerup RB, Lundsgaard D, Iversen L, Kragballe K. Characterization of the interleukin-17 isoforms and receptors in lesional psoriatic skin. The British journal of dermatology. 2009;160(2):319-24.
199. Calautti E, Avalle L, Poli V. Psoriasis: A STAT3-Centric View. International journal of molecular sciences. 2018;19(1).
200. Wolk K, Witte E, Wallace E, Docke WD, Kunz S, Asadullah K, et al. IL-22 regulates the expression of genes responsible for antimicrobial defense, cellular differentiation, and mobility in keratinocytes: a potential role in psoriasis. European journal of immunology. 2006;36(5):1309-23.
201. Zheng Y, Danilenko DM, Valdez P, Kasman I, Eastham-Anderson J, Wu J, et al. Interleukin-22, a T(H)17 cytokine, mediates IL-23-induced dermal inflammation and acanthosis. Nature. 2007;445(7128):648-51.
202. Trifari S, Kaplan CD, Tran EH, Crellin NK, Spits H. Identification of a human helper T cell population that has abundant production of interleukin 22 and is distinct from T(H)-17, T(H)1 and T(H)2 cells. Nat Immunol. 2009;10(8):864-71.
203. Benham H, Norris P, Goodall J, Wechalekar MD, FitzGerald O, Szentpetery A, et al. Th17 and Th22 cells in psoriatic arthritis and psoriasis. Arthritis Res Ther. 2013;15(5):R136-R.
204. Teng MWL, Bowman EP, McElwee JJ, Smyth MJ, Casanova J-L, Cooper AM, et al. IL-12 and IL-23 cytokines: from discovery to targeted therapies for immune-mediated inflammatory diseases. Nature medicine. 2015;21(7):719-29.
205. Watford WT, Hissong BD, Bream JH, Kanno Y, Muul L, O'Shea JJ. Signaling by IL-12 and IL-23 and the immunoregulatory roles of STAT4. Immunol Rev. 2004;202:139-56.
206. Ivanov, II, McKenzie BS, Zhou L, Tadokoro CE, Lepelley A, Lafaille JJ, et al. The orphan nuclear receptor RORgammat directs the differentiation program of proinflammatory IL-17+ T helper cells. Cell. 2006;126(6):1121-33.
207. Lowes MA, Russell CB, Martin DA, Towne JE, Krueger JG. The IL-23/T17 pathogenic axis in psoriasis is amplified by keratinocyte responses. Trends in immunology. 2013;34(4):174-81.
208. Bunn PA, Jr., Foss FM. T-cell lymphoma cell lines (HUT102 and HUT78) established at the National Cancer Institute: history and importance to understanding the biology, clinical features, and therapy of cutaneous T-cell lymphomas (CTCL) and adult T-cell leukemia-lymphomas (ATLL). J Cell Biochem Suppl. 1996;24:12-23.

209. Re GG, Waters C, Poisson L, Willingham MC, Sugamura K, Frankel AE. Interleukin 2 (IL-2) receptor expression and sensitivity to diphteria fusion toxin DAB389IL-2 in cultured hematopoietic cells. Cancer research. 1996;56(11):2590-5.
210. Verma NK, Davies AM, Long A, Kelleher D, Volkov Y. STAT3 knockdown by siRNA induces apoptosis in human cutaneous T-cell lymphoma line Hut78 via downregulation of Bcl-xL. Cell Mol Biol Lett. 2010;15(2):342-55.
211. Geltink RIK, Kyle RL, Pearce EL. Unraveling the Complex Interplay Between T Cell Metabolism and Function. Annual review of immunology. 2018;36:461-88.
212. Birsoy K, Wang T, Chen WW, Freinkman E, Abu-Remaileh M, Sabatini DM. An Essential Role of the Mitochondrial Electron Transport Chain in Cell Proliferation Is to Enable Aspartate Synthesis. Cell. 2015;162(3):540-51.
213. Mills EL, Kelly B, O'Neill LAJ. Mitochondria are the powerhouses of immunity. Nature Immunology. 2017;18(5):488-98.
214. Warburg O. On respiratory impairment in cancer cells. Science. 1956;124(3215):269-70.
215. Carr EL, Kelman A, Wu GS, Gopaul R, Senkevitch E, Aghvanyan A, et al. Glutamine uptake and metabolism are coordinately regulated by ERK/MAPK during T lymphocyte activation. Journal of immunology (Baltimore, Md : 1950). 2010;185(2):1037-44.
216. Fracchia KM, Walsh CM. Metabolic mysteries of the inflammatory response: T cell polarization and plasticity. Int Rev Immunol. 2015;34(1):3-18.
217. Chang C-H, Curtis JD, Maggi LB, Jr., Faubert B, Villarino AV, O'Sullivan D, et al. Posttranscriptional control of T cell effector function by aerobic glycolysis. Cell. 2013;153(6):1239-51.
218. Sena LA, Li S, Jairaman A, Prakriya M, Ezponda T, Hildeman DA, et al. Mitochondria are required for antigen-specific T cell activation through reactive oxygen species signaling. Immunity. 2013;38(2):225-36.
219. Franchina DG, Dostert C, Brenner D. Reactive Oxygen Species: Involvement in T Cell Signaling and Metabolism. Trends in immunology. 2018;39(6):489-502.
220. Mehta MM, Weinberg SE, Chandel NS. Mitochondrial control of immunity: beyond ATP. Nature Reviews Immunology. 2017;17(10):608-20.
221. Nathan C, Cunningham-Bussel A. Beyond oxidative stress: an immunologist's guide to reactive oxygen species. Nature reviews Immunology. 2013;13(5):349-61.
222. Li N, Ragheb K, Lawler G, Sturgis J, Rajwa B, Melendez JA, et al. Mitochondrial Complex I Inhibitor Rotenone Induces Apoptosis through Enhancing Mitochondrial Reactive Oxygen Species Production. Journal of Biological Chemistry. 2003;278(10):8516-25.
223. Murphy MP. How mitochondria produce reactive oxygen species. The Biochemical journal. 2009;417(1):1-13.
224. Lin X, Huang T. Oxidative stress in psoriasis and potential therapeutic use of antioxidants. Free Radic Res. 2016;50(6):585-95.
225. Gostner JM, Becker K, Fuchs D, Sucher R. Redox regulation of the immune response. Redox Rep. 2013;18(3):88-94.
226. Xu C, Kim N-G, Gumbiner BM. Regulation of protein stability by GSK3 mediated phosphorylation. Cell cycle (Georgetown, Tex). 2009;8(24):4032-9.
227. Herzig S, Shaw RJ. AMPK: guardian of metabolism and mitochondrial homeostasis. Nat Rev Mol Cell Biol. 2018;19(2):121-35.
228. Blagih J, Coulombe F, Vincent Emma E, Dupuy F, Galicia-Vázquez G, Yurchenko E, et al. The Energy Sensor AMPK Regulates T Cell Metabolic Adaptation and Effector Responses In Vivo. Immunity. 2015;42(1):41-54.
229. Verbist KC, Wang R, Green DR. T cell metabolism and the immune response. Semin Immunol. 2012;24(6):399-404.
230. Michalek RD, Gerriets VA, Jacobs SR, Macintyre AN, MacIver NJ, Mason EF, et al. Cutting edge: distinct glycolytic and lipid oxidative metabolic programs are essential for

effector and regulatory CD4+ T cell subsets. Journal of immunology (Baltimore, Md : 1950). 2011;186(6):3299-303.
231. Palacios EH, Weiss A. Function of the Src-family kinases, Lck and Fyn, in T-cell development and activation. Oncogene. 2004;23(48):7990-8000.
232. Fayard E, Tintignac LA, Baudry A, Hemmings BA. Protein kinase B/Akt at a glance. J Cell Sci. 2005;118(Pt 24):5675-8.
233. Zhang M, Zhang X. The role of PI3K/AKT/FOXO signaling in psoriasis. Arch Dermatol Res. 2019;311(2):83-91.
234. Huang T, Lin X, Meng X, Lin M. Phosphoinositide-3 kinase/protein kinase-B/mammalian target of rapamycin pathway in psoriasis pathogenesis. A potential therapeutic target? Acta dermato-venereologica. 2014;94(4):371-9.
235. Heinrich PC, Behrmann I, Haan S, Hermanns HM, Muller-Newen G, Schaper F. Principles of interleukin (IL)-6-type cytokine signalling and its regulation. The Biochemical journal. 2003;374(Pt 1):1-20.
236. Camporeale A, Poli V. IL-6, IL-17 and STAT3: a holy trinity in auto-immunity? Front Biosci (Landmark Ed). 2012;17:2306-26.
237. Perez C, Gonzalez-Rincon J, Onaindia A, Almaraz C, Garcia-Diaz N, Pisonero H, et al. Mutated JAK kinases and deregulated STAT activity are potential therapeutic targets in cutaneous T-cell lymphoma. Haematologica. 100. Italy2015. p. e450-3.
238. Long A, O'Connell M, Liskamp RM, Kelleher D. Regulation of CD3 expression in a protein kinase C isozyme-deficient T-cell line. Immunology. 1993;80(4):654-7.
239. Rovedo MA, Krett NL, Rosen ST. Inhibition of glycogen synthase kinase-3 increases the cytotoxicity of enzastaurin. The Journal of investigative dermatology. 2011;131(7):1442-9.
240. Kelleher D, Pandol SJ, Kagnoff MF. Phorbol myristate acetate induces IL-2 secretion by HUT 78 cells by a mechanism independent of protein kinase C translocation. Immunology. 1988;65(3):351-5.
241. Pagliacci MC, Spinozzi F, Migliorati G, Fumi G, Smacchia M, Grignani F, et al. Genistein inhibits tumour cell growth in vitro but enhances mitochondrial reduction of tetrazolium salts: a further pitfall in the use of the MTT assay for evaluating cell growth and survival. Eur J Cancer. 1993;29a(11):1573-7.
242. Garcia R, Bowman TL, Niu G, Yu H, Minton S, Muro-Cacho CA, et al. Constitutive activation of Stat3 by the Src and JAK tyrosine kinases participates in growth regulation of human breast carcinoma cells. Oncogene. 2001;20(20):2499-513.
243. June CH, Ledbetter JA, Gillespie MM, Lindsten T, Thompson CB. T-cell proliferation involving the CD28 pathway is associated with cyclosporine-resistant interleukin 2 gene expression. Molecular and cellular biology. 1987;7(12):4472-81.
244. Antonioli L, Colucci R, Pellegrini C, Giustarini G, Sacco D, Tirotta E, et al. The AMPK enzyme-complex: from the regulation of cellular energy homeostasis to a possible new molecular target in the management of chronic inflammatory disorders. Expert Opinion on Therapeutic Targets. 2016;20(2):179-91.
245. Kelly B, Tannahill GM, Murphy MP, O'Neill LA. Metformin Inhibits the Production of Reactive Oxygen Species from NADH:Ubiquinone Oxidoreductase to Limit Induction of Interleukin-1beta (IL-1beta) and Boosts Interleukin-10 (IL-10) in Lipopolysaccharide (LPS)-activated Macrophages. The Journal of biological chemistry. 2015;290(33):20348-59.
246. Wang X, Li R, Zhao X, Yu X, Sun Q. Metformin Promotes HaCaT Cell Apoptosis through Generation of Reactive Oxygen Species via Raf-1-ERK1/2-Nrf2 Inactivation. Inflammation. 2018;41(3):948-58.
247. Brand MD, Nicholls DG. Assessing mitochondrial dysfunction in cells. The Biochemical journal. 2011;435(2):297-312.
248. Berridge MV, Tan AS. Characterization of the cellular reduction of 3-(4,5-dimethylthiazol-2-yl)-2,5-diphenyltetrazolium bromide (MTT): subcellular localization, substrate dependence, and involvement of mitochondrial electron transport in MTT reduction. Arch Biochem Biophys. 1993;303(2):474-82.

249. Srivastava P, Panda D. Rotenone inhibits mammalian cell proliferation by inhibiting microtubule assembly through tubulin binding. Febs j. 2007;274(18):4788-801.
250. Jiang Q, Yan Z, Feng J. Neurotrophic factors stabilize microtubules and protect against rotenone toxicity on dopaminergic neurons. The Journal of biological chemistry. 2006;281(39):29391-400.
251. Yi JS, Holbrook BC, Michalek RD, Laniewski NG, Grayson JM. Electron Transport Complex I Is Required for CD8+ T Cell Function. The Journal of Immunology. 2006;177(2):852-62.
252. Ozay EI, Sherman HL, Mello V, Trombley G, Lerman A, Tew GN, et al. Rotenone Treatment Reveals a Role for Electron Transport Complex I in the Subcellular Localization of Key Transcriptional Regulators During T Helper Cell Differentiation. Frontiers in immunology. 2018;9:1284.
253. Mohammed F, Gorla M, Bisoyi V, Tammineni P, Sepuri NBV. Rotenone-induced reactive oxygen species signal the recruitment of STAT3 to mitochondria. FEBS Lett. 2020;594:1403-12.
254. Lee M, Hirpara JL, Eu JQ, Sethi G, Wang L, Goh BC, et al. Targeting STAT3 and oxidative phosphorylation in oncogene-addicted tumors. Redox Biol. 2019;25:101073.
255. Cheng X, Peuckert C, Wolfl S. Essential role of mitochondrial Stat3 in p38(MAPK) mediated apoptosis under oxidative stress. Scientific reports. 2017;7(1):15388.
256. Genini D, Brambilla L, Laurini E, Merulla J, Civenni G, Pandit S, et al. Mitochondrial dysfunction induced by a SH2 domain-targeting STAT3 inhibitor leads to metabolic synthetic lethality in cancer cells. Proceedings of the National Academy of Sciences of the United States of America. 2017;114(25):E4924-E33.
257. Erlich TH, Sharkia I, Landolina N, Assayag M, Goldberger O, Berkman N, et al. Modulation of allergic responses by mitochondrial STAT3 inhibitors. Allergy. 2018;73(11):2160-71.
258. Mandal T, Bhowmik A, Chatterjee A, Chatterjee U, Chatterjee S, Ghosh MK. Reduced phosphorylation of Stat3 at Ser-727 mediated by casein kinase 2 - protein phosphatase 2A enhances Stat3 Tyr-705 induced tumorigenic potential of glioma cells. Cellular signalling. 2014;26(8):1725-34.
259. Fendt S-M, Bell EL, Keibler MA, Davidson SM, Wirth GJ, Fiske B, et al. Metformin decreases glucose oxidation and increases the dependency of prostate cancer cells on reductive glutamine metabolism. Cancer research. 2013;73(14):4429-38.
260. Wheaton WW, Weinberg SE, Hamanaka RB, Soberanes S, Sullivan LB, Anso E, et al. Metformin inhibits mitochondrial complex I of cancer cells to reduce tumorigenesis. Elife. 2014;3:e02242-e.
261. Han YH, Kim SH, Kim SZ, Park WH. Antimycin A as a mitochondrial electron transport inhibitor prevents the growth of human lung cancer A549 cells. Oncol Rep. 2008;20(3):689-93.
262. Giorgi-Coll S, Amaral AI, Hutchinson PJA, Kotter MR, Carpenter KLH. Succinate supplementation improves metabolic performance of mixed glial cell cultures with mitochondrial dysfunction. Scientific reports. 2017;7(1):1003.
263. Ehinger JK, Piel S, Ford R, Karlsson M, Sjövall F, Frostner EÅ, et al. Cell-permeable succinate prodrugs bypass mitochondrial complex I deficiency. Nature communications. 2016;7(1):12317.
264. Mills EL, Kelly B, Logan A, Costa ASH, Varma M, Bryant CE, et al. Succinate Dehydrogenase Supports Metabolic Repurposing of Mitochondria to Drive Inflammatory Macrophages. Cell. 2016;167(2):457-70.e13.
265. Gui DY, Sullivan LB, Luengo A, Hosios AM, Bush LN, Gitego N, et al. Environment Dictates Dependence on Mitochondrial Complex I for NAD+ and Aspartate Production and Determines Cancer Cell Sensitivity to Metformin. Cell Metab. 2016;24(5):716-27.

266. MacPherson S, Horkoff M, Gravel C, Hoffmann T, Zuber J, Lum JJ. STAT3 Regulation of Citrate Synthase Is Essential during the Initiation of Lymphocyte Cell Growth. Cell reports. 2017;19(5):910-8.
267. Milkovic L, Cipak Gasparovic A, Cindric M, Mouthuy P-A, Zarkovic N. Short Overview of ROS as Cell Function Regulators and Their Implications in Therapy Concepts. Cells. 2019;8(8):793.
268. Forman HJ, Zhang H, Rinna A. Glutathione: overview of its protective roles, measurement, and biosynthesis. Mol Aspects Med. 2009;30(1-2):1-12.
269. Aquilano K, Baldelli S, Ciriolo MR. Glutathione: new roles in redox signaling for an old antioxidant. Frontiers in Pharmacology. 2014;5:196.
270. Mokhtari V, Afsharian P, Shahhoseini M, Kalantar SM, Moini A. A Review on Various Uses of N-Acetyl Cysteine. Cell J. 2017;19(1):11-7.
271. Mayer MP, Le Breton L. Hsp90: breaking the symmetry. Mol Cell. 2015;58(1):8-20.
272. Schopf FH, Biebl MM, Buchner J. The HSP90 chaperone machinery. Nature Reviews Molecular Cell Biology. 2017;18:345.
273. Whitesell L, Lindquist SL. HSP90 and the chaperoning of cancer. Nat Rev Cancer. 2005;5(10):761-72.
274. Csermely P, Schnaider T, Soti C, Prohaszka Z, Nardai G. The 90-kDa molecular chaperone family: structure, function, and clinical applications. A comprehensive review. Pharmacology & therapeutics. 1998;79(2):129-68.
275. Nathan DF, Vos MH, Lindquist S. In vivo functions of the Saccharomyces cerevisiae Hsp90 chaperone. Proceedings of the National Academy of Sciences. 1997;94(24):12949.
276. Johnson JL. Evolution and function of diverse Hsp90 homologs and cochaperone proteins. Biochimica et biophysica acta. 2012;1823(3):607-13.
277. Gupta RS. Phylogenetic analysis of the 90 kD heat shock family of protein sequences and an examination of the relationship among animals, plants, and fungi species. Mol Biol Evol. 1995;12(6):1063-73.
278. Chen B, Zhong D, Monteiro A. Comparative genomics and evolution of the HSP90 family of genes across all kingdoms of organisms. BMC genomics. 2006;7:156.
279. Wayne N, Bolon DN. Dimerization of Hsp90 is required for in vivo function. Design and analysis of monomers and dimers. The Journal of biological chemistry. 2007;282(48):35386-95.
280. Sidera K, Patsavoudi E. HSP90 inhibitors: current development and potential in cancer therapy. Recent Pat Anticancer Drug Discov. 2014;9(1):1-20.
281. Pick E, Kluger Y, Giltnane JM, Moeder C, Camp RL, Rimm DL, et al. High HSP90 expression is associated with decreased survival in breast cancer. Cancer research. 2007;67(7):2932-7.
282. Wang J, Cui S, Zhang X, Wu Y, Tang H. High expression of heat shock protein 90 is associated with tumor aggressiveness and poor prognosis in patients with advanced gastric cancer. PLoS One. 2013;8(4):e62876.
283. Thomas X, Campos L, Mounier C, Cornillon J, Flandrin P, Le QH, et al. Expression of heat-shock proteins is associated with major adverse prognostic factors in acute myeloid leukemia. Leuk Res. 2005;29(9):1049-58.
284. Le Brazidec JY, Kamal A, Busch D, Thao L, Zhang L, Timony G, et al. Synthesis and biological evaluation of a new class of geldanamycin derivatives as potent inhibitors of Hsp90. Journal of medicinal chemistry. 2004;47(15):3865-73.
285. Tian ZQ, Liu Y, Zhang D, Wang Z, Dong SD, Carreras CW, et al. Synthesis and biological activities of novel 17-aminogeldanamycin derivatives. Bioorganic & medicinal chemistry. 2004;12(20):5317-29.
286. Ferraro M, D'Annessa I, Moroni E, Morra G, Paladino A, Rinaldi S, et al. Allosteric Modulators of HSP90 and HSP70: Dynamics Meets Function through Structure-Based Drug Design. Journal of medicinal chemistry. 2019;62(1):60-87.

287. Butler LM, Ferraldeschi R, Armstrong HK, Centenera MM, Workman P. Maximizing the Therapeutic Potential of HSP90 Inhibitors. Mol Cancer Res. 2015;13(11):1445-51.
288. Marcu MG, Schulte TW, Neckers L. Novobiocin and related coumarins and depletion of heat shock protein 90-dependent signaling proteins. J Natl Cancer Inst. 2000;92(3):242-8.
289. Zhang Z, Banerjee M, Davis RE, Blagg BSJ. Mitochondrial-targeted Hsp90 C-terminal inhibitors manifest anti-proliferative activity. Bioorganic & medicinal chemistry letters. 2019;29(22):126676.
290. Yu XM, Shen G, Neckers L, Blake H, Holzbeierlein J, Cronk B, et al. Hsp90 inhibitors identified from a library of novobiocin analogues. J Am Chem Soc. 2005;127(37):12778-9.
291. Burlison JA, Avila C, Vielhauer G, Lubbers DJ, Holzbeierlein J, Blagg BS. Development of novobiocin analogues that manifest anti-proliferative activity against several cancer cell lines. J Org Chem. 2008;73(6):2130-7.
292. Oh SH, Woo JK, Yazici YD, Myers JN, Kim WY, Jin Q, et al. Structural basis for depletion of heat shock protein 90 client proteins by deguelin. J Natl Cancer Inst. 2007;99(12):949-61.
293. Kim HS, Hong M, Lee SC, Lee HY, Suh YG, Oh DC, et al. Ring-truncated deguelin derivatives as potent Hypoxia Inducible Factor-1alpha (HIF-1alpha) inhibitors. Eur J Med Chem. 2015;104:157-64.
294. Sato N, Yamamoto T, Sekine Y, Yumioka T, Junicho A, Fuse H, et al. Involvement of heat-shock protein 90 in the interleukin-6-mediated signaling pathway through STAT3. Biochemical and biophysical research communications. 2003;300(4):847-52.
295. Basu S, Binder RJ, Ramalingam T, Srivastava PK. CD91 is a common receptor for heat shock proteins gp96, hsp90, hsp70, and calreticulin. Immunity. 2001;14(3):303-13.
296. Kakeda M, Arock M, Schlapbach C, Yawalkar N. Increased expression of heat shock protein 90 in keratinocytes and mast cells in patients with psoriasis. Journal of the American Academy of Dermatology. 2014;70(4):683-90.e1.
297. Stenderup K, Rosada C, Gavillet B, Vuagniaux G, Dam TN. Debio 0932, a new oral Hsp90 inhibitor, alleviates psoriasis in a xenograft transplantation model. Acta dermato-venereologica. 2014;94(6):672-6.
298. Lv J, Zhou D, Wang Y, Sun W, Zhang C, Xu J, et al. Effects of luteolin on treatment of psoriasis by repressing HSP90. Int Immunopharmacol. 2020;79:106070.
299. Caprini E, Cristofoletti C, Arcelli D, Fadda P, Citterich MH, Sampogna F, et al. Identification of key regions and genes important in the pathogenesis of sezary syndrome by combining genomic and expression microarrays. Cancer research. 2009;69(21):8438-46.
300. Fischer TC, Gellrich S, Muche JM, Sherev T, Audring H, Neitzel H, et al. Genomic aberrations and survival in cutaneous T cell lymphomas. The Journal of investigative dermatology. 2004;122(3):579-86.
301. Salgado R, Servitje O, Gallardo F, Vermeer MH, Ortiz-Romero PL, Karpova MB, et al. Oligonucleotide array-CGH identifies genomic subgroups and prognostic markers for tumor stage mycosis fungoides. The Journal of investigative dermatology. 2010;130(4):1126-35.
302. Sibbesen NA, Kopp KL, Litvinov IV, Jønson L, Willerslev-Olsen A, Fredholm S, et al. Jak3, STAT3, and STAT5 inhibit expression of miR-22, a novel tumor suppressor microRNA, in cutaneous T-Cell lymphoma. Oncotarget. 2015;6(24):20555-69.
303. Zhang Q, Raghunath PN, Vonderheid E, Odum N, Wasik MA. Lack of phosphotyrosine phosphatase SHP-1 expression in malignant T-cell lymphoma cells results from methylation of the SHP-1 promoter. Am J Pathol. 2000;157(4):1137-46.
304. Brender C, Nielsen M, Kaltoft K, Mikkelsen G, Zhang Q, Wasik M, et al. STAT3-mediated constitutive expression of SOCS-3 in cutaneous T-cell lymphoma. Blood. 2001;97(4):1056-62.

305. Walia R, Yeung CCS. An Update on Molecular Biology of Cutaneous T Cell Lymphoma. Frontiers in oncology. 2020;9:1558.
306. Ghazawi FM, Alghazawi N, Le M, Netchiporouk E, Glassman SJ, Sasseville D, et al. Environmental and Other Extrinsic Risk Factors Contributing to the Pathogenesis of Cutaneous T Cell Lymphoma (CTCL). Frontiers in Oncology. 2019;9:300.
307. Woetmann A, Lovato P, Eriksen KW, Krejsgaard T, Labuda T, Zhang Q, et al. Nonmalignant T cells stimulate growth of T-cell lymphoma cells in the presence of bacterial toxins. Blood. 2007;109(8):3325-32.
308. Lindahl LM, Willerslev-Olsen A, Gjerdrum LMR, Nielsen PR, Blümel E, Rittig AH, et al. Antibiotics inhibit tumor and disease activity in cutaneous T-cell lymphoma. Blood. 2019;134(13):1072-83.
309. Dulmage BO, Kong BY, Holzem K, Guitart J. What Is New in CTCL—Pathogenesis, Diagnosis, and Treatments. Current Dermatology Reports. 2018;7(2):91-8.
310. Chung CG, Poligone B. Cutaneous T cell Lymphoma: an Update on Pathogenesis and Systemic Therapy. Curr Hematol Malig Rep. 2015;10(4):468-76.
311. Campbell JJ, Clark RA, Watanabe R, Kupper TS. Sezary syndrome and mycosis fungoides arise from distinct T-cell subsets: a biologic rationale for their distinct clinical behaviors. Blood. 2010;116(5):767-71.
312. Jawed SI, Myskowski PL, Horwitz S, Moskowitz A, Querfeld C. Primary cutaneous T-cell lymphoma (mycosis fungoides and Sézary syndrome): Part I. Diagnosis: Clinical and histopathologic features and new molecular and biologic markers. Journal of the American Academy of Dermatology. 2014;70(2):205.e1-.e16.
313. Rittig AH, Lindahl LM, Johansen C, Celis P, Odum N, Iversen L, et al. The MicroRNA Expression Profile Differs Between Erythrodermic Mycosis Fungoides and Sezary Syndrome. Acta dermato-venereologica. 2019;99(12):1148-53.
314. Ralfkiaer U, Lindahl LM, Litman T, Gjerdrum LM, Ahler CB, Gniadecki R, et al. MicroRNA expression in early mycosis fungoides is distinctly different from atopic dermatitis and advanced cutaneous T-cell lymphoma. Anticancer Res. 2014;34(12):7207-17.
315. Krejsgaard T, Odum N, Geisler C, Wasik MA, Woetmann A. Regulatory T cells and immunodeficiency in mycosis fungoides and Sézary syndrome. Leukemia. 2012;26(3):424-32.
316. Berger CL, Wang N, Christensen I, Longley J, Heald P, Edelson RL. The immune response to class I-associated tumor-specific cutaneous T-cell lymphoma antigens. The Journal of investigative dermatology. 1996;107(3):392-7.
317. Abeni D, Frontani M, Sampogna F, Sera F, Bolli S, Corona R, et al. Circulating CD8+ lymphocytes, white blood cells, and survival in patients with mycosis fungoides. The British journal of dermatology. 2005;153(2):324-30.
318. Heald P, Rook A, Perez M, Wintroub B, Knobler R, Jegasothy B, et al. Treatment of erythrodermic cutaneous T-cell lymphoma with extracorporeal photochemotherapy. Journal of the American Academy of Dermatology. 1992;27(3):427-33.
319. Saed G, Fivenson DP, Naidu Y, Nickoloff BJ. Mycosis Fungoides Exhibits a Th1-Type Cell-Mediated Cytokine Profile Whereas Sezary Syndrome Express a Th2-Type Profile. Journal of Investigative Dermatology. 1994;103(1):29-33.
320. Axelrod PI, Lorber B, Vonderheid EC. Infections complicating mycosis fungoides and Sezary syndrome. Jama. 1992;267(10):1354-8.
321. Berger CL, Tigelaar R, Cohen J, Mariwalla K, Trinh J, Wang N, et al. Cutaneous T-cell lymphoma: malignant proliferation of T-regulatory cells. Blood. 2005;105(4):1640-7.
322. Shevach EM. Mechanisms of foxp3+ T regulatory cell-mediated suppression. Immunity. 2009;30(5):636-45.
323. Choi J, Goh G, Walradt T, Hong BS, Bunick CG, Chen K, et al. Genomic landscape of cutaneous T cell lymphoma. Nature genetics. 2015;47(9):1011-9.
324. Fujii K. New Therapies and Immunological Findings in Cutaneous T-Cell Lymphoma. Front Oncol. 2018;8:198.

325. Olsen EA, Rosen ST, Vollmer RT, Variakojis D, Roenigk HH, Jr., Diab N, et al. Interferon alfa-2a in the treatment of cutaneous T cell lymphoma. Journal of the American Academy of Dermatology. 1989;20(3):395-407.
326. Sugaya M, Tokura Y, Hamada T, Tsuboi R, Moroi Y, Nakahara T, et al. Phase II study of i.v. interferon-gamma in Japanese patients with mycosis fungoides. J Dermatol. 2014;41(1):50-6.
327. Netchiporouk E, Litvinov IV, Moreau L, Gilbert M, Sasseville D, Duvic M. Deregulation in STAT signaling is important for cutaneous T-cell lymphoma (CTCL) pathogenesis and cancer progression. Cell Cycle. 2014;13(21):3331-5.
328. Nielsen M, Kaltoft K, Nordahl M, Röpke C, Geisler C, Mustelin T, et al. Constitutive activation of a slowly migrating isoform of Stat3 in mycosis fungoides: Tyrphostin AG490 inhibits Stat3 activation and growth of mycosis fungoides tumor cell lines. Proceedings of the National Academy of Sciences. 1997;94(13):6764.
329. Krejsgaard T, Ralfkiaer U, Clasen-Linde E, Eriksen KW, Kopp KL, Bonefeld CM, et al. Malignant Cutaneous T-Cell Lymphoma Cells Express IL-17 Utilizing the Jak3/Stat3 Signaling Pathway. Journal of Investigative Dermatology. 2011;131(6):1331-8.
330. Vieyra-Garcia PA, Wei T, Naym DG, Fredholm S, Fink-Puches R, Cerroni L, et al. STAT3/5-Dependent IL9 Overexpression Contributes to Neoplastic Cell Survival in Mycosis Fungoides. Clin Cancer Res. 2016;22(13):3328-39.
331. Eriksen KW, Kaltoft K, Mikkelsen G, Nielsen M, Zhang Q, Geisler C, et al. Constitutive STAT3-activation in Sezary syndrome: tyrphostin AG490 inhibits STAT3-activation, interleukin-2 receptor expression and growth of leukemic Sezary cells. Leukemia. 2001;15(5):787-93.
332. Bastidas Torres AN, Cats D, Mei H, Szuhai K, Willemze R, Vermeer MH, et al. Genomic analysis reveals recurrent deletion of JAK-STAT signaling inhibitors HNRNPK and SOCS1 in mycosis fungoides. Genes, Chromosomes and Cancer. 2018;57(12):653-64.
333. McGirt LY, Jia P, Baerenwald DA, Duszynski RJ, Dahlman KB, Zic JA, et al. Whole-genome sequencing reveals oncogenic mutations in mycosis fungoides. Blood. 2015;126(4):508-19.
334. Wozniak MB, Villuendas R, Bischoff JR, Aparicio CB, Martínez Leal JF, de La Cueva P, et al. Vorinostat interferes with the signaling transduction pathway of T-cell receptor and synergizes with phosphoinositide-3 kinase inhibitors in cutaneous T-cell lymphoma. Haematologica. 2010;95(4):613-21.
335. Bali P, Pranpat M, Bradner J, Balasis M, Fiskus W, Guo F, et al. Inhibition of histone deacetylase 6 acetylates and disrupts the chaperone function of heat shock protein 90: a novel basis for antileukemia activity of histone deacetylase inhibitors. The Journal of biological chemistry. 2005;280(29):26729-34.
336. Glaser KB. HDAC inhibitors: clinical update and mechanism-based potential. Biochemical pharmacology. 2007;74(5):659-71.
337. Yu X, Guo ZS, Marcu MG, Neckers L, Nguyen DM, Chen GA, et al. Modulation of p53, ErbB1, ErbB2, and Raf-1 expression in lung cancer cells by depsipeptide FR901228. J Natl Cancer Inst. 2002;94(7):504-13.
338. Golubovskaya V, Wu L. Different Subsets of T Cells, Memory, Effector Functions, and CAR-T Immunotherapy. Cancers (Basel). 2016;8(3):36.
339. Kittipongdaja W, Wu X, Garner J, Liu X, Komas SM, Hwang ST, et al. Rapamycin Suppresses Tumor Growth and Alters the Metabolic Phenotype in T-Cell Lymphoma. Journal of Investigative Dermatology. 2015;135(9):2301-8.
340. Kremer M, Sliva K, Klemke C-D, Schnierle BS. Cutaneous T-cell lymphoma cells are sensitive to rapamycin. Experimental Dermatology. 2010;19(9):800-5.
341. Jain S, Stroopinsky D, Yin L, Rosenblatt J, Alam M, Bhargava P, et al. Mucin 1 is a potential therapeutic target in cutaneous T-cell lymphoma. Blood. 2015;126(3):354-62.
342. Schieke S, Roy S, Khan H, Nihal A, Buethe P. Metabolic dynamics control invasion and dissemination of cutaneous T-cell lymphoma. European Journal of Cancer. 2018;101:S5-S6.

343. Minet E, Mottet D, Michel G, Roland I, Raes M, Remacle J, et al. Hypoxia-induced activation of HIF-1: role of HIF-1alpha-Hsp90 interaction. FEBS Lett. 1999;460(2):251-6.
344. Khan H, Anshu A, Prasad A, Roy S, Jeffery J, Kittipongdaja W, et al. Metabolic Rewiring in Response to Biguanides Is Mediated by mROS/HIF-1a in Malignant Lymphocytes. Cell reports. 2019;29(10):3009-18.e4.
345. Netchiporouk E, Gantchev J, Tsang M, Thibault P, Watters AK, Hughes J-DM, et al. Analysis of CTCL cell lines reveals important differences between mycosis fungoides/Sézary syndrome vs. HTLV-1(+) leukemic cell lines. Oncotarget. 2017;8(56):95981-98.
346. Thaler S, Burger AM, Schulz T, Brill B, Bittner A, Oberholzer PA, et al. Establishment of a mouse xenograft model for mycosis fungoides. Exp Dermatol. 2004;13(7):406-12.
347. Kaltoft K, Bisballe S, Dyrberg T, Boel E, Rasmussen PB, Thestrup-Pedersen K. Establishment of two continuous T-cell strains from a single plaque of a patient with mycosis fungoides. In Vitro Cell Dev Biol. 1992;28a(3 Pt 1):161-7.
348. Krejsgaard T, Vetter-Kauczok CS, Woetmann A, Lovato P, Labuda T, Eriksen KW, et al. Jak3- and JNK-dependent vascular endothelial growth factor expression in cutaneous T-cell lymphoma. Leukemia. 2006;20(10):1759-66.
349. Starkebaum G, Loughran TP, Jr., Waters CA, Ruscetti FW. Establishment of an IL-2 independent, human T-cell line possessing only the p70 IL-2 receptor. Int J Cancer. 1991;49(2):246-53.
350. Duvic M. CD30+ Neoplasms of the Skin. Current Hematologic Malignancy Reports. 2011;6(4):245.
351. Soltan MY, Sumarni U, Assaf C, Langer P, Reidel U, Eberle J. Key Role of Reactive Oxygen Species (ROS) in Indirubin Derivative-Induced Cell Death in Cutaneous T-Cell Lymphoma Cells. International journal of molecular sciences. 2019;20(5):1158.
352. Gough DJ, Corlett A, Schlessinger K, Wegrzyn J, Larner AC, Levy DE. Mitochondrial STAT3 supports Ras-dependent oncogenic transformation. Science (New York, NY). 2009;324(5935):1713-6.
353. Tolcher A, Flaherty K, Shapiro GI, Berlin J, Witzig T, Habermann T, et al. A First-in-Human Phase I Study of OPB-111077, a Small-Molecule STAT3 and Oxidative Phosphorylation Inhibitor, in Patients with Advanced Cancers. Oncologist. 2018;23(6):658-e72.
354. Yoo C, Kang J, Lim HY, Kim JH, Lee M-A, Lee K-H, et al. Phase I Dose-Finding Study of OPB-111077, a Novel STAT3 Inhibitor, in Patients with Advanced Hepatocellular Carcinoma. Cancer Res Treat. 2019;51(2):510-8.
355. Jones M, Wang J, Harmon S, Kling B, Heilmann J, Gilmer JF. Novel Selective Butyrylcholinesterase Inhibitors Incorporating Antioxidant Functionalities as Potential Bimodal Therapeutics for Alzheimer's Disease. Molecules. 2016;21(4):440.
356. Carolan CG, Dillon GP, Gaynor JM, Reidy S, Ryder SA, Khan D, et al. Isosorbide-2-carbamate esters: potent and selective butyrylcholinesterase inhibitors. Journal of medicinal chemistry. 2008;51(20):6400-9.
357. Carolan CG, Dillon GP, Khan D, Ryder SA, Gaynor JM, Reidy S, et al. Isosorbide-2-benzyl carbamate-5-salicylate, a peripheral anionic site binding subnanomolar selective butyrylcholinesterase inhibitor. Journal of medicinal chemistry. 2010;53(3):1190-9.
358. Gaynor JM, Dillon GP, Reidy S, Gilmer JF. Synthesis and structure activity relationships (SAR) of a new class of potent and selective butyrylcholinesterase inhibitors. Chem Biol Interact. 2005;157-158:380-1.
359. Ghosh AK, Brindisi M. Organic carbamates in drug design and medicinal chemistry. Journal of medicinal chemistry. 2015;58(7):2895-940.
360. Li Z, Hogan KA, Cai C, Rieth S. Human Health Effects of Biphenyl: Key Findings and Scientific Issues. Environ Health Perspect. 2016;124(6):703-12.
361. Thode C, Woetmann A, Wandall HH, Carlsson MC, Qvortrup K, Kauczok CS, et al. Malignant T Cells Secrete Galectins and Induce Epidermal Hyperproliferation and

Disorganized Stratification in a Skin Model of Cutaneous T-Cell Lymphoma. Journal of Investigative Dermatology. 2015;135(1):238-46.
362. Krejsgaard T, Lindahl LM, Mongan NP, Wasik MA, Litvinov IV, Iversen L, et al. Malignant inflammation in cutaneous T-cell lymphoma—a hostile takeover. Seminars in Immunopathology. 2017;39(3):269-82.
363. Boumahdi S, de Sauvage FJ. The great escape: tumour cell plasticity in resistance to targeted therapy. Nature Reviews Drug Discovery. 2020;19(1):39-56.
364. Andrique L, Poglio S, Prochazkova-Carlotti M, Kadin ME, Giese A, Idrissi Y, et al. Intrahepatic Xenograft of Cutaneous T-Cell Lymphoma Cell Lines: A Useful Model for Rapid Biological and Therapeutic Evaluation. The American Journal of Pathology. 2016;186(7):1775-85.

Appendix

Target/control	DMSO Raw Data		ST0702 Raw Data		DMSO Average	ST0702 Average	% Change
Reference Spot	8593489	8987076	9034522	9694402	8790282.5	9364462	6.53
p38 α T180/182	1015282	488430	569859	477561	751856	523710	-30.34
ERK 1/2 T202/Y204, T185/Y187	372632	364211	477561	503979	368421.5	490770	33.21
JNK 1/2/3 T183/Y185, T221/Y223	1904609	1888524	1760649	1675724	1896566.5	1718186.5	-9.41
GSK 3 α/β S21/S9	4091773	4289200	3659526	3935112	4190486.5	3797319	-9.38
p53 S392	703362	708628	809345	793163	705995	801254	13.49
Reference Spot	10965098	10853196	9746377	10331302	10909147	10038839.5	-7.98
EGF R Y1086	969810	670757	686894	474094	820283.5	580494	-29.23
MSK 1/2 S276/S360	513658	505818	536494	544821	509738	540657.5	6.07
AMKα1 T183	2594111	2843948	1503589	1623598	2719029.5	1563593.5	-42.49
Akt 1/2/3 S473	889780	982863	631767	628905	936321.5	630336	-32.68
Akt 1/2/3 T308	785268	782754	945632	900789	784011	923210.5	17.75
p53 S46	832260	825673	943220	996177	828966.5	969698.5	16.98
TOR S2448	781958	835429	1026968	1043047	808693.5	1035007.5	27.99
CREB S133	5909342	5552024	6570552	6289630	5730683	6430091	12.20
HSP27 S78/S82	753787	567110	718320	641771	660448.5	680045.5	2.97
AMKα2 T172	788484	747421	731297	822234	767952.5	776765.5	1.15
β-catenin	376387	397581	440317	371591	386984	405954	4.90
p70 S6 kinase T389	1056758	996163	1226708	1081124	1026460.5	1153916	12.42
p53 S15	610654	672617	601060	648333	641635.5	624696.5	-2.64
c-Jun S63	637806	612187	690371	671452	624996.5	680911.5	8.95
Src Y419	631889	626970	568677	559328	629429.5	564002.5	-10.39
Lyn Y397	1293974	1142934	930230	923083	1218454	926656.5	-23.95
Lck Y394	440968	387725	307261	269777	414346.5	288519	-30.37
STAT2 Y689	662825	666646	504611	546446	664735.5	525528.5	-20.94
STAT5a Y694	460488	514362	466122	449887	487425	458004.5	-6.04
p70 S6 kinase T421/S424	1246707	1190329	1399172	1233801	1218518	1316486.5	8.04
RSK 1/2/3 S380/S386/S377	842930	866943	840925	930267	854936.5	885596	3.59

eNOS S1177	716337	697384	741034	745466	706860.5	743250	5.15
Fyn Y420	326785	363344	276521	269012	345064.5	272766.5	-20.95
Yes Y426	498291	430246	293993	261665	464268.5	277829	-40.16
Fgr Y412	355321	283662	167684	172084	319491.5	169884	-46.83
STAT6 Y641	530314	546292	397070	383014	538303	390042	-27.54
STAT5b Y699	514291	523047	431684	462009	518669	446846.5	-13.85
STAT3 Y705	907494	912770	680905	695459	910132	688182	-24.39
p27 T198	675211	670238	424990	466590	672724.5	445790	-33.73
PLC-γ1 Y783	725707	694579	703418	637302	710143	670360	-5.60
Hck Y411	629654	695756	493663	523001	662705	508332	-23.29
Chk-2 T68	1134976	1096520	797022	765980	1115748	781501	-29.96
FAK Y397	1246087	1221441	708921	734071	1233764	721496	-41.52
PDGF Rβ Y751	358669	337933	229109	248520	348301	238814.5	-31.43
STAT5a/b Y694/Y699	823542	917236	734360	818877	870389	776618.5	-10.77
STAT3 S727	1829086	1857425	1629700	1579847	1843255.5	1604773.5	-12.94
WNK1 T60	1920537	1771176	1508247	1521736	1845856.5	1514991.5	-17.92
PYK2 Y402	812128	755061	660761	588061	783594.5	624411	-20.31
Reference Spot	10615066	10620945	13511404	10620945	10618005.5	12066174.5	13.64
PRAS40 T246	3316130	2787519	2149781	1545821	3051824.5	1847801	-39.45
PBS (Negative Control)	382925	470082	287611	335256	426503.5	311433.5	-26.98
HSP60	3673183	3732059	3709022	3771780	3702621	3740401	1.02

Figure A1: Raw Data from HuT78 phosphokinase array (results outlined in Figure 3.7)

Target/control	**Basal**	**IL-2 + DMSO**	**IL-2 + ST0702 (Duplicates)**		**ST0702 Average**	**% change**
Reference Spot	10589517.5	10455778.5	9581526	10290349	9935937.5	-4.97
p38 α T180/182	570002.5	298268.5	469414	451922	460668	54.45
ERK 1/2 T202/Y204, T185/Y187	202553.5	263222	250102	274588.5	262345.25	-0.33
JNK 1/2/3 T183/Y185, T221/Y223	798910	663095	694181.5	623073.5	658627.5	-0.67
GSK 3 α/β S21/S9	3002852	4196769.5	3136961	2541799.5	2839380.25	-32.34
p53 S392	190819.5	203448.5	145293	160563.5	152928.25	-24.83
Reference Spot	11288405	10641367	10867614.5	11278184.5	11072899.5	4.06
EGF R Y1086	98024.5	72548	76174.5	70193.5	73184	0.88

MSK 1/2 S276/S360	619714	492576.5	533961	562020	547990.5	11.25
AMKα1 T183	757826	684333	297993.5	314234.5	306114	-55.27
Akt 1/2/3 S473	244290.5	362525.5	274480.5	216740	245610.25	-32.25
Akt 1/2/3 T308	122318	141387	131456	162237.5	146846.75	3.86
p53 S46	263013.5	265653	181249.5	227739.5	204494.5	-23.02
TOR S2448	187128	223678	135306	150927.5	143116.75	-36.02
CREB S133	2274742	2217748	1819786	2941469.5	2380627.75	7.34
HSP27 S78/S82	954037.5	844085.5	1362887.5	1364842.5	1363865	61.58
AMKα2 T172	250128	233035.5	193715.5	207430.5	200573	-13.93
β-catenin	97929	157572.5	97895	82101.5	89998.25	-42.88
p70 S6 kinase T389	72075	140074.5	119440.5	116627.5	118034	-15.73
p53 S15	60032.5	72738.5	71771	67197.5	69484.25	-4.47
c-Jun S63	174082.5	195531	209603	222340.5	215971.75	10.45
Src Y419	2191076.5	2436415	1498595	2898511.5	2198553.25	-9.76
Lyn Y397	281638.5	312711	276903	337025	306964	-1.84
Lck Y394	140888.5	115272	198909.5	190716.5	194813	69.00
STAT2 Y689	376885.5	331450.5	295744.5	317172.5	306458.5	-7.54
STAT5a Y694	178644	3787300	2655129.5	2829782	2742455.75	-27.59
p70 S6 kinase T421/S424	67475	97543	68570	60751.5	64660.75	-33.71
RSK 1/2/3 S380/S386/S377	91661	115539	144140.5	122981	133560.75	15.60
eNOS S1177	118977.5	132133.5	115072	126521	120796.5	-8.58
Fyn Y420	559794	640350	352134.5	485998	419066.25	-34.56
Yes Y426	199491	200460	194309.5	234166.5	214238	6.87
Fgr Y412	53051.5	44130.5	47781	58572.5	53176.75	20.50
STAT6 Y641	254713.5	323410	210665.5	237617.5	224141.5	-30.69
STAT5b Y699	249871	3513247.5	2315018.5	2425302.5	2370160.5	-32.54
STAT3 Y705	117202.5	357683.5	193046.5	195636.5	194341.5	-45.67
p27 T198	1576046.5	2090504	2055878	1861739	1958808.5	-6.30
PLC-γ1 Y783	145478.5	235674.5	196835.5	216930	206882.75	-12.22
Hck Y411	263908	297374.5	247735.5	227316	237525.75	-20.13
Chk-2 T68	340932.5	361083	299298	274669	286983.5	-20.52
FAK Y397	770715	691314.5	729838	802628.5	766233.25	10.84
PDGF Rβ Y751	129041.5	97007	64318.5	71867.5	68093	-29.81
STAT5a/b Y694/Y699	321003	5045529	3588451.5	3616811	3602631.25	-28.60

STAT3 S727	289595.5	603987.5	346137.5	306341.5	326239.5	-45.99
WNK1 T60	516304	821318.5	567517	455349.5	511433.25	-37.73
PYK2 Y402	205027	190395.5	192799.5	187534.5	190167	-0.12
Reference Spot	9556271	9581499	9142302	8744513.5	8943407.75	-6.66
PRAS40 T246	439676.5	385446.5	425262	361949	393605.5	2.12
PBS (Negative Control)	62633	83905	50864	25472	38168	-54.51
HSP60	2064428.5	2846045.5	2234100.5	2559840	2396970.25	-15.78

Figure A2: Raw Data from PBMC array (results outlined in Figure 3.5)

Thesis Compounds				
Code	**Compound**	**MW (g/mol)**	**Structure**	**Chemical Formula**
1 (ST0702)	Isosorbide-2-aspirinate-5-nicotinate	413.38	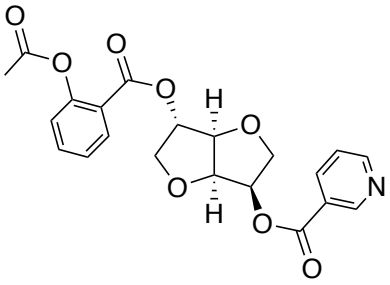	$C_{21}H_{19}NO_8$
2 (ISAL)	Isosorbide-2-salicylate-5-nicotinate	371.35	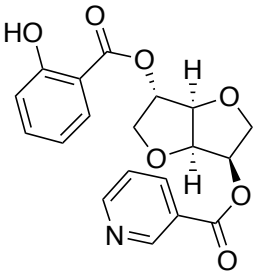	$C_{19}H_{17}NO_7$
3 (ST0701)	Isosorbide-2-aspirinate-5-salicylate	428.39	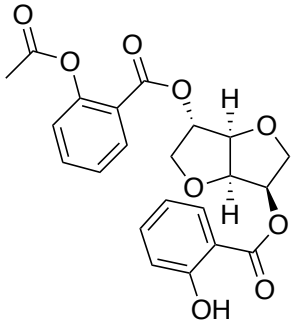	$C_{22}H_{20}O_9$
4	Isosorbide-2 aspirinate-5-isonicotinate	413.38	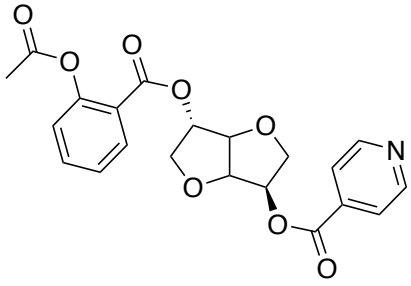	$C_{21}H_{19}NO_8$

5	Isosorbide-5-nicotinate	251.24	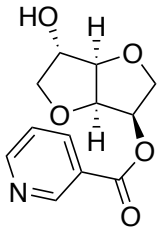	$C_{12}H_{13}NO_5$
6	Isosorbide-2-salicylate-	266.25	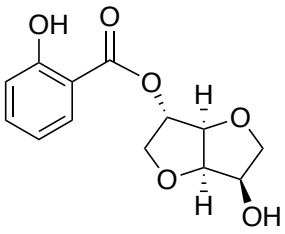	$C_{13}H_{14}O_6$
7	Isosorbide-2-aspirinate	308.29	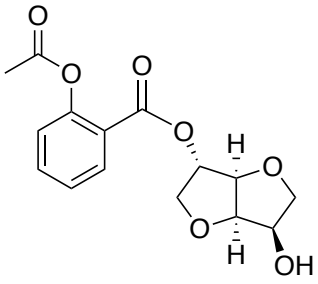	$C_{15}H_{16}O_7$
8	Isosorbide mononitrate	191.14	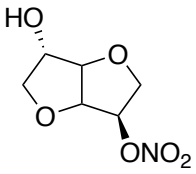	$C_6H_9NO_6$
9a	Isosorbide-2-acetate-5-nitrate	233.18	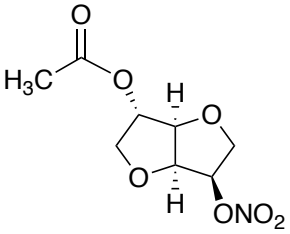	$C_8H_{11}NO_7$
9b	Isosorbide-2-propionate-5-nitrate	247.20	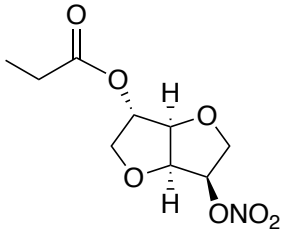	$C_9H_{13}NO_7$

9c	Isosorbide-2-butyrate-5-nitrate	261.23	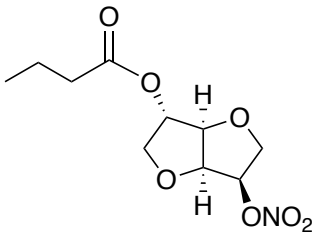	$C_{10}H_{15}NO_7$
9d	Isosorbide-2-valeroate-5-nitrate	275.26	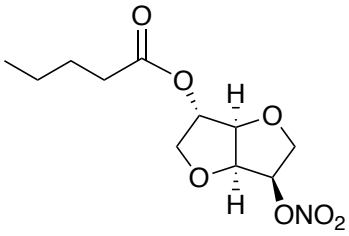	$C_{11}H_{17}NO_7$
9e	Isosorbide-2-benzoate-5-nitrate	295.25	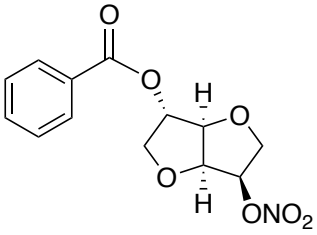	$C_{13}H_{13}NO$
10a	Isosorbide-2-acetate	188.18	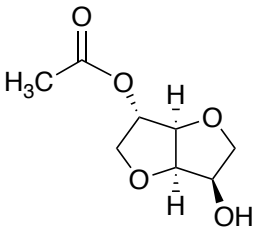	$C_8H_{12}O_5$
10b	Isosorbide-2-propionate	202.21	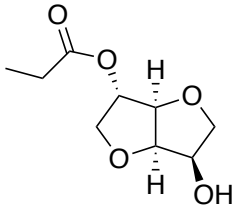	$C_9H_{14}O_5$
10c	Isosorbide-2-butyrate	216.23	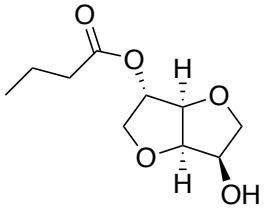	$C_{10}H_{16}O_5$

10d	Isosorbide-2-valeroate	230.26	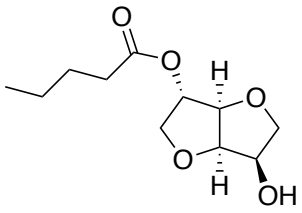	$C_{11}H_{18}O_5$
10e	Isosorbide-2-benzoate	250.25	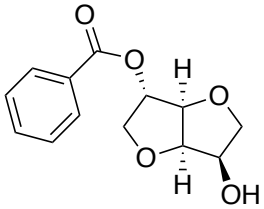	$C_{13}H_{14}O_5$
11a	Isosorbide-2-acetate-5-nicotinate	293.28	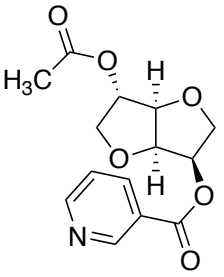	$C_{14}H_{15}NO_6$
11b	Isosorbide-2-propionate-5-nicotinate	307.30	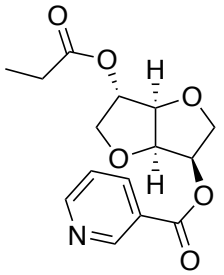	$C_{15}H_{17}NO_6$
11c	Isosorbide-2-butyrate-5-nicotinate	321.33	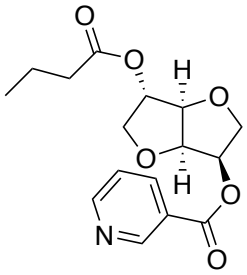	$C_{16}H_{19}NO_6$

11d	Isosorbide-2-valeroate-5-nicotinate	335.36	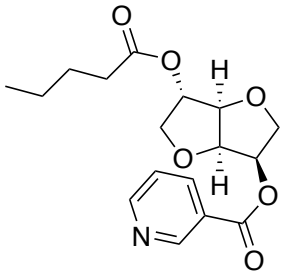	$C_{17}H_{21}NO_6$
11e	Isosorbide-2-benzoate-5-nicotinate	355.35	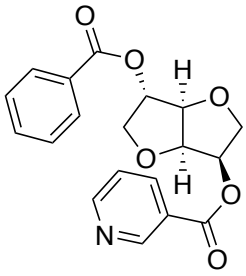	$C_{19}H_{17}NO_6$
12	Isosorbide-2-nicotinate-5-nitrate	296.24	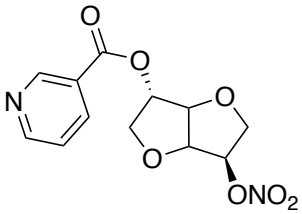	$C_{12}H_{12}N_2O_7$
13	Isosorbide-2-nicotinate	251.24	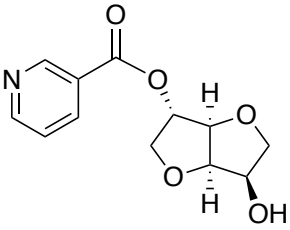	$C_{12}H_{13}NO_5$
14	Isosorbide-2-nicotinate-5-benzoate	355.35	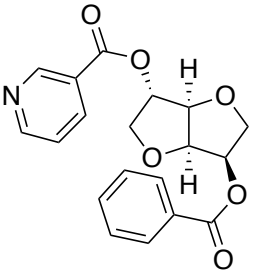	$C_{19}H_{17}NO_6$

15	Isosorbide-2-benzoate-5-isonicotinate	355.35	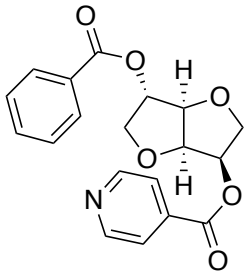	$C_{19}H_{17}NO_6$
16	Isosorbide-2,5-dinicotinate	356.33	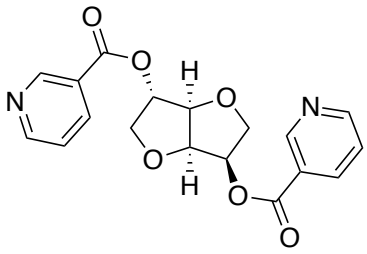	$C_{18}H_{16}N_2O_6$
17	Isomannide	146.14	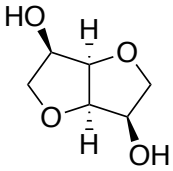	$C_6H_{10}O_4$
18a	Isomannide-2-acetate	188.18	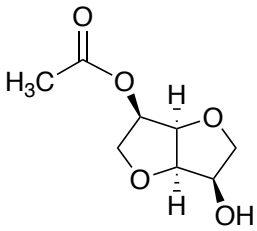	$C_8H_{12}O_5$
18b	Isomannide-2-propionate	202.21	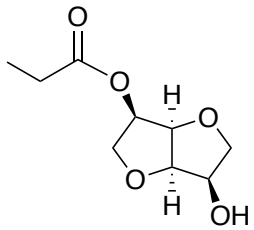	$C_9H_{14}O_5$
18c	Isomannide -2-butyrate	216.23	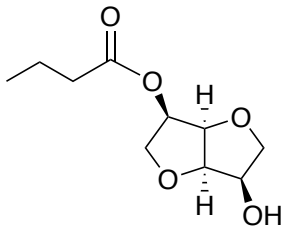	$C_{10}H_{16}O_5$

18d	Isomannide -2-valeroate	230.26	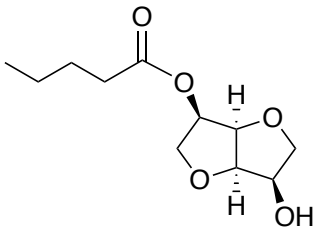	$C_{11}H_{18}O_5$
18e	Isomannide -2-benzoate	250.25	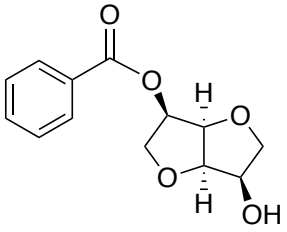	$C_{13}H_{14}O_5$
18f	Isomannide -2-aspirinate	308.29	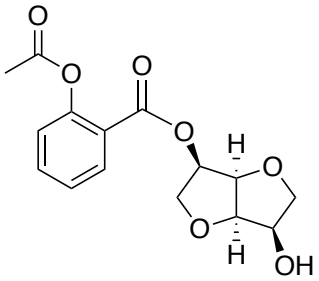	$C_{15}H_{16}O_7$
18g	Isomannide-2-methoxybenzoate	280.28	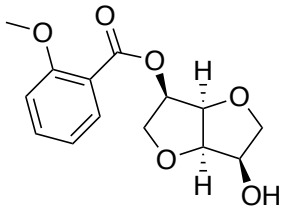	$C_{14}H_{16}O_6$
19a	Isomannide-2-acetate-5-nicotinate	293.28	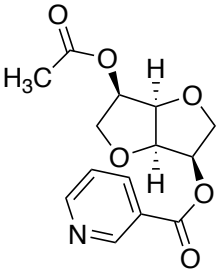	$C_{14}H_{15}NO_6$
19b	Isomannide-2-propionate-5-nicotinate	307.30	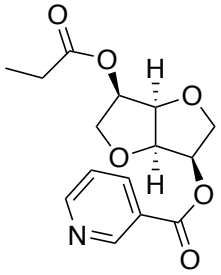	$C_{15}H_{17}NO_6$

19c	Isomannide-2-butyrate-5-nicotinate	321.33	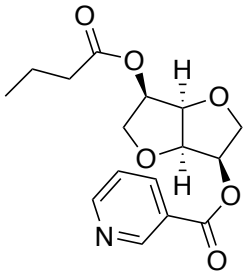	$C_{16}H_{19}NO_6$
19d	Isomannide-2-valeroate-5-nicotinate	335.36	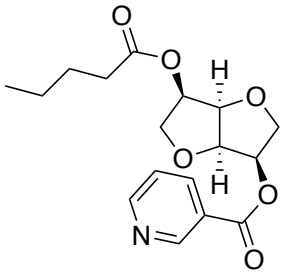	$C_{17}H_{21}NO_6$
19e	Isomannide-2-benzoate-5-nicotinate	355.35	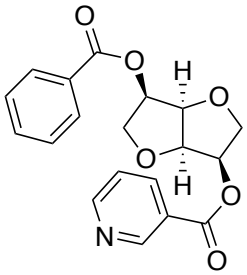	$C_{19}H_{17}NO_6$
19f	Isomannide-2-aspirinate-5-nicotinate	413.38	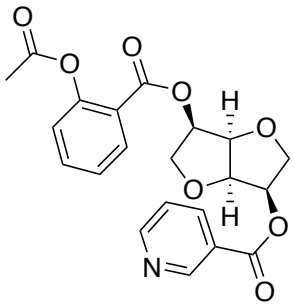	$C_{21}H_{19}NO_8$
19g	Isomannide-2-methoxybenzoate-5-nicotinate	385.37	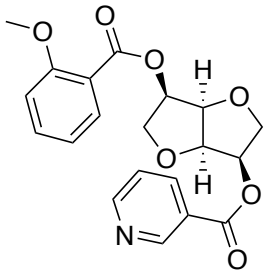	$C_{20}H_{19}NO_7$

20	Isosorbide-2-benzyloxybenzoate-5-nitrate	401.37	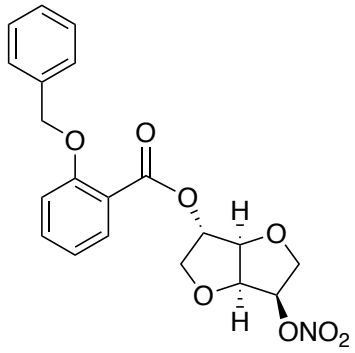	$C_{20}H_{19}NO_8$
21	Isosorbide-2-benzyloxybenzoate	356.37	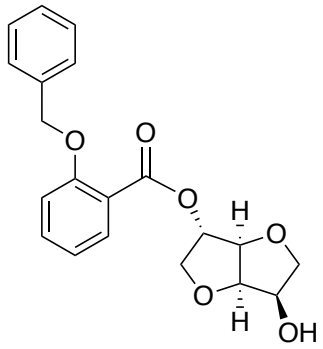	$C_{20}H_{20}O_6$
22	Isosorbide-2-benzyloxybenzoate-5-nicotinate	461.47	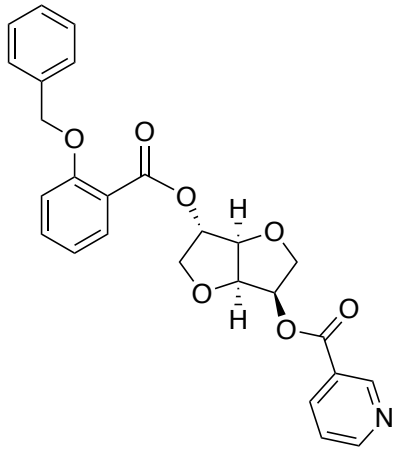	$C_{26}H_{23}NO_7$
23	Isosorbide-5-salicylate	266.25	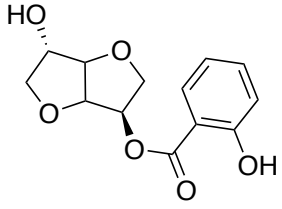	$C_{13}H_{14}O_6$

24	Isosorbide-5-aspirinate	308.29	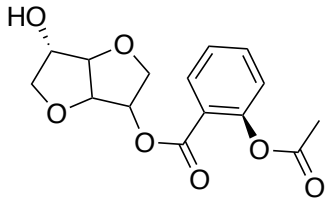	$C_{15}H_{16}O_7$
25	Isosorbide-2-aspirinate-5-nitrate	353.28	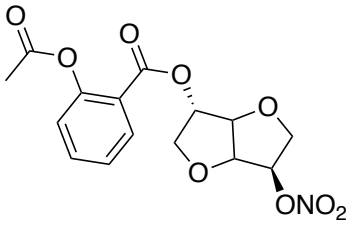	$C_{15}H_{15}NO_9$
26	Isosorbide-2-aspirinate-5-(3-toluate)	426.42	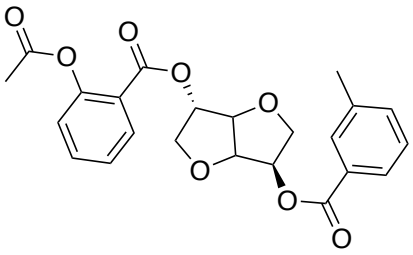	$C_{23}H_{22}O_8$
27	Isosorbide-2-aspirinate-5-(2-toluate)	426.42	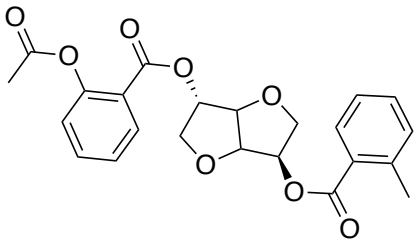	$C_{23}H_{22}O_8$
28	Isosorbide-2-aspirinate-5-(*p*-nitrobenzoate)	457.39	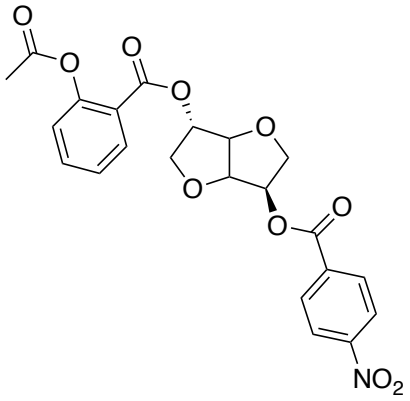	$C_{22}H_{19}NO_{10}$

29	Isosorbide-2-aspirinate-5-acetate	350.32	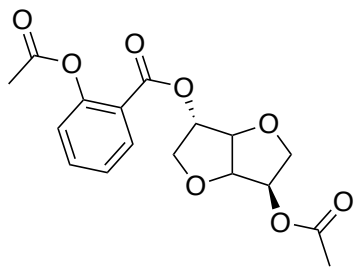	$C_{17}H_{18}O_8$
30	Isosorbide-2-aspirinate-5-(2-chloro-6-methylpyridine)	461.85	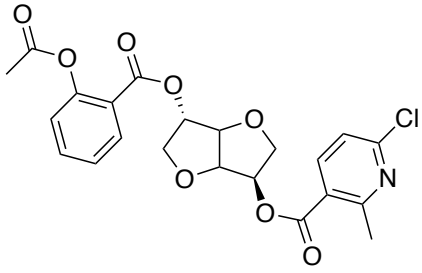	$C_{22}H_{20}ClNO_8$
31	Isosorbide-2-aspirinate-5-(6-chloronicotinate)	447.82	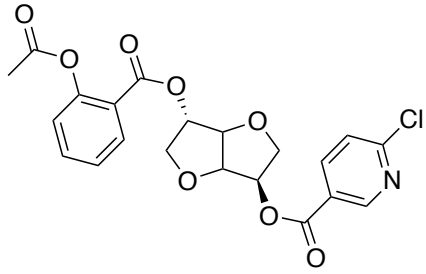	$C_{21}H_{18}ClNO_8$
32	Isosorbide-2-aspirinate-5-(2-methoxybenzoate)	442.42	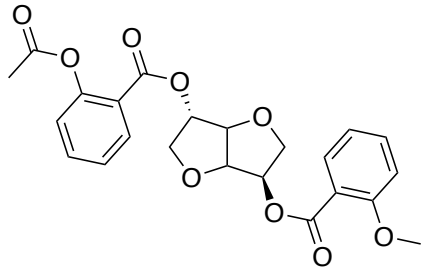	$C_{23}H_{22}O_9$
33	Isosorbide-2-aspirinate-5-(4-methoxy)benzoate	442.42	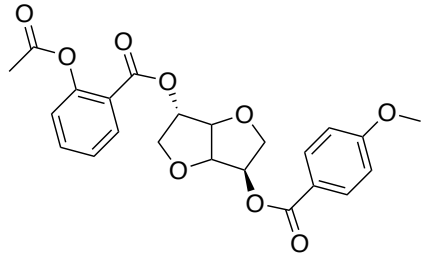	$C_{23}H_{22}O_9$

34	Isosorbide-2-aspirinate-5-(2,5-diethoxybenzoate)	500.50	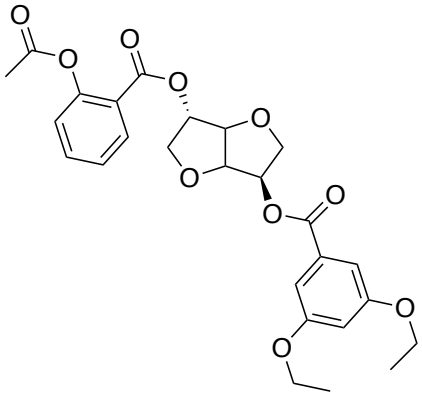	$C_{26}H_{28}O_{10}$
35	Isosorbide-2-aspirinate-5-(4-nitromethyl) benzoate	471.42	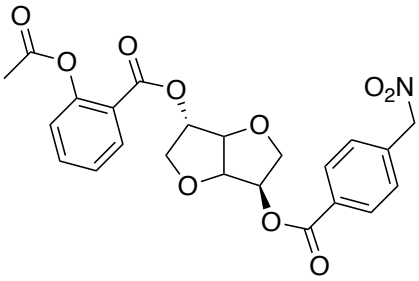	$C_{23}H_{21}NO_{10}$
36	Isosorbide-2-aspirinate-5-(3-chloromethyl) benzoate	460.86	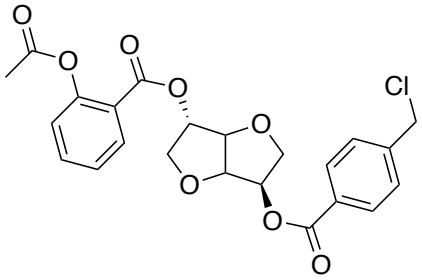	$C_{23}H_{21}ClO_8$
37	Isosorbide-2-aspirinate-5-biphenyl ester	488.49	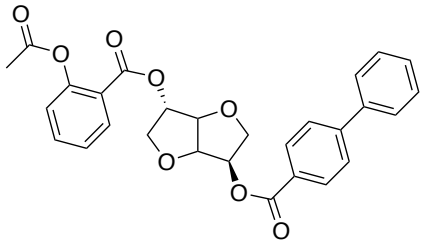	$C_{28}H_{24}O_8$
38	Isosorbide-2,5-biphenyl diester	506.55	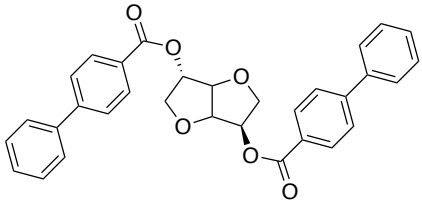	$C_{32}H_{26}O_6$

39	Isosorbide-2,5-disalicylate	386.36	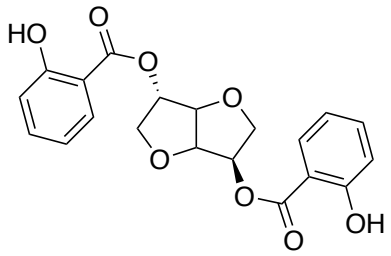	$C_{20}H_{18}O_8$
40	Isosorbide-2-ethylcarbamate	217.22	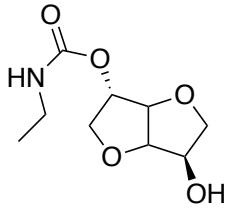	$C_9H_{15}NO_5$
41	Isosorbide-2-ethylcarbamate-5-(*p*-phenylbenzoate)	397.43	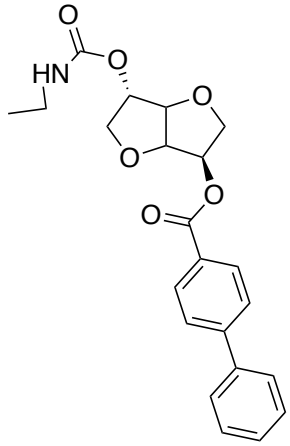	$C_{22}H_{23}NO_6$
42	Isosorbide-2-phenylcarbamate	265.27	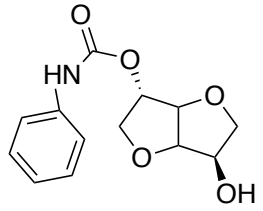	$C_{13}H_{15}NO_5$
43	Isosorbide-2-phenylcarbamate-5-(*p*-nitrobenzoate)	414.37	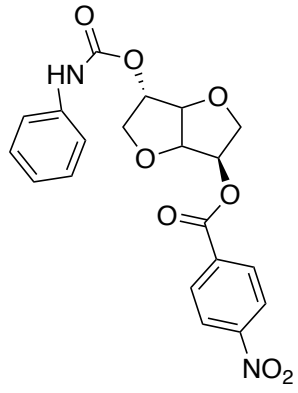	$C_{20}H_{18}N_2O_8$

44	Isosorbide-2-phenylcarbamate-5-nitrate	310.26	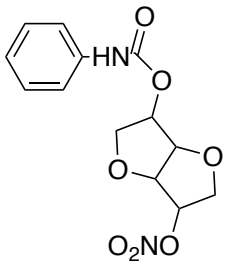	$C_{13}H_{14}N_2O_7$
45	Isosorbide-2-benzylcarbamate-5-(*o*-salicylate)	399.40	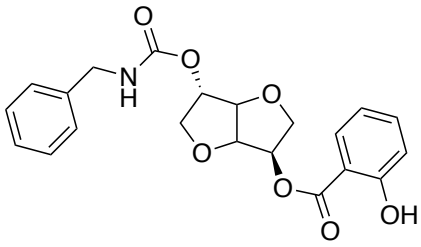	$C_{21}H_{21}NO_7$
46	Isosorbide-2-benzylcarbamate-5-(*p*-aminobenzoate)	398.42	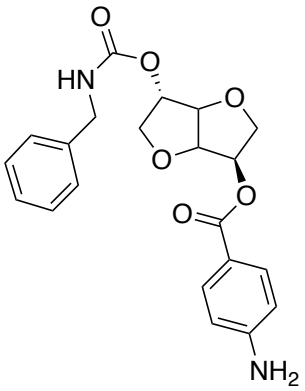	$C_{21}H_{22}N_2O_6$
47	Isosorbide-2-benzylcarbamate-5-nitrate	324.29	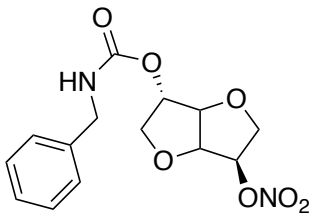	$C_{14}H_{16}N_2O_7$
48	Isosorbide-2-benzylcarbamate-5-(3-salicylate)	399.40	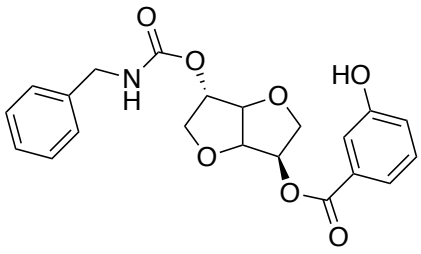	$C_{21}H_{21}NO_7$

49	Isosorbide-2-(2-methoxybenzoate)-5-nitrate	325.27	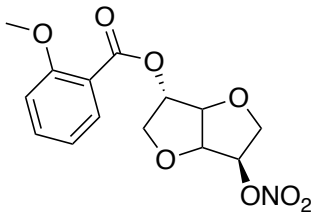	$C_{14}H_{15}NO_8$
50	Isosorbide-2-(3-methoxybenzoate)-5-nitrate	325.27	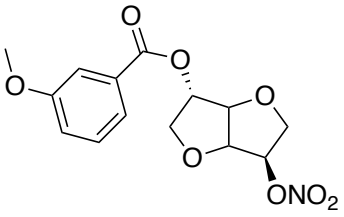	$C_{14}H_{15}NO_8$
51	Isosorbide-2-(4-methoxybenzoate)-5-nitrate	325.27	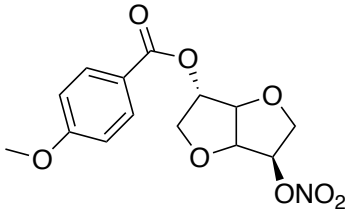	$C_{14}H_{15}NO_8$
52	Isosorbide-2-salicylate-5-isonicotinate	371.35	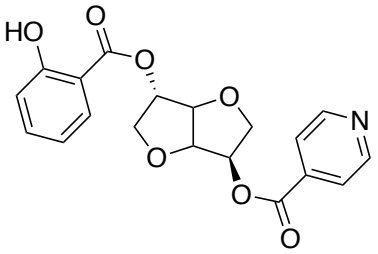	$C_{19}H_{17}NO_7$
53	Isosorbide-2-(3-methoxybenzoate)	280.28	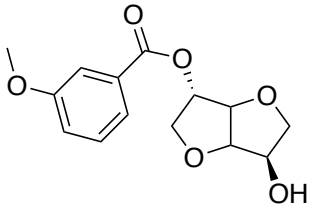	$C_{14}H_{16}O_6$
54	Isosorbide-2-(4-methoxybenzoate)	280.28	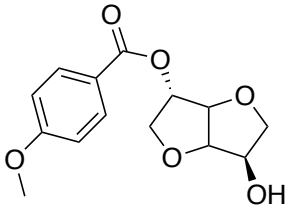	$C_{14}H_{15}NO_8$

55	Isosorbide	146.14	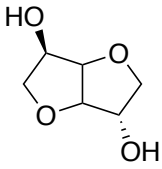	$C_6H_{10}O_4$
56a	Isosorbide-2,5-di-*o*-methoxybenzoate	414.41	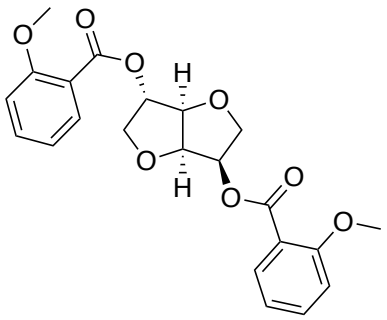	$C_{22}H_{22}O_8$
56b	Isosorbide-2,5-di-*m*-methoxybenzoate	414.41	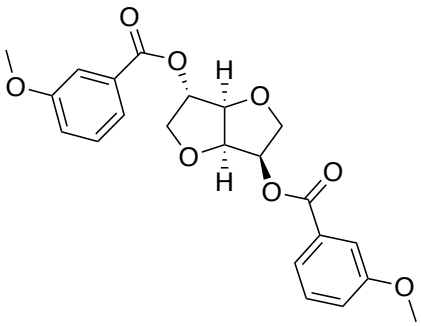	$C_{22}H_{22}O_8$
56c	Isosorbide-2,5-di-*p*-methoxybenzoate	414.41	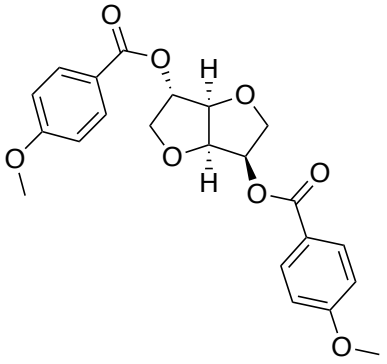	$C_{22}H_{22}O_8$
57a	Isosorbide-2-*o*-methoxybenzoate-5-nitrate	325.27	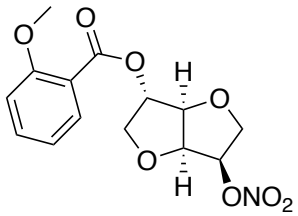	$C_{14}H_{15}NO_8$

57b	Isosorbide-2-*m*-methoxybenzoate-5-nitrate	325.27	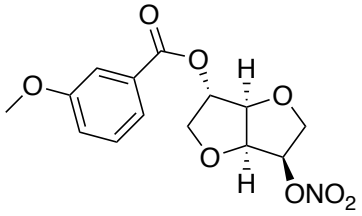	$C_{14}H_{15}NO_8$
57c	Isosorbide-2-*p*-methoxybenzoate-5-nitrate	325.27	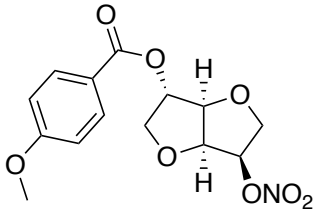	$C_{14}H_{15}NO_8$
58a	Isosorbide-2-*o*-methoxybenzoate	280.27	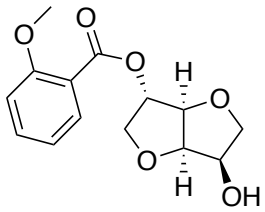	$C_{14}H_{16}O_6$
58b	Isosorbide-2-*m*-methoxybenzoate	280.27	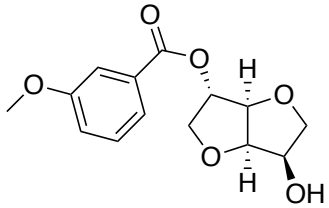	$C_{14}H_{16}O_6$
58c	Isosorbide-2-*p*-methoxybenzoate	280.27	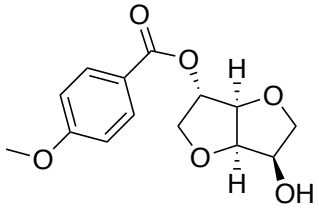	$C_{14}H_{16}O_6$
59a	Isosorbide-2,5-di-*o*,*m*-methoxybenzoate	414.41	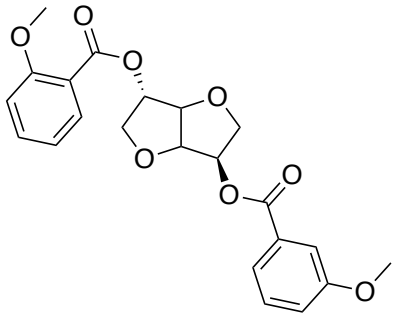	$C_{22}H_{22}O_8$

59b	Isosorbide-2,5-di-*o*,*p*-methoxybenzoate	414.41	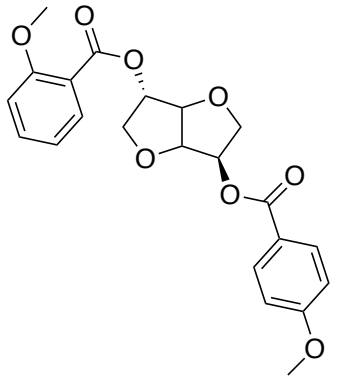	$C_{22}H_{22}O_8$
59c	Isosorbide-2,5-di-*m*,*o*-methoxybenzoate	414.41	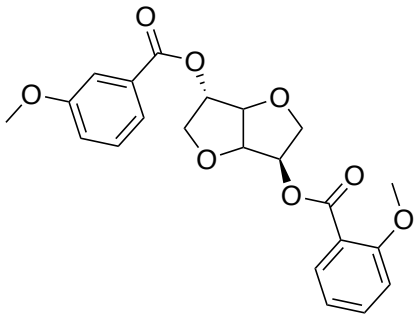	$C_{22}H_{22}O_8$
59d	Isosorbide-2,5-di-*m*,*p*-methoxybenzoate	414.41	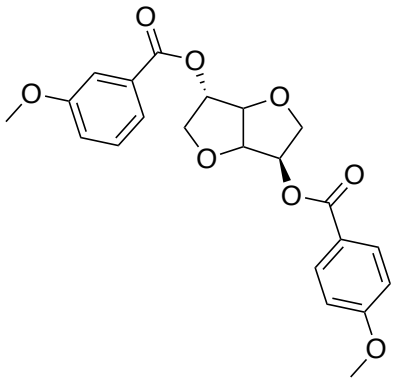	$C_{22}H_{22}O_8$
59e	Isosorbide-2,5-di-*p*,*o*-methoxybenzoate	414.41	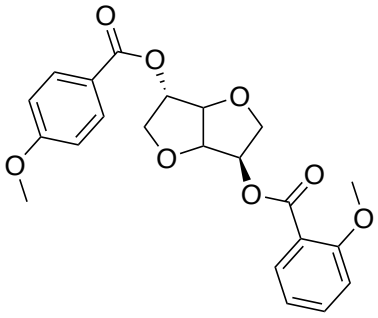	$C_{22}H_{22}O_8$

59f	Isosorbide-2,5-di-*p*,*m*-methoxybenzoate	414.41	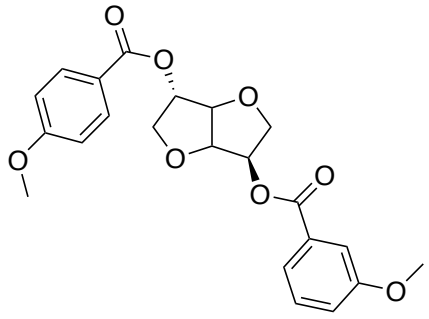	$C_{22}H_{22}O_8$
60a	Isosorbide-2-*o*-methoxybenzoate-5-nicotinate	385.37	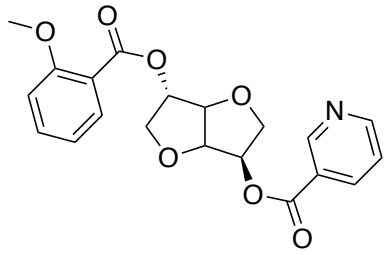	$C_{20}H_{19}NO_7$
60b	Isosorbide-2-*m*-methoxybenzoate-5-nicotinate	385.37	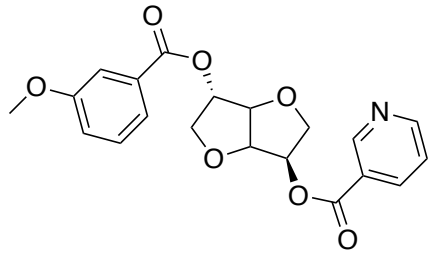	$C_{20}H_{19}NO_7$
60c	Isosorbide-2-*p*-methoxybenzoate-5-nicotinate	385.37	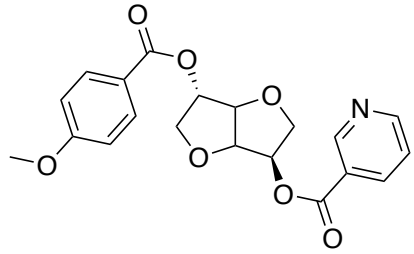	$C_{20}H_{19}NO_7$